Novel Enhancement of HVOF Thermal Sprayed Nanostructured WC-12Co / Inconel-625 Coatings for Tribocorrosion Applications

This thesis is submitted to Dublin City University as the fulfillment of the requirement for award of degree of

Doctor of Philosophy

By

Naif Alharbi

(B.Sc., M.Sc.)

School of Mechanical and Manufacturing Engineering

Dublin City University

Supervisors:

Dr. Joseph Stokes

Prof. Lisa Looney

Dr. Khaled Benyounis

December 2018

Dedication

*This work is dedicated to my
father who passed away during my childhood
&
my beloved mother and wife,
my wonderful brothers, and
my gorgeous sister
for their endless support and
patience
during all my studies abroad,
Without their help, I would have never
finished this achievement*

Thank You

Declaration

I hereby certify that this material, which I now submit for assessment on the programme of study leading to the award of Doctor of Philosophy is entirely my own work, that I have exercised reasonable care to ensure that the work is original, and does not to the best of my knowledge breach any law of copyright, and has not been taken from the work of others save and to the extent that such work has been cited and acknowledged within the text of my work.

Signed: …………………....

(Naif Alharbi)

ID No. 13210434   Date: December 2018

Acknowledgements

Publications Araising from this Research

__Book Chapters__

1- **N. Al Harbi**, K. Y. Benyounis, L. Looney, J. Stokes, Issue 2: Synthesis and Properties of Nanostructured Cermet Coatings, in S. Hashmi (Ed.), Materials Science and Materials Engineering, Elsevier Ltd, 2018.

2- **N. Al Harbi**, K. Y. Benyounis, L. Looney, J. Stokes, Issue 2: Laser Surface Modification of Ceramic Materials, in S. Hashmi (Ed.), Materials Science and Materials Engineering, Elsevier Ltd, 2018.

__Journal Papers__

3- **N. Al Harbi**, K. Y. Benyounis, L. Looney, J. Stokes. Laser modification of HVOF Thermal Sprayed Nanostructured WC-12Co Mixed with Inconel-625 Coatings for Petrochemical Industries" International Journal of Manufacturing Technology and Management (IJMTM) (*accepted with minor revisions).*

__Conference Papers__

4- **N.Al Harbi**, J.Stokes,Optimizing HVOF Spray process parameters and post-heat treatment for Micro/Nano WC–12%Co, mixed with Inconel-625 Powders: A Critical Review, 32nd International Manufacturing Conference (IMC32),September 3-4, 2015, Queens University Belfast,UK.

5- **N.Al Harbi**, K.Y. Benyounis, L. Looney, J.Stokes,The Influence Laser Beam Geometry on the Properties and Microstructure in Laser Re-Melting of Ceramic Materials-A Review, Advances in Materials and Processing Technologies (AMPT), December 14-17, 2015, Madrid,Spain.

6- **N. Al Harbi**, A. Al Hamed, C.P. Karthikeyan, R Padmanabhan, B. S. Yilbas, M. S. J. Hashmi, K. Y. Benyounis, L. Looney, J. Stokes , Laser Treatment of HVOF Thermal Sprayed Nanostructured WC-12Co Mixed with Inconel-625 Coatings for Wear Applications, International Thermal Spray Conference (ITSC), May 10-12, 2016, Shanghai, China.

7- **N. Al Harbi**, K. Y. Benyounis, L. Looney, J. Stokes. Wear and Corrosion Protection and Control Using Tungsten carbide cobalt WC12Co Nanostructured material- Technology Overview, International Thermal Spray Conference (ITSC), May 10-12 2017, Düsseldorf, Germany.

8- **N. Al Harbi**, K. Y. Benyounis, L. Looney, J. Stokes. Design of Experimental Study on the Relationship between Melt-Pool Geometry and Laser-Processing Conditions of Both

Blended and Singular Nanostructured WC-12Co HVOF Thermal Spraying Coating, Advances in Materials and Processing Technologies (AMPT), September 4-7 2018, Dublin, Ireland.

9- **N. Al Harbi**, K. Y. Benyounis, L. Looney, J. Stokes. Design of Experimental Study on the Relationship between Coating Bending Yield Strength and Laser Processing Conditions of Both Blended and Singular Nanostructured WC-12Co HVOF Thermal Spraying Coating, Advances in Materials and Processing Technologies (AMPT), September 4-7 2018, Dublin, Ireland.

Posters

10- **N. Al Harbi**, K. Y. Benyounis, L. Looney, J. Stokes. Design of Experiment Study of the Relationship between roughness and laser processing conditions of Both Blended and Singular Nanostructured WC-12Co HVOF thermal Spraying coating, International Thermal Spray Conference (ITSC), May 10-12 2017, Düsseldorf, Germany.

Awards

A Tell It Straight communication competition finalist for the best-written abstract and presentation, submitted as "Saving Billions of Dollars by Limiting Corrosion" (Dublin City University, 2017, https://www.youtube.com/watch?v=DaViitcFlg0).

Abstract

The HVOF thermal spray process is gradually becoming one of the leading coating techniques taking over traditional electrolytic chrome plating (EHC) due to EHCs harmful effects on the human body. Despite the high quality coatings produced by the HVOF thermal spray system, its role has yet to be validated in the replacement of other traditional coating techniques where specific surface properties are required in particular service operation. Obstacles associated with high-velocity oxy-fuel (HVOF) thermal spray significantly affect coating performance, especially in erosion and corrosion preventive applications. The coating layer therefore must be enhanced with a view to reducing microstructural defects and thereby prolonging the coating's service life.

This research is aimed at examining the effect of using a CO_2 laser system as a post-heat treatment and enhancement procedure applied to two coatings types investigated in this research that were deposited by an HVOF thermally sprayed process onto carbon steel 4041 substrates: firstly, 100% tungsten carbide cobalt (nano-structured) WC-12Co (Infralloy™ S7412) and secondly, WC-12Co nanostructured powder mixed with a nickel chromium alloy (Diamalloy 1005- Inconel 625) at an optimised weight percentage composition of 75% and 25% respectively. The work was carried out through the introduction of experimentally based mathematical models developed by applying response surface methodology (RSM) through Box-Behnken design (BBD), based on three levels of each factor selected, namely laser power, scanning speed and focal position/beam size, using Design of Expert software related to the coating's erosion resistance, melt-pool geometry, mechanical properties and operating cost of the laser treatment. Furthermore, the desirability optimisation approach, based on two criteria (quality and cost), was used for both coatings in conjunction with RSM to determine the optimal combination of the laser parameters to achieve the required laser-treated coating desirability. Different outcomes of surface properties were achieved by varying the laser-processing parameters. The results demonstrate that significant improvement in coating erosion wear (dry and slurry erosion) and mechanical properties (bending strength, surface roughness and microhardness), compared to as-sprayed coating, was achieved after laser treatment in both coating types, especially the singular nanostructured WC-12Co coating. The optimal laser settings found in the quality criteria are 350 W, 37.24 mm and 150.00 mm/min for laser power, focal position and scanning speed, respectively, for the monomial nWC-12Co

coating and 350 W, 45 mm and 300 mm/min for the cost criteria. To the same extent, the optimal setting for the mixed coating for the quality criteria are 169 W, 35 mm and 257.4 mm/min and 250 W, 45 mm and 300 mm/min for the cost criterion. The optimal laser setting mentioned in the quality criteria for the erosive wear, for example, saw an approximately five- to seven-fold reduction in mass loss for dry and slurry erosion in comparison to the untreated monomial nWC-12Co coating. The latter setting created an approximately 7-fold reduction in mass losses for the dry erosion and a 27% reduction in mass losses for slurry erosion compared to their untreated counterparts.

This can mainly be ascribed to the elimination of the discrete splat structure, porosity and microcrevice, as well as the enhanced homogeneity of the nano-scale WC hard ceramic distribution across the metal matrix. Less improvement was seen for the mixed coating as a result of high energy fluence (J/mm^2); the coating surface became rough and gas pockets started forming within the melted zones, creating a porous coating layer that had a negative impact on coating bending strength and erosion performance. Moreover, the results indicate a strong correlation between irradiance and residence time of the laser processing, along with coating composition, with respect to the melt-pool dimensions. Finally, based on the enhancement achieved in the coating properties under the optimal laser settings for both coatings, compared to the untreated ones, the results prove that laser post processing is a cost-effective procedure (aproximately 17% or less of that of HVOF) and therefore will markedly extend the service life of both coatings, saving a lot of money that would be wasted in the case of the untreated ones.

Contents

List of Figures

List of Tables

Nomenclature

Abbreviations

HVOF/ HVAF	High Velocity Oxy/Air Fuel technique
nWC-12Co	Nanocomposite WC-12Co Thermal Spray Powder
MTBF	Mean Time Between Failures
MTTR	Mean Time To Repair
FEA	Finite Element Analysis
ASTM	American Society for Testing Materials
DJH	Diamond Jet Hybrid
DOE	Design of Experiment data analyse software
RSM	Response Surface Methodology
BBD	Box-Behnken Design
CCD	Central composite design
ANOVA	Analysis of Variance
SS	Sum of Squares
df	Degree of freedom
MS	Mean square
HAZ	Heat-Affected Zone
BM	Base Metal
FZ	Fusion Zone
XRD	X-ray Diffraction
SEM	Scanning Electron Microscope
EDS	Energy Diffraction
FMR	Flow Meter Rate
TFT	Thin film transistor
PLC	Programmable Logic Controller
RAID	Redundant Array of Independent Disks
CNC	Computer Numerical Control
CAD	Computer-Aided Drafting
SLPM	Standard Litre Per minute
NLPM	Normal Litres Per minute

TEM	Transverse Electro-Magnetic
MTI	Moving Target Indication
D_m	Melting Depth
t_c	Coating Thickness
R_{qa}	Average Surface Roughness
H_{av}	Average Hardness
P.S.Rebate	The average value of the five Repeated experiments in the DOE marix

Symbols

R^2	Statistical measure of how close the data are to the fitted regression line
P	Number of the Coefficients in the model
n	Number of Experiments
Prob>F	Probability of seeing the observed F value if the null hypothesis is true
P-value	Tests the null hypothesis that data from all groups are drawn from populations with identical means
F-value	Test for comparing model variance with residual (error) variance
λ	Wavelength

CHAPTER 1 - Introduction

This chapter will describe the motivation behind this work and its contribution to the science of surface engineering. In addition, the thesis structure outline is also presented.

1.1 Overview

The long-term wear and deterioration of equipment is certainly the most common form of degradation of components in most industrial plants. According to Bartosik et al. [1], dilapidation of such machines is associated to wear, corrosion and erosion-corrosion effects. In the oil and gas industry, these effects are largely caused by sand particles that are often mixed with crude oil, which has been found to contain different elements, including hydrogen sulphide, carbon dioxide, organic acids, bacteria, as well as water [2]. Consequently, the resultant metal contamination leads to the damage of different machine components. In addition, the degradation process poses a number of safety risks such as contamination of food, environment and even water which are for human and animals' consumption. Such risks are a major concern for both the users and the manufacturers, especially in view of the costs associated with the machinery repairs and compensation in the case of accidents. It is estimated that the effects of wear and corrosion in the oil and gas industry, particularly in developed countries, constitute about 4% of the gross internal product of these countries [3].

The increase in production and operational costs in the oil and gas industry as a result of corrosion and wear effects has, in the recent past, prompted engineers to focus more on effective surface treatment approaches on the manufactured machinery. In particular, the Gulf region, which is undoubtedly one of the richest regions in terms of oil deposits, has attracted significant attention in regard to modern engineering materials due to its harsh environment. This requirement was even magnified in the last two years due to the dramatic turnaround of both the fall in international energy prices to below $75, as illustrated in Figure 1-1, and the rise of crude oil production to compensate for the price drop [4, 5].

Novel Enhancement of HVOF Thermal Sprayed Nanostructured WC-12Co / Inconel-625 Coatings for Tribocorrosion Applications| **Al-Harbi, Naif I**

1
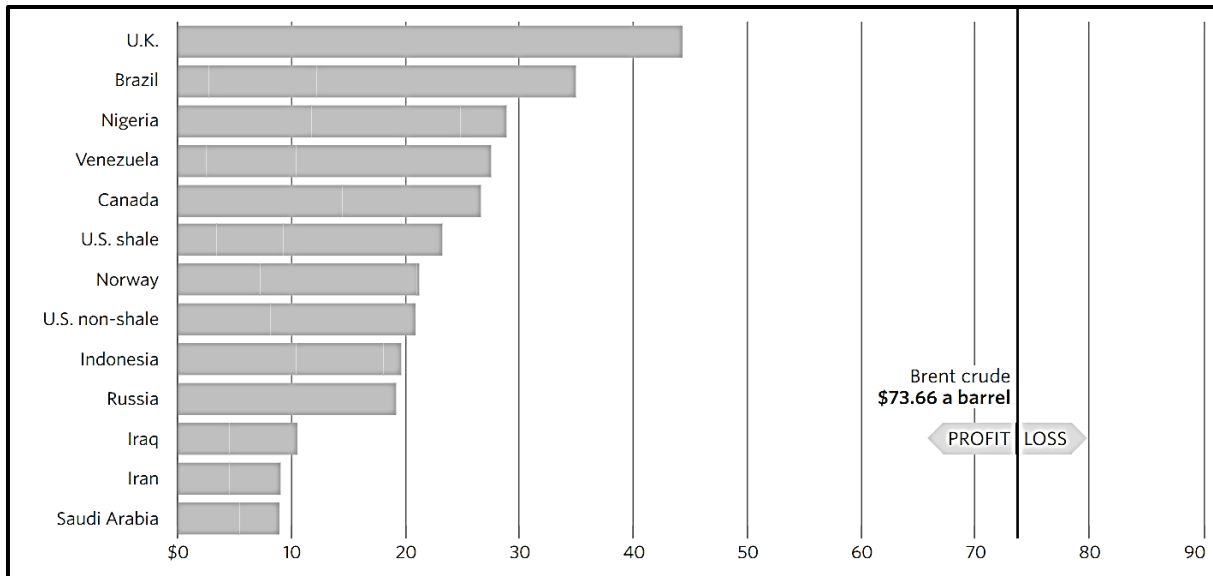
Figure 1-1: Overall cost for production of one barrel of oil as of (May/15/2018) [4].

Most of these serviceable engineering components' surfaces are made of metallic materials which offer varying bonding strengths. However, in such strenuous engineering environments, these components fundamentally require combined erosion and corrosion resistance treatments to provide these surfaces with higher mechanical strength and thereby enhance their surface characteristics. One of the popular surface treatment solutions is hard facing, which consists of coating the bulk material's surface with different layers of different materials; typically, covering an object (substrate) in order to impart some properties to it. In most cases, the property of the coating and those of the substrate differ; hence, the end result is a combination of these properties to form a superior product. There are different methods/processes of depositing coating materials onto the bulk material and these can be classified according to their coating technologies: electrochemical deposition, chemical deposition, chemical vapour deposition (CVD), physical vapour deposition (PVD), thermal spray process, build-up welding and build-up brazing [6]. The selection of a particular process over the other is dependent on the material to be deposited, substrate limitations, the required rate of deposition, the associated coating cost, required process energy, availability of required equipment, the targeted process purity and environmental considerations [7, 8]. One of the most successful and popular thermal spraying techniques is the high velocity oxy-fuel (HVOF) spraying process which has been utilized in many industries because of its flexibility and low cost. In comparison to the other spray techniques, HVOF has proven to be a preferable depositing technique used by industries, especially for temperature sensitive

Novel Enhancement of HVOF Thermal Sprayed Nanostructured WC-12Co / Inconel-625 Coatings for Tribocorrosion Applications| **Al-Harbi, Naif I**

2

materials such as cermet's [9]. Additionally, several characteristics of this technique can also be considered, including: high deposit density and strong adhesion bond to substrates, lower porosity and oxidation, high compressive residual stresses to improve the coating lifetime and cost effectiveness [10]. A typical example of such a coating sprayed by HVOF thermal spray on to metallic substrates are cermet powders, consisting of tungsten carbide (WC) hard particles mixed with some metallic binder such as Co, Co-Cr or Ni. This mixture of WC/metallic binder has been well known since the early 1970's for its excellent wear/erosion resistance [11]. It is being used extensively as coatings for industrial applications which require sliding, abrasion, and erosive wear resistance [9, 12, 13]. Moreover, the nickel-chromium alloy (Inconel-625) coating material is more suitable for applications requiring a coating material with excellent corrosion resistance within corrosive environments. This contributes to a high density coating microstructure provided by the materials, which leads to significantly lower porosity in the coating layer [14].

Due to the corrosive behaviour of some of its chemical compositions, particularly chromium [15, 16], the variation of the mixed powder percentage of feedstock material (e.g. nWC-12Co + Inconel 625 wt. %), can affect the HVOF thermal spray coating performance in erosion-corrosion applications, as mentioned by Al-Hamed [17]. However, some engineering environments are challenging and require composite surface coating microstructures to reach their goal (good wear and corrosion resistance). To achieve this, at least two or more combinations of coating materials may be required for the desired microstructure.

Despite the various types of materials used as coatings for wear and corrosion resistance performance, coating integrity is also important, especially if microstructural defects are detected in the coating layer. Among them, the porosity of the coated layer (confined and interconnected), dark inclusions (oxidization) between the splats, mechanical bonding at the coating/substrate interface and inhomogeneity of the coating structure, all of which have a major effect on its performance, especially in erosion/corrosion preventative applications. In order to further improve the coating quality and to eliminate, or at least reduce the defects listed above, the laser surface modification deserves consideration. Laser processing as a method of post-treatment of pre-coated samples via laser hardening or remelting, offers some advantages in comparison to the traditional treatments, including its chemical cleanliness as well as the fact that there is protection against non-mechanical contact with the surface.

Novel Enhancement of HVOF Thermal Sprayed Nanostructured WC-12Co / Inconel-625 Coatings for Tribocorrosion Applications| **Al-Harbi, Naif I**

3

Additionally, the process is precise, has a controlled thermal profile, is easy to automate and any distortion is controlled through thermal penetration [18]. Many researchers studied the effects of laser melting in the microstructure and properties of HVOF sprayed coating.

Poza et al. [19] studied laser glazing of cold-sprayed coatings and reported that laser glazing reduces interconnected porosity within the coatings. The microstructure of the remelted samples showed a columnar dendritic structure, which had a negative effect on the microhardness value. However, this reduction was still higher than the base metal microhardness value. Laser remelting of HVOF Diamalloy coating with WC blend has been highlighted by Yilbas and Akhtar [20]. They examined the microstructure and morphological variations in the coated layer after laser treatment. It was shown that a treated layer, free from cavities and cracks, as well as a uniform melt could be obtained. A cellular microstructure was noticed with nonuniform sizes and orientations due to the different cooling rate across the thickness of the coated layer. Al-Taha [21], studied the effect of LDL Diode laser in remelting of Inconel 625 coatings blended with WC particles in wear and corrosion performance and found an improvement in corrosion resistance due to removal of the discrete splat structure and micro crevice, and reduction of the compositional gradient between the WC (tungsten carbide) and Inconel 625 matrices. From the above research work, it is clear that the laser treatment significantly enhanced the corrosion resistance of the coating, but in some cases the wear performance deteriorated. However, one of the main important aims of this work is to analyse wear resistance, and enhancing the corrosion resistance by laser treatment, therefore while decreasing the wear resistance performance is not beneficial, particularly in erosion-corrosion (Tribcorrosion) wear applications, such as those found in the oil and gas industry, (oil separation plants and refineries) [22, 23]. Hence, enhancing the corrosion resistance while maintaining wear performance should be considered.

From the literature, the laser processing conditions were found to play an important role in the coating properties, especially in cermet coating materials, with regard to the melting quality, such as the porosity and crack level. Equally some alloying elements (e.g., chromium, carbon) can be eliminated by the formation of new phases, therefore, the proper control of the laser processing conditions, can achieve the desired objectives under investigation.

This research will focus on a detailed investigation of how laser surface modification affects wear/corrosion resistance of two coating material types, namely, 100% tungsten

Novel Enhancement of HVOF Thermal Sprayed Nanostructured WC-12Co / Inconel-625 Coatings for Tribocorrosion Applications| **Al-Harbi, Naif I**

4

carbide cobalt (nano-structured) WC-12Co (Infralloy^{TM} S7412) and 75% WC-12Co (nano-structured powder) mixed with 25% Nickel Chromium alloy (Diamalloy 1005- Inconel 625) [17]. A laser layer treatment was induced onto each applied coating and the performance of the as-sprayed components is compared and given in Chapter 5.

1.2 Contribution to the science of surface engineering

This research investigated the HVOF thermal spray of WC-12Co coating used in the prevention of wear/corrosion on components. Currently, there is great interest in the field of nanostructured materials, whose granular sizes are typically less than 100 nm. With the recent advances in the production of high quality nanoscale powders, including atomisation, colloidal precipitation, mechanical milling, and vapour phase nucleation and growth, the focus of nanostructured materials research is now migrating from one of synthesis to that of processing, as in the fabrication of nanostructured coatings using the HVOF thermal spray process. The nanostructured coatings are extensively tested to extend product life, increase performance and reduce production and maintenance costs; many of such benefits seen in the oil and gas industry. The physical and mechanical properties of HVOF sprayed coatings are strongly influenced by the nano- or micro-structure of the deposit, thus, it depends to a large extent on the physical and chemical states of the particles at the point of impact on the substrate, such as velocity, temperature, degree of melting and oxidant content. To date, most of the research work on laser surface remelting has focused on the conventional WC-12Co coating and the only known research work on WC-12Co nanostructured coatings has been performed by Chen et al. [24]. This was accomplished by selecting only one set of laser parameters settings; hence the effects of varying the laser processing conditions have not been investigated. In addition, blending these hard particles with a nickel chromium alloy (Inconel 625) at an optimised weight percentage composition of 75% to 25% [17], was also not addressed. The literature also shows a gap of knowledge in studying the effect of laser treatments on such coatings and the effects of its processing conditions on mechanical and metallurgical changes. Consequently, the main objective of this research was to obtain detailed knowledge of the effects of the laser surface modification with respect to various mechanical properties and the erosion and erosion–corrosion responses post laser treatment. This research will use design of experiment (DOE) software to analyze experimental data using a DOE approach featuring a number of experiments designed to reveal factors affecting coating performance. Where at the end of this research; the optimum laser parameters for

Novel Enhancement of HVOF Thermal Sprayed Nanostructured WC-12Co / Inconel-625 Coatings for Tribocorrosion Applications| **Al-Harbi, Naif I**

5

each of the research objectives will finally be provided. This is invaluable especially for each of the wear types under investigation in this research (dry erosion and erosion-corrosion) because both experience different environmental conditions in the oil and gas industry; for dry erosion, the material is removed from the target surface by the eroded particles (e.g. coarse and fine sand particles) in a dry stream, which involves mechanical processes only. Common areas affected by such wear in the pipelines include the outer surface, fittings, and oil well drilling. In contrast, the erosion-corrosion wear type, which is also termed aqueous erosion, involves both mechanical and electromechanical processes that affect each other. This is formed as a result of the impignation of solid particles, transported through the petroleum and gas products, that are surrounded by corrosive gases. Common components that are subjected to such aqueous erosion include chock valves, elbows, tees, bends, pumps, separation equipment, and so on, in both upstream and downstream conditions.

Generally in the oil and gas industry, based on economic considerations and its low cost, carbon steel is selected both for the pipelines that extend for thousands of miles and for most of the production components. As part of this, the critical region, which has a short service life as a result of material removal by either dry or aqueous erosion, are coated with a layer of materials with superior mechanical and corrosion properties, such as tungsten carbide, chromium carbide, or boron (containing composites of metallic alloy matrices (e.g. Co, Ni, or Cr)) to extend its lifespan. However, these coatings cannot prevent either type of wear permanently because this implemented layer in the carbon steel surface also has a limited lifetime cycle. Scheduling maintenance at various times is the only way to detect and overcome any coating failure and take control of the situation quickly before any serious damage is done.

To look at the example of the Saudi Aramco company, which is considered the largest oil producer worldwide; it reported that it schedules its maintenance plans, known as testing and inspection (T&I), over its thousands of miles of pipelines every three to five years [23]. Therefore, any alteration arising from extending this period will result in a significant increase in the company's net profit margin as a consequence of the firm saving billions of dollars in maintenance-related expenses (e.g. labour costs, coating or parts replacement, loss of revenue caused by disruption in the supply, and loss of reliability), which are attributed to the operation cost. This could be achieved by optimizing the coating quality to an even greater degree, which is the main aim of this research.

Novel Enhancement of HVOF Thermal Sprayed Nanostructured WC-12Co / Inconel-625 Coatings for Tribocorrosion Applications| **Al-Harbi, Naif I**

6

1.3 Aims and objectives of the research

The research aims to investigate the possibility of improving the wear/corrosion resistance of coatings sprayed onto AISI 4140 carbon steel substrate surfaces by using a 1.5 kW CO_2 Rofin laser and comparing the performance to that of the as-sprayed components.

The coating materials used include the following:

* nWC-12Co
* 75 wt. % nWC-12Co + 25 wt. % Inconel 625

The research work will include the investigation of the metallurgical and morphological changes, mechanical properties and wear and erosion-corrosion performance for various coatings prior to and post laser remelting, to achieve the following objectives:

1. To create operation windows for studying three laser operation conditions to achieve the following: coating with free porosity, crack free and control the melt pool dimension without creating high dilution from the substrate surface, where a very thin layer from the substrate surface is desirable for achieving strong metallurgical bonding and minimal WC hard particles melting.

2. To study the HVOF coating microstructure before and after laser treatment, in terms of coating defects, phase formation and WC hard particles uniformity distribution throughout the coating cross section.

3. To investigate and analyse some of the mechanical properties of the HVOF thermal spray coating before and after laser treatment, where the properties include: hardness, flexibility (bending), and surface roughness.

4. To study and analyse the performance and wear mechanism of the HVOF thermal spray coating under different wear types, namely, erosion wear and erosion-corrosion wear before and after laser treatment with different laser processing conditions.

5. The optimisation of the laser process parameters using design of experiment (DOE) software to analyse the experimental data and to establish the best laser conditions, to yield enhanced wear, erosion-corrosion and mechanical properties listed above. The cost effectiveness of adding laser processing post deposition will be investigated. As an example; if the laser treatment increases the coating lifespan by 100% and the cost of laser processing was significantly less than the coating processing, then, the laser process may be considered an efficient and economic proposal in extending life of the component.

Novel Enhancement of HVOF Thermal Sprayed Nanostructured WC-12Co / Inconel-625 Coatings for Tribocorrosion Applications| **Al-Harbi, Naif I**

7

1.4 Thesis outline

The thesis is comprised of six chapters, as listed in the schematic outline in Figure 1-2, where Chapter 1 is the introduction.

Chapter 2: Explores different aspects related to this research work, first by providing a general background related to the fundamental aspects of wear and corrosion, followed by brief descriptions of the thermal spray coatings. The chapter also reviews the nanostructured materials that were selected in this research (nWC-12Co) in terms of their synthetic process and the scientific justification for using them as a replacement for conventional coating. Also, the chapter covers the general background of the principle of laser energy and laser rapid solidification, and offers a review of the literature regarding laser's potential for improving the wear and corrosion of the HVOF thermal spray coating, along with the influence of laser beam geometry and laser processing parameters on laser remelting of ceramic materials.

Chapter 3; Discusses the materials and equipment that will be used in the experimental work in this research. It includes the two different materials, the equipment, the procedure of blending 75 wt. % nWC-12Co + 25 wt. % Inconel 625, the HVOF thermal spray facility and its spray parameters, laser processing set-up and laser treatment procedure, design of experiments, and the sample surface preparation and its characterization techniques.

Chapter 4; The chapter presents an investigation into the optimization of two laser operation parameters used to melt the two coating materials, namely; scanning speed and laser power. It aims to select the best laser processing conditions for coating layers with minimal or no cracks, low porosity and dilution from the substrate.

Chapter 5; discusses the materials characterization pre the HVOF thermal spray coating, post HVOF coating, and after laser treatment. The characterization will include the coating defects, phase transformation, uniformity distribution across the coating surface. The chapter also presents the values and DOE data analysis for of melt-pool geometry, surface roughness, coating hardness, bending yield strength, dry erosion and erosion-corrosion obtained after laser treatment of the coating according to the experimental arrangements of laser processing conditions created in the DOE. The operating cost effectiveness of using laser processing will be assessed.

Novel Enhancement of HVOF Thermal Sprayed Nanostructured WC-12Co / Inconel-625 Coatings for Tribocorrosion Applications| **Al-Harbi, Naif I**

8

Chapter 6: Provides the current conclusion of this work and the novelty of this research within the area of surface engineering. The chapter concludes with the recommendations for future work.

Chapter 1			
Overview	Contribution to the science of surface engineering	Aims and objectives of the research	Thesis outline

Chapter 2			
Fundamental aspects of wear and corrosion	Thermal Spray Coating	Nanostructured coating: State-of-the-art	Laser Surface Engineering

Chapter 3					
Research Materials	HVOF thermal spray facility and procedure	Laser treatment facility and procedure	Design of experiments	Coating Characterizations	Mechanical and Wear Testing

Chapter 4	
Optimization of the laser processing conditions	Summary of the results

Chapter 5	
Results and discusions	Summary of the results

Chapter 6		
Conclusions	Thesis novelty	Recommended future work

Figure 1-2: Schematic diagram outline the organization of the thesis.

Novel Enhancement of HVOF Thermal Sprayed Nanostructured WC-12Co / Inconel-625 Coatings for Tribocorrosion Applications| **Al-Harbi, Naif I**

9

CHAPTER 2 – Literature Survey

- **Wear and Corrosion in Oil and Gas industry** (1)
- **HVOF Thermal Spray Technology, and State of the Art** (2)
- **Overview of WC-Co coating materials** (3)
- **Laser Surface Modification of Thermal Spray Coatings- Technology Overview** (4)
- **Literature survey summary** (5)
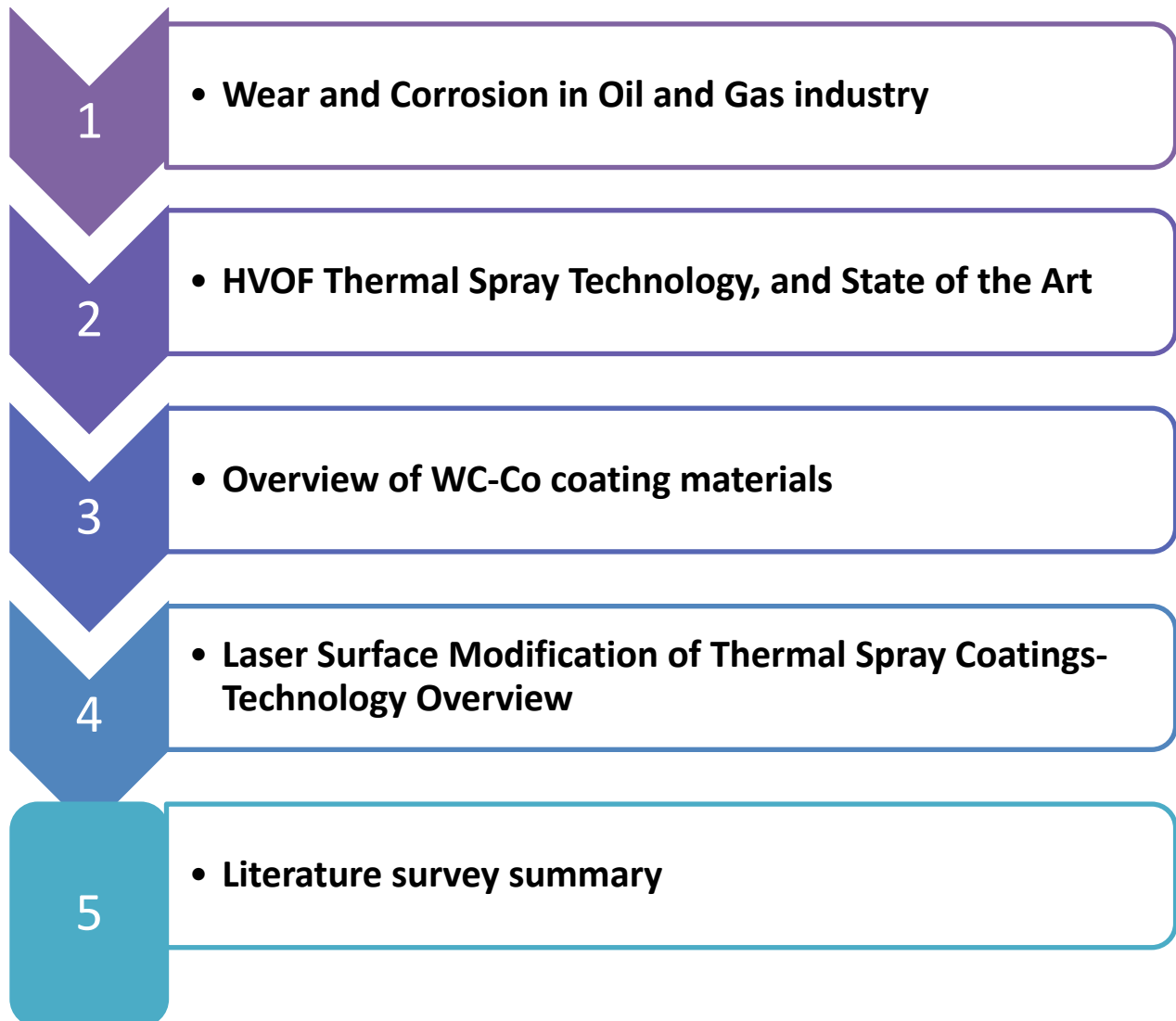
Figure 2-1: The schematic outline of this chapter.

Novel Enhancement of HVOF Thermal Sprayed Nanostructured WC-12Co / Inconel-625 Coatings for Tribocorrosion Applications| **Al-Harbi, Naif I**

10

2.1 Introduction

For engineering components to withstand heavy servicing, they rely on their bulk material properties and characteristics, as well as their surface design. According to Haefer [25], the surface is responsible for the following functions when interacting with thermal, mechanical, chemical, and electrochemical environments:

- Optical behaviour;
- Decorative behaviour;
- Matched interface behaviour;
- Defined tribological behaviour;
- Wear resistance;
- Corrosion resistance.

Surface engineering, a branch of science, manages methods of achieving desired surface requirements [12]. The demands of a particular component's surface property is determined by the particular load conditions under which their final product will operate. Figure 2-2 summarizes the main types of load conditions, divided into surface and volume loads [6].
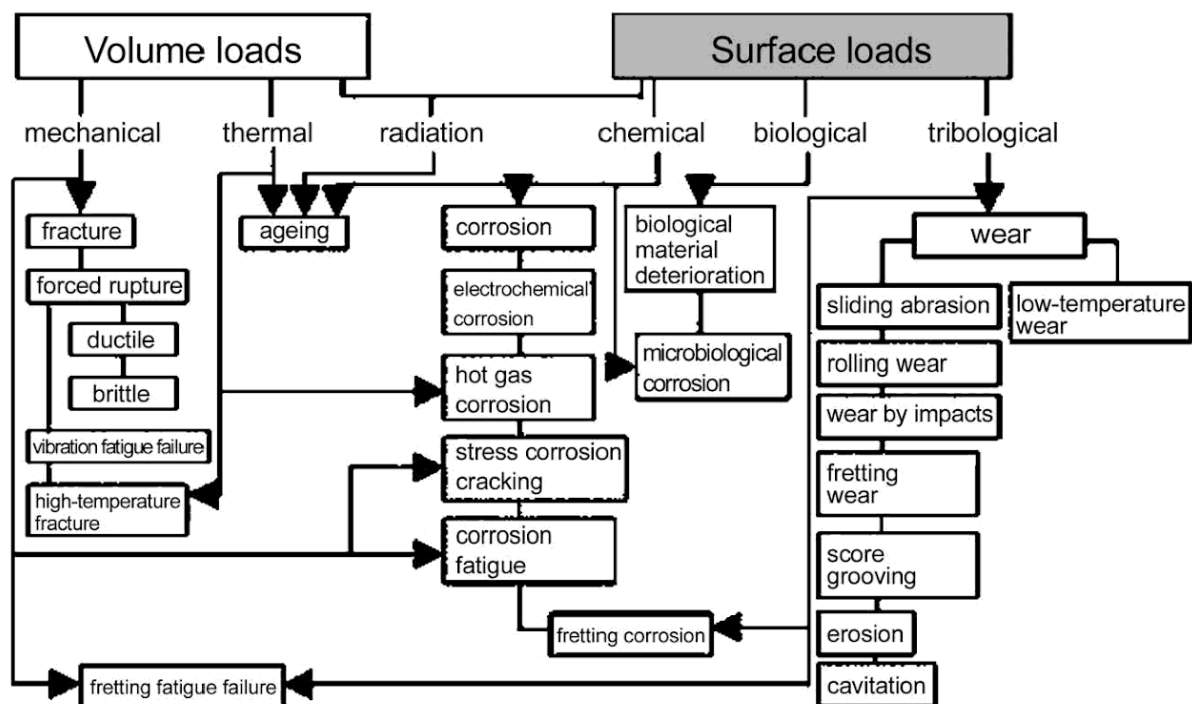
Figure 2-2: The main volume and surface loads on the part's surface, adapted from [6].

Novel Enhancement of HVOF Thermal Sprayed Nanostructured WC-12Co / Inconel-625 Coatings for Tribocorrosion Applications| **Al-Harbi, Naif I**

11

Material behaviour depends heavily on the surface contact area and the environment to which the material is subjected [25]. The surface of a metallic material consists of a matrix (or conglomerate) of individual grains that vary in bond strength and size depending on the manufacturing method and the elements used in forming the grains [12]. The surface of such components may require treatment to enhance surface characteristics. Surface treatments that can change the microstructure of bulk materials include heating and cooling using flame, induction, laser, or electron beam techniques. Another treatment option is mechanical treatment, which is achieved through cold working. Treatments which change the chemistry of a surface, include; nitriding, carburizing, nitrocarburizing, carbonitriding, boriding, chromizing, aluminizing, and siliconizing [12]. Another form of surface treatment is hardfacing, in which the surface of the bulk material is protected with a layer of material whose qualities are superior to those of the bulk material. Hardfacing methods include welding or cladding and coating deposition. Each technique causes either beneficial or detrimental chemical and physical effects on the bulk material [12].

For the oil and gas industry, minimizing wear and corrosion deterioration on the surfaces of mechanical components are a primary concern. Due to their complexity and variety (indicated in Figure 2-2), the main wear and corrosion modes that usually accrue in the oil and gas industry are therefore discussed in the following sections.

2.2 Wear and Corrosion

2.2.1 Tribological Wear

Abrasion wear is the deterioration or gradual loss of the surface of a material caused by relative motion of another material or substance (that is, physical causes). Wear depends on system properties, environmental conditions, the dynamics of relative motion, phase transformations, and chemical reactions [26]. Engineering environments are complex; as often involving the physically and chemically degradation of a component's surface. Lubrication reduces friction and tribological wear, but conventional liquid lubricants tend to fail under extreme conditions—high speed, low pressure, high load, and corrosive environments. Moreover, in other cases lubricants cannot be used, so that a component's performance depends on its surface. Surface coatings and improved tool surfaces can enhance the finished surface of the machined part. The surface topology depends primarily on the process used for forming the material, such as casting, molding, abrading, and cutting.

Novel Enhancement of HVOF Thermal Sprayed Nanostructured WC-12Co / Inconel-625 Coatings for Tribocorrosion Applications| **Al-Harbi, Naif I**

12

Waviness, the error of form, and roughness are components of surface texture that affect the geometrical texture of the material [12].

2.2.1.1 Wear mechanisms

The major categories of wear mechanisms are sliding wear, impact wear, and rolling contact wear. Sliding wear can occur by various mechanisms including adhesion, abrasion, fatigue, erosion, corrosion, and erosion-corrosion. In most cases, sliding wear begins with one mechanism and it can then be preceded by a separate mechanism, which complicates the failure analysis. The only common item between the wear mechanisms is the removal or elimination of the solid materials from the rubbing surface [12]. The impact wear consists of only two mechanisms: two-body impact wear and multi-body impact wear [12]. The rolling contact wear is divided into two mechanisms: pure rolling contact and the rolling-sliding contact.

The standard theoretical wear behaviour over the lifetime of a component is shown in the graph depicted in Figure 2-3, illustrating the mean volume as a function of distance or time [12, 27]. Full details of wear types are detailed specifically by Stokes [12].
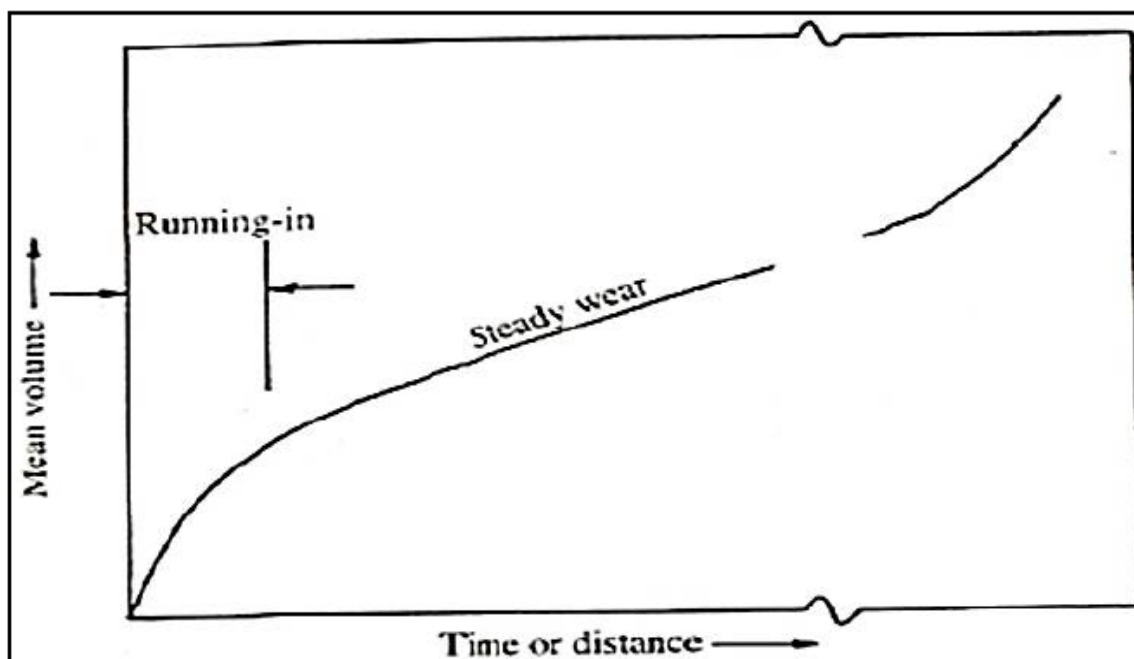
Figure 2-3: Typical wear behaviour of components as a function of time/distance [27].

Novel Enhancement of HVOF Thermal Sprayed Nanostructured WC-12Co / Inconel-625 Coatings for Tribocorrosion Applications| **Al-Harbi, Naif I**

13

2.2.2 Tribochemical (Erosion-Corrosion) Wear

Oil/gas components often fail due to erosion-corrosion wear, therefore its important to focus on such issues. Tribochemical wear is accompanied by the physical and chemical reaction from the environment causing deterioration of a surface, described under the broader category called tribocorrosion or corrosion-erosion wear. Erosion-corrosion occurs because of the presence of carbon dioxide gas, water, and sand particles, which are also produced by hydrocarbons [28]. Carbonic acid, formed when (CO_2) carbon dioxide gas dissolves in water, directly deteriorates metallic materials or dissociates it to a certain degree to form a corrosive solution that destroys the carbon steel materials in service [28]. Depending on the surrounding operating conditions, protective iron carbonate ($FeCO_3$) films usually form on steel surfaces to stop further corrosion attacks. However, this protective film is typically corroded continuously by sand particle collisions, as illustrated in the schematic diagram give in Figure 2-4, exposing new surfaces to further corrosion attacks.
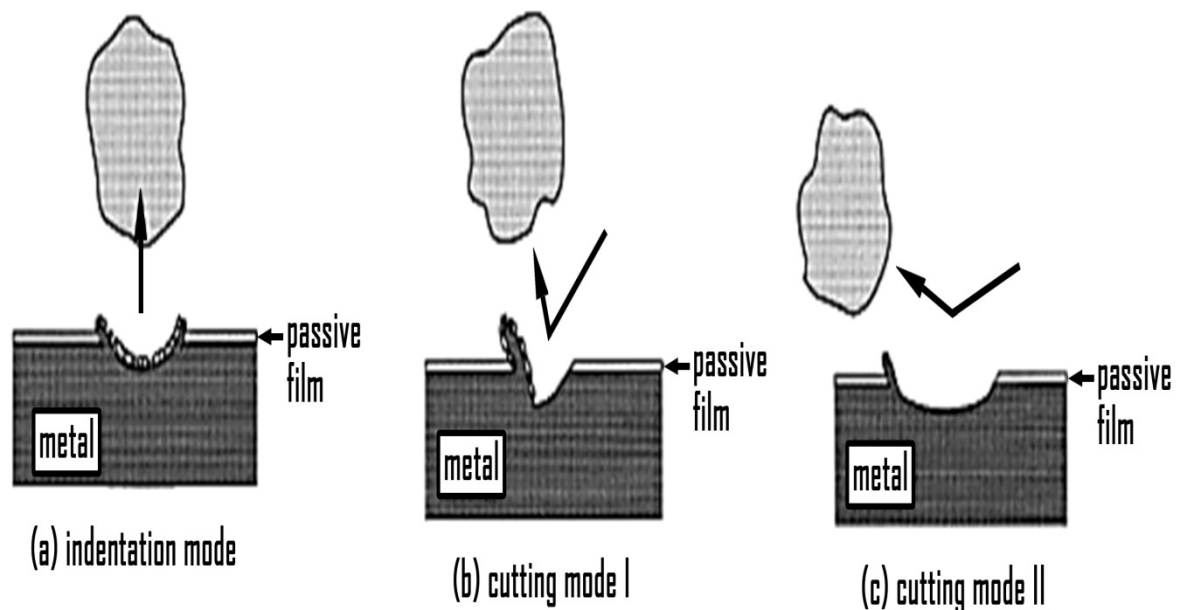
Figure 2-4: Schematic illustrations of the erosion-corrosion wear mechanism [28].

The combined effect of carbon dioxide gas corrosion and sand erosion is called erosion-corrosion [28]. Damage caused by erosion-corrosion is well known to engineers in the oil and gas industry, as the main reason for pipeline components failures such as chokes, tees, elbow, turbine/pump propellors, joints, flanges, and surface and sub-surface safety valves, as shown in Figure 2-5. Poor understanding of erosion-corrosion is the primary cause of such failures [28].

Novel Enhancement of HVOF Thermal Sprayed Nanostructured WC-12Co / Inconel-625 Coatings for Tribocorrosion Applications| **Al-Harbi, Naif I**

14

Figure 2-5: Examples of typical erosion-corrosion damage in the oil and gas industry: (A) a carbon steel pipeline, (B) a choke valve, and (C) a propeller pump [28, 6].

These failures pose a significant threat to the safety of people, the environment, and the operation of oil-field firms because seeping oil and gas may explode. Understanding sand erosion mechanisms in a corrosive environment is essential for the efficient, effective, and reliable service of pipeline components. For erosion-corrosion to occur, shear stress or breakaway velocity must be exceeded in the fluid flow. Localized breakaway will cause a severe corrosion characterized by a shallow horseshoe-shaped or rounded pit. A more general breakaway will lead to uniform material loss depending on the distribution and the orientation of the impacting particles [28].

2.3 Surface Engineering

2.3.1 Overview of coating technology

The surfaces of most serviceable engineering components are made of metallic materials that offer varying bonding strengths. However, in these strenuous engineering environments, such components fundamentally require combined wear and corrosion resistance treatments to

Novel Enhancement of HVOF Thermal Sprayed Nanostructured WC-12Co / Inconel-625 Coatings for Tribocorrosion Applications| **Al-Harbi, Naif I**

15

provide the surfaces with higher mechanical strength and thereby enhance their surface characteristics. Over the last four and a half decades, there has been rapid development in surface engineering, involving the application of traditional and innovative coating technologies to serviceable engineering components and materials. These techniques cause microstructural changes to the surface characteristics of these components and materials for the sole purpose of making them more durable. Coatings are usually applied to an object (substrate) to impart specific properties to it. In most cases, the properties of the coating and of the substrate differ; hence, the end result is a combination of these properties to form a superiour product.

According to Halling [29], the entire coating process involves three main activities, namely selection, transportation, and accumulation of material to the bulk material. The process serves to accomplish the following purposes:

i. Wear protection: Thermal sprayed coatings, such as carbide materials, have good resistance against erosive and abrasive wear;

ii. Corrosion protection: Most materials, especially cast iron and low carbon materials are vulnerable to corrosion; hence, there is a need to protect their surfaces through thermal spray coatings, which are applied using a controlled atmosphere plasma spray and HVOF;

iii. Aesthetic properties: Coatings can improve the surface appearance of the material; and,

iv. Impart insulation characteristics: Thermal sprayed coatings act as thermal barriers (insulators) to lower the temperature of the substrate, thereby extending its life and to improve the working efficiency of the materials through reduced heat loss.

For the coating material to effectively achieve its primary functions (as listed above), it must have certain properties, such as high elastic modulus, hardness, bond strength, low residual stress, and porosity.

There are different methods/processes for depositing coating materials onto the bulk material. These can be classified according to their coating technologies: electrochemical deposition (miscellaneous), chemical deposition, chemical vapor deposition (CVD), physical vapor deposition (PVD), welding build-up or cladding and thermal spray process [30] and Stokes [12] described these techniques in detail (Table. 2-1).

Novel Enhancement of HVOF Thermal Sprayed Nanostructured WC-12Co / Inconel-625 Coatings for Tribocorrosion Applications| **Al-Harbi, Naif I**

16

Advantages	Technology	Disadvantages
+ High hardness value + Good corrosion resistance + Minimal friction with steel contact	**Electrochemical deposition**	− Difficult coating of complex geometries − Environmental problems − Danger of hydrogen embrittlement
+ Very high corrosion resistance + Low temperature process + Suitable for most metal substrates and many non-conducting materials + Uniform coating thickness	**Chemical (elector-less) deposition**	− Expensive − Additional heat treatment necessary
+ Very high hardness value + Good adhesion	**Chemical vapor deposition (CVD)**	− Difficult coating of sharp-edged geometries − Distortion − Disposal of aggressive gaseous waste
+ Dense coating + High adhesion + Low coating process temperature + Allows deposit of pure elements, compounds, and alloys	**Physical vapor deposition (PVD)**	− Low growth rate of coating − Expensive vacuum process − Restriction in terms of part geometry
+ Large variety of materials + Good adhesion + Properties highly controlled through choice of material and process	**Thermal spray process**	− Deposition efficiency of coating process (overspray) − Residual porosity
+ Very high adhesion + Large parts coatable + Inexpensive	**Build-up welding / brazing**	− Coating materials limited − Impact on substrate materials

Table 2–1: Comparison of different coating deposition technologies, adapted from [6].

Novel Enhancement of HVOF Thermal Sprayed Nanostructured WC-12Co / Inconel-625 Coatings for Tribocorrosion Applications| **Al-Harbi, Naif I**

17

2.3.2 Introduction to the thermal spray process

Thermal spray technology is preferred for its advantages over other hard facing processes stated in Table 2-1. Firstly, there are a wide array of materials which have a liquid phase or which are sufficiently ductile that can be used as coatings. Secondly, the thermal stress of the coated surface can be kept low. Thirdly, the coating may be deposited over a large area or a small area. Lastly, some thermal spray equipment are portable [6]. Notable disadvantages of the thermal spray methods include overspray and residual porosity [6].

Thermal spray methods process can be simply defined as a process where a coating is formed from molten or semi-molten droplets [9]. The technology is widely used in major fields in engineering, like automobiles, aerospace, gas turbines and much more. The technology is driven by the particular need to enhance surfaces so that they can withstand aggressive environments [31]. Thermal spraying involves melting and projecting a coating material to the substrate at high speed [31]. The heat is produced by a spray gun after burning an oxygen and fuel gas/fluid mixture, or using an electrical power source. Thermal spray methods are classified into several major groups depending on the source of energy used to melt the coating material. The main groups shown in Figure 2-7, namely; plasma spray methods, combustion flame spray methods, high-velocity oxygen/air-fuel methods, electrical arc methods, and cold gas methods [32]. The current thermal spray techniques coatings currently available in the market can be seen in Figure 2-7. Plasma spray methods include the atmospheric plasma and vacuum plasma spray [32]. High-velocity oxygen/air-fuel methods are differentiated by their designs and the performance of each spray gun [31]. However, all the designs involve similar core principles.

According to Figure 2-8, the temperature of the flame determines the coating materials to be melted and applied on to a surface [33]. Materials that are sensitive to temperature are best sprayed using methods which have lower flame temperatures. Ceramic coatings are mainly deposited using an HVOF thermal spray method since they are highly sensitive to temperature.

Novel Enhancement of HVOF Thermal Sprayed Nanostructured WC-12Co / Inconel-625 Coatings for Tribocorrosion Applications| **Al-Harbi, Naif I**

18
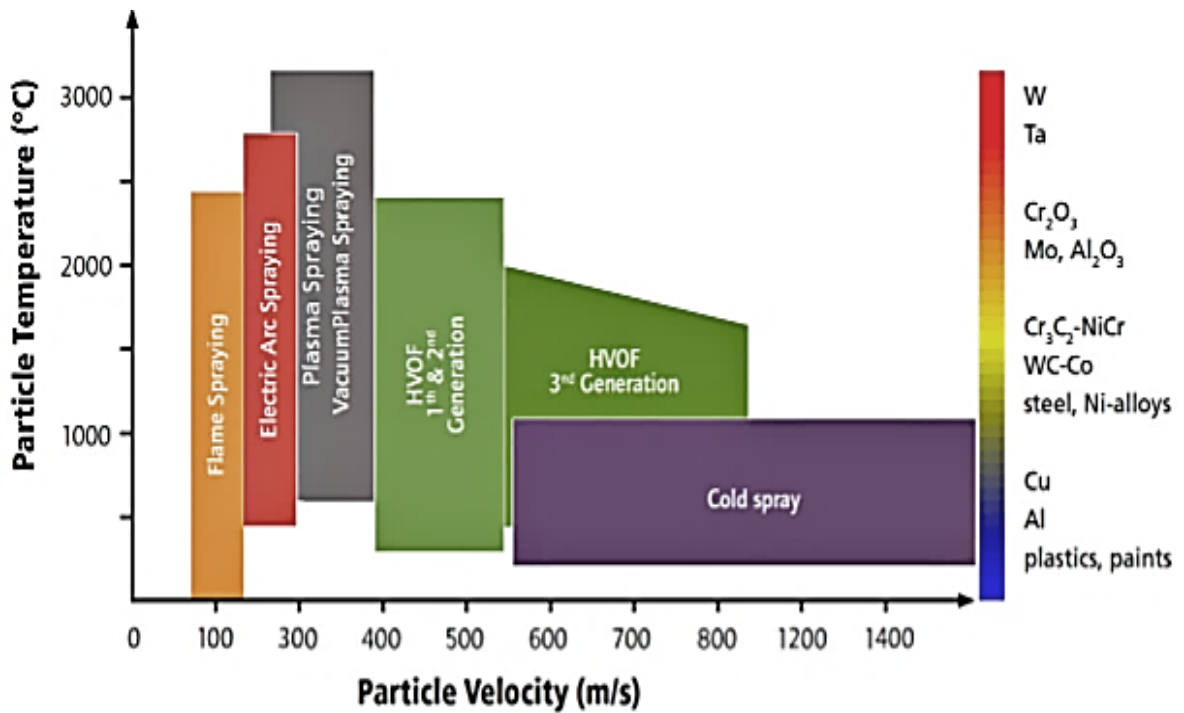
Figure 2-6: Typical particle temperature and velocity for various thermal spray systems [32].
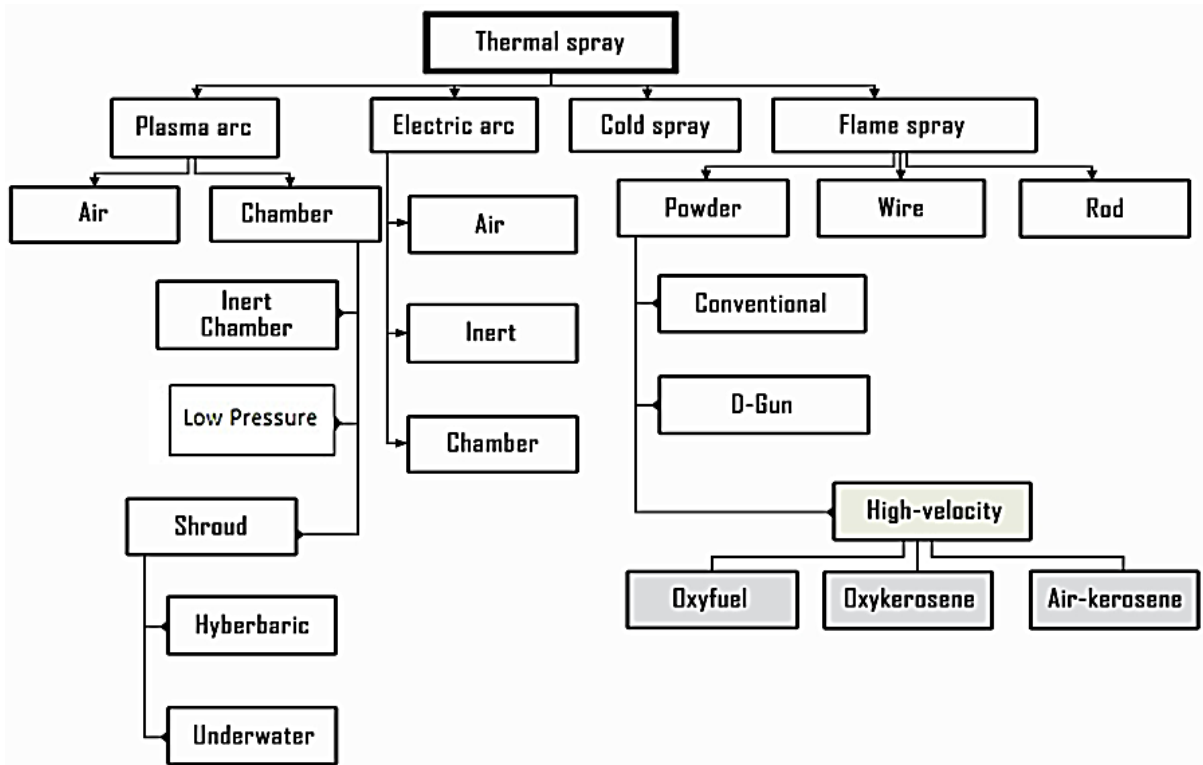
Figure 2-7: Schematic of various techniques of the thermal spray process [26].

Novel Enhancement of HVOF Thermal Sprayed Nanostructured WC-12Co / Inconel-625 Coatings for Tribocorrosion Applications| **Al-Harbi, Naif I**

19
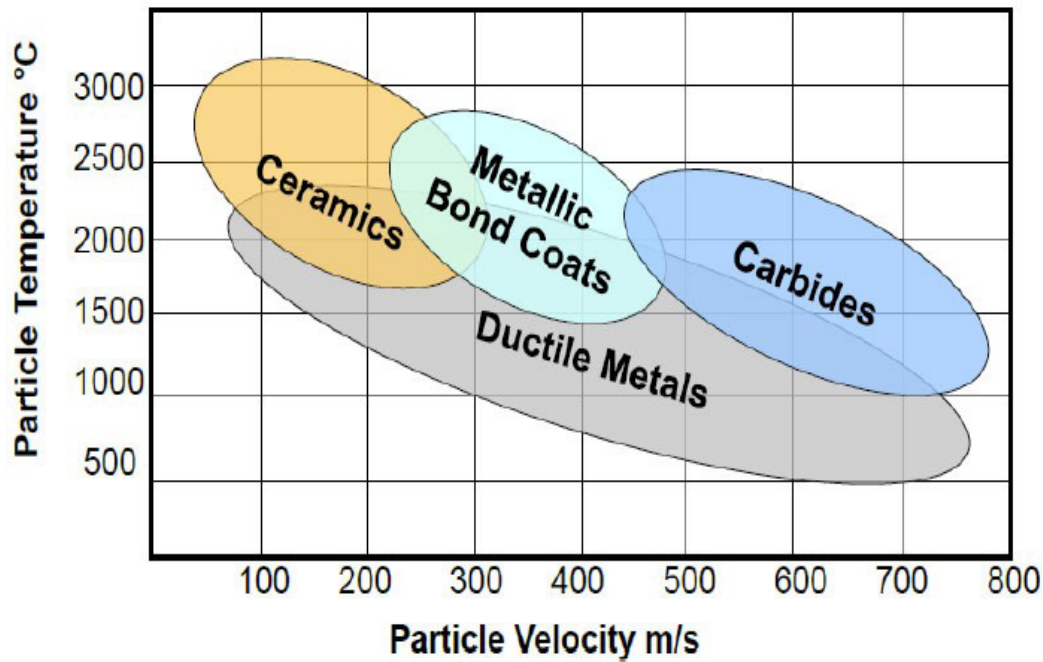
Figure 2-8: Typical particle temperature and velocity for various coating materials [33].

(A) Principles of the thermal spray coating technique

Thermal spraying was invented by a Swiss inventor, Dr. Max Schoop in the early 1900s after observing hot lead shots being projected out of a cannon which then could adhere to almost any surface. This lead to the development and patent of a technique of heating and projecting a metal to build up a material. Schoop used compressed air to project molten material using zinc and tin shots [34]. Figure 2-9 shows a schematic diagram representing the general concept of the thermal spray process.
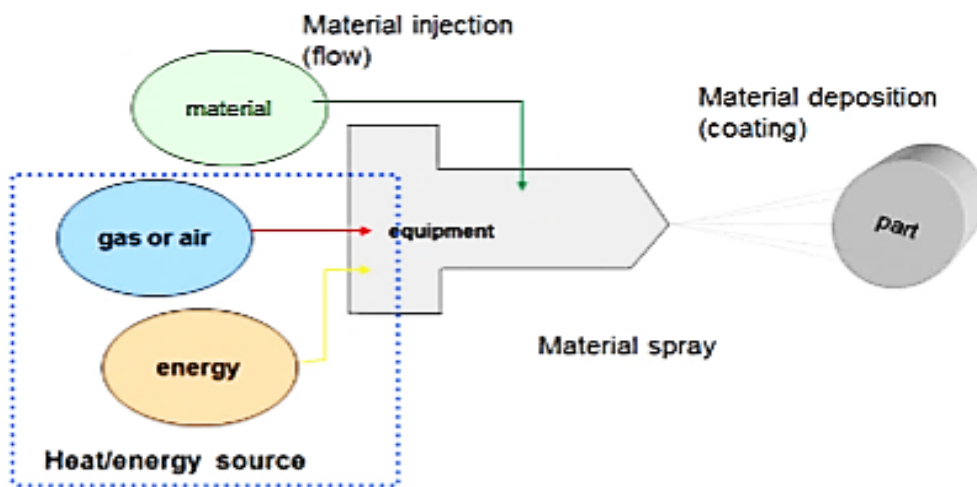
Figure 2-9: Schematic diagram representing the general concept of the thermal spray process [33].

Novel Enhancement of HVOF Thermal Sprayed Nanostructured WC-12Co / Inconel-625 Coatings for Tribocorrosion Applications| **Al-Harbi, Naif I**

20

According to Figure 2-9, the coating process starts with the use of a coating material in the form of wire/rod or powder form. The thermal spray gun is used to supply the required thermal and kinetic energy to the coating material. The thermal (heat) energy melts the coating material while the kinetic (velocity) energy transports the coating to the substrate [35]. The subsequent powder melting process is represented in Figure 2-10.
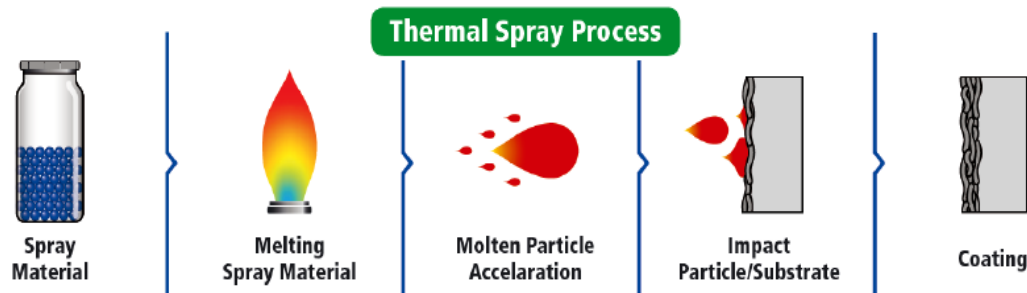
Figure 2-10: Powder melting process steps [32].

(B) The High-Velocity Oxy-Fuel (HVOF) spray

The HVOF spray was developed as an improvement to the conventional powder flame spraying system [31]. The improvement was made possible by the realization that increased velocity of particles produced a better coating density and increased bonding with the substrate [31]. According to Wank [31], this process was developed in the mid-1980s and has become the most important and widely used technique in thermal spraying industrial applications in the recent past. The Continuous Combustion HVOF gun, shown in Figure 2-11, has three main sections: mixing zone, combustion zone, and nozzle. During operation, the gases are mixed and directed to the combustion zone, where the combustion process is initiated, resulting in the expansion of the nozzle.

A combination of kinetic and thermal energy is used to melt and accelerate the powder particles to impart the desired coatings onto the bulk material. This process is characterized by the high impact and high speed of the sprayed powder; thus providing coatings with higher bond strength and less porosity compared to the Detonation Gun process and plasma system [9]. The mechanical interface between the grit blasted substrate and the splats (semi-molten powder) is characterized by mechanical interlocking (explained in the next section). The adhesion strength between them depends on the powder's mechanical properties and the

Novel Enhancement of HVOF Thermal Sprayed Nanostructured WC-12Co / Inconel-625 Coatings for Tribocorrosion Applications| **Al-Harbi, Naif I**

21

substrate's surface roughness [9, 31]. As the spraying continues, the splats build up forming the coating layers.
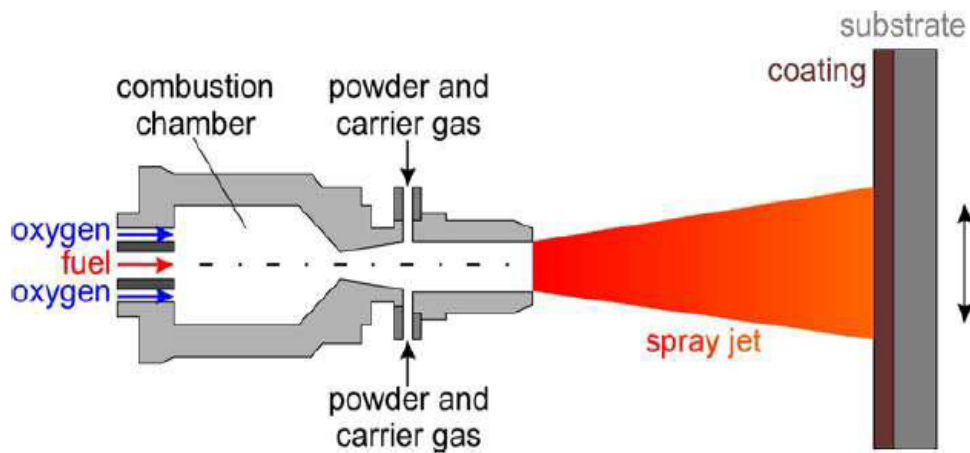
Figure 2-11: Principle of the HVOF thermal spray process [31].

(C) High-Velocity bonding mechanisms

Before coating, the substrate is prepared in a way that enhances bonding. Coating material is then sprayed on the substrate at high speed. The particles of the molten or semi-molten coating material are generally spherical before striking the substrate. Once the particles hits the substrate, they flatten and solidify rapidly upon cooling [26] , as shown in Figure 2-12. The kinetic energy and the temperature of the particles cause stress localization and melting at the point of impact with the substrate, thereby causing a mechanical bond with the substrate upon cooling. The continued impact of coating particles, followed by solidification, results in a microstructure that is strongly bonded to the substrate [26].

Novel Enhancement of HVOF Thermal Sprayed Nanostructured WC-12Co / Inconel-625 Coatings for Tribocorrosion Applications| **Al-Harbi, Naif I**

22

(A)

In-Flight
Particles

Particles Mechanically
Locked to the substrate

Asperities

(B)

Mechanical Bonding

20 μm   EHT = 15.00 kV   Signal A = SE1   Date :23 Apr 2017   ZEISS
WD = 11.5 mm   Photo No. = 8583   Time :0:45:13
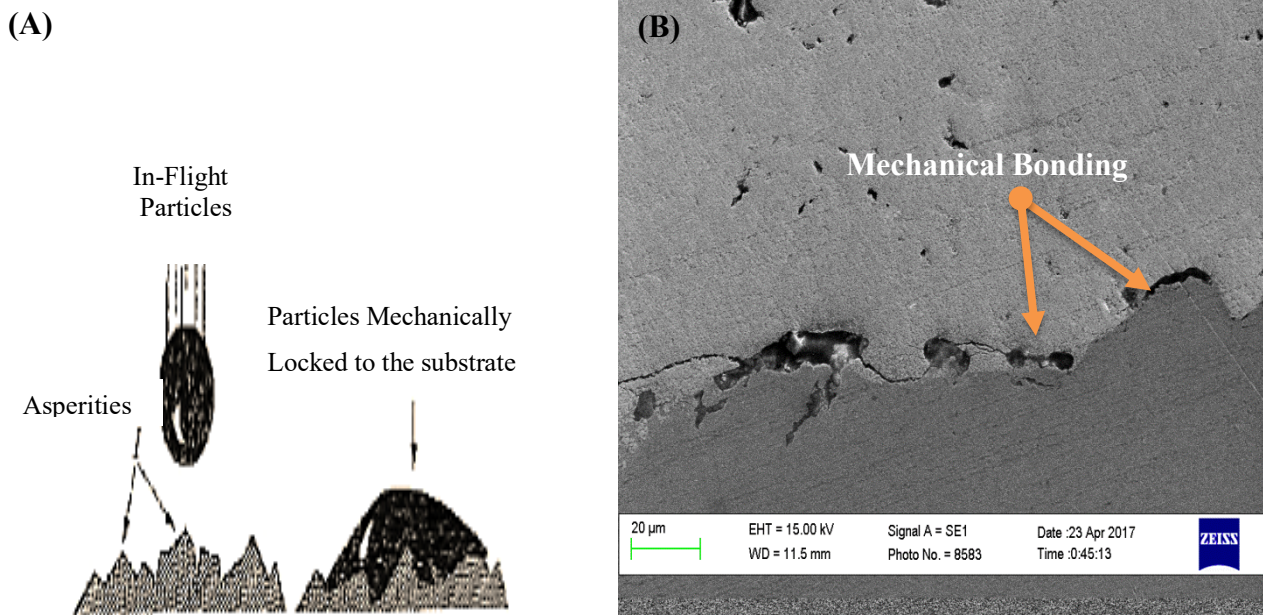
Figure 2-12: (A) at coating/substrate interface [26], and (B) optical micrograph of the HVOF sprayed WC-Co coating at the coating/substrate interface.

2.4 Tungsten carbide cobalt (WC-Co)

The WC-Co composites can be formed through co-precipitation of tungsten and cobalt salts in a liquid phase. Carburization then takes place to form WC-Co particles. Suitable precipitation components such as guanidine salts can be employed, which provide benefits of complete pyrolysis of the remains at significantly lower temperatures and costs as well as lower molecular weight compared to other organic amines. The main advantage of the WC-Co composites as coating materials is their high hardness, resistance to wear, and high-temperature strength.

According to Yao et al. [36], the WC has a simple hexagonal crystal structure. It has two atoms per unit cell with a c/a ratio of 0.976. This hexagonal lattice has half of its six-fold coordinated carbon atom positions unoccupied. The WC then joins Co to form the WC-Co composite. WC-Co composite (irregular in shape) is better suited for coatings due to its low erosion rate compared to other coatings [37], and are harder and tougher [36]. Properties of these composites depend on the composition and microstructure, in which case, increasing the cobalt percentage decreases the hardness whereas decreasing the cobalt percentage increases the hardness [36].

Novel Enhancement of HVOF Thermal Sprayed Nanostructured WC-12Co / Inconel-625 Coatings for Tribocorrosion Applications| **Al-Harbi, Naif I**

23

2.4.1 Nanostructured WC-Co Cermet Coatings

Cermet is a composite material composed of metallic and non-metallic ceramic with both ionic and covalent bonds mostly used as coatings to protect materials against wear and corrosion. Cermet's are excellent coating materials since their properties are closely correlated to their structure [38-40]. Cermet have better mechanical properties due to the presence of ionic-covalent bond in addition to making them brittle materials for coating applications. It is important to note that any material used as protection against wear and corrosion should provide good bonding with the substrate without deteriorating/affecting the mechanical properties of the parent materials. The use of cermets as wear and corrosion resistant materials can be facilitated by the presence of the ion-covalent bond that eliminates the development of linear defaults in the atomic pile, in an attempt to oppose the metallic element of the substrate.

Other advantages of cermet's as coating materials include: excellent resistance against corrosion, high elastic modulus, high melting point temperature, lightness, high breaking point, high mechanical strength, high hardness and enhanced electrical insulation properties due to ion-covalent liaisons.

Since the electronic structure of ceramics allows metallic type conductivity for metal carbides and nitrides (such as TiC, TiN, WC etc.), there exists conductive ceramics. The simple chemical compounds e.g. nitrides, carbides, carbo-nitrides and flourides of transition metals such as Hf, Zr, Fe, Ni, and Co and the composites are the most suitable materials for achieving corrosion and wear surface protection. This is because, these compounds show superior properties such as surface hardness, excellent adhesion to several materials and resistant to corrosion because of their chemical nature. The wettability of the hard carbide phase by the metal matrix affects both the mechanical properties and structure of cermets. To ensure enhanced wettability, binder materials such as nickel are extensively utilized due to excellent wettability obtained from interaction of the d-levels electrons that are not saturated [41].

To overcome the present challenge of high wear resistance desired for coating materials in many engineering applications and to increase its service live, there are recent attempts to reducing the typical size of the hard carbide atom, as can be seen in Figure 2-13. This will translate to reduced mean free path between the particles of carbide thus increasing wear

Novel Enhancement of HVOF Thermal Sprayed Nanostructured WC-12Co / Inconel-625 Coatings for Tribocorrosion Applications| **Al-Harbi, Naif I**

24

resistance and fracture toughness. Wear resistance in the carbide material is attained due to exposure of the matrix to the corrosive/harsh setting over very small proportions. Therefore, nanostructured WC-Co composites have proved potential materials to replace standard macrostructure WC-Co and hard chromium on wear parts due to increased toughness and hardness.
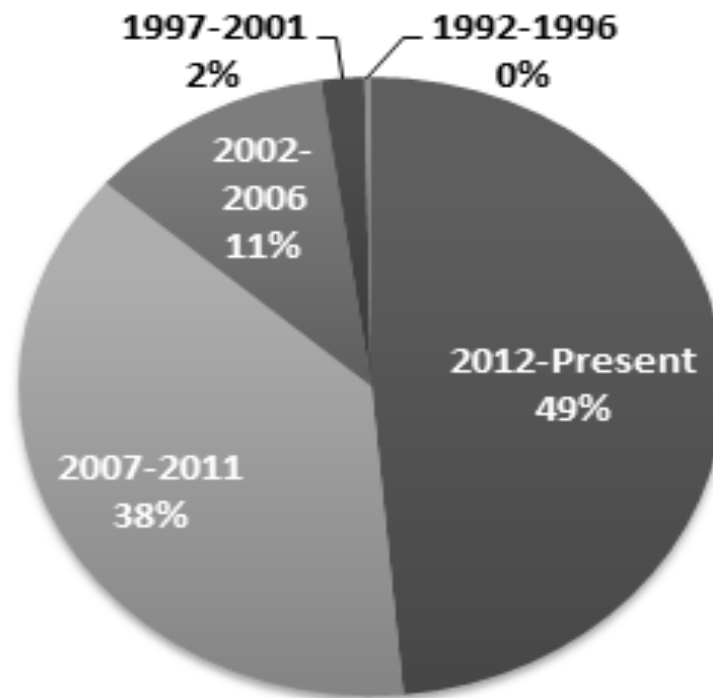
Figure 2-13: Percentage breakdown of the publications relating to Nanostructured coating (as of 10/11/2016) using Scopus search engine. Words used during research (nano+coating) in; [Article Title, Abstract, Keywords].

However, the inherent limitations of nanostructured WC-Co cermet coatings such as low shear modulus, Young's modulus and bulk modulus are the main driving force for consideration and investigation of new generation of nanostructures FeCu cermets with the objective of having coatings with better elastic constants. Further details on the synthesis and the properties of nanostructured cermet coatings, can be found at the following published work [42].

Novel Enhancement of HVOF Thermal Sprayed Nanostructured WC-12Co / Inconel-625 Coatings for Tribocorrosion Applications| **Al-Harbi, Naif I**

25

2.4.2 Alloy Powders mixed with WC-Co cermet for erosion- corrosion applications

In spite of widespread use of composites that contain carbides such as chromium carbide or tungsten carbide that provide superior coating resistance to pure water in nanoscale level, several components in oil and gas industry suffer collision erosion. Collision erosion occurs in component parts such as pump chokes and ball valves where small hard particles are eroded inside corrosive liquid streams. The corrosion properties of metallic binders used in such environments need consideration. Consequently, cobalt as binder matrices for carbide is not an appropriate choice for erosion-corrosion environment as documented by Kumari et al. [43] and Ahmed et al. [44]. Modifications thus have to be performed on metallic materials either by blending cermet with alloy coating powders such as nickel-based alloys or by use of coating powder with another metallic material such as Cr_3C_2-NiCr and WC-CoCr.

In a study conducted by Gérard [45], advanced thermal spray technology makes possible wear resistant coatings on surfaces of engines made of magnesium or aluminium. According to this research, engine tests on diesel and gasoline engines decrease the coefficient of friction and reduces the consumption of fuel by 2 to 4%. Moskowitz's [46] research conducted earlier was in line with these findings as the researcher also discovered significant economic and technical advantages of thermal spray coatings in providing solution to plant equipment problems. The researcher noted that modifying High Velocity-Oxy Fuel (HVOF) process using unique inert gas shrouding led to low-oxide and high-density metallic alloys. In this regard, the research discovered that coatings of corrosion-resistant alloys such as Hastelloy C-276 and type 316L stainless steel can act as true barriers to corrosion. Al-Hamed [17] conducted a related research to identify the developments of WC-12Co nanostructured coatings specifically concerning modification of WC-12Co through the addition of Inconel-625 HVOF thermal spray coatings to improve its mechanical property performance above conventional micro-structured coatings. The results of this research, demonstrated that the use of proper HVOF controlled parameters can significantly improve the performance of the nanostructured WC-12Co coating.

Sidhu et al. [47] also conducted research to determine the behaviour of hot corrosion of HVOF, where, High Velocity-Oxy Fuel sprayed Stellite-6 and NiCrBSi coatings on a Ni-Based Superalloy. At the end of the experiment, the researchers recorded that coatings deposited on nickel-based super-alloys exhibited better resistance to hot corrosion, than those

Novel Enhancement of HVOF Thermal Sprayed Nanostructured WC-12Co / Inconel-625 Coatings for Tribocorrosion Applications| **Al-Harbi, Naif I**

26

un-coated. In so far NiCrBSi provided reliable resistance, Stellite-6 coated super-alloys performed better. Hidalgo et al. [48] research investigated the behaviour of sprayed NiCrBSiFe and WC- NiCrBSiFe alloys that were used within coal-fired boiler combustor and subjected to conditions that initiated a post-combustion gas atmosphere. Reyes and Neville [49] conducted an experiment that aimed at assessing electrochemical and mechanical erosion in liquid-solid slurry using cobalt-based and nickel-based alloys. Degradation of the alloy-coated parts displayed distinctive electrochemical behaviour. It became apparent that simple replacement of materials with harder cermet is never enough. Cobalt-based bit body materials exhibited better coating than the cobalt-based alloys. Further details of the erosion-corrosion of WC-12Co with the addition of Ni based alloys, can be seen in the published work of Ahmed et al. [50].

2.5 Laser Surface Engineering

2.5.1 Lasers

Lasers are referred to as powerful flashlight beams [51]. This scholar argues that there is a difference between an ordinary light and the laser light, which can be likened to the difference that exists between the ripples in a person's bathtub and the ocean's large waves. The author [51], narrates that the workings of lasers are like moving a hand back and forth within a bathtub and creating very strong waves. As the hand keeps moving with the waves, the waves become larger. The same thing can be done in the ocean a few million times and the result will be mountainous waves towering over one's head [51]. A laser creates something resembling that with light waves as well. Lasers often start off with weak light. However, they add more and more energy until the light waves become highly concentrated. Therefore, a laser can be described as a powerful light beam which can zoom miles into the sky or cut through metal.

2.5.2 Laser Surface Rapid Solidification

The shape of the solid-liquid interaction regulates the microstructural characteristics of the surface during the process of solidification. Moreover, the physical and chemical composition—as well as the thermal condition of the melted layer of the material—are highly essential to the nature and stability of the resultant solid-liquid interaction [26].

Novel Enhancement of HVOF Thermal Sprayed Nanostructured WC-12Co / Inconel-625 Coatings for Tribocorrosion Applications| **Al-Harbi, Naif I**

27

What's more, the temperature gradient, the growth rate, and the composition of the alloy all define the morphology of the solidification. These factors are critical in the interaction between the liquid and solid states of the material, which may lead to planar, cellular, or dendritic growth. In addition, the temperature gradient and the growth rate are vital in determining the cooling rate, which may affect the scales of solidification by microstructures and their shapes, as shown in Figure 2-14 [26, 52].
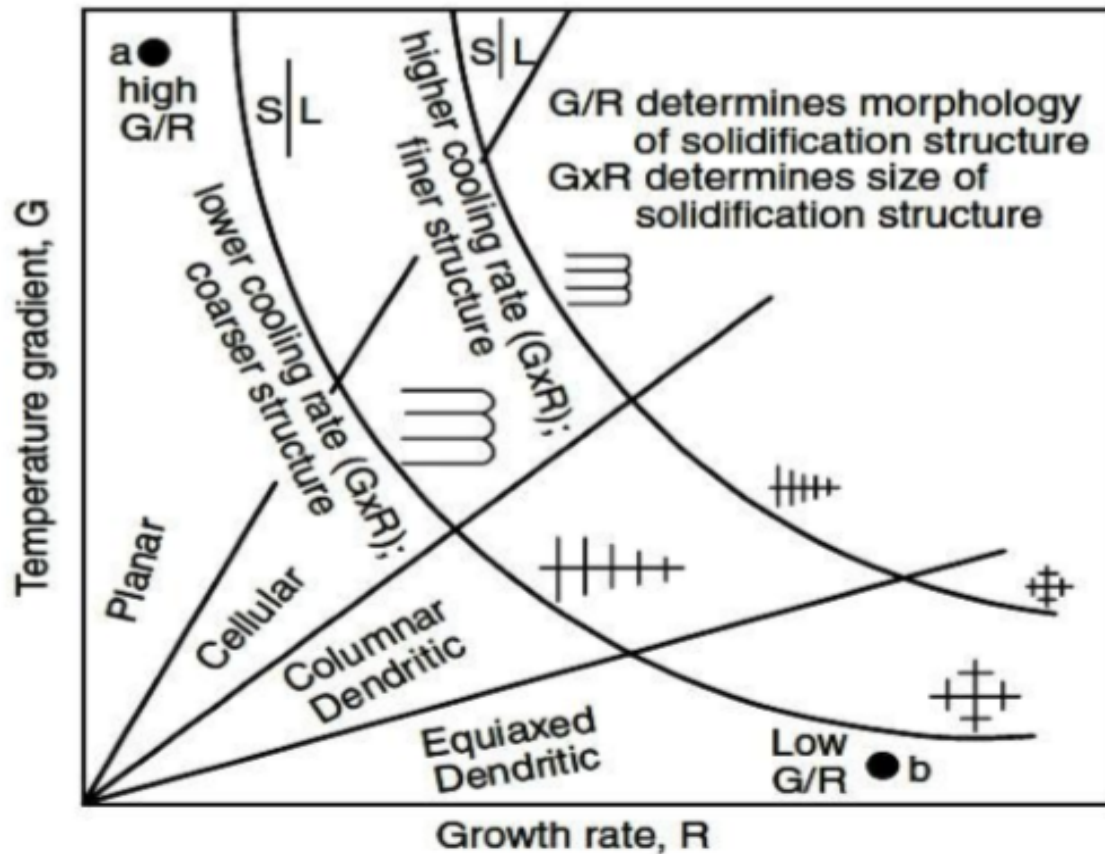
Figure 2-14: Effect of temperature gradient (°C/mm) on growth rate (μm/s) for the size and morphology of the solidification structure [52].

Cooling rates are extremely high during laser treatments because of the conditions of the stated treatments, however the solidification velocity and temperature gradient can be relatively high. Superior materials with distinct properties, whether physical or mechanical, can be produced because of the extremely fast solidification process from the laser melting [26, 52].

In comparison, the cooling rate decreases from its maximum level on the surface of the material to its minimum level at the bottom of the molten pool. Additionally, the cooling

Novel Enhancement of HVOF Thermal Sprayed Nanostructured WC-12Co / Inconel-625 Coatings for Tribocorrosion Applications| **Al-Harbi, Naif I**

28

rate also decreases from a maximum rate at the centre of the molten pool to the its minimum at the edge of the molten pool. Such discrepancies in cooling lead to microstructure variations in the molten pool of the material [52].

As a result of the high cooling rates of scanning lasers, the undercooled liquid produces protruding structures during the solidification process. Such protrusions eventually grow and develop into cellular or dendritic microstructures, as shown in Figure 2-15 [26, 52].
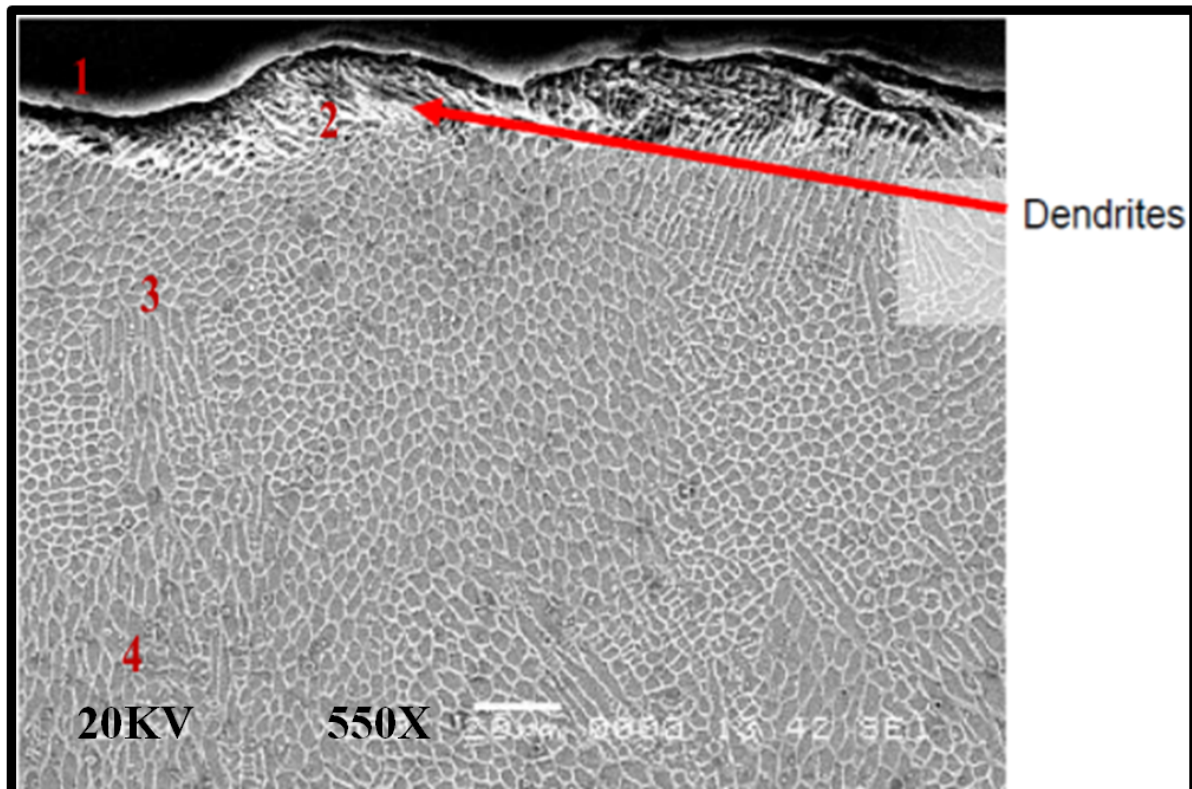
Figure 2-15: SEM micrograph of cross-section for the Inconel 625 coating after laser treatment. Shows: (1) coating top surface, (2) fine dendritic microstructure, (3) fine cellular region, and (4) coarse cellular region. Treated by diode laser with 57 W/mm^2 and 100 mm/s scanning speed [21].

The slow processing conditions of the scanning laser treatment create a coarser texture of dendritic microstructures, as seen in Figure 2-16 (A). More important, the scanning laser treatment with high-speed cladding or solidification conditions produces finer dendritic structures because of the better alignment of atoms or particles caused by the higher state of energy and interactions, as shown in Figure 2-16 (B) [26, 53].

Novel Enhancement of HVOF Thermal Sprayed Nanostructured WC-12Co / Inconel-625 Coatings for Tribocorrosion Applications| **Al-Harbi, Naif I**

29
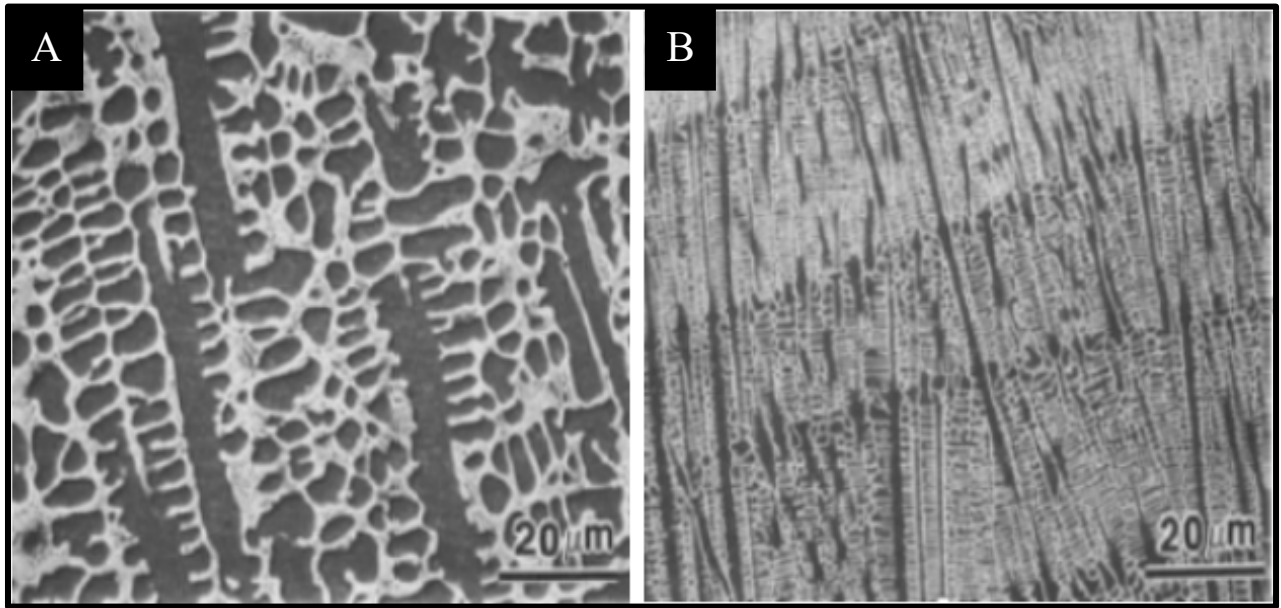
Figure 2-16: SEM morphology for the Stellite 6 coating cladded at the top stainless steel substrate with two different scanning speeds: (a) low scanning speed of 1.67 mm/s, and (b) fast scanning speed of 167 mm/s [53].

Furthermore, columnar growth dendrites, as shown in Figure 2-17, are usually created by nucleation, in most cases involving substrate-quenched alloys in scanning laser treatments, which usually occur at the surface area within the contact of the affected substrate. Varying microstructures may be created by rapid solidification induced by high-powered laser treatments in different materials [26, 54].
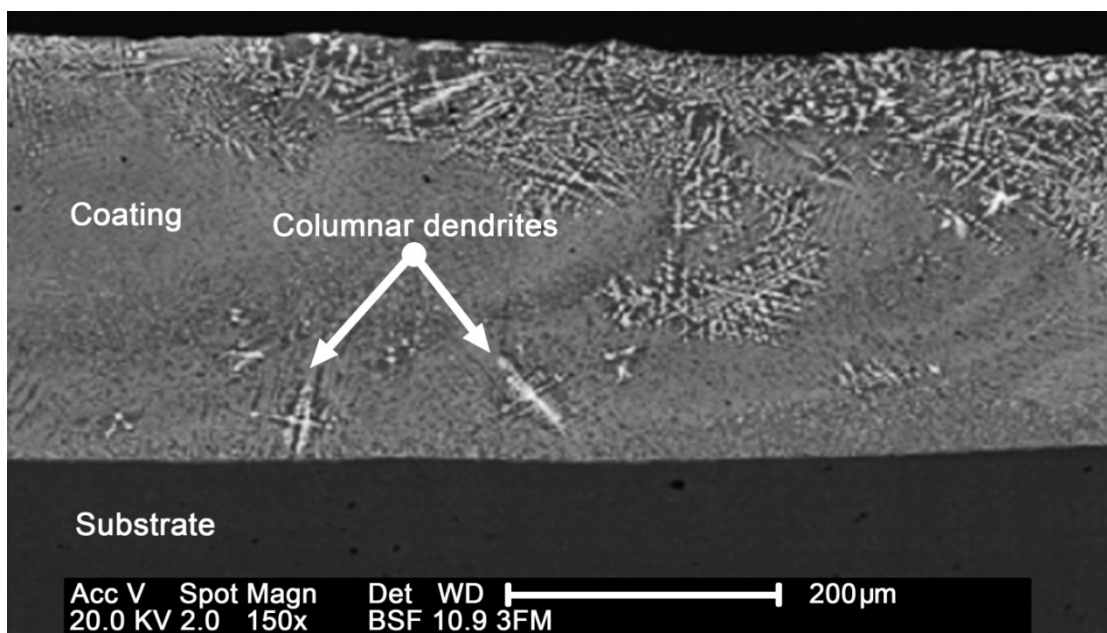
Figure 2-17: SEM morphology for fully melted Inconel 626+42 wt. % WC MMC coating. Shows columnar dendrites growth at the coating/substrate interface [54].

Novel Enhancement of HVOF Thermal Sprayed Nanostructured WC-12Co / Inconel-625 Coatings for Tribocorrosion Applications| **Al-Harbi, Naif I**

30

2.5.3 Effects of laser treatment on wear resistance and hardness of HVOF coatings

There have been numerous attempts to improve the wear resistance and hardness of the HVOF coatings through laser treatment.

According to the study by Chen et al. [24], wear resistance was diminished after the laser remelting of WC-12 wt.% Co HVOF coatings on a microscale and nanoscale level, which lessened the carbide size and fracture of the carbide. Liu et al. [54], examined the relationship between laser surface treatment and the wear performance and corrosion of Inconel 625-sprayed and WC-based HVOF coatings. Corrosion and wear resistance of the HVOF coatings can be achieved through laser treatment by lessening the micro-galvanic force and through the elimination of the discrete splat-structure, as well as micro-crevice and porosity. Furthermore, the results have shown that the selection of proper processing parameters of the said coatings have led to better wear resistance and hardness of the HVOF coatings as well as better porosity and corrosion resistance. This is further supported by Figure 2-18. Also, it can be seen in the figure, doubling the load applied to the same samples would not necessary double the volumetric wear loss, which was confirmed by the typical wear behaviour discussed previously in Figure 2-3.
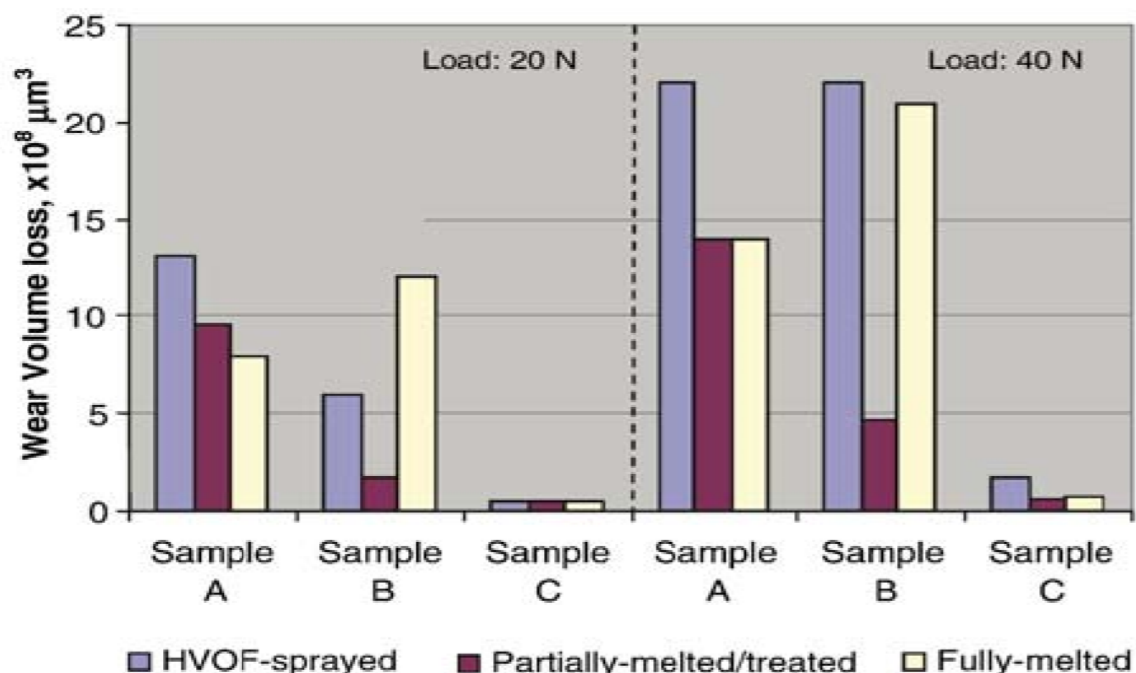
Figure 2-18: Comparison of wear volume loss of HVOF Inconel 625 mixed with the WC particles coating with different applied load, WC contents and melting depth [54].

Novel Enhancement of HVOF Thermal Sprayed Nanostructured WC-12Co / Inconel-625 Coatings for Tribocorrosion Applications| **Al-Harbi, Naif I**

31

On the other hand, Kumari et al. [55], On the other hand, Kumari et al. [55], conducted research which indicated that the micro-hardness increased after laser post treatment of thermally sprayed Ni-WC coatings. They showed Micro-hardness may be increased during the post-deposition treatment; however, it depended on the laser scanning speed and the composition of the coating.

Lastly, Zhang et al. [56], examined the wear performance of Ni – Cr_3C_2 and Ni – WC and its relationship with the scanning laser treatment. Results indicated that the discrepancies in the micro-hardness of the coatings can be attributed to the difference in the solidified structure. Such findings agree with Figure 2-19.
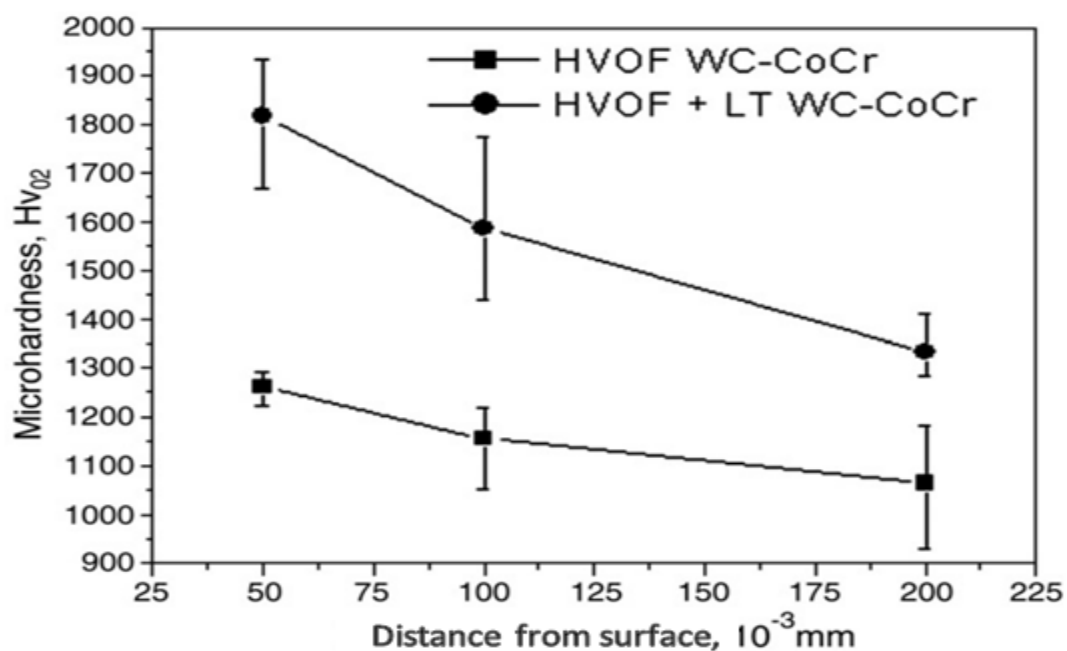
Figure 2-19: Micro-hardness of the HVOF WC-CoCr coating pre- and post-heat treatment [56].

2.5.4 Effects of laser treatment on microstructure and corrosion of HVOF coatings

Generally, laser treatment improves the surface composition of a material through homogenization and leads to a higher density of HVOF coatings by removing porosity, which prevents entry of the substrate. Past studies have also shown that microstructure and corrosive properties can be improved further through this type of laser treatment.

Wu et al. [57], conducted research wherein proper processing led to improved dendritic growth and better corrosion resistance of nickel-based and tungsten carbide coatings. According to Yilbas et al. [58], the laser-controlled melting on Inconel 625-based coatings

Novel Enhancement of HVOF Thermal Sprayed Nanostructured WC-12Co / Inconel-625 Coatings for Tribocorrosion Applications| **Al-Harbi, Naif I**

32

improved the corrosion resistance of the material and reduced the pores on the surface, as shown in Figure 2-20.
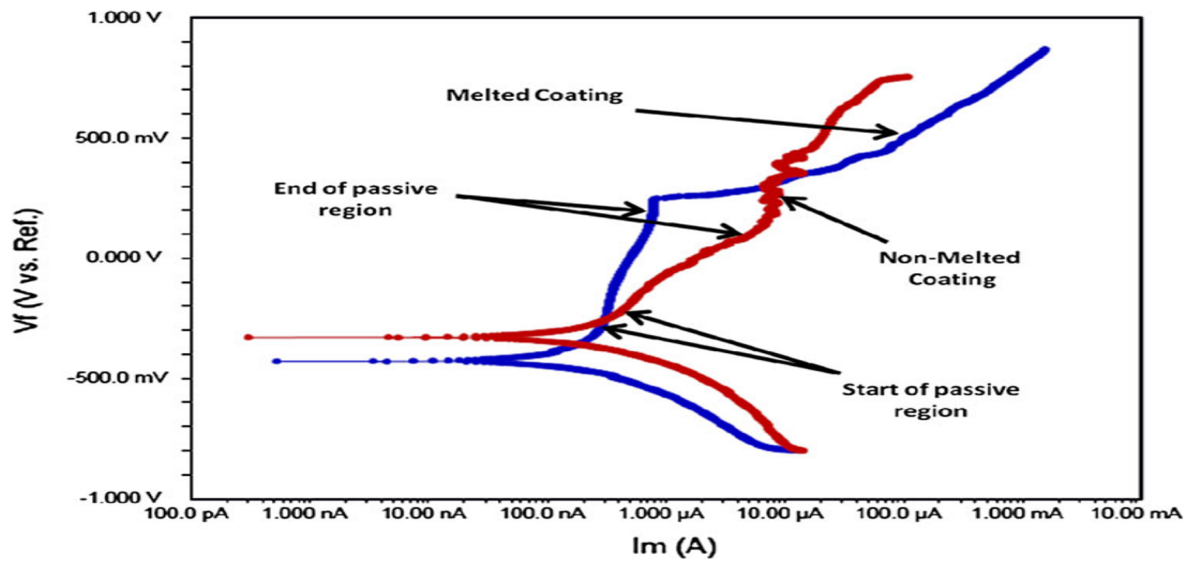
Figure 2-20: Polarization curves of the HVOF Inconel 625 -12wt. % WC coating before and after laser treatment [58].

On the other hand, Liu et al. [54], also conducted a study which indicated that faceted dendritic micro-structures were created through high-power laser diode treatments of (58% Inconel 625 + 42% WC (wt.%)) coatings and these structures were held to be beneficial for the wear performance and corrosive resistance of the coatings. Such findings are supported by Figure 2-21.
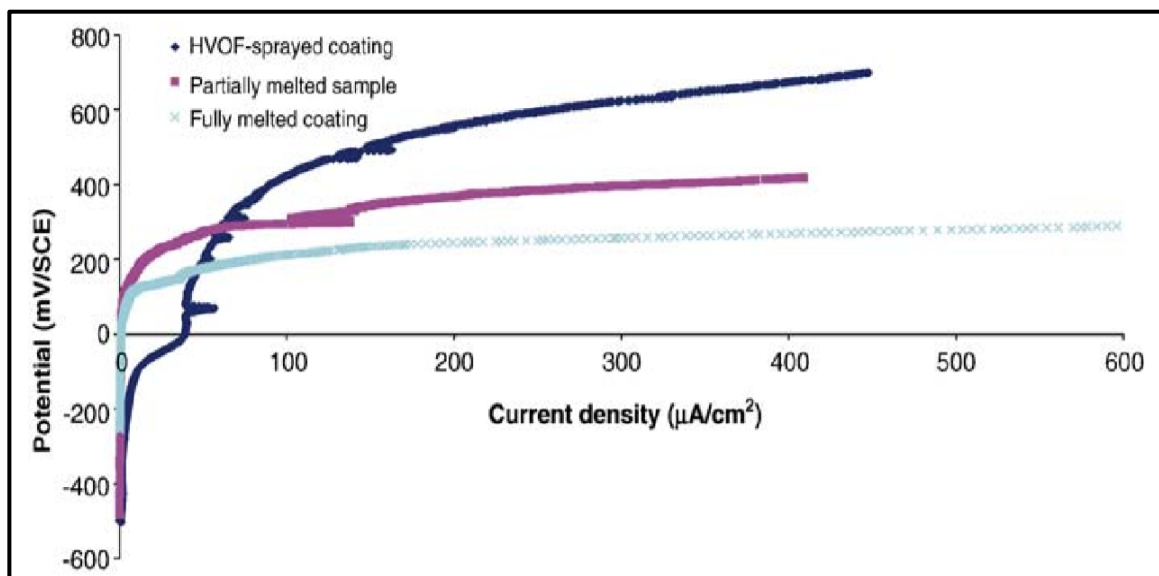
Figure 2-21: Polarization curves of the HVOF Inconel 625 -22wt. % WC coating before and after laser treatment at different melt depths [54].

Novel Enhancement of HVOF Thermal Sprayed Nanostructured WC-12Co / Inconel-625 Coatings for Tribocorrosion Applications| **Al-Harbi, Naif I**

33

Kumari et al. [55], also pointed out that the differences in corrosive resistances of coatings may be caused by variances in the scanning speeds of laser treatments. Such variances also produce differences in micro-structure and porosities in coatings. Yilbas et al. [20], have shown that crack initiation in coatings can be caused by differences in the composition of coatings. Laser treatment can help further reduce the number of defective sites in these coatings. Lastly, Tuominen et al. [59], have conducted a study which showed that laser remelting of Inconel 625 coatings produced homogenization. This led to better micro-structures with better corrosive resistance of the material.

2.5.5 The influence of laser beam geometry and laser processing parameters on laser remelting of ceramic materials

The use of laser treatment to coat materials has been growing in popularity in various industries of late. Such a treatment is usually performed using either circular or rectangular beam geometry—usually, as already discussed, to enhance a coating by eliminating pores and nonuniform distribution of the coating elements, thereby helping create homogenous coating properties. However, during laser treatment of ceramic materials, thermally induced cracks can be created during melting and rapid solidification when the elastic stress of the treated material exceeds its fracture strength. This stress builds up during the cooling stage as a result of the thermal gradients that develop in the treated region—for each element's various degree and rate of thermal contraction are in tension with its neighbours' [60]. Furthermore, stress results when elements in the untreated region that are proximate to the treated zone restrain the treated elements during contraction [60]. The relatively high thermal stress of ceramic materials results from their brittleness, low thermal conductivity, and high melting temperature—properties that produce significant thermal gradients and variances in cooling rate during the laser treatment process. This, in turn, leads to thermal shock, giving rise to cracks in the treated surface, particularly at the centerline of laser beam track and at the edges. These cracks shorten a coating's service life [60].

Research has shown that to achieve a good laser remelting operation that is characterized by few or no cracks and little to no porosity, heat transfer conditions should be altered to provide a constant cooling rate that smooths the transition from plastic to elastic regions on the treated surface [60-71]. Some researchers have succeeded in forming crack-free ceramic surface materials, whether by adding an extra process, such as techniques of heating and postheating, or by optimizing the single-step processing conditions of a single

Novel Enhancement of HVOF Thermal Sprayed Nanostructured WC-12Co / Inconel-625 Coatings for Tribocorrosion Applications| **Al-Harbi, Naif I**

34

laser beam through selection of optimal parameters and/or use of different laser beam geometry—as temperature distribution over the surface of a material can vary, increasing natural convection and heat radiation in the surface material. In this work, which seeks to reduce operation costs; single-step processing is a particular area of interest for its susceptibility to being made more cost-effective and practical as well as simpler [60]. This section reviews influence of laser parameters and beam profiles for achieving crack-free laser treatment. The section concludes by considering which beam geometry is best suited to treating ceramic materials among four conventional types of beam profile available in the market—circular, line, rectangular, or elliptical (ovaloid)—and ultimately identifying the elliptical profile as the best choice for melting the surface of ceramic materials. In the process, the criteria used to reach this conclusion are supplied. Further detailed literature on the Laser Surface Modification of Ceramic Materials, can be found at the following published work [72].

(A) Brief summary on author's published work [72]

The literature and the drawings in Table 2-1 of the main four beam profile selected in this section show that the beam that produces lower heating and cooling rates during the laser treatment will not crack the surface with the highest hardness in the elliptical beam. It has the similar advantage of the Rec-L beam, namely, a long interaction time, and the added advantage of its geometric feature—a leading and trailing edge—to provide progressive increasing or decreasing line density per unit length in the direction of the scan. Subsequently, low heating and cooling rates will be achieved at a longer processing speed and smaller power density to attain the required melting depth compared to the other conventional beams, making it a more cost-effective procedure. Based on this literature, it is also evident that the laser processing conditions should be optimized prior to the final laser treatment. Beam diameter, scanning speed, and power density will play the main roles, apart from the beam geometry of the thermal stress build-up, during the laser treatment. Furthermore, to avoid thermal shock during the laser treatment and account for homogeneous properties across the coating materials, using a laser beam with uniform density and continuous mode is preferable.

Novel Enhancement of HVOF Thermal Sprayed Nanostructured WC-12Co / Inconel-625 Coatings for Tribocorrosion Applications| **Al-Harbi, Naif I**

35
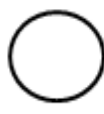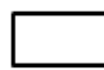
Circular	Rectangular		Line	Elliptical
	Rec-L	Rec-S		
◯ ↑U	▯ ↑U	▭ ↑U	▬ ↑U	⬭ ↑U

Table 2-1: Main beam geometry used in this research.

2.6 Literature Survey Summary

- The oil and gas industry experience a series of problems, such as wear and erosion-corrosion which severely affect the merging profits of oil and gas firms. The necessity of having superior coating with long service life has increased especially in the last two years as a result of rapid reduction of oil and gas prices from above 100 dollar per barrel to less than 75 dollar currently as discussed in chapter one. Therefore, having superior coating with long service life will protect the environment and decrease the money that is spent as labour cost, coating or part replacement, loss of revenue due to disruption in the supply (unplanned shutdown) and unreliability.

- The nanostructure WC-Co coating has great potential to replacing the conventional microstructure powder materials, and its uses have increased recently, particularly in the oil and gas industry. This contributes to nanostructure WC-Co coating's superiority in some of its intrinsic and extrinsic properties in comparison to the conventional materials, which are mainly morphological as it has a high dense coating and lower porosity. Also due to the superiority of some of its mechanical properties, for instance having higher hardness, yield strength and fractural toughness when compared with microstructure materials that have been made possible due to the reduced free path between cobalt caused by reducing the WC carbide size. However,

Novel Enhancement of HVOF Thermal Sprayed Nanostructured WC-12Co / Inconel-625 Coatings for Tribocorrosion Applications| **Al-Harbi, Naif I**

36

the inherent limitations of nanostructured WC-Co coatings is its low elastic stability and high sensitivity to high temperature when sprayed by thermal spray that cause them to decarburize, which eventually affects the wear and corrosion resistance of the coating. Inconel 625 on the other hand has excellent corrosion and erosion-corrosion resistance when used in corrosive environments and this contributes to a high dense coating microstructure provided by the materials and due to the corrosive behaviour of some of its chemical compositions (e.g., chromium, nickel).

- Due to the economic considerations, the oil/gas industry uses carbon steel for its pipelines and most of its production components. In low-life cycle regions, due to dry erosion (e.g., some regions of pipelines' outer surface and fittings), components are usually coated with a layer of materials with superior mechanical properties (e.g., high hardness, bending strength, and toughness) that perform better under dry erosion wear condition. One class of coating widely used for such wear type includes hard particles carbides (e.g., WC, Cr_3C_2, and TiC) in metallic alloy matrices such as Ni, Cr, or Co. [38-40]. In the mixture of carbides/ metallic binders, as the carbide particles become smaller and the metallic binder ratio decreases, erosion wear performance improves. For aqueous erosion (erosion-corrosion) wear, which usually occurs in an inner region involving a wet environment (such as valves, elbows, and pumps), regardless of the high mechanical properties required for such wear, the corrosion properties will be considered. Such properties are usually managed by selecting an appropriate coating mixture containing chemical compositions with enhanced corrosive resistance behaviour under a corrosive environment and by detecting no or low coating layer morphological defects that create a path for electrochemical reactions, for example, porosity and cracks.

- Despite the high-quality coatings produced by the HVOF thermal spray system, it has yet to produce a defect-free coating. Some of the disadvantages the HVOF thermal spray coating process is its porosity within the coated layer, mechanical bonding at the coating/substrate interface and non-uniform distribution of the coating elements have a major effect on its performance, especially in erosion/corrosion preventative applications. Conversely, post heat-treatment application on HVOF coatings were targeted to improve the coating wear, corrosion resistance, and other mechanical properties by reducing the composition gradient between the matrix and hard phase

Novel Enhancement of HVOF Thermal Sprayed Nanostructured WC-12Co / Inconel-625 Coatings for Tribocorrosion Applications| **Al-Harbi, Naif I**

37

through promoting some inter-diffusion in the coating and improving the adhesion bonding between coating and substrate. Up to now, most of the previous work on laser surface treatment of HVOF thermal sprayed coatings has concentrated on attempts to improve the corrosion, wear resistance, and metallurgical properties of conventional WC-Co coating. The metallurgical changes, wear, and corrosion performance for nanostructure WC-Co after the laser treatment process were not examined in detail. In addition, blending the nanostructure WC-Co powder with a nickel chromium alloy (Inconel 625) at an optimised weight percentage of 75% to 25%, respectively, has not been investigated. The open literature review shows that there is a gap in the knowledge on aspects of laser treatment using these two coating types and assessment of performance of such treated coatings. Consequently, the main objective of this thesis has focused on determining the relationship between the laser processing conditions and the resulting coating mechanical and tribological properties for the two coating types under study, through to the development of process models (using design-of-experiment techniques). Finally, the optimal laser process conditions to achieve high performance and superior properties for each response will be found with help of statistical design-of-experiment software.

- A literature review clearly shows that to produce a laser-treated coating free from porosity and cracks, prevent dilution from the substrate, and control the melting of hard particles inside the melting pool that negatively impact coating properties and limit the optimization objectives for providing a coating with superior wear and corrosion performance in critical regions/ components in the oil and gas industry, appropriate laser processing conditions and the geometry of laser-beam should be considered.

Novel Enhancement of HVOF Thermal Sprayed Nanostructured WC-12Co / Inconel-625 Coatings for Tribocorrosion Applications| **Al-Harbi, Naif I**

38

CHAPTER 3 - Experimental Methods

1. • **Research materials**

2. • **Substrate materials design and fabrication**

3. • **HVOF thermal spray facility and thermal spray procedure**

4. • **Laser treatment facility and laser treatment procedure**

5. • **Design of experiments**

6. • **Coating characterization techniques and procedures**

7. • **Mechanical testing of the coating**

8. • **Erosion and Erosion-Corrosion wear testing of the coating**
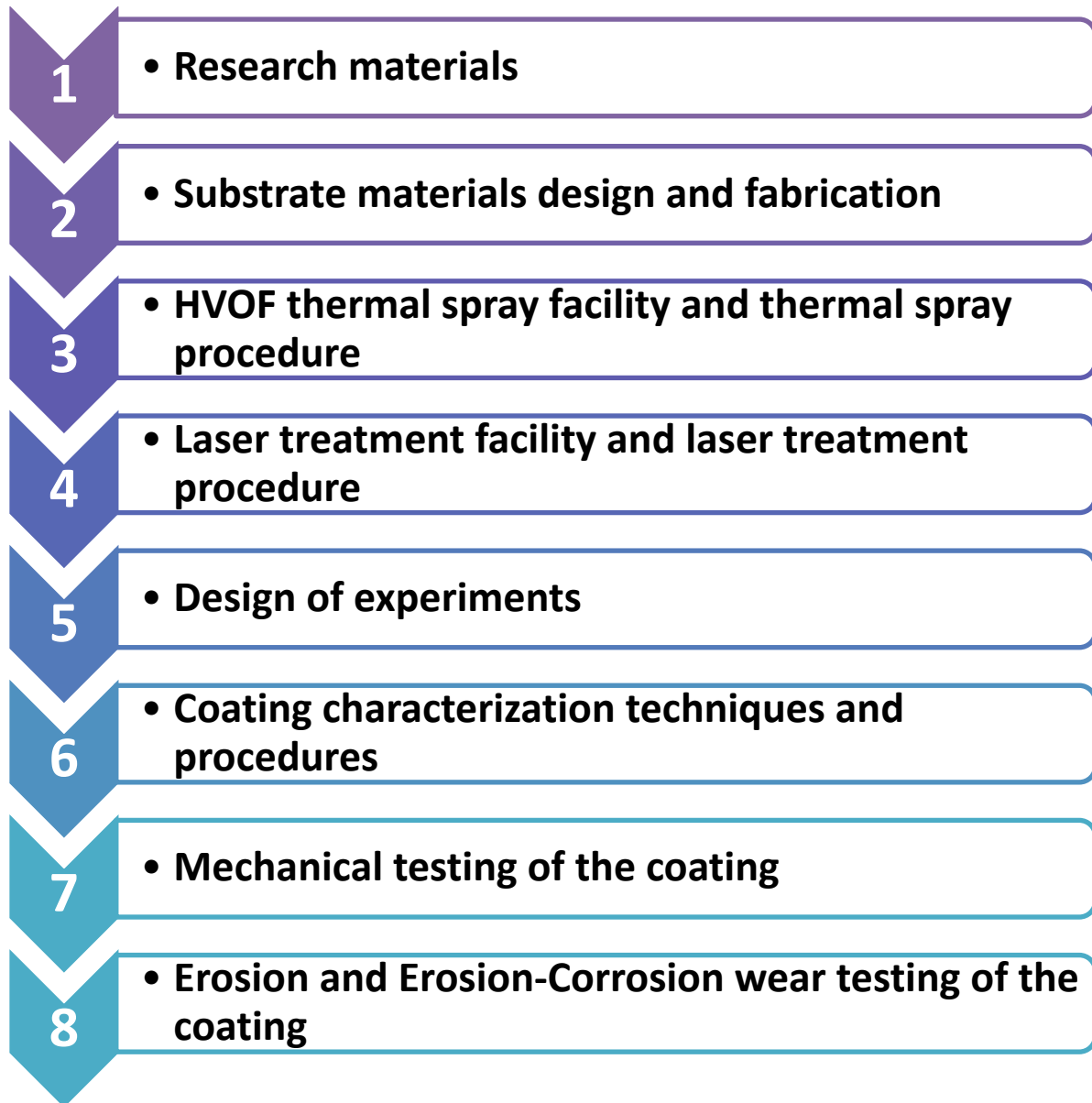
Figure 3-1: The schematic outline of this chapter.

Novel Enhancement of HVOF Thermal Sprayed Nanostructured WC-12Co / Inconel-625 Coatings for Tribocorrosion Applications| **Al-Harbi, Naif I**

39

3.1 Research materials

The two feedstock materials used in this investigation were superfine nanostructured Infralloy™ S7412 and Inconel 625 (Ni-Cr alloy) Diamalloy 1005. The chemical composition of these powders and their average particle size are given in Table 3-1, the coating characteristic of each material and its typical applications are briefly described, and the blending process for the mixed coating types is explained in the following subsections.

Product	Chemical composition %					Powder particle size
Infralloy™ S7412	Co			WC		45+5 μm
	12			Balance		
Diamalloy 1005	Cr	Mo	Fe	Nb	Ni	45+11μm
	21.5	9	2.5	3.7	Balance	

Table 3-1: Powder particle size and chemical compositions [14, 73].

3.1.1 Infralloy™ S7412 WC-12Co (nanostructured)

This is a superfine, nanostructured tungsten carbide/cobalt powder material that has an 88:12 composition ratio of carbide to cobalt. This powder is available on the market under the commercial name Infralloy™ S7412 and is supplied by Informat Corporation. As shown in Figure 3-2, when observed under a microscope, the materials are shown to have a spherical morphology; they have a 45+5 μm particle size and many superfine tungsten grains ranging between 100 and 500 nm in length that are distributed uniformly within the cobalt matrix [73].

Recently, nanostructure tungsten carbide powders and coatings have increased, either as a substitute for it's equivalent microstructure size powder or as a mixture of both (multimodal, mixed micro and nano) powders. This increased usage is partly explained by its superiority for use in conventional materials. Its advantages primarily lie in its morphological and mechanical nature; it produces a relatively high-density coating containing less than 3% porosity, and a higher hardness and fractural toughness than microstructure materials, such as

Novel Enhancement of HVOF Thermal Sprayed Nanostructured WC-12Co / Inconel-625 Coatings for Tribocorrosion Applications| **Al-Harbi, Naif I**

40

Diamalloy 2004, because of the free path reduction between cobalt surrounding smaller WC grain sizes [74].

Figure 3-2: SEM micrograph of the nanostructure of WC-12Co (Infralloy^{TM} S7412).

3.1.2 Diamalloy 1005 (Inconel 625)

This gas-atomized nickel chromium superalloy powder material is commercially known as Diamalloy 1005, developed by Sulzer Metco (Oerlikon Metco is the new owner). Under microscopic observation, this powder exhibits a uniform spherical particle size range of 45+11 μm, as shown in Figure 3-3 [75]. The alloy material provides a coating characterized by a high-tensile bond strength (above 69 MPa) and good oxidation resistance at temperatures not exceeding 870°C [14].

Diamalloy 1005 is suitable for applications requiring a coating material that has excellent corrosion resistance for different corrosive environments, which contributes to the high-density coating microstructure the material provides and leads to low porosity in the coating layer [14].

Novel Enhancement of HVOF Thermal Sprayed Nanostructured WC-12Co / Inconel-625 Coatings for Tribocorrosion Applications| **Al-Harbi, Naif I**

41
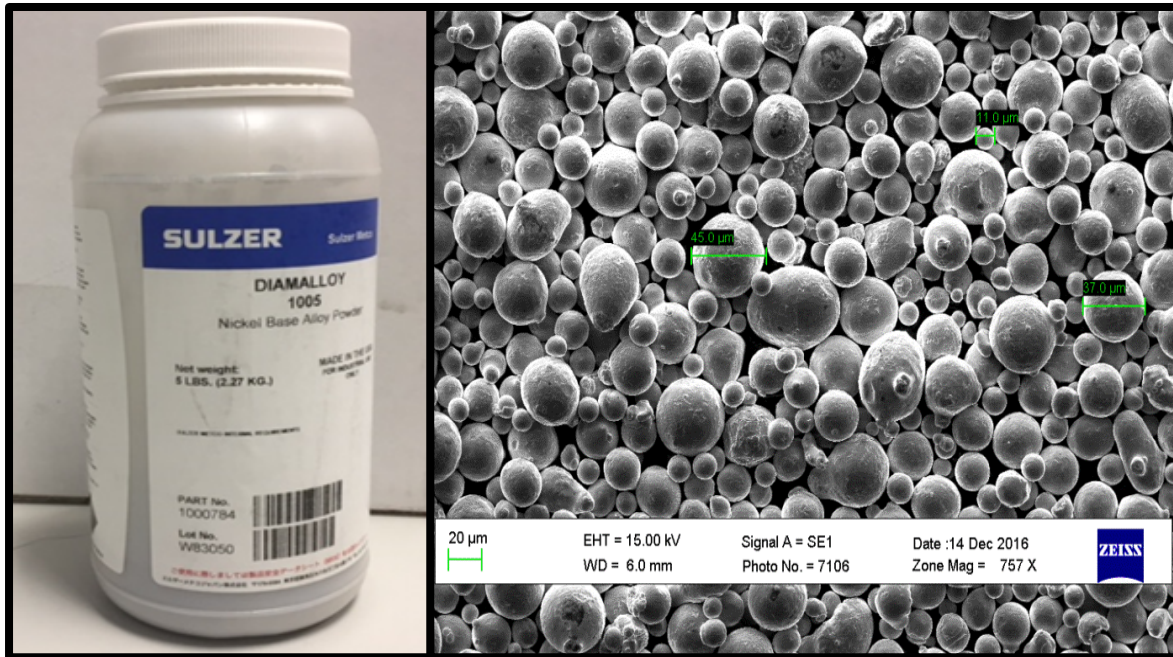
Figure 3-3: SEM micrograph of the Ni-Cr alloy (Diamalloy 1005).

3.1.3 Coating blending

The two powders of the mixed coating type (75 wt. % nWC-12Co + 25 wt. % Inconel 625) were mixed at the optimized percentage weights measured by the KERN KB digital balance with an accuracy of ±0.03 g and a maximum capacity of 1 Kg, as shown in Figure 3-4. This mixing took place inside a spray booth under extraction. Protective equipment that complied with the standards and safety data sheet for the two materials (i.e. glasses, full face-dust mask with a scale number FFP3 filter, clothes, and latex gloves) should be used while mixing the powder. This was done to prevent the powder from contacting the skin, causing respiratory issues and to prevent the powder from being contaminated by the environment inside the lab. It is necessary for the two powders to be homogeneously distributed prior to the thermal spray process. However, after the two powders were mixed inside the spray booth under the assigned weight, they formed into two separate layers separated by a clear boundary, as illustrated in Figure 3-5, and because of the different bulk densities and shapes of the particles of each of the powders, the small particles escaped downward while the large particles remained at the top of each layer.

Novel Enhancement of HVOF Thermal Sprayed Nanostructured WC-12Co / Inconel-625 Coatings for Tribocorrosion Applications| **Al-Harbi, Naif I**

42
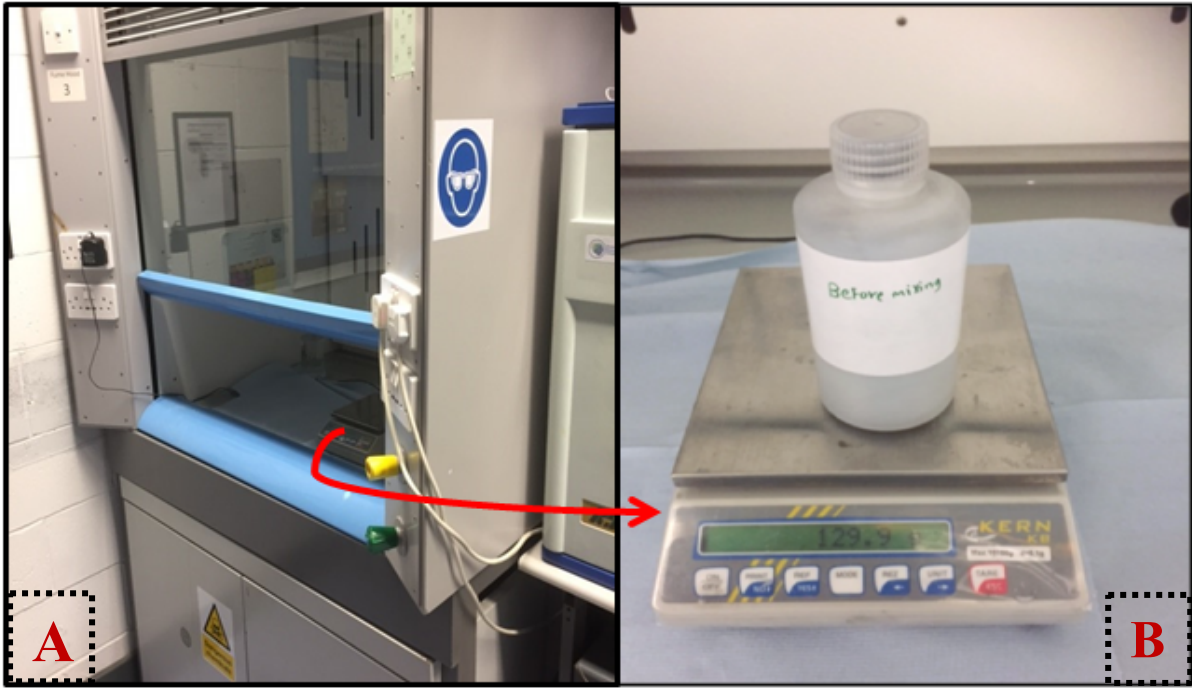
Figure 3-4: Powder mixing for the blended coating type, (A) Fume hood, and (B) Highly accurate KERN KB digital balance.
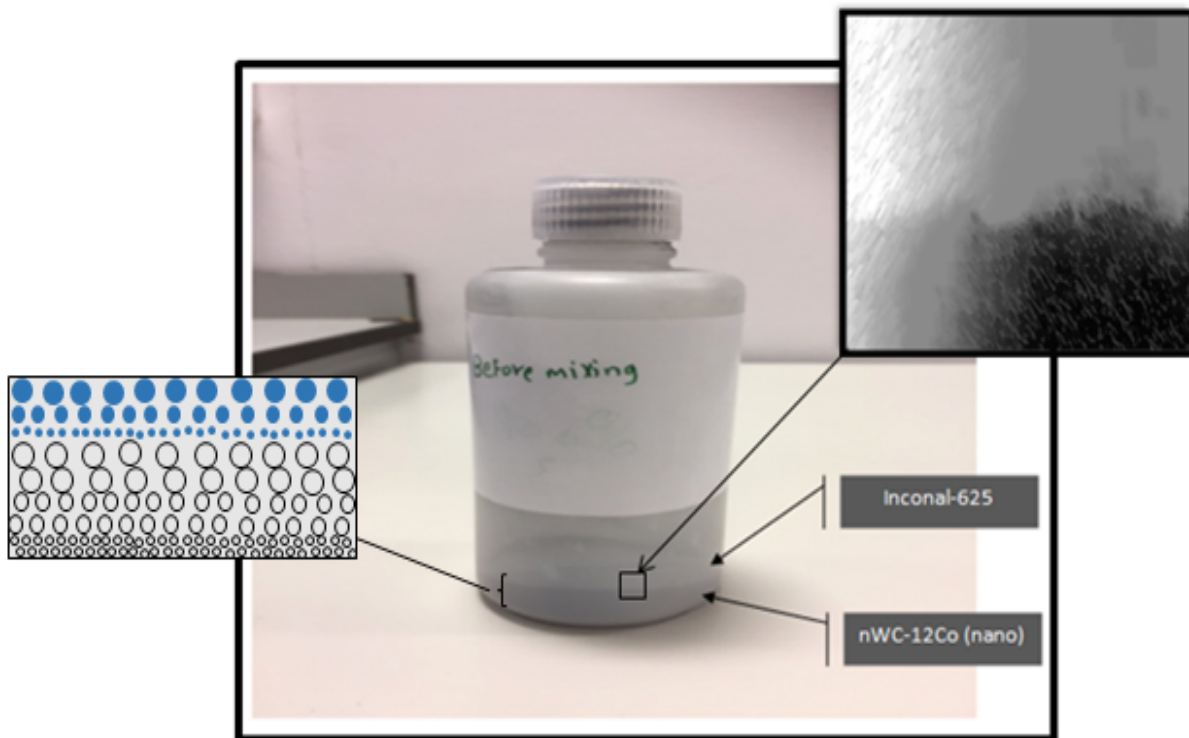
Figure 3-5: The two powders in one container were mixed by the blending device.

Novel Enhancement of HVOF Thermal Sprayed Nanostructured WC-12Co / Inconel-625 Coatings for Tribocorrosion Applications| **Al-Harbi, Naif I**

43

In addition due to the inhomogeneous distribution of the coating powder, issue arise during thermal spraying, as a result of the segregation between the large and small particles, caused by differences in the particles' density, size, and resilience [76]. If the differences in particle size distribution are reduced, this segregation is likely not to happen. Hence, the two powdered materials must be properly mixed. Three standard mixing devices are commonly used in the industry to blend powders: Retsch Turbula, Kenice statics, and the V-shaped drum mixer. The latter was used for this research, as shown in Figure 3-6; this blender is made of two cylinders joined at a 90° angle, which forms the V-Shape. The angle between both the cylinders and the centerline is 45° as shown in Figure 3-6. The drum has a capacity of 2 litres, but it should not be fully filled with powder; as there needs to be enough space for the powder material to move freely through the legs and apex inside the drum of both the vertical and horizontal axes to ensure that the powder material has been completely mixed. The blending took the following stages: the coating materials for the mixed coating were filled to the assigned weight fraction as discussed earlier, connected to the lathe machine, and left to rotate at 40 rpm for 30 minutes, as recommended by Bauman et al. [77].

Figure 3-6: DCU V-Shape blender used for mixing the powder.

Novel Enhancement of HVOF Thermal Sprayed Nanostructured WC-12Co / Inconel-625 Coatings for Tribocorrosion Applications| **Al-Harbi, Naif I**

44

3.2 Substrate materials

The substrate used for this investigation is made from a 4-mm-thick sheet that is classified by the American Iron and Steel Institute as AISI 4140 and that is widely used for several applications in the oil and gas sectors (e.g pump shaft, valves, stem assemblies and bearings), supplied by MIR Steel UK Ltd. It is provided in sheet form in a size of 1.250 × 1 m, and it is cut using a high-precision laser cutting machine into different shapes according to the ASTM standards testing dimensions' requirements, described in detail in the following two sections.

The AISI 4140 contains low carbon of ferritic phase, which provides a body-centered cubic structure at room temperature. Alloyed with alloy steel of the AISI 41×× series; it has a low carbon content of 0.15%, which makes it more ductile than any other higher-carbon steel that lead to lower hardness and tensile strength. It has a chromium content of 0.05%, this is relatively small and not enough for it to be categorized as stainless steel, which would make it unsuitable for corrosion and erosion-corrosion resistance applications. It also contains 0.79% manganese combined with 0.013% Sulphur to prevent brittleness; both of these elements offer proper toughness and are suitable for post-heat treatment, and the 0.011% molybdenum will ensure the uniformity of the hardness and the high strength. A summary of the chemical composition and mechanical properties of the selected substrates are listed in Table 3-2.

<table>
<tr><td rowspan="6">Sheet Thickness 4 mm</td><td>Chemistry</td><td colspan="14">Chemical Analysis (%)</td></tr>
<tr><td rowspan="3">Elements</td><td>C</td><td>Mn</td><td>P</td><td>S</td><td>Cr</td><td>Mo</td><td>Ni</td><td>Cu</td><td>V</td><td>Al</td><td>N</td><td>Si</td><td>Ce</td><td>Fe</td></tr>
<tr><td>.15</td><td>.79</td><td>.005</td><td>.013</td><td>.05</td><td>.011</td><td>.8</td><td>.11</td><td>.005</td><td>.058</td><td>.006</td><td>.01</td><td>.308</td><td>Balance</td></tr>
<tr><td>Material Properties</td><td colspan="14">Mechanical properties</td></tr>
<tr><td>Properties</td><td colspan="4">Tensile strength (T.S)</td><td colspan="3">Yield strength (Y.S)</td><td colspan="3">Modulus of Elasticity (E.L)</td><td colspan="4">Hardness (HV)</td></tr>
<tr><td>Value (units)</td><td colspan="4">655 (MPa)</td><td colspan="3">350-380 (MPa)</td><td colspan="3">180-190 (GPa)</td><td colspan="4">250 (Hardness Vickers)</td></tr>
</table>

Table 3-2: The chemical composition and mechanical properties of the selected substrate [17].

Novel Enhancement of HVOF Thermal Sprayed Nanostructured WC-12Co / Inconel-625 Coatings for Tribocorrosion Applications| **Al-Harbi, Naif I**

45

3.2.1 Substrate/Specimen design

The selected substrate, purchased from MIR Steel UK Ltd., has been sent to a domestic fabrication company for high-precision laser cutting work using a Bystronic Sprint 3015 Laser cutting machine. The sheet was cut into four different shapes according to the ASTM standards for the required dimensions of mechanical testing, wear and erosion-corrosion characterization as required in this research. Drawings of the shapes and the dimensions of each of the four designs (Figure 3-7) were previously created using the Creo Parametric software and sent to the fabrication company to simplify their manufacturing operations. The optical photographs of the substrates after they were laser-cut are shown in Figure 3-8.

ASTM D-790-07 bending sample

ASTM A370 Corrosion and erosion test disc sample
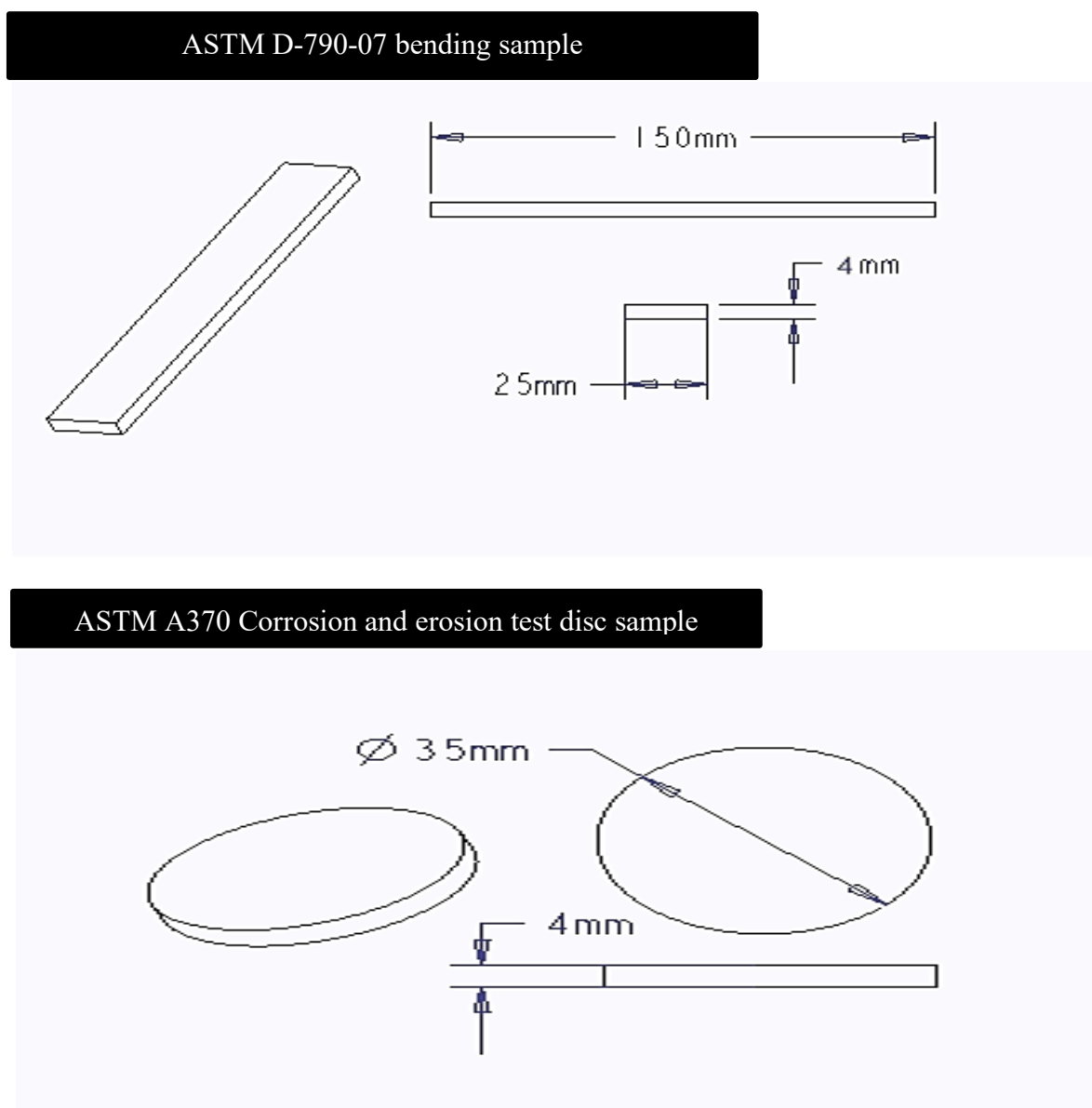
Figure 3-7: Drawing of the two substrate shapes that were used in the research labeled with their ASTM standard code.

Novel Enhancement of HVOF Thermal Sprayed Nanostructured WC-12Co / Inconel-625 Coatings for Tribocorrosion Applications| **Al-Harbi, Naif I**

46

The two substrate shapes include the following:

ASTM D-790-7: This substrate is a rectangular shape that will be used according to the standard for the three-point bending test, and also used for the coating morphological and microstructure characterization pre/post the laser treatment.

ASTM A370: This substrate is a disc shape that was used according to the standard for the erosion and erosion-corrosion tests.
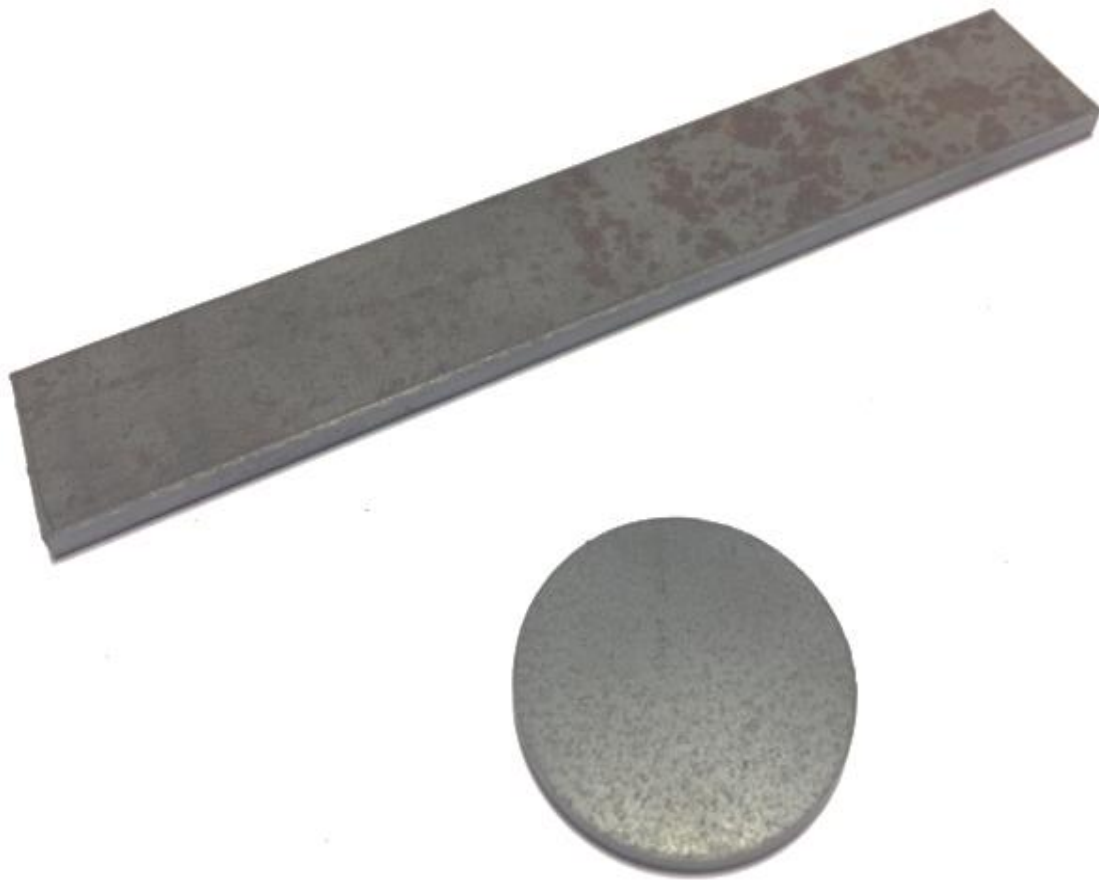
Figure 3-8: Optical photograph of the two substrate types after laser cutting.

Novel Enhancement of HVOF Thermal Sprayed Nanostructured WC-12Co / Inconel-625 Coatings for Tribocorrosion Applications| **Al-Harbi, Naif I**

47

3.2.2 Coating design

The coating locations for the four substrates are shown in Figure 3-9. According to the standard shown in the schematic, the coating will cover one side of all the substrates.
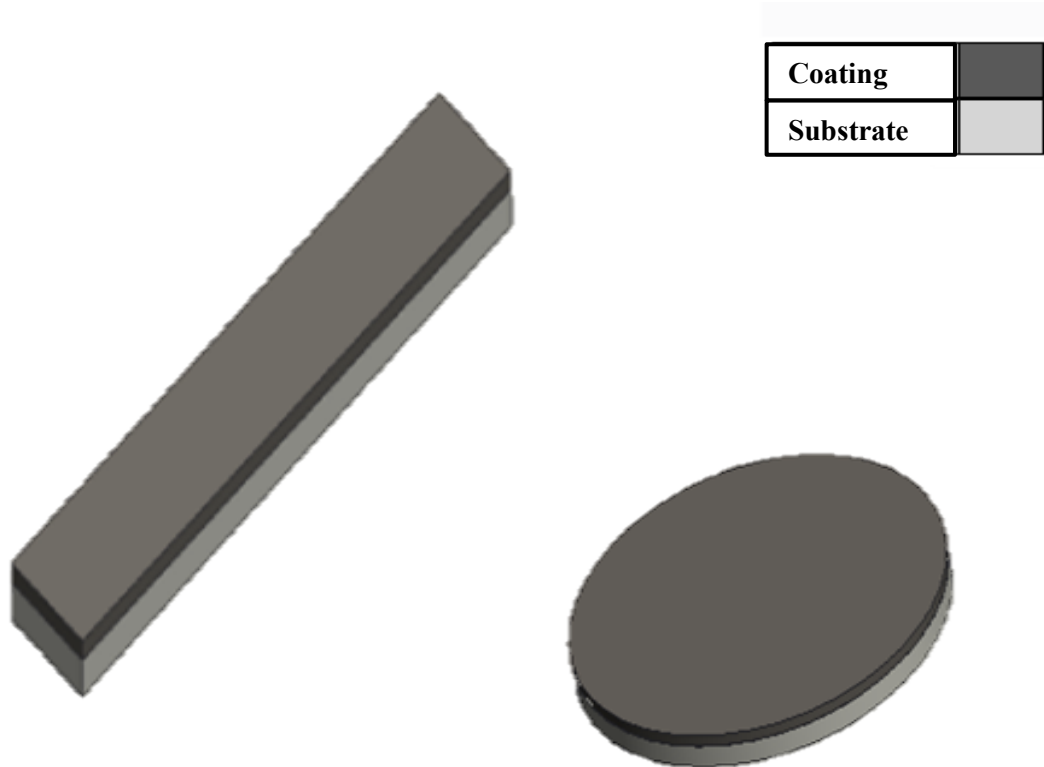
Coating	
Substrate	

Figure 3-9: Schematic of the desired coating location on the different substrate shapes.

3.3 HVOF thermal spray facility

As the thermal spray facilities in DCU were out of commission, the coating was performed at the Oerlikon Company in Switzerland with the auther in attendance using the MultiCoat HVOF spray system, shown in the schematic diagram in Figure 3-10. The company, Oerlikon Metco, is a global leader in the fields of thin film, vacuum propulsion, textile, and precision technologies. In the field of thermal spray coating, Oerlikon stands out as the undisputed leader; it is credited with developing innovative precision technologies and solutions that are highly efficient and reliable. One such technology is the MultiCoat HVOF spray system used in the coating. Due to its semi-automatic HOVF spray system, the technology has numerous advantages, including [78]:

Novel Enhancement of HVOF Thermal Sprayed Nanostructured WC-12Co / Inconel-625 Coatings for Tribocorrosion Applications| **Al-Harbi, Naif I**

48

- The simplicity of operation and the reduced cost;
- The quality that is assured because of the reliability of the process;
- The versatility of the process (i.e., the system can easily be adapted to perform a wide range of tasks);
- The ability to maximize the quality and uniformity of the coating.
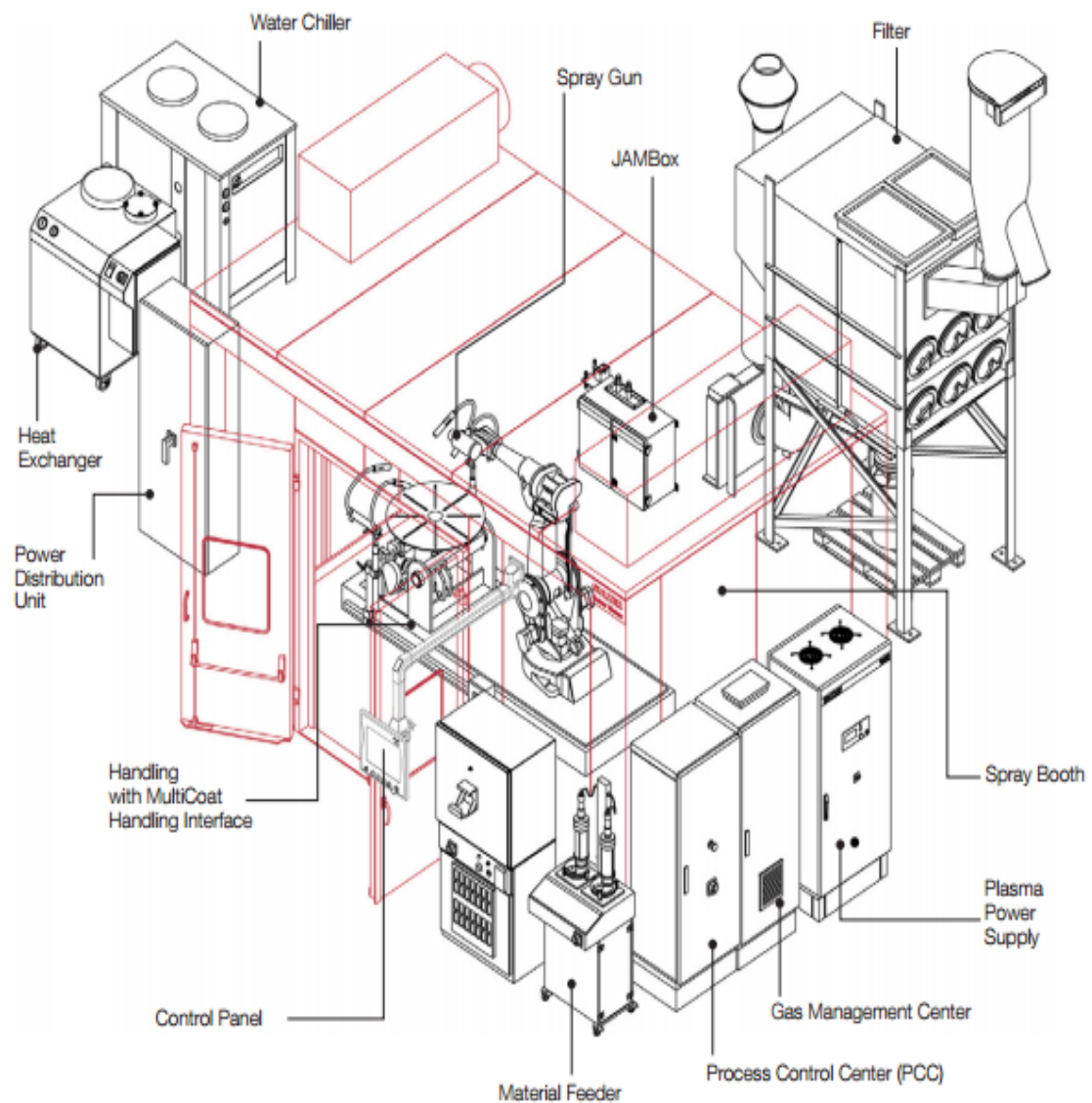
Figure 3-10: Schematic layout of the MultiCoat HVOF thermal spray system used for the coating [78].

Novel Enhancement of HVOF Thermal Sprayed Nanostructured WC-12Co / Inconel-625 Coatings for Tribocorrosion Applications| **Al-Harbi, Naif I**

49

3.3.1 MultiCoat HVOF spray system features

Like other thermal spray systems, the MultiCoat HVOF system used in this research is designed to be a fully self-contained manufacturing system. In this sense, the system can operate in isolation as a solo production unit, but it can also be designed to operate as part of a larger production line. In Figure 3-11, the components of the MultiCoat HVOF system are divided into three primary categories: key components, handling components, and peripheral components [79].
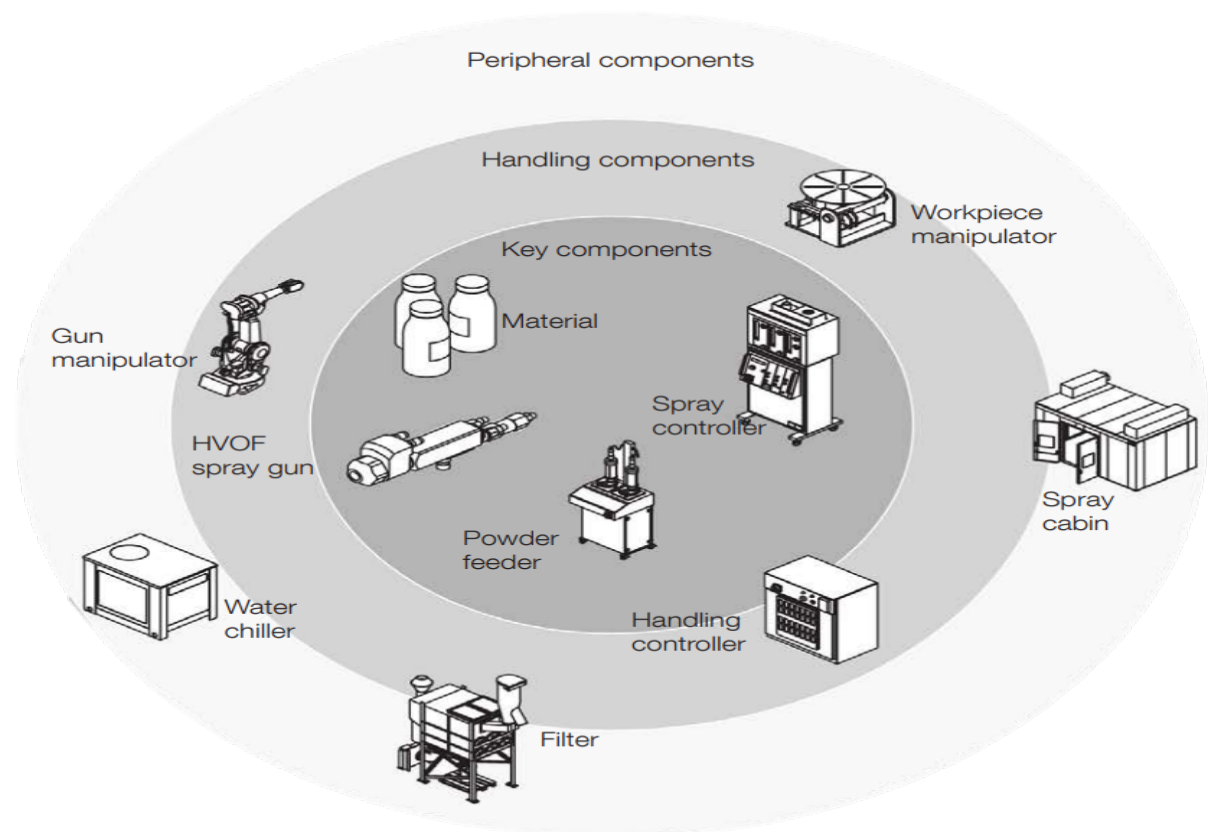
Figure 3-11: Component categories of the MultiCoat HVOF thermal spray system [79].

(A) Key components

The core components are critical for the operation of the system. These elements include the material to be used for the coating, the feed and delivery system for the coating material, a thermal spray gun used in the coating process to propel the coating material toward the workpiece, and a system for controlling the process and other components [79]. In some instances, an AC to DC power converter may be required, but this would depend on the spray process

Novel Enhancement of HVOF Thermal Sprayed Nanostructured WC-12Co / Inconel-625 Coatings for Tribocorrosion Applications| **Al-Harbi, Naif I**

50

employed. The selected thermal spray process also determines whether a heat exchanger for the spray gun or a heater is required [79].

(B) Handling components

These components control the movements of the spray gun and synchronize the gun and the relative position of the gun with the work-piece.

(C) Peripheral components

These components fall under one of four sub-categories: environmental (this includes, for example, the exhaust system, air filter component, and soundproof cabin), safety elements (e.g., warning devices and components for monitoring gas), productivity elements (e.g., software for reporting and managing the work-piece), and components for managing the quality (e.g., spray plum monitoring and diagnostics, which are commonly used for process control) [79].

3.3.2 Powder feeder

A 9MP DJ feeder, as show in Figure 3-12, was used for this research, to ensure superior powder feed precision. The 9MP series of feeders are equipped with closed-loop computerized feed rate monitoring and control [80]. The feeder enables a user to program the feed rate limits and thereby set appropriate and consistent feed rates for any given application [80]. The device operates optimally for a wide range of feed powder states, ranging from fine to coarse powder and from low- to high-density powder [80].

Within the 9MP DJ feeder, delivery of the coating material to the spray gun is maintained through a combination of fluidization, gravity, the use of carrier gas, and a pressure differential within the hopper. The coating powder is fed into the tapered hopper through gravity to the gas fluidization area at the base of the hopper. A vibrator at the base of the hopper assists the gravity and fluidization feed. The powder moves out of the hopper aided by the carrier gas, which flows through the fluidization area to the pickup shaft and pushes the powder toward the spray gun. The powder feed rate is increased by an increase in pressure differential.

The control system for the feeder is driven by a microprocessor weighing device that continuously checks the weight of the hopper. An alarm alerts an operator when the feeder is

Novel Enhancement of HVOF Thermal Sprayed Nanostructured WC-12Co / Inconel-625 Coatings for Tribocorrosion Applications| **Al-Harbi, Naif I**

51

not operating optimally or when the hopper is empty. Using the control panel, an operator can enter a desired feed rate or a known hopper pressure.
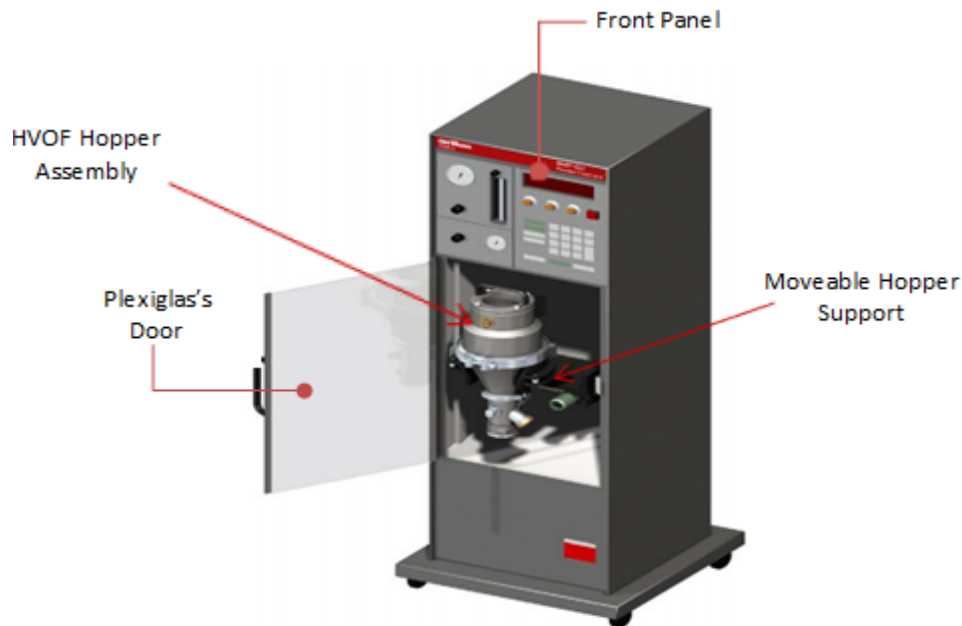
Figure 3-12: The 9MP DJ powder feeder used in the HVOF facility [80].

3.3.3 DJM 2700 HVOF gas fluid gun

In this research, a machine mount Diamond jet (DJ) gun that has a water-cooled air cap was used in conjunction with a DJ 2701 air cap (7.14 mm diameter). The gun had both a diverging and a converging nozzle section. This gun is also referred to as the 3rd generation HVOF spray gun, and it is appropriate for carbide powders and used with propane and natural gas, as shown in Figure 3-13.

The DJ relies on fuel gas, oxygen, and air to produce a high-pressure annular flame. The flame is a source of energy for melting the powder material [81]. A diverging or a converging nozzle running at a supersonic speed is used to accelerate the gas stream, which propels the powdered particles toward the substrate [81]. The individual particles deform plastically when they make contact with the substrate. The coating is characterized by high density, fine and predictable chemistries, and homogeneous microstructures [81]. The coating material is focused on the center of the flame using axial powder injection. This alignment

Novel Enhancement of HVOF Thermal Sprayed Nanostructured WC-12Co / Inconel-625 Coatings for Tribocorrosion Applications| **Al-Harbi, Naif I**

52

eliminates the buildup of the coating material on the walls of the extended air cap, minimizing wear and tear. A water sensing interface unit, DJC2600, is required for the system where the water-cooled HVOF DJ gun is used [82]. The unit signals the DJC series controller when the gun water level falls below the required limits for safety. In such a case, an HVOF system shutdown is initiated [82].
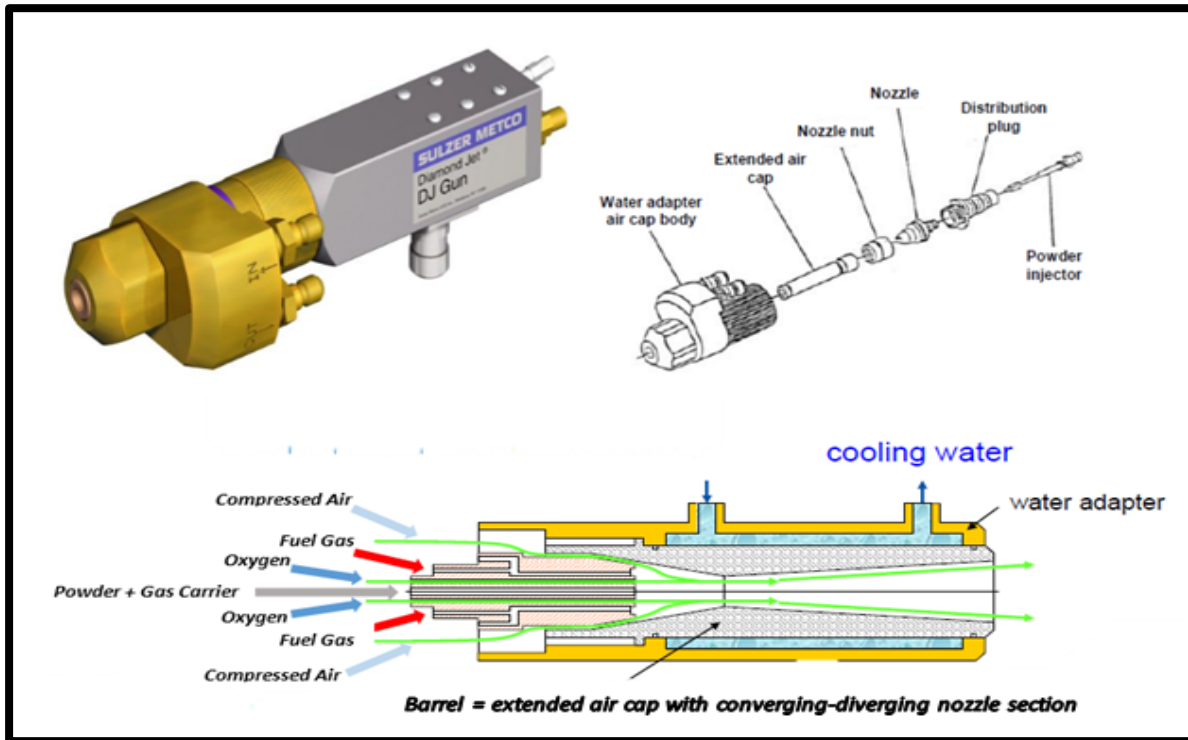
Figure 3-13: Schematic of water-cooled DJM2700 gun with DJ 2701 air cap used in the HVOF facility [83].

3.3.4 Gas management center (GMC)

The gas management center (GMC) contains nitrogen, oxygen, and propane cylinder gas isolated by the GMC HVOF gas tank to prevent pressure reduction caused by cold weather, as shown in Figure 3-14. Oxygen at a high pressure is supplied and serves as the oxidant for the composition process. Three 88-kg oxygen cylinders were used to achieve a high pressure. Three 75-kg cylinders of propane were also used as the fuel gas during the composition process to achieve the required pressure and flow rates. To maintain the pressure of the propane used in the composition process, a vaporized system was used with nitrogen as the back-filled pressure gas. In addition, the pressure of the air compressed through the gun was regulated by control units that were adjusted accordingly. The gas parameters were set in accordance with directives from the companies supplying the conventional microstructure

Novel Enhancement of HVOF Thermal Sprayed Nanostructured WC-12Co / Inconel-625 Coatings for Tribocorrosion Applications| **Al-Harbi, Naif I**

53

WC-12Co powder material (Oerlikon) for the singular nWC-12Co coating, and the optimised recommendation for the spraying of mixed powder, obtained from a PhD student's research at Dublin City University [17]. The recorded gas pressures were (10.34, 5.17, and 4.82 bar) for the oxygen, air, and fuel, respectively, for the mixed coating, and (10.34, 6.2, and 6.8 bar) for the oxygen, air, and fuel, respectively, for the singular nWC-12Co coating.

Figure 3-14: GMC HVOF gas management centre used in the research [79].

3.3.5 DJC spray controller

The Oerlikon Metco MultiCoat Controller with MultiCoat Vision software provides limitless thermal spray versatility and unrivaled process control—all in a single package [78]. The MultiCoat system features superb abilities, including a unique twin-brain management process and an industrial-grade PC known as the PLC to log data and supervise the entire spraying process [78]. The PLC is matched with two RAID-1 technology hard disks to minimize data loss. The MultiCoat system is easy to set up because of its modular plug-and-play component design, which represents a quantum leap over all previous controllers. This technology offers the best of both worlds by combining an enhanced technique with user-friendly, high-resolution touchscreen graphics, flexible spray equipment, system component

Novel Enhancement of HVOF Thermal Sprayed Nanostructured WC-12Co / Inconel-625 Coatings for Tribocorrosion Applications| **Al-Harbi, Naif I**

54

configuration choices, and robust recipe management [78]. The technology also allows the MultiCoat system to accommodate a variety of spray guns, power sources, and power feeders. This flexibility is enhanced by remote robot controllers that are customized to fit the needs of the various applications. The ability of the MultiCoat system to handle up to four separate thermal spray processes from a single operating station is an outstanding feature of the system [78].

Figure 3-15: (Left) MultiCoat process control center (PCC) used in the research, and (Right) MultiCoat control panel on wheel-stand used in the experiments [78].

3.4 HVOF thermal spray procedure

This section describes the details of the coating process procedure adopted by the author. The process started with the samples surface preparation procedure, continued with the samples holding technique and coating system parameters, and concluded with the coating process.

3.4.1 Substrates surface preparation

The following procedure was followed for preparing the substrate:

- Sample was placed in a magnetic holder, as shown in Figure 3-17.
- First, the samples were cleaned using acetone; then, their edges were smoothed using a grinder.

Novel Enhancement of HVOF Thermal Sprayed Nanostructured WC-12Co / Inconel-625 Coatings for Tribocorrosion Applications| **Al-Harbi, Naif I**

55

- Samples were cleaned for a second time using acetone before being grit-blasted using the standard grit blasting method (Figure 3-16(A)). This process was performed manually; a handheld gun was used to spray grits of under 152 mm spraying distance 90° from the part that had 3.8 bar of compressed air pressure. The 90° spraying angle between the two sides of the vertical direction of the blasted surface was used to avoid having irregular surface roughness. Honite 13 particles were used as the blasting media and had the following chemical composition (provided by Guyson): 95.65% Al_2O_3, 2.42% Ti_2O_2, 0.92% SiO_2,0.12 % Fe_2O_3,0.35% CaO and 0.22% MgO. The particle sizes ranged between 106 and 212 μm, and the particles were white in colour and spherical in shape, as shown in Figure 3-16-B. The angle and distance from which blasting occurred were estimated, leading to some variations; closer blasting distances increased the impact of powder particles, resulting in particles sticking to the substrate's surface. Some contamination from the sand particles was expected at the coating–substrate interface. Generally, this contamination should not exceed 25% per cross-sectional area of the interface, because any more would affect the bond strength at the coating–substrate interface.
- Finally, masking was used to cover the samples and prevent oxidation from occurring. The samples were then grouped according to the coating types and were coated immediately after.
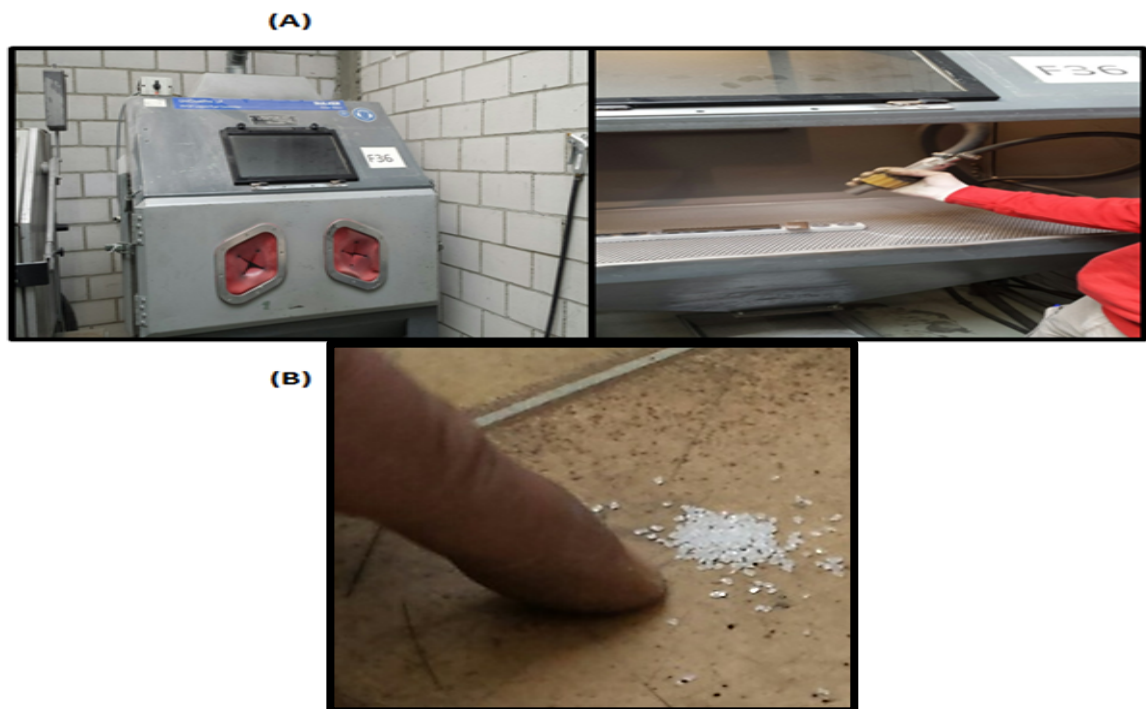
Figure 3-16: (A) Empire grit-blasting machine used to rough and clean the sample surface, and (B) Honite 13 powder particles were used.

Novel Enhancement of HVOF Thermal Sprayed Nanostructured WC-12Co / Inconel-625 Coatings for Tribocorrosion Applications| **Al-Harbi, Naif I**

56
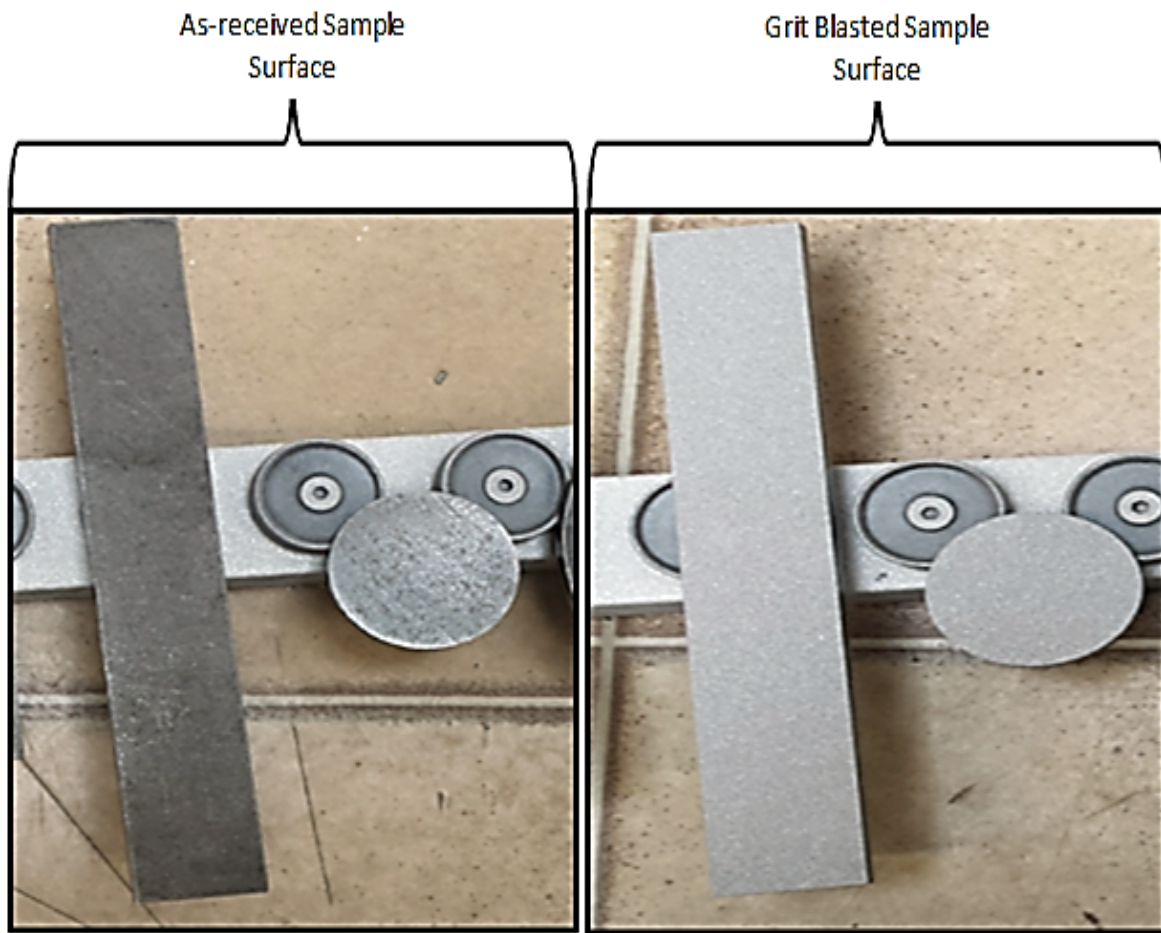
Figure 3-17: Sample surfaces before and after the grit-blasting process.

3.4.2 Substrate setup for deposition

A 305-mm diameter turntable was used to hold the samples while the turntable rotated, as shown in Figure 3-18. Sixteen samples, each separated by a 1-cm distance, could be sprayed simultaneously. Through the MultiCoat Process Control center, the turntable was set to rotate at a speed of 83 rpm, and the powder flow rate was set to 38 rpm for the two coating types, providing an application rate in the range of 8.3 to 10 um/pass. Prior to the coating process, the substrate was preheated to 165°C for one full cycle to remove any moisture and minimize the effects of thermal expansion of the coating process.

Novel Enhancement of HVOF Thermal Sprayed Nanostructured WC-12Co / Inconel-625 Coatings for Tribocorrosion Applications| **Al-Harbi, Naif I**

57
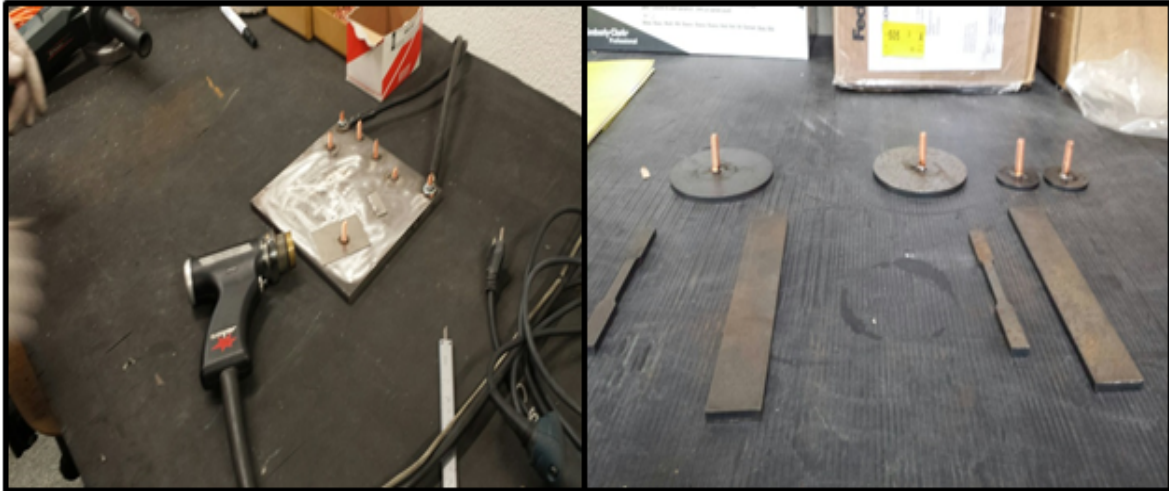
Figure 3-18: (A) The disc shape sample brazed by copper screws to be tightened to rectangular steel afterward, and (B) Samples placed in the turntable tightened to the standard fixture.

3.4.3 Coating system parameters

The spray parameters are considered the dominant factors that affect the coating quality. Table 3-3 provides the recommended parameters provided by the powder manufacturer, Oerlikon, for the conventional microstructure WC-12Co type used for the singular nWC-12Co powder. For the mixed powder, the optimized parameters were obtained from previous research at Dublin City University [17].

Novel Enhancement of HVOF Thermal Sprayed Nanostructured WC-12Co / Inconel-625 Coatings for Tribocorrosion Applications| **Al-Harbi, Naif I**

58

Powder Name		Infralloy S7412	Mixed powder
Powder Chemical Composition		nWC-12Co	75 wt. % nWC-12Co + 25 wt. % Inconel 625
Oxygen flow	[NLPM]	240	272
Air flow	[NLPM]	375	367
Fuel gas type		Propane	Propane
Fuel flow	[NLPM]	70	70
lambda value		0.94	0.88
Carrier Gas Flow(N$_2$)	[SLPM]	14.7	12.5
Powder feed rate	[g/min]	38	38
Hoper back pressure	[mbar]	1.4	1.4
Vibrator Pressure	[mbar]	240	206
Spray distance	[mm]	203	178
Rotation speed	[RPM]	83	83
Translation speed	[mm/s]	4.0	4.0
Surface speed	[m/min]	80	80
Step	[mm/pass]	3	3
No. of passes	#	32	28
Application rate	μm/pass	8.6	9.5
Substrate cooling	type; direction	4 x Ventury 5 bar	4 x Ventury 5 bar
Cooling power	[kW]	3.6	5.0

Table 3-3: Recommended parameters used for spraying the two powder types.

Because of the sensitivity of the nanostructures used in this study, the nitrogen carrier gas flow rate for singular nWC-12Co coating was increased from the recommended value, 12.5 SLPM, to 14.7 SLPM. This increases the velocity and results in a lower flame temperature for the coating materials, as shown in the example for the CR_3C_2-20NiCr coating materials in Figure 3-19. Subsequently, it will lead to the nanoscale WC particles having shorter dwell time and being exposed to lower flame temperatures during spraying; consequently, there will be less decarburization in the carbides.

Novel Enhancement of HVOF Thermal Sprayed Nanostructured WC-12Co / Inconel-625 Coatings for Tribocorrosion Applications| **Al-Harbi, Naif I**

59
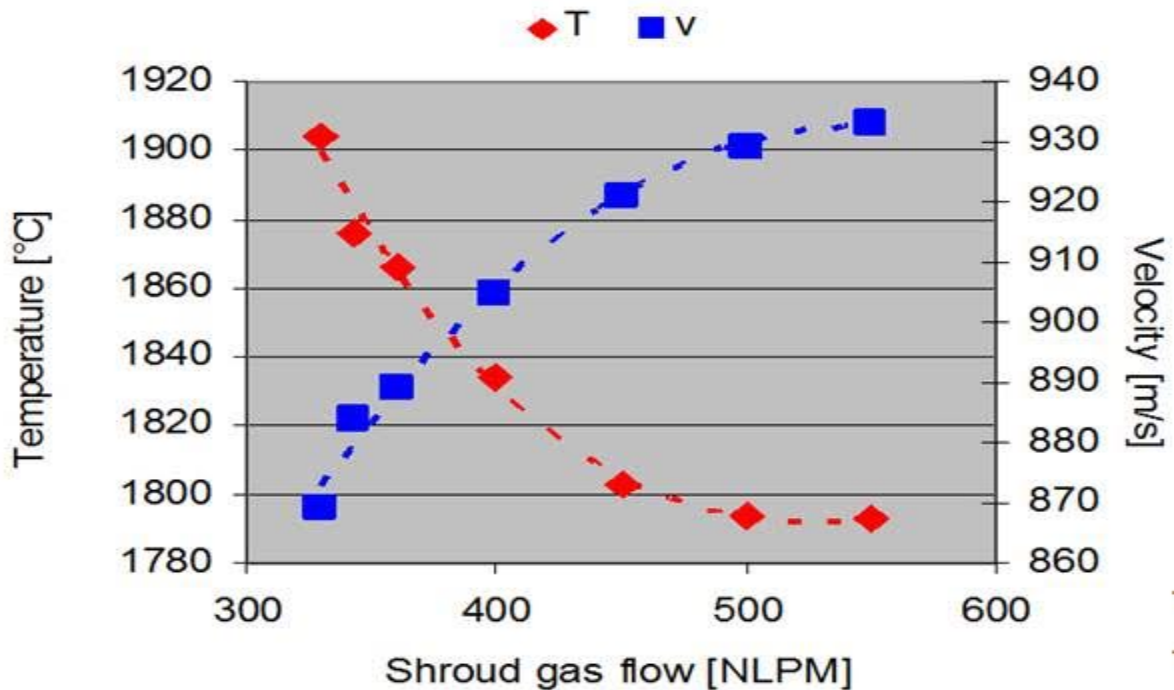
Figure 3-19: Influence of shroud gas flow on the partial velocity (V) and temperature (T) for the CR_3C_2-20NiCr coating sprayed by the WOKA7105 gun [83].

3.4.4 Thermal spray process

The process begun by filling the DJ powder feeder with the assigned powder (either nWC-12 Co or a mixed powder type) and then manually installing the DJM2700 gun to the Fanuc robot, as shown in Figure 3-20 (A). The required spray distance was adjusted manually; a ruler was used to measure the distance between the gun nozzle and the substrate, as shown in Figure 3-20 (B). The DJC spray controller controlled the process, and user inputs were fed through the MultiCoat control panel.

The MultiCoat control panel contains software that provides features for all the thermal spray components. It includes functions that enable parameter data to be logged into tables and monitors all the thermal spray processes, as shown in Figure 3-20 (D). An operator pre-sets all the necessary parameters before the thermal process is initiated.

At system startup, the thermal spray process adheres to a series of stages. First, there is the initiation of oxygen, propane gas, and gun air. Then, the Fanuse robot moves to the DJC2700 Hydrogen Pilot located at one corner of the thermal spray booth and ignites the gun, as shown

Novel Enhancement of HVOF Thermal Sprayed Nanostructured WC-12Co / Inconel-625 Coatings for Tribocorrosion Applications| **Al-Harbi, Naif I**

60

in Figure 3-20 (C). The turntable then starts rotating, and a few minutes later, the powder feed is automatically initiated.

The angle from the spray gun to the work-piece is 90°. The air cooling system was used in this experiment, as shown in Figure 3-20 (E), to provide cooling to the work-piece to prevent the materials from shrinking by overheating during the thermal spray process.
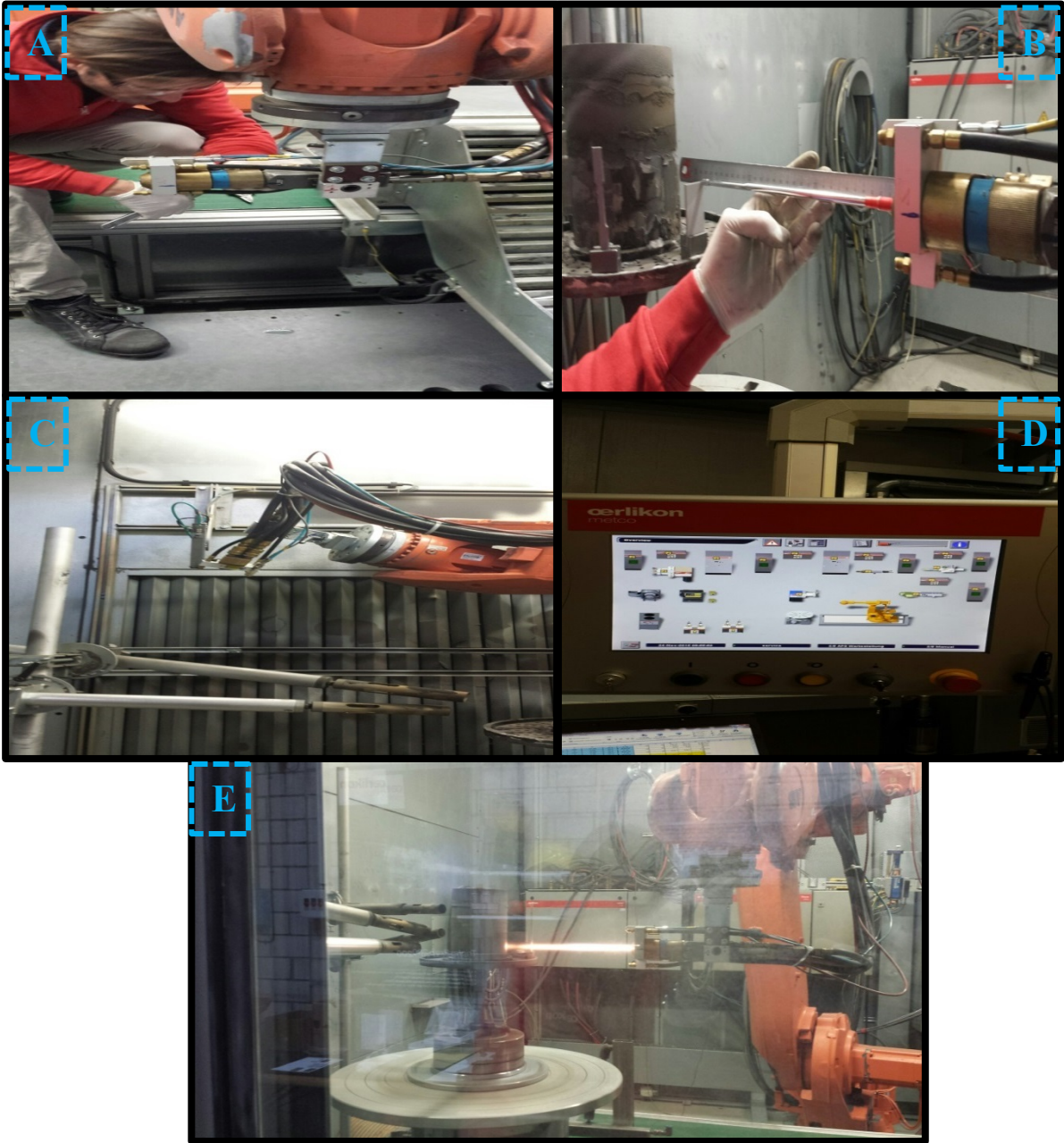
Figure 3-20: Images of the HVOF thermal spray process used in the research.

Novel Enhancement of HVOF Thermal Sprayed Nanostructured WC-12Co / Inconel-625 Coatings for Tribocorrosion Applications| **Al-Harbi, Naif I**

61

3.5 Laser treatment facility

The CO_2 laser employed in the present study involves the Rofin DC-015 diffusion-cooled CO_2 slab layer model, the specifications of which are explained in Table 3-4 (conducted in DCU). The laser optical resonator shown in Figure 3-21 comprises two parallel RF-electrodes and two mirrors (rear and front). From the RF field, the laser gas is usually excited between the electrodes, which are cooled by water. A linearly-polarized beam at a 45° angle is generated by the resonator design.

Parameters	Specifications
Wavelength (λ)	10.6 μm
Output Power Range	150–1500 W
Beam Quality Factor	K > 0.9
Operation Mode	Pulsed and Constant
Beam Propagation Parameter (M^2)	1.11
Laser Gas	ROFIN-SINAR Special-Premix
Pulse Width	26 μs

Table 3-4: Specification of the Rofin DC-015 CO2 laser system [84].

1. Laser beam
2. Laser beam telescope
3. Output mirror
4. Cooling water connection
5. High frequency excitation
6. Cooling water connection
7. Rear Mirror
8. Active zone (slab)
9. Waveguiding electrodes
10. Grounding (earthling)
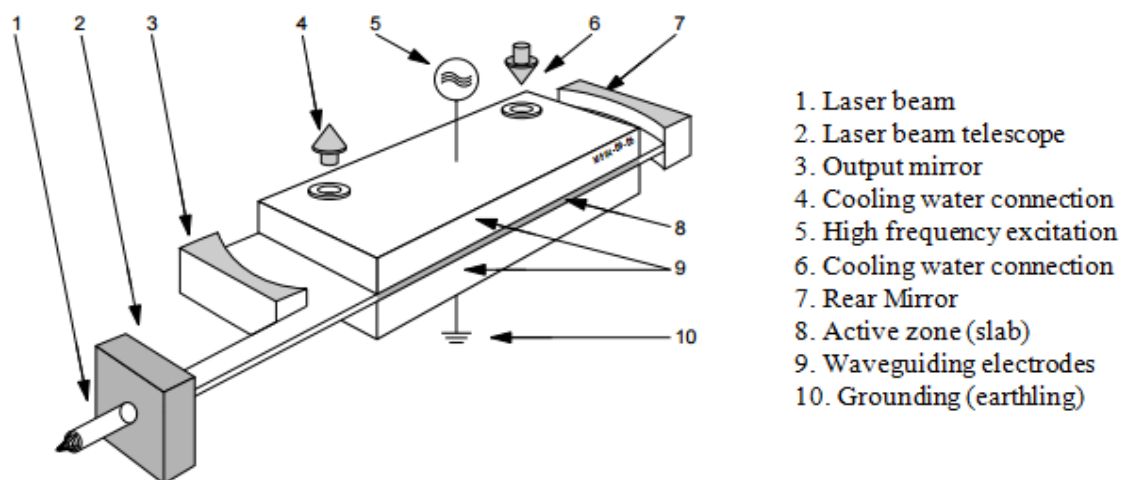
Figure 3-21: Laser resonator of the CO_2 laser [84].

Novel Enhancement of HVOF Thermal Sprayed Nanostructured WC-12Co / Inconel-625 Coatings for Tribocorrosion Applications| **Al-Harbi, Naif I**

62

3.5.1 CNC motion system

The laser system functions in combination with the CNC motion system. Specifically, the MTI 0505 scientific motion system was used. According to the demonstration in Figure 3-22, the motion system comprises a machining table (XY) that had a 500-mm movement range in two directions (500 X 500 mm). The table has optical rotary encoders that provide a motion resolution of about 1.25 μm. The velocity of movement in the two directions can vary between 1 mm/min and 5,000 mm/min. The initial acceleration might reach about 2 m/s^2 [85].

The control system CNC motion scheme is integrated with a laser control system. As such, the control console can regulate the laser power and the motion system simultaneously using the touchscreen on the TFT displays [85]. The jet or nozzle system that comprises the focusing components is fixed on a vertical linear variable displacement transducer (LVDT) and allows for a 150-mm vertical adjustment of the central position. In addition, the nozzle ensures that a continuous flow of compressed air (nitrogen, oxygen, or argon) is conveyed to the ray in a coaxial manner.
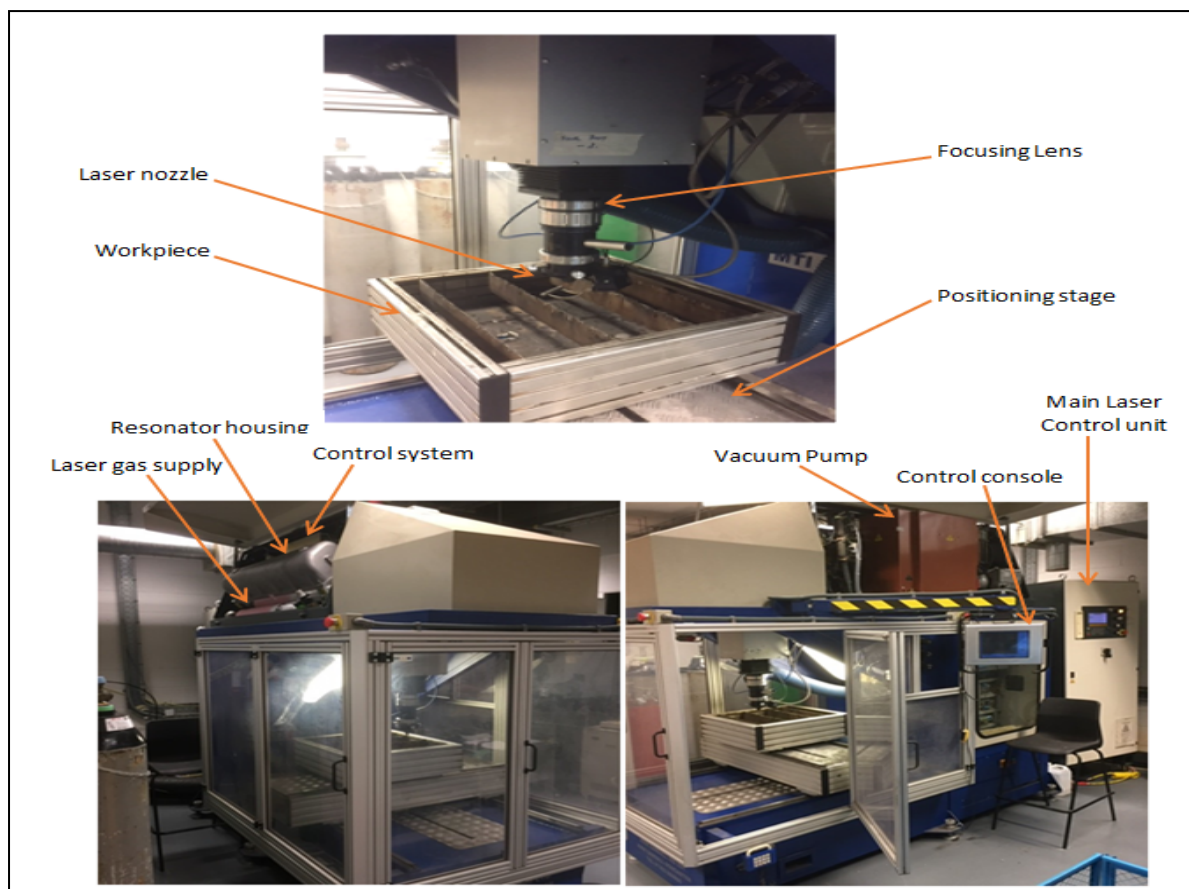
Figure 3-22: Rofin dc-015 CO$_2$ laser system main components.

Novel Enhancement of HVOF Thermal Sprayed Nanostructured WC-12Co / Inconel-625 Coatings for Tribocorrosion Applications| **Al-Harbi, Naif I**

63

3.6 Laser treatment procedure

A 1.5 PW kW CO_2 Rofin laser provided by Mechatronic Industries Ltd., as described earlier, was used to perform the laser melting. The 90° incident angle of the laser beam with the treated surface was maintained to perform homogeneous laser beam irradiation to the coated samples. Compressed argon was supplied coaxially as a shielding gas at a constant pressure of 0.5 bar to reduce oxidation from the treated surface. The laser treatment was performed using a laser beam of elliptical spot shape, where the long dimension moved with the scanning direction and had a uniform density distribution, as shown in the modelled beam profiles in Figure 3-23. To eliminate or reduce the thermal shocks during laser treatment, the continuous operational mode was applied. The overlap ratio was maintained at 40% to achieve a flatter-based hardened zone along the melt pool depth. Another three processing parameters and their relationships to the coating quality were studied by applying the three-level Box-Behnken design of experiment (DOE) in this research (described later).

The three control parameters used for the coating quality and implemented as factors in the DOE experiment were:

1. Laser average power, P (W);
2. Scanning speed, U (mm/min);
3. And focal point position (beam size), F (mm).
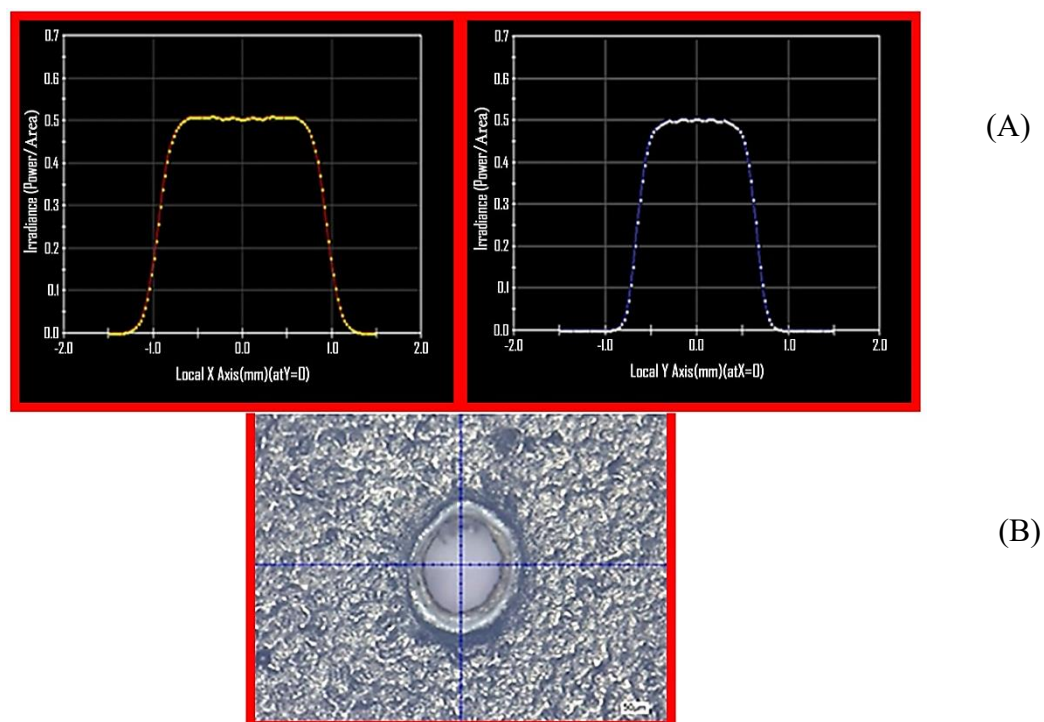
Figure 3-23: (A) The modeled beam profiles at a focal position of ≈ +25 showing the Top-Hat elliptical beam profile, and (B) The geometry validated experimentally by laser alignment paper.

Novel Enhancement of HVOF Thermal Sprayed Nanostructured WC-12Co / Inconel-625 Coatings for Tribocorrosion Applications| **Al-Harbi, Naif I**

64

Based on the results presented in the next chapter of the laser optimization, a Box-Behnken design (Section 3.7.2) featuring three levels (3^n) was developed. Table 3-5 shows the selected levels for each of the three control factors, and their corresponding DOE coding units are presented in the top row.

DOE Coding	Units	Notation	Limits		
			-1	0	1
Power	W	P	150	250	350
Scanning Speed	mm/min	U	150	225	300
Focal Position	mm	F	+35	+40	+45

Table 3-5: The selected levels of the three control factors based on the laser optimization results.

Table 3-6 provides the full list of all possible experimental arrangements that could result from these levels. These comprise of 17 runs, five of which are repeated at the center point (P.S:13, 14, 15, 16, 17) and marked by an asterisk for the repeatability analysis.

Run No.	Laser Power (W)	Focal Position (mm)	Scanning Speed (mm/min)
P.S.1	150	35	225
P.S.2	350	35	225
P.S.3	150	45	225
P.S.4	350	45	225
P.S.5	150	40	150
P.S.6	350	40	150
P.S.7	150	40	300
P.S.8	350	40	300
P.S.9	250	35	150
P.S.10	250	45	150
P.S.11	250	35	300
P.S.12	250	45	300
P.S.13*	250	40	225
P.S.14*	250	40	225
P.S.15*	250	40	225
P.S.16*	250	40	225
P.S.17*	250	40	225

Table 3-6: The laser control-run experiments and *Repeated experiments.

Novel Enhancement of HVOF Thermal Sprayed Nanostructured WC-12Co / Inconel-625 Coatings for Tribocorrosion Applications| **Al-Harbi, Naif I**

65

3.7 Design of Experiments (DOE)

Concerning the analysis of variance (ANOVA), the Design-Expert software was employed to test for the adequacy of the created simulations [85]. The F-test based on the lack-of-fit test was utilized to examine the statistical significance of the models regarding the terms of every model in the equation for regression (model equation). The F-values usually indicate the factor of influence. For higher F-values, this implies that the factor has significant influence. Additionally, the p-value (Prob. > F) of the model, as well as the terms, were calculated using software with the ANOVA methodology. When the p-values do not surpass the level of significance (for example α = 0.10), then the model was accepted to be adequate in the confidence interval of (1- α) [85]. Moreover, if the p-value for the lack-of-fit test goes beyond the significance level, the model was observed to sufficiently fit the data.

The R^2 values involve the calculation of the extent of variation about the mean that is depicted in the model. When R^2 is near to 1, the variance is minimal about the mean. The adjusted R^2 value usually measures the extent of variation about the mean that is adjusted for the quantity of terms within the model. The variation amongst the adjusted R^2 and predicted R^2 should be less than 0.2 [85]. If the difference is larger than 0.20, then there is a problem with the model or the used data.

The sufficient precision ratios usually measure the signal to noise proportions. For a ratio larger than four, there is adequate model discrimination. Further, it means that the model can navigate the design region. The significance testing of the terms of the model as well as the decision to consider them in the model equation was conducted using a step-by-step regression technique. The regression technique was employed to fit a second-order polynomial equation that involves the experimental data as well as to determine the applicable model terms for the depth and width for each of the results. Therefore, the created model equations comprised solely the terms that have a significant impact on the response.

Generally, the model is adequate when the successions of the hypothesis demonstrated in Table 3-7 are real. Also, it is important to accomplish the adjusted R^2 and predicted R^2 values from the model that are as high as possible towards R^2 to ensure a best-fit model. Accordingly, the best scenarios occur when all three values are close to one.

Novel Enhancement of HVOF Thermal Sprayed Nanostructured WC-12Co / Inconel-625 Coatings for Tribocorrosion Applications| **Al-Harbi, Naif I**

66

Term	Set Acceptable Levels
Model Prob > F	<0.05
Lack of fit Prob > F	<0.05
R^2	Between 0.6 and 1
Predicted R^2 – Adjusted R^2	≤ 0.2

Table 3-7: Minimum values set for module acceptance.

For the present study, the significance value was taken as $\alpha = 0.05$ to ensure that the 95% level of confidence is achieved in the established models. Additionally, the predicted R^2 as well as the adjusted R^2 should be within 0.20 of each another. Otherwise, a problem arises with the model or the data. When the adequate precision ratios are larger than four, there is adequate model discrimination.

3.7.1 Optimization approach in Design-Expert software

The optimization component within the Design-Expert software usually searches for a mixture of factor levels that concurrently meet the specifications (optimization criteria) on each of the responses as well as the process factors (the numerous response optimization) [86]. The graphical and numerical optimization approaches were employed in the research by selecting the preferred objectives for each response and factor. The numerical optimization approach entails merging the goals into a desirability function (D). Within the Design-Expert software, the numerical optimization attribute discovers a point or additional points within the factors field that can make the most of the objective function.

For the graphical optimization that has several responses, the software will define areas whereby the requirements concurrently accomplish the suggested criteria by overlapping or superimposing the crucial response outlines on a contour scheme [86]. Thus, the pictorial search for the best compromise can be achieved. When handling several responses, it is advisable to undertake a numerical optimization first since it is not possible to discover a practical area. Accordingly, the graphical optimization portrays the region of feasible response values within the factor space. In case the fields do not meet the optimization requirements, they will be shaded. Figure 3-24 demonstrates the flowchart for the optimization phases used by the Design-Expert software.

Novel Enhancement of HVOF Thermal Sprayed Nanostructured WC-12Co / Inconel-625 Coatings for Tribocorrosion Applications| **Al-Harbi, Naif I**

67
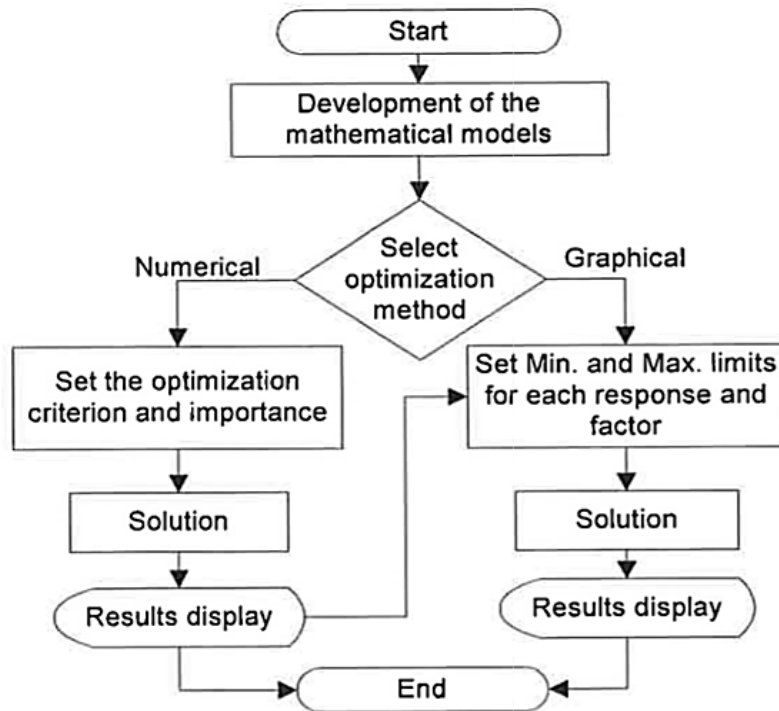
Figure 3-24: Flowchart of the optimization steps used by the Design-Expert software [86].

3.7.2 Box-Behnken Design (BBD)

Box-Behnken design (BBD) is one of the most two popular experimental design types of Responses surface methodology (RSM) DOE design which exists for developing second-order models, where the second one are the central composite design (CCD) [87].

A group of techniques related to the study of how different variables influence a controlled experiments outcome are referred to like the design of experiments. Once the independent factors or variables that affect the process or product are identified, their effects on dependent responses or variables are investigated. The Box-Behnken Design is used in Response Surface Methodology to achieve the following objectives [87]:

- Obtain at least three levels, by placing each independent variable at one of three values that are equally spaced. These independent variables are normally coded as -1, 0 and +1.

- The placement of the independent variables outlined above should be designed in a way that they would fit a quadratic model. The quadratic model in question should

Novel Enhancement of HVOF Thermal Sprayed Nanostructured WC-12Co / Inconel-625 Coatings for Tribocorrosion Applications| **Al-Harbi, Naif I**

68

contain; an intercept, squared terms, a product of two independent variables and linear terms.

- There should be a reasonable fraction of the count of coefficients and the count of experimental points in the quadratic model. This translates to designs of between 1.5 and 2.6.

- The distance from the center should be used to determine the estimation variance. This can be achieved by designs that have 4 – 7 factors. The distance from the center is not supposed to change a lot in the smallest cube that has the experimental points.

By searching for design with likable/agreeable estimation variance properties, the 7 factors design is found first followed by similar designs for other numbers. Each design is like a combination of a full/fractional (two-level) factorial design that has an incomplete block design. A given number of independent variables are put through all of the factorial design's combinations in each block as the other independent values stay fixed at the central values. For example, three factors translate to a total of 12 design points which have five center points totaling 17 points. This happens despite the fact that 12 distinctive combinations account for less than a half of the total combinations with an equal level count, but they provide enough information for 10 polynomial coefficients [88].
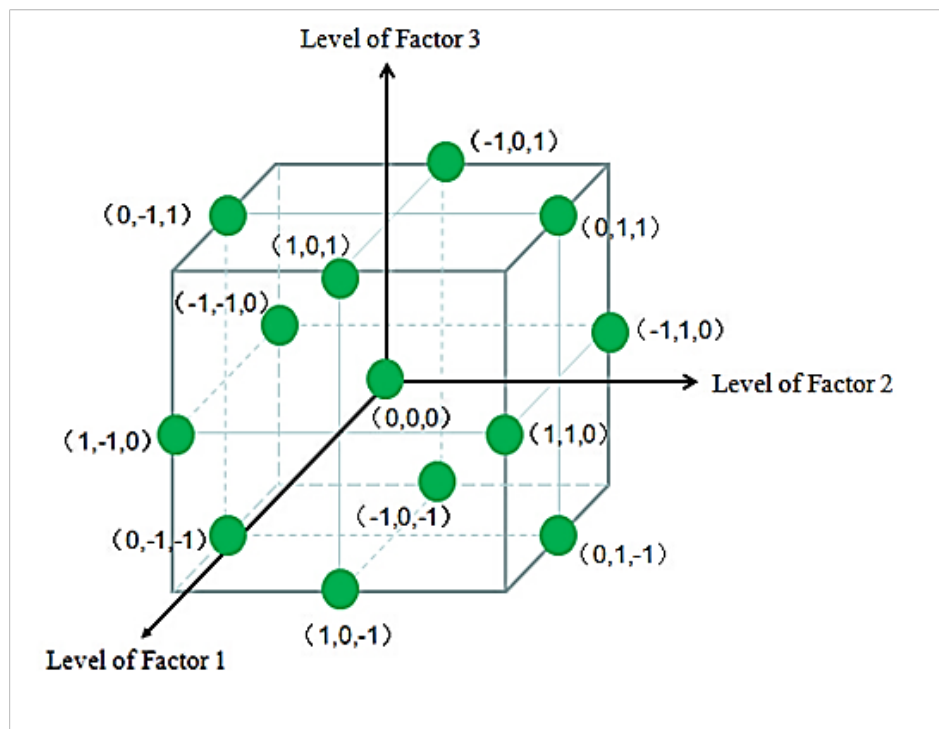
Figure 3-25: Layout of BBD (Box–Behnken design).

Novel Enhancement of HVOF Thermal Sprayed Nanostructured WC-12Co / Inconel-625 Coatings for Tribocorrosion Applications| **Al-Harbi, Naif I**

69

(A) BBD analysis of the design

The equations below can be employed to obtain the 10 coefficients that are inside the polynomial. Equations 3-7 and 3-1 to 3-4 can be used for this purpose. Equations 3-1 to 3-4 can be used to obtain the sum of squares squares for every term of the BBD, and to obtain the sum of squares designed with less than three factors. In the case where A, B, D1, and C1 are constants for the 3 factors designs; the three constants become 1⁄8, 1⁄4, 1⁄4, and -1⁄16 respectively [87].

$$b_0 = \bar{y}_o \qquad\qquad Equation\ 3-1$$

$$b_i = A \sum_{u=1}^{N} x_{iu}\, y_u \qquad\qquad Equation\ 3-2$$

$$b_{ii} = D_1 \sum_{u=1}^{N} x^2{}_{iu}\, y_u \ + \ C_1 \sum_{i=1}^{N} x^2{}_{ii}\, y \ - \ (\bar{y}_o\,/\,s) \qquad\qquad Equation\ 3-3$$

$$b_{ij} = D_1 \sum_{u=1}^{N} x_{iu}\, x_{ju} y_u \qquad\qquad Equation\ 3-4$$

$$ss_{b_i} = A \sum_{i=1}^{N} (x_i\, y_i)^2 \qquad\qquad Equation\ 3-5$$

$$ss_{b_{ij}} = D_1 \sum_{u=1}^{N} (x_{iu}\, x_{ju} y_u)^2 \qquad\qquad Equation\ 3-6$$

$$ss_{b_{ii}} = D_0 \sum_{ii=1}^{N} y_u + \sum_{u=1}^{N} b_{ii}\, x^2{}_{iu} y_u \ - \ \sum_{u=1}^{N} (y_n)^2 /N \qquad\qquad Equation\ 3-7$$

Novel Enhancement of HVOF Thermal Sprayed Nanostructured WC-12Co / Inconel-625 Coatings for Tribocorrosion Applications| **Al-Harbi, Naif I**

70

(B) The Main Features Of The BBD Design

Below is a list of the major features of Box-Behnken design in its application in Response Surface Methodology designs [86]:

- The design points are assigned to specific positions

- Each factor in this design has three levels

- The main purpose of the BBD design in RSM is to estimate a quadratic model.

- This design is engineered to give the strong coefficient estimates close to the center of the design space, weaker coefficient estimates at the cube corners because there are no design points

- The BBD design is very sensitive to bad runs and missing information

- In the BBD design, the operability area and the area of interest are similar.

3.8 Coating characterization technique and equipment

A characterization technique refers to a technique in which a unique signature or profile of a given material is developed based on the material's unique characteristics. In case a structure consist of a combination of traces of materials (a mixture or impure substance), the characteristic profile will display overlapping signatures which can be studied carefully to reveal the composition of the structure. Coating characterization, on the other hand, is used to evaluate the characteristic microstructural features or the composition of the coating substance. In coating characterization, the technique is not limited to profile determination but rather it can also be applied to a depth profile in the quest for defects analysis, and physical as well as chemical characteristics in the quest for understanding the coating decomposition when subjected to wear and tear. Powder and coating characterization can be studied using techniques such as: scanning electron microscopy (SEM), energy dispersive X-ray spectroscopy (EDS), as well as x-ray diffraction (XRD) techniques.

Novel Enhancement of HVOF Thermal Sprayed Nanostructured WC-12Co / Inconel-625 Coatings for Tribocorrosion Applications| **Al-Harbi, Naif I**

71

3.8.1 Sample metallography surface preparations

Preparation of the samples for metallographic analysis is a critical step in the thermal spray coating process. Good preparation results in high-quality coatings characterization. For this experiment, the ASTM E192003 standard was used in the metallography preparation. The ASTM E192003 standard specifies five critical steps to be followed in preparing the sample: sectioning, cleaning, mounting, grinding, and polishing, which are described as follows.

(A) Sectioning

Sectioning of the samples in this experiment was designed to minimize the size of the sample so that it could perfectly fit into the mounting machine. The samples were held with care to avoid destroying the interface between the coatings and the substrate. The samples were sectioned by use of diamond cutting wheel as shown in Figure 3-26, with water being used as a lubricant. To avoid overheating, the diamond wheel was set at a low speed of 0.3 mm/s to prevent coating de-lamination and distortion.
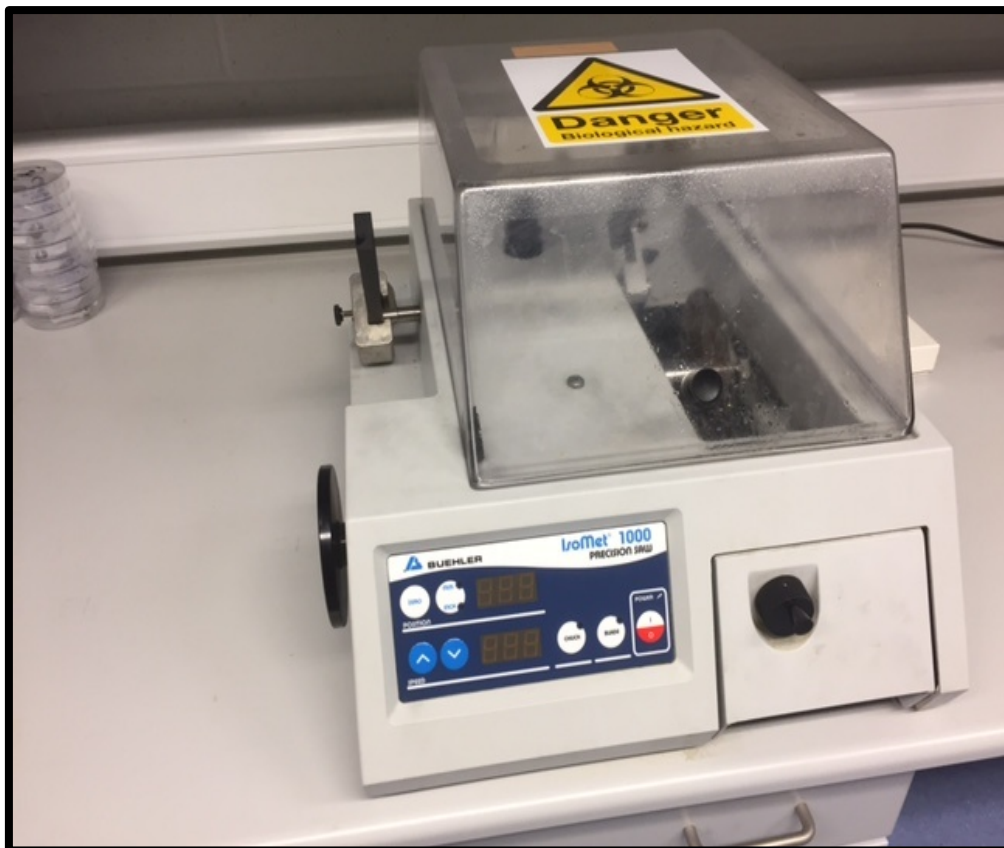
Figure 3-26: Isomet 1000 series sectioning machine used to cut the coated samples.

Novel Enhancement of HVOF Thermal Sprayed Nanostructured WC-12Co / Inconel-625 Coatings for Tribocorrosion Applications| **Al-Harbi, Naif I**

72

(B) Cleaning

After sectioning, the preparation of the samples commenced with cleaning, aimed at removing any dirt on the surface of the samples. Acetone, an organic solvent, was used in the cleaning process to remove any fluid contaminants from the sample surface. Then, the clean samples were left to dry at room temperature.

(C) Mounting

The thermal spray coating samples were mounted to ensure they maintain their original structure of the sample during polishing and grinding. In this step, it was critical to consider several criteria, such as adequate mechanical strength, good adhesion to the specimen, ease-of-handling. In this research, a hot-press SimpliMet 2000 series 50 mm mounting machine (Figure 3-27) from the Buehler manufacturing company was used.

To hold the sample in its position, a black phenolic powder was used as the resin. A cylinder was used to contain the sample and the remaining space was filled with the resin. The temperature was maintained at 150° and 3 bar pressure for ten minutes to embed the sample.
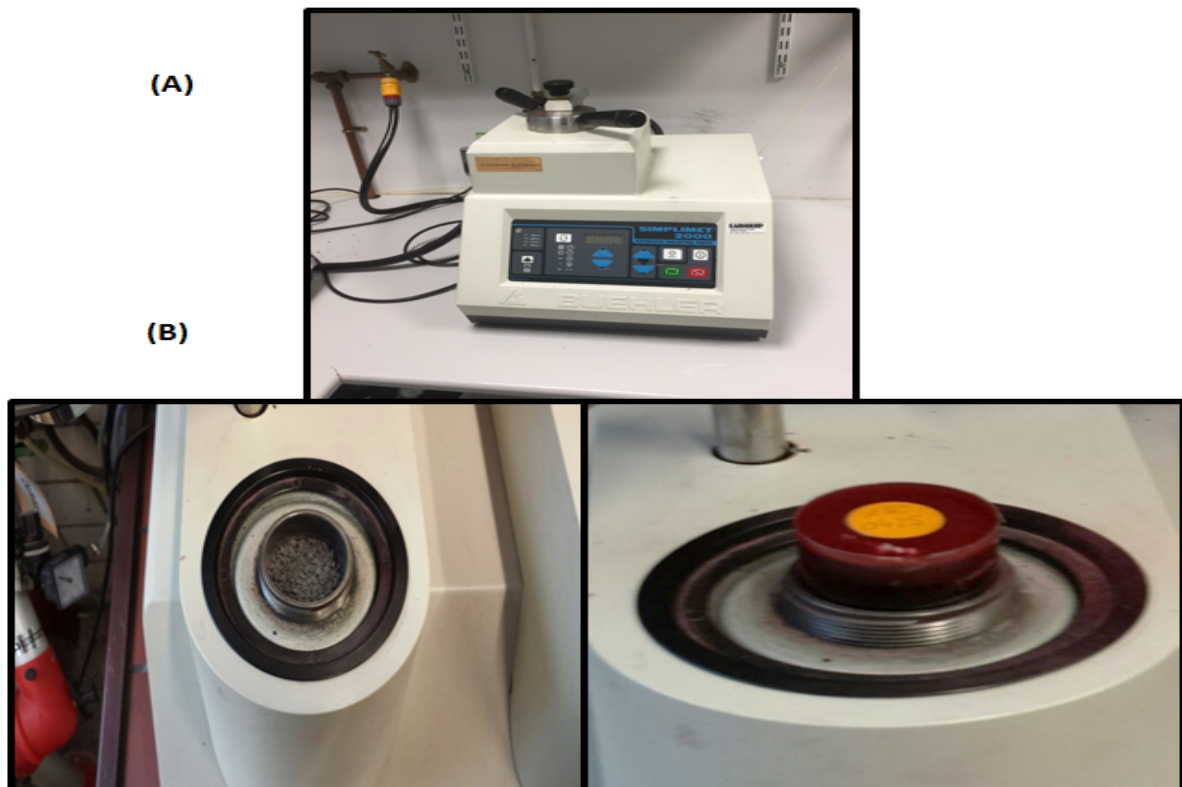
Figure 3-27: (A) Hot-press SimpleMet 2000 series used for samples mounting, and (B) Before and after pressurizing the resin.

Novel Enhancement of HVOF Thermal Sprayed Nanostructured WC-12Co / Inconel-625 Coatings for Tribocorrosion Applications| **Al-Harbi, Naif I**

73

(D) Grinding

The grinding process was performed using a semi-automatic METKON machine (Figure 3-28). The samples were ground in steps using different grit sizes while water was used as a lubricant. The machine used could grind six samples at once. The first step of the grinding process (also called the planar grinding) involved the use of a P60 silicon carbide paper that was meant to remove any damage that may have been induced during the sectioning. This step lasted for 4 min. Subsequent 4-min steps involved the use of silicon carbide papers with fine grits, specifically; P240, P400, P800, P1200, and P2000. After every step, the samples were thoroughly cleaned with water to remove staked grinded partials. The fine grit grinding was meant to remove any damage induced during the planner grinding, and each step involved use of contact pressure at 130 kPa.

Figure 3-28: Semi-automatic METKON grinding and polishing machine used for the samples.

(E) Polishing

This step aimed at giving samples a reflective flat surface. The METKON machine was using to polish the samples with a TEXTMET PERF cloth paper. Polishing entailed performing the process by use of different sizes of diamond particles: sizes 9, 6, 3, and 0.5 µm. Each polishing step lasted 5 min and was performed under a contact pressure of between 90 and 150 kPa.

Novel Enhancement of HVOF Thermal Sprayed Nanostructured WC-12Co / Inconel-625 Coatings for Tribocorrosion Applications| **Al-Harbi, Naif I**

74

(v) Chemical Etching

The last step of the metallographic sample preparation involved chemical etching of the laser-treated samples. To reveal the microstructure and the melt-pool geometry, the laser-treated samples for the two coating types were chemically etched with Murakami's reagent (10 gram NaOH, 10 gram potassium ferricyanide, and 100 ml of distilled water) and 5% nitric acid made with distilled water. The nitric acid was applied to the substrate carbon steel to define the melt depth boundary when the beam irradiation reached it. The samples were mechanically etched using cotton cloth for 1–2 min, rinsed with isopropyl alcohol followed by distilled water to remove all traces of the solution, and finally dried using a blower.

3.8.2 Scanning electron microscopy (SEM)

Scanning electron microscopy was used in the research to analyze the powder materials and coating prior to and after laser treatment. SEM provides good structural morphology analysis as well as crystallographic arrangement of the coating materials. Figure 3-29 shows the SEM equipment developed by EVOLS 15 that was applied in this research.

1. Aperture adjusting micrometers
2. Nitrogen supply regulator
3. Nitrogen control ball valve
4. Stage control Joystick
5. Chamber door
6. Keyboard Console
7. Plinth
8. Chamber door movement
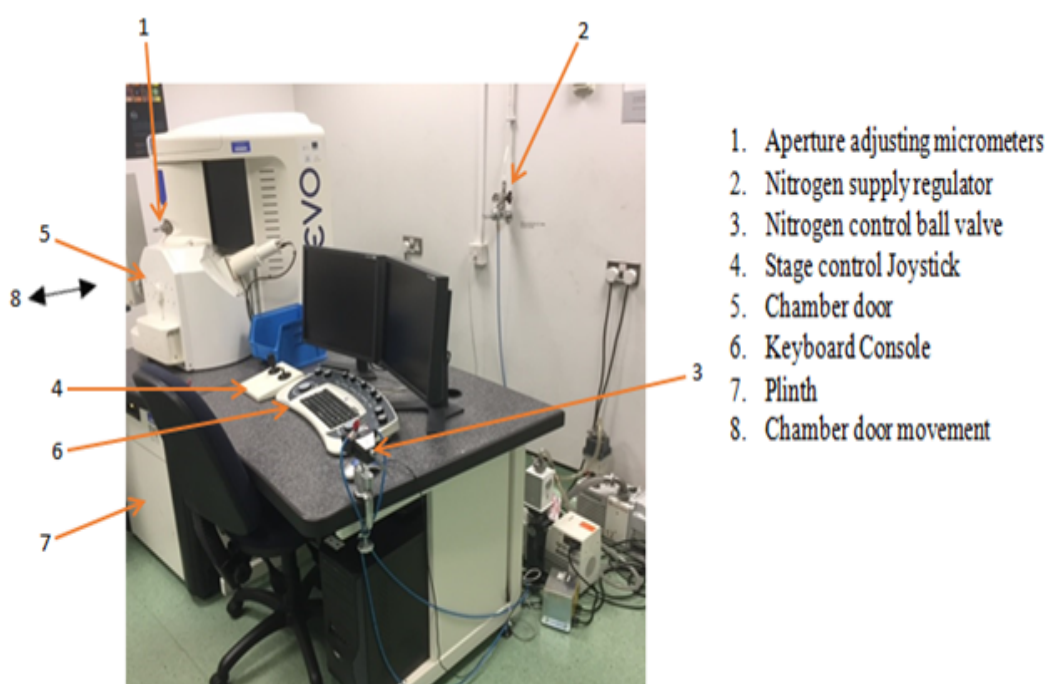
Figure 3-29: DCU EVOLS 15 scanning electron microscopy (SEM) used in the research to analyze the powder and the coating before and after laser treatment.

.

Novel Enhancement of HVOF Thermal Sprayed Nanostructured WC-12Co / Inconel-625 Coatings for Tribocorrosion Applications| **Al-Harbi, Naif I**

75

Scanning electron microscopy operates by directing a beam of electrons to the sample under investigation. The directed electron beam has very high kinetic energy that must produce an effect after collision with the sample that happens to be in its path. Upon striking the sample, the electron-sample interaction results in the emission of either a photon or an electron from the sample and corresponding effects from each point of the irradiated sample are mapped onto the display screen. The display reveals vital information, such as texture or external morphology, physical (crystal orientation), and chemical (identity or composition) characteristics. Different materials will obviously display different signals on the screen owing to the different nature and uniqueness of the materials. Figure 3-30 shows a schematic representation of the SEM operation principle. The electron beam produced from the electron gun is accelerated and focused toward the sample through a series of anodes and magnetic deflection systems, respectively [89].
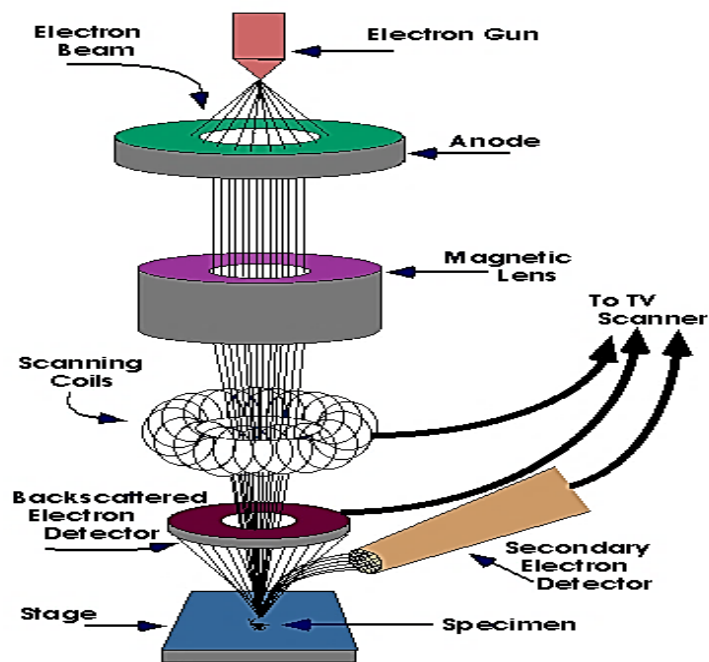
Figure 3-30: Schematic diagram of the operation of a SEM [90].

3.8.3 Energy dispersive x-ray spectroscopy (EDS)

Energy dispersive x-ray spectroscopy was used in the research to analyze the powder materials and coating prior and after laser treatment. EDS is used mainly in determining the

Novel Enhancement of HVOF Thermal Sprayed Nanostructured WC-12Co / Inconel-625 Coatings for Tribocorrosion Applications| **Al-Harbi, Naif I**

76

elemental identity of the coating material. Each element existing in nature has a corresponding unique characteristic x-ray radiation — radiation is produced from a material when it is impinged upon by high energy radiation, a photon or an electron beam. Energy dispersive x-ray spectroscopy makes use of this principle by providing the initial radiation that is used to strike the sample and providing a detection mechanism of the secondary radiations produced after initial radiation and sample bombardment [91]. By studying the secondary radiations, the chemical identity of the sample can be inferred, leading to an ideal revelation of the elements within the sample. Figure 3-31 shows the EDS equipment used in the research and Figure 3-32 shows the schematic EDS diagram.

Figure 3-31: DCU EDAX series energy dispersive x-ray spectroscopy (EDS) used in the research to analyze the powder and the coating before and after laser treatment.
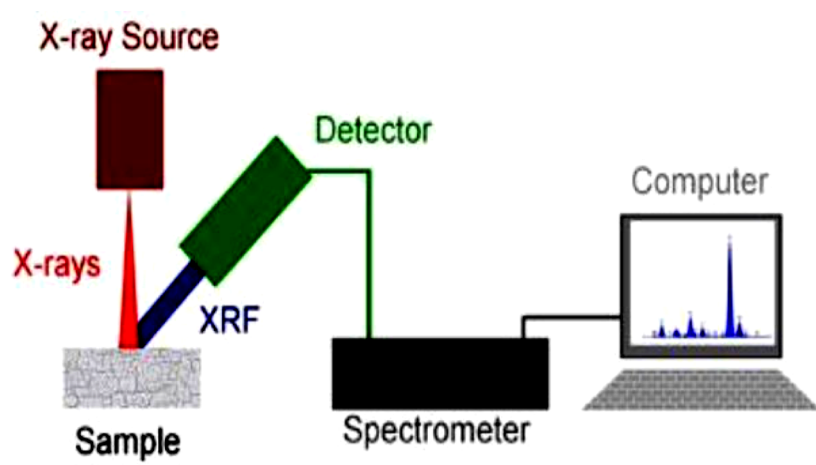
Figure 3-32: Schematic diagram of energy dispersive x-ray spectroscopy (EDS) [91].

Novel Enhancement of HVOF Thermal Sprayed Nanostructured WC-12Co / Inconel-625 Coatings for Tribocorrosion Applications| **Al-Harbi, Naif I**

77

3.8.4 X-ray diffraction (XRD)

X-ray diffraction was used in the research to analyze the powder materials and coating pre and post laser treatment. Unlike EDS, XRD does not reveal the coating identity directly but rather provides potential information that can be used to infer the crystal structure of the coating and possible estimation of the defects and material stress. XRD is a characterization technique in which samples to be characterized are placed on the path of the x-ray to scatter them, after which the scattered x-ray pattern is studied and based on the scattering angle and the signature, one can infer meaning on the interatomic spacing, crystal arrangement and crystal orientation. Through phase analysis and signature comparison, the coating identification can be possible. However, this would involve a tedious process of comparing the signature of the material against the available database of signatures of XRD. The challenge becomes even greater when the material used in the coating is not a pure sample, as the signature would comprise of an overlapping pattern. Figure 3-33 shows the XRD equipment used in this research. Note the evacuated window that safeguards the user against the harmful effect of x-ray radiation [17].
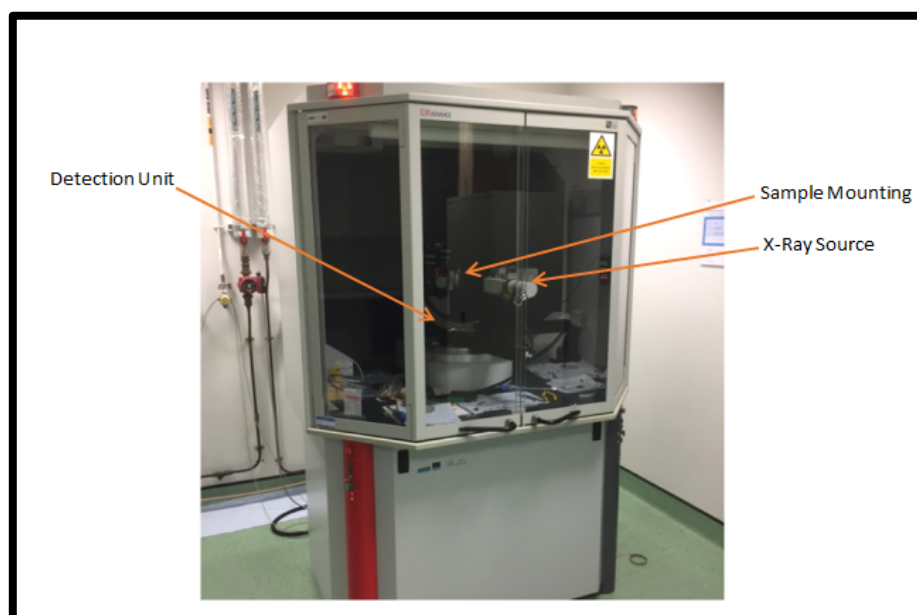
Figure 3-33: DCU X-ray diffraction (XRD) equipment used in this research to analyze the powder materials and coating prior and after laser treatment.

In a powdered XRD, the crystalline structure of the powder provides a three-dimensional diffraction grating comparable to the x-ray wavelength. This grating is similar to the crystalline lattice of the material under a probe; thus, the study of crystal morphology and

Novel Enhancement of HVOF Thermal Sprayed Nanostructured WC-12Co / Inconel-625 Coatings for Tribocorrosion Applications| **Al-Harbi, Naif I**

78

atomic spacing as well as associated irregularities is possible with XRD. Furthermore, XRD forms a material's unique fingerprint based on the constructive interference of the diffracted monochromatic x-ray and the incident rays from the sample. Constructive interference occurs when the Bragg's condition is satisfied, namely:

$$n\lambda = 2d \sin\theta \qquad\qquad Equation\ 3-8$$

where n is an integer, λ is the wavelength of the x-ray, d is the lattice interplanar spacing, and Ɵ is the diffraction, or Bragg's angle. Further parameters are shown in Figure 3-34.
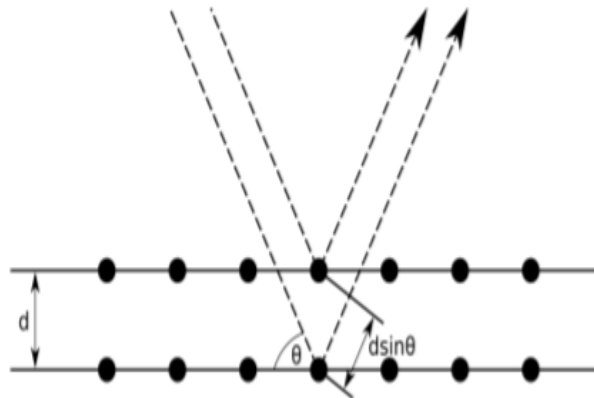
Figure 3-34: Bragg's x-ray diffraction [17].

3.8.5 Light microscope

A light microscope was used in the research to analyze the powder materials and coating prior and after laser treatment. Furthermore, the porosity of the coating will be measured by using the image analysis tools available in the VHX digital light microscope. Figure 3-35 shows the VHX digital light microscope that will be applied and can produce a magnification in the range of 0.1 to 5,000 times the original size, by varying either the image or object distance or even changing the lens through advanced charged coupled detector (CCD) zooming optics.

Novel Enhancement of HVOF Thermal Sprayed Nanostructured WC-12Co / Inconel-625 Coatings for Tribocorrosion Applications| **Al-Harbi, Naif I**

79
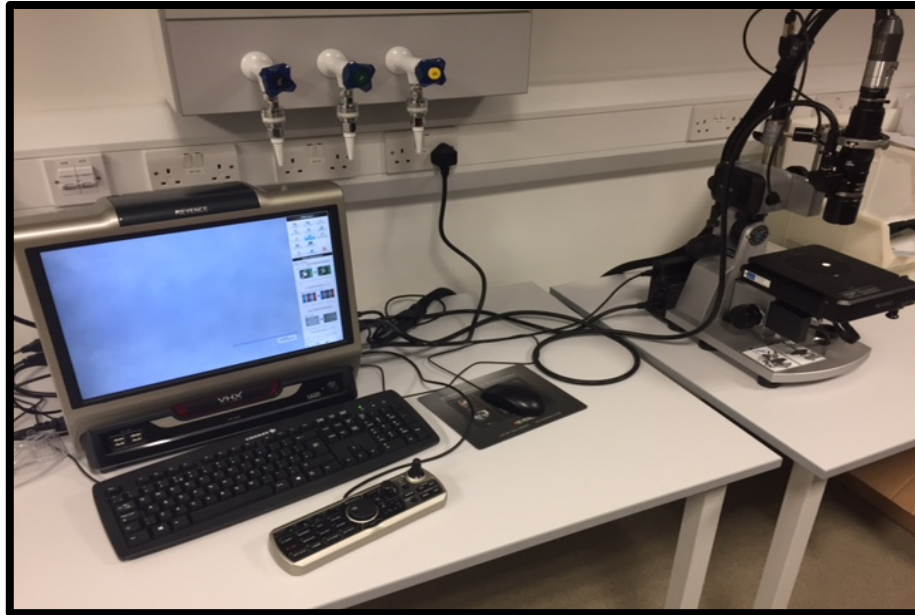
Figure 3-35: DCU VHX digital light microscope used in the research.

The VHX digital light microscope is characterized by a high resolution as well as the ability to take measurement parameters for improved quality of work, especially in hardness indentation, texture, and assessment of wear and tear. Figure 3-36 shows an image obtained from the VHX digital light microscope displaying the porosity of the sample illuminated.
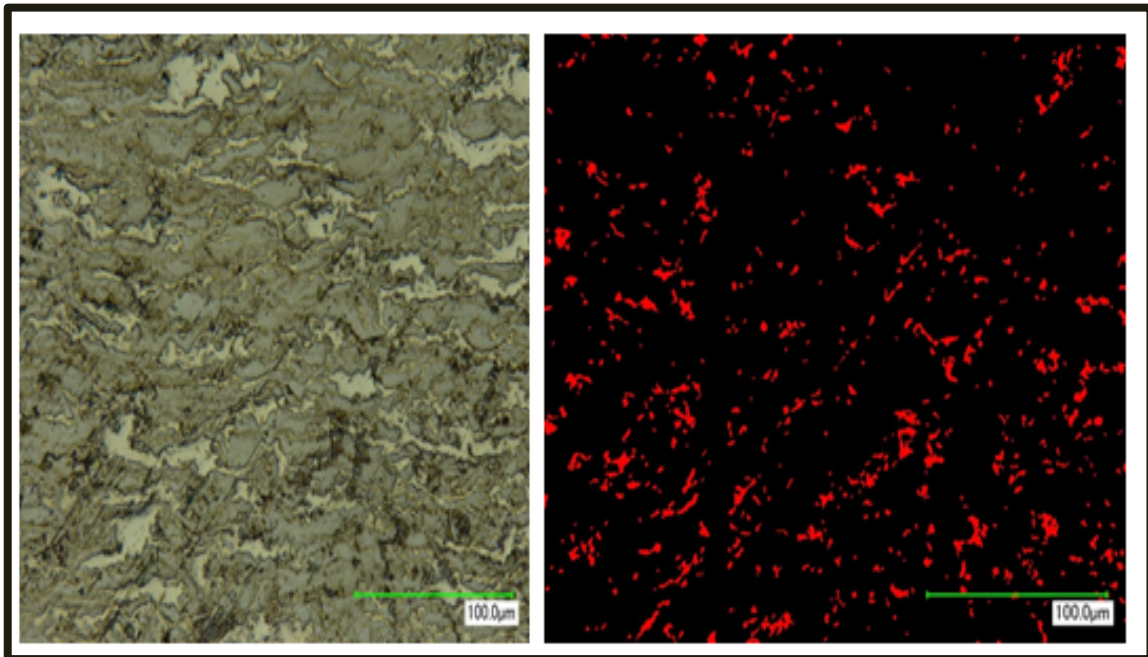
Figure 3-36: Porosity indicated by the VHX digital light microscope with the image analysis tool.

Novel Enhancement of HVOF Thermal Sprayed Nanostructured WC-12Co / Inconel-625 Coatings for Tribocorrosion Applications| **Al-Harbi, Naif I**

80

3.9 Mechanical performance of the coating

Different coatings have different mechanical properties that determine the performance of the material being coated. While oil/gas omponents may fail due to erosion/corrosion, but in some applications in the oil and gas industry may require particular mechanical properties, therefore a clear understanding of the correlation between mechanical properties and specific wear rate is required. A series of mechanical tests can be performed on a coating surface to verify the different coating parameters. These tests include, but are not limited to: hardness and roughness, viscoelastic properties, tensile strength, and fatigue. In this stage of the research, a mechanical test for coating surface roughness, as well as surface micro hardness and flexural behaviour (three points bending test), were measured.

3.9.1 Surface roughness measurements

Surface roughness measurements were used to analyze the coating's surface roughness pre and post laser treatment. The surface roughness features of the HVOF thermally coated spray arise because of surface irregularities, such as unmelted particles, different cooling rates, and/or variations in the gun transfer. Figure 3-37 shows a Dektak 150 surface roughness testing machine used in this research.
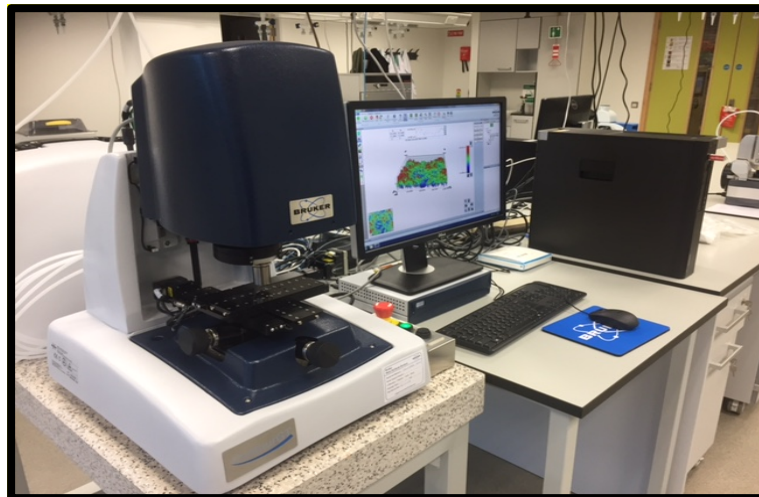
Figure 3-37: Dektak 150 surface roughness testing machine used in the research.

The equipment used provides a high-surface roughness resolution measurement by moving the stylus over the surface coating to be measured. For different applications and levels of roughness required, a stylus with another sensitivity can be applied.

Novel Enhancement of HVOF Thermal Sprayed Nanostructured WC-12Co / Inconel-625 Coatings for Tribocorrosion Applications| **Al-Harbi, Naif I**

81

3.9.2 Micro hardness measurements

Micro hardness measurements were used to analyze the coating cross-section hardness pre and post laser treatment in increments of 50 μm along the coating depth (Figure 3-38). Each reading was taken laterally four times to ensure the repeatability and uniformity of the tests.
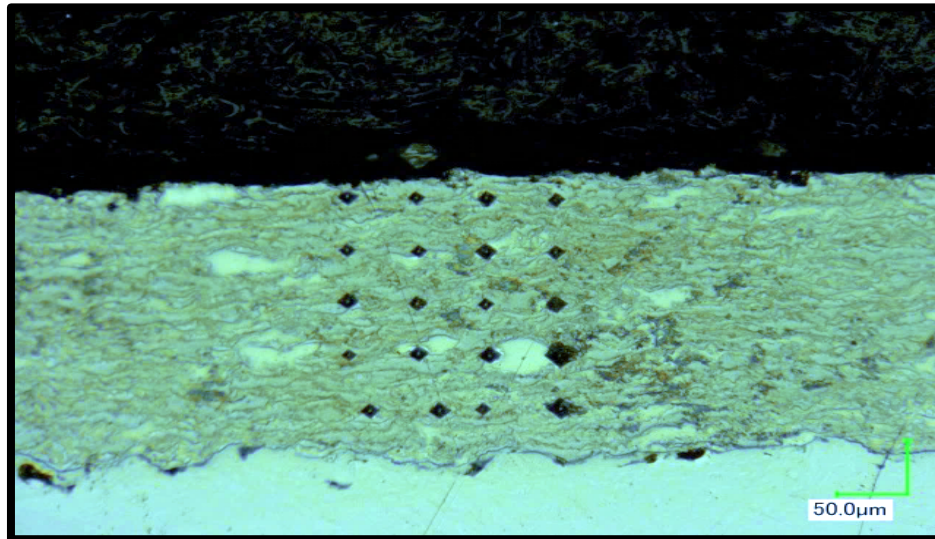
Figure 3-38: Indentation lateral and along the depth of the tested sample with increments of 50 μm.

The micro hardness test measures the indentation and cracks to determine the material's resilience or resistance to potential indenters resulting in a small, thin-sized deformation. The test can also measure the surface-to-core hardness in addition to the conditions of the surface, such as carburization, decarburization, or even grinding burns. The results from the micro-hardness test can be used to evaluate the following: effective hardening depth, core hardness, hardness conformity, and/or macro constituents' hardness necessary in estimating the quality of protection through the coating. Figure 3-39 shows a Leitz Miniload Micro Hardness testing machine used in this research. The work was performed using a pyramid-shaped indenture under a 100-g load, as recommended in the standard test method for Vickers hardness testing of ceramic materials (ASTM E 92).

Novel Enhancement of HVOF Thermal Sprayed Nanostructured WC-12Co / Inconel-625 Coatings for Tribocorrosion Applications| **Al-Harbi, Naif I**

82

Figure 3-39: Leitz Miniload Micro Hardness tester used.

3.9.3 Three point bending test

The three point bending test was performed to help investigate the flexural behaviour of the HVOF thermal spray coated samples pre and post the laser treatment. The equipment used for the testing was the Zwick T1-FR005TN.A50 and the testing procedure was conducted at room temperature. The setup of the system is shown in Figure 3-40.
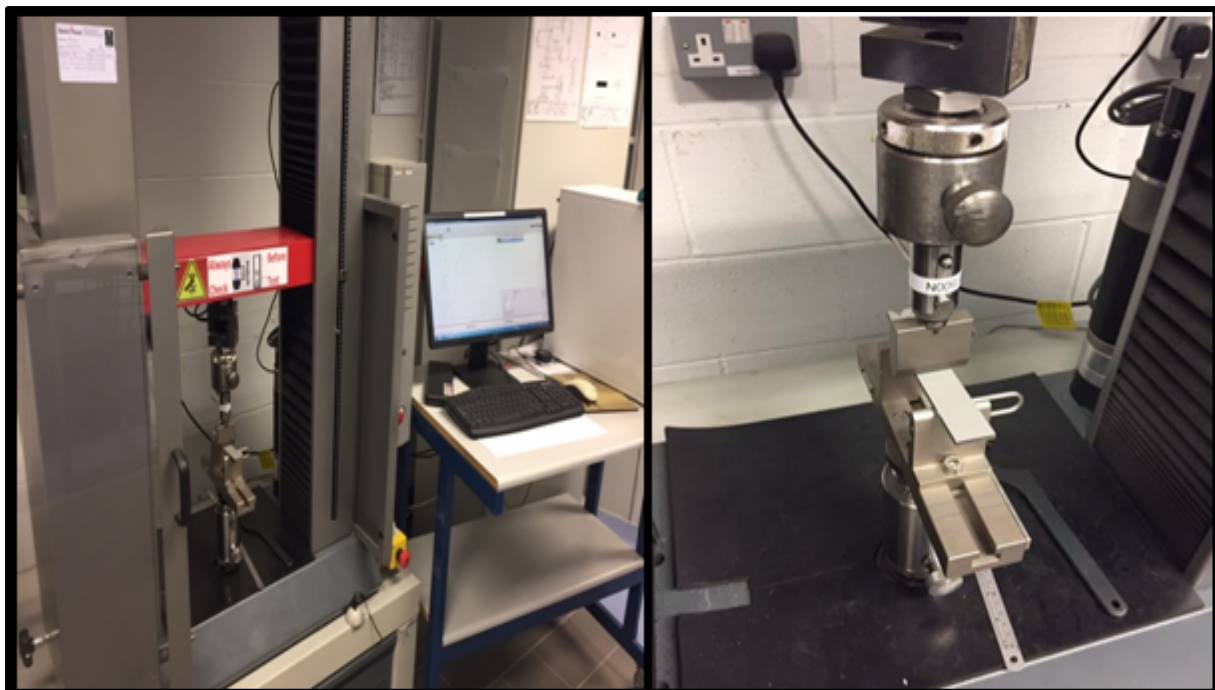
Figure 3-40: DCU Zwick 5KN Electro-Mechanical bending testing machine setup.

Novel Enhancement of HVOF Thermal Sprayed Nanostructured WC-12Co / Inconel-625 Coatings for Tribocorrosion Applications| **Al-Harbi, Naif I**

83

The machine measures flexure using the crosshead travel encoder by compensating the deformation of the machines. The modulus of flexure is determined between either 10 % and 50 % FMax or 10 % and 25 % of FMax [91]. The ratio of the span to the thickness of the specimen is determined using the definition stated in article 32.1 of ASTM [91]. Therefore, the specimen is subjected only to low shear forces. The specimen was a rectangular shape as described earlier and the geometry of the test is shown in Figure 3-41. The speed of the crosshead used was 1.0 mm/min, and it was stopped when the coating failed or the deflection reached 6%. During the testing process, 36 samples were tested. The test data was collected using the electronic equipment.
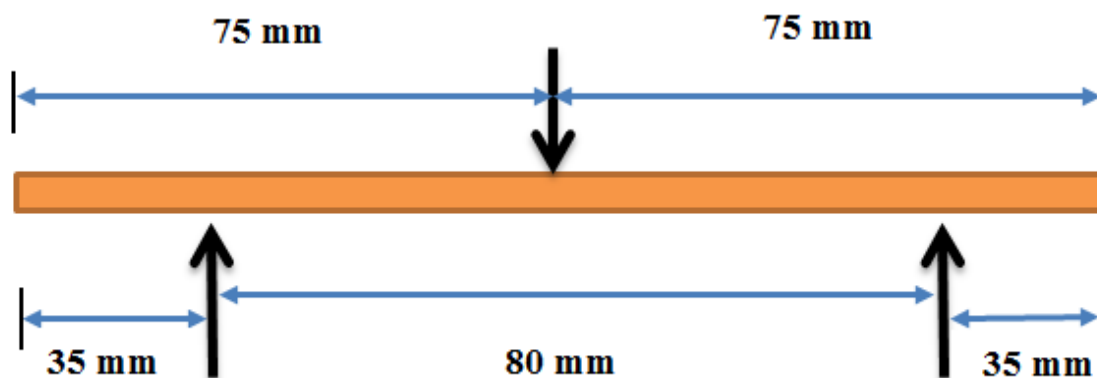
Figure 3-41: Geometry of the three point bending test.

Novel Enhancement of HVOF Thermal Sprayed Nanostructured WC-12Co / Inconel-625 Coatings for Tribocorrosion Applications| **Al-Harbi, Naif I**

84

3.10 Erosion and erosion-corrosion wear testing for the coating

The working environment in the oil and gas industries is harsh and damaging to machine parts, particularly as a result of erosion-corrosion. To prevent this, an appropriate coating is applied to the most vulnerable parts and assessed for performance prior to use through suitable erosion-corrosion tests.

In the current study, two such tests – dry and slurry – were employed to assess the performance of a coating before and after laser treatment, to analyze how laser processing conditions affect the erosion mechanisms. Both tests were conducted using an air jet blasting machine, as per ASTM G 73 standard, with each lasting for about 50 minutes.

3.10.1 Dry erosion test

For each coating type, a dry erosion test was conducted on both an untreated and a laser-treated sample. As mentioned, an air jet blasting machine, with a jet nozzle internal diameter of 10 mm, was used to perform the test, as shown in Figures 3–42. The distance between the nozzle and the test sample was maintained at 100 mm. Prior to testing, samples were appropriately cleaned using acetone and dried to remove dirt and loosely bonded materials, and weighted.

The samples were weighed using the electronic balance, also shown earlier in Figures 3–4, to assess the effect of the erosion test on their weight, hence the performance of the coating. Then, they were clamped in a fixture to expose them to the high-speed sand particles being emitted from the nozzle. The particles were accelerated using a pressure of 7 bar and set to bombard the test sample perpendicular at an angle of 90°.

The test parameters are presented in Table 3-8. Among them are the erodent particle size and type, both of which were selected based on the application and machinery requirements prevalent in the oil and gas industries.

Novel Enhancement of HVOF Thermal Sprayed Nanostructured WC-12Co / Inconel-625 Coatings for Tribocorrosion Applications| **Al-Harbi, Naif I**

85

Figure 3-42: DCU air jet blasting machine used for the dry erosion test.

Test Parameters	Values
Particle material	Honite
Particle size (µm)	106-212
Standoff distance (mm)	150
Jet nozzle diameter (mm)	10
Impact angle	90°
Test time (min)	50
Pressure spray (Bar)	7
Erodent feed rate (kg/s)	0.0289

Table 3-8: Dry erosion test Conditions.

Novel Enhancement of HVOF Thermal Sprayed Nanostructured WC-12Co / Inconel-625 Coatings for Tribocorrosion Applications| **Al-Harbi, Naif I**

86

3.10.2 Slurry erosion test

Erosion and corrosion adversely affect the performance and reliability of the mechanical equipment, plants, and pipelines used in the oil and gas industries. Accordingly, evaluation of a coating's wear resistance under conditions of erosion and corrosion—achievable through slurry erosion tests—is essential. Various techniques have been proposed for evaluating a coating's behaviour under such conditions; in this study, a bath of corrosive slurry was used to expose the corrosive liquid to the test sample, due to the limitation of equipment been available in Dublin City University as shown in Figure 3-43. To avoid corrosion of the workpiece steel area, a sponge was fitted into the corrosive liquid so that only the coating's surface side came into direct contact with the corrosive liquid through sponge absorption from the slurry bath. The sample surface area of the portion of coated sample exposed to the corrosive liquid was 96.2 cm^2, and the slurry was composed of sea water (pH 8.2) prepared according to ASTM D 1141-98 and simulating the Ph of the corrosive environment when drilling for oil by Aramco in Saudi Arabia [23]. This was achieved by dissolving 245.34 g of sodium chloride and 40.94 g of anhydrous sodium sulfate in 8 to 9 L of water, then adjusting the pH to 8.2 by adding 0.1 N of sodium hydroxide [23].
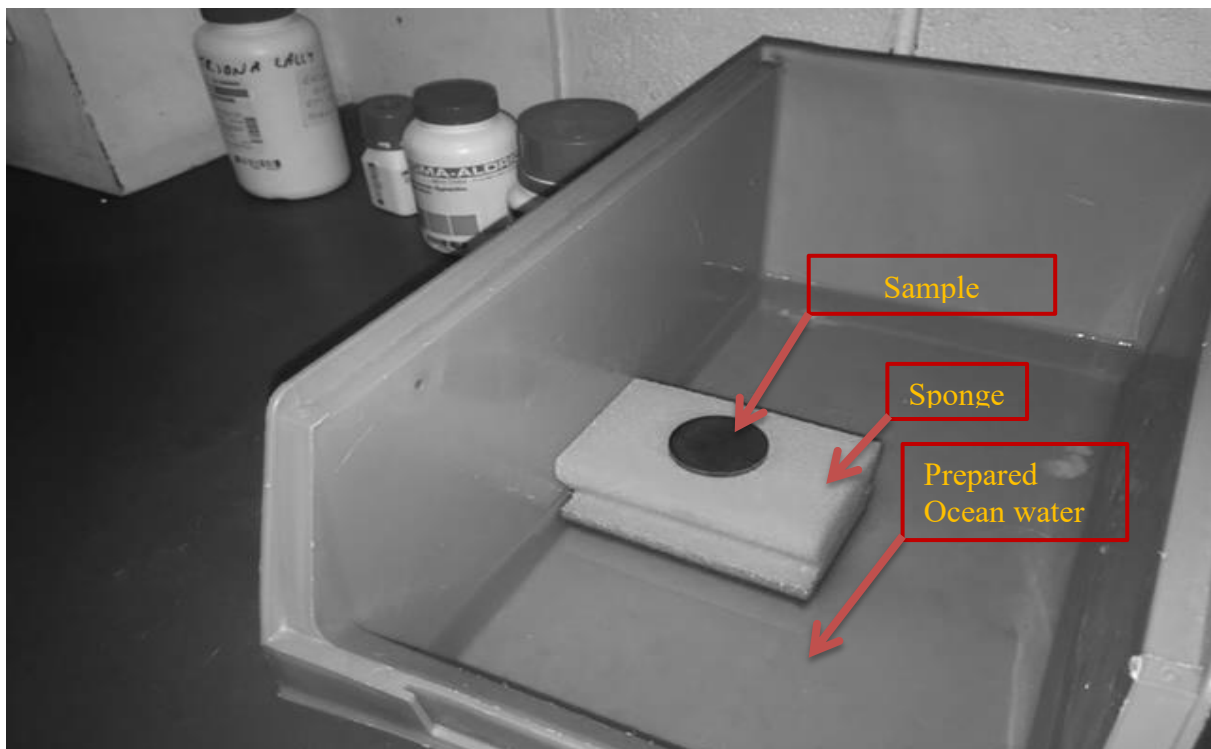
Figure 3-43: Photograph of the Erosion–corrosion slurry bath used in the current Research.

Novel Enhancement of HVOF Thermal Sprayed Nanostructured WC-12Co / Inconel-625 Coatings for Tribocorrosion Applications| **Al-Harbi, Naif I**

87

The following steps were followed during the slurry erosion test. The coated sampels were weighed by the electronic balance which had an accuracy of $\pm$ 0.001 g, then the sample in the coating layer side was left on the wet sponge for 48 hours, the sample was removed under wet conditions and immediately exposed to erosion testing (on its coated face). Finaly, as mentioned earlier, test samples were appropriately cleaned using acetone, dried to remove moisture, and weighed after every test. A summary of the test parameters is shown in Table 3-9 below.

Test Parameters	Values
Particle material	Honite
Particle size (μm)	106-212
Standoff distance (mm)	150
Jet nozzle diameter (mm)	10
Impact angle	90°
Pressure spray (Bar)	6
Sand Particle impingination (min)	50
Corrosive liquid contact (hrs)	48
Corrosive slurry	Prepared Ocean water (pH 8.2)

Table 3-9: Conditions of the Slurry erosion test.

Novel Enhancement of HVOF Thermal Sprayed Nanostructured WC-12Co / Inconel-625 Coatings for Tribocorrosion Applications| **Al-Harbi, Naif I**

88

CHAPTER 4 - Optimization of Laser Operating Conditions

4.1 Introduction

This chapter presents a preliminary investigation of the influence of laser processing conditions, namely laser power and scanning speed, on the melting of the two coating types. The aim was to find the adjustable range of laser power and scanning speed at three levels, to optimise a treated coating that is free of cracks and porosity and with minimal or no dilution of the substrate materials. Laser processing, were carried out at the focal position of -35 above the sample surface, producing a 3.22 × 2.3 mm beam size. This was the smallest beam size used and represented the worst-case scenario for the thermal stress created during the laser treatment because of the short interaction time, as discussed in Chapter 2. Later, -40 and -45 will be added to the three-level Box-Behnken design of experiment (DOE) as further two levels of the focal position, to analyze its effect on the coating quality.

4.2 Definition of optimization objectives

Single linear laser tracks were produced by moving the laser beam with a scanning speed of 300–1500 mm/min and a laser power of 300–1300 W. The combination of these laser processing conditions provided a set of resident time and energy fluences with a range of 0.0021–0.0107 ms and 0.1082–2.0311 J/mm^2, respectively. These are given by:

$$F = P_0 t_0 / A \qquad\qquad Equation\ 4-1$$

where F is the laser fluence, P_0 is the input laser power, A is the beam cross-sectional area, and t_0 is the beam resident time, which is expressed by D/U, where D is the beam diameter at the center line in the scanning direction and U is the laser scanning speed.

No overlap was used, so as to precisely define the laser processing conditions to the corresponding cross-section. An optical photograph of the upper surfaces of some of the laser tracks is shown in Figure 4-1. All processing conditions and corresponding cross-section observations are presented in Tables 4-1 and 4-2 near the end of this chapter.

Novel Enhancement of HVOF Thermal Sprayed Nanostructured WC-12Co / Inconel-625 Coatings for Tribocorrosion Applications | **Al-Harbi, Naif I**

89
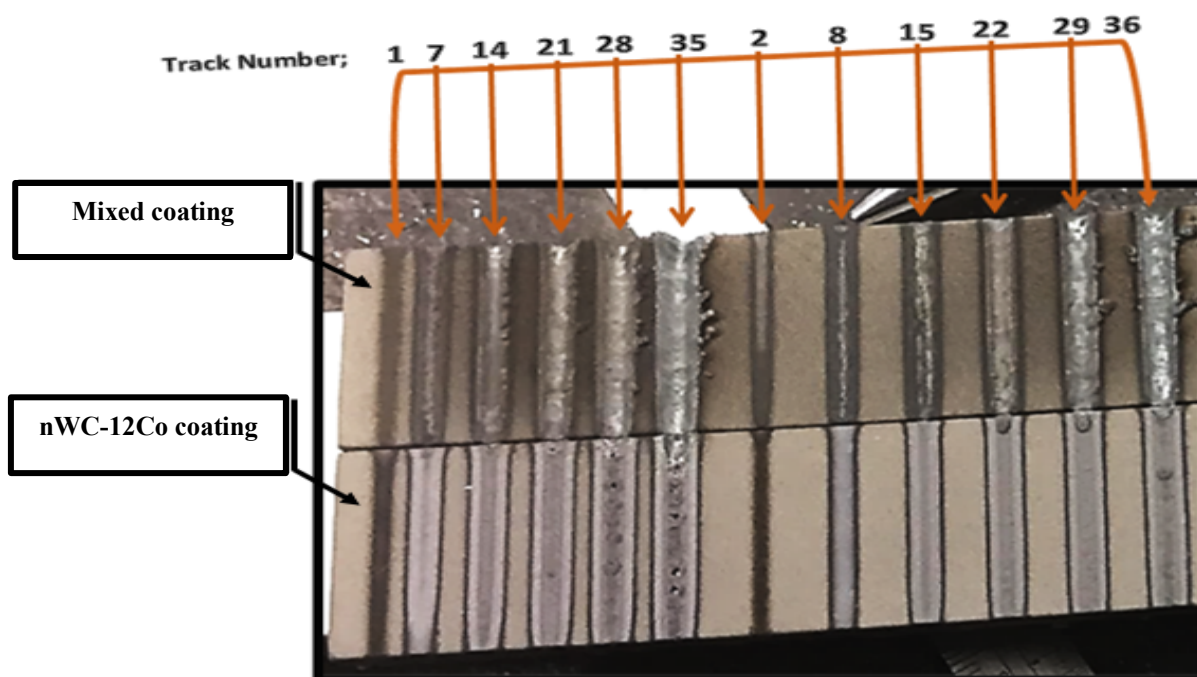
Figure 4-1: Optical photograph of some of the laser tracks.

The optimum laser conditions were determined by the appropriate laser power and scanning speed ranges according to the following conditions:

- Suitable melt that will allow partial melting of the HVOF coating (melt depth < coating thickness) or full melt with a minimal melting of the substrate (melt depth ≥ coating thickness), as shown in Figure 4-2 and Figure 4-4(A).
- Melt layer that is free of porosity and cracks.

4.3 Melting depth of HVOF coating

4.3.1 Partial melting within the laser-treated coating

In this method, the depth of the laser-melted layer is less than that of the coating thickness, meaning that the interface between the coating layer and substrate is not affected. When expressed mathematically, the ratio of the melt depth to the coating thickness can be less than a single unit as a result of partial heating. Within the partially melted surface of the coating, only the top layers are affected while the interfacial bond strength remains the same. Melting occurs at a relatively lower melting point; the surface becomes smoother after the laser treatment, with minimal cracks, as observed under magnification (see Figure 4-3). Under

Novel Enhancement of HVOF Thermal Sprayed Nanostructured WC-12Co / Inconel-625 Coatings for Tribocorrosion Applications | **Al-Harbi, Naif I**

90

these conditions, residual tensile stress could develop at a high laser scanning speed, as seen in Figure 4-7(B). The rapid cooling of the coating causes lateral cracks in the coating layer and/or separations of the substrate and coating. Importantly, the laser parameters must be adjusted to avoid coating delamination along with coating defects such as porosity and cracks.
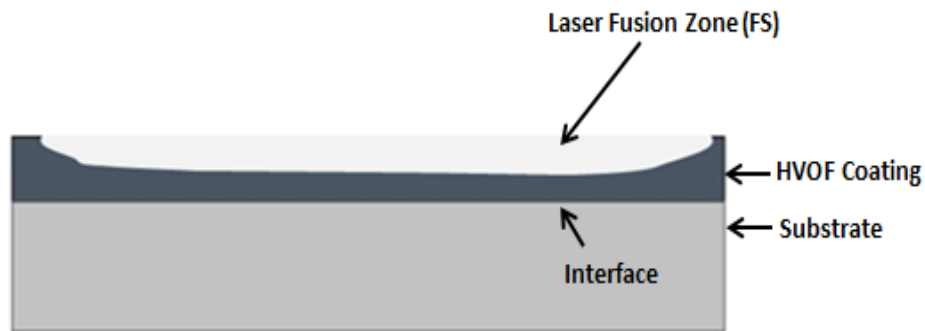
Figure 4-2: Schematic showing partial melting of HVOF coating.
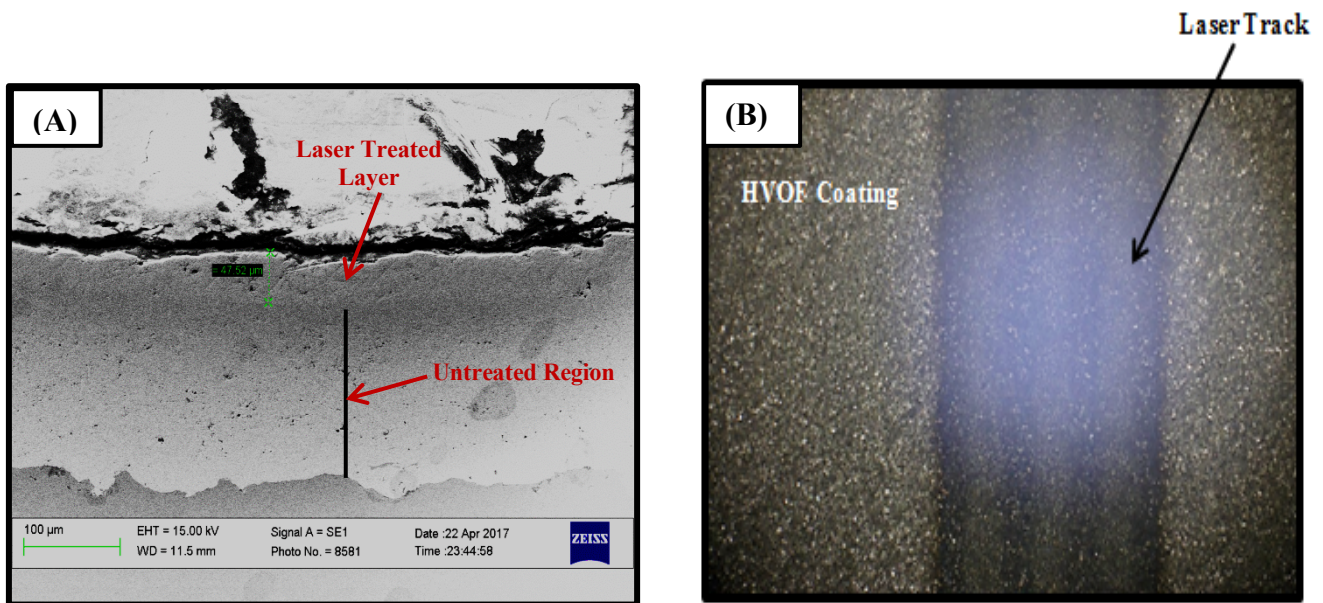
Figure 4-3: Laser-treated nWC-12Co HVOF coating at 300 W, 300 mm/min: (A) SEM image of the cross-section showing the partially melted surface that is free of cracks and low porosity, and (B) Microscope image from the top surface showing the surface becoming smoother.

Novel Enhancement of HVOF Thermal Sprayed Nanostructured WC-12Co / Inconel-625 Coatings for Tribocorrosion Applications | **Al-Harbi, Naif I**

91

4.3.2 Full melting within the laser-treated coating

When the HVOF coating is melted completely, the melting depth will be greater than or equal to the coating thickness, as demonstrated in the schematic in Figure 4-4. Minor dilutions can be introduced by such melting. In some cases the interface between the coating and the substrate is melted. Dilution does not occur when there is no melting of the interface between the coating and the substrate. Full melting, in which minor dilution is favorable removes the splat bonding structure and pores in HVOF coatings when coupled with sufficient temperatures for solidification of the microstructures into bonding with the substrate. The net effect is a shift from mechanical to fusion-based bonding. Consequently, the bond strength between the coating and substrate will be enhanced due to the elimination of defects (porous strips) in the interface, as shown in Figure 4-5(B).
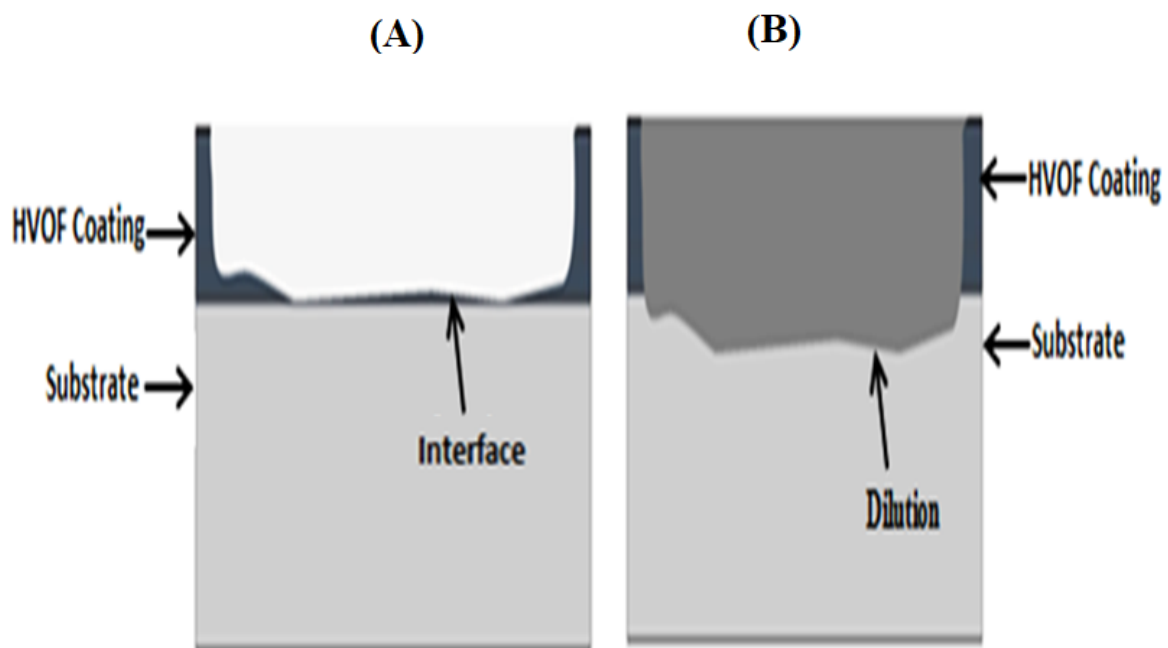
Figure 4-4: Schematic showing full melting of HVOF coating: (A) Full melting without substrate dilution, and (B) Full melting with substrate dilution.

Novel Enhancement of HVOF Thermal Sprayed Nanostructured WC-12Co / Inconel-625 Coatings for Tribocorrosion Applications | **Al-Harbi, Naif I**

92
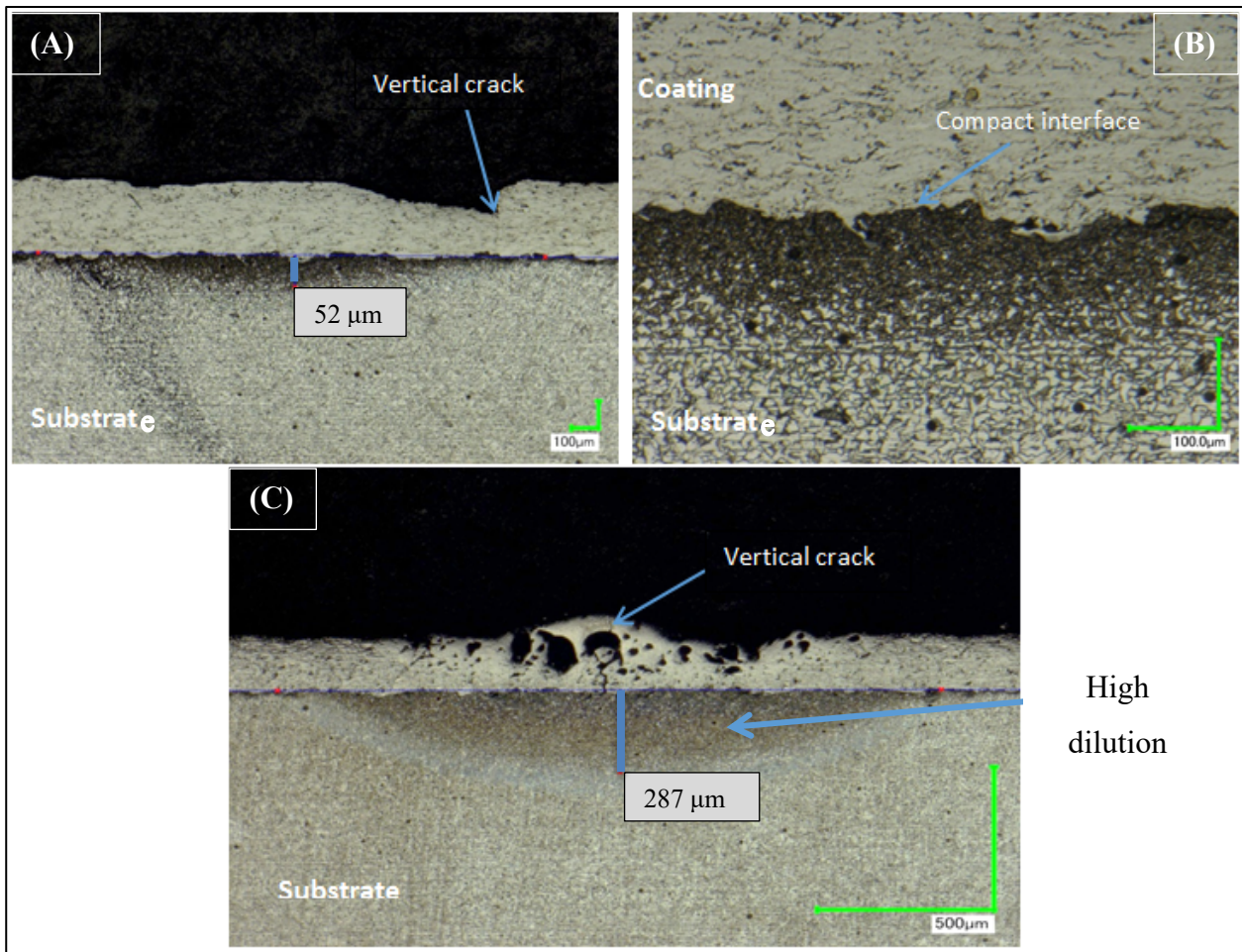
Figure 4-5: Microscope image of laser-treated HVOF coating: (A, B) Full melting with minor dilution, and (C) Full melting with high dilution.

4.4 Formation of porosity within laser-treated surface layer

For the purposes of this study, the term "porosity" refers to gas pockets within the melted zones. The gases are produced from the reaction of metal oxides and carbon to form carbon monoxide and carbon dioxide [92, 93]. Although they typically accumulate in the melted pool, they are released in the process of cooling because of the reduced solubility in solids [94]. In practical terms, insufficient time is available for solubility, and when at certain times the quantity of these gases is more than can be dissolved in the solids in the melted pools [94].

Accordingly, the parameters of the laser must be adjusted so that porosity can be minimized during laser processing. In particular, reducing the laser speed (with a high interaction time) and selecting the appropriate level of power density can help allow sufficient time for air bubbles to escape from the melted pool. In this research, when the laser treatment was conducted at high scanning speeds and laser power, the gas pockets started to

Novel Enhancement of HVOF Thermal Sprayed Nanostructured WC-12Co / Inconel-625 Coatings for Tribocorrosion Applications | **Al-Harbi, Naif I**

93

form within the laser-melted layer in both coating types, as shown in Figure 4-6. Vertical cracks were also observed at the melting layer (see Figure 4-6 (A)). Porosity can be reduced by proper selection of scanning speeds and power density, while the scanning time should be set to enable a longer interaction time in which the gases can dissolve. In this work, the optimum parameters for the power and scanning speed of laser treatment should be less than 500 W and 500 mm/min, respectively, for reducing the effects of porosity in both coating types.
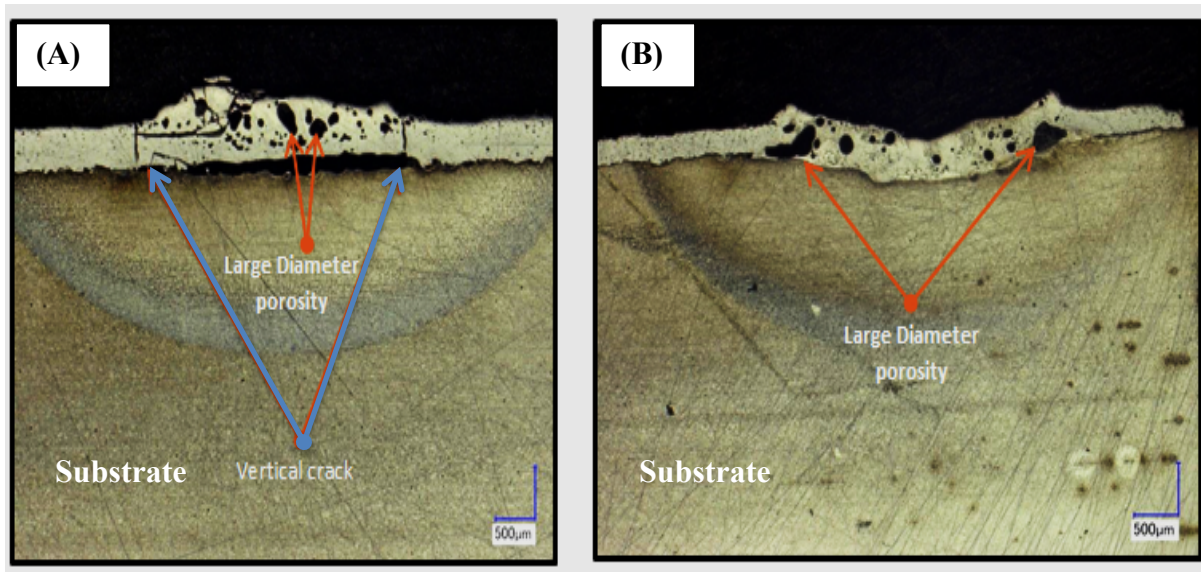
Figure 4-6: Porosity in laser-treated surface: (A) Porosity near the surface and a vertical crack in 75 wt. % nWC-12Co + 25 wt. % Inconel 625 HVOF laser-treated coating (900 W, 1500 mm/min), and (B) Porosity in 75 wt. % nWC-12Co + 25 wt. % Inconel 625 HVOF laser-treated coating (900 W, 1300 mm/min).

4.5 Crack formation within laser-treated HVOF coating

Thermal gradients causes cracking to occur during the treating process in laser coating by exerting thermal stress on the coating and substrate. Due to the high laser speed and a greater power level, this effectively increases the thermal stress, both factors enhance the cracking of the HVOF coating [95]. The stress also increases in the cooling step, causing cracks to occur in the melted layer because the coating material is not sufficiently strong to withstand the high solidifying rate [26, 95]. In addition, the HVOF coating and the substrate do not expand/contract to the same level during the thermal process, thus shrinkage of the melted pool can create residual stress in melted coating [96, 97]. The results of some studies prove that the reliability of any laser-treated material depends on the scanning speed deployed [26, 98, 99].

Novel Enhancement of HVOF Thermal Sprayed Nanostructured WC-12Co / Inconel-625 Coatings for Tribocorrosion Applications | **Al-Harbi, Naif I**

94

The results of the current study demonstrate that the laser treatment of the two different HVOF coatings can enable crack-free zones when the laser scanning speed is ≤ 300 mm/min; hence, the higher the speed, the greater the quantity and magnitude of the cracks created in the process. Thus, to reduce the number and sizes of cracks, low scanning speeds must be employed to allow a longer interaction time. Concurrently, the use of low power levels avoids the possibility of high dilution from the coating substrate.

Scanning speed and power parameters can be optimized for every form of HVOF coating to reduce the chances of cracks forming within the treated zone in the nWC-12Co HVOF and mixed HVOF coatings. Both coating types exhibit significant cracking potential, particularly at high scanning speeds (see Figure 4-7). The crack concentrated at the laser track edges, as illustrated in Figure 4-7(A), was the product of stress that occurred as a result of the elements from the untreated region surrounding the treated zone restraining the treated elements during the contraction [60]. What is more, considering the high scanning speeds and relatively low power at that level, it would only create partial melting of the coating layer; the same phenomenon caused a lateral crack to occur between the treated and untreated regions of the coating, as shown in Figure 4-7(B).
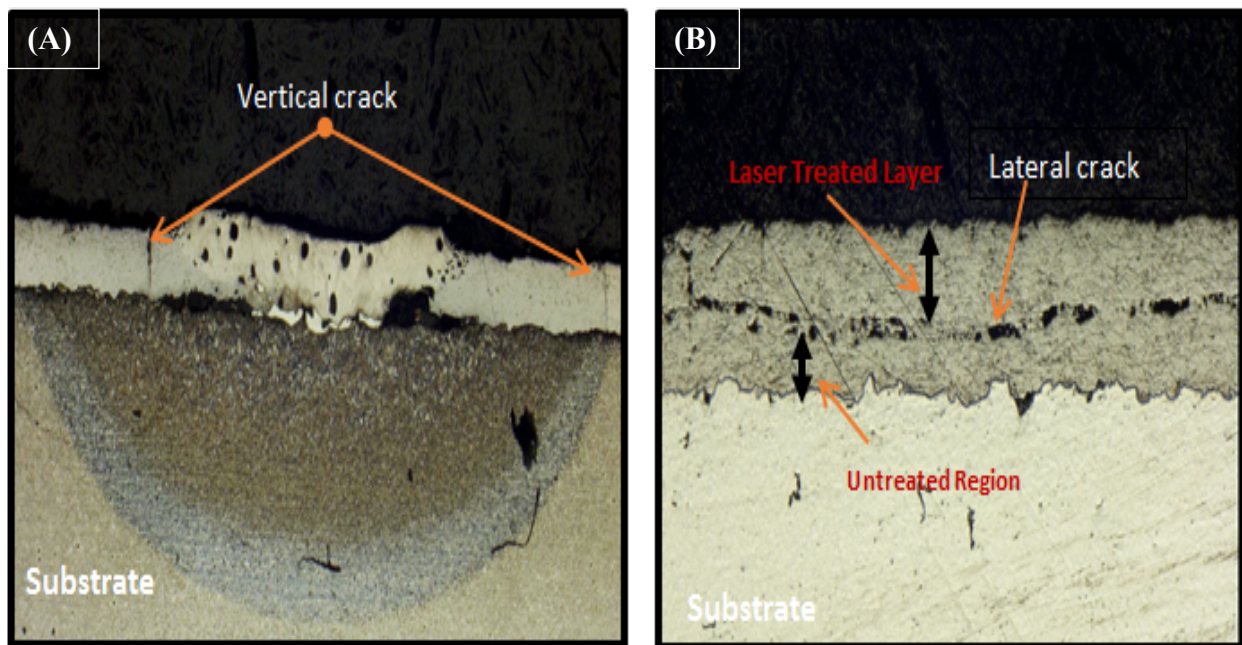
Figure 4-7: Cracks in laser-treated coating: (A) Vertical cracks in full melting of nWC-12Co HVOF coating at 900 W, 700 mm/min, and (B) Lateral crack in partial melting of WC HVOF coatings (500 W, 1300 mm/min).

Novel Enhancement of HVOF Thermal Sprayed Nanostructured WC-12Co / Inconel-625 Coatings for Tribocorrosion Applications | **Al-Harbi, Naif I**

95

4.6 Optimal laser operation for coating enhancement

In Figures 4-8 and 4-9, the laser operating thresholds are presented while showing the regions where no cracks were present and porosity was noticed in both coatings. A ratio is shown at the y-axis that defines the ratio of melt depth to the coating thickness. When the ratio is less than 1, the coating is partially melted. In this condition, only the upper deposits of the coatings are melted, with no interference with the interfacial bonds' strength that exists from the coating to the substrate. When the ratio is greater than 1, complete melting of the coatings occurs, which can even affect the coating/substrate interface. The graphs clearly show, as predicted, that the melt depth for all samples is a function of the scanning speed and laser power. Specifically, a greater depth is caused by a low scanning speed and high power; thus, a short residence time between the laser beam and treated surface will result in shorter melt depths and vice versa.
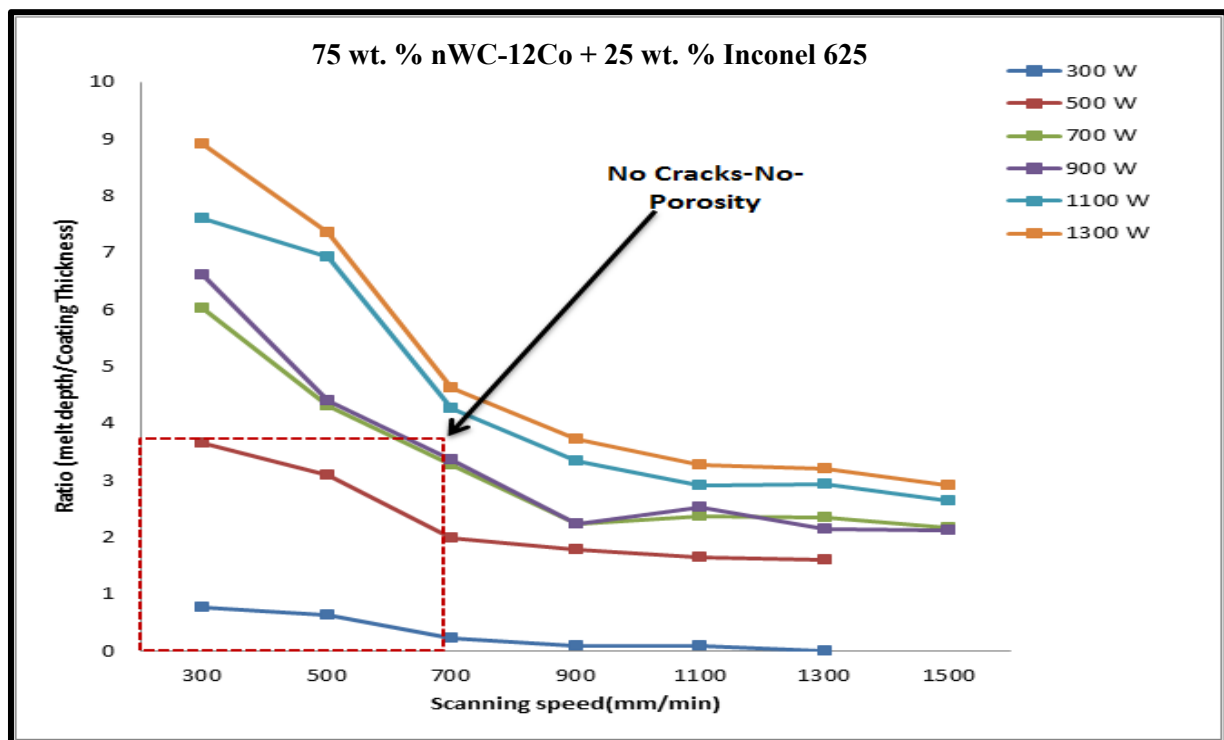
Figure 4-8: Optimal laser operation for mixed coating, to produce a coating free of cracks and porosity.

Novel Enhancement of HVOF Thermal Sprayed Nanostructured WC-12Co / Inconel-625 Coatings for Tribocorrosion Applications | **Al-Harbi, Naif I**

96
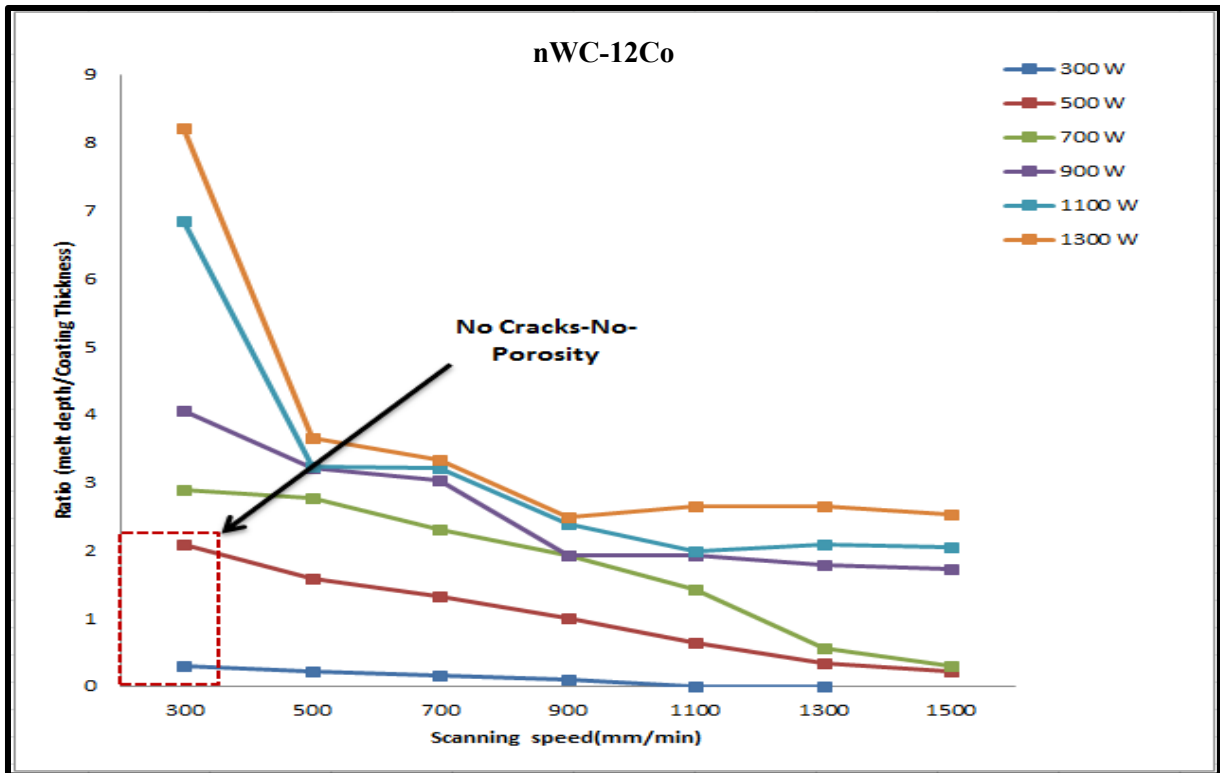
Figure 4-9: Optimal laser operation for nWC-12Co coating, to produce a coating free of cracks and porosity.

The previous figures (4-8 and 4-9) illustrate that both coating types had confirmed cracks under certain laser conditions. The window that provides optimum conditions for both laser treated coating within minimal or no cracks was wider for the mixed coat than for the singular nWC-12Co coating. The observation from the graph is attributed to WC content whereby the singular nWC-12Co coating has a high content of WC particles, which reduces the fracture strength as compared to mixed coating [24]. The conclusion is similar to the results presented by Chen [24], who used a laser with a power rating of 5 kW CO_2, as well as to those of Al-Taha [21], who used a 1.5 kW diode laser on 22 wt. % –42 wt. % WC-Inconel 625 coatings.

From these figures (4-8 and 4-9), one can also observe that a singular nWC-12Co coating had a lower melting depth than the mixed coating. This is a result of the thermal conductivity increasing linearly with increasing the WC concentration, as described by Liu et al. [54].

Novel Enhancement of HVOF Thermal Sprayed Nanostructured WC-12Co / Inconel-625 Coatings for Tribocorrosion Applications | **Al-Harbi, Naif I**

97

Track no.	Power (W)	Speed (mm/min)	Residence Time (ms)	Laser Fluence (J/mm²)	Cross Section Observation		
75 wt. % nWC-12Co + 25 wt. % Inconel 625							
					Best	Moderate	Worst
Track-1	300	300	0.0107	0.4687	Partial melting, no cracks, no porosity		
Track-2	300	500	0.0064	0.2812	Partial melting, no cracks, no porosity		
Track-3	300	700	0.0046	0.2009	Low melting, no cracks, no porosity		
Track-4	300	900	0.0036	0.1562	Low melting, cracks, no porosity		
Track-5	300	1100	0.0029	0.1278	Low melting, cracks, no porosity		
Track-6	300	1300	0.0025	0.1082	No melting		
Track-7	500	300	0.0107	0.7812	Full melting, no cracks, porosity		
Track-8	500	500	0.0064	0.4687	Full melting, no cracks, porosity		
Track-9	500	700	0.0046	0.3348	Full melting, no cracks, porosity		
Track-10	500	900	0.0036	0.2604	Full melting, cracks, porosity		
Track-11	500	1100	0.0029	0.2130	Full melting, cracks, porosity		
Track-12	500	1300	0.0025	0.1803	Full melting, cracks, low porosity		
Track-13	500	1500	0.0021	0.1562	Full melting, cracks, low porosity		
Track-14	700	300	0.0107	1.0936	Full melting, cracks, porosity		
Track-15	700	500	0.0064	0.6562	Full melting, cracks, porosity		
Track-16	700	700	0.0046	0.4687	Full melting, cracks, porosity		
Track-17	700	900	0.0036	0.3645	Full melting, cracks, porosity		
Track-18	700	1100	0.0029	0.2983	Full melting, cracks, porosity		
Track-19	700	1300	0.0025	0.2524	Full melting, cracks, porosity		
Track-20	700	1500	0.0021	0.2187	Full melting, cracks, porosity		
Track-21	900	300	0.0107	1.4061	Full melting, cracks, low porosity		
Track-22	900	500	0.0064	0.8437	Full melting, cracks, porosity		
Track-23	900	700	0.0046	0.6026	Full melting, cracks, porosity		
Track-24	900	900	0.0036	0.4687	Full melting, cracks, porosity		
Track-25	900	1100	0.0029	0.3835	Full melting, cracks, porosity		
Track-26	900	1300	0.0025	0.3245	Full melting, cracks, porosity		
Track-27	900	1500	0.0021	0.2812	Full melting, cracks, porosity		
Track-28	1100	300	0.0107	1.7186	Full melting, cracks, porosity		
Track-29	1100	500	0.0064	1.0311	Full melting, cracks, low porosity		
Track-30	1100	700	0.0046	0.7365	Full melting, cracks, low porosity		
Track-31	1100	900	0.0036	0.5729	Full melting, cracks, porosity		
Track-32	1100	1100	0.0029	0.4687	Full melting, cracks, porosity		
Track-33	1100	1300	0.0025	0.3966	Full melting, cracks, porosity		
Track-34	1100	1500	0.0021	0.3437	Full melting, cracks, porosity		
Track-35	1300	300	0.0107	2.0311	Coating delamination		
Track-36	1300	500	0.0064	1.2186	Coating delamination		
Track-37	1300	700	0.0046	0.8705	Partial coating delamination		
Track-38	1300	900	0.0036	0.6770	Full melting, cracks, porosity		
Track-39	1300	1100	0.0029	0.5539	Full melting, cracks, porosity		
Track-40	1300	1300	0.0025	0.4687	Full melting, cracks, no porosity		
Track-41	1300	1500	0.0021	0.4062	Full melting, cracks, porosity		

Table 4-1: The observation of all laser tracks carried out during the laser optimization process for mixed coating.

Novel Enhancement of HVOF Thermal Sprayed Nanostructured WC-12Co / Inconel-625 Coatings for Tribocorrosion Applications | **Al-Harbi, Naif I**

98

				nWC-12Co			
Track no.	Power (W)	Speed (mm/min)	Residence Time (ms)	Laser Fluence (J/mm^2)	Cross Section Observation		
					Best	Moderate	Worst
Track-1	300	300	0.0107	0.4687	Partial melting, small cracks, no porosity		
Track-2	300	500	0.0064	0.2812	Partial melting, no cracks, no porosity		
Track-3	300	700	0.0046	0.2009	Low melting, no cracks, no porosity		
Track-4	300	900	0.0036	0.1562	Low melting, cracks, no porosity		
Track-5	300	1100	0.0029	0.1278	No melting		
Track-6	300	1300	0.0025	0.1082	No melting		
Track-7	500	300	0.0107	0.7812	Full melting, no cracks, porosity		
Track-8	500	500	0.0064	0.4687	Full melting, no cracks, porosity		
Track-9	500	700	0.0046	0.3348	Full melting, no cracks, porosity		
Track-10	500	900	0.0036	0.2604	Full melting, cracks, porosity		
Track-11	500	1100	0.0029	0.2130	Full melting, cracks, porosity		
Track-12	500	1300	0.0025	0.1803	Full melting, cracks, low porosity		
Track-13	500	1500	0.0021	0.1562	Full melting, cracks, low porosity		
Track-14	700	300	0.0107	1.0936	Full melting, cracks, porosity		
Track-15	700	500	0.0064	0.6562	Full melting, cracks, porosity		
Track-16	700	700	0.0046	0.4687	Full melting, cracks, porosity		
Track-17	700	900	0.0036	0.3645	Full melting, cracks, porosity		
Track-18	700	1100	0.0029	0.2983	Full melting, cracks, porosity		
Track-19	700	1300	0.0025	0.2524	Full melting, cracks, porosity		
Track-20	700	1500	0.0021	0.2187	Full melting, cracks, porosity		
Track-21	900	300	0.0107	1.4061	Full melting, cracks, low porosity		
Track-22	900	500	0.0064	0.8437	Full melting, cracks, porosity		
Track-23	900	700	0.0046	0.6026	Full melting, cracks, porosity		
Track-24	900	900	0.0036	0.4687	Full melting, cracks, porosity		
Track-25	900	1100	0.0029	0.3835	Full melting, cracks, porosity		
Track-26	900	1300	0.0025	0.3245	Full melting, cracks, porosity		
Track-27	900	1500	0.0021	0.2812	Full melting, cracks, porosity		
Track-28	1100	300	0.0107	1.7186	Full melting, cracks, porosity		
Track-29	1100	500	0.0064	1.0311	Full melting, cracks, low porosity		
Track-30	1100	700	0.0046	0.7365	Full melting, cracks, porosity		
Track-31	1100	900	0.0036	0.5729	Full melting, cracks, porosity		
Track-32	1100	1100	0.0029	0.4687	Full melting, cracks, porosity		
Track-33	1100	1300	0.0025	0.3966	Full melting, cracks, porosity		
Track-34	1100	1500	0.0021	0.3437	Full melting, cracks, porosity		
Track-35	1300	300	0.0107	2.0311	Full melting, cracks, porosity		
Track-36	1300	500	0.0064	1.2186	Full melting, cracks, porosity		
Track-37	1300	700	0.0046	0.8705	Full melting, cracks, porosity		
Track-38	1300	900	0.0036	0.6770	Full melting, cracks, no porosity		
Track-39	1300	1100	0.0029	0.5539	Partial coating delamination		
Track-40	1300	1300	0.0025	0.4687	Coating delamination		
Track-41	1300	1500	0.0021	0.4062	Coating delamination		

Table 4-2: The observation of all laser tracks carried out during the laser optimization process for nWC-12Co coating.

Novel Enhancement of HVOF Thermal Sprayed Nanostructured WC-12Co / Inconel-625 Coatings for Tribocorrosion Applications | **Al-Harbi, Naif I**

99

4.7 Summary of the results

In conclusion, the laser operation window for each coating type was established and the impact of changes to the laser power and scanning speed on the porosity, cracking, and melting depth of the treated coating were evaluated. The formation of porosity was noticed under selected laser processing conditions, resulting in higher energy fluence (J/mm^2) (energy delivered per unit area) which led to evaporation of the coating at the elevated temperature and the release of gases that were at amounts beyond their solubility limits in the solid or when the gas bubbles were trapped in the melting zones because of the high scanning speed, providing insufficient time for the gas molecules to be released [92, 93]. Furthermore, crack nucleation under certain laser processing conditions, because of the high thermal stress, was observed, which was found to be directly proportional to the increase in the laser power and scanning speed [95].

The optimisation window of the laser operating conditions for the mixed coating was obviously lasrger for crack-free growth, compared to the singular nWC-12Co coating. This was due to the higher WC hard particle content in the nWC-12Co coating, which caused low fracture strength [24]. Finally, the high melting depth, which was one of the features to be avoided and depends on a high rate of dilution from the substrate, can deteriorate the properties of the coating material.

The melt depth was found to be directly proportional to the increase in the laser power and to the reduction in laser scanning speed or to the irradiance (W/mm^2) and residence time (in ms) in the case of a varying laser beam size. The melting depth for the mixed coating was higher than that for the nWC-12Co coating as a result of the higher WC hard particle content, which reduced the temperature increase and its gradient in the treated coating, as the thermal conductivity rises with increasing WC concentration [24, 54]. Moreover, the melting depth appeared to be greater when the laser beam was applied to the substrate, due to the low melting point of carbon steel compared to that of the coating material.

The two coating materials clearly required vastly different laser conditions to produce a laser melted coating that was defect-free (without porosity, cracks, or high dilution) when the focal position was fixed at +35 mm, yielding a laser beam spot size of 3.22 mm × 2.3 mm. Because of time constraints over the course of this research, the process parameters in Table 4-3 were selected as variables for both coatings.

Novel Enhancement of HVOF Thermal Sprayed Nanostructured WC-12Co / Inconel-625 Coatings for Tribocorrosion Applications | **Al-Harbi, Naif I**

100

DOE Coding level	-1	0	1
Power (W)	150	250	350
Focal Position (mm)	+35	+40	+45
Scanning Speed (mm/min)	150	225	300

Table 4-3: Different levels for the three control parameters (power, focal position, and scanning speed) chosen in this study for a comprehensive DOE analysis.

Novel Enhancement of HVOF Thermal Sprayed Nanostructured WC-12Co / Inconel-625 Coatings for Tribocorrosion Applications | **Al-Harbi, Naif I**

101

CHAPTER 5 - Results and Discussion

5.1 Introduction

This chapter is devided into two sections; the first section covers the discussion and based on coating characterization pre and post the application of HVOF thermal spray as well as the results summary of the two as-sparayed coatings and powders. The characterization included the following: powder morphology, powder mixing quality, coating defects, phase transformation and uniformity of element distribution across the coating cross-section, porosity levels, surface roughness, microhardness, three-point bending stress, Dry erosion and Slurry Erosion . Furthermore, for the sake of comparison, the XRD analysis of the nickel chromium alloy (Diamalloy 1005–Inconel 625) powder, coating, along with SEM images of the top surface, has been presented. These were sprayed as coating materials with similar spray parameters as the mixed coating shown in Table 3-3, Chapter 3.

The second section provided the characterisation of the laser treated HVOF coating such that carried out for the as-sprayed coating and the analysis of the experimental data by design of the experimental (DOE) for the melt-pool geometry, all the mechanical behavior excluding the microhardening properties (as simply measured to link its values to the different properties evaluated in the research), and the tribological laser-treated results, finishing off with the laser parameters' optimization and cost analyses. For simplicity, this section will contain the following three parts after the initial characterization such as; XRD analysis, coating top surface and cross-section analysis:

1. Melt-pool geometry and mechanical behaviour of laser treated coatings

    - Melt-Pool Dimensions (Width and depth)
    - Surface roughness
    - Hardness
    - Flexural strength

2. Tribological behaviour of laser treated coatings

    - Dry Erosion
    - Slurry Erosion

Novel Enhancement of HVOF Thermal Sprayed Nanostructured WC-12Co / Inconel-625 Coatings for Tribocorrosion Applications | **Al-Harbi, Naif I**

102

3. Optmization and cost analysis

- Laser Parmeters optimization based on the research objectives, such as yielded the optimal Mechanical and Tribological behaviour.

- Cost analysis based on optimum laser setting for the HVOF coating and laser operating process.

In addition, the singular 100% nWC-12 Co powder/coating and the 75 wt. % nWC-12Co + 25 wt. % Inconel 625 will sometimes be referred to as monomial and mixed respectively.

5.2 Powders

Two powder types were used in this research: a singular 100% nWC-12 Co powder and a mixed powder with 75% nWC-12Co (Infralloy^{TM} S7412) blended with 25% Nickel Chromium alloy (Diamalloy 1005–Inconel 625) for the production of HVOF coatings.

5.2.1 Powders morphological observation

Figures 5-1 and 5-2 show the morphology of the two coating powders as observed through SEM. Figure 5-1 shows the agglomerated nature of the powder through its circular geometry of the particle sizes in the range of 45 + 5 μm for nWC-12Co and almost oval in shape with smooth surface and powder size range of 11 ± 44 μm for Inconel 625 powders, as shown in Figure 5-2. According to the manufacturer's details, the particle dimensions were in the range of 45 + 5 μm for both powders; hence, the values obtained were consistent with the theoretical values for the mixed-type powder as can be explained in the following section. When a smaller section of the image was magnified, some tiny pores were observed in the agglomerated powder of nanoscale WC particles with binder as compared to the magnified image of SEM morphology for the Inconel 625 powder, as shown in Figure 5-2. The smooth surface with uniform grain structure, even at higher magnification, of the Inconel 625 powder can be attributed to some of the powder's original chemical constituents such as Nickel (Ni) [100]. Magnani et al. [101] states that the agglomeration nature of the nWC-12Co powder leads to homogeneous heating/deposition during the thermal spray.

Novel Enhancement of HVOF Thermal Sprayed Nanostructured WC-12Co / Inconel-625 Coatings for Tribocorrosion Applications | **Al-Harbi, Naif I**

103
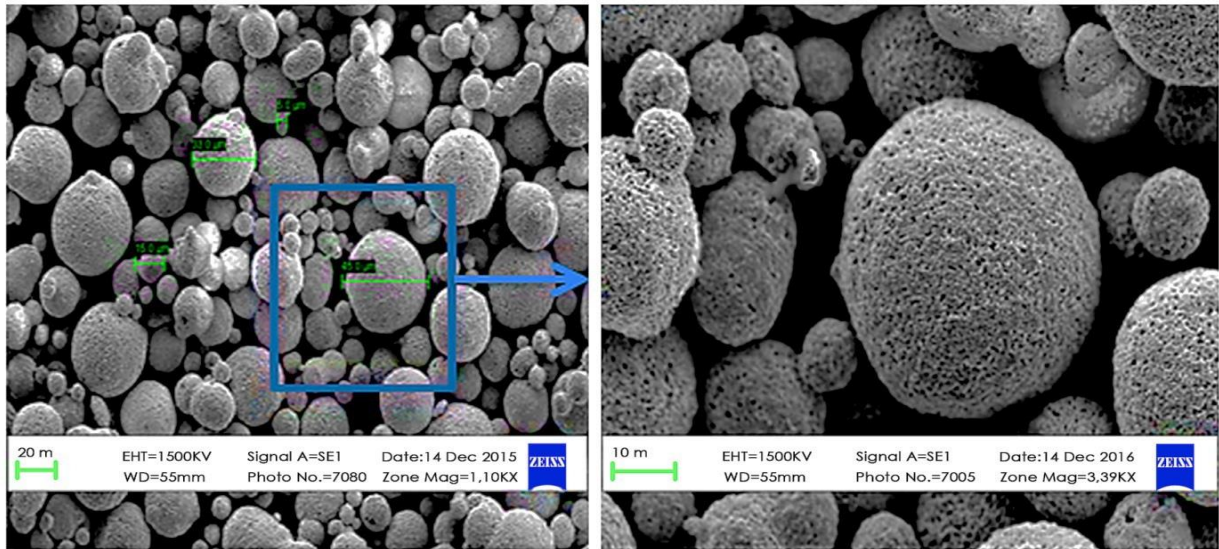
Figure 5-1: SEM morphology of the nWC-12Co (Infralloy™ S7412) powder.
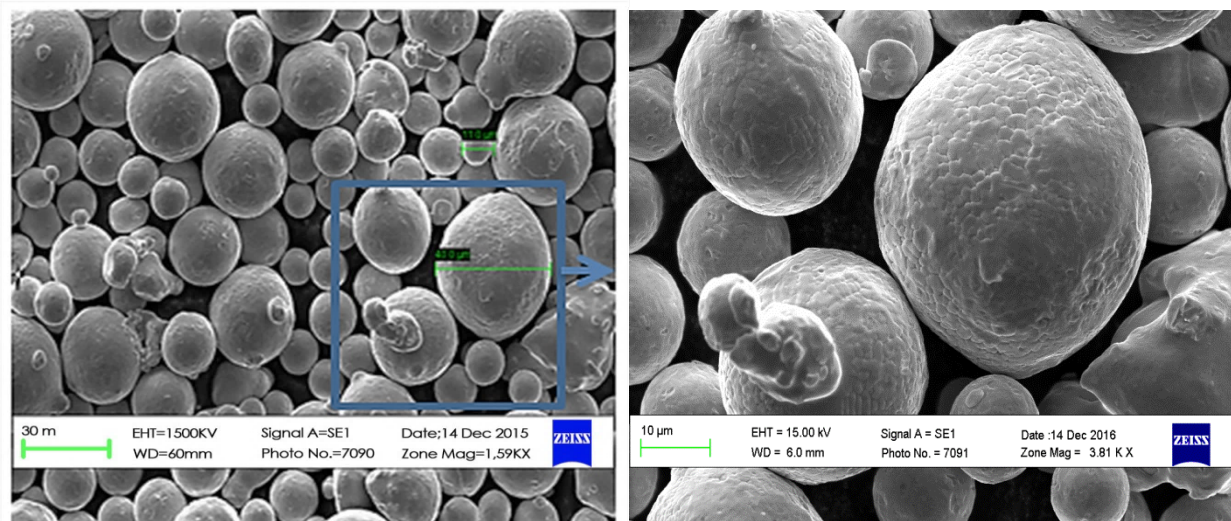
Figure 5-2: SEM morphology of the Inconel 625 powder.

5.2.2. Post mixing of the mixed coating powder

The two powders (75 wt. % nWC-12Co + 25 wt. % Inconel 625) were mixed with the aim of achieving homogeneity in the mixture as reflected in the final result. After taking samples of the powder following mixing and using the EDS imaging mapping tool as shown in Figure 5-4, the results showed that there was homogeneous distribution of the powder types and sizes. In addition, the measured particle diameters were found to be consistent with the particle size in the range of 5 to 45 μm. In this case, the homogeneity of the mixture's components effectively surpassed the cohesive forces between the unique components. Thus, the

Novel Enhancement of HVOF Thermal Sprayed Nanostructured WC-12Co / Inconel-625 Coatings for Tribocorrosion Applications | **Al-Harbi, Naif I**

104

possibility of clusters of a particular mixture component was eliminated with the equal distribution of all the components within the entire mixture.

Nonetheless, in the zoom-in view of the SEM image in Figure 5-4, it is still possible to distinguish the two components of the mixture based on their associated textures within the homogeneous mixture, which can be noted through the clear identification of the two elements W and Ni within the mixture Figure 5-4 (B, C). In addition, the particle-size distribution analysis measurement of the diameter ranges for the mixed powder 75 wt. % nWC-12Co + 25 wt. % Inconel 625 (as shown in Figure 5-3) revealed that very large particles and very small particles existed in the mixture, irrespective of the component, and were tending to be free and not clustered around other particles of the same size range as in the case of small-sized particles, especially in the range of 5 – 20 μm of diameter. Similar results were reported by Abdollah and Mateos et al. [102, 103]. However, as can be seen from the particle size distribution analysis in Figure 5-3, the majority of the mixed-powder particles' size was in the range of 5 to 20 μm (above 85%).
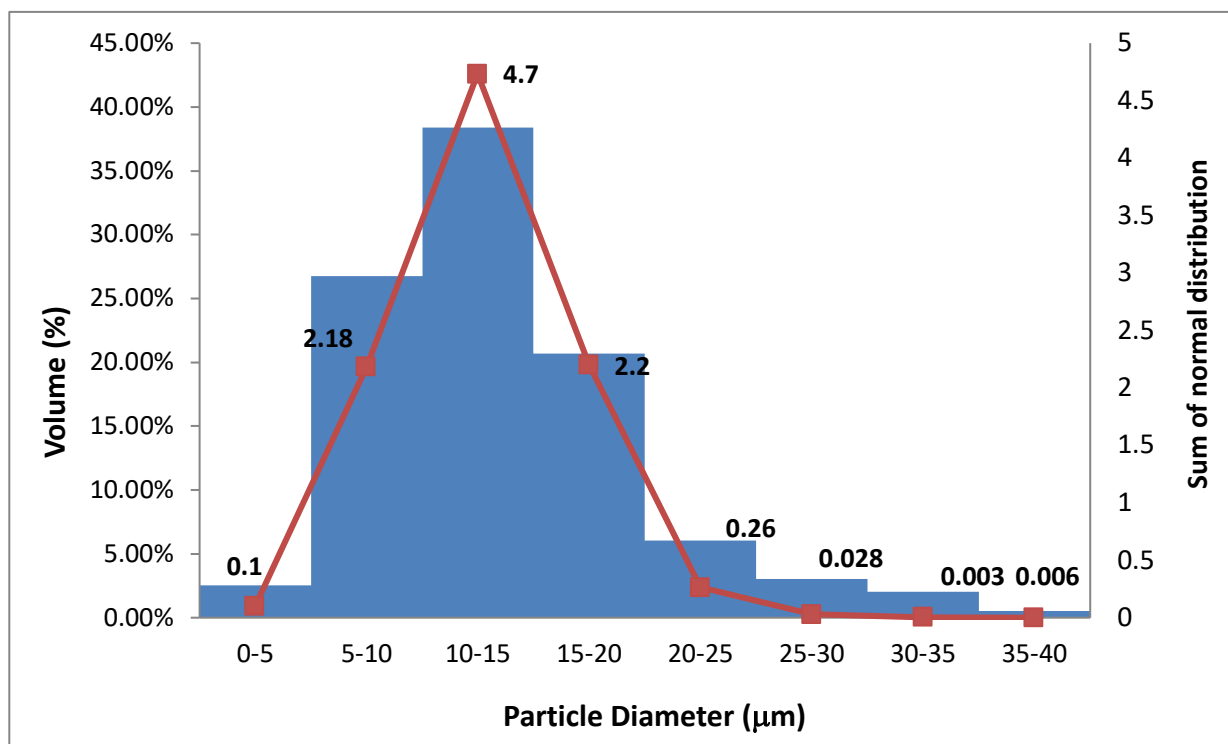
Figure 5-3: Particle size distribution analysis to measure the diameter ranges for the mixed powder 75 wt. % nWC-12Co + 25 wt. % Inconel 625.

Novel Enhancement of HVOF Thermal Sprayed Nanostructured WC-12Co / Inconel-625 Coatings for Tribocorrosion Applications | **Al-Harbi, Naif I**

105
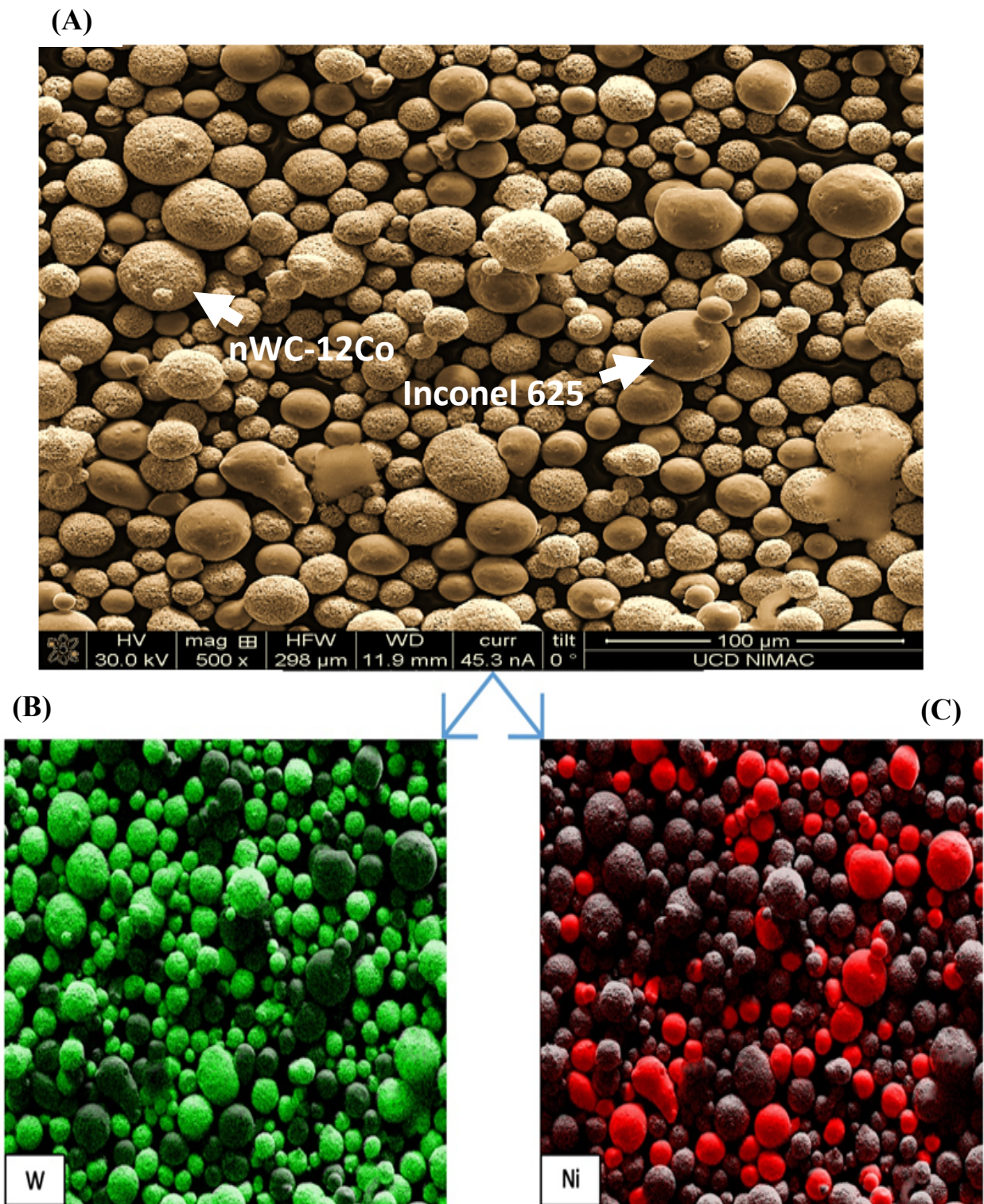
Figure 5-4: EDS element mapping of the mixed powder (75 wt. % nWC-12Co + 25 wt. % Inconel 625) (A) by picking one element of each powder type,(B) nWC-12Co powder, and (C) Inconel 625 powder, where the top image is the SEM location of the element mapping.

Novel Enhancement of HVOF Thermal Sprayed Nanostructured WC-12Co / Inconel-625 Coatings for Tribocorrosion Applications | **Al-Harbi, Naif I**

106

5.2.3 Powders XRD analysis

Figure 5-5 shows the XRD analysis of the nWC-12Co, Inconel 625 and the mixed stock powders. According to the results of the individual XRD of the powders (nWC-12Co, as well as the mixture 75 wt. % nWC-12Co + 25 wt. % Inconel 625), the respective patterns were dominated by the individual elements, compounds and phases. The XRD pattern of nWC-12Co powder of Figure 5-5 (A), had peak positions/intensities and distribution of the primary crystalline phases WC and Co. The greater intensity and higher numbers of WC peaks, in comparison to the cobalt (Co), can be attributed to the higher percentage of WC nanoparticles in the starting powder material (WC-12Co).

Meanwhile, the XRD pattern of the Inconel 625 and mixed stock powder (Figures 5-5 B and C), patterns overlaped with the intensities of the mixed powder. Although the two patterns look similar, a closer look reveals the additional peaks corresponding to the peaks of the other powders in the mixture, which were individual Ni and Cr elements. In addition, new crystalline NiCrCo and NiCr phases were detected, whereas Mo, Fe and Nb, which were originally found in the Inconel 625, were not detected [17]. In terms of WC particles, the WC phase in nWC-12Co powder had a higher peak intensity than that of the mixture 75 wt. % nWC-12Co + 25 wt. % Inconel 625, which could have contributed to the differences in percentage of WC in both coating powders.

Novel Enhancement of HVOF Thermal Sprayed Nanostructured WC-12Co / Inconel-625 Coatings for Tribocorrosion Applications | **Al-Harbi, Naif I**

107
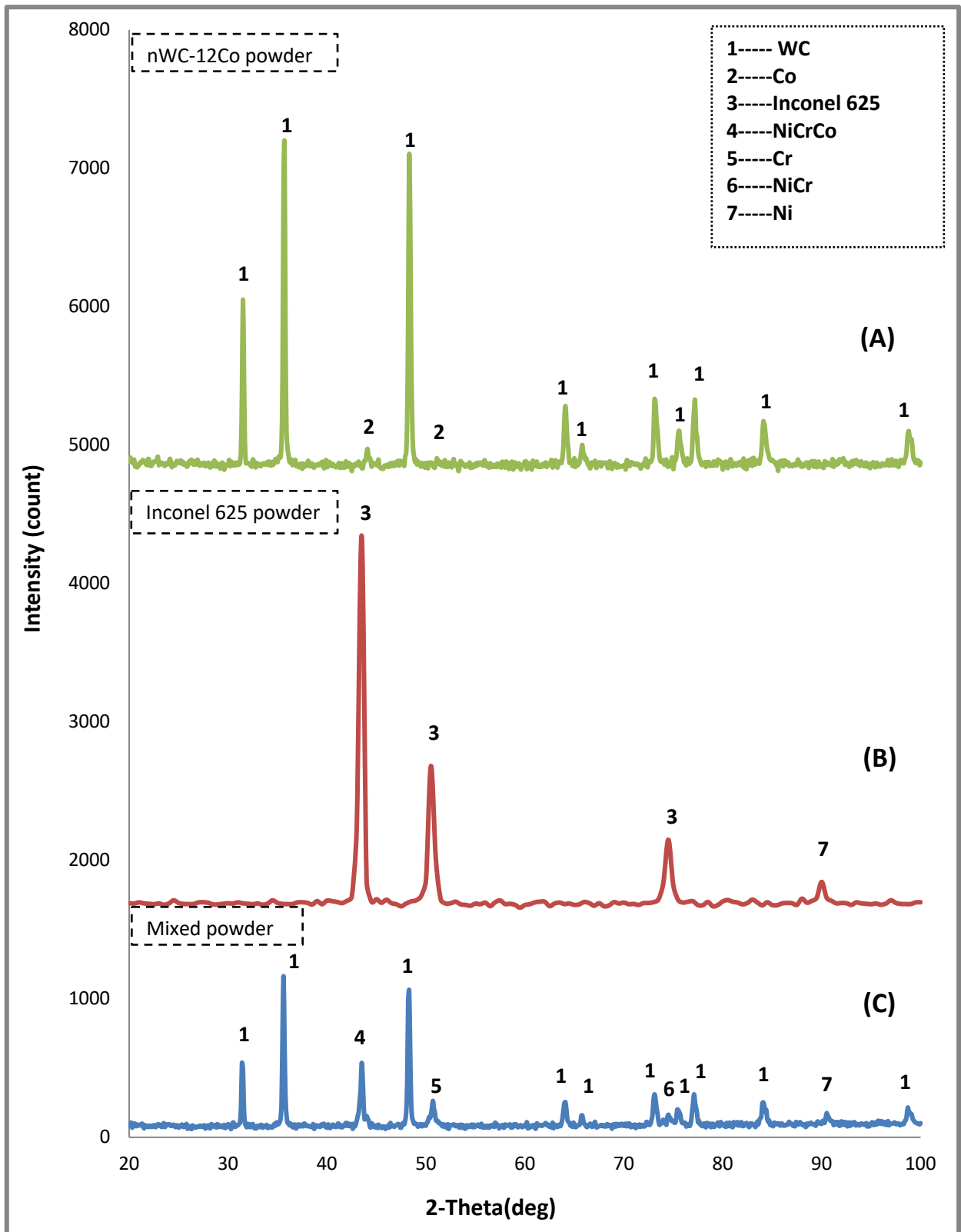
Figure 5-5: XRD pattern of the nWC-12Co,Inconel 625 and 75 wt. % nWC-12Co + 25 wt. % Inconel 625 stock powders.

Novel Enhancement of HVOF Thermal Sprayed Nanostructured WC-12Co / Inconel-625 Coatings for Tribocorrosion Applications | **Al-Harbi, Naif I**

108

5.3 As-sprayed coating

5.3.1 Surface views of HVOF coatings

Figures 5-6 to 5-8 illustrates the SEM views of the surface of the HVOF coating for nWC-12Co (5-6), Inconel 625 (5-7) and mixed example 75% nWC-12Co and 25% Inconel 625 (5-8). Due to the non-uniform solidification and different particle sizes, some surfaces experienced some porosity and/or micro-cracks, and in occasionally unmelted granules on the coated surface. The insufficient heat supplied during HVOF spraying resulted in some unmelted particles, thus more heat would have been required than that supplied to completely melt the coating powders binder matrix and form a dense microstructure. During solidification, the difference between the expansivity rates of the mixture components resulted in an unequal cooling rate and consequently resulted in the formation of micro-cracks and pores. Micro-cracks represent lines of surface weakness separating unjointed surfaces, while pores can be identified by small holes within the surface.

In general, the monomial nWC-12Co HVOF coatings appeared denser than the mixed and Inconel 625 coatings, which can be attributed to the particles being sprayed at a higher speed, as explained in Table 3-3, Chapter 3. This allowed for the closing of more voids in the microstructure. Furthermore, only the metal cobalt (Co), which forms 12% of each of the powder particles, should be melted during the spraying process, while the nanoscale WC hard particles will maintain their hard phase throughout the entire coating process. This finding was further confirmed by comparing the coating with and without a level of WC particles in Figures 5-7 (B) and 5-8 (B); despite both coatings being sprayed with the same parameters, the coating without WC inclusion appeared to have a larger number of unmelted particles than the one mixed with nWC-12Co powder particles.

In order to measure the surface roughness in more detail, the morphology of the surface was investigated using DEKTAK 150 mapping. This clearly showed both the 2D and 3D profiles of the coated surface. From the profiles, the areas of inhomogeneity could be clearly observed, as shown in Figures 5-9 and 5-10. Table 5-1 displays the average surface roughness (R_a) and average surface area ratio (S_{dr}) from four different readings.

Novel Enhancement of HVOF Thermal Sprayed Nanostructured WC-12Co / Inconel-625 Coatings for Tribocorrosion Applications | **Al-Harbi, Naif I**

109
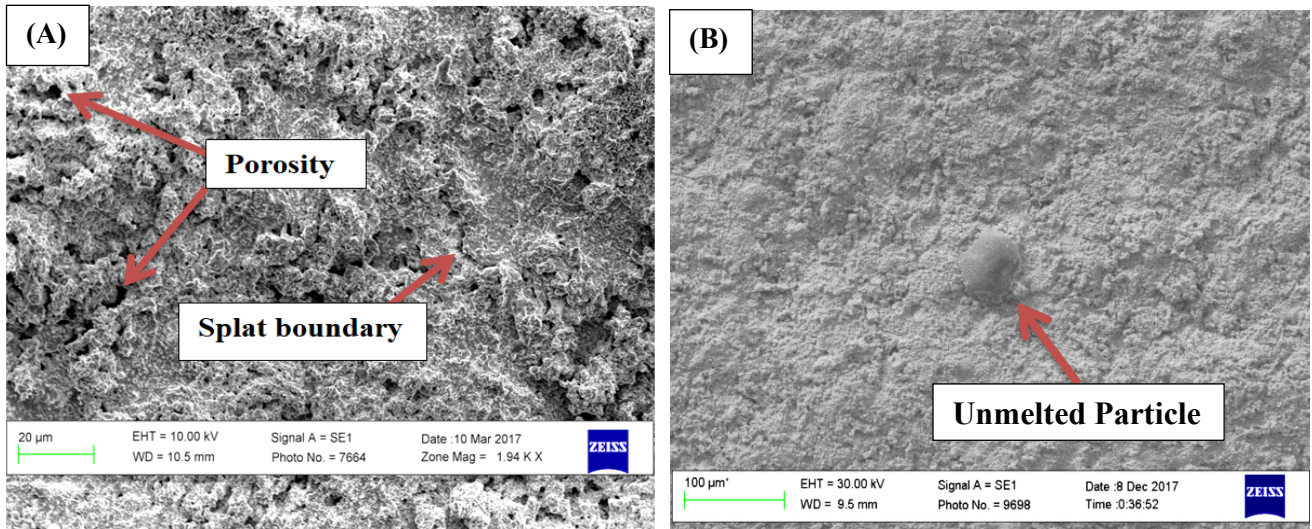
Figure 5-6: SEM micrograph of the top surface of nWC-12Co HVOF coatings with (A) high magnification and (B) low magnification.
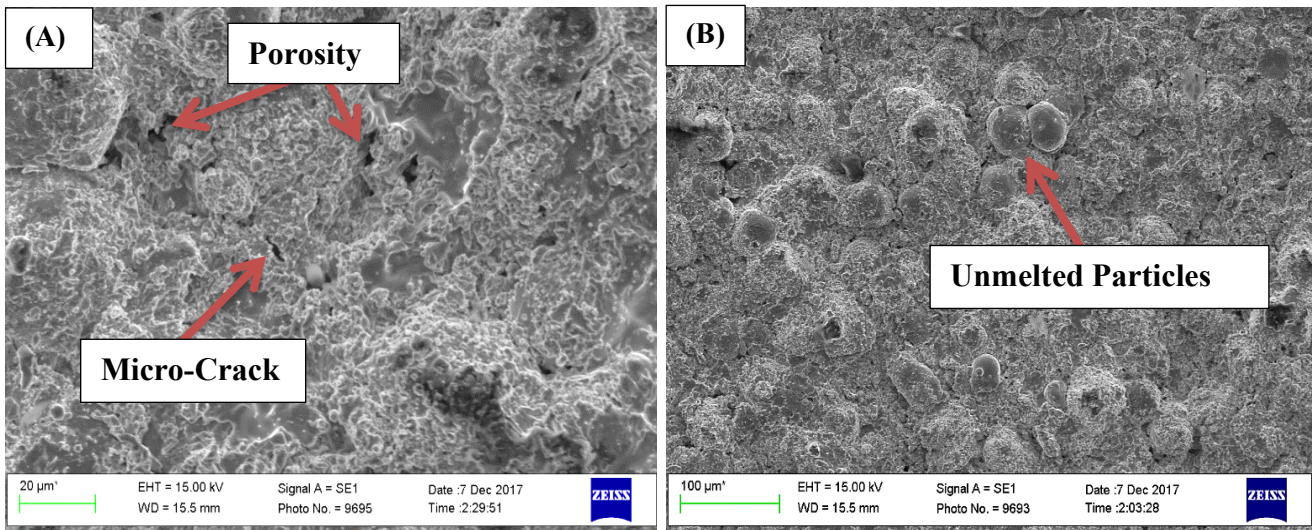
Figure 5-7: SEM micrograph of the top surface of Inconel 625 HVOF coatings with (A) high magnification and (B) low magnification.
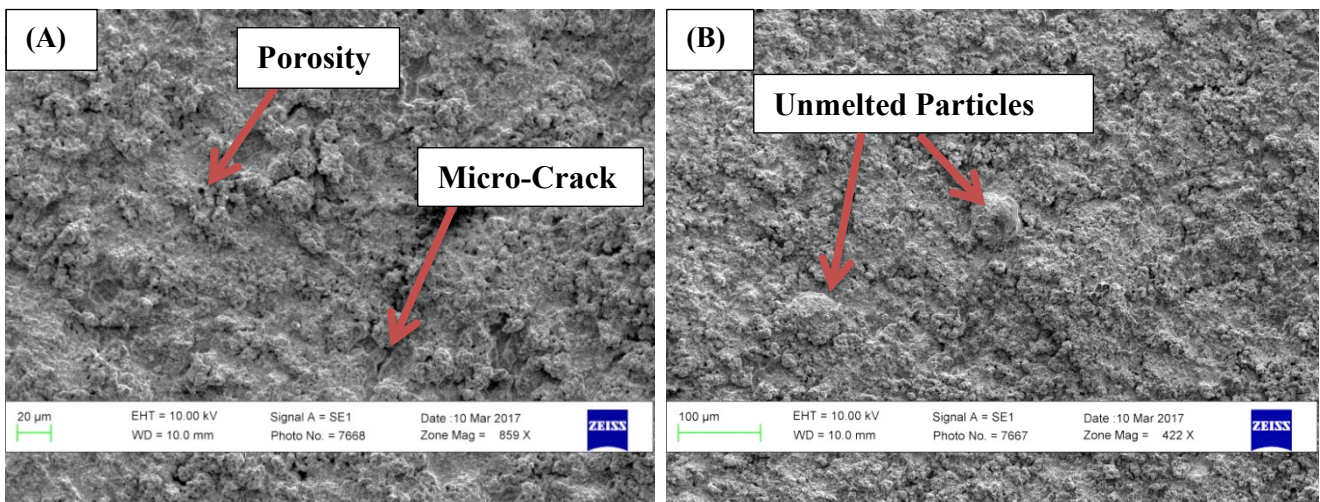
Figure 5-8: SEM micrograph of the top surface of 75 wt. % nWC-12Co + 25 wt. % Inconel 625 HVOF coatings with (A) high magnification and (B) low magnification.

Novel Enhancement of HVOF Thermal Sprayed Nanostructured WC-12Co / Inconel-625 Coatings for Tribocorrosion Applications | **Al-Harbi, Naif I**

110
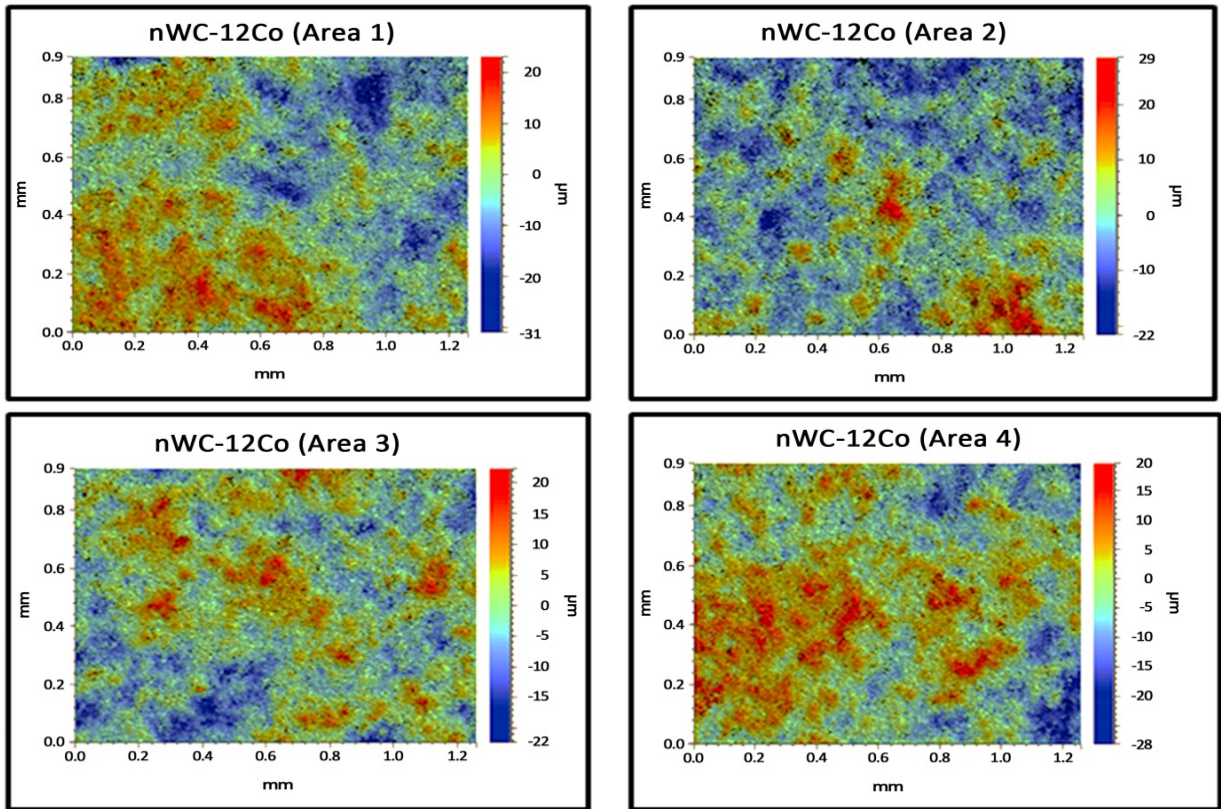
(A)
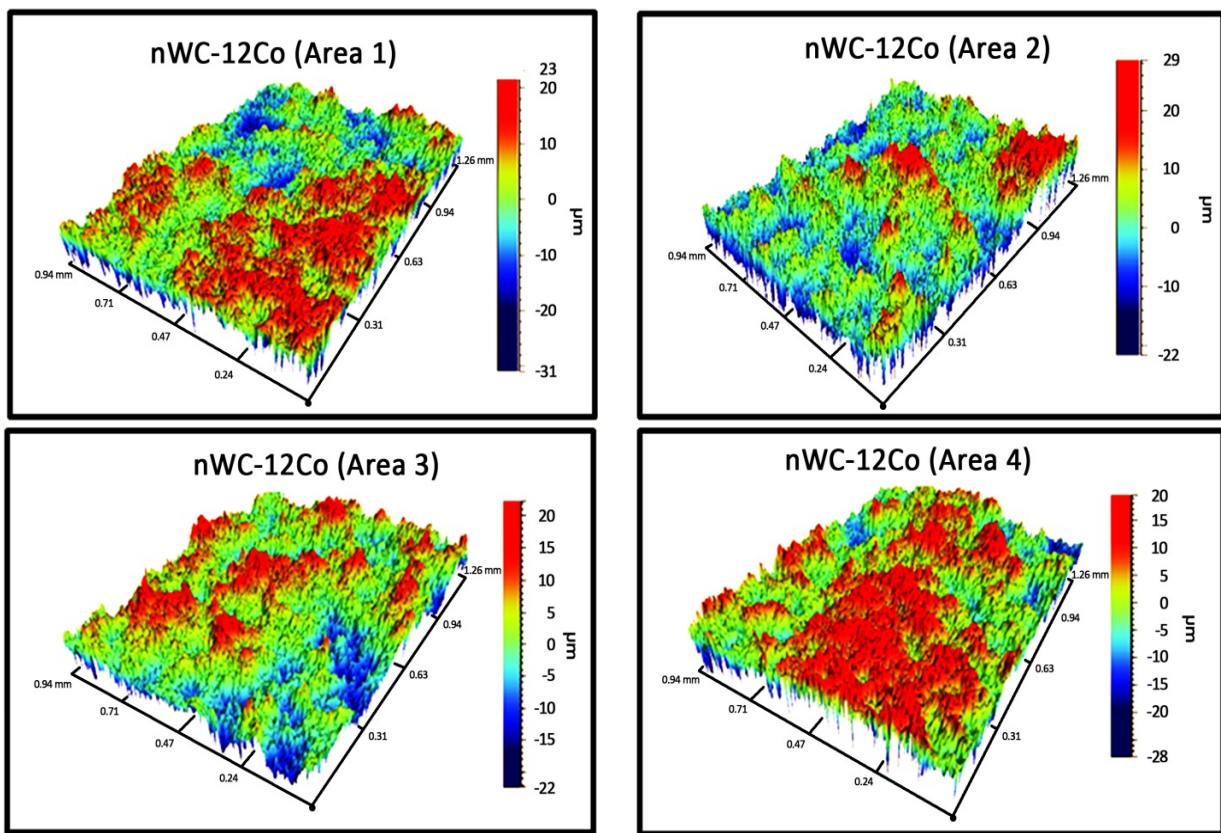
(B)

Figure 5-9: surface profiles (A) and (B) 3D profiles in four different areas on monomial nWC-12Co coating surface.

Novel Enhancement of HVOF Thermal Sprayed Nanostructured WC-12Co / Inconel-625 Coatings for Tribocorrosion Applications | **Al-Harbi, Naif I**

111
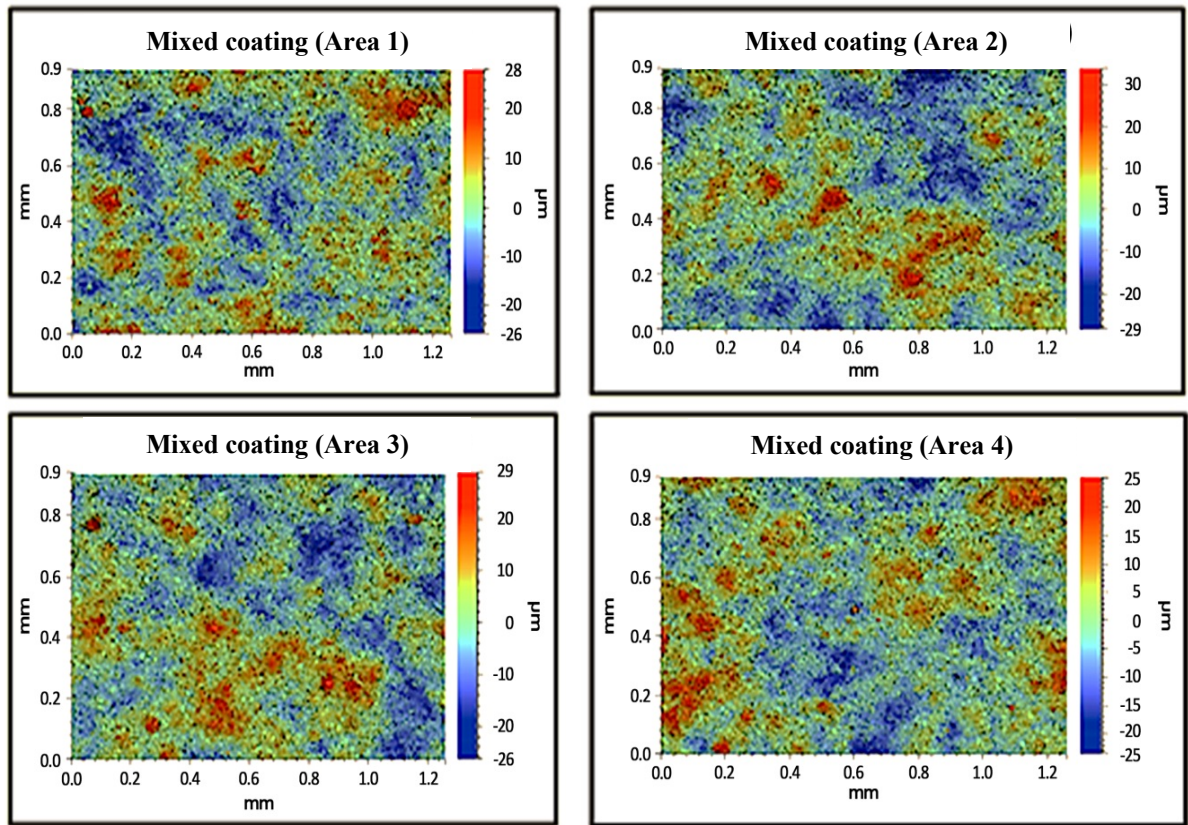
(A)
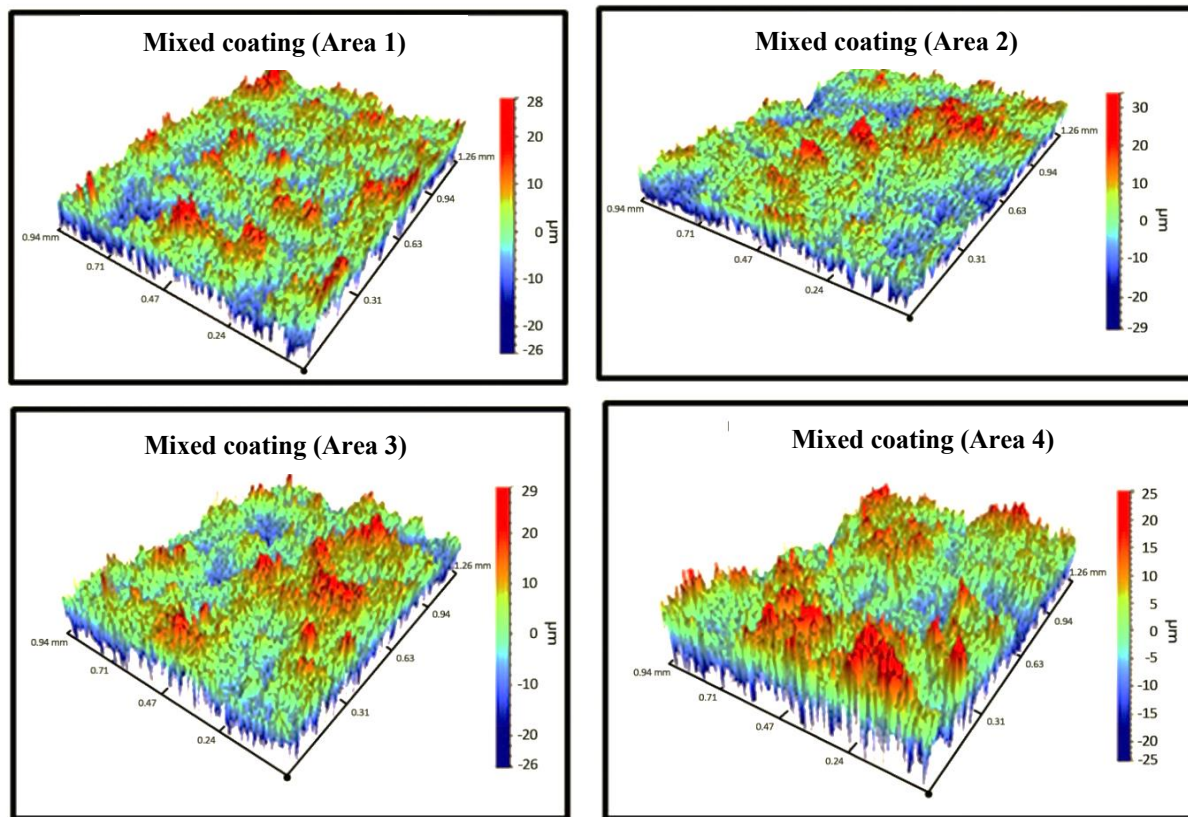
(B)

Figure 5-10: 2D surface profiles (A) and (B) 3D profiles in four different areas on 75 wt. % nWC-12Co + 25 wt. % Inconel 625 coating surface.

Novel Enhancement of HVOF Thermal Sprayed Nanostructured WC-12Co / Inconel-625 Coatings for Tribocorrosion Applications | **Al-Harbi, Naif I**

112

HVOF Coating	Average Surface Roughness R_{qa} (μm)	Average Surface Area Ratio S_{dr} (%)
Monomial nWC-12Co	5.24	226.2
Mixed coating	5.58	305.17

Table 5-1: The average surface roughness and surface area ratio for the as-sprayed coatings.

In conclusion, the monomial nWC-12Co coating has the lowest surface roughness, which can be attributed to the reasons discussed earlier, due to the small size of tungsten carbide (WC) nanoscale particles that could easily melt during the HVOF thermal spray and form a uniform splat buildup, revealing a smoother surface. This result matches findings from an earlier study carried out by Al-Hamed [17], which stated that increasing the composition percentage of nanostructured WC-12Co particals in the coating over that of Inconel 625 can decrease the surface roughness.

5.3.2 Cross sectional view of the HVOF coatings

The detailed microstructure of the two-coating cross section (75 wt. % nWC-12Co + 25 wt. % Inconel 625 and monomial nWC-12Co) can be observed in Figures 5-11 to 5-17, where both coating types exhibit a nonhomogeneous microstructure and have a series of coating defects. The cross-sectional microscope views were achieved by sectioning the samples perpendicular to the longitudinal axis. For the 75 wt. % nWC-12Co + 25 wt. % Inconel 625 coating (Figure 5-11), the cross section shows that unmelted or partially molten splats were embedded into the carbon steel substrate surface, forming a bond that contained a number of boundary defects such as contamination and micro-separation (porous strips) along the coating/substrate interface.

The porous strips at the coating/substrate interface region indicated volume shrinkage of the coating that accrued at the interface region, along with a low processing temperature, resulting only in mechanical bonding. The porosity presence along the cross section in the high magnification micrograph (Figure 5-12(A)) can be categorized as interconnected porosity that were formed as gaps between the semi-melted coating droplets, particularly between Inconel 625 and nWC-12Co particles.

Novel Enhancement of HVOF Thermal Sprayed Nanostructured WC-12Co / Inconel-625 Coatings for Tribocorrosion Applications | **Al-Harbi, Naif I**

113
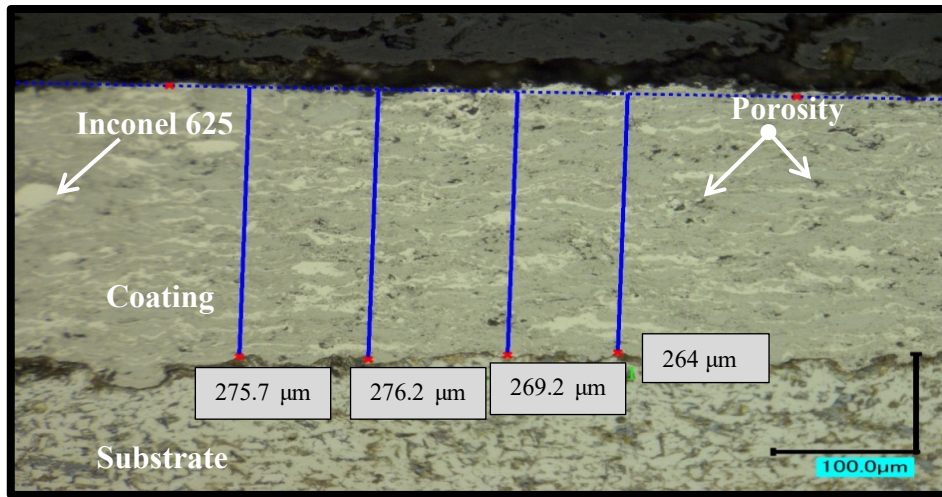
Figure 5-11: Microscope image of cross section of 75 wt. % nWC-12Co + 25 wt. % Inconel 625 HVOF coating.
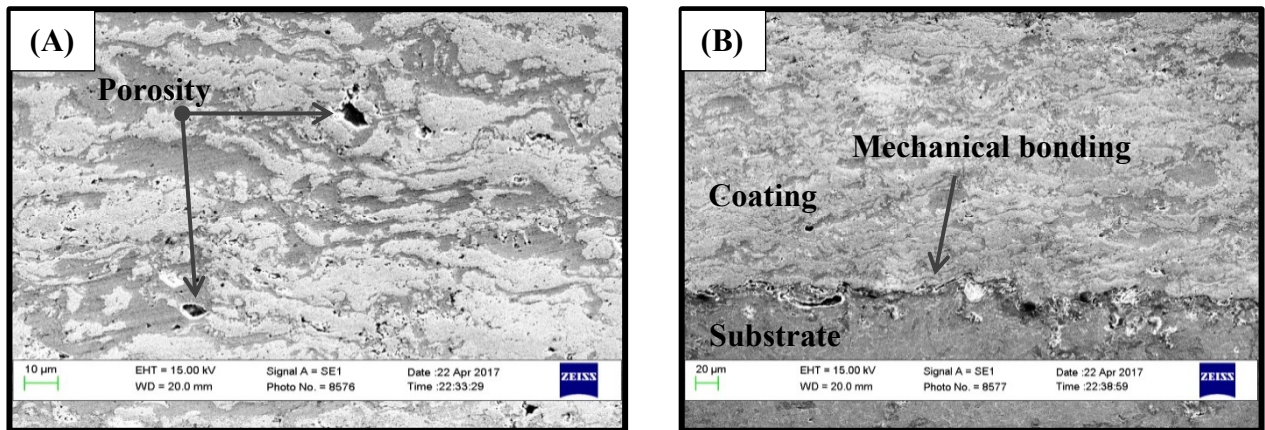
Figure 5-12: SEM micrographs of 75 wt. % nWC-12Co + 25 wt. % Inconel 625 HVOF coating at typical structure (A) and at the coating/substrate interface (B).

Figure 5-13 presents the EDS analysis of the chemical composition at different locations for the 75 wt. % nWC-12Co + 25 wt. % Inconel 625 HVOF coating. As described earlier, the porosity in the 75 wt. % nWC-12Co + 25 wt. % Inconel 625 HVOF coating is interconnected and concentrated between the semi-melted splats boundaries of the two different coatings, as shown in the Figure 5-13. From the results of this Figure, the dark phase is the Inconel 625 matrix, the white phase been the WC nanoscale particles, and the gray phase is the Co binder surrounding WC hard particles.

Further chemical analysis was done by EDS near the splat boundary of an Inconel 625 splat, as illustrated in Figure 5-13 (points 1, 2). It was noted that there is a significant increase in oxygen at the point close to the Inconel 625 splat boundary in comparison to the interior region point (1). This may be caused by the coating particles' outer surface coming into contact with oxygen, in comparison to the interior region of the splats. This oxidation comes

Novel Enhancement of HVOF Thermal Sprayed Nanostructured WC-12Co / Inconel-625 Coatings for Tribocorrosion Applications | **Al-Harbi, Naif I**

114

as a result of Inconel 625 splats combined with excessive unburnt oxygen formed during the thermal spray process, which is characterized by the segregation of chromium and niobium oxides from the Ni-rich matrix as reported by two detailed EDS analyses by Boudi and Al Fadhil et al. [104, 105]. In addition, in the EDS analysis, the Si and Al compounds were noted, which may have been due to the surface preparation process (such as silicon carbide paper used in the grinding process and aluminium oxide grit blasting materials used for substrates surface preparation).
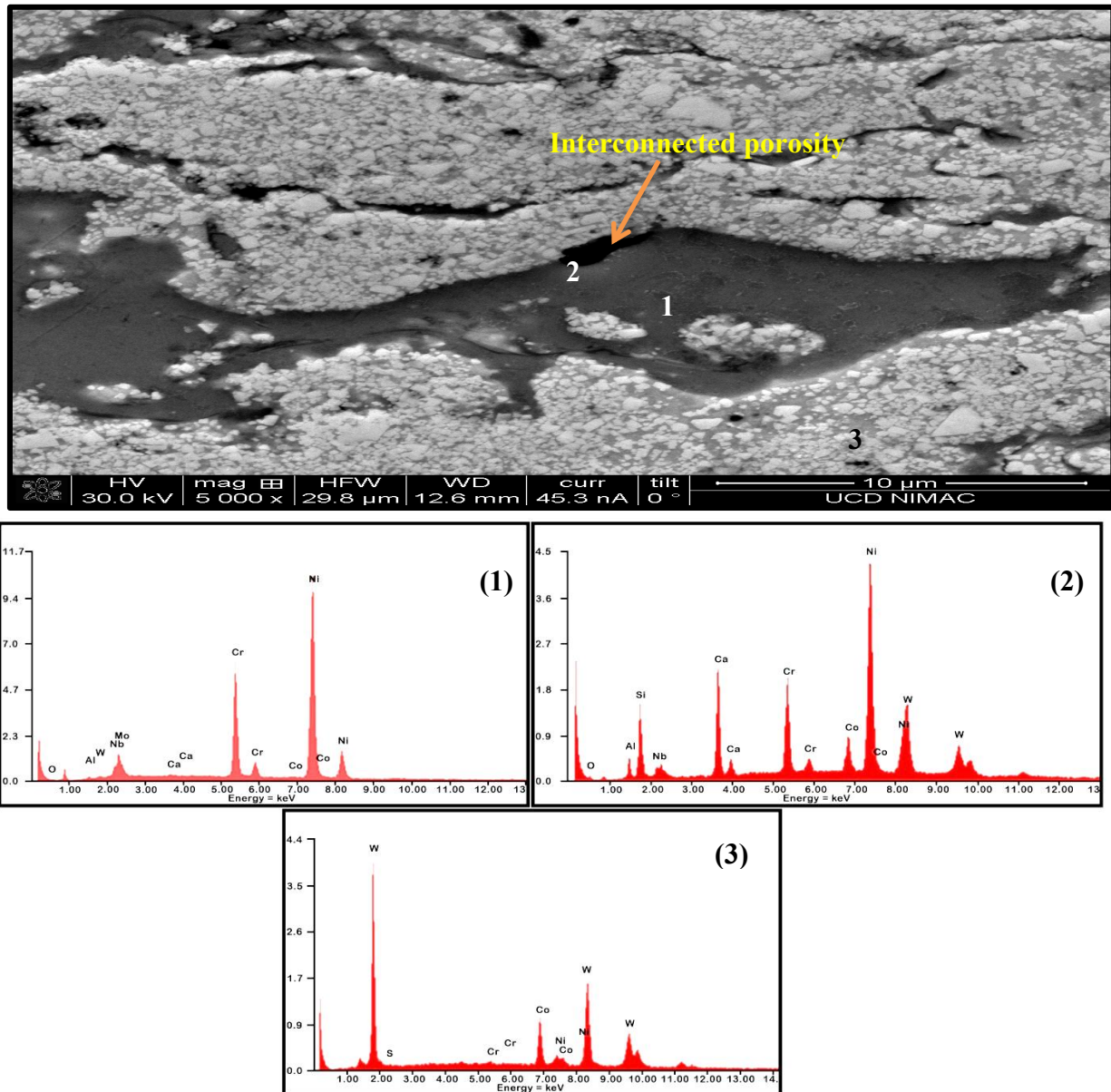
Element	Ni	W	Co	Cr	Nb	Mo	Al	C	Si	O	Total (wt. %)
Area 1	64.10	2.40	0.23	19.51	4.49	7.58	0.81	0.36	0	0.52	100
Area 2	31.33	33.40	4.72	8.72	3.45	0.74	1.95	7.71	5.83	2.15	100
Area 3	2.32	84.42	12.43	0.71	0	0	0	0	0.12	0	100

Figure 5-13 EDS results analysis of various locations in 75 wt. % nWC-12Co + 25 wt. % Inconel 625 HVOF coating (1) dark matrix, (2) dark matrix near splat boundary, and (3) white and gray phases.

Novel Enhancement of HVOF Thermal Sprayed Nanostructured WC-12Co / Inconel-625 Coatings for Tribocorrosion Applications | **Al-Harbi, Naif I**

115

detailed microstructure of monomial WC-12Co cross section (Figures 5-14 and 5-15) shows a non-uniform distribution of the WC pieces embedded in a metal binder matrix (cobalt); the microstructure exhibits different gray shades: the bright regions are the WC-rich carbide regions, also associated with the decarburizations, and the dark are the Co-rich binder regions. Some porosity and micro voids can also be seen along the coating cross section, plus a number of boundary defects, such as contamination and micro-separation (porous strips) along the coating/substrate interface.

This contamination occurred due to the high impact of grit particles during the grit blasting process, as this process was done manually (the gun was handheld), sprayed under a 152 mm spraying distance and at a 60° spraying angle, where this spraying distance and angle were estimated, which led to some variability (in turn, closer distance creates a high impact of powder particles, and subsequently, the particles stick in the substrate surface).
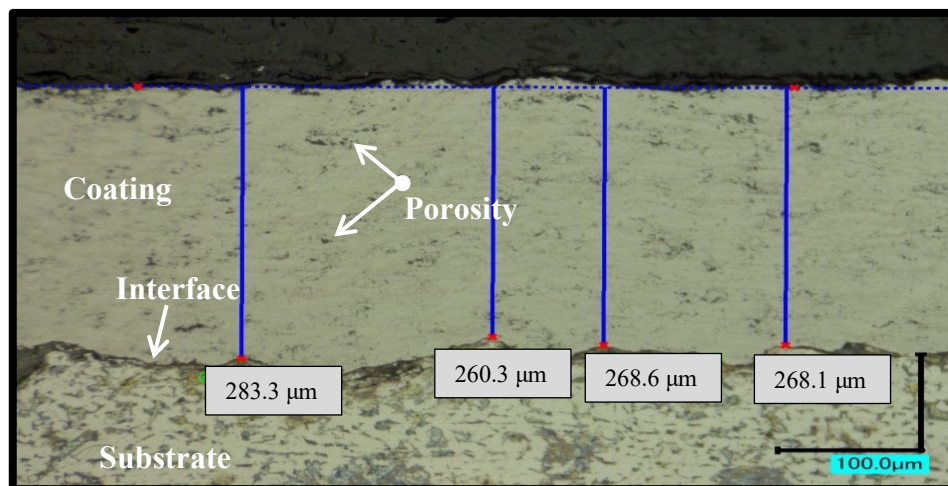
Figure 5-14: Microscope image of cross section of nWC-12Co HVOF coating.
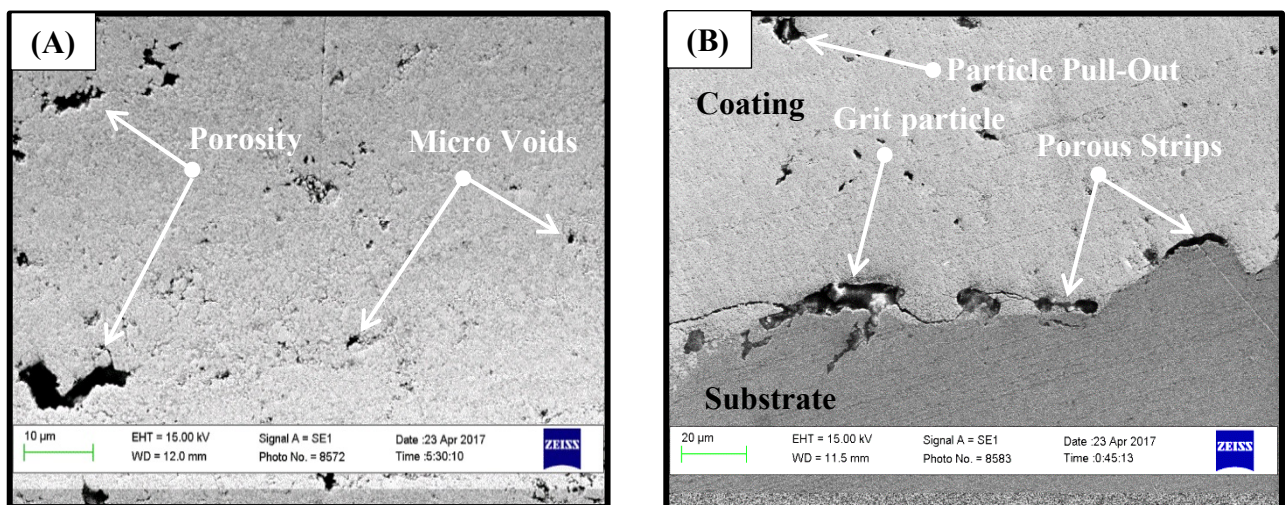
Figure 5-15: SEM micrographs of nWC-12Co HVOF coating at typical structure (A) and at the coating/substrate interface (B).

Novel Enhancement of HVOF Thermal Sprayed Nanostructured WC-12Co / Inconel-625 Coatings for Tribocorrosion Applications | **Al-Harbi, Naif I**

116

The porosity along the cross section comes as the result of some semi-melting particles during the thermal spraying of the monomial nWC-12Co HVOF coating, where the micro-voids come as a consequence of either partial semi-melting of the coating droplets or decomposition of carbon elements.

According to the spraying parameters outlined in Table 3-3, Chapter 3, the particles were injected into a flame temperature of almost 2870°C, which resulted in a 1997°C particle deposition temperature and 646 m/s deposition velocity (all measured by a Tecnar Accuraspray-G3C system). Under this condition, nWC-12Co was either partially or completely molten, as the binder matrix starts to melt and forms the eutectic binder phase at a temperature of 1495°C, where WC melts and starts decomposition to a less-hard phase at 1250°C, and it decomposes by losing one of its carbon atoms, forming W_2C and C as free carbon; it should be noted here that the melting point of a WC binary system alone, unblended with cobalt binder, is above 2750°C [23, 106]. However, the combination will lower the WC dissolution temperature to 1250°C, due to the increase in the wettability of WC when blended together with cobalt as presented in Figure 5-16. This free carbon was created by WC decomposition, and it combines with excessive unburned oxygen formed during the thermal spraying process and from carbon monoxide and dioxide gases (CO and CO_2), resulting in micro-voids inside the coating.

Furthermore, it can be noted from the microstructure that some particles pull out, leaving spherical porous gaps, and this contributes to WC-12Co brittleness, as ductile binder cobalt (12%) is at a relatively small percentage. Furthermore, from the EDS analysis in Figure 5-17 of the chemical composition at two different locations for the monomial nWC-12Co HVOF coating, it can be seen that voids are located at regions with high tungsten carbide weight percentage as illustrated in Figure 5-17 (point 1) in comparison to another region (point 2).

Temperature Scale

WC Decomps. at 1250 °C	Co Melts at 1495 °C	W2C Melts at 2785°C	Co Boils at 2870 °C	W Melts at 3410 °C	C Melts at 3500 °C	C Boils at 4827 °C	W Boils at 5660 °C
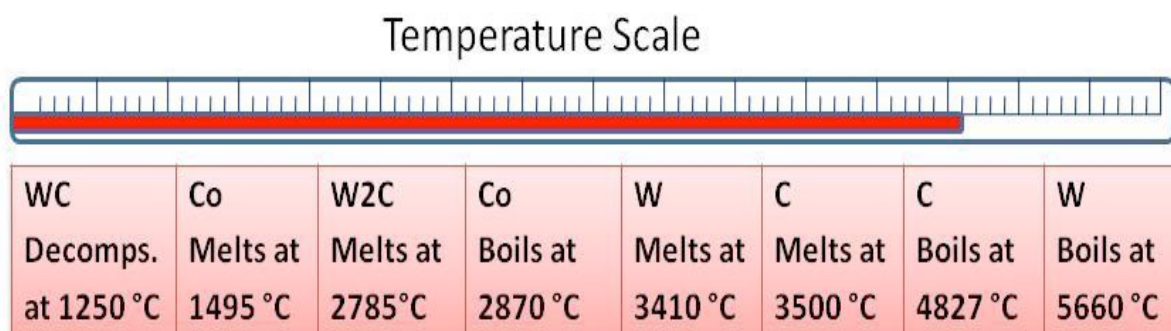
Figure 5-16: The sequence of WC-Co reaction to high temperature [23].

Novel Enhancement of HVOF Thermal Sprayed Nanostructured WC-12Co / Inconel-625 Coatings for Tribocorrosion Applications | **Al-Harbi, Naif I**

117

Element	W	Co	C	O	Total (wt. %)
Area 1	94.79	5.21	0	0	100
Area 2	81.84	16.39	1.13	0.64	100
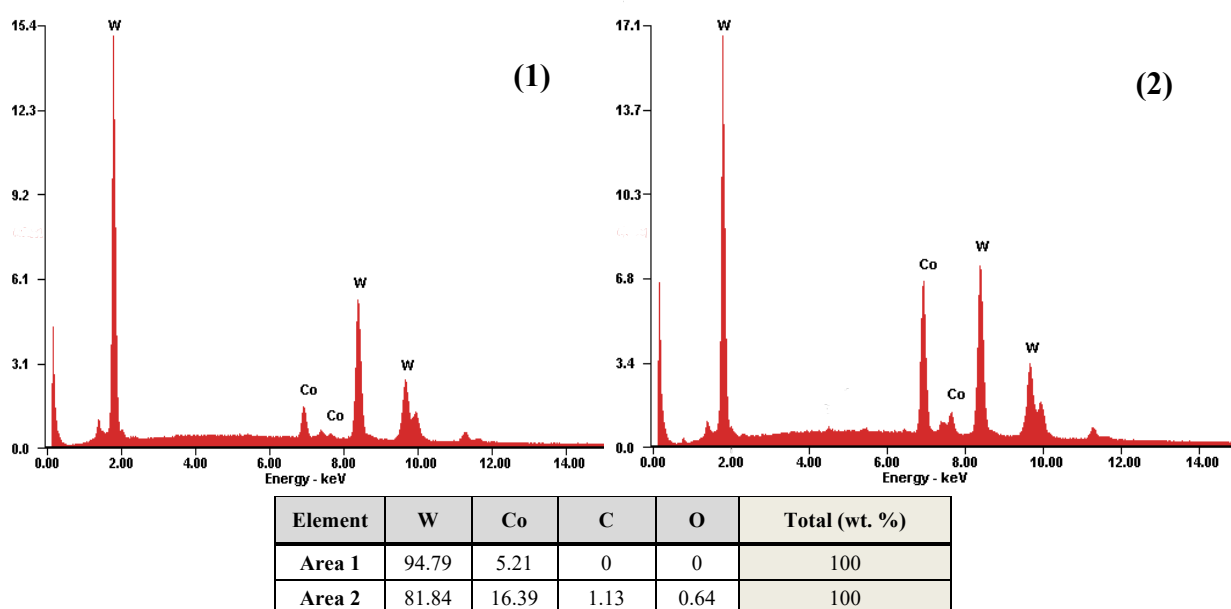
Figure 5-17: EDS results analysis of nWC-12Co HVOF coating (1) near void boundary and (2) for nWC-12Co coating.

The coating thickness for the two coatings has been measured from four different readings (as shown in Figure 5.11 and 5.11) , and the average values of the four measurements and their standard deviation are shown in Table 5-2.

Novel Enhancement of HVOF Thermal Sprayed Nanostructured WC-12Co / Inconel-625 Coatings for Tribocorrosion Applications | **Al-Harbi, Naif I**

118

Coating	Thickness (μm)	Standard Deviation (μm)
Monomial nWC-12Co	~ 270.1	9.6
Mixed coating	~ 274.6	3.82

Table 5-2: As-sprayed coatings thickness measurement results.

5.3.3 Element mapping of as-sprayed coatings

In order to further investigate the elemental distribution of the HVOF coatings' cross section, EDS was used to obtain elemental mapping, as illustrated in Figure 5-18 and 5-19. Figure 5-18 shows the elemental mapping images of the 75 wt. % nWC-12Co + 25 wt. % Inconel 625 HVOF coating. In accordance with expectations, the coating has a non-uniform composition in which various elements are concentrated at specific locations. Three different regions were observed, including the matrix or Inconel 625 area containing Ni, Cr, and Mo (Nb and Fe, had not been added) and the binder areas surrounding the WC particles, are Co, as well as the WC particles. In addition, the 75 wt. % nWC-12Co + 25 wt. % Inconel 625 coating showed the presence of oxygen, especially along the Inconel 625 inter-splat boundaries and close to the top surface.

In comparison to the mixture of the two powders, the SEM image for a monomial nWC-12Co coating shown in Figure 5-19 illustrates how difficult it is to distinguish between the mapping of where there is amorphous Co binder and where there is a high ratio of WC hard particles. However, by taking different points by EDS, as can be seen in Figure 5-19, the results show that there was an inhomogeneous distribution of nanoscale WC hard particles and Co binder. In addition, the oxygen elements were traced across the coating layer as well, but due to small quainaty and scattered as individuals without forming clustered region in comparsion to the ones noticed in the mixed coating, hadnot been provided as difficluts to visiually clearified.

However, this is the inhomogeneous distribution of the coating element, which was available in both coatings types and will have a significant impact on their performance. As it results in a coating with uneven mechanical properties along its cross section, it will cause a reduction in its resistance to wear and corrosion [26].

Novel Enhancement of HVOF Thermal Sprayed Nanostructured WC-12Co / Inconel-625 Coatings for Tribocorrosion Applications | **Al-Harbi, Naif I**

119
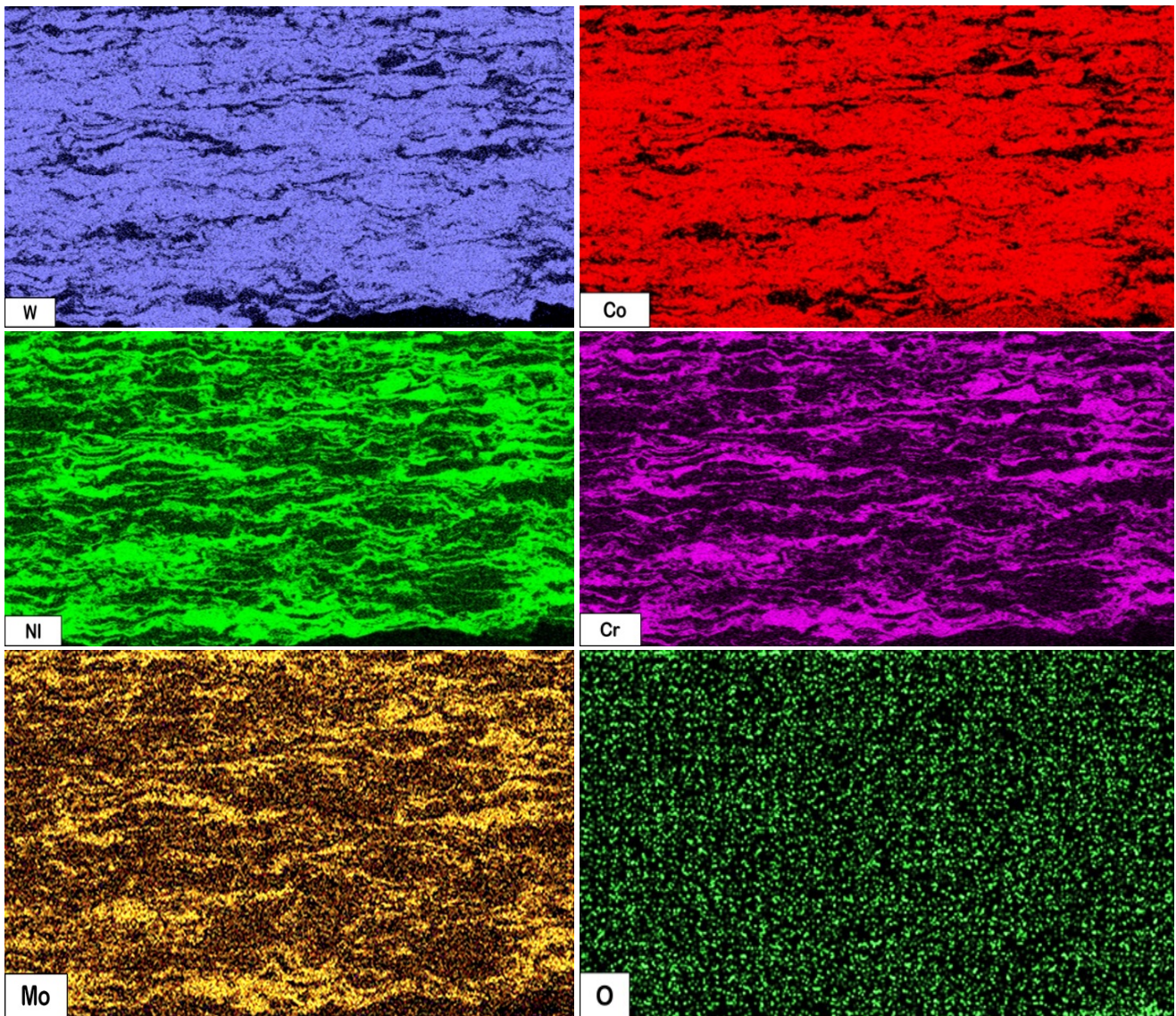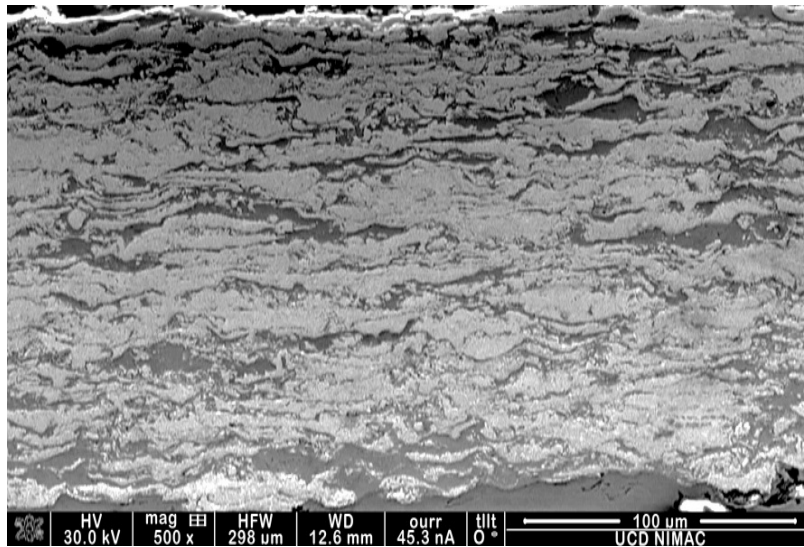
Figure 5-18: EDS element mapping of the 75 nWC-12Co + 25 Inconel 625 (wt. %) HVOF coating, where the top image is the original SEM image.

Novel Enhancement of HVOF Thermal Sprayed Nanostructured WC-12Co / Inconel-625 Coatings for Tribocorrosion Applications | **Al-Harbi, Naif I**

120
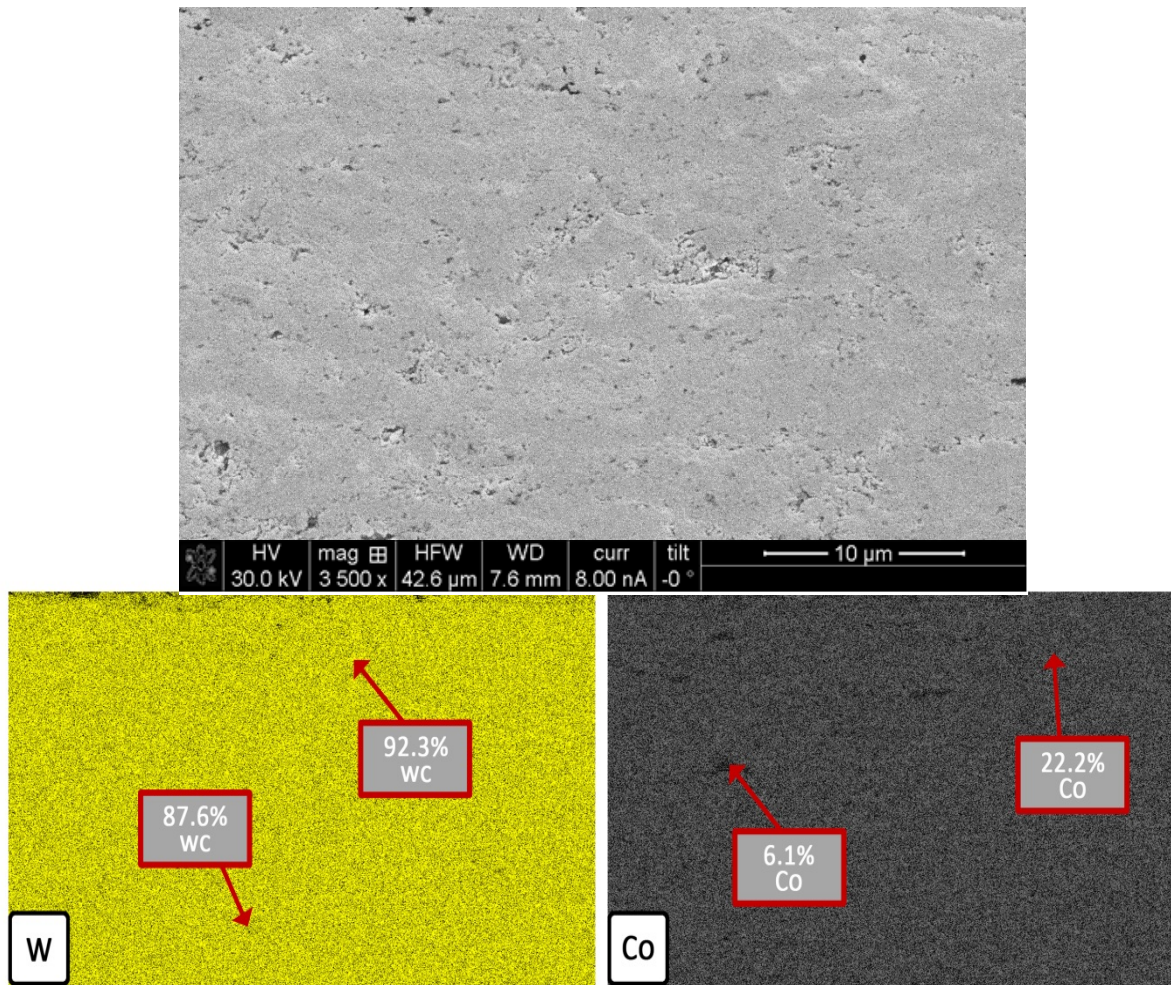
Figure 5-19: EDS element mapping of the nWC-12Co HVOF coating, where the top image is the SEM location of the element mapping.

5.3.4 XRD analysis of HVOF coatings

The XRD patterns were used to identify the elements of the coating material, and the method had the effective capacity of determining whether the deposit material was comprised of the mixture by analysing the resulting phases. The XRD results (Figure 5-20) for the monomial nWC-12Co HVOF coating showed similar peak positions with lower intensities for the WC crystalline phase in the respective coating powder, as provided in previsualised form in Figure 5-5. Furthermore, as a consequence of the process of thermally spraying the powders with the intention of obtaining a dense coating feature, decarburisation occurred within the nanostructured particles, effectively changing the carbon ratio within the mixture. This change of the carbon yielded the formation of a new W_2C phase between about 36° and 39°, with very low peak intensity. The loss of carbon from the nanoscale WC particles, which

Novel Enhancement of HVOF Thermal Sprayed Nanostructured WC-12Co / Inconel-625 Coatings for Tribocorrosion Applications | **Al-Harbi, Naif I**

121

would later interact with oxygen, would lead to the formation of less hard phases such as W_2C and W, which in turn would decrease the resistance to wear and corrosion [17]. The result also indicated small peak for the cobalt (Co), similarly to what was observed previously in the starting nanostructured powder, as shown in Figure 5-5.

For the mixed and the Inconel 625 coating, shown in Figure 5-21, in both coatings all peaks had significantly reduced to their corresponding powders and certain elements were dispersed from some of the phases. For the mixed coating at the bottom of the figure, new phases can be observed at 2Θ of about 36° and 48° in comparison to the figure without thermal spraying (Figure 5-5). The new crystalline phases included W_2C and CO_6W_6C. The intensity peak of the crystalline phase of W_2C for the mixed coating was slightly higher than the one observed for the nWC-12Co HVOF coating, which could be attributed to the different spray parameters used. As the mixed coating was sprayed at a lower volumetric flow rate by the nitrogen carrier gas, this yielded to the coating powder that had been sprayed at a lower dwell time with a higher flame temperature. Consequently, the decomposition of carbon from the nanoscale carbide particles would be greater.
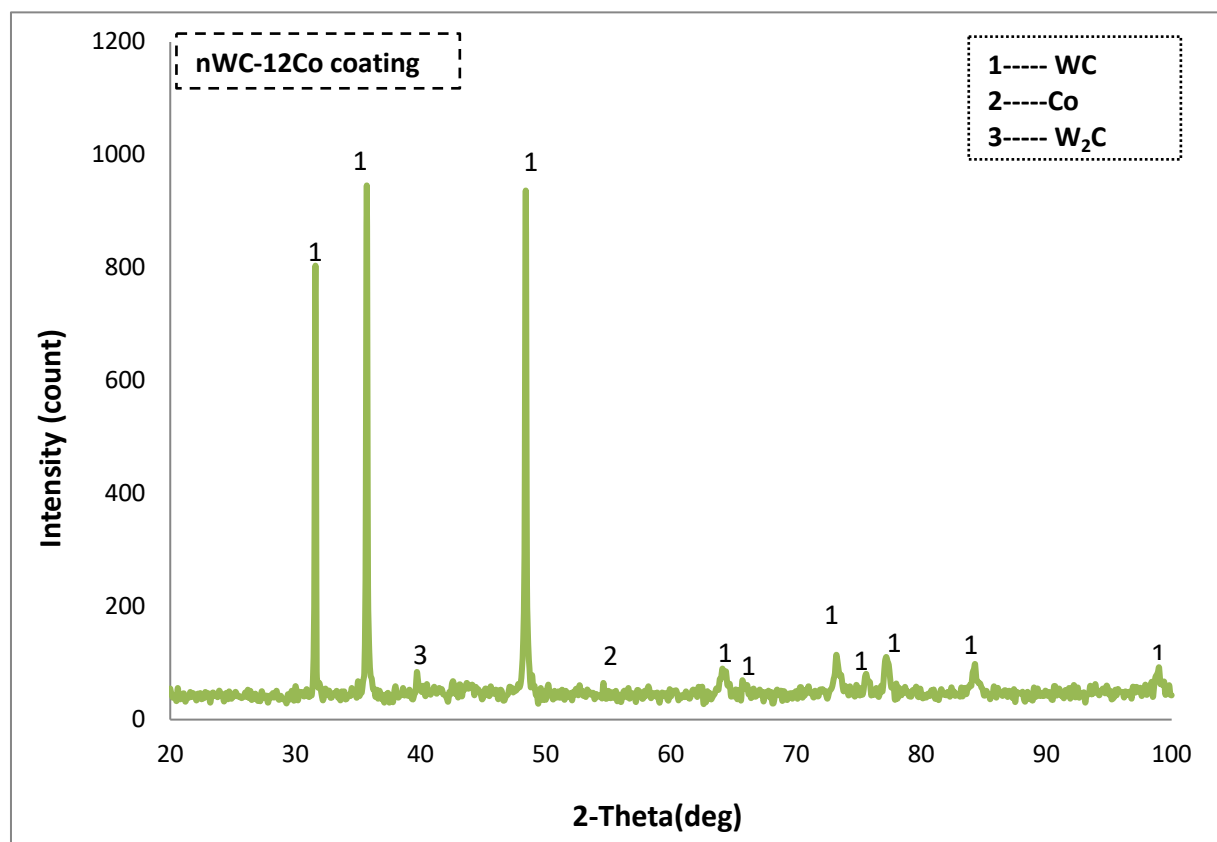
Figure 5-20: XRD pattern of the nWC-12Co HVOF coating.

Novel Enhancement of HVOF Thermal Sprayed Nanostructured WC-12Co / Inconel-625 Coatings for Tribocorrosion Applications | **Al-Harbi, Naif I**

122
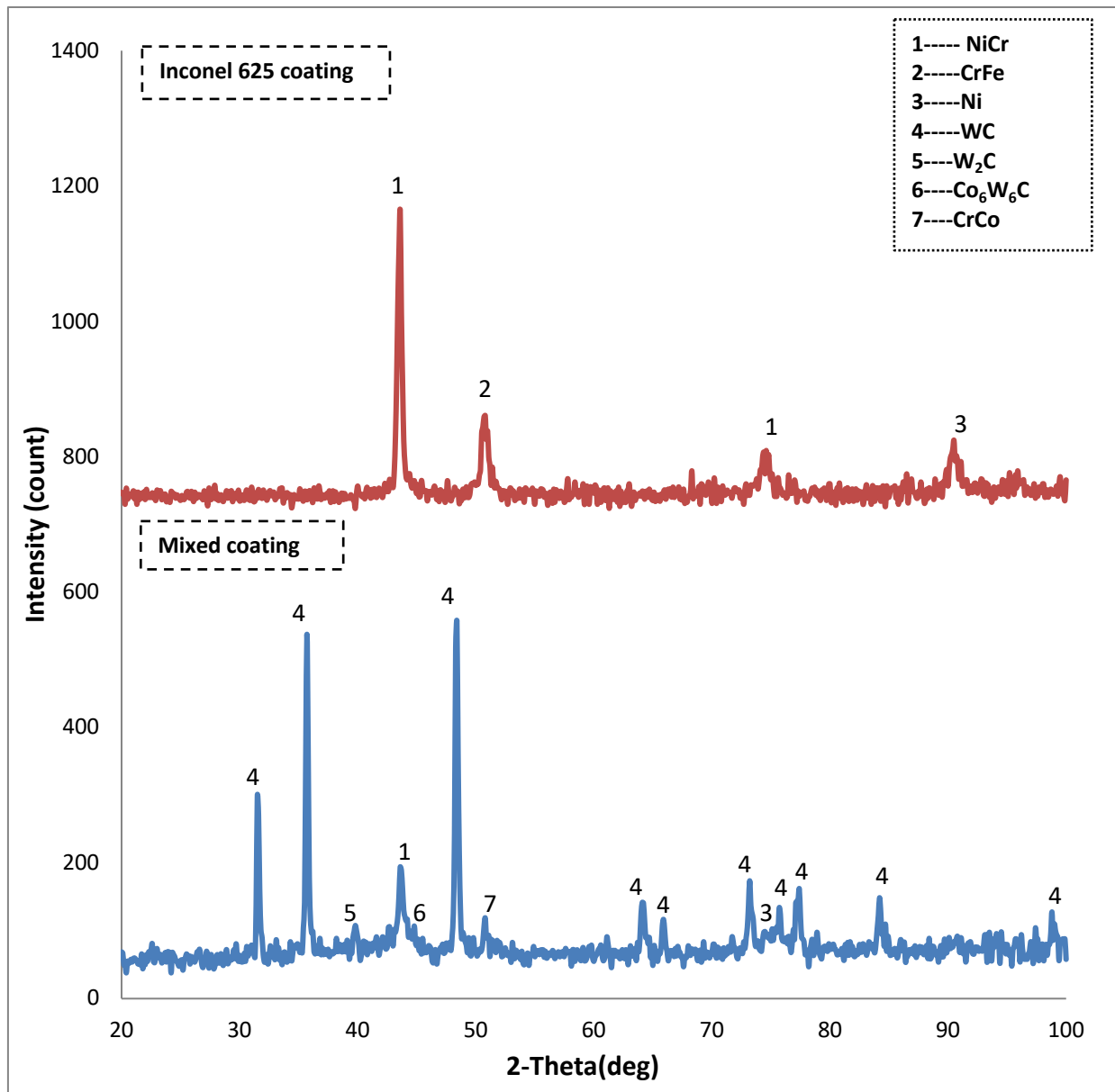
Figure 5-21: XRD pattern of the Inconel 625 and 75 wt. % nWC-12Co + 25 wt. % Inconel 625 HVOF coatings.

5.3.5 Porosity measurements of HVOF coatings

The procedure for porosity measurement of HVOF coatings was carried out by a VHX digital light microscope in this experiment. The measurements were taken at the center of the coating cross section of a width of 150 μm and a height of 100 μm. Table 5-3 shows the measurement of porosity for the two coatings. The combination of 75 wt. % nWC-12Co and 25 wt. % Inconel 625 had the highest porosity of approximately 4.9 %, while the coating from nWC-12Co alone achieved a porosity of about 3.5 %.

Novel Enhancement of HVOF Thermal Sprayed Nanostructured WC-12Co / Inconel-625 Coatings for Tribocorrosion Applications | **Al-Harbi, Naif I**

123

HVOF Coating	Porosity (%)
Monomial nWC-12Co	~ 3.5
Mixed coating	~ 4.9

Table 5-3: Porosity measurements for the two coating types.
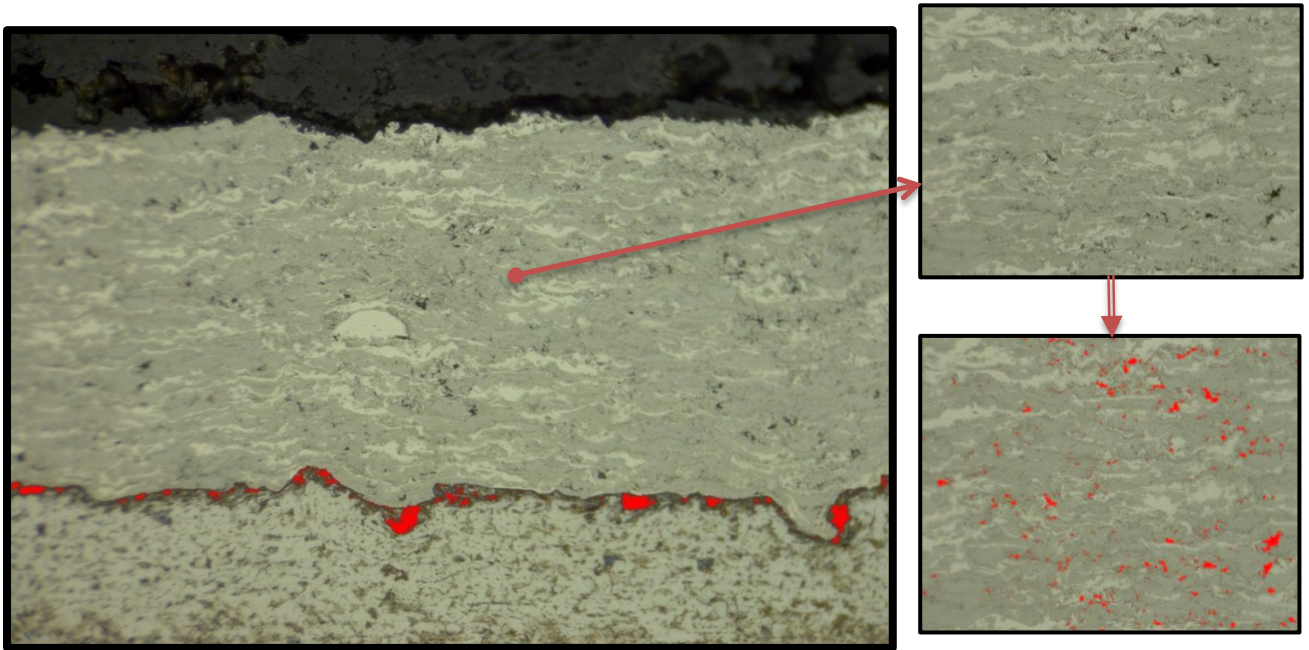
Figure 5-22: Porosity within 75 wt. % nWC-12Co + 25 wt. % Inconel 625 HVOF coating.
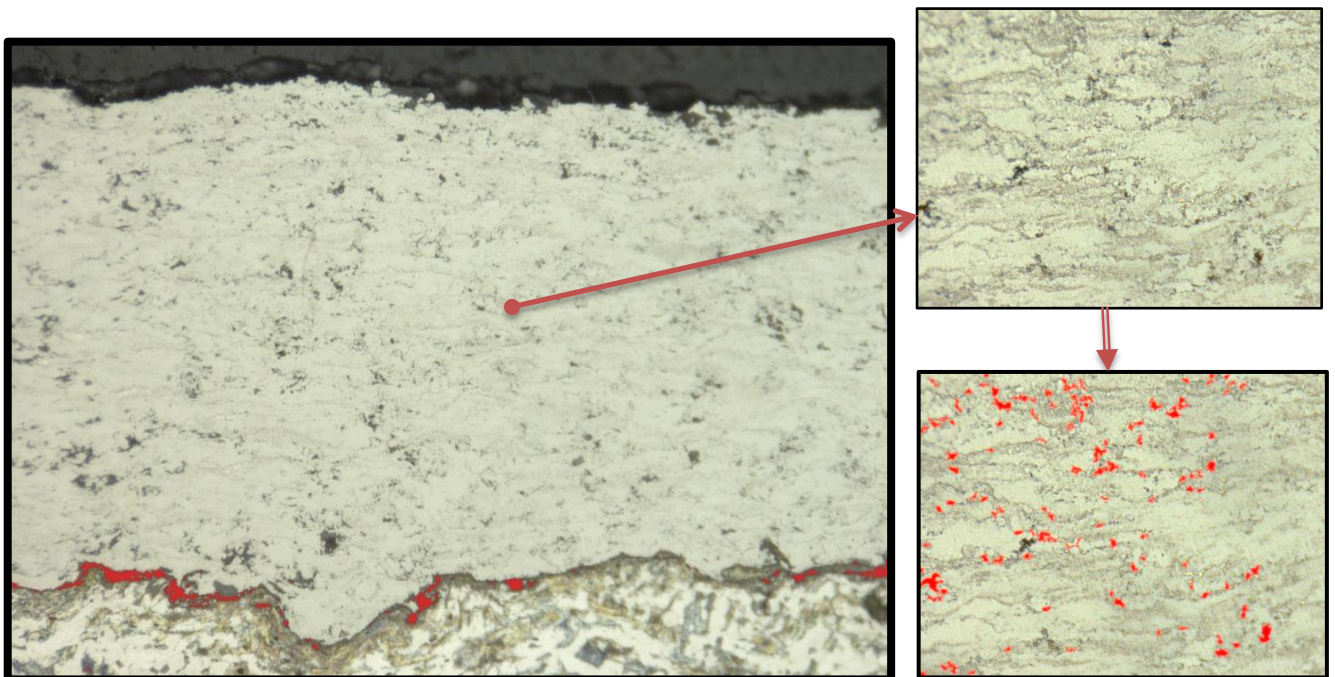
Figure 5-23: Porosity within nWC-12Co HVOF coating.

Novel Enhancement of HVOF Thermal Sprayed Nanostructured WC-12Co / Inconel-625 Coatings for Tribocorrosion Applications | **Al-Harbi, Naif I**

124

Apart from the porosity within the coatings, porosity is also present at the interface between the coating and substrate as shown by the red-coloured indications in each of the figures.

In summary, the the 75 wt. % nWC-12Co + 25 wt. % Inconel 625 mixed coating had a higher porosity, which contributed to a large amount of unmelted or semi-melted particles, which creates interconnected porous holes between coating droplets, particularly between Inconel 625 and nWC-12Co particles.

5.3.6 Microhardness performance of as-sprayed coatings

The Vickers hardness test method was used to measure the hardness of the two as sprayed coating, and the results are displayed in Table 5-4. The variation of microhardness along the depth for the as-sprayed coatings are shown in Figure 5-24, which shows inconsistent change both along the depth and cross-sectional microhardness for each HVOF-sprayed coating. This was the reason for the relatively high standard deviation that existed following the presence of the discrete splats, micro-cracks, and pores, as well as the different ratio of WC hard phase. This was especially true for the mixed coating as at different locations, the indentions mark were observed to partially or totally penetrate the less hard metal alloy of semi-melted Inconel 625 particles as shown in Figure 5-25(B).
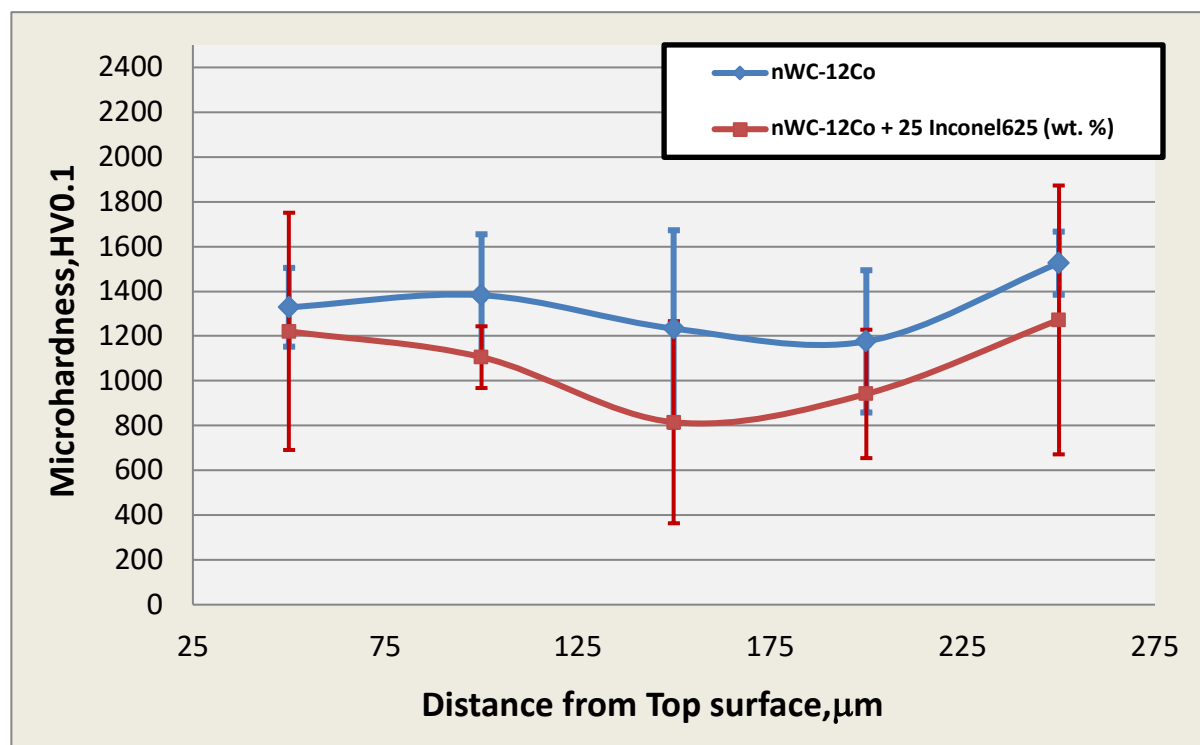
Figure 5-24: Microhardness profiles along the coating depth for nWC-12 Co and 75 wt. % nWC-12Co + 25 wt. % Inconel 625 HVOF as-sprayed coatings.

Novel Enhancement of HVOF Thermal Sprayed Nanostructured WC-12Co / Inconel-625 Coatings for Tribocorrosion Applications | **Al-Harbi, Naif I**

125
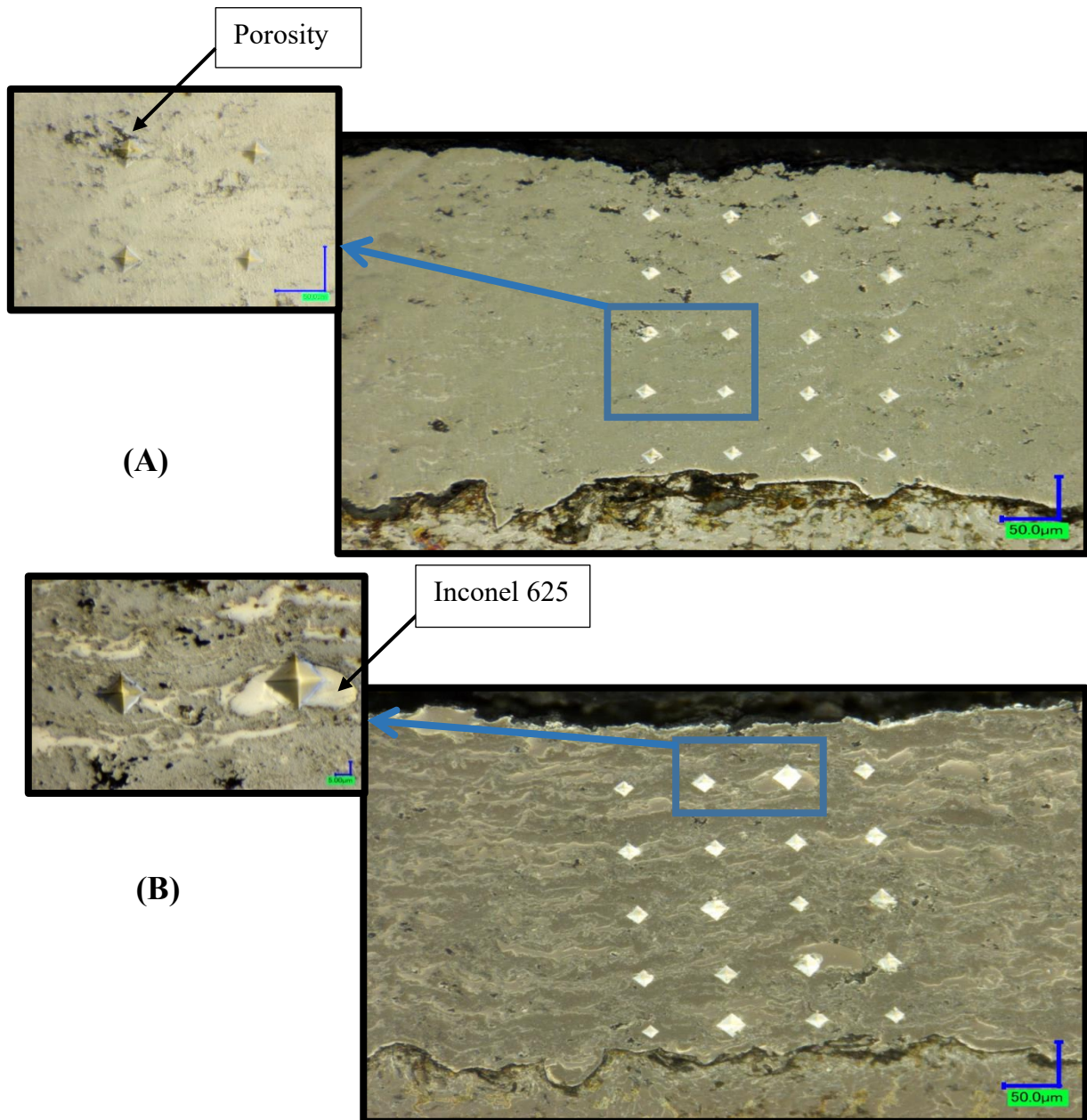
Figure 5-25: The indentation shapes in the cross section of the Vickers hardness tester in (A) nWC-12Co HVOF coating, and (B) 75 wt. % nWC-12Co + 25 wt. % Inconel 625 HVOF coating.

Sample	Max (H$_V$)	Min (H$_V$)	Average (H$_V$)	Std. Dev (H$_V$)
Monomial nWC-12Co coating	1845	826	1329.15	312
Mixed coating	1970	511	1071.05	370.1
Substrate	162	170	167	3.5

Table 5-4: Vickers microhardness results (HV0.1) for nWC-12 Co , 75 wt. % nWC-12Co + 25 wt. % Inconel 625 HVOF as-sprayed coatings and substrate.

Novel Enhancement of HVOF Thermal Sprayed Nanostructured WC-12Co / Inconel-625 Coatings for Tribocorrosion Applications | **Al-Harbi, Naif I**

126

In accordance with the expectations, the average microhardness increased with the increasing of WC content, similar to the results of a study by Rakhes [26]. In addition, it was noted that the coating hardness increased near to the coating/ substrate interface. This was due to the tensile residual stresses found nearer the interface compared to the centre or at the top area of HVOF coating layer [17].

5.3.7 Three-point bending test of as-sprayed coatings

The flexural strength of particular objects is related to a number of factors, as documented by Kramaker et al. [107] and illustrated in Equation 5-1:

$$\sigma = \frac{1.5 \times F}{W \times D} \times \frac{L}{D} \qquad\qquad Equation\ 5-1$$

Here, F, L, W and D represent the flexural load, span length, specimen width and thicknesses, respectively. According to the equation, both coated samples had similar conditions, the only difference being shown through the test carried out on the workpieces; the thickness (D) was slightly smaller for one of the samples, which was attributed to the $\sim$ 270 μm coating layer added to the 4 mm workpiece. Furthermore, a clearly important step was to compare the different coatings. The thickness of both should have been the same; as the flexural strength decreases, the coating thickness should increase.

The flexural behaviour of the two different HVOF thermal spray-coated samples, along with the uncoated base metal, was examined using the three-point bending tests; these were repeated three times for consistency and the average recorded. The stress strain curve, as seen in Figure 5-26, showed a similar behaviour for the two As-sprayed coatings that were sprayed using the same coating system. In terms of flexural stress, the singular nWC-12Co coating had a higher flexural strength (622 MPa) than did the mixed coating and the uncoated substrate (601 and 503 MPa, respectively) for the same strain. Moreover, a higher force was needed to bend the singular nWC-12Co coating, in comparison to that required for the mixed coating and substrate (2.36, 2.28 and 1.68 kN, respectively).

The lower elastic limit for the mixed coating, in comparison to the nWC-12Co coating, can be attributed to the reduction of the coating stiffness (Young modules) when Inconel 625 was mixed with the nWC-12Co powder as a result of decreasing the ratio of the nanoscale WC carbides in the coating layer [17, 23]. Such a finding also appears in a study conducted

Novel Enhancement of HVOF Thermal Sprayed Nanostructured WC-12Co / Inconel-625 Coatings for Tribocorrosion Applications | **Al-Harbi, Naif I**

127

by Li et al. [108], who indicated that they incorporated titanium (10–20%) by volume as a reinforcement for the HVOF sprayed hydroxyapatite (HA) that coated the metallic surface; the overall Youngs modules then improved significantly. Furthermore, the nWC-12Co coating had a denser coating, with lower porosity and higher micro-hardness, which was also linked broadly to the higher ratio of the nano-scale WC in the monomial nWC-12Co in comparison to the mixed coating, as explained earlier. Similar trends were observed in two previous studies [17, 23], whose authors concluded that increasing the composition percentage of nanostructured WC-12Co in the coating over that of Inconel 625 would enhance the yield strength. Where the amount of load required for the coating to start bending was related to the coating hardness, the latter increased as further loading was needed to make it bend. In addition, because of the availability of high oxygen content that was scattered mainly along the Inconel 625 splats and, in particular, on either side of the coating, in the free surface region and in the bottom between the coating/substrate interface, as clarified earlier in the EDS element mapping in Figures 5–18 and the EDS of the various locations in the mixed coating in Figures 5–13, differences arose in the stiffness of the coating layer. This, in turn, triggered the crack initiation and propagation along either side of the coating layer.

Because the three-point bending was applied on the coated surface side, the coating section of the workpiece on the free side (top region) was subjected to compression stresses only. Meanwhile, internal stress developed on the bottom of the coating at the coating/substrate interface as a result of the compression-shearing force arising from the different stiffnesses between the coating and substrate. This created local stress concentrations, particularly in the defects sited between the coating/substrate material interface (high oxide content splats, porous strips at the coating/substrate interface, unmelted particles and micro-voids). This side of the coating was considered the most responsible for crack initiation, as reported in numerous experimental studies such as that carried out by Yilbas et al. [109] and those by Arif et al. and Dahham, which included simulation works [110, 111]. A notable point here is that generally, the stress located in the defects site is higher than the mean internal stresses and is usually the source of the cracks. Thus, as a result, when the critical stresses for the crack propagation reach either of the defects available in the coating/substrate interface, the crack will be initiated and, as the loading condition continues further during the test, the crack propagation will extend further until it divides the coating into two separate parts. Consequently, the internal stresses will finally be relaxed and relieved in the coating/substrate

Novel Enhancement of HVOF Thermal Sprayed Nanostructured WC-12Co / Inconel-625 Coatings for Tribocorrosion Applications | **Al-Harbi, Naif I**

128

interface, where the crack configuration and morphology are dependent on the type of powder selected as the coating and the thickness of the same, as reported by Watanabe et al. [112]. However, in general, the results showed that adding this small layer (~ 270 μm) of either of the coating types to the 4 mm-thick workpiece will significantly enhance its toughness and correspondent resistance to failure when bending. Figure 5-27 shows an optical photograph of the surface of the uncoated workpiece and the two coated samples after the three-point bending test. No signs of cracks are evident for the uncoated sample in comparison to those shown in the coated samples, which also explains the different behaviour of the plastic region between the two coated samples shown in Figure 5-26. Here, both samples show the breaking point as being between 2% and 3% for the deflection, which was not the case for the maximum deflection assigned earlier of 6% for the untreated sample. However, such behaviour is expected and considered typical of the flexural curve for the ductile metallic material, which is usually characterised as having long elongation before fracturing in the plastic region. Figure 5-27 and 5-28 shows the optical and the SEM images respectively under high magnification showing the morphology for the two coated samples after the three-point bending test. It is clear that the crack for the mixed coating looks smaller (Figure 5-28 B) and much narrower (closely spaced) in comparsion to the monomial nWC-12Co crack (Figure 5-28 A), which may be due to the higher ratio of metallic binder that may lead to smother crack propagation. In addition, higher ultimate bending strength along the stresses axis was reached by the monomial nWC-12Co (Figure 5-26).
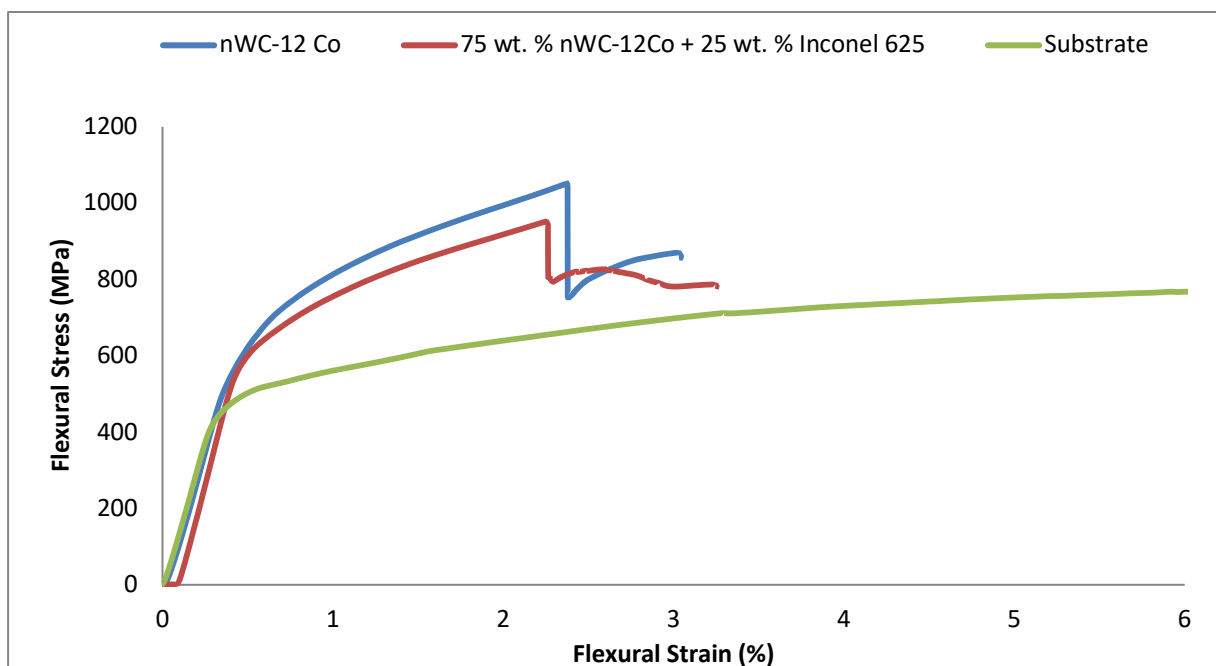
Figure 5-26: Flexural prosperity resulting from applying the three-point bending test to substrate and as-sprayed coatings.

Novel Enhancement of HVOF Thermal Sprayed Nanostructured WC-12Co / Inconel-625 Coatings for Tribocorrosion Applications | **Al-Harbi, Naif I**

129
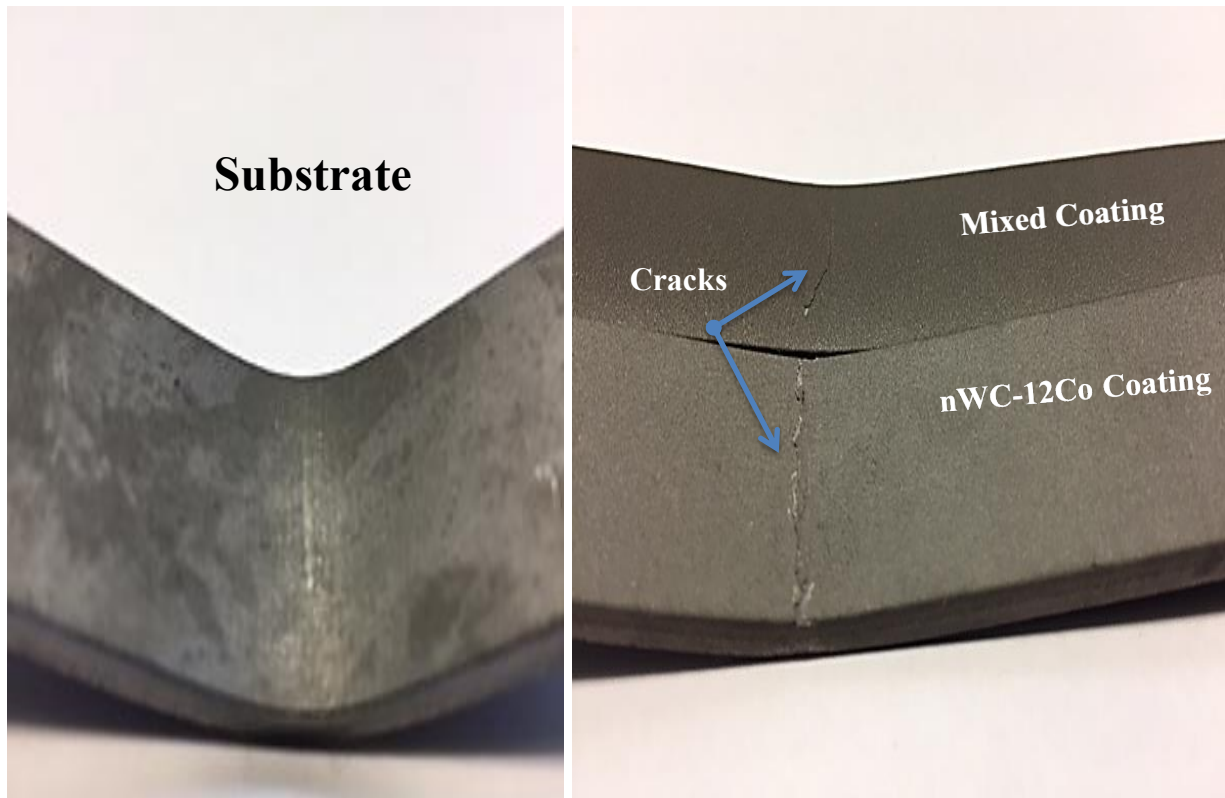
Figure 5-27: Optical photographs of the of the central regions of the substarte and two as-sprayed coatings after the three point bending test.
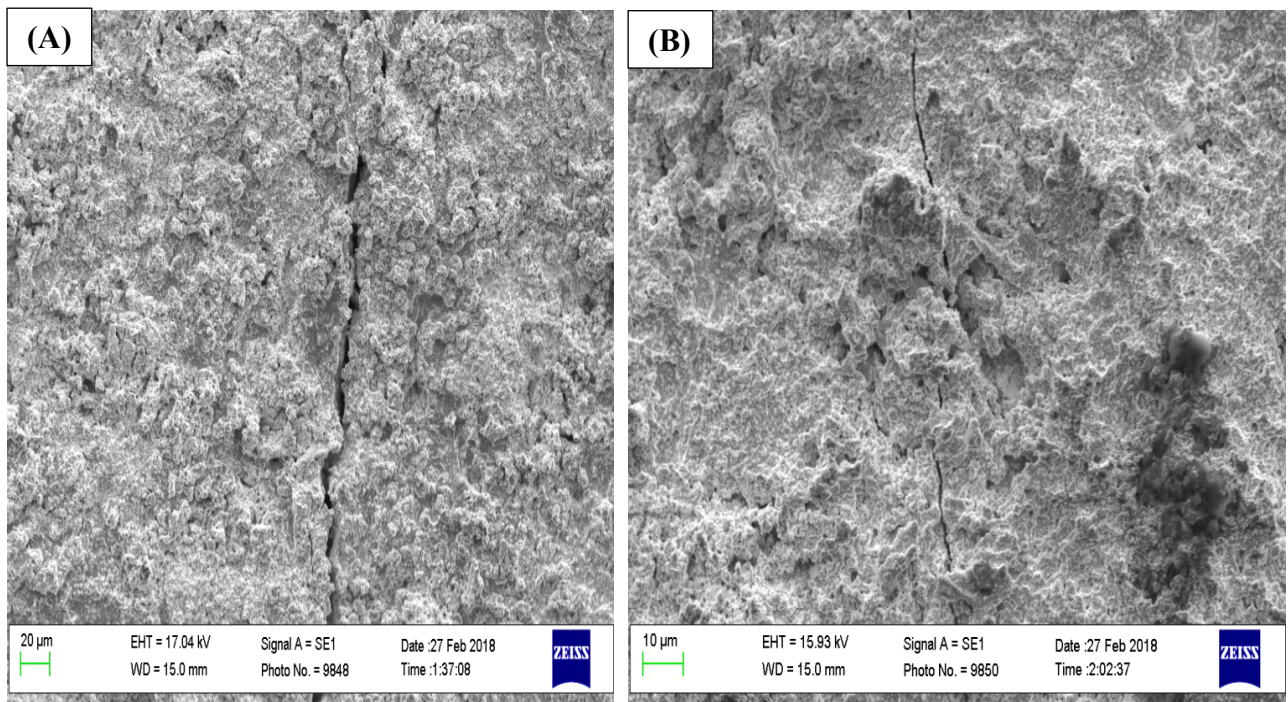
Figure 5-28: SEM micrographs with high magnification of the surface cracks inititation during the three point bending test for the two as-sprayed coatings; (A) monomial nWC-12Co coating and (B) Mixed coating.

Novel Enhancement of HVOF Thermal Sprayed Nanostructured WC-12Co / Inconel-625 Coatings for Tribocorrosion Applications | **Al-Harbi, Naif I**

130

5.3.8 Dry erosion test of the as-sprayed coatings

Dry erosion is considered one of the most widespread types of wear in the oil and gas industry. It is usually the result, as explained earlier in the literature chapter, of a high-energy impact by hard particles on the subjected surface in a dry environment. However, the erosion mechanism occurs to different degrees at various conditions, based on the particles' sizes and properties, the erosion angle, the environmental temperature during the erosion and so on. For this research, tests were carried out for all samples under the same conditions and according to ASTM G 73, as discussed in detail in the Experimental Methods chapter.

The results of the dry erosion of the two as-sprayed coatings and the uncoated workpiece are presented in Figure 5-29 in the form of mass loss (g). As can be clearly seen from the results, the monomial nWC-12Co coating showed the lowest mass loss, followed by the mixed coating, and finally the uncoated workpiece had the highest loss, that is 0.765g, 1.46g and 6.59g respectively. This also translates to an erosion rate of the mass loss over a 50-minute test period compared to the total mass (in percentage form) of 3.11%, 5.78% and 29.7% respectively.
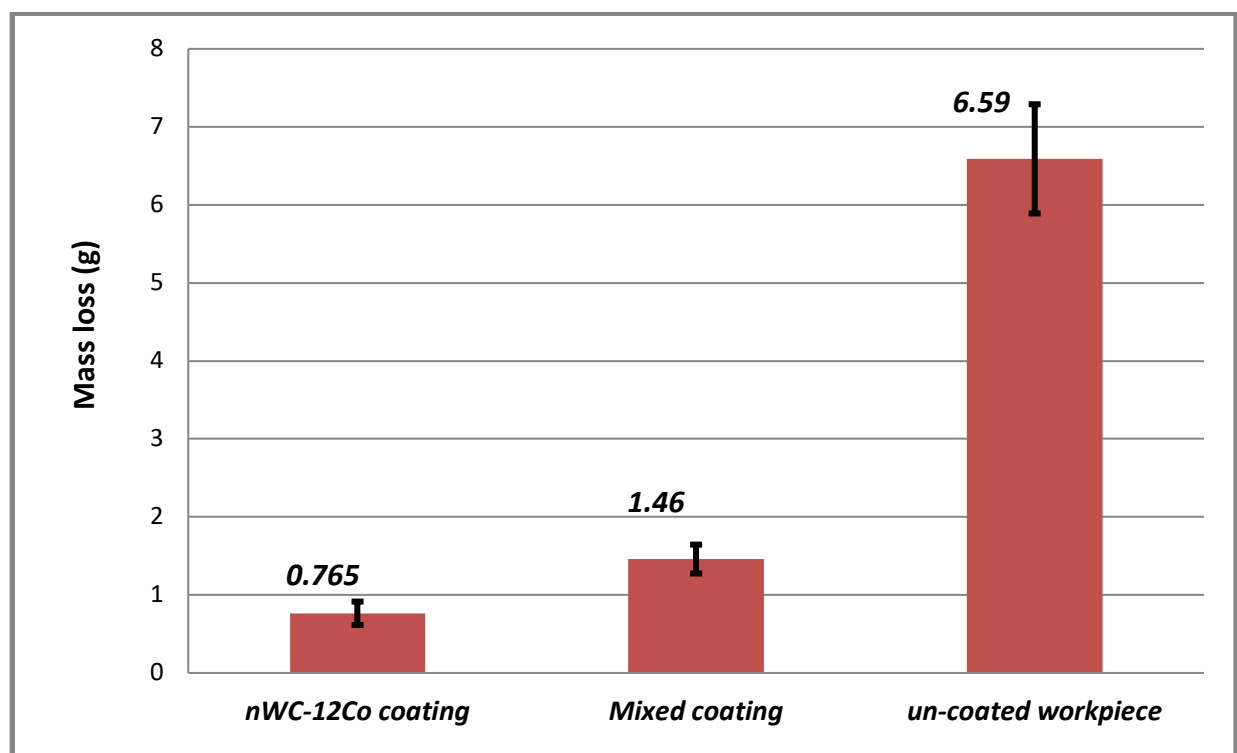
Figure 5-29: The mass losses resulting from dry erosion of the uncoated workpiece and the two as-sprayed coatings.

Novel Enhancement of HVOF Thermal Sprayed Nanostructured WC-12Co / Inconel-625 Coatings for Tribocorrosion Applications | **Al-Harbi, Naif I**

131

The lower mass loss for the nWC-12Co coating, compared to those for the mixed coating, is expected and may be linked for two different reasons. Firstly, it has a higher microhardness based on the average taken throughout the cross-section of the two coating layers (shown earlier in Table 5-4), or more importantly, for those measured close to the coating's top surface because this region will initially resist hard particles' impact on the surface. Secondly, the mixed coating has the highest presence of non-melted and semi-melted particles of the over the monomial nWC-12Co coating, which was also clarified earlier in the investigation into the surfaces of the two as-sprayed coatings and their corresponding roughness. The amount of unmelted particles plays a significant role in the erosion rate, along with crack propagation, as reported in the experimental work carried out by A1 Fadhli [113], who investigated the erosion and corrosion of Inconel-625 powder coatings when deposited on three different metallic surfaces. However, in general, the results show that the coating layer had a major impact in terms of reducing the erosion wear rate of the workpiece.

Figure 5-30 shows the eroded area of the two coated samples and the uncoated workpiece, indicating a strong correlation between the size and morphology of the eroded area, the ability of the surface to resist the eroded particles and the element composition of the target surface. For instance, the eroded area was much smaller for the monomial nWC-12Co coating surface and greater for the mixed coating and uncoated workpiece respectively. Furthermore, the surface topology of the monomial nWC-12Co coating was rough in appearance compared to the mixed coating and the uncoated workpiece, which looked the same. This may be attributed to the low amount of the soft binder matrices (12% cobalt) in the monomial nWC-12Co coating, with the result that when the eroded particles hit the coating surface, the WC nano-scale hard particles were pulled out or the full semi-melted powder particles were removed, leaving small pits in the eroded area.

Novel Enhancement of HVOF Thermal Sprayed Nanostructured WC-12Co / Inconel-625 Coatings for Tribocorrosion Applications | **Al-Harbi, Naif I**

132
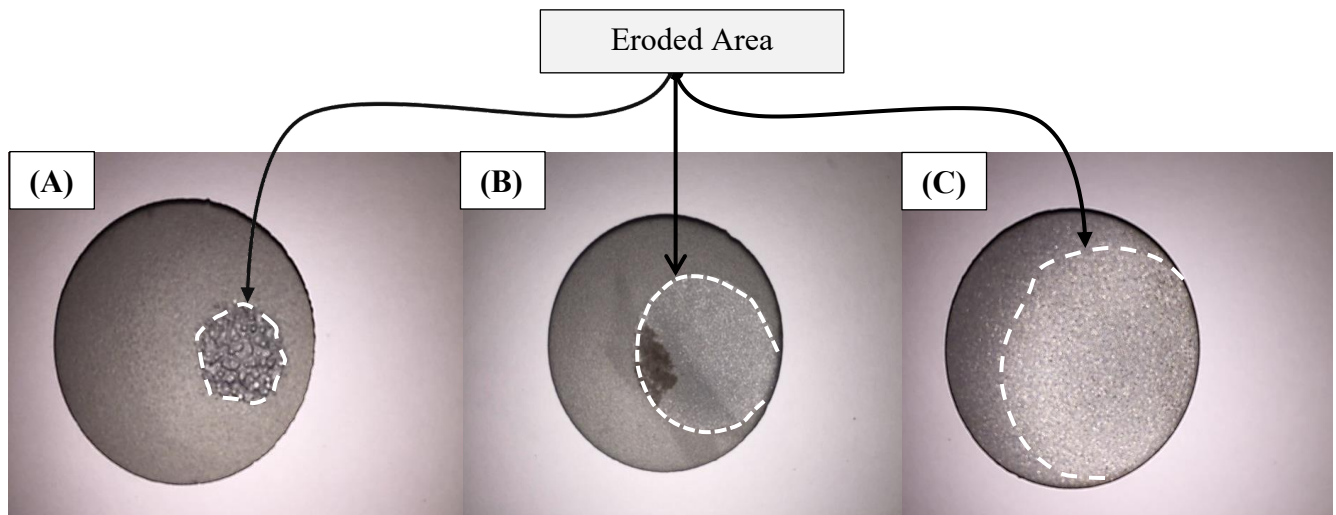
Figure 5-30: Optical photographs of the samples showing the eroded area for (A) nWC-12Co coating, (B) Mixed Coating and (C) Un-coated workpiece.

5.3.9 Slurry erosion test of the as-sprayed coatings

The results of the slurry erosion-corrosion testing for the the two as-sprayed coatings and the uncoated workpiece are presented in Figure 5-31 in terms of mass loss. However, as previously mentioned, this wear type is considered the most common for slurry handling equipment and results in huge maintenance costs for companies, due to equipment failure, material replacement, and downtime. The only difference between this wear mechanism and dry erosion wear is the presence of the corrosive liquid during the wear processing.

The test results and the microscope images, can be seen in Figures 5-31 and 5-32 respectively, each of which reveal that no significant erosion-corrosion damage was observed for the two as-sprayed coatings and the uncoated workpiece after exposure to erosion-corrosion, in contrast to the damage noted for the dry erosion. Two reasons for this difference are possible. One explanation is that the slurry solution that remained on the surface might have reduced the abrasion impact of the grit particles. A second possible reason for the different results is that the grit sand particles were sprayed at the target surface at a lower speed, according to the standard followed: the dry erosion test was carried out at 7 bar of pressure and the slurry erosion at 6 bar. However, the results for the dry erosion followed the same pattern, with the monomial nWC-12Co coating showing the lowest mass loss (within 0.29 g), followed by the mixed coating's mass loss (within 0.41 g), and finally the uncoated workpiece's mass loss (within 0.75 g). The explanation for the greatest coating material loss

Novel Enhancement of HVOF Thermal Sprayed Nanostructured WC-12Co / Inconel-625 Coatings for Tribocorrosion Applications | **Al-Harbi, Naif I**

133

for the mixed coating (almost four times greater) is the same as that for the dry erosion result: due to the hardness of the material and the higher number of unmelted particles with their corresponding lower microstructure porosity.
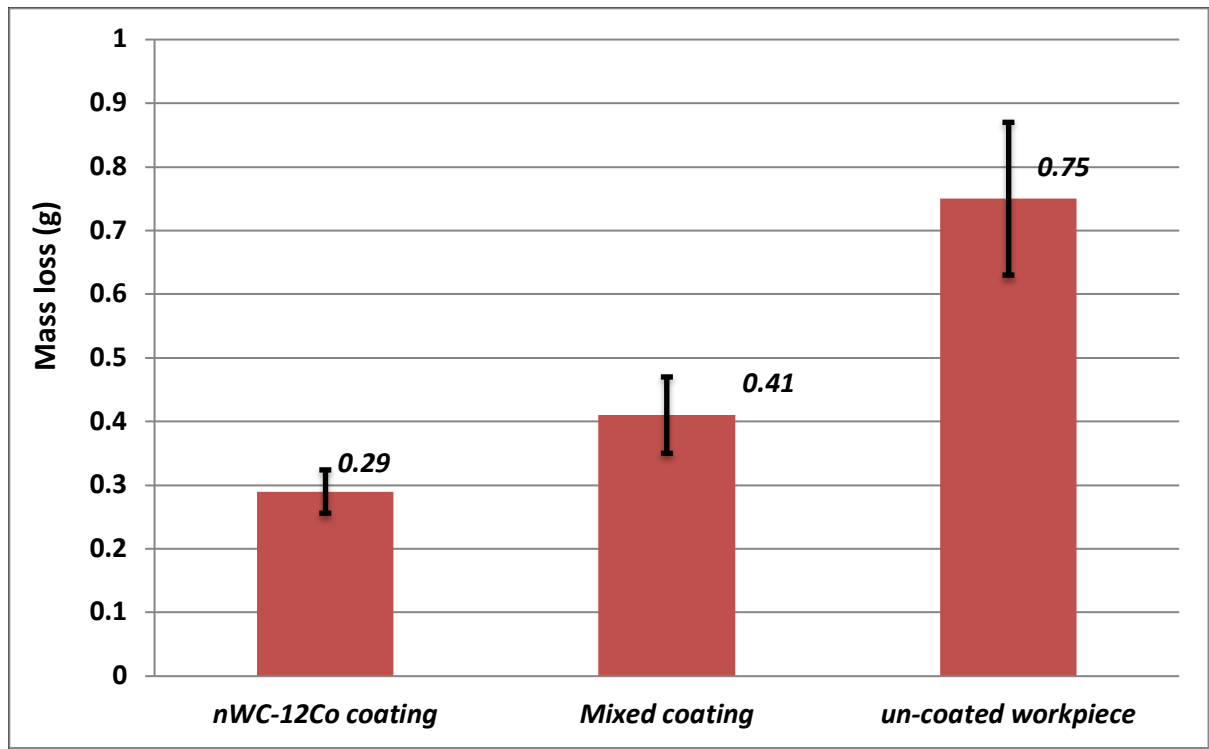
Figure 5-31: The mass loss resulting from slurry erosion of the uncoated workpiece and the two as-sprayed coatings.

Figure 5-32 presents the microscopic images taken after corrosive liquid contact and then after the grit blasting process. Clearly, the corrosion effect for the uncoated sample is very high in comparison to the two coated samples, with yellow discolouration affecting much of the workpiece sample. By contrast, in the coated samples, the effects of 48 hours of contact of the corrosive liquid appeared to be insignificant and are characterised by yellow spots that are scattered over the coating surface. Furthermore, after the erosion process, the corroded region was completely removed from the two coated samples, but not from the uncoated workpiece, revealing that the corrosion penetrated deeper into the uncoated sample.

Novel Enhancement of HVOF Thermal Sprayed Nanostructured WC-12Co / Inconel-625 Coatings for Tribocorrosion Applications | **Al-Harbi, Naif I**

134
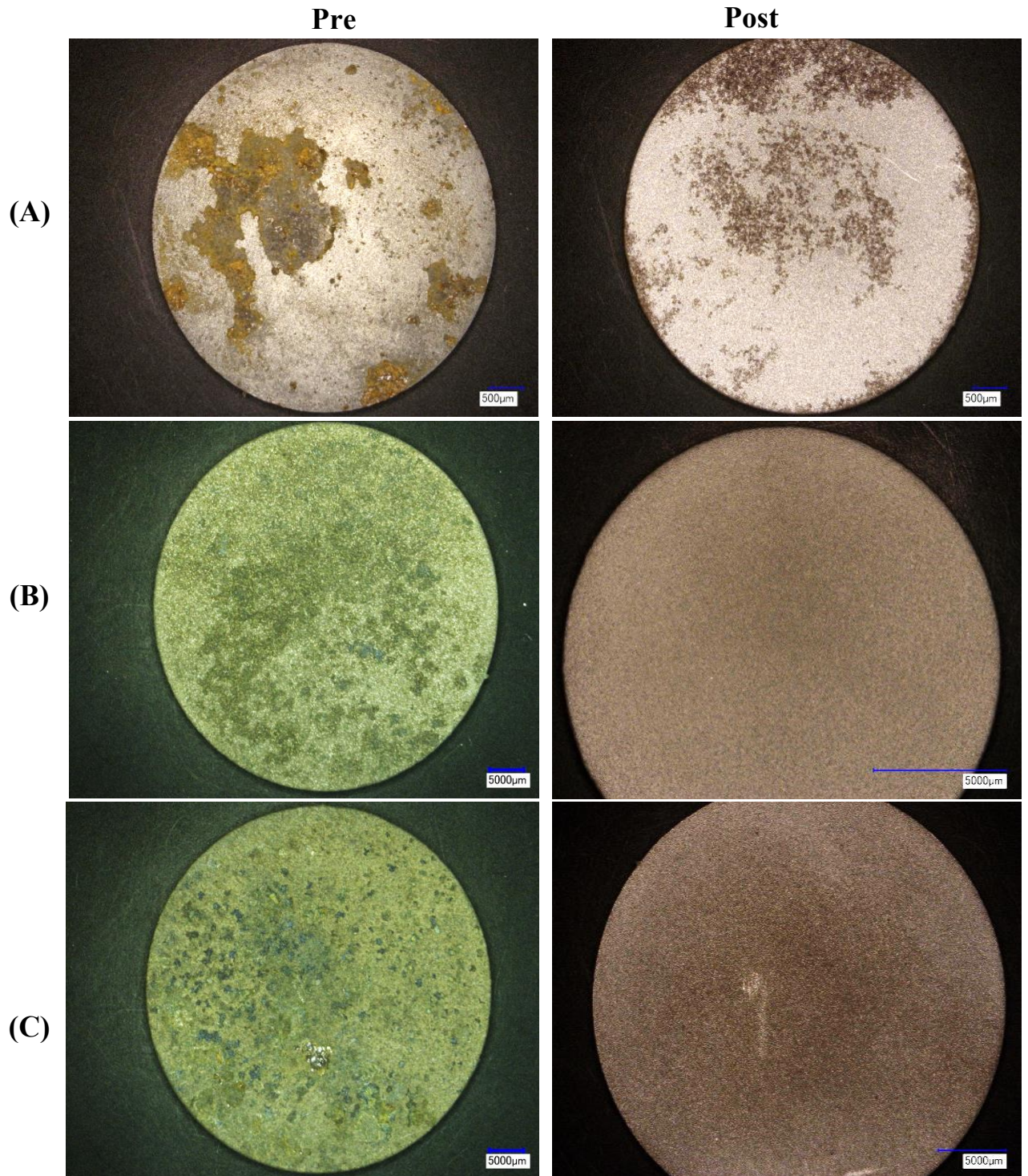
Figure 5-32: Microscopic images of the samples showing the eroded area for (A) Uncoated workpiece, (B) Mixed coating, and (C) Monomial nWC-12Co coating, pre (after contact with corrosion liquid) and post grit blasting.

5.4 Summary of the results of the as-sprayed coatings

➤ The surface of the two coating types (monomial nWC-12Co and mixed) showed some unmelted particles with pores, micro-crevices, and micro-cracks.

➤ The surface roughness along with surface ratio was slightly lower in monomial nWC-12Co coating in comparison to the mixed coating. This could be attributed to the increased tungsten carbide (WC) nanoscale particles content. The R_{qa} was $\sim$ 5.58 μm for the mixed and $\sim$ 5.24 μm for monomial nWC-12Co HVOF Coating.

➤ The cross section of the two HVOF coatings show lamellar splat structure with some defects, such as porosity, micro-separation (porous strips) along the coating/substrate interface, and lack of chemical homogeneity.

➤ The monomial nWC-12Co coating shows lower porosity percentage compared to the mixed coating, which contributed to the large amount of unmelted or semi-melted particles, and this created interconnected porous holes between coating droplets between the Inconel 625 and nWC-12Co particles.

➤ The EDX analysis showed the presence of high oxides in Inconel 625 splat boundaries in comparison to the centre region, where the porosity in the monomial nWC-12Co was located around the region with a high tungsten carbide rate.

➤ The microhardness and flexural strength for monomial nWC-12Co was higher than the mixed coating; this contributed to a higher WC hard particle content. This may also be due to the smaller amount of micro-cracks and pores in the coating layer.

➤ The phases observed by XRD for the monomial nWC-12Co stock powder were WC and Co, while the phases observed in mixed stock powder were WC, NiCrCo, NiCr, Cr and Ni. After the coating process, most phases were retained except for the disappearance of one of the cobalt (Co) peak along with the formation of a W_2C new crystalline phase in the nWC-12Co HVOF coating, and W_2C and Co_6W_6C in the mixed coating. A free peak of cobalt was also evident as a joint reaction with Nikel (Ni) and Chromium (Cr) formed for the mixed coating, suggesting that it appeared as a reaction with Tungsten, Chromium and Carbon to form Co_6W_6C and CrCo phases respectively.

➤ The results for the dry erosion and slurry erosion demonstrated the best performance for the monomial nWC-12Co coating, in comparison to the mixed coating in the form of mass loss. This contributed initially to the higher microhardness, especially for those measured close to the coating's top surface, because this region will initially resist the hard particle impact on the surface, and the amount of unmelted particles.

Novel Enhancement of HVOF Thermal Sprayed Nanostructured WC-12Co / Inconel-625 Coatings for Tribocorrosion Applications | **Al-Harbi, Naif I**

136

5.5 Melt pool geometry of the laser treated coatings

Experiments have been carried out to investigate the effects of laser processing conditions, based on their impact on the melt pool's dimensions. By understanding and predicting the geometry of the melt pool's profile behaviour, the hope is that this can be linked to the coating integrity and the resultant mechanical and wear properties of the two coating types. Furthermore, by selecting the appropriate laser processing settings for any future work, the required melt pool can be reached and the overlap movement assigned according to the setting selected. As explained earlier in Chapter 4 and the published work [72], a high rate of dilution from the substrate, as the result of an extreme melting depth, can deteriorate the properties of the coating material by mixing them with the substrate properties, which are usually lower. Meanwhile, selecting inappropriate overlapping without taking into account the changes made to the track width by the setting chosen will yield inconsistent results and may create an unnecessary addition of heat to the treated zone, potentially resulting in an inhomogeneous microstructure.

Various research studies have been conducted on the influence of laser processing parameters on the melt pool's geometry. One of these was, carried out by White et al. [114], which focused on ALSiMg alloy powder treated with an M2 SLM fibre laser machine. The Analysis of Variance (ANOVA) and a response thick plate numerical model were used to analyse the data for three control factors—laser power; scanning speed; and hatch spacing (as they related to two different responses, track width and melt depth). The results indicated that, as the energy per unit increased, such as through the use of low scanning speed, high power and low hatching spacing, so did the melt pool's depth and track width. In a mathematical analysis conducted by Al-Taha [21], who used lump parameter techniques to predict the melt depth as a function of laser power on Inconel 625 coating, cladded using a 1.5 kW diode laser by WC particles at three different percentages (0%, 9.3% and 47%), the prediction of the melt pool agreed with the trend of the experimental findings. As both these studies showed, the melt depth increased when the laser power was increased. However, for the measurements recorded at different locations, a significant error was shown between the results. In this case, assumptions were made during the numerical analysis as follows: the coating would have constant thermal properties, a homogeneous structure and a uniform laser melting process. Furthermore, the author reported that the constitution of the coating material played a significant role in the melt depth's behaviour.

Novel Enhancement of HVOF Thermal Sprayed Nanostructured WC-12Co / Inconel-625 Coatings for Tribocorrosion Applications | **Al-Harbi, Naif I**

137

Four laser tracks were created for each run. The measurements were taken in the normal scanning direction, the melt pool's width and depth measured for each sample in four different locations, and the average taken. The measurements were taken at the edge of the heat-affected zone, as shown in Figures 5-34 and 5-35. Notably, it was extremly difficult to identify the melt zone's, especially for laser settings that produced a low energy input such as P.S.7, P.S.3 and P.S.5.

Two interesting phenomena were noted (as shown in Figure 5-36) the tracks' width was magnified at the edges of the sample as the laser travelled back and forth. This may have contributed to the short residence time between the laser beam leaving the sample and returning again to make the next track, whereby the latter would be preheated by the immediate vicinity of its predecessor. Moreover, the track width and depth of the laser tracks were consistent in their dimensions, after the second track because the first two passes stabilised the inherited heat that formed between the laser tracks, as shown in Figure 5-34 (B).
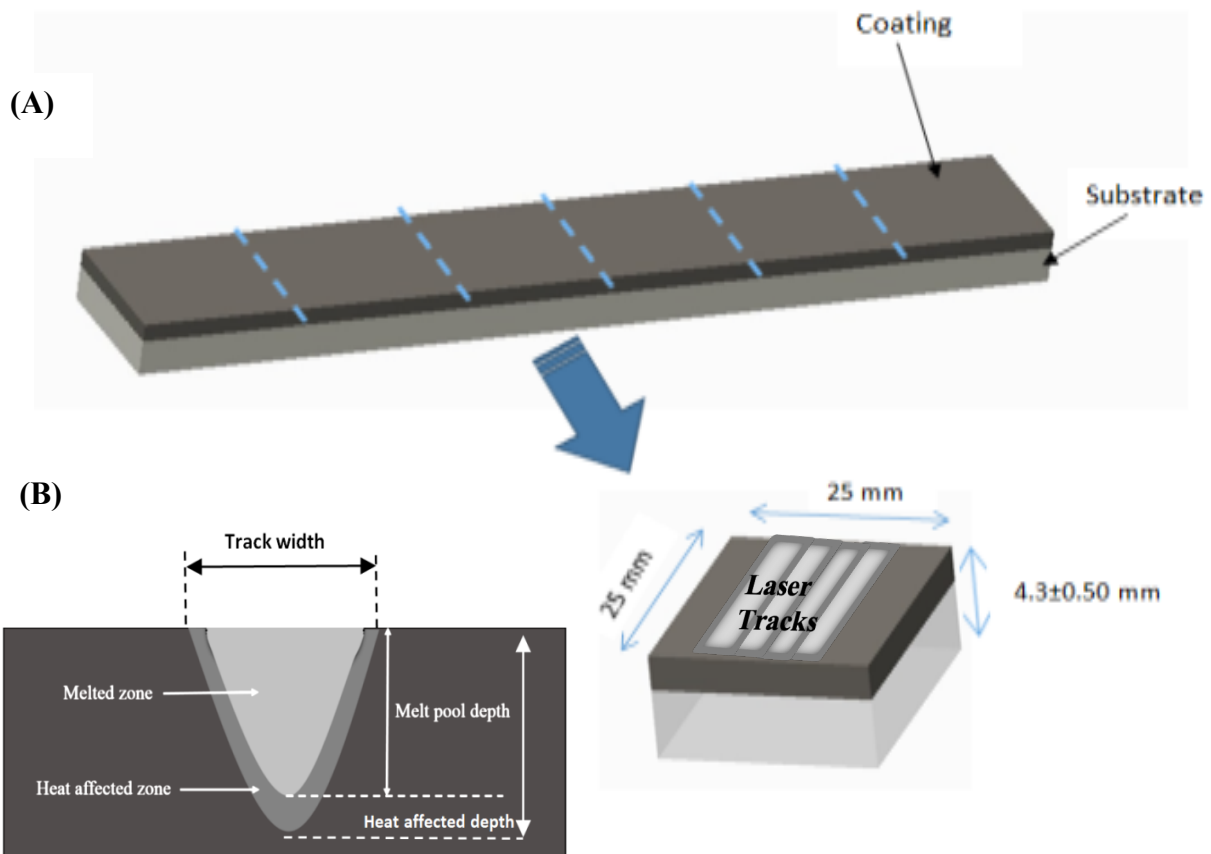
Figure 5-33: (A) Schematic diagram of the sample's dimensions prepared for laser processing and (B) schematic diagram showing melt pool profile and geometry for a single laser track.

Novel Enhancement of HVOF Thermal Sprayed Nanostructured WC-12Co / Inconel-625 Coatings for Tribocorrosion Applications | **Al-Harbi, Naif I**

138
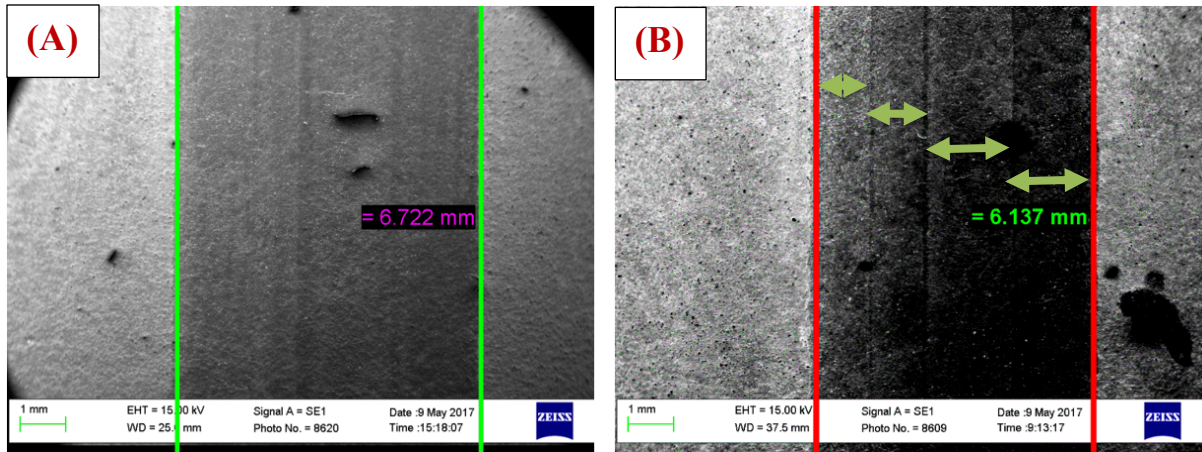
Figure 5-34: Measuring melt pool width for (A) P.S.6 for nWC-12Co coating and (B) P.S.11 for the mixed coating. Track width increased gradually in the first passes (left to right).
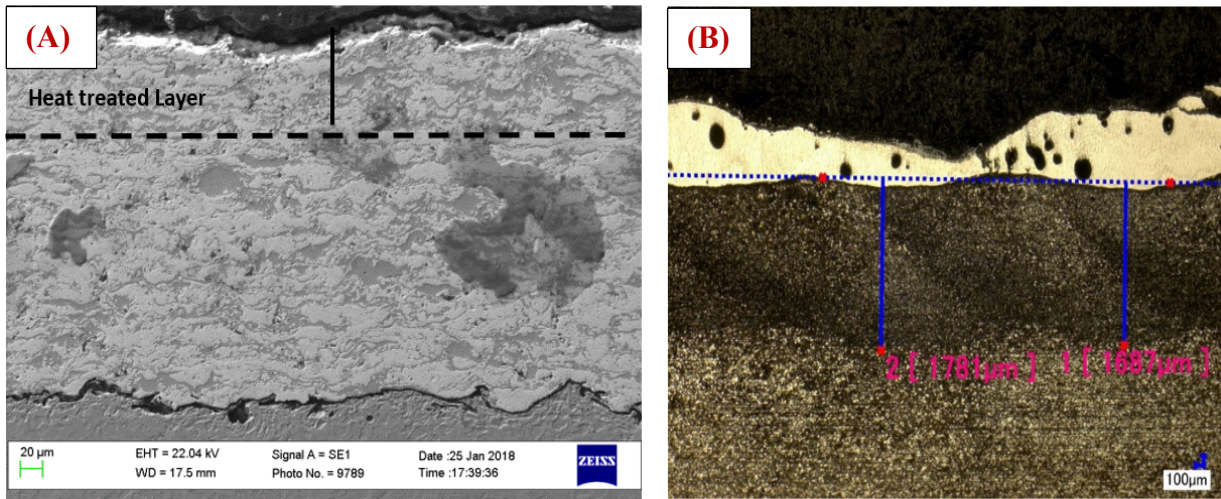
Figure 5-35: Measuring melt pool depth for the mixed coating for (A) P.S.11 within partial melting and (B) P.S.6 with high melting depth, creating dilution from the substrate.
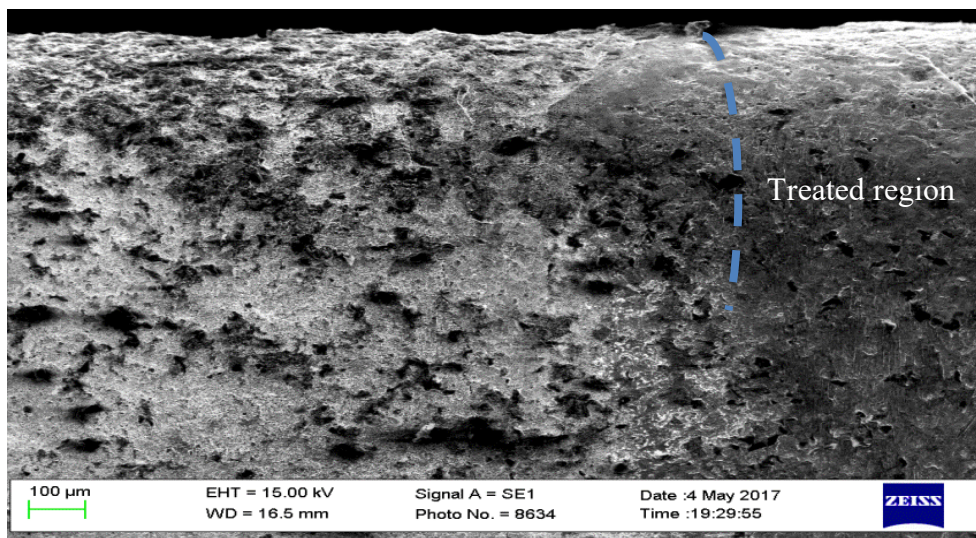
Figure 5-36: SEM image of the sample edge without sectioning, showing the laser track magnifying in width at the edge.

Novel Enhancement of HVOF Thermal Sprayed Nanostructured WC-12Co / Inconel-625 Coatings for Tribocorrosion Applications | **Al-Harbi, Naif I**

139

Figures 5-37 and 5-38 show the variation of the melt pool dimensions according to the various laser settings. In the results, the significant effects of the laser condition selected in the melt pool geometry can be clearly seen. However, for both figures, the results show that the change in the mixed coating for each of the laser settings was greater, matching the results found earlier in the operation windows created in Chapter 4 for selecting the optimal level of the three control factors. Overall, the P.S.6 laser setting provided the highest change for both melt depth and width for both coating types.
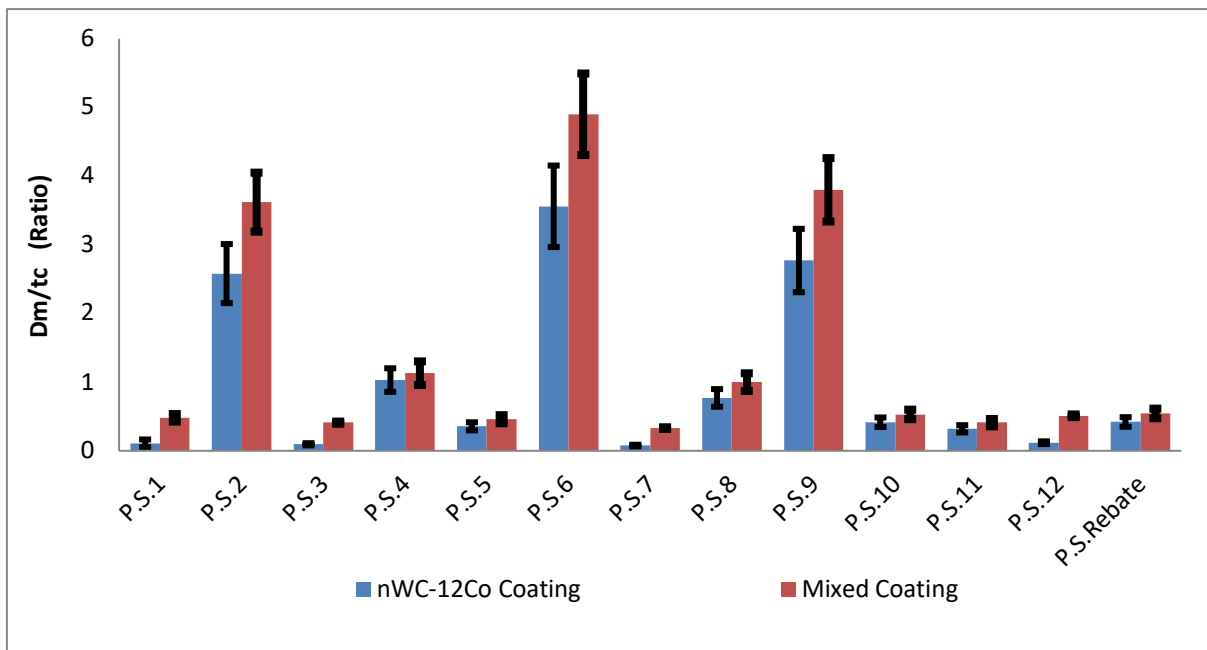
Figure 5-37: Melt depth to the coating ratio (D_m/t_c) for the laser-treated two coatings tested using various laser settings.
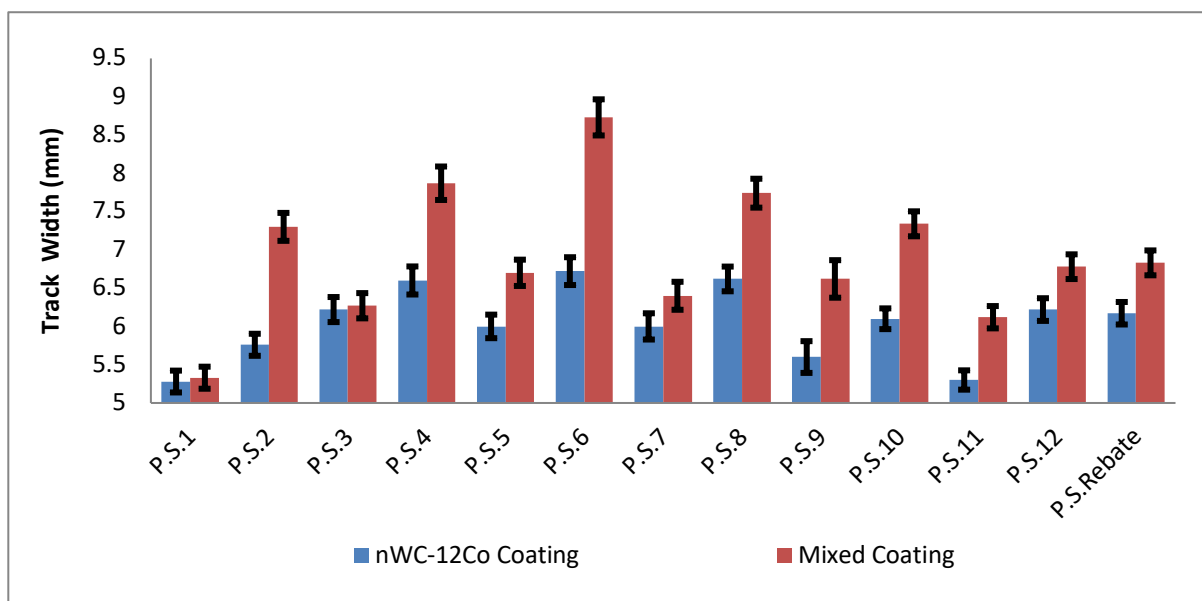
Figure 5-38: The average of four tracks width for the laser-treated two coatings tested using various laser settings.

Novel Enhancement of HVOF Thermal Sprayed Nanostructured WC-12Co / Inconel-625 Coatings for Tribocorrosion Applications | **Al-Harbi, Naif I**

140

5.5.1 Development of the mathematical model for track width dimension

It should be noted that at the start, the width of the four tracks apart from the modification carried out by the laser processing condition inputs were equal to 5.52, 6.24, and 6.96 mm for focal positions +35, +40, and +45 mm, respectively.

The Design of Experiment V7 software was used to derive the mathematical model to show the effects of the considered input factors: laser power, focal position, and scanning speed to the width of the heat-affected zone of four tracks that were measured at the top surface. The ANOVA tables for both laser-treated coatings are shown in Table 5-5 and Table 5-6. The quadratic model was selected to fit the data for both laser-treated coatings as it showed all three variables and their significance levels within each coating. In this study, various acceptable levels were determined in order to evaluate the two coating models. To begin with, model probability (significance) and lack of fit probability (non significance) had to satisfy a criteria of < 0.05 for a variable to be termed significant. In a 95% confidence interval, a probability of above 0.05 was required to justify a null hypothesis. In the situation where the probability was less than 0.05, the null hypothesis was rejected and concluded that there is a significant difference.

In terms of the R values, an acceptable level for R^2 was, found to rest between 0.6 and 1. In a regression model, R squared represents the extent to which variables are dependent on each other and ranges from 0 to 1. Zero in a regression model represents no dependence, while 1 represents total dependence. R squared represents the magnitude of dependence, not the type of dependence. The acceptable level for predicted R^2 – adjusted R^2 should be ≤ 0.2, while the, acceptable levels for adequate precision should be > 4. Table 5-5 and 5-6 shows the results obtained in the analysis. Clearly, the data presented in the ANOVA tables for both laser-treated coatings indicate that the modules match the acceptable levels assigned.

From the ANOVA tables, the power and focal position were the primary factors for controlling the track width of the laser-treated monomial nWC-12Co, and the scanning speed was a secondary effect; whereas for the laser-treated mixed coating, all three factors—power, scan speed, and focal position—had a strong influence on width. Significant interactions up to the second order can be observed for all three factors for both laser-treated coating types, indicating that the response was not linear and would be very sensitive to change in the levels of each of the factors.

Novel Enhancement of HVOF Thermal Sprayed Nanostructured WC-12Co / Inconel-625 Coatings for Tribocorrosion Applications | **Al-Harbi, Naif I**

141

Source	Sum of Squares	DF	Mean Square	F value	Prob > F	
Model	0.0021	6	0.0004	78.22	< 0.0001	significant
A-Laser Power	*0.0004*	*1*	*0.0004*	*95.49*	*< 0.0001*	
B-Focal Position	*0.0011*	*1*	*0.0011*	*242.28*	*< 0.0001*	
C-Scanning Speed	*0.0000*	*1*	*0.0000*	*2.38*	*0.1542*	
BC	*0.0000*	*1*	*0.0000*	*9.81*	*0.0107*	
A²	*0.0001*	*1*	*0.0001*	*14.65*	*0.0033*	
B²	*0.0005*	*1*	*0.0005*	*108.80*	*< 0.0001*	
Residual	*0.0000*	*10*	*4.488E-06*			
Lack of Fit	*0.0000*	*6*	*5.362E-06*	*1.69*	*0.3186*	*not significant*
Pure Error	*0.0000*	*4*	*3.176E-06*			

R-Squared   **0.97**   Adj.R^2 = 0.96

Adeq.Precision = 28.91   Pred.R^2 = 0.92

Table 5-5: ANOVA analysis for laser-treated monomial nWC-12Co coating track width.

Source	Sum of Squares	DF	Mean Square	F value	Prob > F	
Model	9.21	8	1.15	385.11	< 0.0001	significant
A-Laser Power	*6.02*	*1*	*6.02*	*2014.79*	*< 0.0001*	
B-Focal Position	*1.04*	*1*	*1.04*	*349.39*	*< 0.0001*	
C-Scanning Speed	*0.6903*	*1*	*0.6903*	*231.02*	*< 0.0001*	
AB	*0.0342*	*1*	*0.0342*	*11.45*	*0.0096*	
AC	*0.1190*	*1*	*0.1190*	*39.83*	*0.0002*	
A²	*0.2979*	*1*	*0.2979*	*99.70*	*< 0.0001*	
B²	*0.7130*	*1*	*0.7130*	*238.60*	*< 0.0001*	
C²	*0.3505*	*1*	*0.3505*	*117.28*	*< 0.0001*	
Residual	*0.0239*	*8*	*0.0030*			
Lack of Fit	*0.0146*	*4*	*0.0037*	*1.58*	*0.3351*	*not significant*
Pure Error	*0.0093*	*4*	*0.0023*			

R-Squared   **0.99**   Adj.R^2 = 0.99

Adeq.Precision = 84. 3   Pred.R^2 = 0.97

Table 5-6: ANOVA analysis for laser-treated mixed coating track width.

Novel Enhancement of HVOF Thermal Sprayed Nanostructured WC-12Co / Inconel-625 Coatings for Tribocorrosion Applications | **Al-Harbi, Naif I**

142

The final mathematical models for both laser-treated coatings' track width in terms of coded factors, which can be used to make predictions about the response for given levels of each factor were found to be as follows:

nWC-12Co Coating (Track Width) = +0.16 - 7.319E-003 * A - 0.012 * B + 1.155E-003 * C +1.632E-003 * AB + 5.730E-004 * AC -3.318E-003 * BC - 3.958E-003 * A^2 + 0.011 * B^2 + 2.087E-004 * C^2 *Equation* $5-2$

Mixed Coating (Track Width) = +6.84 + 0.87 * A + 0.36 * B -0.29 * C - 0.093 * AB -0.17* AC - 0.015 * BC + 0.27 * A^2 - 0.41* B^2 + 0.29* C^2 *Equation* $5-3$

Where A is laser power, B is focal position and C is scanning speed and the equation in terms of coded factors can be used to make predictions about the response for given levels of each factor. By default, the high levels of the factors are coded as +1, and the low levels of the factors are coded as -1. The coded equation is useful for identifying the relative impact of the factors by comparing the factor coefficients. It should be noted here that the first numbers in both equations are constants (0.16 and 6.84*)*.

From the above equations one can rank the dependence as follows: $-B > B^2 >> -A > -A^2 > -BC > AB > C > AC > C^2$ for the monomial nWC-12Co coating. It can be establish that for the laser-treated monomial nWC-12Co coating, the focal position (B) had the highest effect amongst the three factors both as itself (B) and squared (B^2) on track width, followed by laser power (A); the scanning speed (C) was one of the lowest. In addition, as an interaction, the focal position and scanning speed combination (BC) had the most significant relationship in terms of track width.

Ranking the dependence of the laser treated mixed coating results: $A > -B^2 > B > -C = C^2 > A^2 > -AC > -AB > -BC$. Here, the laser power was the most significant factor in track width as individual (A) and focal position as squared (B^2) followed by focal position (B). For the laser-treated mixed coating, the laser power and scanning speed (AC) combination also exhibited the most significant relationship. Generally, the model for the laser-treated mixed coating was statistically more significant in track width response compared to the laser-treated monomial nWC-12Co coating model. However, the difference between the two was very small as the R squared values were 0.99 and 0.97 for the mixed coating and the monomial nWC-12Co coating, respectively.

Novel Enhancement of HVOF Thermal Sprayed Nanostructured WC-12Co / Inconel-625 Coatings for Tribocorrosion Applications | **Al-Harbi, Naif I**

143

Figure 5-39 is a normal plot for laser-treated monomial nWC-12Co coating (track width), showing that the residuals had a linear relationship, which indicated that the residuals were normally distributed. Therefore, ANOVA could be carried out on observations for the track width of this laser-treated coating.
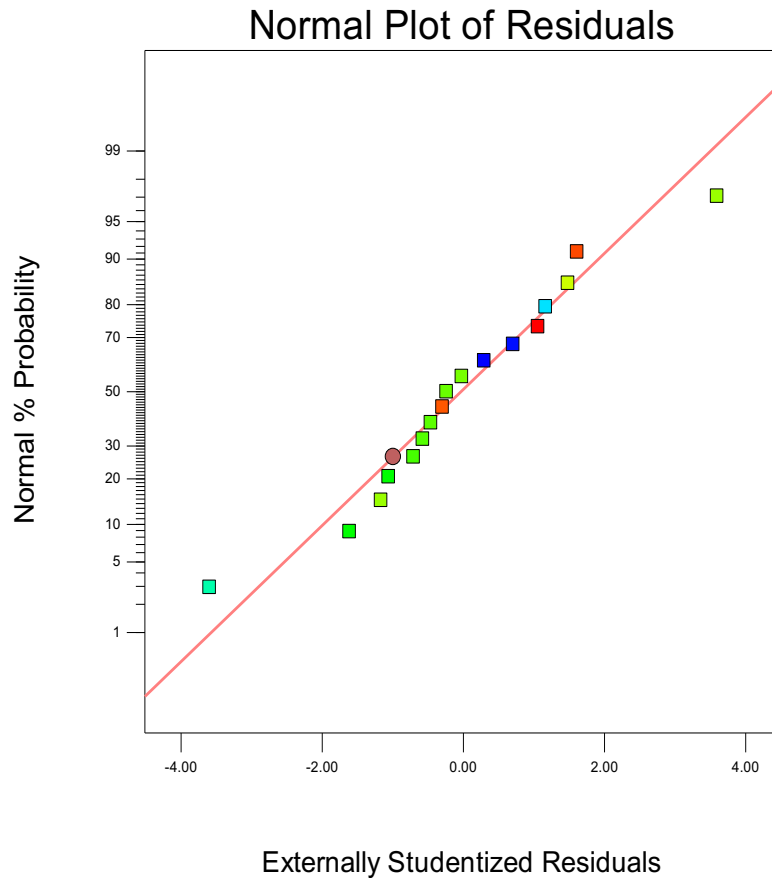
Figure 5-39: Normal plot residual of laser-treated monomial nWC-12Co coating track width (mm).

In addition, the relationship between the actual and predicted value was linear, indicating that the difference between them was small as shown in Figure 5-40 for the monomial nWC-12Co coating (track width). The same criterion was observed for the mixed coating track width, and for the sake of brevity, is provided in Appendix A-1 of this research.

Novel Enhancement of HVOF Thermal Sprayed Nanostructured WC-12Co / Inconel-625 Coatings for Tribocorrosion Applications | **Al-Harbi, Naif I**

144

Figure 5-40: Predicted versus actual plot for laser-treated monomial nWC-12Co coating track width (mm).

The final mathematical model determined by the DOE software for both laser-treated coatings to be used to predict the optimized values of track width response with regards to actual factors is given in Equation 5-4 and 5-5.

nWC-12Co Coating (Track Width) = +0.89211-2.30259E-005 * Laser Power - 0.035533 * Focal Position + 3.33483E-004 * Scanning Speed + 3.26314E-006 * Laser Power * Focal Position + 7.64051E-008 * Laser Power * Scanning Speed - 8.84703E-006 * Focal Position * Scanning Speed - 3.95757E-007 * Laser Power² + 4.29706E-004 * Focal Position² + 3.70948E-008 * Scanning Speed²   Equation 5 − 4

Mixed Coating (Track Width) = -22.92025 +7.95000E-003 * Laser Power + 1.44430 * Focal Position - 0.019647 * Scanning Speed - 1.85000E-004 * Laser Power * Focal Position - 2.30000E-005 * Laser Power * Scanning Speed - 4.00000E-005 * Focal Position * Scanning Speed + 2.66000E-005 * Laser Power² - 0.016460 * Focal Position² + 5.12889E-005 * Scanning Speed²   Equation 5 − 5

Novel Enhancement of HVOF Thermal Sprayed Nanostructured WC-12Co / Inconel-625 Coatings for Tribocorrosion Applications | **Al-Harbi, Naif I**

145

5.5.2 DOE results of track width

For track width analysis, the main factors of concern (as explained in paragraph one of 5.5.1) were the laser power (A) and scanning speed (C), it is reasonable to state that the increase of the track width is a function of increasing the beam size, controlled by increasing the focal position height (B). Figures 5-41 and 5-42 illustrate the perturbation plot, showing the effects of each of the three factors on the track width of both laser-treated coatings. From the graphs, it can be observed that track width increased with increasing laser power. In the same manner, one can argue that track width reduced slightly in almost linear manner with increasing scanning speed. This finding can be used to prove that track width was directly proportional to an increase in the energy input either by increasing the laser power level or increasing the interaction time controlled by the scanning speed in a quadratic manner (A, A^2, C, and C^2 terms in the coded equations). From the two perturbation plots, one can establish that the behaviours of both coatings regarding the laser conditions were similar. However, it can be noted that the rate of the track width change for the mixed coating was higher than that of the monomial nWC-12Co coating. This happened, as explained earlier, due to the higher WC hard particle content; as a result, the temperature conductivity rose along with its gradient in the treated coating [24, 54]. Furthermore, a significant difference can be clearly observed between the two levels of focal position (B) of +35 mm and +45 mm in the rate of broadening the track width. This might be attributed to a reduction of the power density as the beam size increased with raising the focal position (B). The most appropriate conclusion that can be drawn from the mathematical model relation developed is that there was direct proportionality between increasing the laser power, focal position, and track width and inverse proportionality between increasing the scanning speed and track width.

Novel Enhancement of HVOF Thermal Sprayed Nanostructured WC-12Co / Inconel-625 Coatings for Tribocorrosion Applications | **Al-Harbi, Naif I**

146
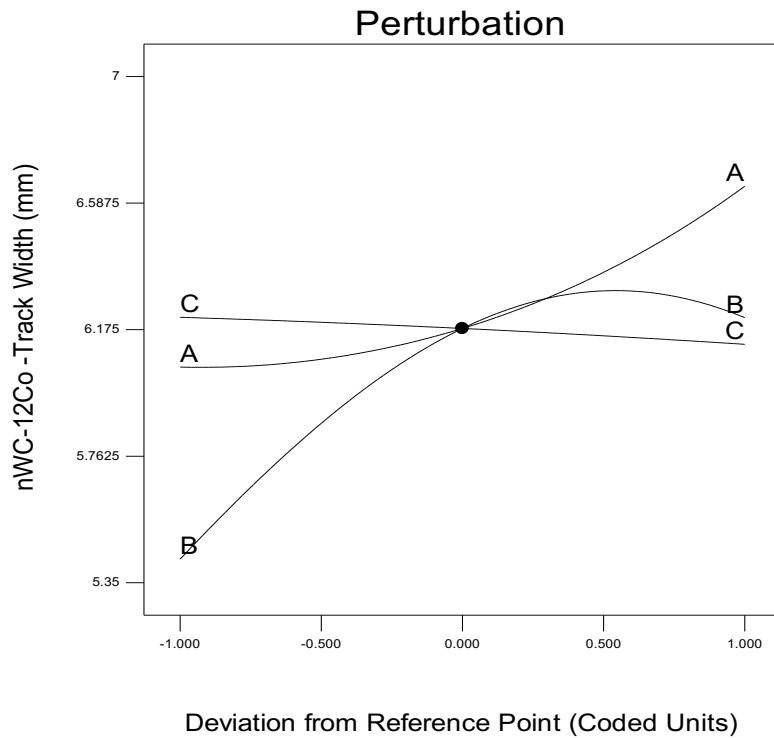
Figure 5-41: Perturbation plot for laser-treated monomial nWC-12Co coating track width.
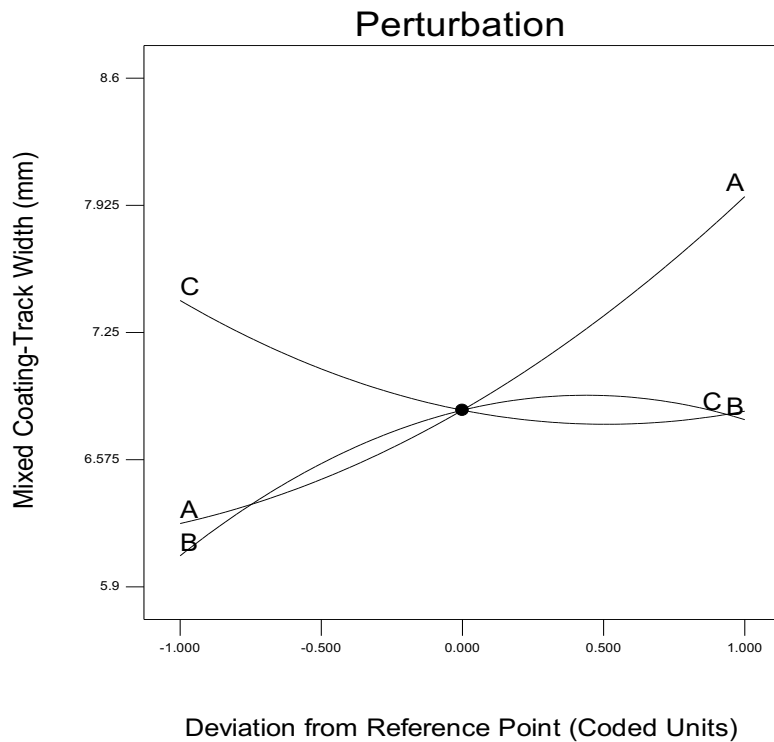
Figure 5-42: Perturbation plot for laser-treated mixed coating track width.

Novel Enhancement of HVOF Thermal Sprayed Nanostructured WC-12Co / Inconel-625 Coatings for Tribocorrosion Applications | **Al-Harbi, Naif I**

147

5.5.3 Development of the mathematical model for melt depth dimension

In this case, melt depth, was observed, this is the perpendicular height of the bore created during the process of melting. In order to understand the impact of both coatings and the relationship between these coatings and melt depth, the ratio of melt depth to coating thickness (D_m/t_c) was applied. This ratio was established by dividing the depth of the bore created during the process of melting by the thickness of the respective coating. The goal here was to establish the impact of laser power, focal position, and scanning speed on melt depth. In order to establish this relationship, ANOVA was conducted with a quadratic model. Acceptable levels were applied such as; < 0.05 for model probability, and lack of fit was not significant, R^2 value above 95%, ≤ 0.2 for predicted R^2 – adjusted R^2, and an adequate precision of > 4; therefore according to the results, the two models were acceptable. The ANOVA tables for the two coating types (Table 5-7 and 5-8) show that all factors (laser power, focal position and scanning speed) had a strong significance in the ratio of melt depth to coating thickness (D_m/t_c). With the number of interactions, some higher orders were still significant. Furthermore, the scanning speed seemed to be more important in influencing depth in comparison to the width for the laser-treated monomial nWC-12Co coating.

Source	Sum of Squares	DF	Mean Square	F value	Prob > F	
Model	17.99	9	2.00	448.47	< 0.0001	significant
A-Laser Power	*6.04*	*1*	*6.04*	*1354.06*	*< 0.0001*	
B-Focal Position	*1.48*	*1*	*1.48*	*331.25*	*< 0.0001*	
C-Scanning Speed	*5.88*	*1*	*5.88*	*1318.06*	*< 0.0001*	
AB	*0.59*	*1*	*0.59*	*132.14*	*< 0.0001*	
AC	*2.05*	*1*	*2.05*	*460.01*	*< 0.0001*	
BC	*0.54*	*1*	*0.54*	*120.86*	*< 0.0001*	
A^2	*0.33*	*1*	*0.33*	*73.72*	*< 0.0001*	
B^2	*0.27*	*1*	*0.27*	*61.12*	*< 0.0001*	
C^2	*0.68*	*1*	*0.68*	*153.12*	*< 0.0001*	
Residual	0.031	7	4.458E-003			
Lack of Fit	*0.014*	*3*	*4.735E-003*	*1.11*	*0.4419*	*not significant*
Pure Error	*0.017*	*4*	*4.250E-003*			

R-Squared   **0.99**   Adj.R^2 = 0.99

Adeq.Precision = 68.43   Pred.R^2 = 0.98

Table 5-7: ANOVA analysis for laser-treated monomial nWC-12Co coating (D_m/t_c).

Novel Enhancement of HVOF Thermal Sprayed Nanostructured WC-12Co / Inconel-625 Coatings for Tribocorrosion Applications | **Al-Harbi, Naif I**

148

Source	Sum of Squares	DF	Mean Square	F value	Prob > F	
Model	4.31	9	0.48	531.42	< 0.0001	significant
A-Laser Power	1.34	1	1.34	1485.80	< 0.0001	
B-Focal Position	0.39	1	0.39	432.96	< 0.0001	
C-Scanning Speed	1.31	1	1.31	1449.50	< 0.0001	
AB	0.17	1	0.17	193.48	< 0.0001	
AC	0.48	1	0.48	529.56	< 0.0001	
BC	0.24	1	0.24	263.31	< 0.0001	
A^2	0.086	1	0.086	95.46	< 0.0001	
B^2	0.14	1	0.14	155.65	< 0.0001	
C^2	0.12	1	0.12	132.55	< 0.0001	
Residual	6.310E-003	7	9.014E-004			
Lack of Fit	3.346E-003	3	1.115E-003	1.51	0.3417	*not significant*
Pure Error	2.964E-003	4	7.409E-004			

R-Squared   **0.99**   Adj.R^2 = 0.99

Adeq.Precision = 70. 63   Pred.R^2 = 0.98

Table 5-8: ANOVA analysis for laser-treated mixed coating (D_m /t_c).

The final mathematical models for both laser-treated coatings (D_m /t_c) in terms of coded factors that can be used to make predictions about the response for given levels of each factor were found to be as follows:

$nWC\text{-}12Co\ Coating\ (D_m\ /t_c) = + 0.42 + 0.87 * A - 0.43 * B - 0.86 * C - 0.38 * AB - 0.72$
$* AC + 0.37 * BC + 0.28 * A^2 + 0.25 * B^2 + 0.40* C^2$ $Equation\ 5-6$

$Mixed\ Coating\ (D_m\ /t_c) = + 0.74 + 0.41 * A - 0.22 * B - 0.40 * C - 0.21 * AB - 0.35 * AC +$
$0.24 * BC + 0.14 * A^2 + 0.18 * B^2 + 0.17* C^2$ $Equation\ 5-7$

From the above equations, several observations can be made. Can rank the dependence as follows: A > -C > -AC > -B > C^2 > -AB > BC > A^2 > B^2 for the monomial nWC-12Co coating. First, the laser power itself (A) had the highest impact, followed by the scanning speed both itself (C) and their interaction (AC) on D_m/t_c for monomial nWC-12Co coating. In terms of squared factor, the scanning speed (C^2) followed by the laser power (A^2) had the most significant factors as squared on D_m/t_c for the monomial nWC-12Co coating.

Ranking the dependence of the laser treated mixed coating results: A > -C > -AC > BC > -B > -AB > C^2 > B^2 > A^2. Shows the mixed coating also behaving in the same manner as the

Novel Enhancement of HVOF Thermal Sprayed Nanostructured WC-12Co / Inconel-625 Coatings for Tribocorrosion Applications | **Al-Harbi, Naif I**

149

laser-treated monomial nWC-12Co coating for A, C and AC factors. The only difference between these factors was their levels and the total level of response for mixed coatings was higher than that of the monomial nWC-12Co coating. In addition, as a squared factor, the (C^2) for the scanning speed had the highest impact.

Figure 5-43 is a normal plot for laser-treated monomial nWC-12Co coating (D_m/t_c), showing that the residuals exhibited a linear relationship, which indicates that the residuals were normally distributed. Therefore, ANOVA could be carried out on observations of the melt depth of this coating.
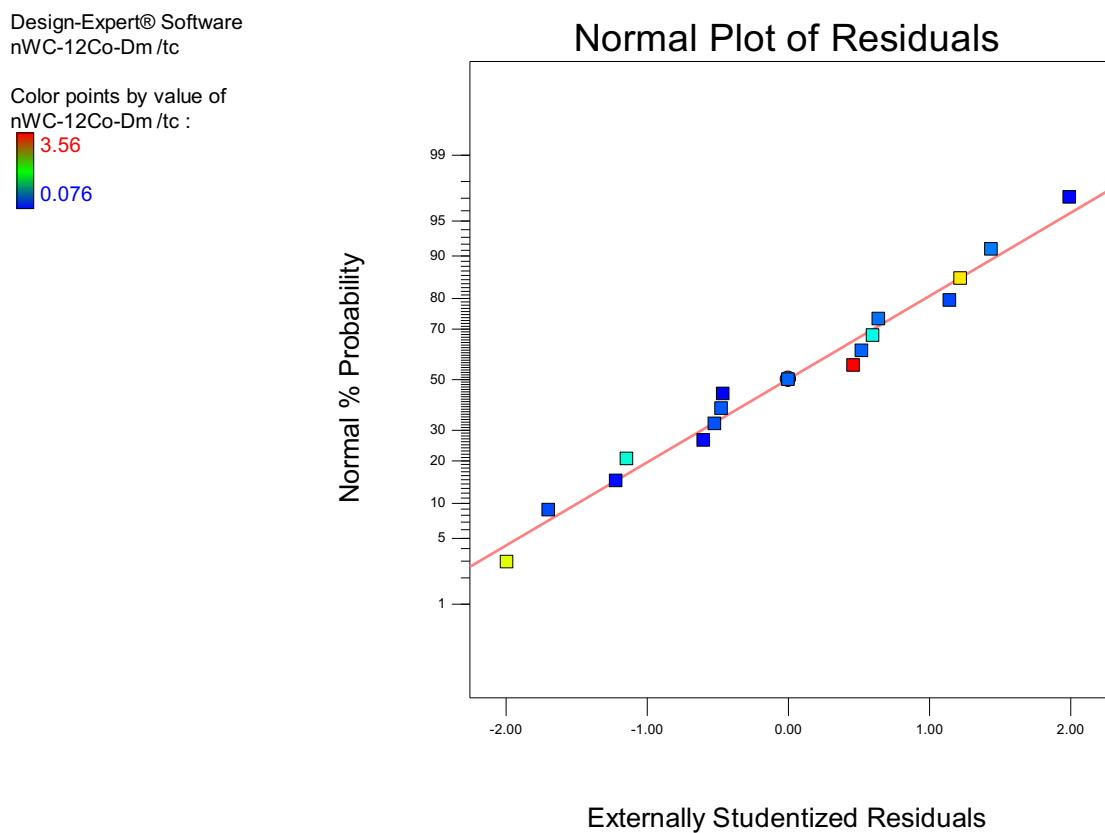
Figure 5-43: Normal plot residual of residuals for laser-treated monomial nWC-12Co coating (D_m/t_c).

In addition, the relationship between the actual and predicted value was linear, indicating that the difference between them was small as shown in Figure 5-44 for the laser-treated monomial nWC-12Co coating (D_m/t_c). The same criteria were observed for the mixed coating (D_m/t_c), and for the sake of brevity, is provided in Appendix A-2 of this research.

Novel Enhancement of HVOF Thermal Sprayed Nanostructured WC-12Co / Inconel-625 Coatings for Tribocorrosion Applications | **Al-Harbi, Naif I**

150
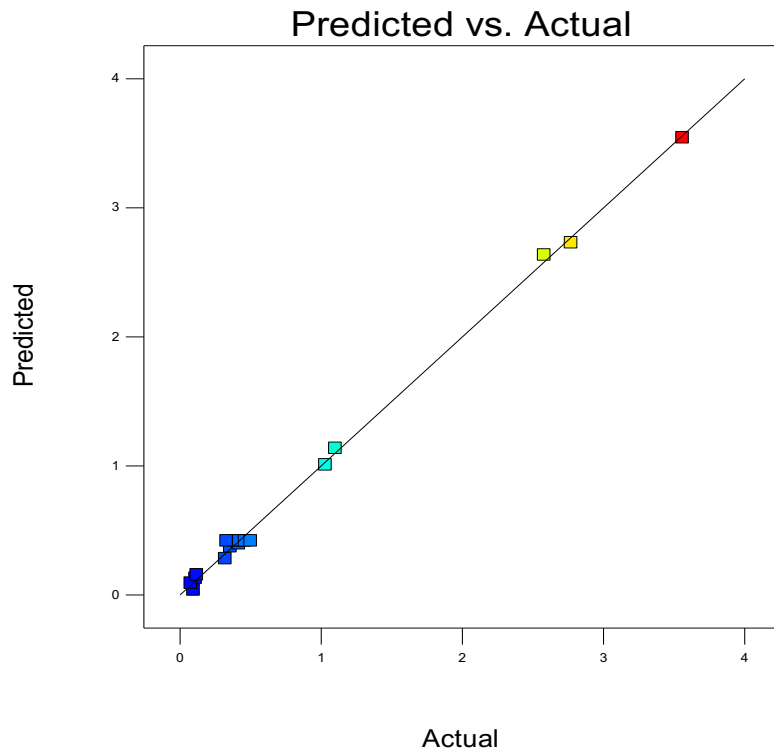
Figure 5-44: Predicted versus actual plot for laser-treated monomial nWC-12Co coating (D_m /t_c).

The final mathematical model determined by the DOE software for both laser-treated coatings to be used to predict the optimized values of melt depth to coating thickness (D_m/t_c) response with regards to actual factors is given in Equation 5-8 and 5-9.

nWC-12Co Coating (D_m /t_c) = +21.66916 + 0.046898 * Laser Power - 0.92825 * Focal Position - 0.058917 * Scanning Speed - 7.67500E-004 * Laser Power * Focal Position - 9.54667E-005 * Laser Power * Scanning Speed + 9.78667E-004 * Focal Position * Scanning Speed + 2.79375E-005 * Laser Power^2 + 0.010175 * Focal Position^2 + 7.15778E-005 * Scanning Speed^2 *Equation* 5 − 8
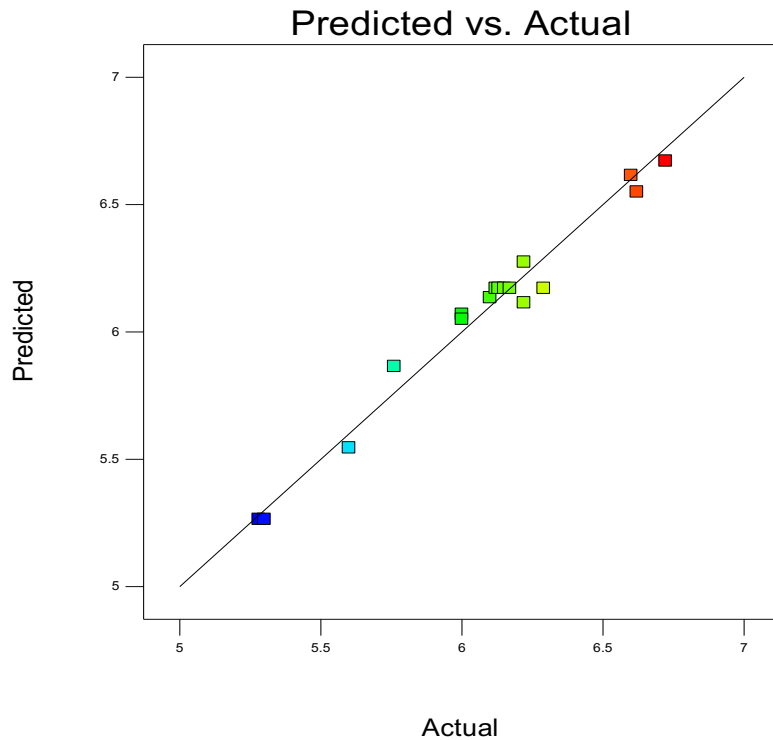
Mixed Coating (D_m /t_c) = +15.86509 + 0.024012 * Laser Power - 0.67006 * Focal Position - 0.033333 * Scanning Speed - 4.17616E-004 * Laser Power * Focal Position - 4.60602E-005 * Laser Power * Scanning Speed + 6.49587E-004 * Focal Position * Scanning Speed + 1.42960E-005 * Laser Power^2 + 7.30167E-003 * Focal Position^2 + 2.99471E-005 * Scanning Speed^2 *Equation* 5 − 9

Novel Enhancement of HVOF Thermal Sprayed Nanostructured WC-12Co / Inconel-625 Coatings for Tribocorrosion Applications | **Al-Harbi, Naif I**

151

5.5.4 DOE results of melt depth dimensions

As can be noted from the perturbation plots, for both coatings in figures 5-45 and 5-46, the ratio of melt depth to coating thickness increased in a cubic growth manner with an increase in laser power and interaction time by lowering the scanning speed. However, the scanning speed (C) seemed to have had a pronounced effect on melt depth in comparison to the track width discussed in the previous section. It is also clear that increasing the size of the laser beam reduced the melt depth. In comparison, increasing the laser beam size as a function of raising the focal position (B) would increase the energy per unit length, due to the lengthened interaction time. This reduction in melt depth can be attributed to the variation of power density. It can be noted that the power density varied inversely with the beam size [115]. When the size of a bean was too large, the power concentration area was too large, and hence, power density was less. On the other hand, if the beam size was small, power was concentrated on a small area, and thus, power density increased, as a result providing intense energy that was able to melt the treated surface to a greater depth. This can be clearly established from the mathematical models in equations 5-6 and 5-7 for both coatings. Laser power, or what can be referred to as power density when divided into the laser beam area, was the main factor in determination of depth. Since power density here was being controlled by focal position/beam size, one can state with confidence that beam size was a factor in determination of melt depth. Furthermore, increasing beam size by raising the focal position (B) increased the melt pool circumference as well as, potentially, the quantity of heat radiation emitted from the outer surface region and the degree of heat conduction seen between the melting region along the depth and the adjacent unmelted region.

Novel Enhancement of HVOF Thermal Sprayed Nanostructured WC-12Co / Inconel-625 Coatings for Tribocorrosion Applications | **Al-Harbi, Naif I**

152
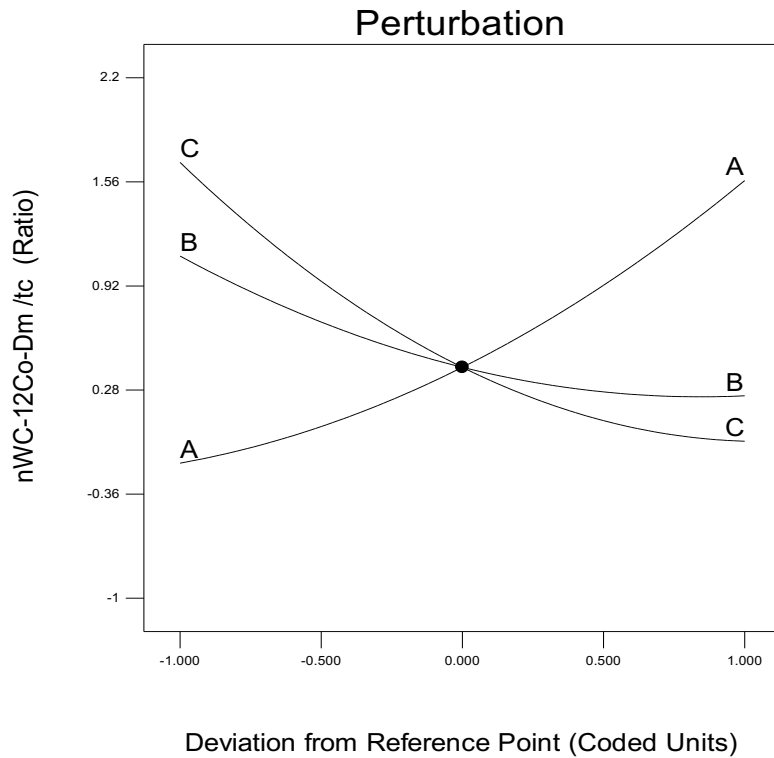
Figure 5-45: Perturbation plot for laser-treated monomial nWC-12Co coating (D_m /t_c).
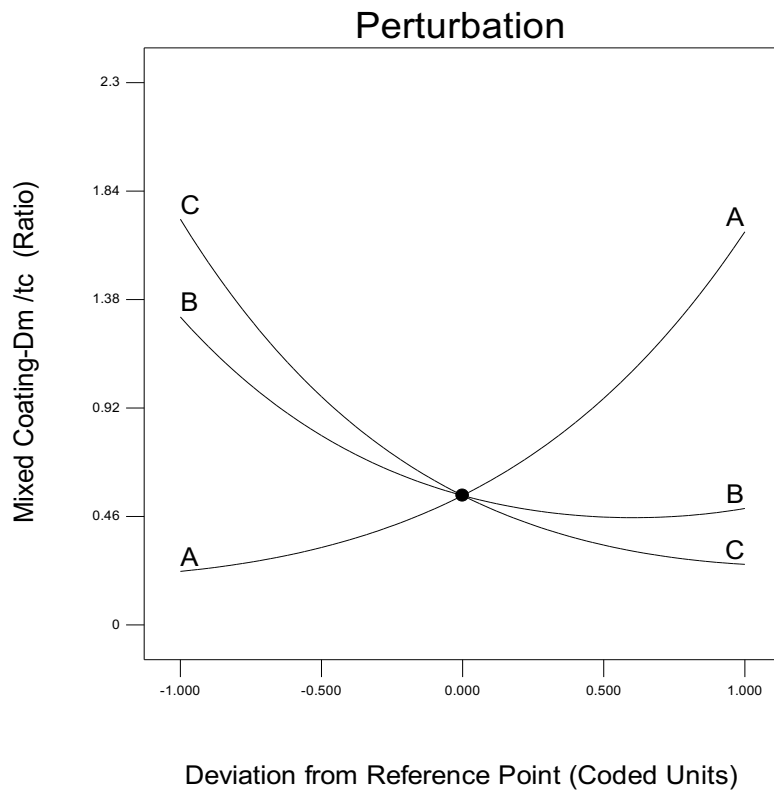
Figure 5-46: Perturbation plot for laser-treated mixed coating (D_m /t_c).

Novel Enhancement of HVOF Thermal Sprayed Nanostructured WC-12Co / Inconel-625 Coatings for Tribocorrosion Applications | **Al-Harbi, Naif I**

153

This can be further clarified in Figure 5-47, which shows the interaction plot between laser power and focal position to the laser-treated monomial nWC-12Co coating (D_m/t_c) when scanning speed of 225 mm/min is used. A difference can be seen between different focal positions in terms of melt depth. It can be observed that the higher the focal position, the greater the beam size and the lower the melt depth. The smaller beam size (+35 mm) magnified the effect of laser power to the melt depth response, in contrast to results seen with the larger beam size (+45 mm). The same trend was seen with the laser-treated mixed coating, as shown in Figure 5-48. What this essentially means is that laser power was a factor of beam size. With a larger beam size, power density would be minimized. Thus, laser power was a most significant factor in determining melt depth. one can conclude that the melt depth was inversely proportional to the beam size, which was controlled by focal positions and directly proportional between increasing the laser power and reducing the scanning speed [21, 114, 115].
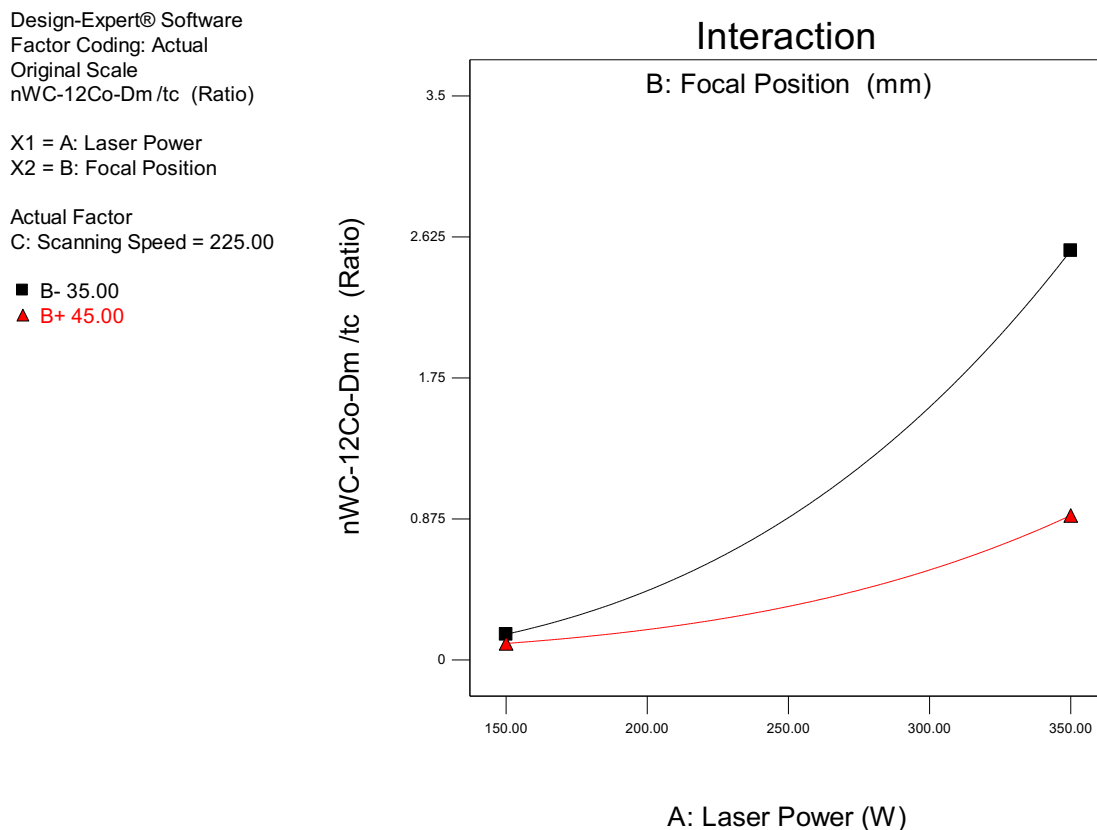
Figure 5-47: Interaction between laser power and focal position relative to monomial nWC-12Co coating (D_m/t_c) response.

Novel Enhancement of HVOF Thermal Sprayed Nanostructured WC-12Co / Inconel-625 Coatings for Tribocorrosion Applications | **Al-Harbi, Naif I**

154
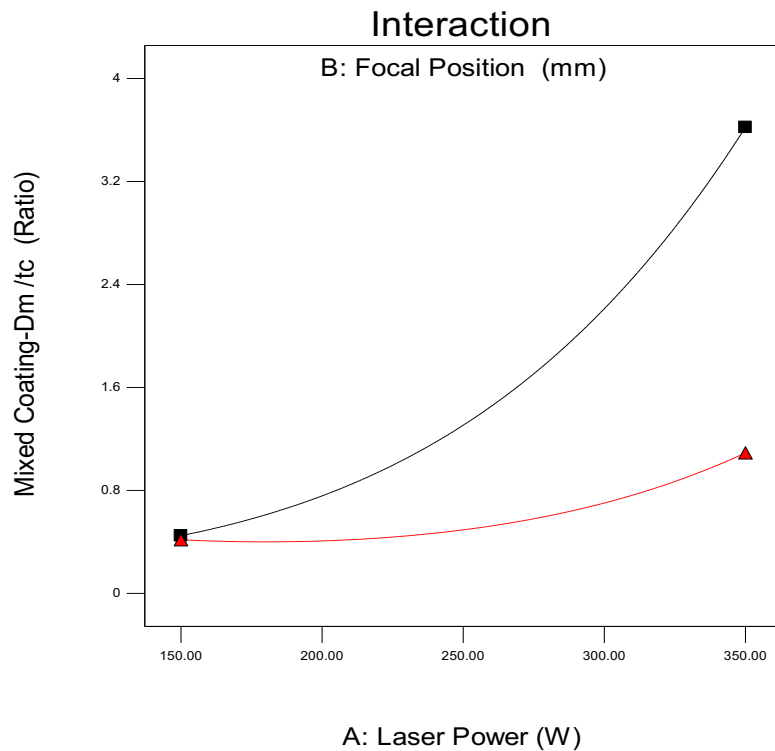
Figure 5-48: Interaction between laser power and focal position relative to mixed coating (D_m/t_c) response.

In summary, the dimensions in response to the three factors (laser power, scanning speed, and focal position) controlling melt pool track width and depth, as evidenced by the ratio of melting depth to coating thickness, were statically analyzed for both coatings. For melt pool track width, the primary factors of concern were laser power (A) and scanning speed (C), with increases to melt pool tracks reasonable for the focal position level (B), the beam size being larger. Track widths for both coatings increased with energy density (high power, slow scanning speed) as energy input per unit length was greater. For ratio of melt depth to coating thickness (D_m/t_c), all factors were under consideration, with the ratio of melt depth to coating thickness for both coatings found to be the same, and for the same reason found for the track width, in terms of laser power and scanning speed. However, contrary to expectations, (D_m/t_c) varied inversely with beam size (specifically when increasing focal position levels), even though beam interaction time had lengthened. This finding might be attributable to a reduction in power density; power was found to be the dominant factor for both coatings as verified by the ANOVA tables and the coded equations. In general, for both melt pool tracks' width and depth (D_m/t_c), the mixed coating showed greater dimensional changes than the monomial nWC-12Co coating.

Novel Enhancement of HVOF Thermal Sprayed Nanostructured WC-12Co / Inconel-625 Coatings for Tribocorrosion Applications | **Al-Harbi, Naif I**

155

5.6 Surface views of laser-melted HVOF coatings

A smooth coating surface with a low degree of roughness, that does not require surface preparation, is not only aesthetically pleasing, but also contributes to wear rate and fatigue failure [113, 116-124]. For instance, the smoother the surface, the more the volumetric wear rate decreases, because of the lack of friction resistance [116].

According to Menezes et al., the coefficient of friction, as well as wear, depends on the surface roughness [117]. The observer should note that in the process of a dry contact, the condition of friction will increase when the surface becomes rougher. However, this condition correlates inversely with the weight of the load exerted. As noted by Riyadh et al. [118], the surface roughness of Al-Si alloy contributed greatly to the asperities shape of R_a and strongly influenced the rate of wear [119].

Figures 5-49 to 5-54 show the surface morphology for the two HVOF coatings after laser treatment according to different energy inputs (from lowest to highest). For the laser-treated monomial nWC-Co coating, as can be seen in Figures 5-49 to 5-51, as the laser's energy input increased, the surface became more homogeneous with excellent sealing effects. That is, the smooth surface was the result of melting the unmelted particles that were noted from their as-sprayed top coating surface in Figures 5–6 and their corresponding interconnected porosity (voids). Nevertheless, a few shallow voids were noted, but did not appear to have great depth along the coating layer observed in the laser settings, which provided insufficient laser energy levels. these did not completely change the phase of the semi-melted particles, such as that shown in P.S.10 in Figure 5-49. In addition, the homogeneity of the coating elements along the surface was enhanced further by increasing the energy input, as can be seen from the differences between P.S.8 and P.S.4 in Figures 5-50 and 5-51 respectively. Some local spherical protuberances of cobalt-rich regions was observed in P.S.8, which was confirmed by EDS analyses, despite the voids being completely eliminated.

For the laser-treated mixed coating, as shown in Figures 5-52 to 5-54, the microstructure of the mixed coating was similar to that found for the monomial nWC-Co coating, regarding the homogeneity of the coating element, due to increasing the thermal energy. However, increasing the energy input, formed a rougher surface and bubbles were created during the laser melting, which coalesced and escaped, leaving holes at the coating surface. In addition, the coating surface became rougher and the bubble holes increased in

Novel Enhancement of HVOF Thermal Sprayed Nanostructured WC-12Co / Inconel-625 Coatings for Tribocorrosion Applications | **Al-Harbi, Naif I**

156

quantity and diameter as the energy input was increased, as shown in Figures 5-53 and 5-54 respectively.
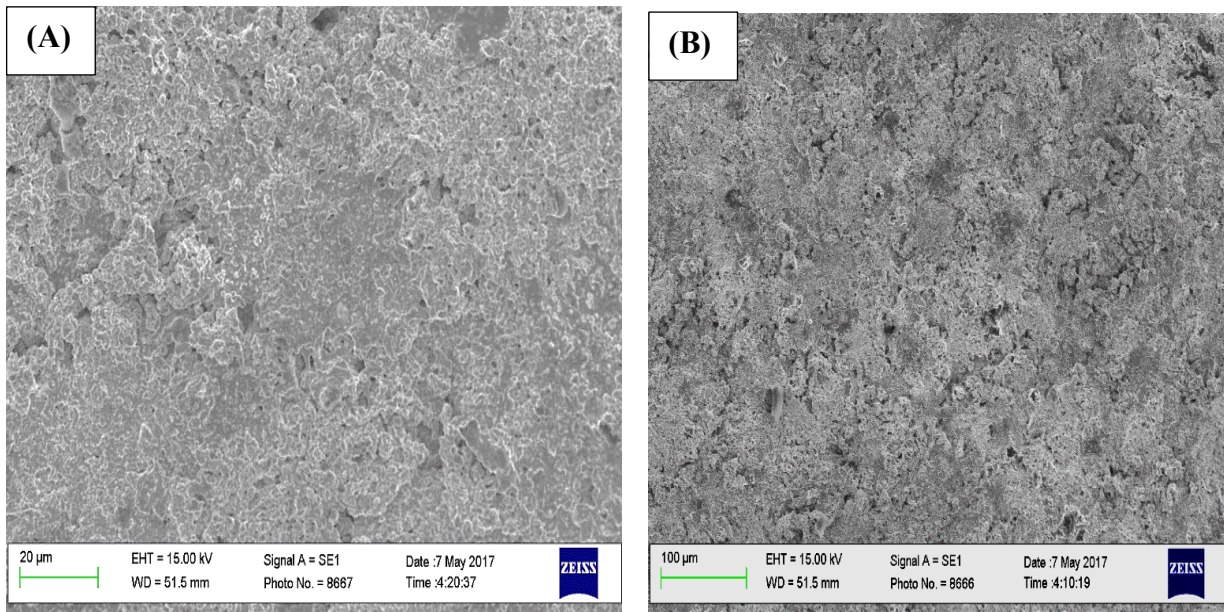
Figure 5-49: SEM micrograph of laser-treated top surface of nWC-12Co HVOF coatings (P.S.10, within R_{qa} = 3.18 μm) with (A) high magnification and (B) low magnification.
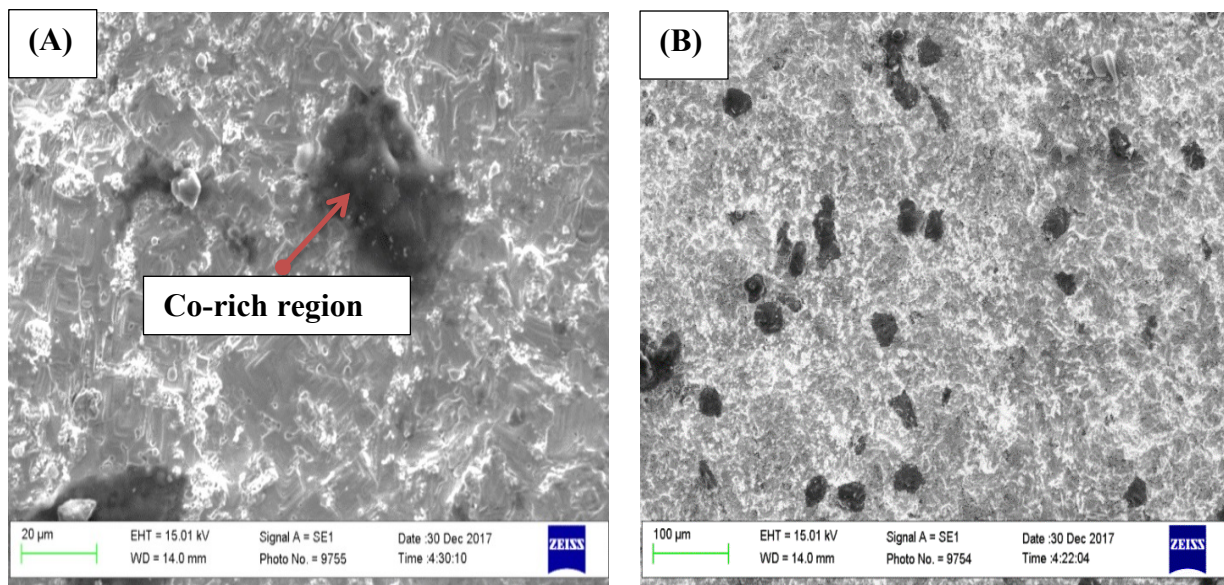
Figure 5-50: SEM micrograph of laser treated top surface of nWC-12Co HVOF coatings (P.S.8, within R_{qa} =2.77 μm) with (A) high magnification and (B) low magnification.

Novel Enhancement of HVOF Thermal Sprayed Nanostructured WC-12Co / Inconel-625 Coatings for Tribocorrosion Applications | **Al-Harbi, Naif I**

157
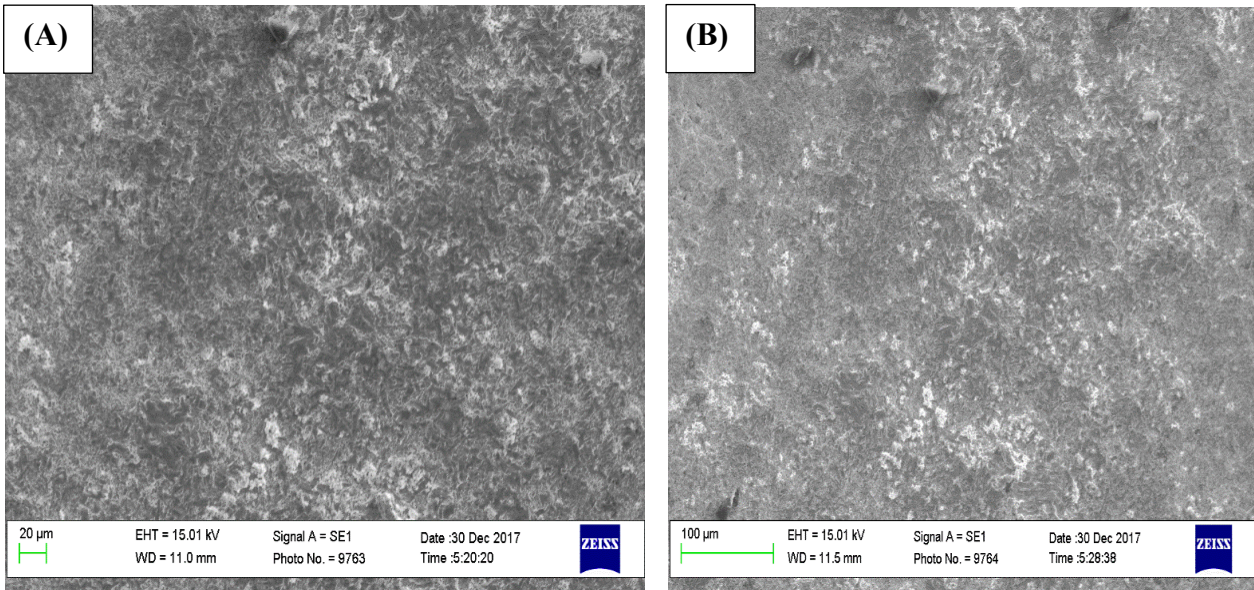
Figure 5-51: SEM micrograph of laser-treated top surface of nWC-12Co HVOF coatings (P.S.4, within R_{qa} = 3.17 μm) with (A) high magnification and (B) low magnification.
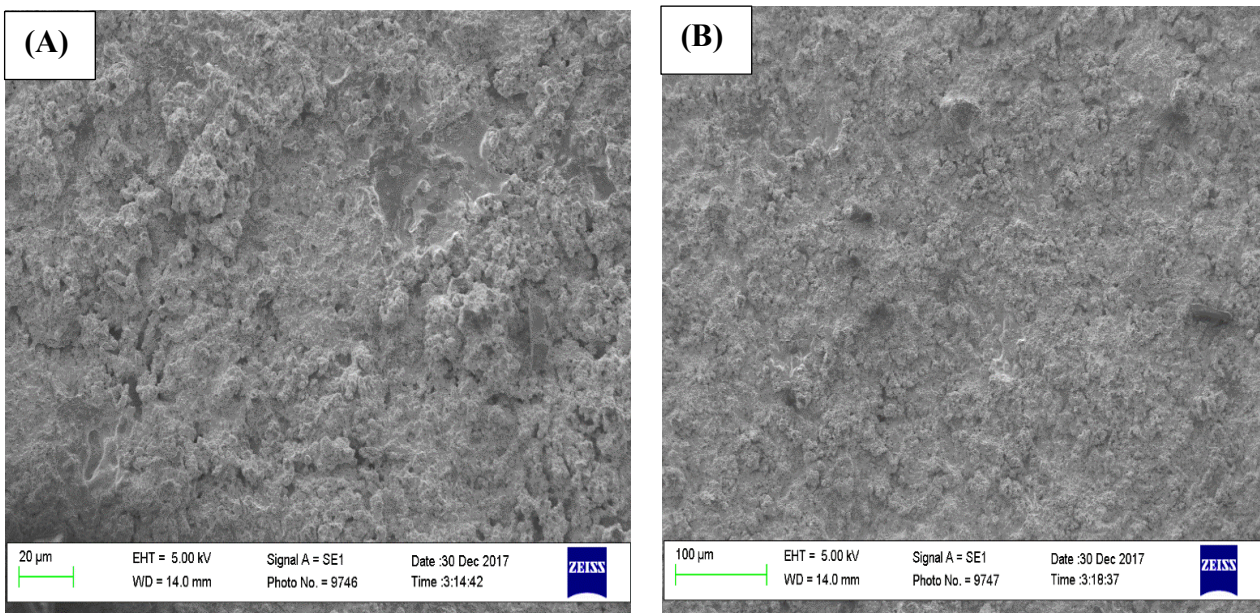
Figure 5-52: SEM micrograph of laser-treated top surface of mixed HVOF coatings (P.S.10, within R_{qa} = 3.99 μm) with (A) high magnification and (B) low magnification.

Novel Enhancement of HVOF Thermal Sprayed Nanostructured WC-12Co / Inconel-625 Coatings for Tribocorrosion Applications | **Al-Harbi, Naif I**

158
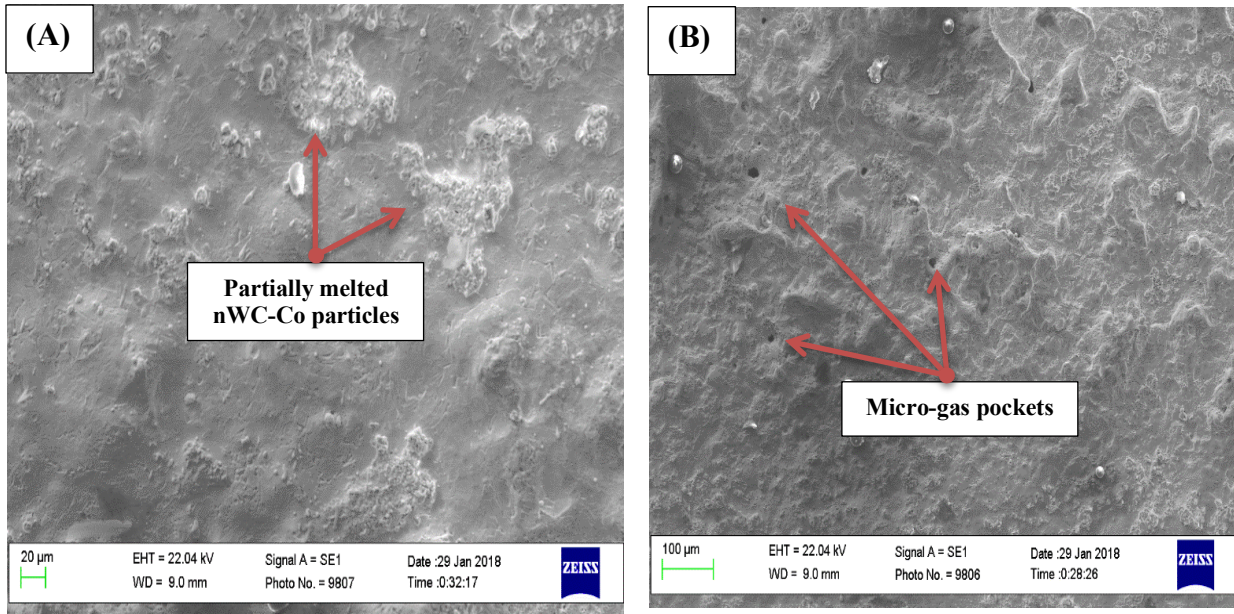
Figure 5-53: SEM micrograph of laser-treated top surface of mixed HVOF coatings (P.S.12, within R_{qa} = 4.1 µm) with (A) high magnification and (B) low magnification.
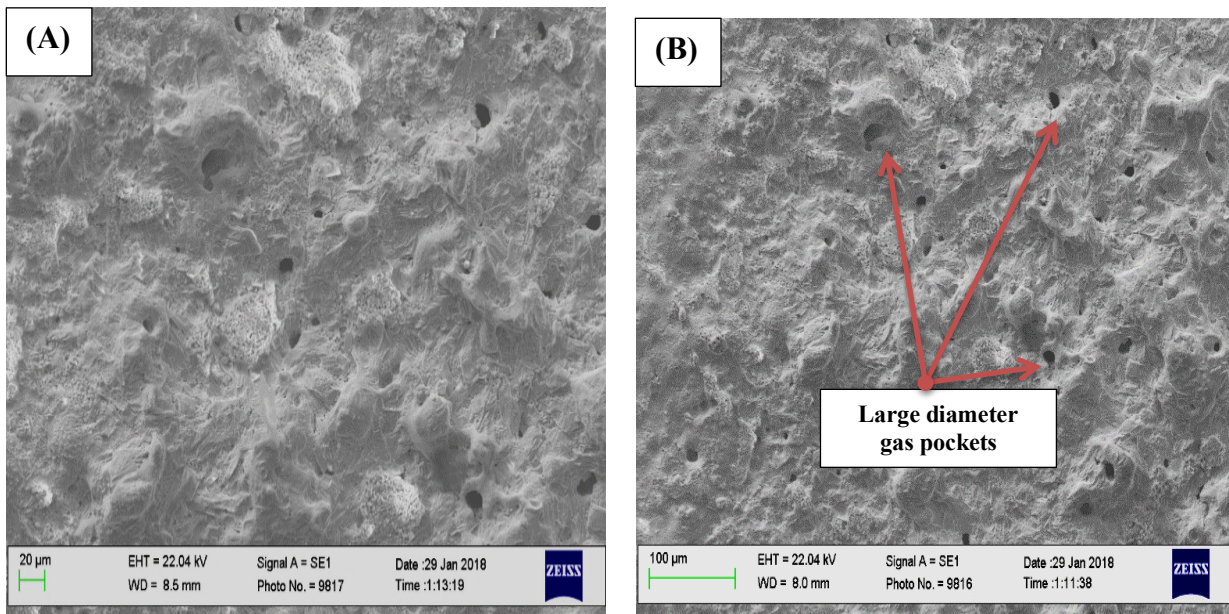
Figure 5-54: SEM micrograph of laser-treated top surface of mixed HVOF coatings (P.S.8, within R_{qa} = 10.95 µm) with (A) high magnification and (B) low magnification.

The different responses of the two coating surfaces' roughness to the laser processing conditions may have contributed to the different ratio of binder metrics in the coating layer. As the mixed would have contained a higher ratio of metallic binder matrices, as a result of blending the 25% of Inconel 625 (Ni-Cr alloy) metals with the nWC-12Co HVOF coatings that already contained 12% cobalt, it eventually formed 34% binder matrices in the mixed coating layer in comparison to only 12% of the monomial nWC-12Co coating. Consequently

Novel Enhancement of HVOF Thermal Sprayed Nanostructured WC-12Co / Inconel-625 Coatings for Tribocorrosion Applications | **Al-Harbi, Naif I**

159

, this high amount of metallic binders possibly became unstable during any laser settings that provided high-energy input and rapidly solidified to form a rough surface, simply because of the time (in milliseconds) for the laser beam to leave the treated region. Such behaviour of the mixed coating with the laser processing action was similar to that seen in the work carried out by Evan et al. [120], who noted that the surface roughness of the 316L stainless steel metallic sample increased when enhancing the irradiance and resident time of the laser processing. Such findings were further confirmed by studying the surface profile in 2D of the laser setting amongst the created DOE matrix that provided the highest energy input, which was P.S.6 (P = 350 W, F = 40 mm, and U = 150 mm/min), as shown in Figure 5-55 (along with optical photographs of the two laser-treated surfaces). The amplitude of the surface roughness picks, average surface roughness, and average surface area ratio were significantly higher for the mixed coating in comparison to the monomial nWC-12Co HVOF coatings.
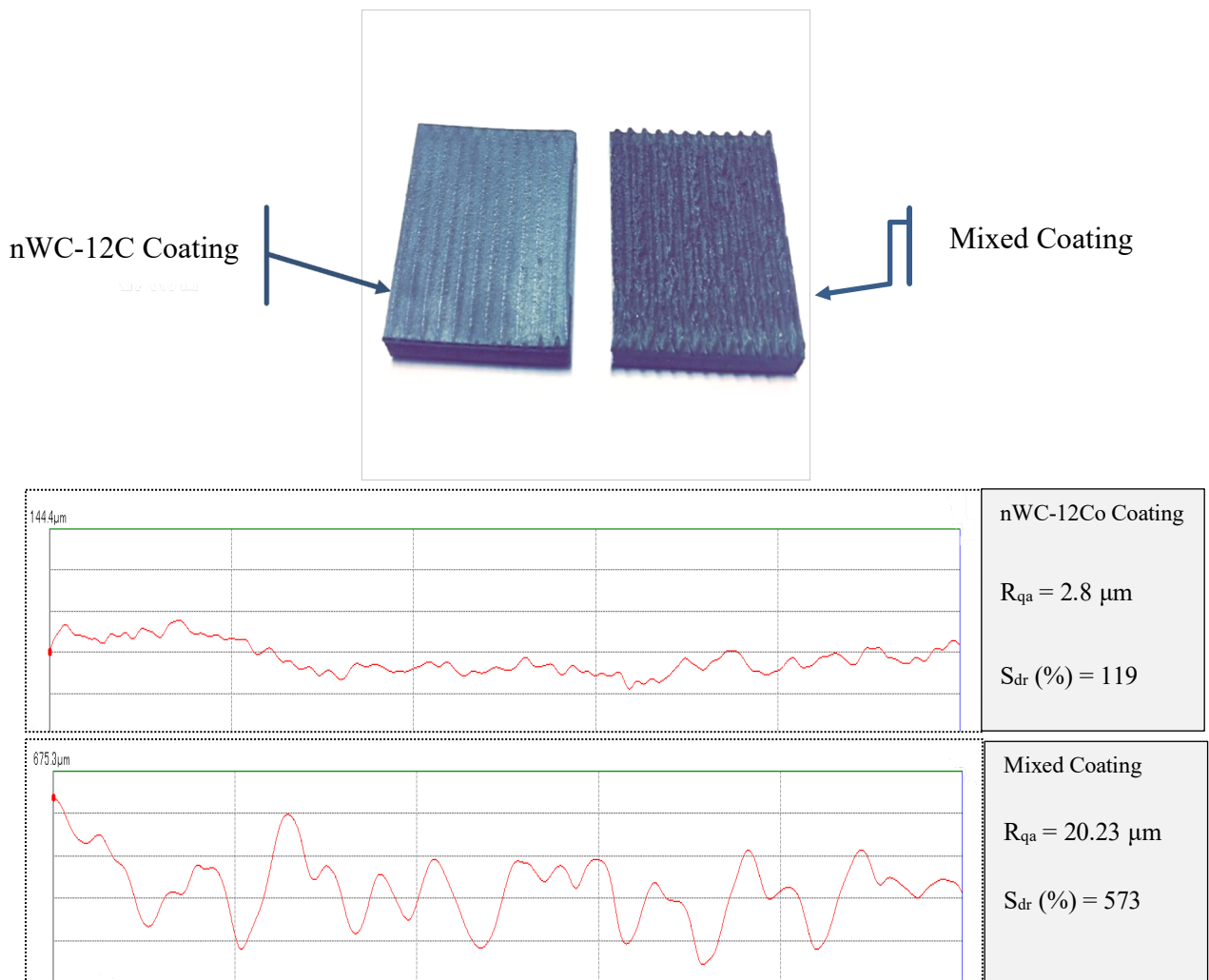
Figure 5-55: Optical photograph and surface profile for the two laser-treated coatings' roughness measurement of P.S.6 (within P = 350 W, F = 40 mm, and U = 150 mm/min).

Novel Enhancement of HVOF Thermal Sprayed Nanostructured WC-12Co / Inconel-625 Coatings for Tribocorrosion Applications | **Al-Harbi, Naif I**

160

The results of the average roughness for both coatings, before and after the laser treatment according to the DOE matrix (given in Table 3–6), are summarized in Figures 5-56 and 5-57. Clearly, as a result of the melting of the top surface, the surface roughness of the monomial nWC-12Co HVOF under all laser settings reduced significantly with a small standard deviation of 0.22. P.S.9 and P.S.8 provided the lowest surface roughnesses with approximately 100% reduction of 2.7 and 2.77 μm respectively, compared to the as-sprayed coating of 5. 24 μm. Meanwhile, for the mixed coating, the variation and standard deviation was significantly high at 6.47, where P.S.1 and P.S.12 provided the lowest surface roughnesses of 3.01 and 3.69 μm respectively.
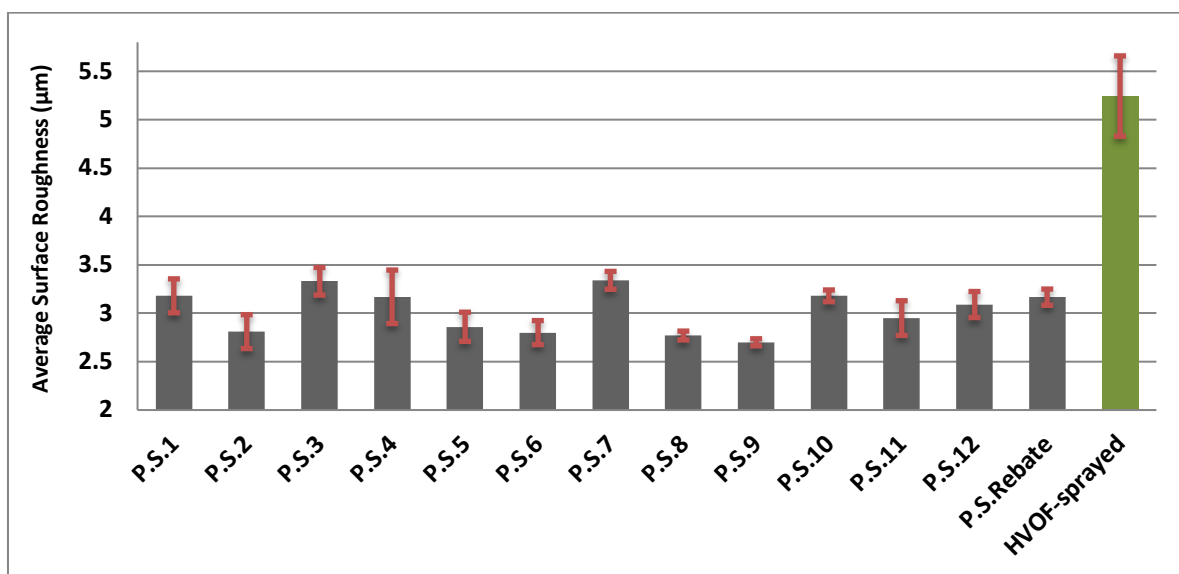
Figure 5-56: Surface roughness of the nWC-12Co HVOF coating before and after the laser treatment under the various laser settings.
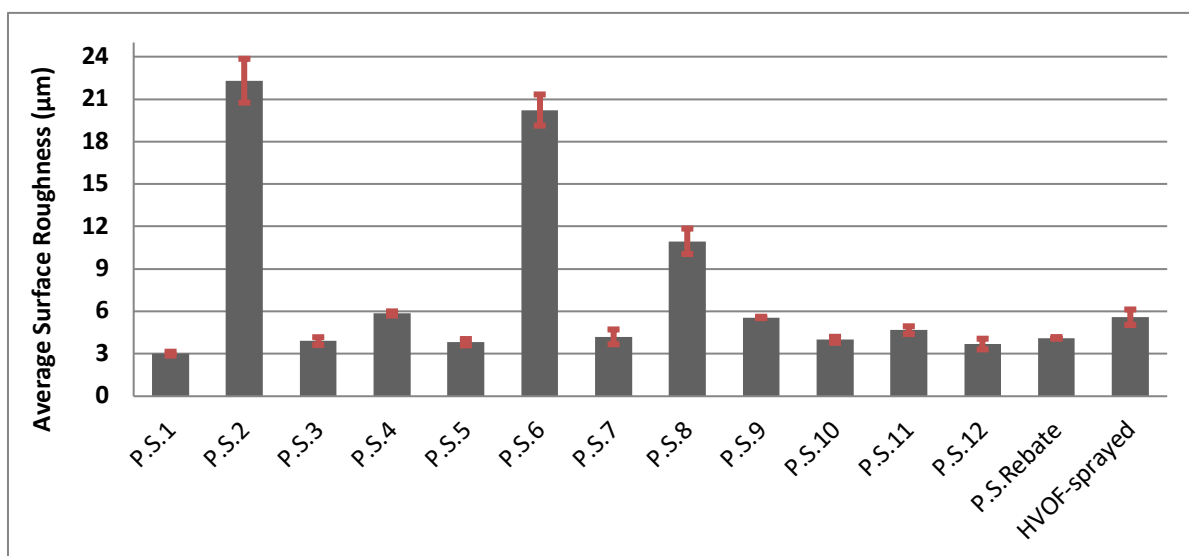
Figure 5-57: Surface roughness of the mixed HVOF coating before and after the laser treatment under the various laser settings.

Novel Enhancement of HVOF Thermal Sprayed Nanostructured WC-12Co / Inconel-625 Coatings for Tribocorrosion Applications | **Al-Harbi, Naif I**

161

5.6.1 Development of the mathematical model for surface roughness

Similarly to what was carried out for melt-pool dimensions, the design of experiment (DOE) analysis was used to derive the mathematical model to show the effects of considered input factors—namely, laser power, focal position, and scanning speed—on the laser-treated coating surface roughness of the two coating types. The quadratic model, which was selected to fit the data for both coatings, showed R^2 value of 0.91 for the laser-treated monomial nWC-12Co coating and 0.99 for the mixed coating. To determine the modules to be used in the analysis, several acceptable levels were set up as follows: the model probability and lack of fit probability, R^2, and the differences between the predicted R^2, adjusted R^2, and adequate precision. For this study, all of these were above the minimum level set for module acceptance, as clarified in the two AVOVA tables for both laser-treated coatings (see Table 5.9 for the monomial nWC-12Co and Table 5.10 for the mixed coating). As can be seen from the Prob>F value in the AVOVA tables, the laser power and focal position had the most significant effects on the surface roughness of both laser-treated coatings, whereas the scanning speed showed that this factor had only secondary effects. Furthermore, significant interactions took place up to the second order for all factors in the laser-treated mixed coating and the scanning speed for the laser-treated monomial nWC-12Co. This indicates that the response is not linear and is highly sensitive to changes in the levels of these factors.

Source	Sum of Squares	DF	Mean Square	F value	Prob > F	
Model	0.6116	6	0.1019	18.31	< 0.0001	significant
A-Laser Power	0.1682	1	0.1682	30.21	0.0003	
B-Focal Position	0.1596	1	0.1596	28.67	0.0003	
C-Scanning Speed	0.0465	1	0.0465	8.35	0.0161	
AC	0.0650	1	0.0650	11.68	0.0066	
BC	0.0289	1	0.0289	5.19	0.0459	
C²	0.1433	1	0.1433	25.74	0.0005	
Residual	0.0557	10	0.0056			
Lack of Fit	0.0308	6	0.0051	0.8271	0.6030	not significant
Pure Error	0.0249	4	0.0062			

R-Squared	**0.91**	Adj.R^2 = 0.86	
Adeq. Precision = 16.13		Pred.R^2 = 0.73	

Table 5-9: ANOVA analysis for laser-treated monomial nWC-12Co coating surface.

Novel Enhancement of HVOF Thermal Sprayed Nanostructured WC-12Co / Inconel-625 Coatings for Tribocorrosion Applications | **Al-Harbi, Naif I**

162

Source	Sum of Squares	DF	Mean Square	F value	Prob > F	
Model	0.1741	8	0.0218	547.90	< 0.0001	significant
A-Laser Power	*0.1087*	*1*	*0.1087*	*2736.95*	*< 0.0001*	
B-Focal Position	*0.0089*	*1*	*0.0089*	*223.35*	*< 0.0001*	
C-Scanning Speed	*0.0017*	*1*	*0.0017*	*41.73*	*0.0002*	
AB	*0.0185*	*1*	*0.0185*	*464.62*	*< 0.0001*	
AC	*0.0027*	*1*	*0.0027*	*67.50*	*< 0.0001*	
A²	*0.0280*	*1*	*0.0280*	*705.01*	*< 0.0001*	
B²	*0.0009*	*1*	*0.0009*	*21.76*	*0.0016*	
C²	*0.0042*	*1*	*0.0042*	*106.06*	*< 0.0001*	
Residual	*0.0003*	*8*	*0.0000*			
Lack of Fit	*0.0001*	*4*	*0.0000*	*0.7060*	*0.6280*	*not significant*

R-Squared **0.99** Adj.R^2 = 0.996

Adeq. Precision = 80 Pred.R^2 = 0.992

Table 5-10: ANOVA analysis for laser-treated mixed coating surface roughness.

The final mathematical models for both coatings' laser-treated surface roughness, in terms of coded factors that can be used to make predictions about the response for given levels of each factor, were found to be as follows:

*nWC-12Co coating (roughness) = +0.32 + 0.016 * A - 0.016 * B - 8.559E-003 * C -6.411E -003 * AB + 0.013 * AC + 0.010 * BC + 4.621E-003 * A² - 3.294E-005 * B² +0.020 *C^2* $Equation\ 5-10$

*Mixed coating (roughness) = + 0.49 - 0.12 * A + 0.033 * B + 0.014 * C + 0.068 * AB + 0.026 * AC - 4.770E-003 * BC - 0.082 * A² + 0.014 * B² - 0.032 *C^2* $Equation\ 5-11$

Based on the above equations, for nWC-12Co one can point out that all factors have some impact on surface roughness. Can rank the dependence as follows: C^2 > A = -B > AC > BC > C > AB > A^2 > B^2 for the monomial nWC-12Co coating. It can be establis h, from the results and the literature, that the factors are related to each other. For the monomial nWC-12Co, the most important factors are the laser power (A) and focal position (B) as itself within equal values, but the opposite sign (opposite effect), where the latter indicates the opposite response to the surface roughness. As a squared factor and paired interaction, the **(**C^2**)** for the scanning

Novel Enhancement of HVOF Thermal Sprayed Nanostructured WC-12Co / Inconel-625 Coatings for Tribocorrosion Applications | **Al-Harbi, Naif I**

163

speed and laser power within the same, as combined effects (AC), had the most significant impact on the surface roughness respectively.

Ranking the dependence of the laser treated mixed coating results: -A >> -A^2 > AB > B > -C^2 > AC > C = B^2 > -BC. The laser power (A), its square (A^2) and laser power combined with focal position (AB) had the most significant impact on the surface roughness of this coating.

Figure 5-58 is a normal plot for laser-treated monomial nWC-12Co coating surface roughness, showing that the residuals have a linear relationship, which indicates that they are normally distributed. Thus, ANOVA can be carried out on observations for the surface roughness of this coating.
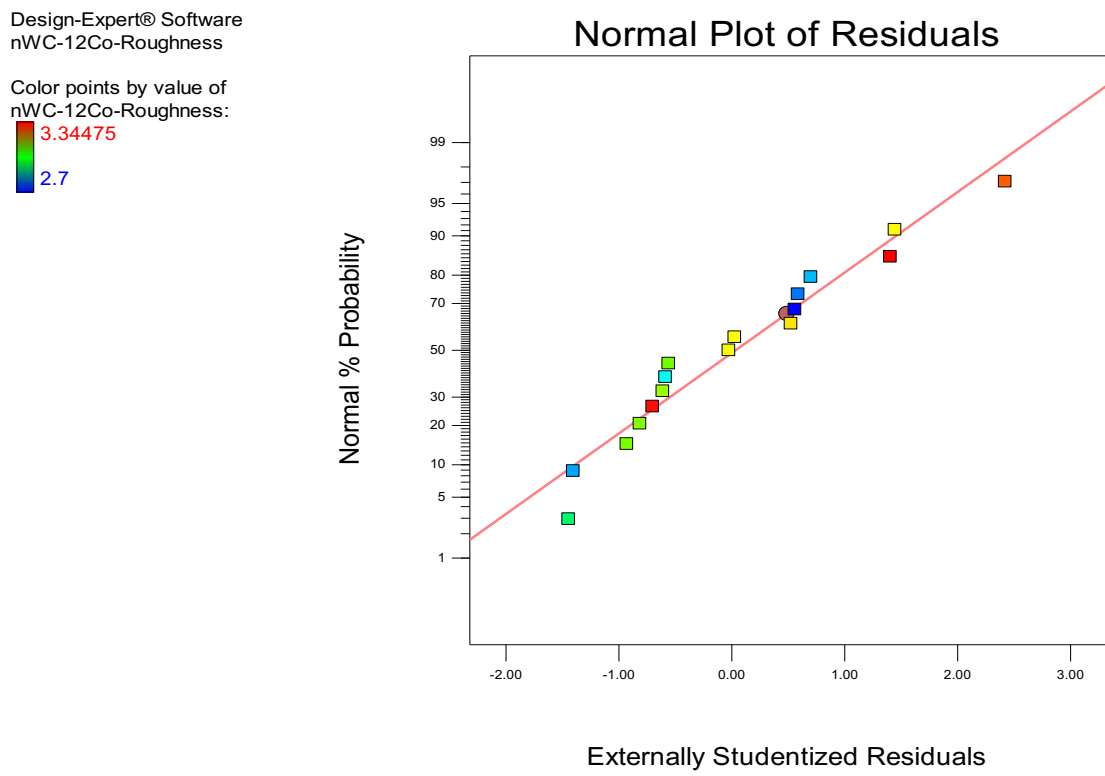
Figure 5-58: Normal plot residual of laser-treated monomial nWC-12Co coating surface roughness (µm).

In addition, the relationship between the actual and predicted value is linear, which indicates that the difference between them is small, as shown in Figure 5-59 for the monomial nWC-12Co coating (surface roughness). The same criteria were observed for the mixed coating track width, which for the sake of brevity, is provided in Appendix B of this research.

Novel Enhancement of HVOF Thermal Sprayed Nanostructured WC-12Co / Inconel-625 Coatings for Tribocorrosion Applications | **Al-Harbi, Naif I**

164
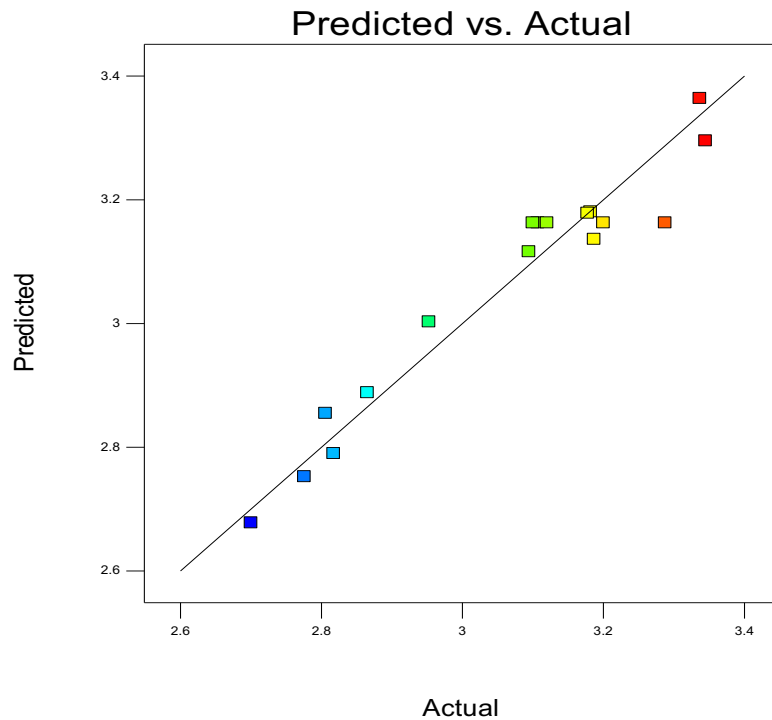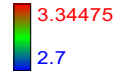
Figure 5-59: Predicted versus actual plot for laser-treated monomial nWC-12Co coating surface roughness (μm).

The final mathematical model determined by the DOE software for both laser-treated coatings to be used to predict the optimized values of roughness response with regards to actual factors is given in Equation 5-12 and 5-13.

$nWC\text{-}12Co\ Coating\ (roughness) = +0.85795 + 3.31686E\text{-}005 * Laser\ Power - 6.02065E\text{-}003 * Focal\ Position - 3.27545E\text{-}003 * Scanning\ Speed - 1.28218E\text{-}005 * Laser\ Power * Focal\ Position + 1.79619E\text{-}006 * Laser\ Power * Scanning\ Speed + 2.73701E\text{-}005 * Focal\ Position * Scanning\ Speed + 4.62051E\text{-}007 * Laser\ Power^2 - 1.31769E\text{-}006 * Focal\ Position^2 + 3.59439E\text{-}006 * Scanning\ Speed^2$
$\qquad\qquad\qquad\qquad\qquad\qquad\qquad\qquad\qquad\qquad\qquad Equation\ 5-12$

$Mixed\ Coating\ (roughness) = +2.03696 - 3.29887E\text{-}003 * Laser\ Power - 0.070295 * Focal\ Position + 2.36825E\text{-}003 * Scanning\ Speed + 1.35854E\text{-}004 * Laser\ Power * Focal\ Position + 3.45205E\text{-}006 * Laser\ Power * Scanning\ Speed - 1.27188E\text{-}005 * Focal\ Position * Scanning\ Speed - 8.15555E\text{-}006 * Laser\ Power^2 + 5.73164E\text{-}004 * Focal\ Position^2 - 5.62351E\text{-}006 * Scanning\ Speed^2$
$\qquad\qquad\qquad\qquad\qquad\qquad\qquad\qquad\qquad\qquad\qquad Equation\ 5-13$

Novel Enhancement of HVOF Thermal Sprayed Nanostructured WC-12Co / Inconel-625 Coatings for Tribocorrosion Applications | **Al-Harbi, Naif I**

165

5.6.2 DOE results of surface roughness

Figures 5.60 and 5.62 are perturbation plots showing the effect of each factor on the surface roughness response for both laser-treated coatings. From these graphs, one may observe that most of the factors have different effect on the coating surface roughness for the two coating types. That is to say, either direct or inverse proportionality exists when the levels of the factors are increased with result to the surface roughness. According to the perturbation plot for the laser-treated monomial nWC-12Co coating in Figure 5-60, which was taken in the central level (Level 0), the surface roughness slows an almost similar behaviour as that noted for the focal position and laser power with melt depth DOE analyses.

The observer may see that as the laser power increases (A), the surface roughness of the laser-treated monomial nWC-12Co coating decreases in a quadratic manner, while the surface roughness increases in a linear fashion due to increasing levels of the focal position (B). Laser power and focal position, as explained earlier in the ANOVA table, and the final coded equation (Equation 5-10) are the most influential variables in the determination of surface roughness. As laser power levels increase, so will the energy input. Where the focal position gets higher, the beam size will become bigger, which will lead to a reduction of the power density (power/area), as explained earlier in the melt depth DOE static analyses. The relationship or interaction between these two factors and the surface roughness response can be represented by the contour plot, as seen in Figure 5.61.

For the scanning speed, a pronounced effect can be seen on the laser roughness when changing the levels of the scanning speed. However, in general, the scanning speed in the lowest-level region (between 150 and 225 mm/min) shows that the surface roughness increases with increased the scanning speed (150 to 225 mm/min) as a result of lowering the energy per unit length, which is a by-product of shortening the interaction time of the beam within the treated surface. However, in the highest-level region of the scanning speed (between 225 and 300 mm/min), increased speed acts oppositely to what was noticed in the previous region of the surface roughness response, which might contribute to the effects of changing other factors (laser power and scanning speed).

Novel Enhancement of HVOF Thermal Sprayed Nanostructured WC-12Co / Inconel-625 Coatings for Tribocorrosion Applications | **Al-Harbi, Naif I**

166
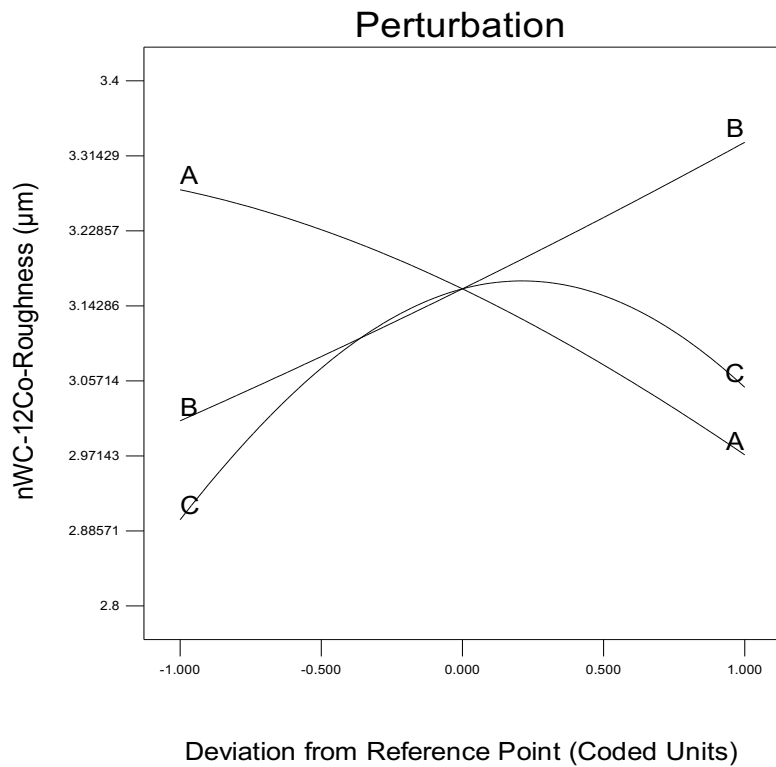
Figure 5-60: Perturbation plot for laser treated monomial nWC-12Co coating surface roughness.
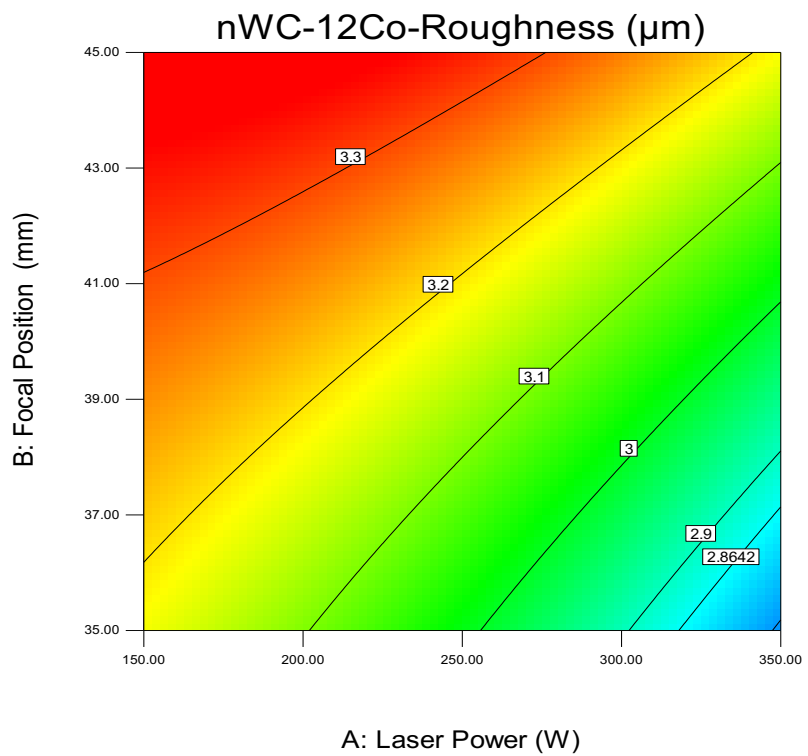
Figure 5-61: Contour plot of the laser treated monomial nWC-12Co coating for the focal position versus the laser power.

Novel Enhancement of HVOF Thermal Sprayed Nanostructured WC-12Co / Inconel-625 Coatings for Tribocorrosion Applications | **Al-Harbi, Naif I**

167

For the mixed coating, the Perturbation plot (shown in Figure 5-62), shows the surface roughness to reduced at lower energy levels; then, as the energy rises by increasing the laser power or lowering the focal position, the surface roughness increases. However, laser power has a major effect on roughness compared to the other two factors at their maximises. For the focal position, the surface roughness seems different. As previously explained, increasing the focal position will lower the energy density; consequently, the surface roughness for the mixed coating shows a slight reduction and increased focal position levels/beam size. This outcome could be further clarified by presenting the significant differences between the two focal positions that provided the smallest (+35 mm) and largest beam size (+45 mm) in their interaction via applying laser power to the mixed-coating's surface roughness, as shown in Figure 5-63. However, the higher impact of the focal position for the laser treated monomial nWC-12Co coating clearly increases surface roughness or decreases it for the compressed mixed coating. A similar interaction plot shows the melt pool geometry static analyses between the laser power and the focal position, which could be attributed to findings reported by Yasa et al. [121], who found that by using a bigger laser beam, the number of laser tracks along the surface will be smaller; subsequently, the number of transaction regions between the tracks that formed valleys will be minimised and create a smother surface.
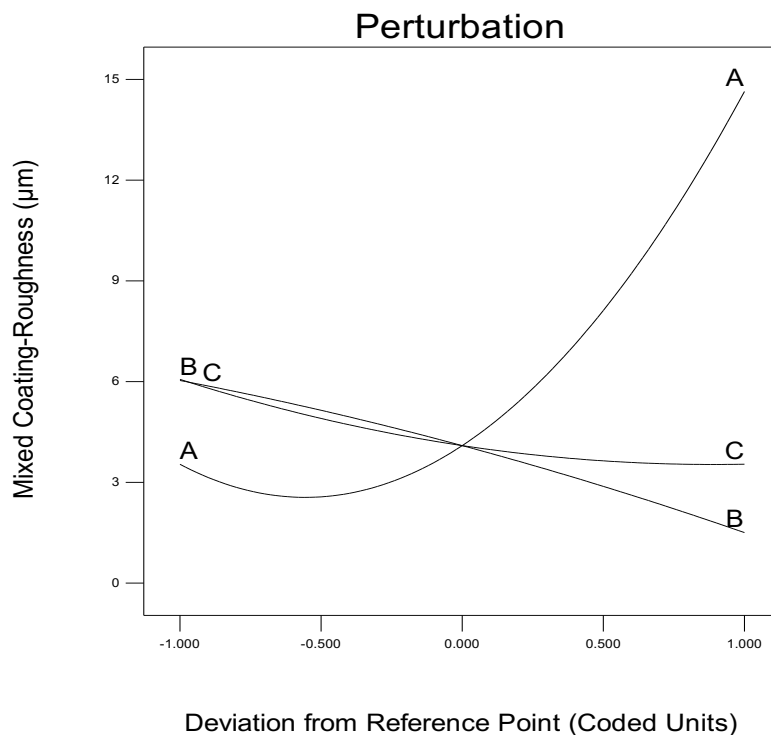
Figure 5-62: Perturbation plot for laser treated mixed Coating surface roughness.

Novel Enhancement of HVOF Thermal Sprayed Nanostructured WC-12Co / Inconel-625 Coatings for Tribocorrosion Applications | **Al-Harbi, Naif I**

168
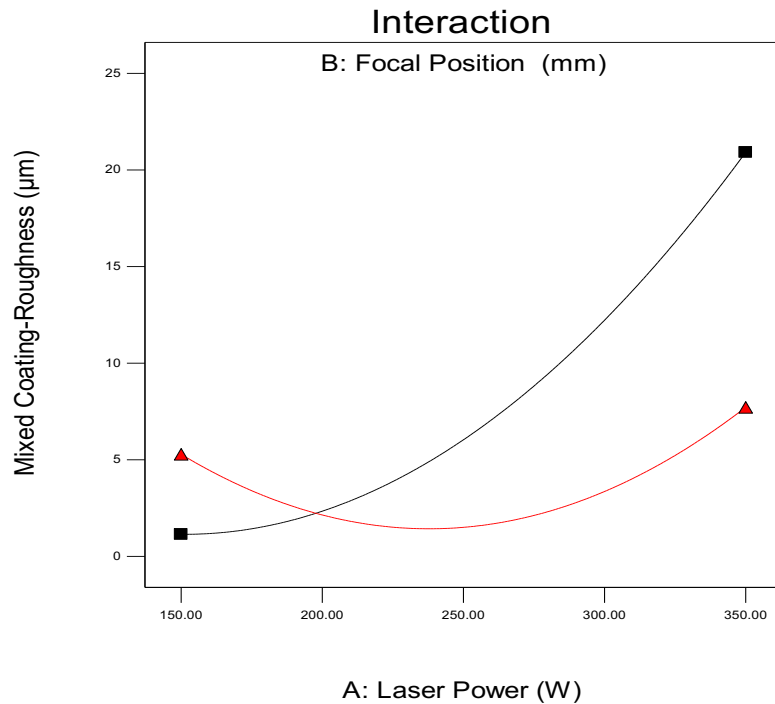
Figure 5-63: Interaction between the laser power and the focal position to the mixed coating surface roughness.

In summary, the effect on surface roughness of the two laser-treated coatings for the three control factors under investigation (laser power, scanning speed and focal position) behave oppositely at some levels of energy input for the mixed-coating type. For the monomial nWC-12Co coating, surface roughness decreased as energy input increased (high laser power, low scanning speed and large beam size). A large beam size, increased by increasing the focal position, will lower the power density, and the focal position and power were noted as the dominate factors for both coating types. At low-energy input, the mixed coating will fully melt or partially melt the unmelted coating powder in the outer surface of the coating, reducing surface roughness. However, at some energy input levels, the surface roughness starts to increase within the increased energy input as the high number of metallic binders become unstable under the laser settings, forming a rough surface. Furthermore, the results show that apart from the effect of changing the laser beam size controlled by the focal position in the power density on the surface roughness of the two coatings, increasing the laser beam size will reduce the surface roughness as a result of reducing the number of tracks required to treat the same area. This outcome explains why the surface roughness for the mixed coating that provided the highest energy input and the ratio of melt depth to coating thickness (D_m/t_c) P.S.6 (focal position = +45) was lower than the P.S.2 (focal position = +35).

Novel Enhancement of HVOF Thermal Sprayed Nanostructured WC-12Co / Inconel-625 Coatings for Tribocorrosion Applications | **Al-Harbi, Naif I**

169

5.7 XRD of laser-treated HVOF coatings

Figures 5-64 and 5-65 illustrate the XRD patterns of the two coatings after laser treatment under two different energy inputs. According to the initial observation of the peaks before (in Figures 5-20 and 5-21) and after the laser-melting process of the two coatings, the peaks were less intense and larger than those observed for the as-sprayed coatings. Furthermore, after closed examination of the peaks, one can observe that the full width at half maximum (FWHM) of the XRD peaks was bordering on the laser-melting coatings to a greater degree than that of those obtained for the as-sprayed coating. This indicates that the crystallite became smaller after the laser melting processing. The results for the monomial nWC-12Co-sprayed coating, prior to treatment, indicate that it contained Co, WC and W_2C compounds only. However, as can be observed in Figure 5-64, the laser melting process, under two different heat inputs (P.S.4 being the lowest and P.S.6 the highest), resulted in the emergence of new phases; pure cobalt (Co) and a small amount of eta crystalline phases of unbrittle carbides (Co_6W_6C) under low-energy inputs, compared to the XRD pattern of the monomial nWC-12Co-sprayed coating (Figure 5-20). Furthermore, during the higher-energy input as in P.S.6, shown in the same figure, phase W was noted as individual and small amounts of brittle eta carbides (Co_2W_4C) along with new phases that were also noted in the low-energy input: unbrittle eta carbides (Co_6W_6C) and Co. The increase in the amount of W_2C and eta carbides Co_6W_6C at both laser-processing energy inputs, along with the presence of the W phase and brittle eta carbides (Co_2W_4C) as new phases in the high-energy input (P.S.6), demonstrates the growing release of carbon from the WC into the surroundings as a result of high temperature melt. Furthermore, one can clearly see that the degree to which the carbons decarburized increased in line with the amount of heat energy input, which either explains the rise in the peak intensity and quantity of W_2C components or reveals the W phase and brittle eta carbides (Co_2W_4C) as new phases for the P.S.6, in comparison with the P.S.4, which yields lower-energy input. The eta carbides' phases (Co_6W_6C and Co_2W_4C) were formed as a result of the reaction between the Co and WC phase during the laser melting processing [26]. However, the Influence of Eta-Phase on Wear characteristics of WC-Co Carbides was experimented on by Formisano et al.[122]. The results show that the wear resistance depends on the size and distribution of the Eta-phase. The samples that show the greater increase in performance, compared to the stoichiometric one, are those with lower carbon content. They have a gradually smaller Eta-phase size with a larger distribution.

Novel Enhancement of HVOF Thermal Sprayed Nanostructured WC-12Co / Inconel-625 Coatings for Tribocorrosion Applications | **Al-Harbi, Naif I**

170

Figure 5-65 shows the XRD patterns of the mixed coatings after the laser treatment under two different energy inputs. First, the observer should note that the XRD analyses could not be carried out in the sample treated at the highest-energy inputs, such as P.S.6 or P.S.2 respectively amongst the DOE metrix shown in Table 3-6, as these laser settings provided high energy inputs that yielded high surface roughness (above 20 μm) where the XRD only penetrated to a depth of 10–20 μm, even after polishing, therefore the coating's top surface fractured because of large gas pockets in the coating layers (as will be discussed in the following section).

The results of the XRD patterns of the mixed coating, under different energy inputs (P.S.10 and P.S.4), can be seen in Figure 5-65. At low-energy inputs, the result for P.S.10, as can be seen, shows it to have been composed of almost the same phases as were seen for the as-sprayed mixed coating in Figure 5-21. The only minor differences to be noted are the disappearance of cobalt as an interaction with chromium (CrCo) between 50 and 55° of 2θ, along with the vanishing of nickel peak between 70 and 80° of 2θ. However, such results are as expected because the only change under this low-energy input is usually characterised by partial melting of the coating's top layer surface and partial reduction of this region's defects. Under high-input energy, as can be seen in the same figure in comparison to the XRD patterns of the as-sprayed mixed HVOF coating and in laser treatment under low-input energy (P.S.10), the eta carbide phases (Co_6W_6C and Co_2W_4C) became the major phase in contrast to the WC phase, which was a major phase prior to laser processing. Furthermore, the pattern indicates a greater magnitude of the W_2C phase along with W and Cr_2O_3, further new phases that had not been found under the low-energy input. The observer should note here that the degree of decarburization of carbons from the WC was higher in the mixed coating of P.S.4 than that found in P.S.6 of the monomial nWC-12Co coating, despite the latter providing a higher-energy input. This may be attributed to the increases in the wettability level of nano-scale WC carbides, caused by increasing the ratio of binder matrix in the coating layer [106].

Similar finding confirm the effect of the binder ratio in the decomposition of WC in WC/Co coating carried out by Chivavibul et al. [123], the results revealed that the increase in the cobalt content from 12 to 25 wt.% led to higher degree of dissolution of WC carbides and finally to lower a reduction in hardness and toughness.

Novel Enhancement of HVOF Thermal Sprayed Nanostructured WC-12Co / Inconel-625 Coatings for Tribocorrosion Applications | **Al-Harbi, Naif I**

171
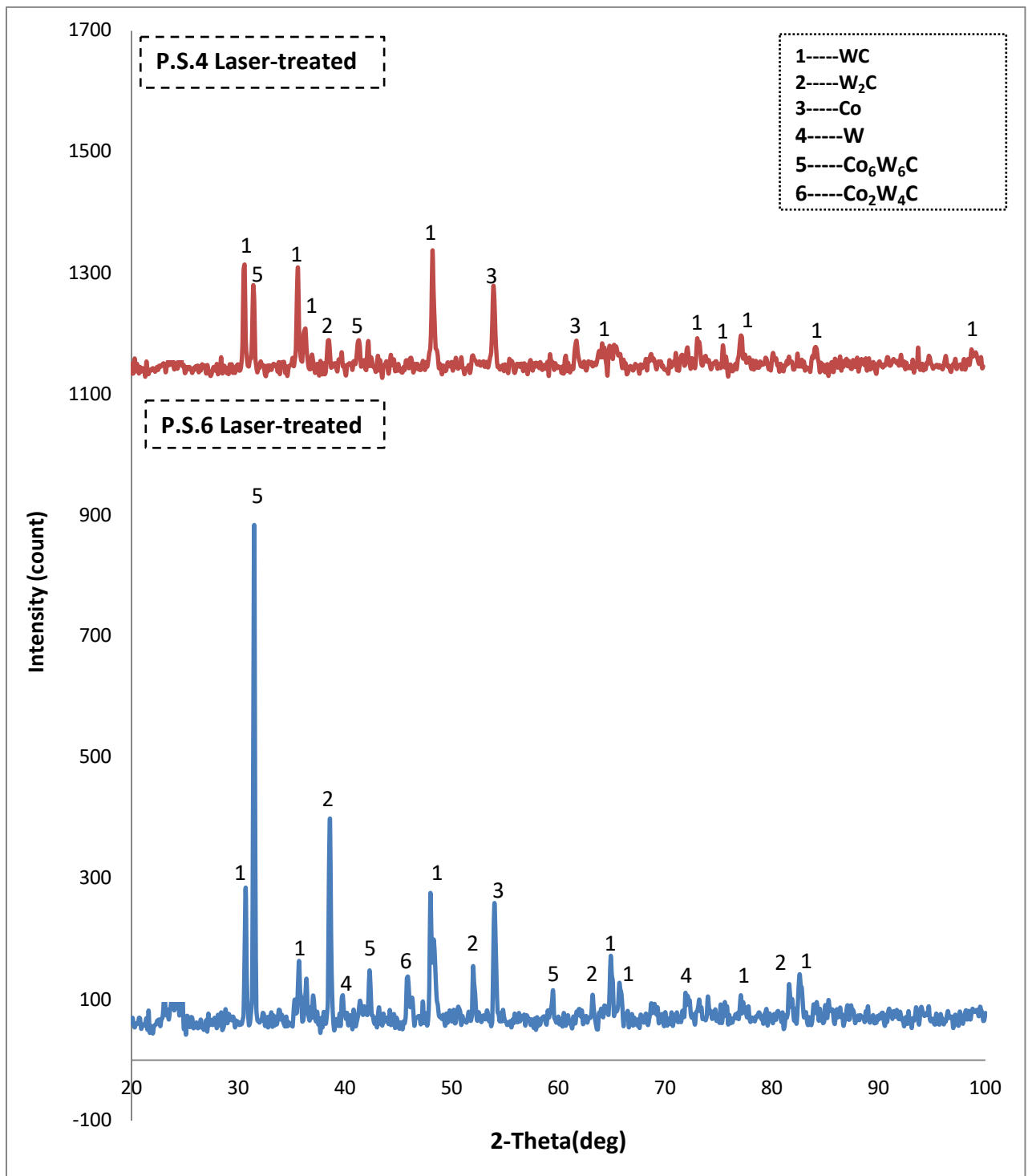
Figure 5-64: XRD results for laser-treated monomial nWC-12Co HVOF coating under different energy inputs, P.S.4 being the lowest and P.S.6 the highest.

Novel Enhancement of HVOF Thermal Sprayed Nanostructured WC-12Co / Inconel-625 Coatings for Tribocorrosion Applications | **Al-Harbi, Naif I**

172
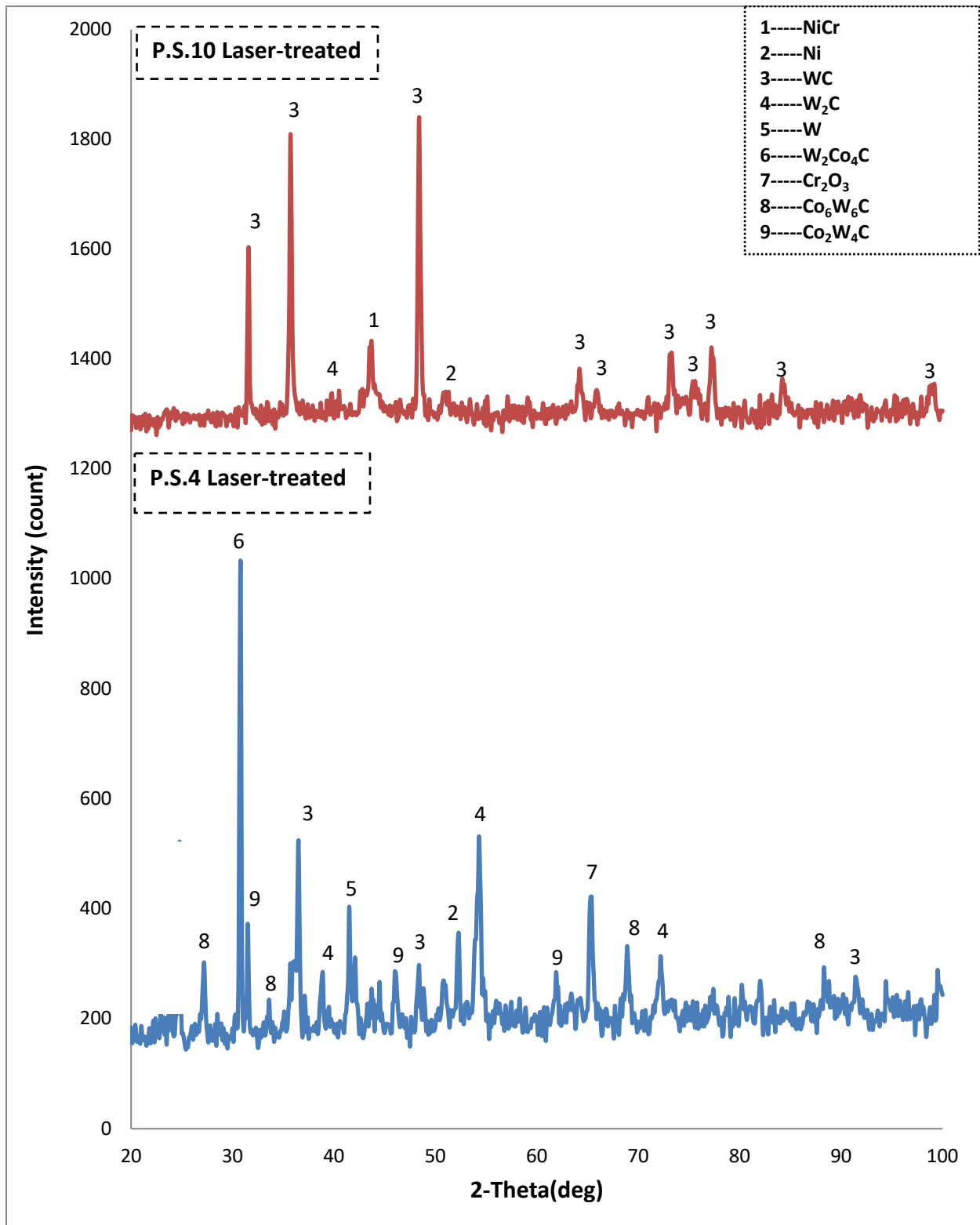
Figure 5-65: XRD results for laser-treated nWC-12Co HVOF coating under different energy inputs, P.S.10 being the lowest and P.S.4 the highest.

Novel Enhancement of HVOF Thermal Sprayed Nanostructured WC-12Co / Inconel-625 Coatings for Tribocorrosion Applications | **Al-Harbi, Naif I**

173

5.8 Cross-section of laser-treated HVOF coatings

The cross-section of the two HVOF coatings, nWC-Co and the mixed ones, after laser treatment under different energy inputs (from lowest to highest) are shown in Figures 5- 66 to 5- 69 and 5- 71 to 5- 73 respectively. The laser processing under low energy for the nWC-Co HVOF coating demonstrates that only the top region of the coating layer was melted, as can be seen in P.S.8 in Figure 5-66, and the melting region shows a smooth surface with a homogeneous structure, along with a low porosity level and no sign of cracks.

Below the melting region lay the heat-treated region; that is, the temperature was not sufficient to reach the melting temperature of the nWC-Co HVOF coating. Therefore, the microstructure's homogeneity appears to have become lower as it went further to the substrate side, as evidenced by, for example, the splat boundaries and small gaps appearing in this region. Furthermore, the interface between the coating and substrate was not affected by the laser treatment and porous strips that were noted in the as-sprayed coating available.

When using a laser setting that provided higher-energy input (moderate), such as P.S.4 and its corresponding cross-section shown in Figure 5-67, the results demonstrate that a full melting of the coating layer was achieved that almost provided the ideal microstructure of a coating layer. The latter is characterized by a smooth surface with no visible unmelted splats, cracks, or porosity, except that available in micro-levels in the region close to the substrate, which may be attributed to the low temperature level reached in that region in comparison to its upper counterpart. This also explains the deformation of solid geometry shown between the coating and substrate regions, which may be attributed to a lack of sufficient heat to achieve a perfect change from mechanical to fusion bonding; furthermore, during the cooling stage, the coating and substrates begin to shrink at uneven strain properties, leading to the formation of distortion geometries. Moreover, the chemical etching of P.S.4 shows the formation of a fine dendrites phase under this laser setting, located in the upper region of the laser-treated coating layer as shown in Figure 5-68.

Novel Enhancement of HVOF Thermal Sprayed Nanostructured WC-12Co / Inconel-625 Coatings for Tribocorrosion Applications | **Al-Harbi, Naif I**

174
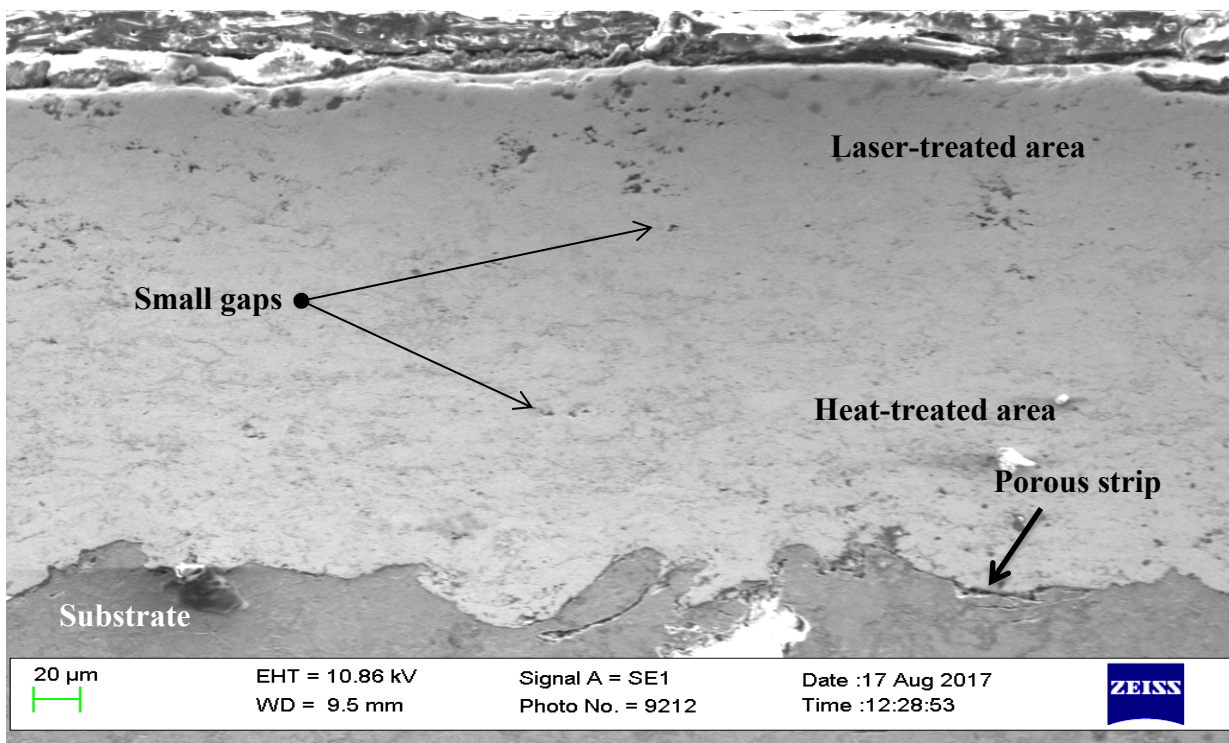
Figure 5-66: SEM micrograph of cross-section of laser-treated nWC-Co coating (P.S.8).
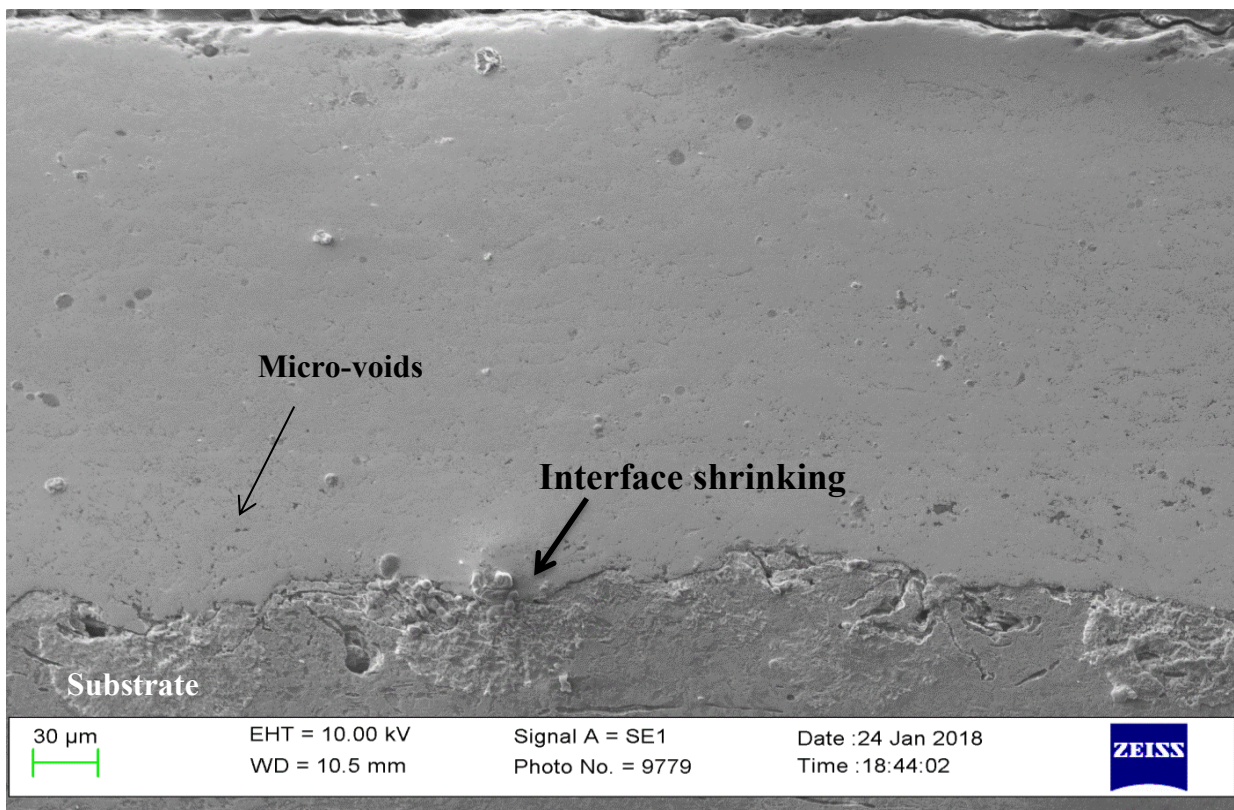
Figure 5-67: SEM micrograph of cross-section of laser-treated nWC-Co coating (P.S.4).

Novel Enhancement of HVOF Thermal Sprayed Nanostructured WC-12Co / Inconel-625 Coatings for Tribocorrosion Applications | **Al-Harbi, Naif I**

175
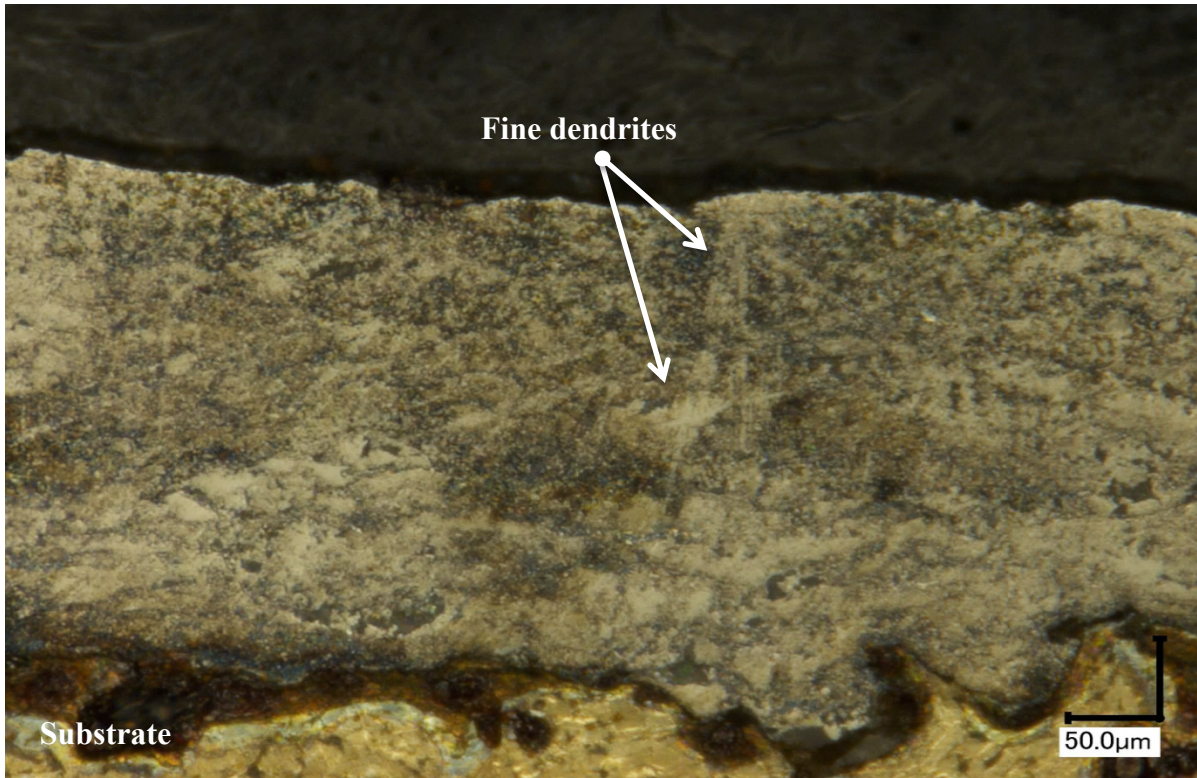
Figure 5-68: Microscope image of laser-treated HVOF coating (P.S.4) following chemical etching, showing fine dendrites phase close to the free surface region.

The cross-section of the laser setting P.S.6, which provided the highest energy amongst the DOE matrix shown in Figure 5-69, which displays a clear formation of the SEM micrograph under this setting, which yielded a smooth surface with no sign of cracks and unmelted splats along the coating layer. However, distortion defects were scattered along the coating layer and mainly concentrated in its upper region, which may have formed as a result of the high thermal energy used under this laser setting. In contrast to what was observed earlier in Figures 5-66 and 5-67 for P.S.8 and P.S.4 respectively, because of the high energy, the interface between the HVOF coating and substrate changed completely, from mechanical bonding within porous strips to fusion bonding. This was confirmed even further by the EDS line scan for the constitution elements of this coating (tungsten and cobalt), along with iron (Fe) for the substrate used along the coating layer depth as shown in Figure 5-70. Obviously, in the interface denoted by the red circle (A1), different elements intersected at that region and the metallurgical bonding between the coating and substrate was created.

Novel Enhancement of HVOF Thermal Sprayed Nanostructured WC-12Co / Inconel-625 Coatings for Tribocorrosion Applications | **Al-Harbi, Naif I**

176
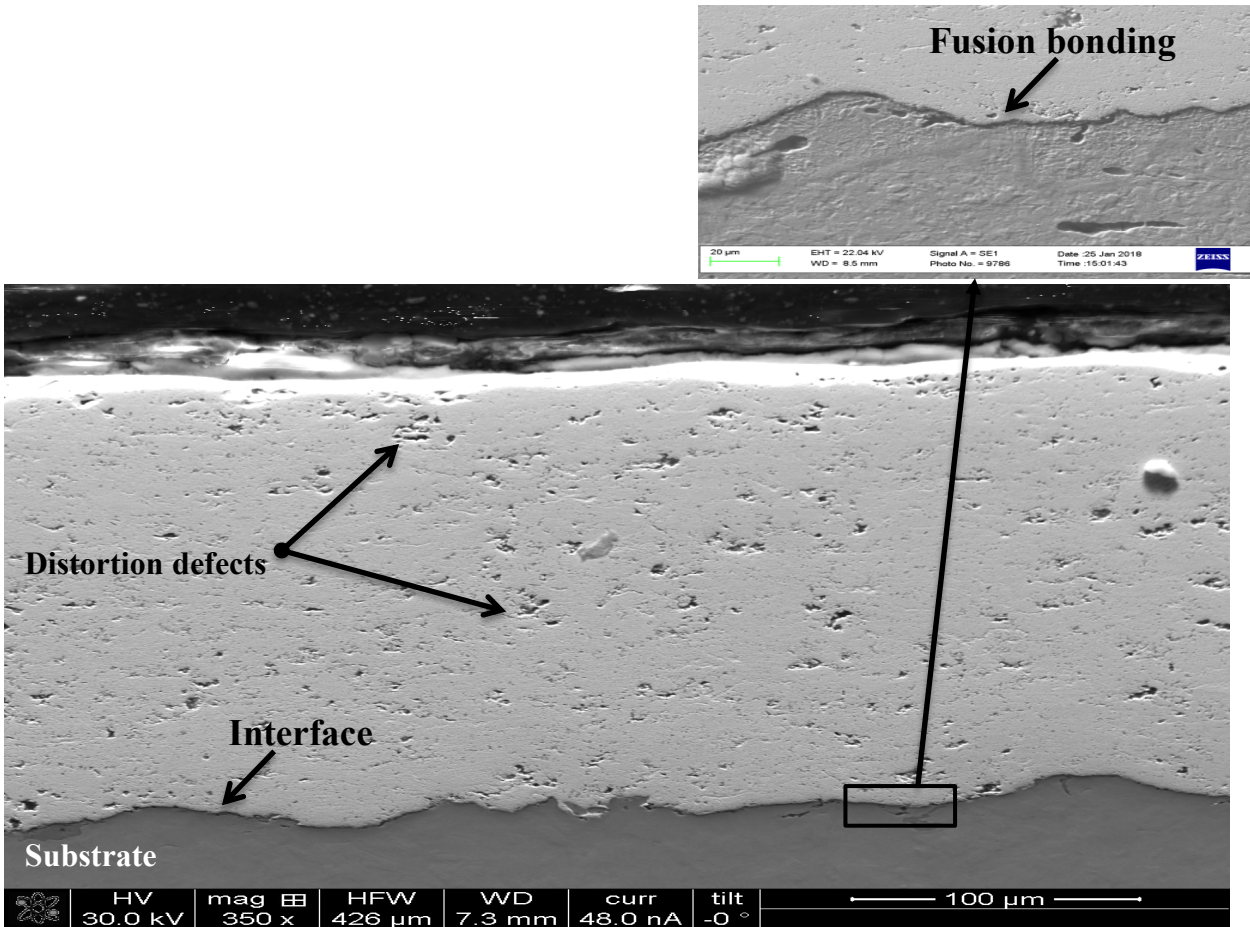
Figure 5-69: SEM micrograph of cross-section of laser-treated nWC-Co coating (P.S.6).
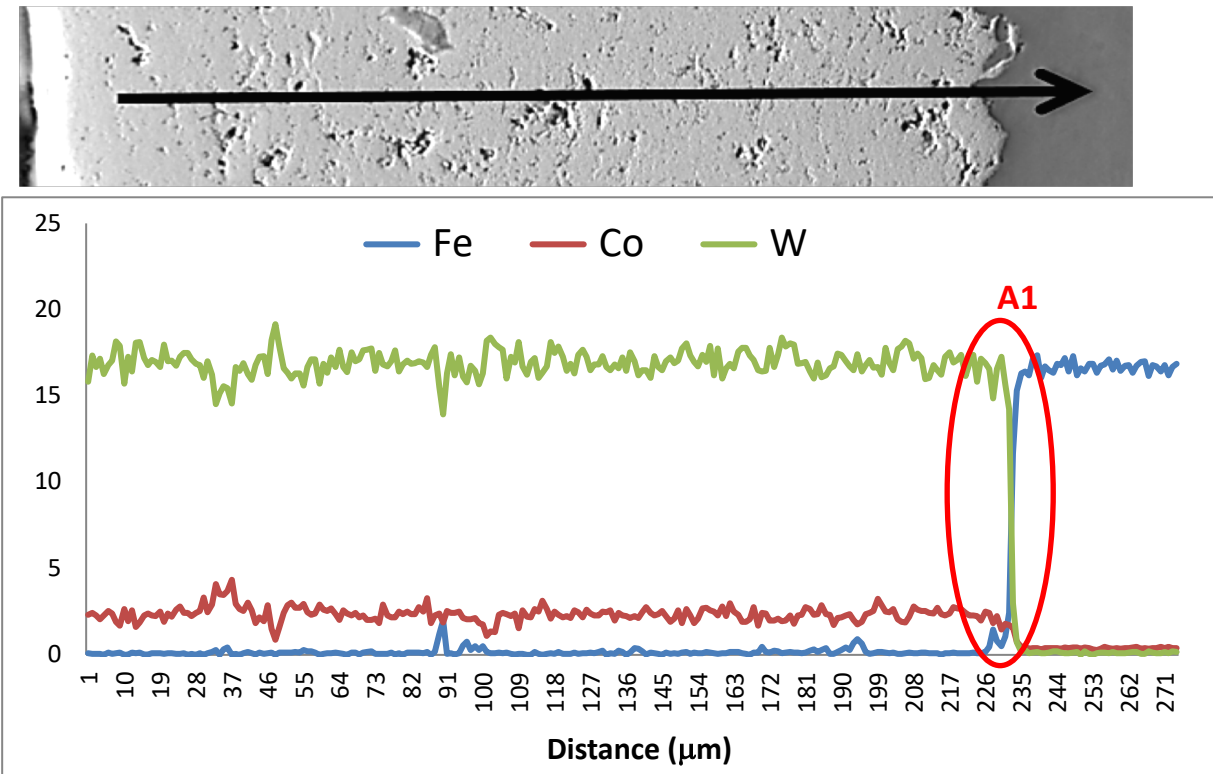
Figure 5-70: EDS line scan of laser-treated nWC-Co HVOF coating (P.S.6), into the interface location.

Novel Enhancement of HVOF Thermal Sprayed Nanostructured WC-12Co / Inconel-625 Coatings for Tribocorrosion Applications | **Al-Harbi, Naif I**

177

For the mixed coating under the same concept, the cross-section of the laser-treated coating layer under three laser settings can be seen from Figures 5-71 to 5-73. Figure 5-71 shows an SEM micrograph of a cross-section for a partial melting of P.S.1, which was laser-treated at a low-energy input, which had a laser power of 150 W, 225 mm/min scanning speed, and the lowest focal position height and provided the smallest beam size of +35 mm. This laser setting only melted the upper region of the coating layer, resulting in a significant reduction of a number of coating defects that were observed in the untreated laser coating shown in Figure 5-11. The roughness was slightly reduced at the surface and significantly reduced in the interconnected porosity at the upper region between the different coating particles, in comparison to the heat-treated region that was close to the substrate side. Furthermore, a closer inspection of the upper region clearly reveals partial homogeneity of the coating elements' distribution along the microstructure, whereas, as explained earlier, the dark phase is Inconel 625 powder and the white phase is the WC nanoscale particles.

Figure 5.72 shows an SEM micrograph of a cross-section of a fully melted mixed HVOF coating for P.S.9. The fusion bond at the interface between the coating and the substrate was created by the laser treatment. Comparing the cross-section between P.S.1 and P.S.9, in which the laser setting of the latter provided a higher-energy input, the homogeneity was significantly enhanced by increasing the energy input, especially in the region close to the top surface because the microstructure appeared to be almost "one colour". This gives the impression that the elements were redistributed evenly along the coating layer at this region; after the laser re-melting process, the microstructure looked denser with a lower amount of visible unmelted splats, with their corresponding interconnected porosity level, than can be seen in P.S.1. However, at this energy level, the surface looked rougher and the gas pockets formed close to the top free surface as a result of the higher energy fluence (J/mm^2) (energy delivered per unit area) when air bubbles did not have sufficient time to escape from the melted pool, as discussed in detail in Chapter 4 of this thesis. Here, the source of the gas could have been the porosity present in the HVOF coating or the reaction of metallic oxides with carbon to form CO and CO_2. The concentration of the gas pockets at the near-surface region was a consequence of this region receiving the total energy absorbed by the laser beam, which was dissipated in the form of temperature conductivity transmitted through the coating layer.

Novel Enhancement of HVOF Thermal Sprayed Nanostructured WC-12Co / Inconel-625 Coatings for Tribocorrosion Applications | **Al-Harbi, Naif I**

178
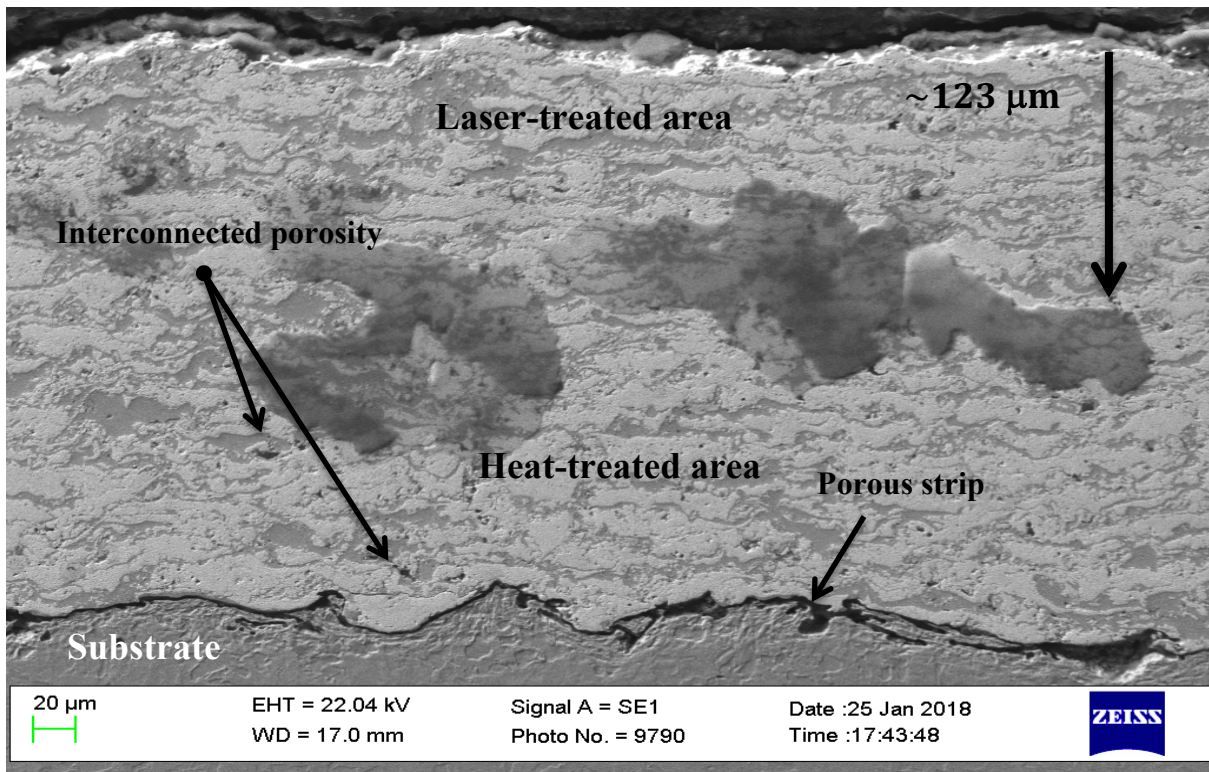
Figure 5-71: SEM micrograph of cross-section of laser-treated mixed coating (P.S.1).
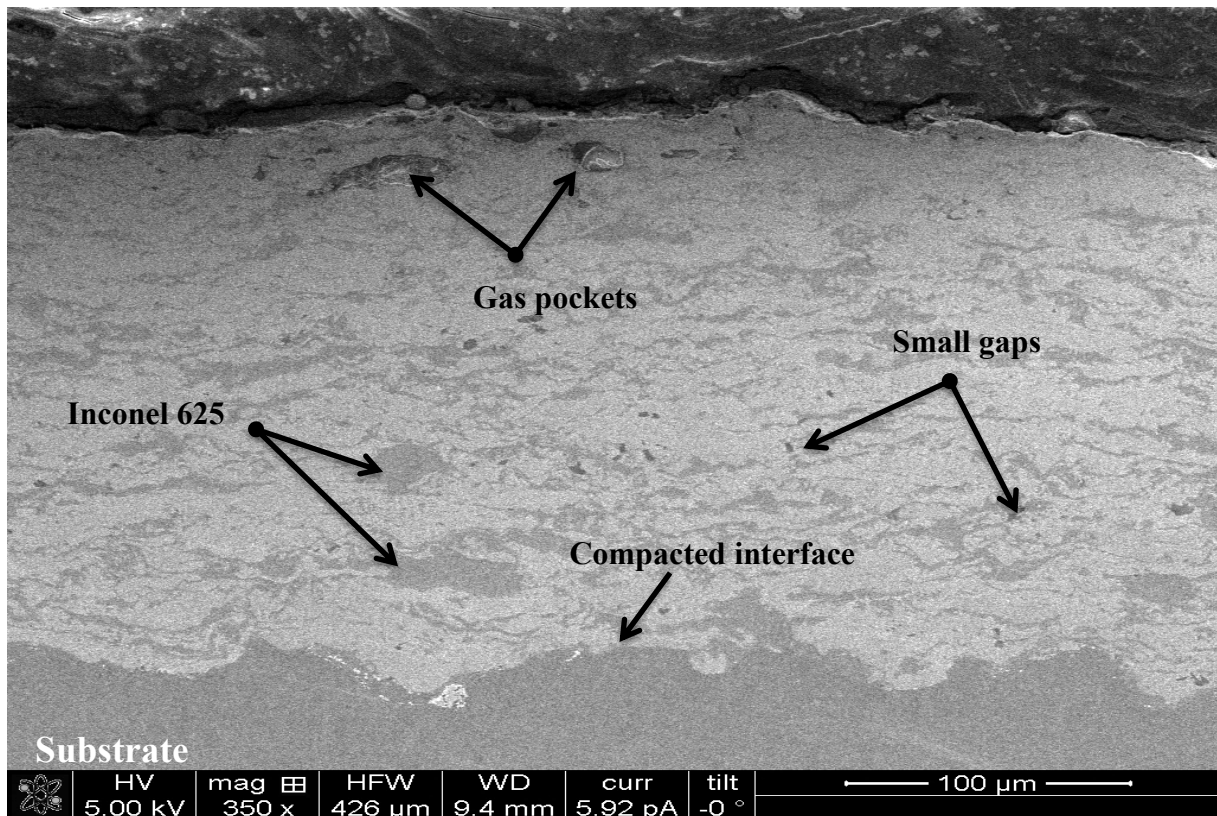
Figure 5-72: SEM micrograph of cross-section of laser-treated mixed coating (P.S.9).

Novel Enhancement of HVOF Thermal Sprayed Nanostructured WC-12Co / Inconel-625 Coatings for Tribocorrosion Applications | **Al-Harbi, Naif I**

179

Similarly to what was conducted for the laser-treated monomial nWC-12Co coating, Figure 5-73 presents the cross-section of the laser-treated mixed HVOF coating under the highest energy input among the DOE matrix (P.S.6). It can be clearly seen from this SEM micrograph that the surface became rougher and the diameter and quantity of the gas pockets significantly increased. This is a result of the higher energy input applied. The coating/substrate clearly compacted and formed metallurgical bonding between the two surfaces. The EDS line scan along the depth of the coating layer, and the corresponding results, are presented in Figure 5-74. The elements selected for the coating were tungsten, nickel, and chromium, while iron (Fe) was chosen for the substrate. Obviously, the interface denoted by the red circle (A1) confirms that different elements intersected at that region and that metallurgical bonding between the coating and substrate was created. In addition, by comparing the upper region of the laser-treated coating layer with its lower counterpart, denoted by the red circle (A2), the observer can unequivocally see that the former was more homogeneous then the lower one, as can be seen the concentration of the elements are fluctuating and that attributed to lower thermal energy reached to this region in comparison the upper one to sufficiently re-melted and the elements evenly distribute it.
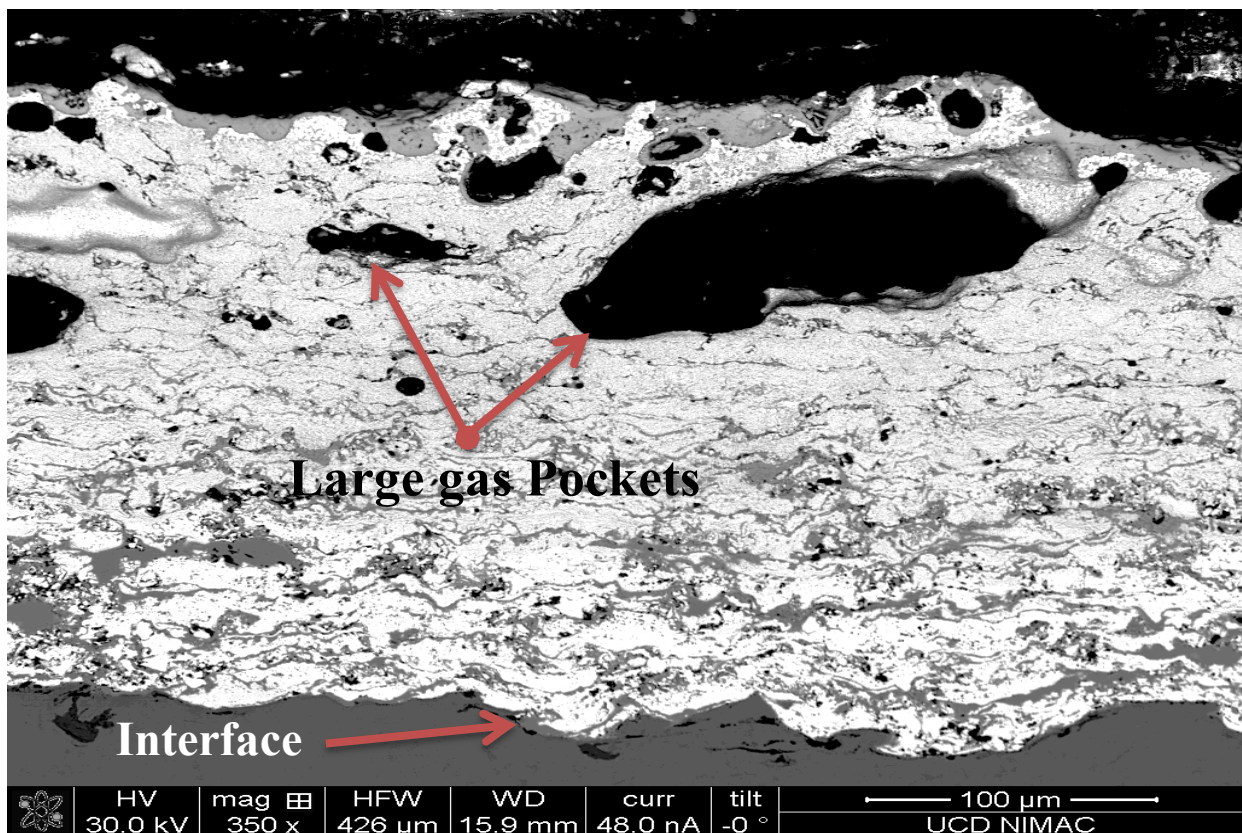
Figure 5-73: SEM micrograph of cross section of laser treated the mixed coating (P.S.6).

Novel Enhancement of HVOF Thermal Sprayed Nanostructured WC-12Co / Inconel-625 Coatings for Tribocorrosion Applications | **Al-Harbi, Naif I**

180
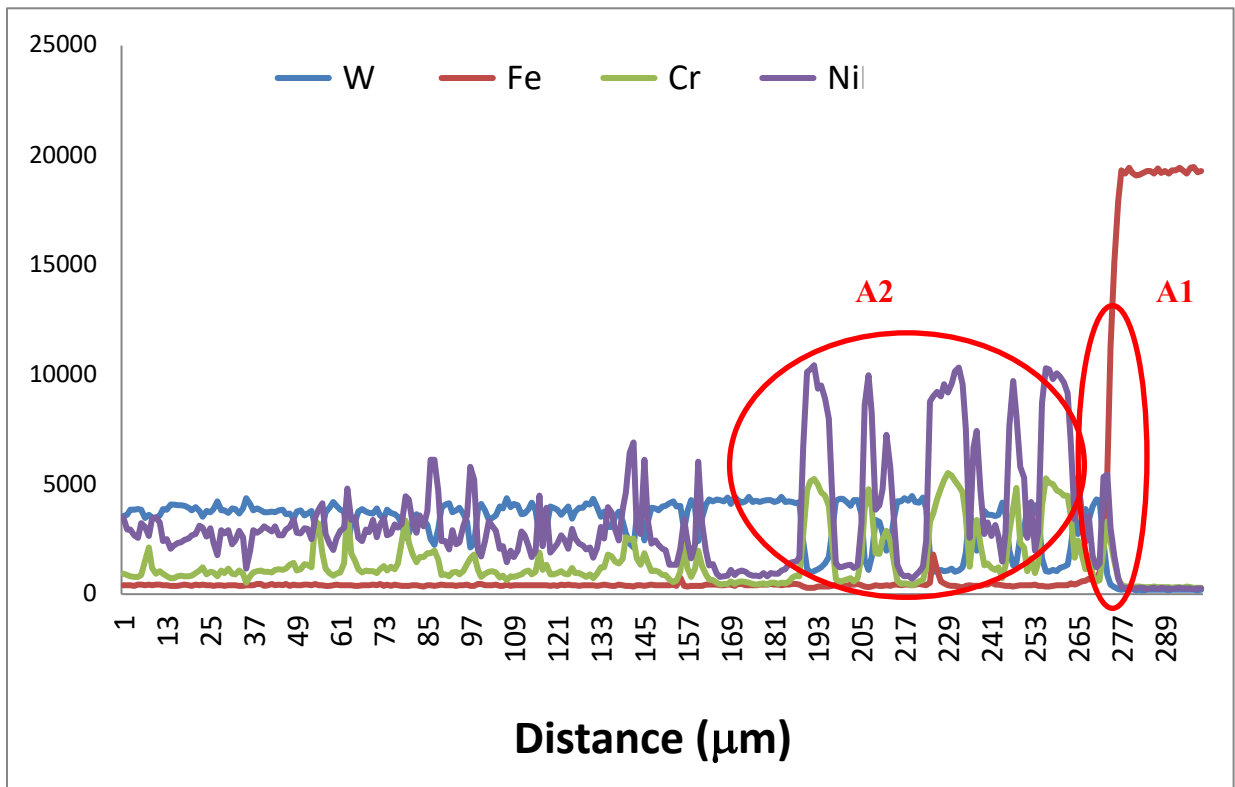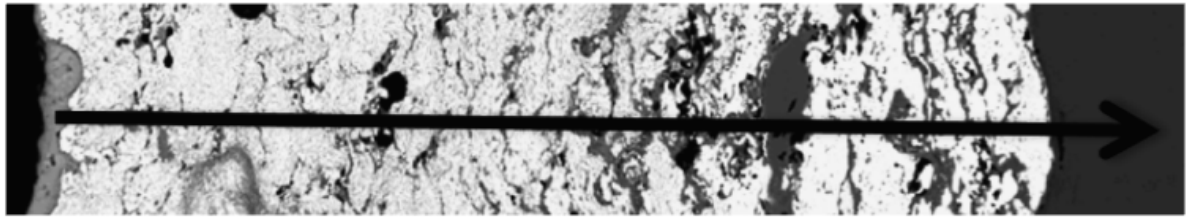
Figure 5-74: EDS line scan of laser treated Mixed HVOF coating (P.S.6), into the interface location.

5.8.1 Element mapping of laser treated HVOF coatings

Homogeneity of the both HVOF coatings after laser treatment can also be observed by the EDS measurement. Figure 5.75 illustrates the EDS elemental mapping of the laser partially melted mixed coating of P.S.10. Three elements of the mixed coating were selected namely Nickel, chromium and cobalt. As clearly can be seen, the laser treated region (top area) has homogeneous distribution of the three different elements that under investigation. Which indicated significant improvement in coating homogeneity in comparison to EDS element mapping measurement that was taken earlier for the mixed as-sprayed coating that shown in Figure 5-18. In addition, aluminium EDS mapping was taken to evaluate the contamination by the grit blasting materials that used for substrates surface preparation, as can be seen the result indicate and confirm the availability of the remained aluminium oxide particles after

Novel Enhancement of HVOF Thermal Sprayed Nanostructured WC-12Co / Inconel-625 Coatings for Tribocorrosion Applications | **Al-Harbi, Naif I**

181

the preparation process and that indicated by the bright colour in the coating /substrate interface region.
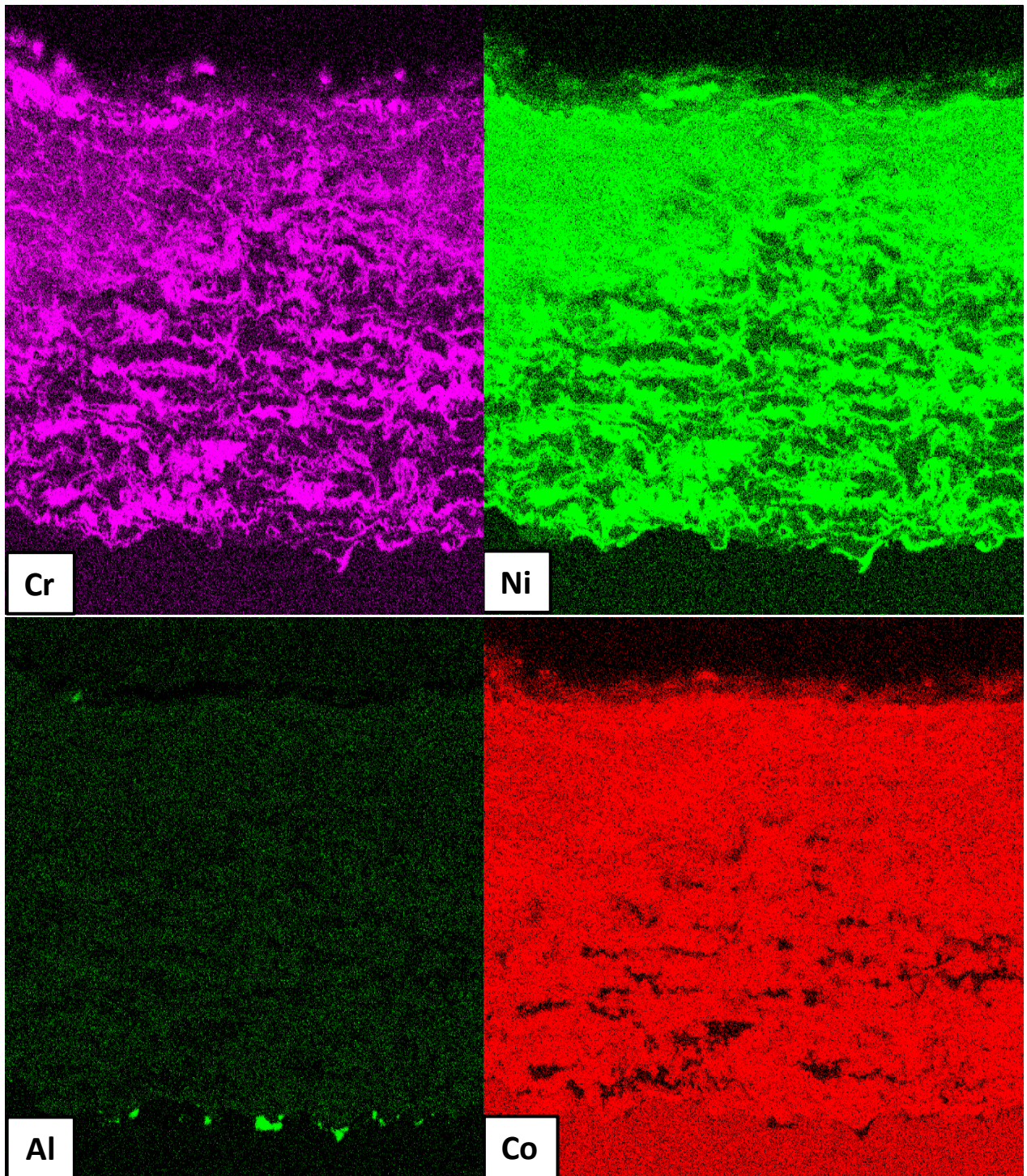
Figure 5-75: EDS element mapping of the laser treated mixed HVOF coating (P.S.10) with Partially melting of the coating layer.

Novel Enhancement of HVOF Thermal Sprayed Nanostructured WC-12Co / Inconel-625 Coatings for Tribocorrosion Applications | **Al-Harbi, Naif I**

182

Figure 5-76 illustrates the EDS reading in three different areas along the laser treated nWC-Co coating layer depth (P.S.4), with almost full melting of the coating layer was achieved under this laser sitting as discussed earlier. Looking to the percentage of the constitution elements of this monomial coating (the tungsten and the cobalt) as given in the table within Figure 5-76, the percentages were almost constant along the depth of the coating layer, which confirms the homogeneity of the coating elements in the coating layer as result of laser remelting which significantly improved, compared to the EDS element mapping that carried out for the as-sprayed coating earlier in Figure 5-19. The EDS analysis reveals also a higher dissolution of W and C in the cobalt phase in comparison to the EDS analysis carried out earlier in Figure 5-17 for as-sprayed coating at two different locations. This was expected due to the higher operating temperature resulting from laser post processing. Where the high ratio of the free carbon in the upper (A1) relative to the middle (A2) and the bottom area (A3), resulting can happened also due a higher temperature reached to the surface region in comparison to another two areas. Furthermore the Fe and Al percentage were highest in the area the close to the steel substrate (A3).
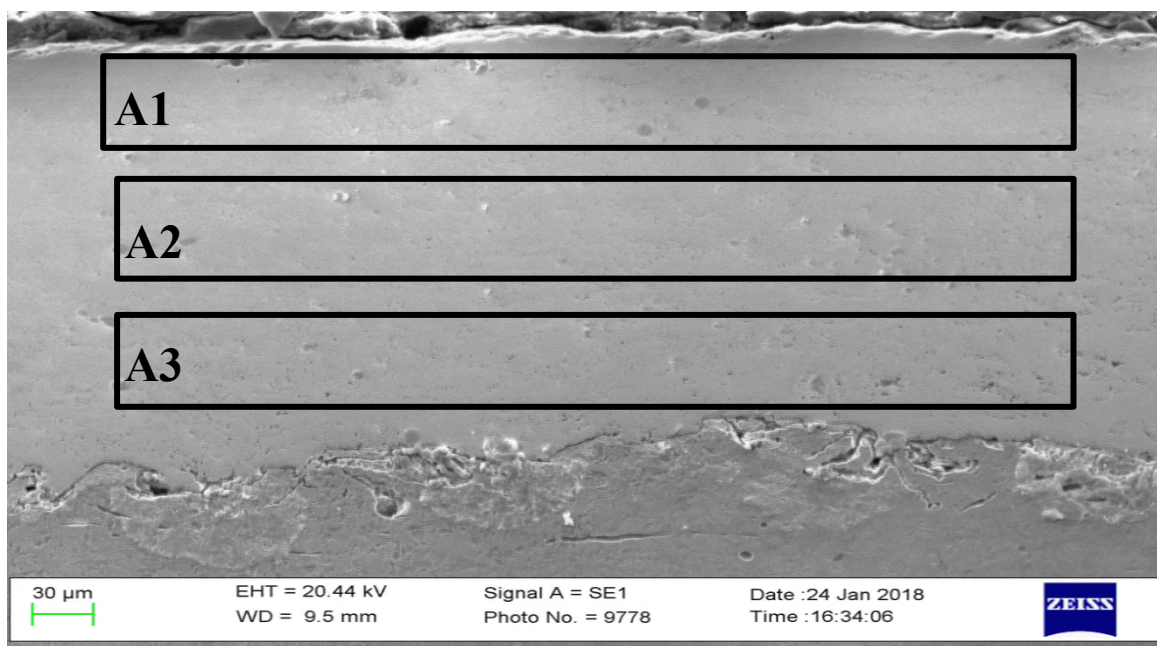
Element	W	Co	C	Fe	Al	Total (wt. %)
Area 1	73.87	11	13.9	0.11	0.12	100
Area 2	75.07	10.87	13.79	0.15	0.12	100
Area 3	73.92	10.89	13.79	0.26	1.14	100

Figure 5-76: EDS results of different areas of nWC-Co HVOF coating after laserTreatment.

Novel Enhancement of HVOF Thermal Sprayed Nanostructured WC-12Co / Inconel-625 Coatings for Tribocorrosion Applications | **Al-Harbi, Naif I**

183

5.8.2 Porosity measurements of laser treated HVOF coatings

Figure 5.77 illustrates the results of porosity measured for both HVOF coating types after laser treatment. The measurement were taken close to the surface region of the laser treated coating layer, as the various laser sitting provided different laser melting depth at the coating layer. Compared to the porosity before laser treatment which was 3.5 % and 4.9 %, the porosity level for the monomial nWC-12Co and it was then mixed with the coating, there is significant reduction of porosity after laser treatment. P.S.4 and P.S.2 has the lowest porosity after laser treatment for the nWC-Co HVOF coating of 0.46 and 0.7% respectively, and P.S.10 and P.S.12 has the lowest porosity after laser treatment for the mixed coating of 0.8 and 0.9 % respectively, and as discussed in details in literature chapter coating with low porosity level is an important factor for protecting the substrate in corrosive environments. Furthermore; the results show a strong correlation between the porosity levels of the coating layer (laser treated and as-sprayed) and the surface roughness, there was a linear relation between both of them; high surface roughness indicating high porosity and vice versa. Two porosity measured samples for each of the laser treated coating types are presented in Figures 5-78 to 5-81.
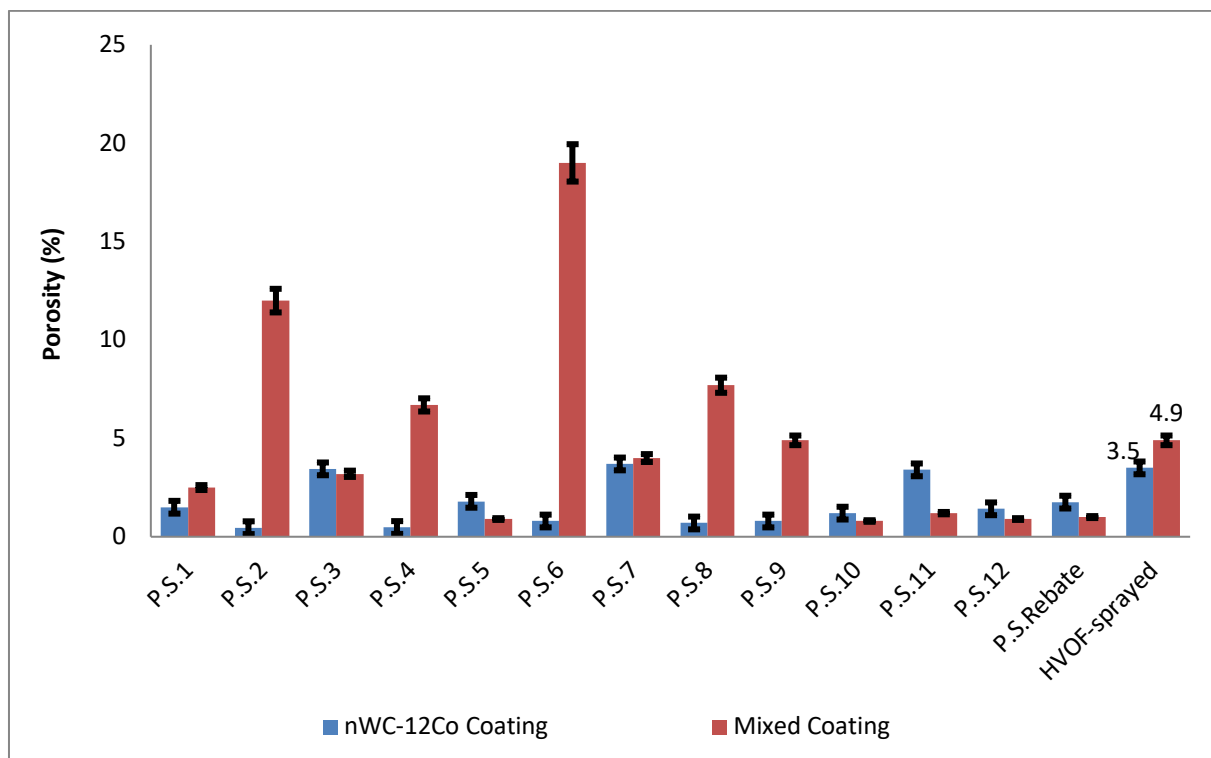
Figure 5-77: Measurement of porosity of various HVOF coatings before and after laser treatment.

Novel Enhancement of HVOF Thermal Sprayed Nanostructured WC-12Co / Inconel-625 Coatings for Tribocorrosion Applications | **Al-Harbi, Naif I**

184
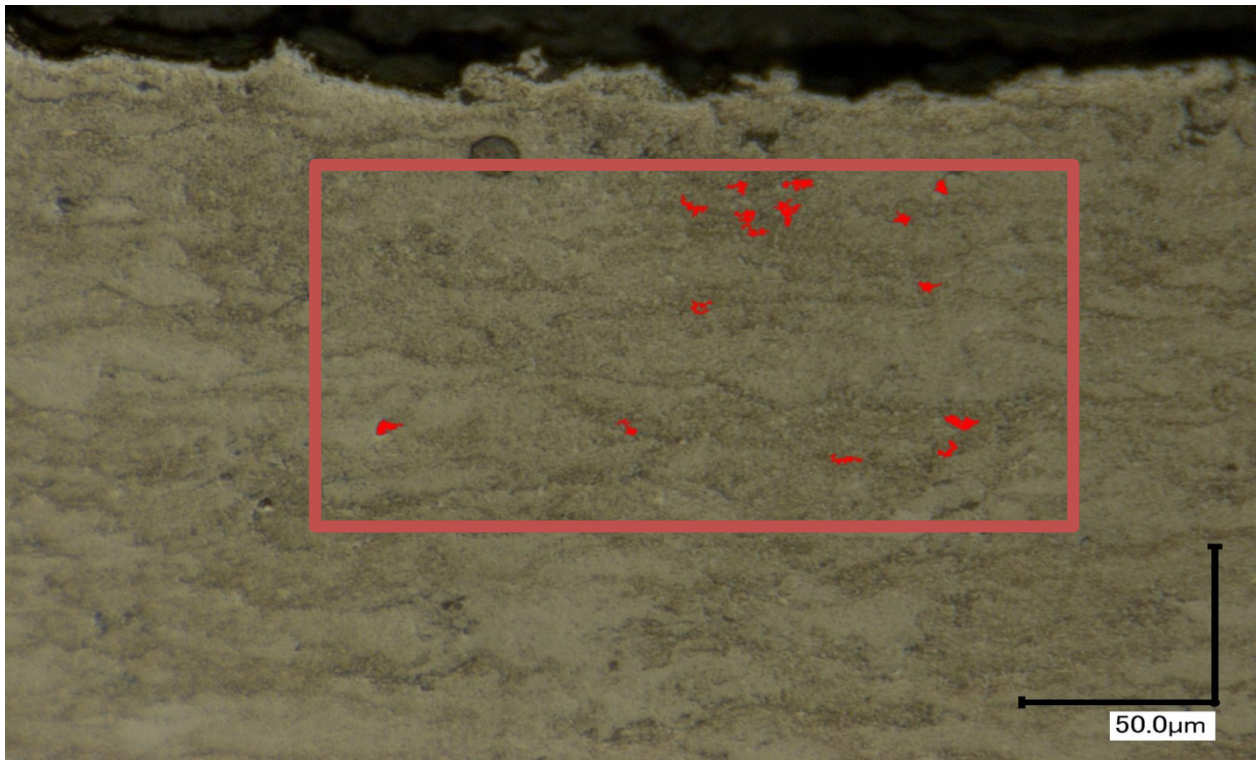
Figure 5-78: Porosity of laser nWC-Co HVOF coating after laser Treatment (P.S.5).
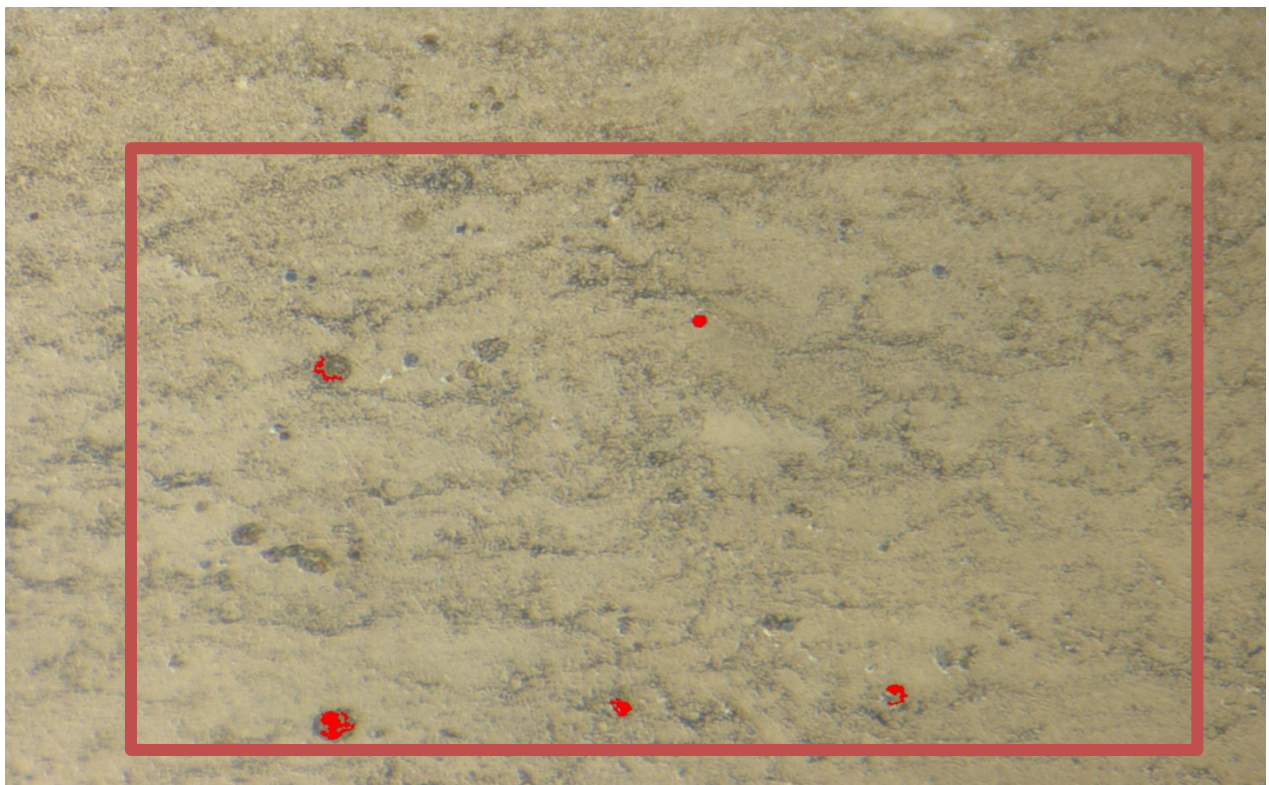
Figure 5-79: Porosity of laser nWC-Co HVOF coating after laser Treatment (P.S.4).

Novel Enhancement of HVOF Thermal Sprayed Nanostructured WC-12Co / Inconel-625 Coatings for Tribocorrosion Applications | **Al-Harbi, Naif I**

185
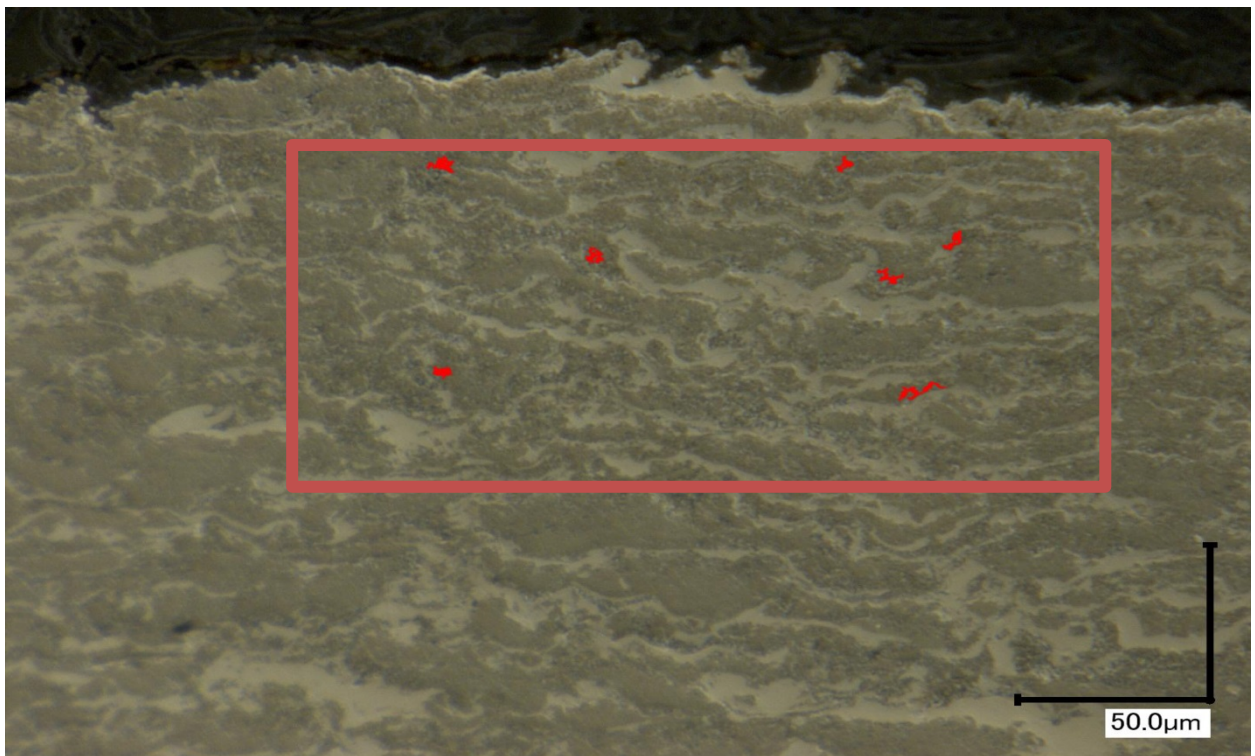
Figure 5-80: Porosity of laser mixed HVOF coating after laser Treatment (P.S.12).
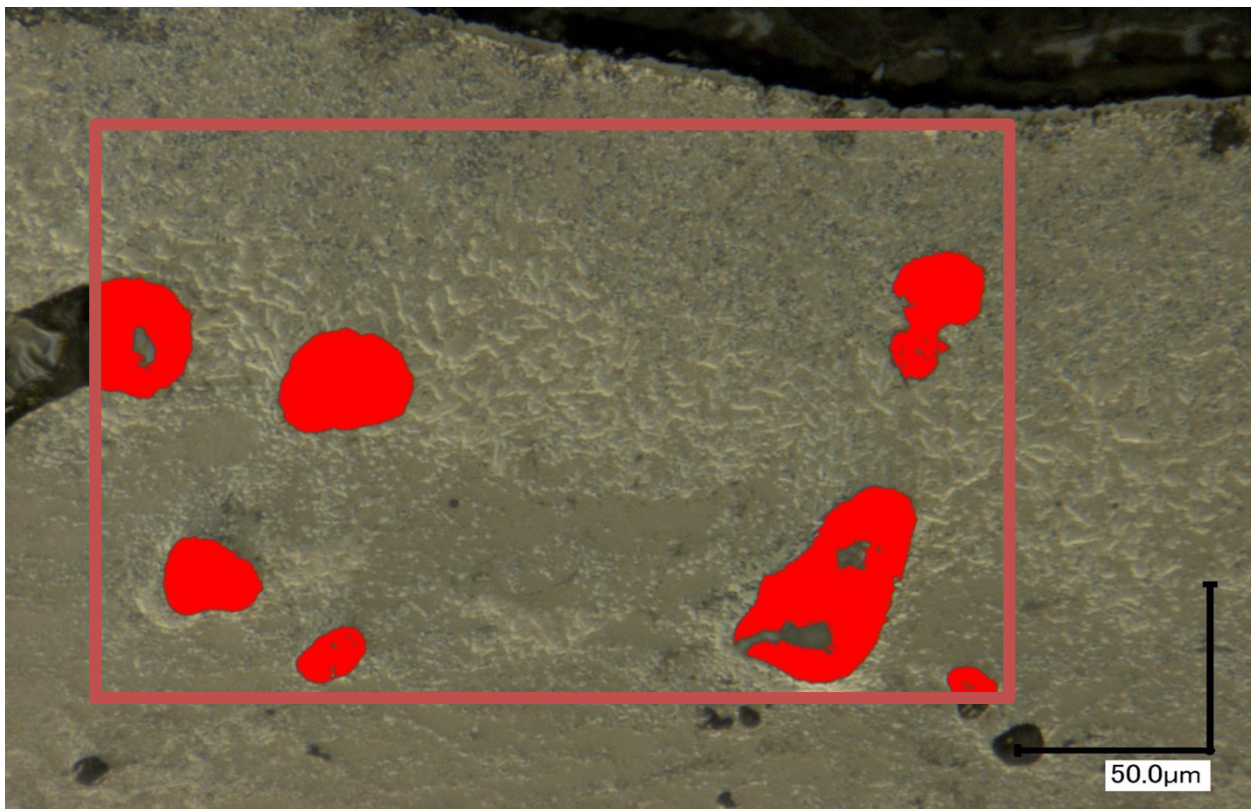
Figure 5-81: : Porosity of laser mixed HVOF coating after laser Treatment (P.S.2).

Novel Enhancement of HVOF Thermal Sprayed Nanostructured WC-12Co / Inconel-625 Coatings for Tribocorrosion Applications | **Al-Harbi, Naif I**

186

5.9 Microhardness of laser-treated HVOF coatings

The average of the microhardness for the two as-sprayed coatings, taken from 20 readings along the coating depth and width and under a 100 g load, was 1329.15 and 1071.05 $HV_{0.1}$ for the monomial nWC-12Co and the mixed coating respectively. Under the same procedure, the average Vicker hardness was measured after the laser treatment under the various laser settings formed from the DOE matrix in Tables 3–6, and the results are presented in Figure 5-83. During the measurement of the microhardness for the laser-treated mixed coating along its cross-section, a problem arose when taking the measurement in the samples treated under energy input, resulting in a coating layer with gas pockets as discussed earlier. The alternative solution was to take the measurement in the overlap zone between the laser tracks; as was found in this region, the gas pockets were significantly smaller in comparison to the central region of the laser beam, as shown for the laser treatment (P.S.4) of the mixed coating in Figure 5-82. This can be attributed to the central region of the laser beam during laser processing, which is surrounded by the region with the high temperature, meaning that the conductivity of the temperature is focused along the depth side only. This is not the case for the sides of the laser beam, which, at one of its sides, is surrounded by the untreated region, and the temperature dissipation takes in two sides, along the depth and on one side of the laser beam. This also explains why the heat-affected zone shape along the depth of the treated surface will always have a hemispherical shape, no matter which laser beam profile is selected [124].
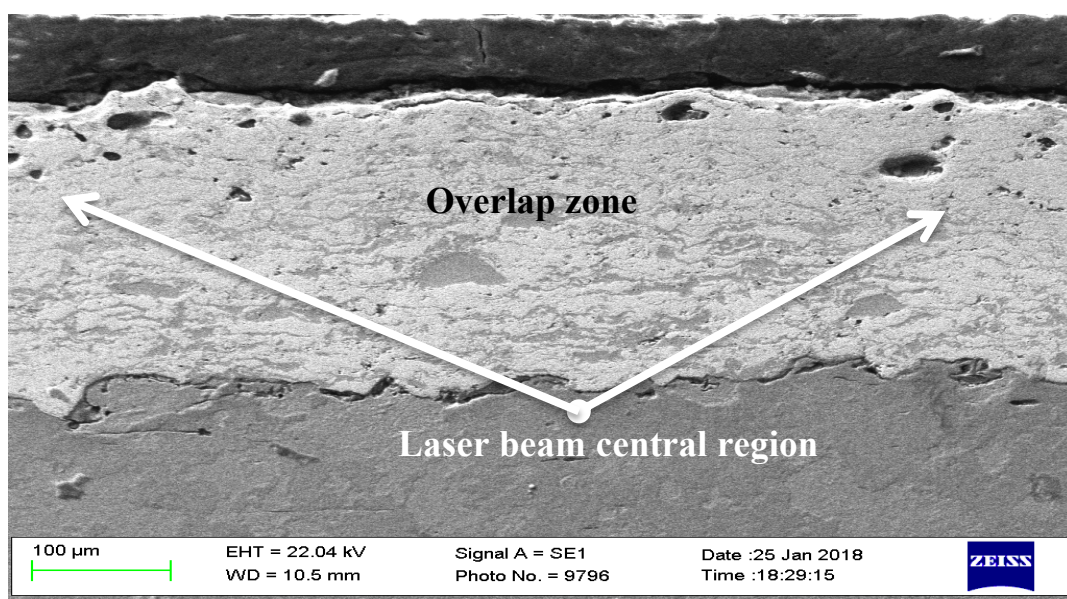
Figure 5-82: The region of the microhardness measured for the laser settings providing gas pockets in the mixed coating layer.

Novel Enhancement of HVOF Thermal Sprayed Nanostructured WC-12Co / Inconel-625 Coatings for Tribocorrosion Applications | **Al-Harbi, Naif I**

187

The results for the two coatings, as can be seen in Figure 5-83, were significantly improved after the laser treatment for a number of settings. This was caused by the enhancement of the coating elements' homogeneity along the cross-section of the coating layer and the elimination of several defects that were noticed in the HVOF as-sprayed coatings, such as micro-cracks and porosity (as shown in Figure 5-25). The P.S.4 and P.S.1 laser settings provided the highest average microhardness for monomial nWC-12Co of 1840 and 1592 $HV_{0.1}$ respectively. For the mixed coating, P.S.6 and P.S.4 provided the highest microhardness of 1305 and 1239 $HV_{0.1}$ respectively. However, the enhancement of the microhardness's average value for laser-treated monomial nWC-12Co was still higher after the laser treatment, and the magnitude of positive changes in a percentage form was greater as well. This may, as explained earlier in the as-sprayed HVOF coating microhardness performance discussion, be the result of the higher ratio of nano-scale hard phase carbide in the starting powder of the monomial nWC-12Co coating type. Other causes might be two factors observed after the laser processing; first, despite the melt depth of the mixed coating being greater under the same laser setting in comparison to the monomial nWC-12Co, as discussed earlier in the melt-pool dimension characterisation, this did not provide better homogeneity of elements, as can be seen in the EDS line scanning for both coatings under the P.S.6 setting (as shown in Figures 5-70 and 5-74). This is attributed to the mixed coating, which is composed of two different coating types; as a result, a higher-energy input is required to fully integrate the elements of the two types and redistribute the homogeneity along the coating layer. Second, the degree of WC particle decomposition in the mixed coating was greater than in the monomial nWC-12Co, as discussed earlier in the XRD analyses section. This was caused by the increase in the wettability brought about by increasing the binder matrices ration surrounding the nano-scale WC hard particles. Consequently, the large ratio of nano-scale WC particles decomposed to a softer W_2C, W phase, and the total average microhardness of the coating was reduced. For the same reason, this P.S.4 had a higher value of average microhardness than the P.S.6 for the laser-treated HVOF monomial nWC-12Co.

Novel Enhancement of HVOF Thermal Sprayed Nanostructured WC-12Co / Inconel-625 Coatings for Tribocorrosion Applications | **Al-Harbi, Naif I**

188
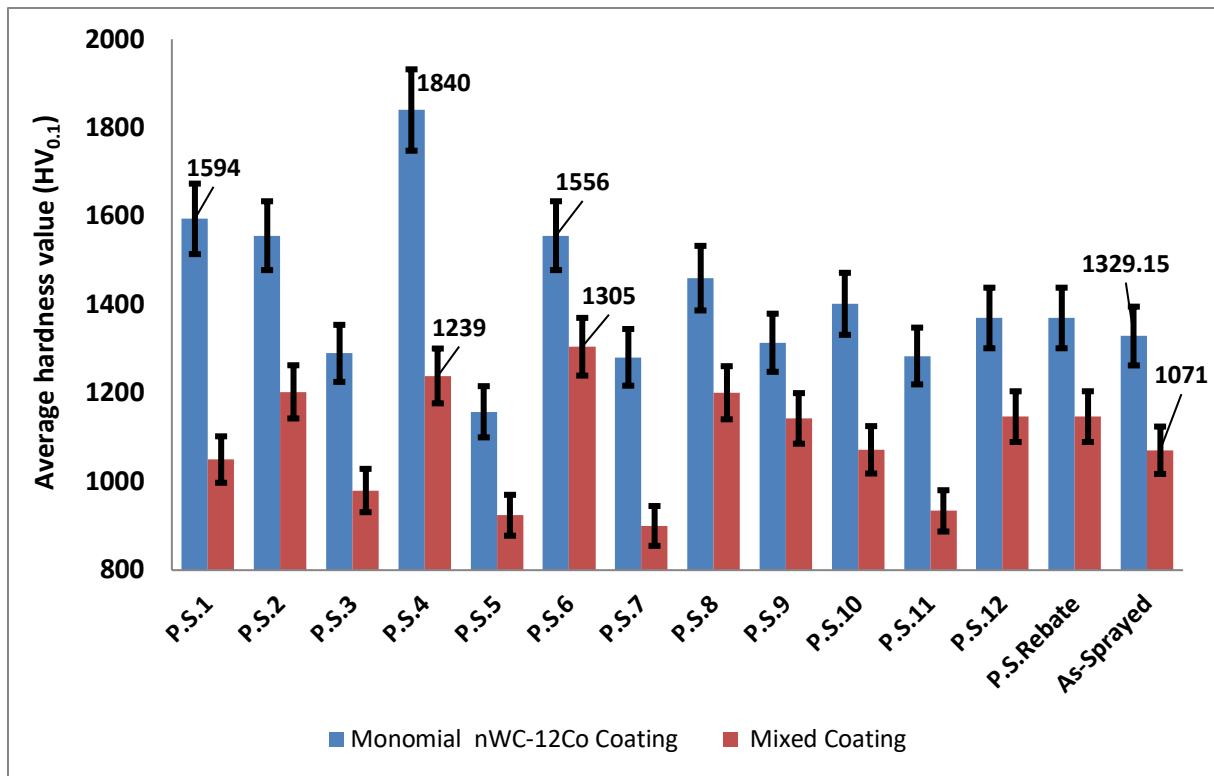
Figure 5-83: Average Vickers hardness value for the two coating types before and after the laser treatment.

Figures 5-84 and 5-85 show the variation of microhardness along the depth for the two coatings before and after laser treatments. Here, P.S.1 provided partial melting of the coating layer for both coatings, while P.S.4 and P.S.6 provided a fully melted coating layer for the monomial nWC-12Co and mixed coating respectively. Due to the elimination of coating defects and enhancement of the coating element's homogeneity after laser processing, the top region of the two coatings under the various laser settings, showed higher microhardness with lower standard deviation to the same region, was measured for the two sprayed coatings. However, the microhardness of the partially melted layer was only increased within the top layer of the coating and began to reduce significantly as it receded from the surface coating region, which can be explained by the fact that the temperature was not, or only slightly reached, the lower region of the coating and no change was made to their microstructure. However, the microhardness results for the laser treated P.S.4 within full melting of monomial nWC-12Co coating layer shows a better result to that obtained by Zhang et al. [56] and their finding presented in figure 2-20 of literature chapter, for HVOF WC-CoCr coating after laser treatment while for the mixed coating under both laser sittings the microhardness slightly lower.

Novel Enhancement of HVOF Thermal Sprayed Nanostructured WC-12Co / Inconel-625 Coatings for Tribocorrosion Applications | **Al-Harbi, Naif I**

189
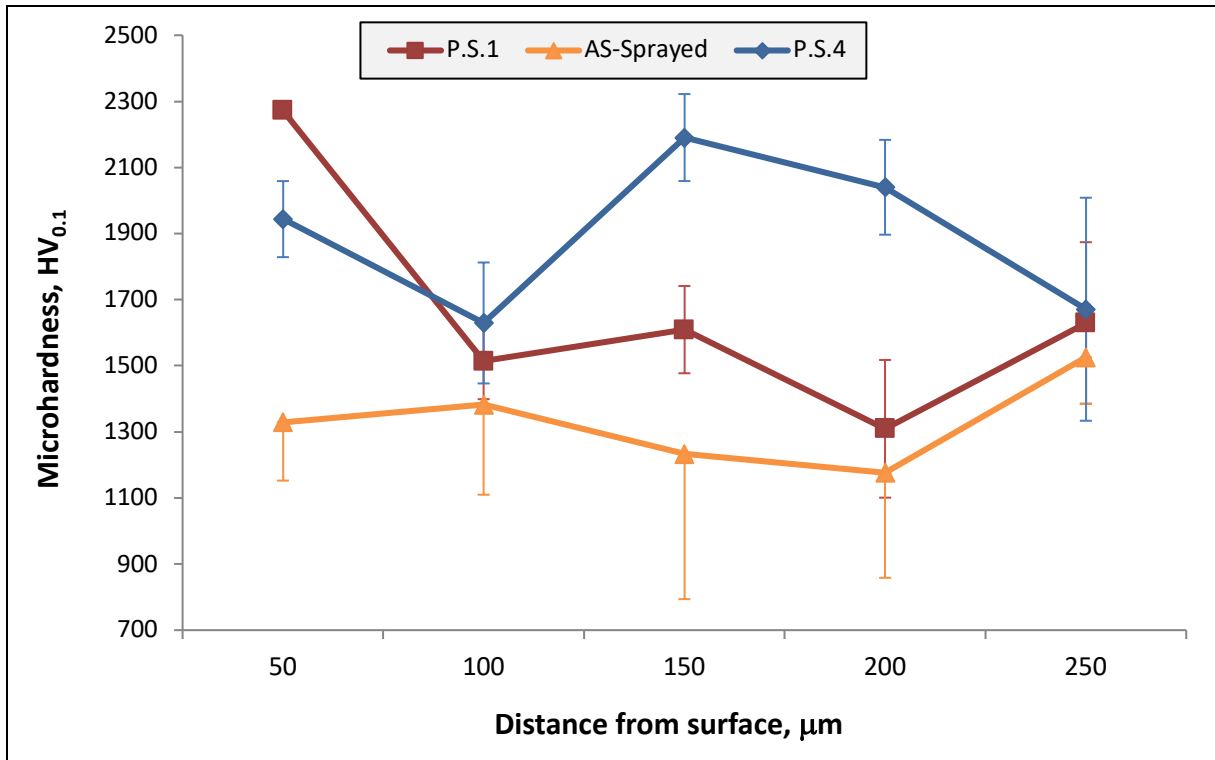
Figure 5-84: Micro hardness profiles along the coating depth for nWC-12 Co coating pre- and post-heat treatment.
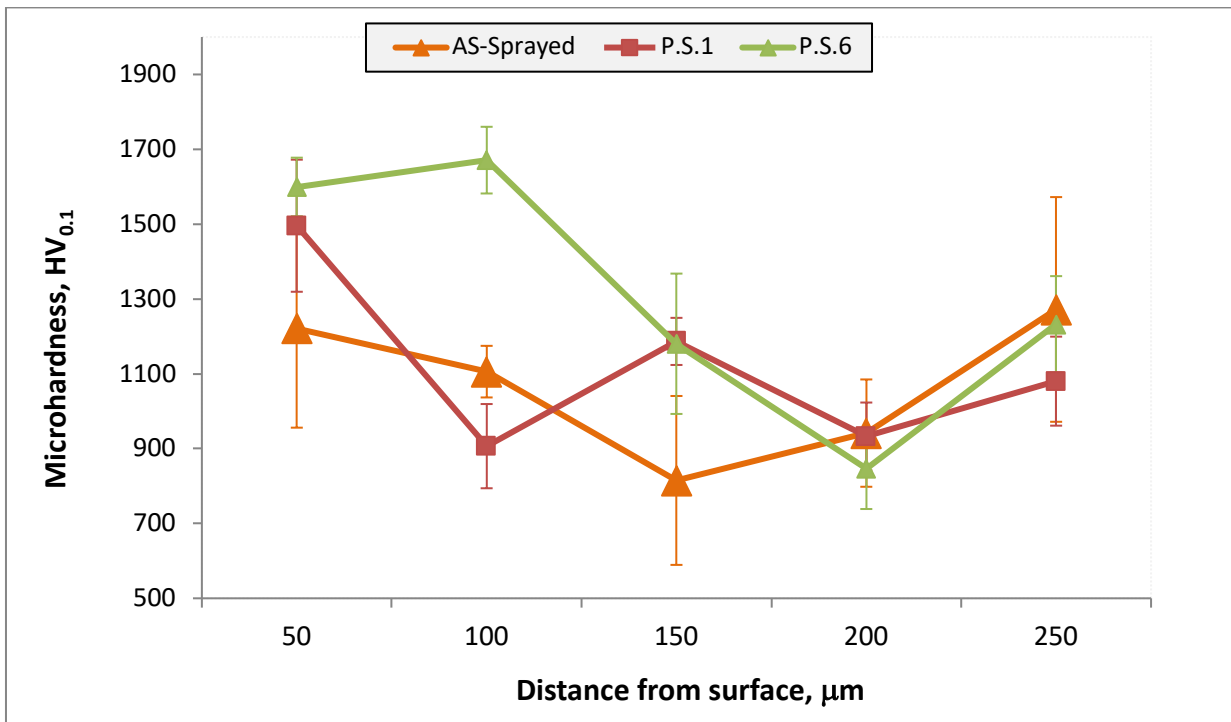
Figure 5-85: Micro hardness profiles along the coating depth for the mixed coating pre- and post-heat treatment.

Novel Enhancement of HVOF Thermal Sprayed Nanostructured WC-12Co / Inconel-625 Coatings for Tribocorrosion Applications | **Al-Harbi, Naif I**

190

5.10 Three point bending of laser-melted HVOF coatings

In the oil and gas industry, some components such as the ball valves, elbows, joints and so on, are subjected to high operation pressure due to crude oil pumping and abrasive attacks that are caused by different particles with large diameter and due to chips been pulled-out from the coating surface. Such a situation can result in the early degradation of the coating system thus reducing its service life. That is the reason why a coating with high yield strength resistance is one of the most desirable properties that can enable materials to withstand severe conditions mentioned above. Figure 5-86 and 5-87 shows the results that were obtained for the flexural strength and the maximum load measured at the elastic region of the coating for each laser setting according to the DOE matrix along with the values that were characterised earlier for the two as-sprayed coating respectively. Each test was repeated for three times for consistency and the average was taken. As shown, the results show a significant improvement in the elastic limit for the two types of coating after the laser treatment under various laser settings. The main reasons for the improvement are the significant enhancement of the region irradiated by the laser beam such as the improvement of the coating micro hardness and the elimination of a number of coating microstructure defects that acts as crack initiation centres during the bending process. The defects include porosity and discontinuity of the interfacial properties across the coating and the substrate. The laser treatment also enhances the homogeneity of the coating elements along the coating microstructure. As shown in both figures (Figure 5-75 and Figure 5-76), for the laser treated monomial nWC-Co coating; P.S.6 followed by P.S.4 laser settings provided the highest flexural strength and corresponding maximum load of 738, 684 MPa and 2.8, 2.6 KN respectively. When the laser setting of P.S.6 are used, the additional tolerance level observed are 118 MPa and 0.44 KN respectively for the monomial nWC-Co coating. In the case of the mixed coating, a minimal improvement was seen after the laser processing compared to the monomial coating. However, P.S.10 and P.S.3 provided the highest elastic limit of 650 and 630 MPa and a maximum load carrying capacity of 2.47 and 2.39 KN respectively for the laser treated mixed coating. For example, P.S.10 had a 49 MPa and 0.19 KN higher strength and load capacity respectively compared to the as-sprayed mixed HVOF coating. When comparing the elastic limit and the maximum load for the P.S.10 of the mixed coating to the values obtained for the untreated as-sprayed monomial nWC-Co HVOF coating, it can be seen that the mixed coating after treating with laser settings of P.S.10 was higher. Generally however, the monomial nWC-Co HVOF coating performed better over the as-sprayed mixed coating for a number of reasons as

Novel Enhancement of HVOF Thermal Sprayed Nanostructured WC-12Co / Inconel-625 Coatings for Tribocorrosion Applications | **Al-Harbi, Naif I**

191

discussed earlier, and due to the benefit of the higher ratio of nano-scale hard phase WC particles contained in the monomial nWC-Co HVOF coating.
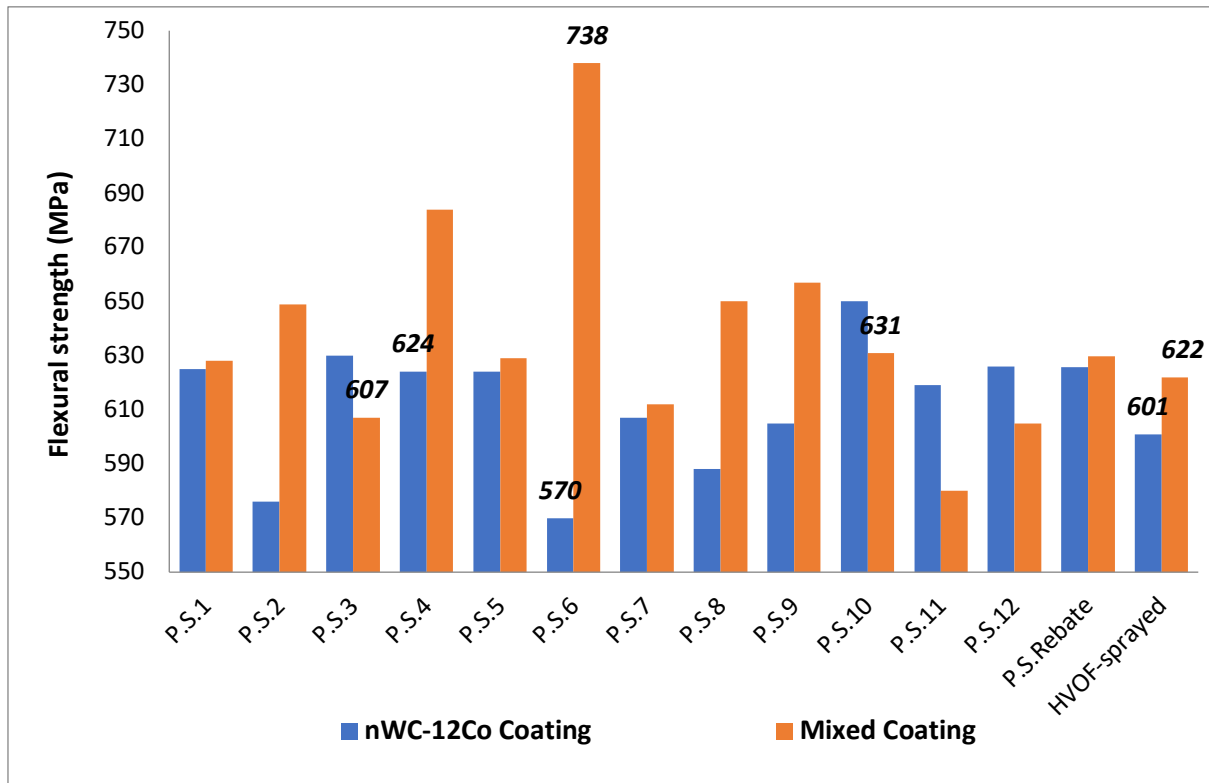
Figure 5-86: Flexural/Bending strength value for the two coating types before and after the laser treatment under the various laser settings.
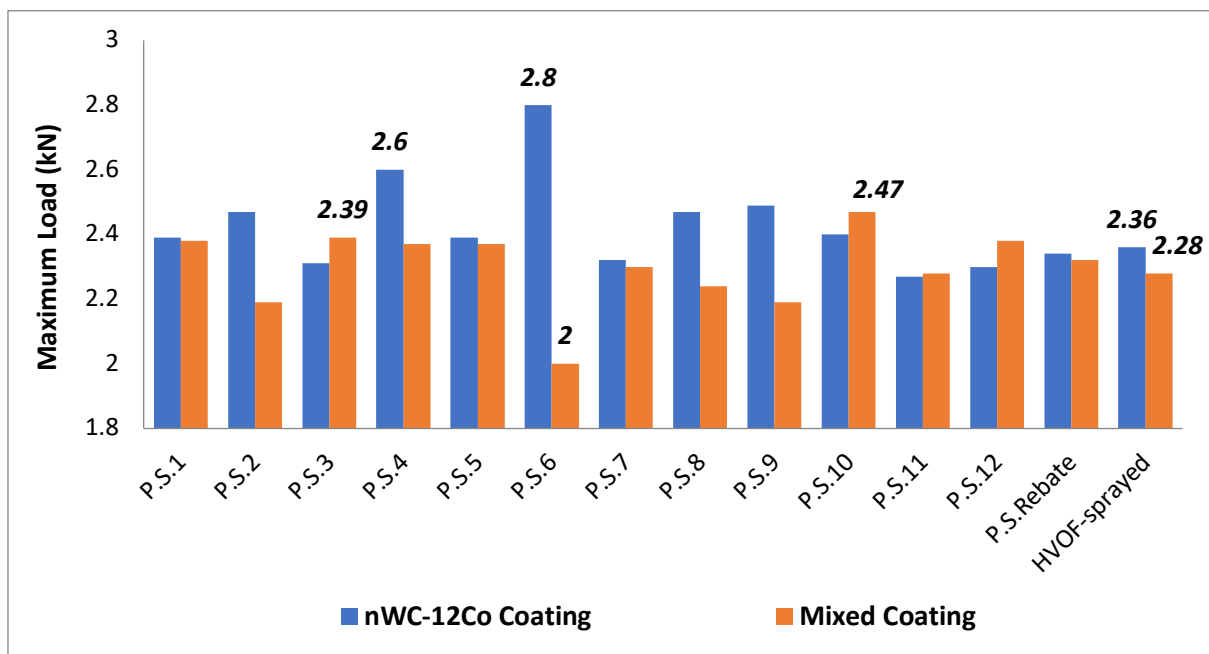
Figure 5-87: Maximum load required to undergo the bending test for the two coating types before and after the laser treatment under the various laser settings.

Novel Enhancement of HVOF Thermal Sprayed Nanostructured WC-12Co / Inconel-625 Coatings for Tribocorrosion Applications | **Al-Harbi, Naif I**

192

5.10.1 Effect of the amount of the energy input on bending yield strength

The elasto-plastic behaviour of the two as-sprayed coatings along with their laser treatment at two different energy input is shown in Figures 5-88 and 5-89. The P.S.6 laser setting provided the highest energy input amongst the DOE metrix as discussed earlier.

The as-sprayed coating and the laser treated monomial nWC-Co HVOF coating that were treated under the two different laser settings showed similar elastic behaviour to particular bending stress/load prior, reaching a yield point of up to $\approx 540\,\text{MPa}$. These coatings then started to behave differently in a gradual rate upwards to theor breaking point in the plastic region of each sample [109]. However, the two laser-treated samples in both laser settings (P.S.6 and P.S.4) gave a higher elastic limit and holding load compared to the untreated coating. The P.S.6 laser setting had higher elasto-plastic behaviour and the maximum load in the elastic region compared to the P.S.4 settings. However, the P.S.4 laser setting provided a coating with a higher value of microhardness and lower porosity level as shown earlier (Figures 5-83 and 5-77 respectively). The different response to the bending process might be attributed to the change that was made in the bonding between the coating/substrate interface (from the mechanical contact with numerous porous strips to the fusion bonding as confirmed earlier in the SEM micrograph), and the EDS line scanning shown in Figure 5-69 and 5-70. This was not the case for P.S.4. As a result, the local shear stresses were considered to be the main cause of coating failure that were created due to the large differences in mechanical properties of the coating and the substrate in the defects region. This did not occur in the case of P.S.6 setting in contrast to either the untreated coating or the treatment of the coating with P.S.4 laser setting. This might also explain the abnormal behaviour of P.S.6 settings after the breaking point, which clearly differs with all the other samples for both coatings in Figures 5-88 and 5-89. A ripple type pattern is seen in the energy relaxation curve after breaking point for P.S.6 where the other samples drop sharply. The reason could be attributed to the total gradual elimination along the transverse extension of the coating in the high stress region of the coating, as seen in Figure 5-90 (C). However, as the bending load increases, both the treated and untreated coatings behave in a similar way.

Novel Enhancement of HVOF Thermal Sprayed Nanostructured WC-12Co / Inconel-625 Coatings for Tribocorrosion Applications | **Al-Harbi, Naif I**

193
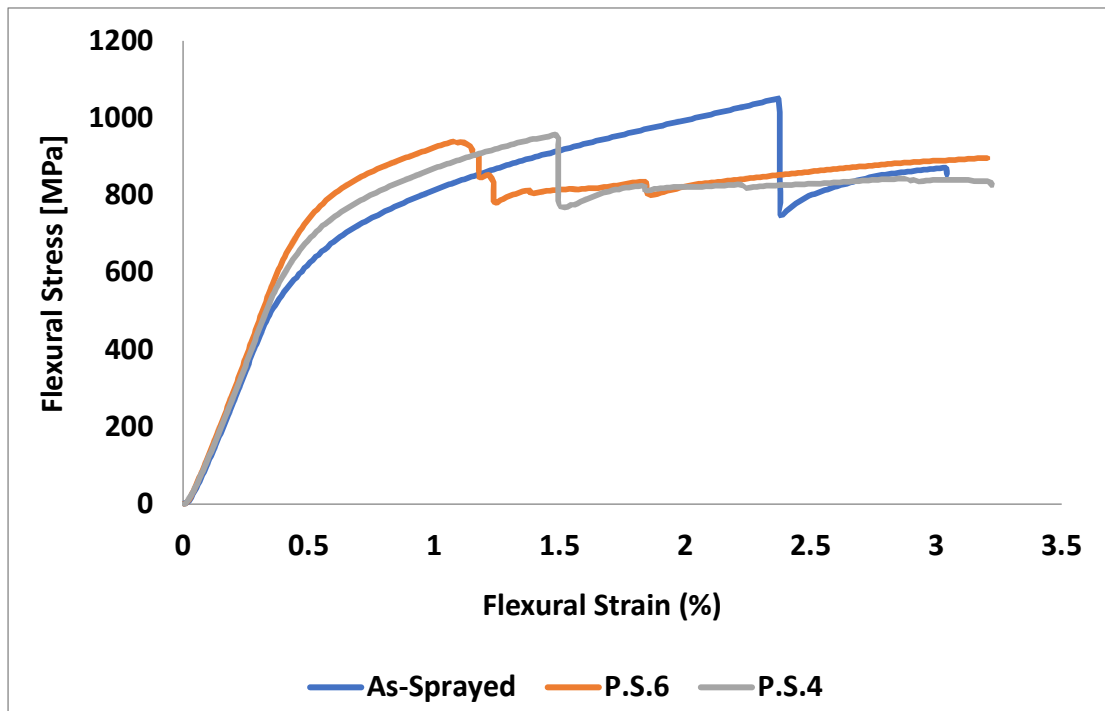
Figure 5-88: A comparison between bending flexure stress of monomial nWC-12Co HVOF coating before and after laser treatment under two different laser settings.

Figure 5-89 shows the elasto-plastic behaviour of the mixed as-sprayed HVOF coating before and after the laser treatment at two different energy inputs. The P.S.10 provided the highest elastic limit and holding load among all the varying laser settings for the treated mixed HVOF coating. The laser setting that provided the highest energy input (P.S.6) setting gave the lowest flexural stress and holding load as shown in Figures 5-86 and 5-87. The results indicate that by treating the mixed coating to a particular level of energy such as the P.S.10 level, the plastic region can support higher load levels (2.47 KN) and flexural stress (650 MPa) in comparison to the untreated coating. The early termination of the elastic limit and the reduction of the loading capacity for the mixed HVOF coating that is treated with high energy, results in the formation of bubbles (5-90 (F)) that leaves holes in the coating layer. Consequently, the holes act as the source of the crack initiation and results the failure of the coating. Therefore, an appropriate laser setting should be considered for avoiding the gas pockets formation in the coating layer and it must have an inverse relationship with the bending strength response.

Novel Enhancement of HVOF Thermal Sprayed Nanostructured WC-12Co / Inconel-625 Coatings for Tribocorrosion Applications | **Al-Harbi, Naif I**

194
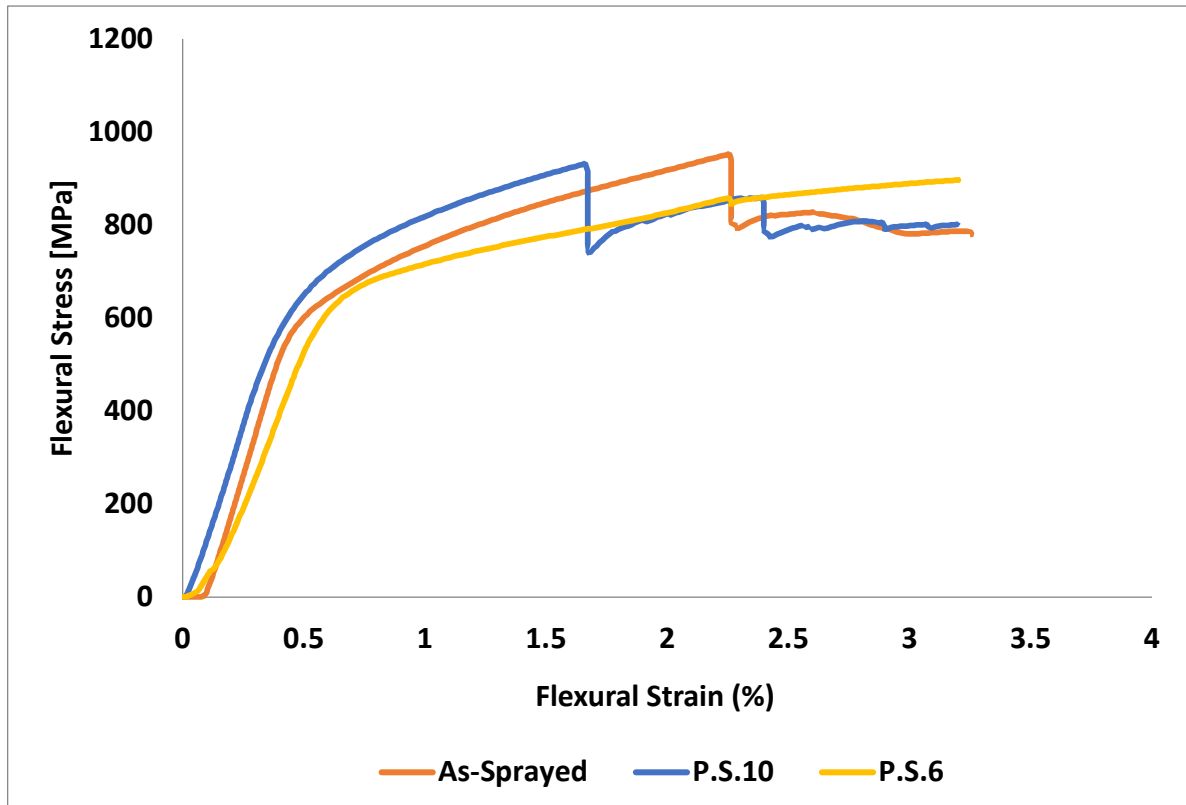
Figure 5-89: A comparison between bending flexure stress of the mixed HVOF coating before and after laser treatment under two different laser settings.

Figure 5-90 shows the SEM images of the morphology for the two HVOF coatings after laser treatment under different energy inputs (from lowest to highest) after the three-point bending test. Contrary to what was noticed earlier for the as-sprayed coatings where the coating failure looked at the types of cracks that were formed as seen in Figure 5-28, the deformation after the laser treatment ranged from detaching delamination from the coating layer to different degrees, to the total delamination of the coating (peeling off from the substrate surface) as in P.S.6 for the laser treated monomial nWC-12Co. The laser setting with the highest energy input, yielded gas pockets within the coating layer similar to the one shown in P.S.6 for the mixed coating (Figure 5-90 (F)). The gas pockets form crack initators and produce different failure than that found for the other coating types (Figure 5-90 (A) to (E)).

Novel Enhancement of HVOF Thermal Sprayed Nanostructured WC-12Co / Inconel-625 Coatings for Tribocorrosion Applications | **Al-Harbi, Naif I**

195
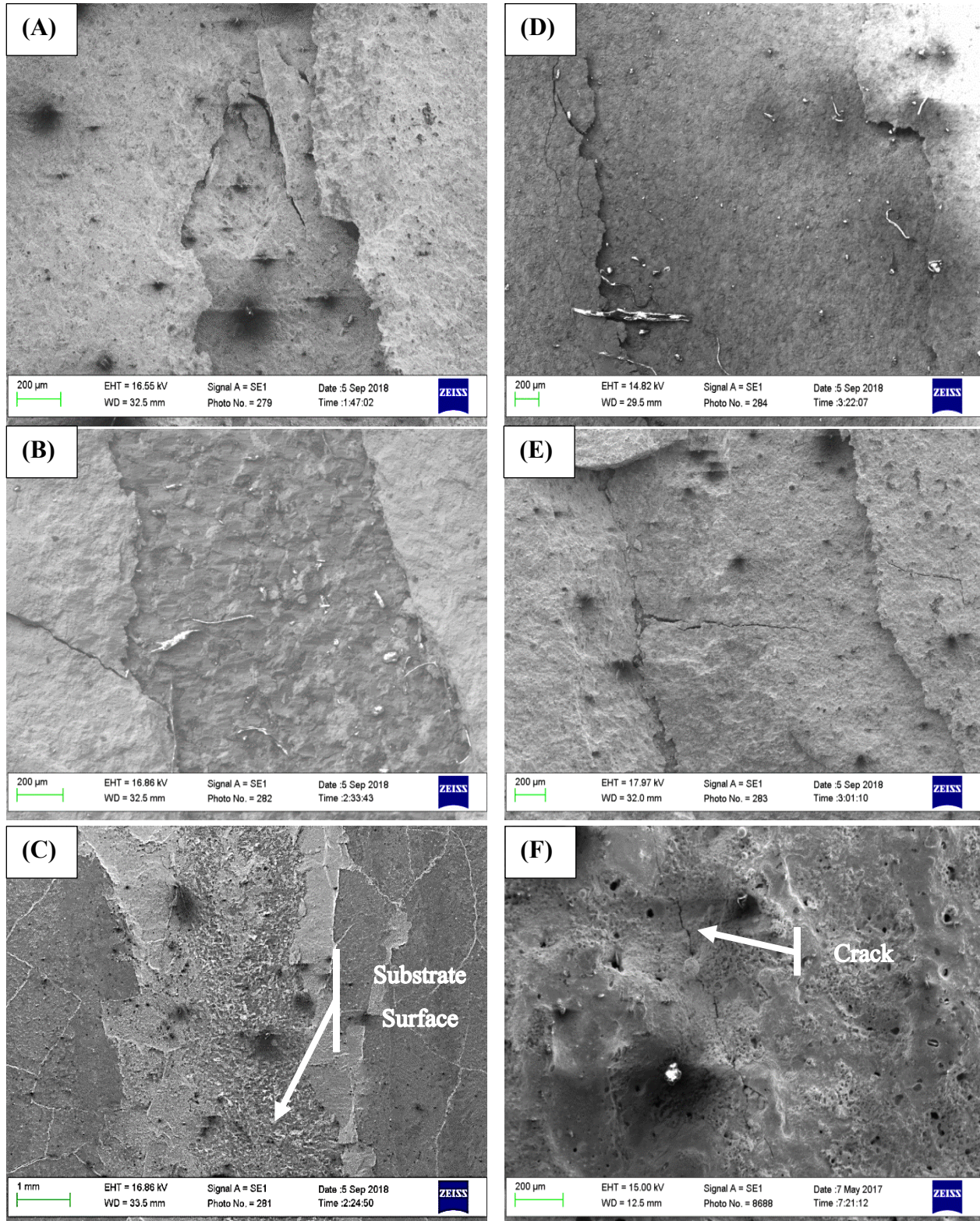
Figure 5-90: SEM micrographs of the surface failures morphology during the three point bending test for the two laser treated coatings ; (A) monomial nWC-12Co— partially-melted (P.S.1), (B) monomial nWC-12Co — almost fully-melted (P.S.4),(C) monomial nWC-12Co —fully-melted (P.S.6), (D) mixed coating— partially-melted (P.S.11), (E) mixed coating— partially-melted (P.S.10), (F) mixed coating— fully -melted (P.S.6).

Novel Enhancement of HVOF Thermal Sprayed Nanostructured WC-12Co / Inconel-625 Coatings for Tribocorrosion Applications | **Al-Harbi, Naif I**

196

5.10.2 Development of the mathematical model for yield strength deformation

The design of experiment (DOE) analysis was used to analyse the data obtained by the experimental measurement of the yield strength and the process factors - laser power, focal position, and the scanning speed - under three different levels. The quadratic model was used to fit the data as it showed a high R^2 value of 0.97 and 0.975 for the laser treated monomial nWC-12Co and the mixed coating yield strength response (< 0.05), respectively (see Table 5-11 for the monomial nWC-12Co coating and Table 5-12 for the mixed nWC-12Co coating). The ANOVA tables show that the lack of fit was not significant and the adequate precision was more than 0.4 within values of predict R^2 and adjusted R^2 close to each other (i.e. differences less than 0.2). The laser power and the scanning speed are the primary factors for controlling the yield strength of the laser-treated monomial nWC-12Co coating. The focal position had a secondary effect. For the laser-treated mixed coating, the laser power and the focal position are the primary factors for the yield strength whereas the scanning speed has a secondary effect. Moreover, there are significant interactions up to the second order in the laser power for both coatings, the focal position for the monomial, and the scanning speed for the mixed. This indicates that the response is not linear and is very sensitive to changing levels.

Source	Sum of Squares	DF	Mean Square	F value	Prob > F	
Model	18886.44	8	2360.80	45.26	< 0.0001	significant
A-Laser Power	7503.13	1	7503.13	143.83	< 0.0001	
B-Focal Position	21.13	1	21.13	0.4050	0.5423	
C-Scanning Speed	5408.00	1	5408.00	103.67	< 0.0001	
AB	784.00	1	784.00	15.03	0.0047	
AC	1260.25	1	1260.25	24.16	0.0012	
BC	650.25	1	650.25	12.46	0.0077	
A²	2520.80	1	2520.80	48.32	0.0001	
B²	895.80	1	895.80	17.17	0.0032	
Residual	417.33	8	52.17			
Lack of Fit	330.53	4	82.63	3.81	0.1118	not significant
Pure Error	86.80	4	21.70			

R-Squared   **0.97**   Adj.R^2 = 0.95

Adeq. Precision = 29.3   Pred.R^2 = 0.82

Table 5-11: ANOVA analysis for the laser-treated monomial nWC-12Co coating yield strength data.

Novel Enhancement of HVOF Thermal Sprayed Nanostructured WC-12Co / Inconel-625 Coatings for Tribocorrosion Applications | **Al-Harbi, Naif I**

197

Source	Sum of Squares	DF	Mean Square	F value	Prob > F	
Model	6796.39	9	755.15	30.64	< 0.0001	significant
A-Laser Power	2048.00	1	2048.00	83.08	< 0.0001	
B-Focal Position	1378.12	1	1378.12	55.91	0.0001	
C-Scanning Speed	10.13	1	10.13	0.41	0.5420	
AB	462.25	1	462.25	18.75	0.0034	
AC	306.25	1	306.25	12.42	0.0097	
BC	361.00	1	361.00	14.65	0.0065	
A^2	1667.41	1	1667.41	67.64	< 0.0001	
B^2	259.46	1	259.46	10.53	0.0142	
C^2	315.04	1	315.04	12.78	0.0090	
Residual	172.55	7	24.65			
Lack of Fit	55.75	3	18.58	0.64	0.6299	not significant

R-Squared   **0.975**   Adj.R^2 = 0.943

Adeq. Precision = **49.72**   Pred.R^2 = 0.845

Table 5-12: ANOVA analysis for the laser-treated mixed coating yield strength data.

The final mathematical models for both laser-treated coatings' yield strength in terms of coded factors that can be used to make predictions about the response for given levels of each factor were found to be as follows:

nWC-12Co coating (Bending) = +1.582E-003 -7.091E-005 * A -4.035E-006 * B +6.222E-005 * C -3.348E-005 * AB +3.482E-005 * AC -3.349E-005 * BC -5.642E-005 * A^2 +3.523E-005 * B^2 +3.896E-006 *C^2 $Equation\ 5-14$

Mixed coating (Bending) = +625.80 -16.00 * A +13.13 * B -1.13 * C +10.75 * AB +8.75 * AC -9.50 * BC -19.90 * A^2 +7.85 * B^2 -8.65 * C^2 $Equation\ 5-15$

Where A is laser power, B is focal position and C is scanning speed. From the equations above the dependence on bending strength can be ranked as follows: -A > C > -A^2 > B^2 > AC > BC > -AB > -B > C^2 for the monomial nWC-12Co coating and the following can be noted; for the laser-treated monomial nWC-12Co coating yield strength, among the three factors, the laser power (A) had the highest negative effect, followed by a positive effect by the scanning speed (C). As squared, the laser power (A^2) had the highest negative effect. Almost all the factors interact with each other as paired interaction in equal value.

Novel Enhancement of HVOF Thermal Sprayed Nanostructured WC-12Co / Inconel-625 Coatings for Tribocorrosion Applications | **Al-Harbi, Naif I**

198

For the mixed coating yield strength response, the dependence rank as follow: $-A^2 > -A > B > AB > BC > AC > -C^2 > B^2 > -C$. The laser power had the highest negative effect, both as squared (A^2) and itself (A). Focal position (B) is next. As paired interaction, the focal position with laser power and with scanning speed (AB, -BC) had the most significant impact on the yield strength, respectively.

Figure 5-91 is a normal plot for the laser-treated monomial nWC-12Co coating yield strength. The plot shows that the residuals have a linear relationship, which implies that they are normally distributed. Hence, ANOVA can be carried out on observations for the yield strength of this coating.

.
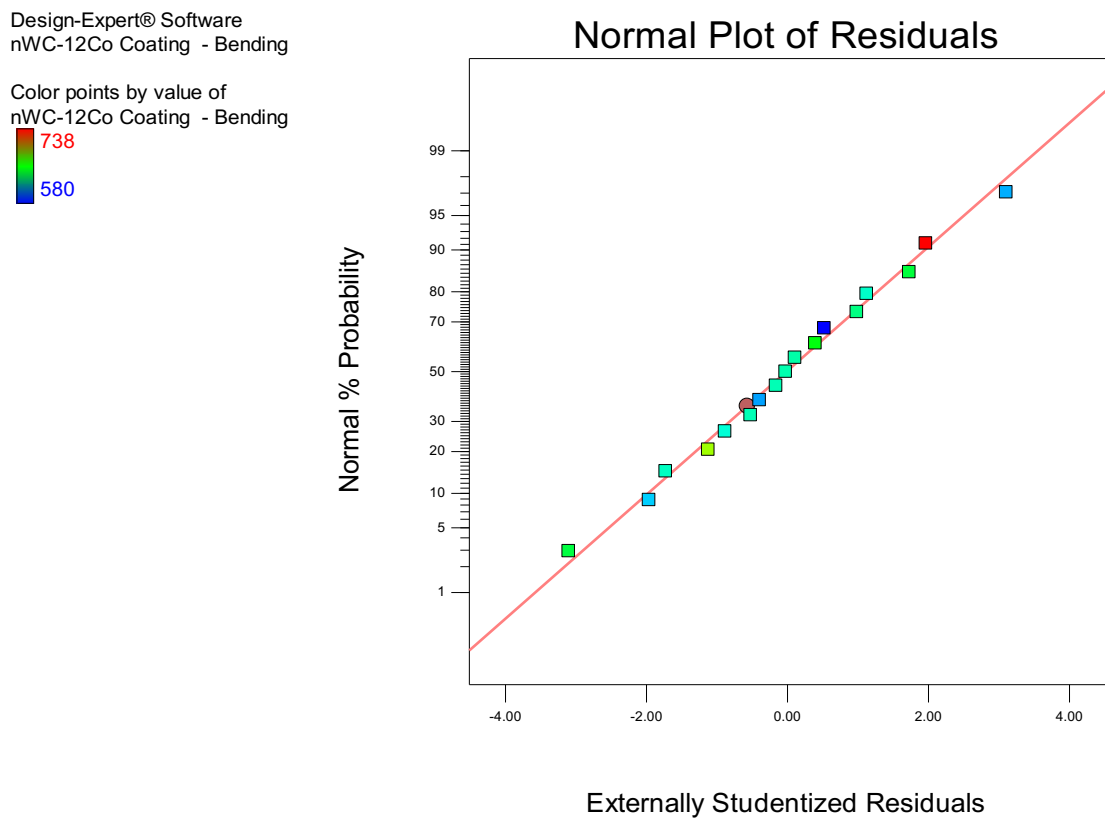
Figure 5-91: Normal plot residual of laser-treated monomial nWC-12Co coating for yield strength (MPa).

In addition, the relationship between the actual and predicted value is linear, thus, indicating that the difference between them is small, as shown in Figure 5-92 for the monomial nWC-12Co coating (yield strength). The same was observed for the mixed coating yield strength, which for the sake of brevity, is provided in Appendix C of this research.

Novel Enhancement of HVOF Thermal Sprayed Nanostructured WC-12Co / Inconel-625 Coatings for Tribocorrosion Applications | **Al-Harbi, Naif I**

199
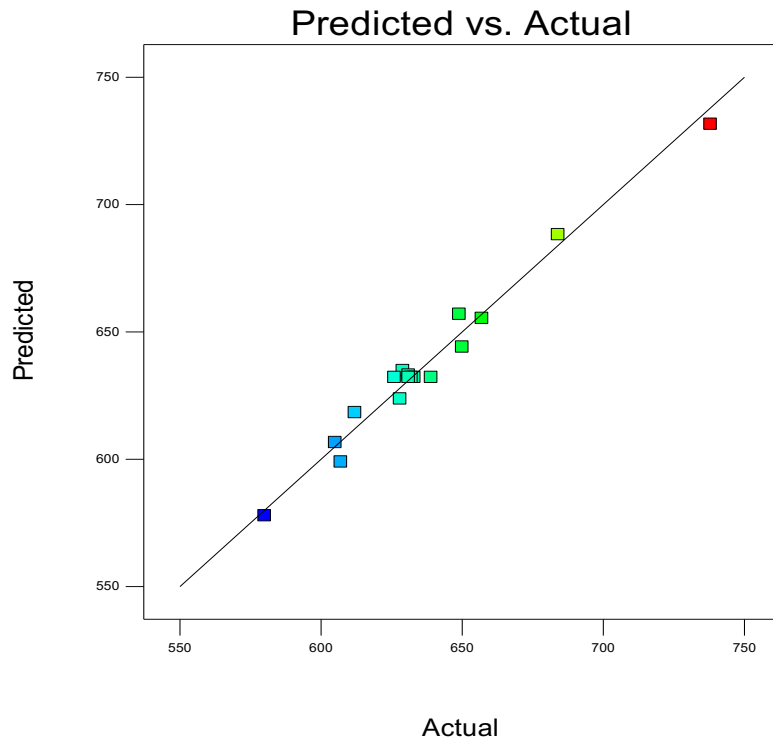
Figure 5-92: Predicted versus actual plot for laser-treated monomial nWC-12Co coating for yield strength (MPa).

The final mathematical model determined by the DOE software for both laser-treated coatings to be used to predict the optimized values of yield strength response with regards to actual factors is given in Equation 5-16 and 5-17.

nWC-12Co Coating (Bending) = +2.32960E − 003 + 3.74589E-006 * Laser Power - 7.67059E-005 * Focal Position + 2.92959E-006 * Scanning Speed - 6.69668E-008 * Laser Power * Focal Position + 4.64287E-009 * Laser Power * Scanning Speed - 8.93076E-008 * Focal Position * Scanning Speed - 5.64203E-009 * Laser Power^2 + 1.40918E-006 * Focal Position^2 + 6.92535E-010 * Scanning Speed^2 *Equation* 5 − 16*

Mixed Coating (Bending) = +916.97500 - 0.28750 * Laser Power - 22.17000 * Focal Position + 1.39867 * Scanning Speed + 0.021500 * Laser Power * Focal Position + 1.16667E-003 * Laser Power * Scanning Speed - 0.025333 * Focal Position * Scanning Speed - 1.99000E-003 * Laser Power^2 + 0.31400 * Focal Position^2 - 1.53778E-003 * Scanning Speed^2 *Equation* 5 − 17*

Novel Enhancement of HVOF Thermal Sprayed Nanostructured WC-12Co / Inconel-625 Coatings for Tribocorrosion Applications | **Al-Harbi, Naif I**

200

5.10.3 DOE results of yield strength

Figures 5.93 is a perturbation plot showing the effect of each factor on the yield strength response for laser-treated monomial nWC-12Co coating. From these graphs changing of the beam size as a function of raising the focal position did not seem have had a significant effect on the yield strength of laser treated monomial nWC-12Co coating. However, the central level (Level 0), seems to give a better yield strength than the lowest and the highest level (-1 and 1). It can be clearly seen that the yield strength of this coating increased with the increase in laser power in a quadratic manner (A and A^2). The yield strength also decreases in a nearly linear behaviour with an increase in scanning speed. The relationship between the laser power effects to the yield strength of the monomial nWC-12Co coating and the scanning speed can be seen in contour plot that is shown in the Figure 5-94 for approximately wide range value setting for B (focal position). It is evident that the yield strength increases with the increase in energy input (high laser power and slow scanning speed) [125]. Moreover, the contour plot shows that the laser power is slightly more significant to the yield strength as compared to the scanning speed.
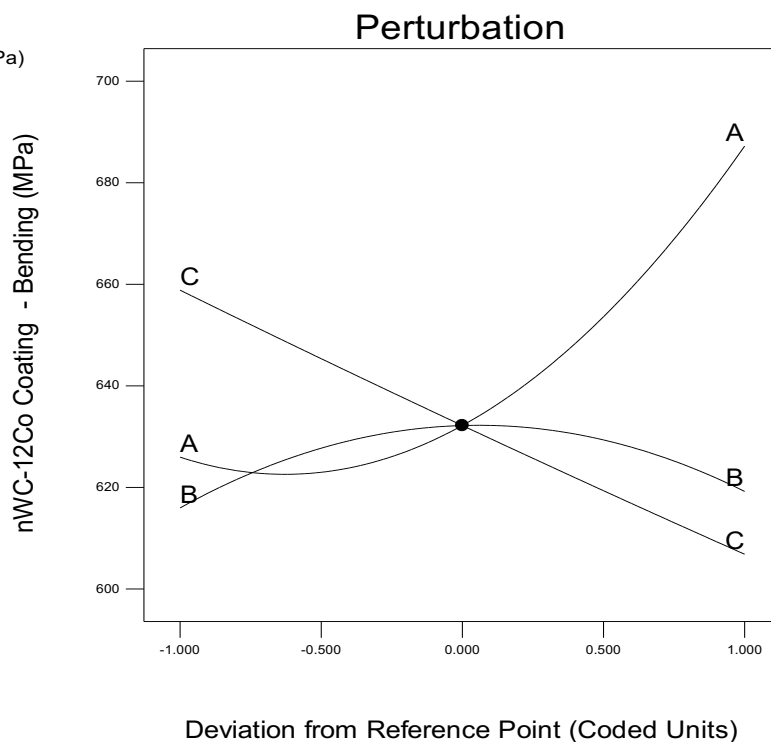
Figure 5-93: Perturbation plot for laser-treated monomial nWC-12Co coating for yield strength response.

Novel Enhancement of HVOF Thermal Sprayed Nanostructured WC-12Co / Inconel-625 Coatings for Tribocorrosion Applications | **Al-Harbi, Naif I**

201
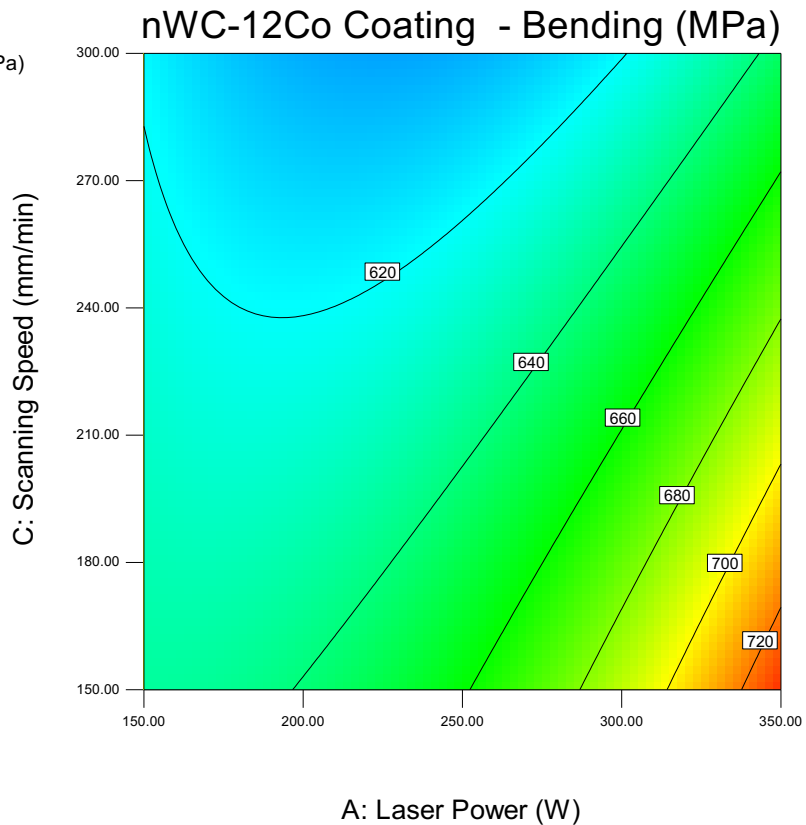
Figure 5-94: Contour plot of the laser treated monomial nWC-12Co coating yield strength response versus the scanning speed and the laser power.

Figure 5.95 is a perturbation plot that shows the effect of each of the three factors on the yield strength in response to laser-treated mixed coating. The graphical plot shows that the yield strength for the mixed coating increases proportionally with the increase in energy input to a certain level, for example the mixed coating increases as a function of laser power and focal position factors, particularly over the lowest-level region (between 150 and 250 W for the laser power). As the laser power further increases; the yield strength starts to reduce sharply as a result of the gas pockets formed due to the high energy input. Similarly, increasing the beam size (focal position B influence) as a function of an increased focal position will lead to a reduction in the power density (Power/Area). The laser power is the dominant factor for the laser-treated mixed coating in yield strength response as presented in final mathematical equation (Equation $5-15$).

The scanning speed does not have a significant impact on the yield strength of the mixed coating. However, as the contour plot that describes the relationship between the laser power

Novel Enhancement of HVOF Thermal Sprayed Nanostructured WC-12Co / Inconel-625 Coatings for Tribocorrosion Applications | **Al-Harbi, Naif I**

202

and the effects of the scanning speed to the yield strength of the mixed coating taken in the central level (Level 0) for the focal position factor is shown in Figure 5-96. The change in yield strength resulting from the change in the level of the scanning speed is very little and the elastic limit decrease with the increase in scanning speed [125]. Additionally, the interaction between the most influencing factors (laser power and focal position) to the yield strength response of the mixed coating that take in the lowest level for the scanning speed (Level -1) can be seen in the contour plot in Figure 5-97. As it is evident, the increased yield strength for the mixed coating is a function of the power density (power/area). The use of low energy input is desirable to obtain a high yield strength for this coating type, which can be done either by lowering the laser output power or increasing the beam diameter size as a function of raising the focal position. The reason as explained earlier is that, increasing the laser power, induces high energy input into the coating layer. As a result, the gas pockets are formed within the coating layer. On the other hand, increasing the beam diameter decreases the density of heat flux. Consequently, the limit of gas pockets formation will extend to some level.
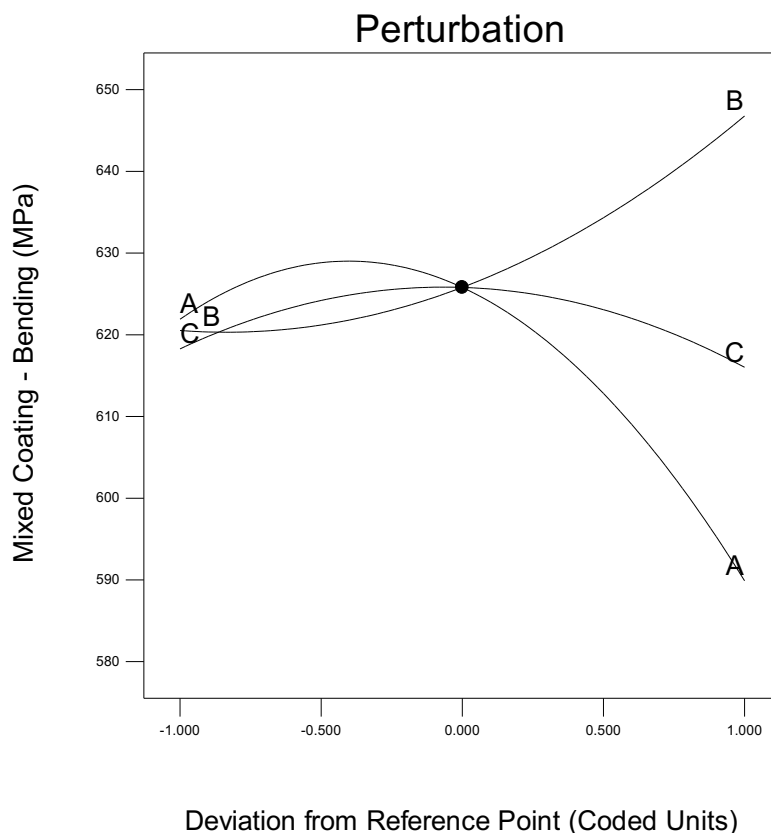
Figure 5-95: Perturbation plot for laser-treated mixed coating for yield strength response.

Novel Enhancement of HVOF Thermal Sprayed Nanostructured WC-12Co / Inconel-625 Coatings for Tribocorrosion Applications | **Al-Harbi, Naif I**

203
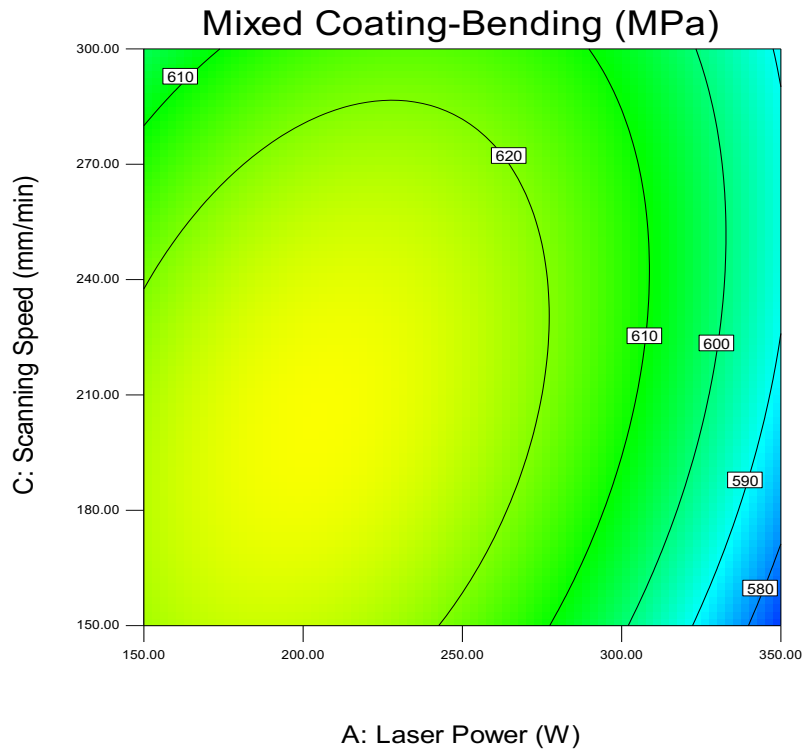
Figure 5-96: Contour plot of the laser treated mixed coating yield strength response versus the scanning speed and the laser power.
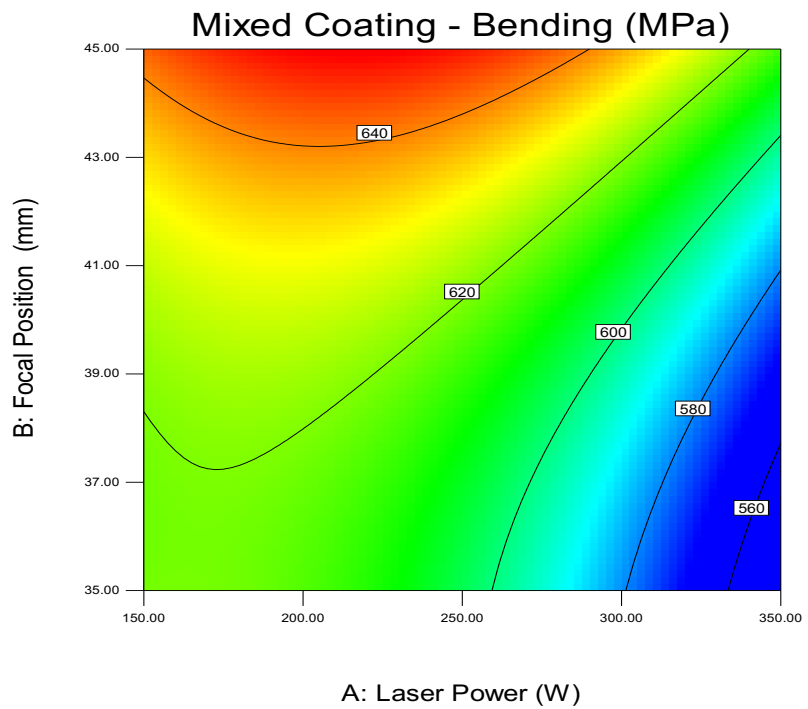
Figure 5-97: Contour plot of the laser treated mixed coating yield strength response versus the f focal position and the laser power.

Novel Enhancement of HVOF Thermal Sprayed Nanostructured WC-12Co / Inconel-625 Coatings for Tribocorrosion Applications | **Al-Harbi, Naif I**

204

5.11 Dry erosion of laser-melted HVOF coatings

Figure 5-98 shows the mass losses for the laser-treated samples of both coating types under various laser settings along with the values that were characterised earlier for the two as-sprayed coating respectively. Erosion rate results were obtained twice for each laser-treated coating, and the average taken, before and after cleaning. A significant reduction was seen in mass losses for different laser settings compared to the untreated coatings. For example, the nWC-12Co coating P.S.9, P.S.8 and P.S.4 samples provided the lowest mass losses, 0.13, 0.135 and 0.14 g, respectively, an approximately five- to six-fold reduction in mass. For the mixed coating, mass losses after the laser processing seemed lower in comparison to the monomial nWC-12Co coating. However, P.S.7 and P.S.1 provided the lowest mass losses, almost fifty percent lower, within 0.75 and 0.8 g, respectively, compared to 1.46 g for the untreated mixed coating. Furthermore, the mass losses for the mixed coating types treated under high energy inputs (e.g. P.S.6, P.S.2, P.S.9, P.S.8 and P.S.4, respectively) were higher (above 2.5 g) in comparison to the untreated mixed coating. Conversely, those laser settings provided the lowest mass losses for the monomial nWC-12Co coating. This might be attributed to the coating composition and significant improvement after laser treating of the coating microstructural/surface integrity, leading to a dense coating microstructure which is free of pores, cracks and un-melted particles; low roughness; formation of new phases; and microhardness of the region close to the surface. However, the improvement of surface microhardness does not usually lead to better wear performance, as reported by Pau, Li and Jayakumar et al, respectively [126–128]. This is because a number of other properties should be studied simultaneously (e.g. toughness and Young's module) to fully understand the coating mechanism, as clarified by Weng et al. [129]. However, this was not the case for the mixed coating because high energy input laser settings produced a rough surface, with gas cavities that were scattered beneath and on the top of the coating surface. Consequently, this led the top-layer coating to be easily removed due to fracturing by erosion particles during testing, as can be seen for P.S.4 in Figure 5-99 (D).

Novel Enhancement of HVOF Thermal Sprayed Nanostructured WC-12Co / Inconel-625 Coatings for Tribocorrosion Applications | **Al-Harbi, Naif I**

205
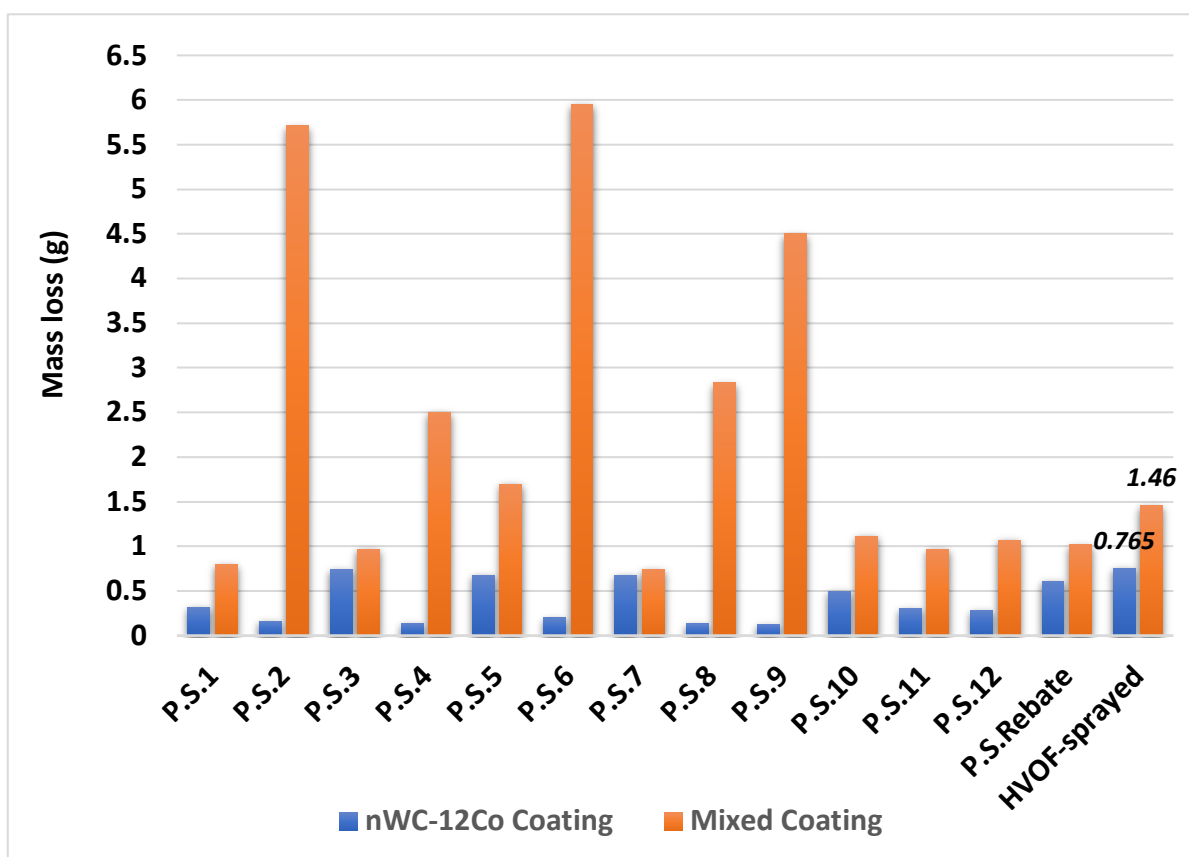
Figure 5-98: Dry erosion value for the two coating types before and after laser treatment under various laser settings.

Figure 5-99 shows the laser-treated samples after the dry erosion results under different laser energy inputs. The eroded area and mass losses were clearly different in each sample based on coating composition and laser setting. For example, the erosion effects were much smaller in the monomial nWC-12Co coating under those laser settings (P.S.9 and P.S.4) compared to P.S.7 and P.S.4 for the mixed coating under the same erosion condition. Although the gas pockets that formed in P.S.4, laser settings led the sand-eroded particles to easily fracture the coating top layer to form high mass losses, this was not the case for the laser settings that provided lower specific energy and smaller mass losses, such as that of P.S.7 (Figure 5-99 (C)), As a result, lower energy inputs, in general, seemingly yielded better erosion wear resistance for the mixed coating. Similar findings were noted by Weng et al. [130] in the laser cladding of a Co-based composite coating on T6AL-alloy. These authors found that a lower energy input led to better resistance, owing to more TiB$_2$ bulks being retained in the coating layer.

Novel Enhancement of HVOF Thermal Sprayed Nanostructured WC-12Co / Inconel-625 Coatings for Tribocorrosion Applications | **Al-Harbi, Naif I**

206
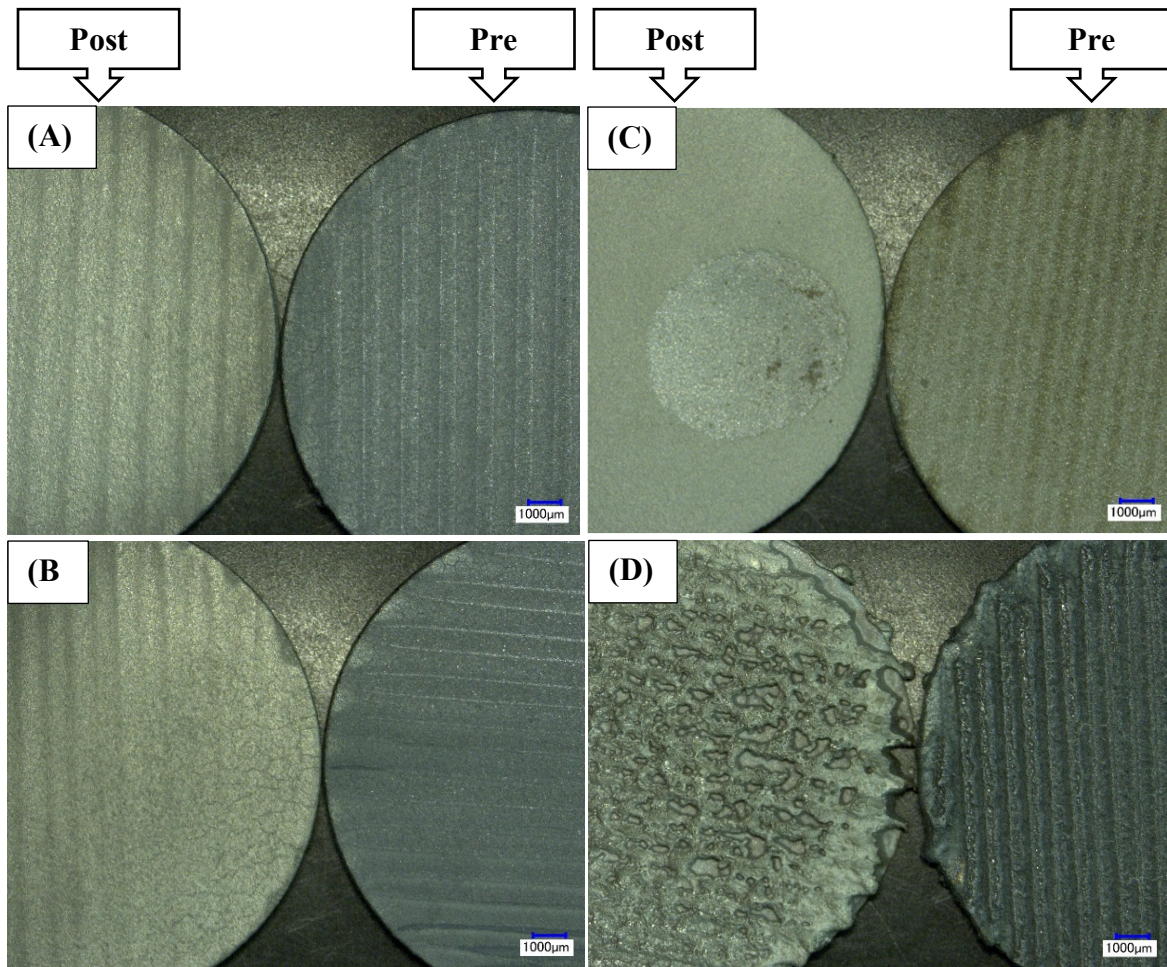
Figure 5-99: Optical photographs of laser-treated samples for both coating types before and after the dry erosion test. (A) P.S.9 nWC-12Co coating, (B) P.S.4 nWC-12Co coating, (C) P.S.7 mixed coating and (D) P.S.4 mixed coating.

5.11.1 Development of the mathematical model for dry erosion results

A design of experiment (DOE) analysis was again used to analyse the data obtained via the experimental measurement of the dry erosion results. The quadratic model was also used to fit the data. Tables 5-13 and 5-14 show the ANOVA tables for both laser-treated coatings (monomial and the mixed nWC-12Co coating types, respectively). The ANOVA indicates no significant lack of fit and a significant modle (< 0.05), with the predicted R^2 and adjusted R^2 close to each other (less than 0.2). Clearly, the laser power and the focal position are the primary factors for controlling dry erosion for the laser-treated monomial coating, while the scanning speed has a secondary effect. For the laser-treated mixed coating, all factors had a significant effect on the dry erosion resistance response in the mixed coating. Moreover, significant interactions took place up to the second order in the focal position for the monomial and all factors (laser power, focal position and scanning speed) for the laser-treated

Novel Enhancement of HVOF Thermal Sprayed Nanostructured WC-12Co / Inconel-625 Coatings for Tribocorrosion Applications | **Al-Harbi, Naif I**

207

mixed coating. This result indicates that the response is not linear and will be more sensitive to changes in the levels of those factors.

Source	Sum of Squares	DF	Mean Square	F value	Prob > F	
Model	0.8224	8	0.1028	31.61	< 0.0001	significant
A-Laser Power	0.3983	1	0.3983	122.45	< 0.0001	
B-Focal Position	0.0703	1	0.0703	21.62	0.0016	
C-Scanning Speed	0.0011	1	0.0011	0.3468	0.5722	
AB	0.0529	1	0.0529	16.26	0.0038	
BC	0.0380	1	0.0380	11.69	0.0091	
A²	0.0252	1	0.0252	7.75	0.0238	
B²	0.1579	1	0.1579	48.53	0.0001	
C²	0.0556	1	0.0556	17.08	0.0033	
Residual	0.0260	8	0.0033			
Lack of Fit	0.0103	4	0.0026	0.6552	0.6540	not significant
Pure Error	0.0157	4	0.0039			

R-Squared	0.97	$Adj.R^2 = 0.938$
Adeq. Precision = 16.29		$Pred.R^2 = 0.85$

Table 5-13: ANOVA analysis of the laser-treated monomial nWC-12Co coating dry erosion data.

Source	Sum of Squares	DF	Mean Square	F value	Prob > F	
Model	48.13	9	5.35	766.71	< 0.0001	significant
A-Laser Power	20.38	1	20.38	2921.29	< 0.0001	
B-Focal Position	4.99	1	4.99	715.24	< 0.0001	
C-Scanning Speed	7.30	1	7.30	1046.04	< 0.0001	
AB	2.87	1	2.87	411.29	< 0.0001	
AC	1.18	1	1.18	168.78	< 0.0001	
BC	3.03	1	3.03	434.06	< 0.0001	
A²	5.88	1	5.88	843.29	< 0.0001	
B²	0.36	1	0.36	51.45	0.0002	
C²	1.53	1	1.53	219.18	< 0.0001	
Residual	0.049	7	6.975E-003			
Lack of Fit	0.040	3	0.013	6.08	0.0569	not significant
Pure Error	8.780E-003	4	2.195E-003			

R-Squared	0.99	$Adj.R^2 = 0.997$
Adeq. Precision = 79.34		$Pred.R^2 = 0.98$

Table 5-14: ANOVA analysis of the laser-treated mixed coating dry erosion data.

Novel Enhancement of HVOF Thermal Sprayed Nanostructured WC-12Co / Inconel-625 Coatings for Tribocorrosion Applications | **Al-Harbi, Naif I**

208

The final mathematical models for both laser-treated coatings' dry erosion, in terms of coded factors that can be used to make predictions about the response for given levels of each factor, were found to be as follows:

nWC-12Co coating (Dry erosion) = +0.62 -0.22 * A +0.094 * B -0.012 * C -0.11 * AB
-0.016 * AC -0.098 * BC -0.077 * A² -0.19 * B² -0.11 * C² $\qquad$ *Equation 5 − 18*

Mixed coating (Dry erosion) = +1.02 +1.60 * A -0.79 * B -0.96 * C -0.85 * AB -0.54 * AC
+0.87 * BC +1.18 * A² +0.29 * B² +0.60 * C² $\qquad$ *Equation 5 − 19*

Where A is laser power, B is focal position and C is scanning speed. The above equations rank the dependence for the monomial nWC-12Co coating as follows: $-A \gg -B^2 > - AB = C^2 > B > -BC > -A^2 > -AC > -C$. Moreover, the laser-treated monomial nWC-12Co coating dry erosion showed, among the three factors, that laser power (A) had the highest negative effect, followed by a positive effect for the focal position (B). As squared, the focal position (B^2) had the highest negative effect, whereas in combined effects, the laser power within the conjoined focal position (AB) had the most significant impact on dry erosion for the laser-treated monomial nWC-12Co coating.

For the mixed coating dry erosion response, dependence was ranked as follows: $A > A^2 > -C > BC > -AB > -B > C^2 > -AC > B^2$. The laser power had the highest positive effect, both as itself (A) and squared (A^2). Scanning speed (-C and C^2) was next. As a paired interaction, the focal positions with scanning speed and laser power (BC, -AB) had the most significant impact on dry erosion.

Figure 5-100 is a normal plot for the laser-treated monomial nWC-12Co coating dry erosion. The plot shows that the residuals have a linear relationship, which implies that they are normally distributed. Hence, an ANOVA can be carried out on observations for the dry erosion of this coating.

Novel Enhancement of HVOF Thermal Sprayed Nanostructured WC-12Co / Inconel-625 Coatings for Tribocorrosion Applications | **Al-Harbi, Naif I**

209
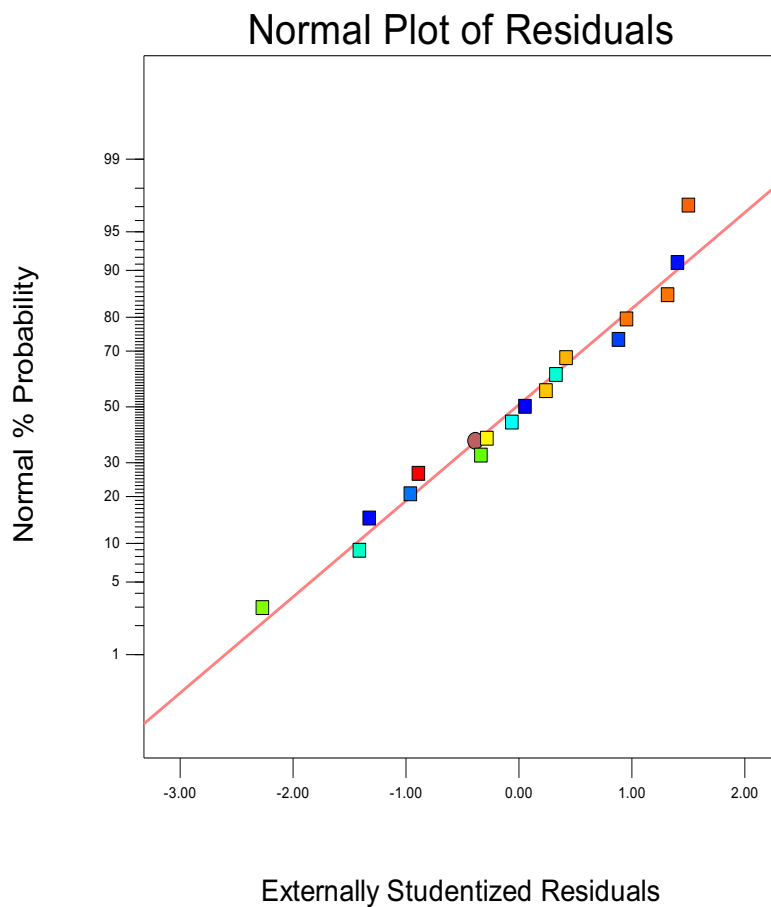
Figure 5-100: Normal plot residual of laser-treated monomial nWC-12Co coating for dry erosion (g).

In addition, the relationship between the actual and predicted value is linear, indicating that the difference between them is small, as shown in Figure 5-101 for the monomial nWC-12Co coating (dry erosion). The same was observed for the mixed-coating dry erosion, which for the sake of brevity, is provided in Appendix D of this research.

Novel Enhancement of HVOF Thermal Sprayed Nanostructured WC-12Co / Inconel-625 Coatings for Tribocorrosion Applications | **Al-Harbi, Naif I**

210
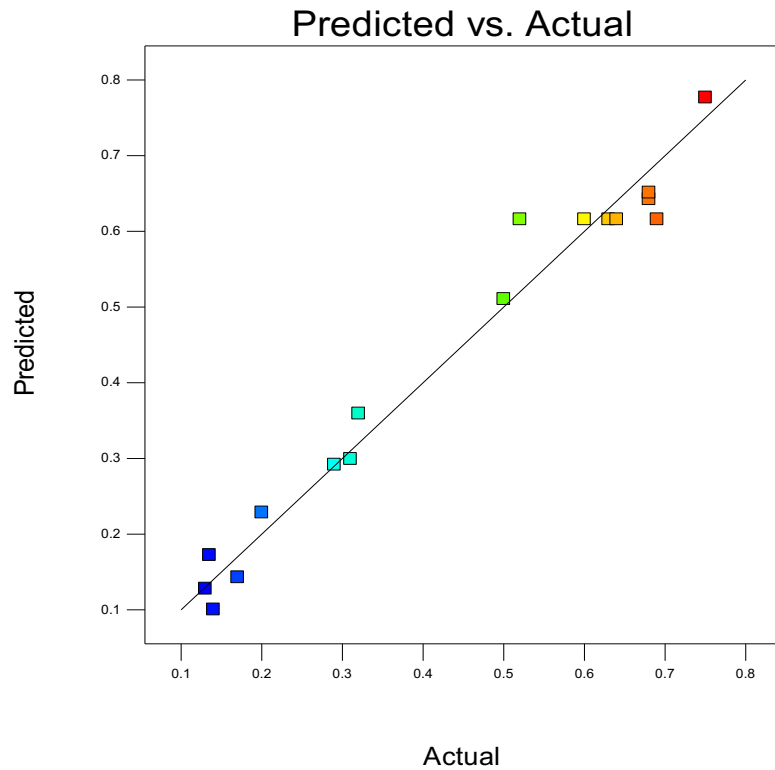
Figure 5-101: Predicted versus actual plot for laser-treated monomial nWC-12Co coating for dry erosion (g).

The final mathematical model determined by the DOE software for both laser-treated coatings to be used to predict the optimised values of dry erosion response with regards to actual factors is given in Equations 5-20 and 5-21.

*nWC-12Co Coating (Dry erosion) = -18.21191 +0.011325 * Laser Power +0.75435 * Focal Position +0.019973 * Scanning Speed -2.30000E-004 * Laser Power * Focal Position -2.16667E-006 * Laser Power * Scanning Speed -2.60000E-004 * Focal Position * Scanning Speed -7.73750E-006 * Laser Power^2 -7.74500E-003 * Focal Position^2 -2.04222E-005 * Scanning Speed^2*   *Equation* 5 − 20

*Mixed Coating (Dry erosion) = +37.58358 +0.040888 * Laser Power -1.19070 * Focal Position -0.13566 * Scanning Speed -1.69375E-003 * Laser Power * Focal Position -7.23333E-005 * Laser Power * Scanning Speed +2.32000E-003 * Focal Position * Scanning Speed +1.18194E-004 * Laser Power^2 +0.011677 * Focal Position^2 +1.07122E-004 * Scanning Speed^2*   *Equation* 5 − 21

Novel Enhancement of HVOF Thermal Sprayed Nanostructured WC-12Co / Inconel-625 Coatings for Tribocorrosion Applications | **Al-Harbi, Naif I**

211

5.11.2 DOE results of dry erosion

Figures 5–102 to 5–104 show a perturbation plot effect of each of the three control factors (laser power, focal position and scanning speed) and the interaction of the most dominant factor, the laser power (A) within focal position (B) and scanning speed (C), respectively, with the dry erosion response for laser-treated monomial nWC-12Co coating. These graphs show a strong similarity in the effects of each of the three factors' responses to the mass losses and the surface roughness, seen earlier in Figure 5-60 for the laser-treated monomial nWC-12Co coating. The same is also true for the mixed coating, as shown in Figures 5–105. That is, a smother surface will lead to lower mass losses as a result of the lack of friction resistance by the coating surface when it gets blasted by the grit particles [116]. However, as can be seen in Figure 102, the mass losses of the laser-treated monomial nWC-12Co coating significantly decrease with increasing laser power in an almost cubic manner. The dry erosion seems different for the focal position. As previously explained, increasing the focal position (B) will lower the energy density because the beam size will get larger. Consequently, the mass losses for the laser-treated monomial nWC-12Co coating show a slight increase in the low-level region (approximately between -1 and 0.5 as a coded value for the focal position). This result can be further clarified by presenting the significant differences between the two focal positions that provided the smallest (+35 mm) and largest beam size (+45 mm) in their interaction with the laser power to the laser-treated monomial nWC-12Co coating mass loss response. As shown in Figure 5-103, the lowest focal position (B) /beam size (+35 mm) will lead to better performance in dry erosion mass losses compared to the highest one (+45 mm). However, at a laser power (A) of approximately > 320 W, the largest beam size (+ 45) starts to behave more pleasingly. This might be attributed to a number of reasons, such as degree of dissolution of WC carbides as a function of increasing the laser energy input level [23, 122] and the large beam size providing lower surface roughness, as reported by Yasa and Kruth [121] and confirmed earlier in the surface roughness results discussion.

Novel Enhancement of HVOF Thermal Sprayed Nanostructured WC-12Co / Inconel-625 Coatings for Tribocorrosion Applications | **Al-Harbi, Naif I**

212

Figure 5-102: Perturbation plot for laser-treated monomial nWC-12Co coating dry erosion results.

Figure 5-103: Interaction between the laser power and the focal position to the monomial nWC-12Co coating dry erosion results.

Novel Enhancement of HVOF Thermal Sprayed Nanostructured WC-12Co / Inconel-625 Coatings for Tribocorrosion Applications | **Al-Harbi, Naif I**

213

From the perturbation plot given in Figure 5-102 and the interaction between laser power and scanning speed in Figure 5-104, the scanning speed (C) clearly shows insignificant effects in the mass losses of the laser-treated monomial nWC-12Co coating. This finding matches an experiment carried out by Hemmati et al. [131], who studied the effect of the laser-cladding speed on the hardness and wear performance of laser-deposited stainless steel coatings. The results show that the increase in solidification rate, as a function of increasing the scanning speed of the laser beam interaction with the target surface, did not create any change in the hardness and wear rate of these coatings. However, in this research both focal position (B) /beam size and scanning speed control the resident time of the laser beam with the target surface. The resident time of the laser beam as explained in the literature chapter in Figure 2-15, will determine the morphology and size solidification structure. This result can be explained by the interaction between the focal position and scanning speed (BC) being greater than that between laser power and scanning speed (-0.098 BC, 0.016 * AC, respectively).

Design-Expert® Software
Factor Coding: Actual
nWC-12Co-Dry Erosion (g)

X1 = C: Scanning Speed
X2 = A: Laser Power

Actual Factor
B: Focal Position = 40.00

■ A- 150.00
▲ A+ 350.00
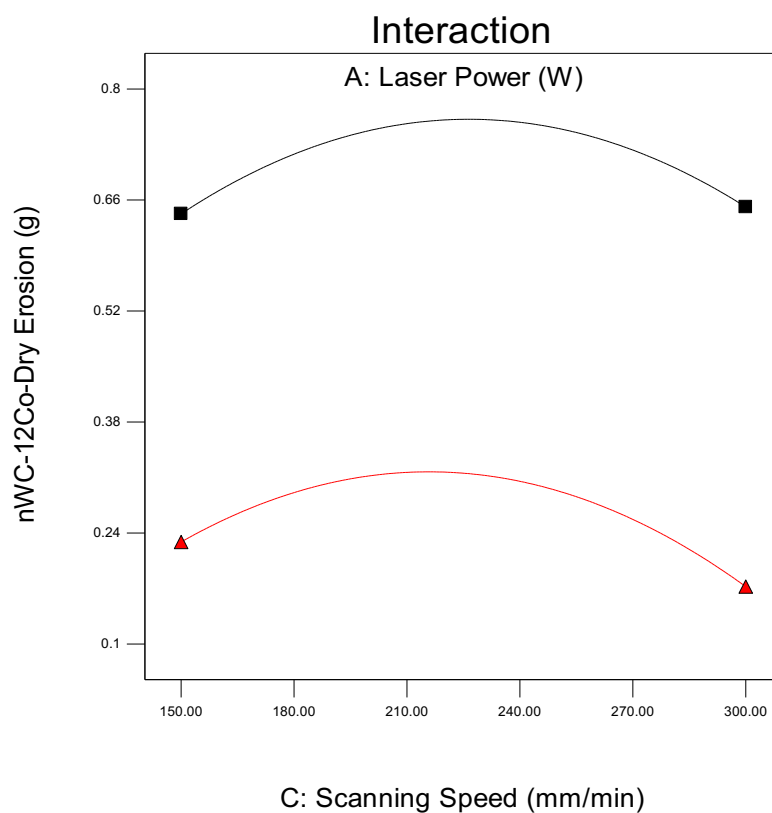
Figure 5-104: Interaction between the laser power and the scanning speed to the monomial nWC-12Co coating dry erosion results.

Novel Enhancement of HVOF Thermal Sprayed Nanostructured WC-12Co / Inconel-625 Coatings for Tribocorrosion Applications | **Al-Harbi, Naif I**

214

For the mixed coating, the perturbation plot (Figure 5-105) shows that the mass losses decrease at lower energy levels; then, as the energy rises, by either increasing the power density (amping up the laser power (A) and reducing the focal position/beam size (B)) or lowering the scanning speed (C) (lengthening the interaction time), mass losses increase. However, laser power has a major effect on mass losses for the laser-treated mixed coating compared to the other two factors, as presented in the coded mathematical model (Equation 5-19) and in the perturbation plot in Figure 5-105. Nevertheless, looking to the effect of laser power in mass losses response in the low-level region (between 0 to 1) to the high-level region (-1 to 1), the rate of mass losses in the high-level region is seen to significantly magnify as the laser power increases. This is may be due as previously explained, the coating layer of the laser-treated mixed coating, under a particular energy level, starts to become rougher and gas pockets start forming in the coating layer, increasing in quantity and diameter as the energy input increases. Consequently, both will have a negative impact on the resistance of the high-impact energies of the sand-eroded particles and lead the top coating layer to be easily removed during the dry erosion testing.

Design-Expert® Software
Factor Coding: Actual
Mixed Coating-Dry Erosion (g)

Actual Factors
A: Laser Power = 250.00
B: Focal Position = 40.00
C: Scanning Speed = 225.00
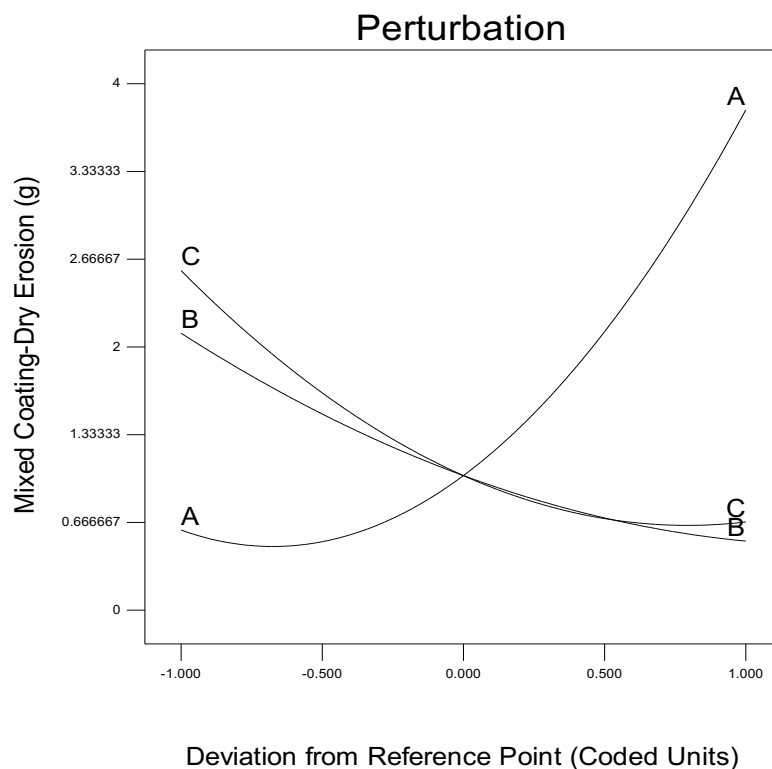
Figure 5-105: Perturbation plot for laser-treated mixed coating dry erosion results.

Novel Enhancement of HVOF Thermal Sprayed Nanostructured WC-12Co / Inconel-625 Coatings for Tribocorrosion Applications | **Al-Harbi, Naif I**

215

Figures 5-106 to 5-108 show the contour plots of the interaction between laser power and focal position, laser power and scanning speed, and scanning speed and focal position, respectively. Clearly, all contour plots show that the dry erosion response behaves more satisfactorily under a low specific energy level. Furthermore, the plots show and confirm that laser power is slightly more significant regarding dry erosion, followed by scanning speed, with focal position as the lowest.
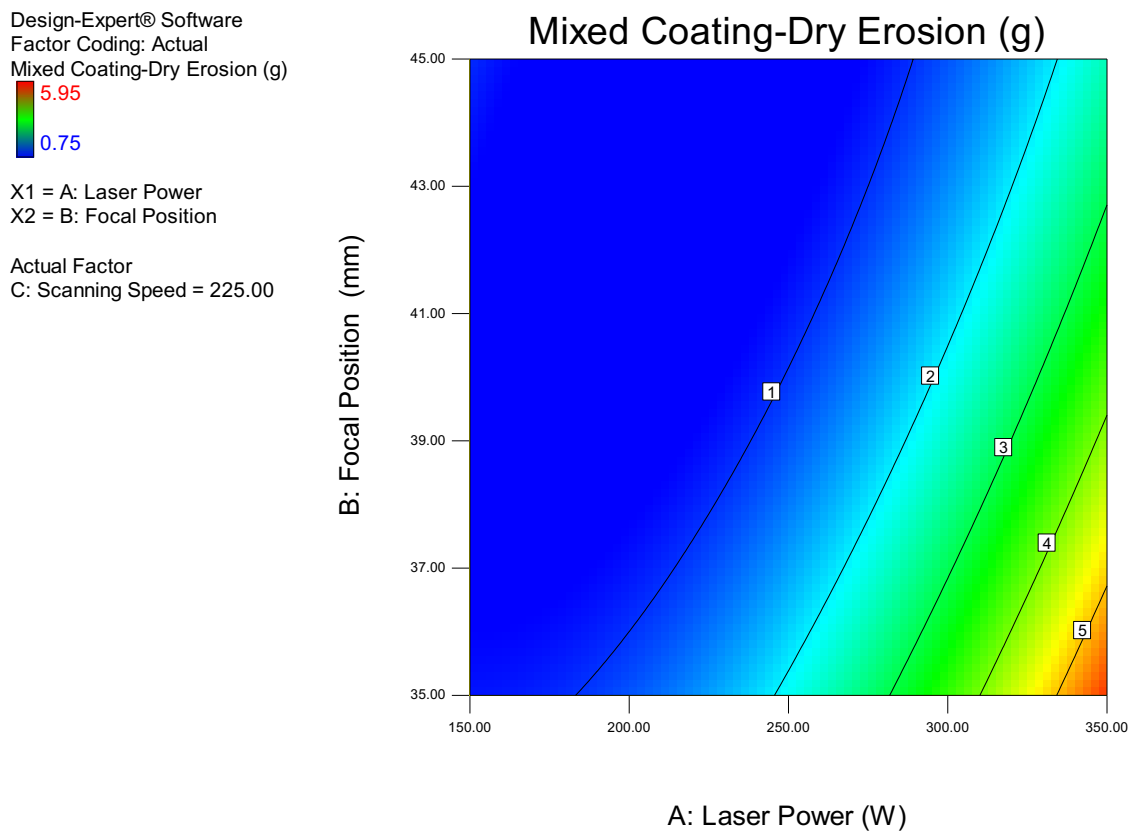
Figure 5-106: Contour plot of the laser-treated mixed coating dry erosion response versus the focal position and the laser power.

Novel Enhancement of HVOF Thermal Sprayed Nanostructured WC-12Co / Inconel-625 Coatings for Tribocorrosion Applications | **Al-Harbi, Naif I**

216

Figure 5-107: Contour plot of the laser-treated mixed coating dry erosion response versus the scanning speed and the laser power.

Figure 5-108: Contour plot of the laser-treated mixed coating dry erosion response versus the scanning speed and the focal position.

Novel Enhancement of HVOF Thermal Sprayed Nanostructured WC-12Co / Inconel-625 Coatings for Tribocorrosion Applications | **Al-Harbi, Naif I**

217

5.12 Slurry erosion of laser-melted HVOF coatings

The erosion wear caused by hard particles becoming ingrained into a surface is one of the most common types of wear that damages the components in the oil and gas industry. The erosion of these components is further accelerated by the corrosion process of the surface as a result of corrosive liquid [132–136].

The results of the slurry erosion-coated samples, before and after laser processing under the different laser settings in terms of mass losses, are presented in Figure 5-109. P.S.2 and P.S.4, amongst all the laser settings used to treat the monomial nWC-12Co coating, had the lowest mass losses via the slurry erosion testing, followed by P.S.8, within which losses increased slightly. The amount of mass losses for these laser settings ranged from 0.055 to 0.065 g, forming a remarkable reduction of the mass losses noted for the untreated monomial nWC-12Co coating (0.29 g). The improvement was a reduction in mass of approximately four to five times after laser-treating the monomial nWC-12Co coating under these settings and almost 13 times in comparison to the uncoated workpiece. For the mixed coating, the magnitude of the mass reduction after the laser processing under the best laser settings (P.S.10, P.S.7, and P.S.12) was somewhat smaller than what was achieved for the monomial nWC-12Co coating. However, the P.S.10 and P.S.7 laser settings yielded the lowest mass losses for this coating type of 0.265 and 0.31 respectively. The improvement was an almost 64% reduction in losses, as was the case for P.S.10 in comparison to 0.41 g for the untreated mixed coating.

Clearly, as per what was mentioned earlier for the dry and slurry erosion of HVOF coatings along with uncoated workpiece characterisation, the erosion rates in dry particles' impact are about five orders of magnitude higher than those in slurry erosion testing. A similar observation was noted by Al-Hamed [17] in his investigation of the erosion performance of mixing three coating powder materials (Micro/Nano WC-12Co and Inconel-625) and in another research work conducted by Hawthorne et al. [137]. The latter conducted their work by evaluating the performance of ten HVOF coatings under two different angles (20° and 90°) under both dry and slurry erosion (six WC cermets with Co/Ni-based matrices, CrC–NiCr composite and three metallic alloys), concluding that the erosion rates in dry particles' impact were about three orders higher in magnitude than those in slurry erosion results. This was attributed to the slurry tests being mitigated by the water medium to the erosion particles during the blasting process. Moreover, the WC–12Co cermet coating was

Novel Enhancement of HVOF Thermal Sprayed Nanostructured WC-12Co / Inconel-625 Coatings for Tribocorrosion Applications | **Al-Harbi, Naif I**

218

found to be more susceptible to slurry erosion damage than the WC–10Co–4Cr matrix coating. The authors also found that the removal of the matrix after four hours' exposure to the aqueous slurry impingement was more evident in the pure cobalt matrix coating than the cobalt–chrome alloy matrix. They concluded that, by using the cobalt as a binder matrix for hard carbides, the cobalt matrix can be made more electrochemically active and will be more susceptible to corrosion than the cobalt–chrome alloy matrix carbides [137]. Meanwhile, the corrosion rate of the WC-Co coating will be higher and faster when increasing the cobalt metallic matrix contents [138, 139].
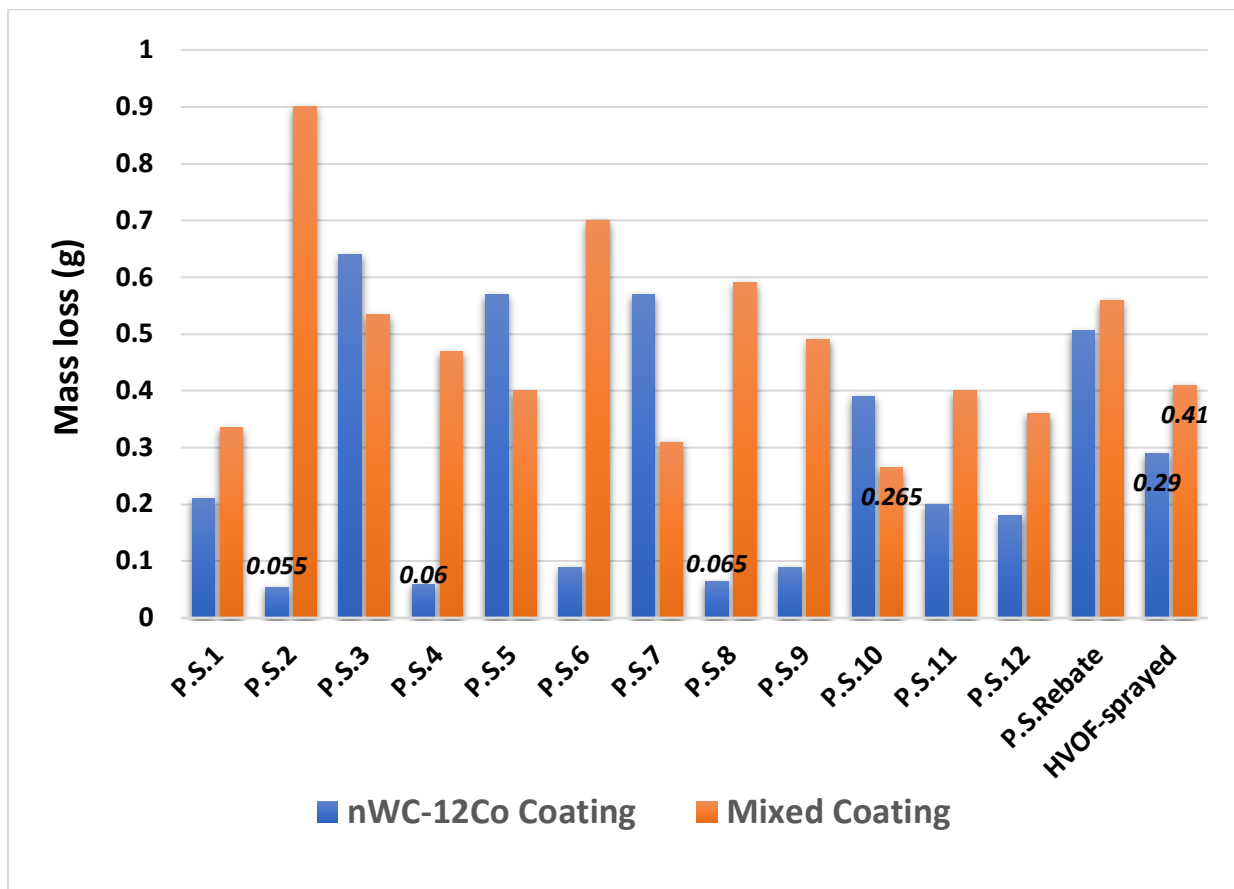
Figure 5-109: Slurry erosion value for the two coating types before and after laser treatment under various laser settings.

The reason as explained by Liu and Singh et al. [54, 139], due to the microgalvanic force forms as a result of the difference in the electrochemical potential in the interface between the ceramic phases as effective cathodes and the anodic metal matrix that surrounds them. Consequently, in terms of lowering the corrosion rate, the selection of an appropriate metal matrix containing metallic materials such as chromium and/or Molybdenum is more preferable, having been proven in numerous studies to offer greater resistance to localised

Novel Enhancement of HVOF Thermal Sprayed Nanostructured WC-12Co / Inconel-625 Coatings for Tribocorrosion Applications | **Al-Harbi, Naif I**

219

corrosion while being more compatible with the hard phases [54, 140–141]. This may explain why the mixed coating performed better under the slurry erosion testing than the monomial nWC-12Co coating under a similar laser setting, providing low-energy inputs such as P.S.3, P.S.7 and P.S.10, as shown in Figure 5-109. Similarly, the corrosion effect for the untreated monomial nWC-12Co coating was more noticeable at the coating top surface after 48 hours of contact with the corrosive liquid in comparison to the untreated mixed coating in Figure 5-32. As was noted for both coatings when laser-treated under low energy inputs, the coating top surface was characterised by a dark colour for both, a sign that those samples were surface-rich with the binder matrix. As a result, for the laser-treated monomial nWC-12Co coating, the corrosion rate was significantly high after 48 hours of contact with the corrosive environment and prior to the grit particles blasting process, as shown in the optical photographs for P.S.5 and P.S.3 in Figures 5-110 (A) and (B), leading to weakening of the coating top surface, which could then easily be removed by the blasting process. However, this was not the case for the mixed coating, as shown in Figure 5-111 (A) and (B) for P.S.12 and P.S.10 respectively, where the coating top surface shows a significant improvement in the corrosion resistance effect after contact with the corrosive liquid, which is obviously linked to the modification of the metal occasioned by mixing the Inconel 625 nickel-chromium alloy with the monomial nWC-12Co powders. In contrast, with increasing energy inputs, the WC concentration gradually changed towards the coating's outer surface, reducing the dramatic composition gradient between the metallic matrix and the hard phase and elimination of the porosity, which is also caused by the formation of various new phases for the laser-treated monomial nWC-12Co coating. The degree of the passivation was enhanced and a number of laser settings showed almost zero corrosion effect after the corrosion medium contact and low mass losses, such as those shown in Figures 5-110 (C) and (D) for P.S.4 and P.S.2 respectively. For the mixed coating, as was clarified earlier in the high laser energy input, the gas pockets will form in the coating layer's outer surface and beneath it, where their quantity and diameter size will increase proportionally with the increase of the laser energy input at a particular level. Consequently, those pores create paths for corrosive fluids to attack the substrate material and create a high corrosion rate, as shown in the optical photographs in Figures 5-111 (C) and (D) for P.S.8 and P.S.6 respectively, and eventually the mass losses, after the grit blasting, will significantly increase in comparison to the untreated coating.

Novel Enhancement of HVOF Thermal Sprayed Nanostructured WC-12Co / Inconel-625 Coatings for Tribocorrosion Applications | **Al-Harbi, Naif I**

220
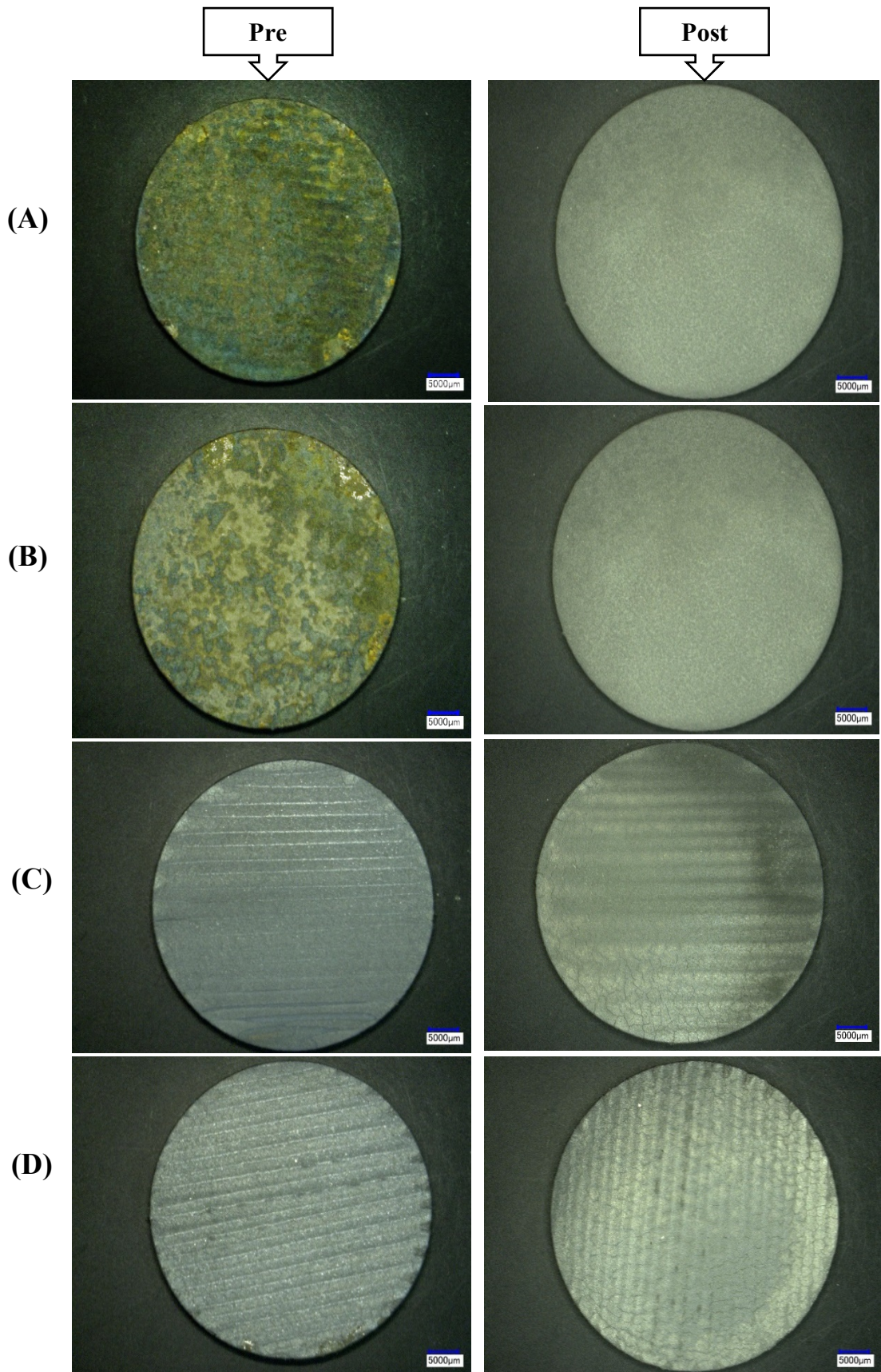
Figure 5-110: Optical photographs of laser-treated samples for the monomial nWC-12Co coating pre (after contact with corrosion liquid) and post grit blasting. (A) P.S.5, (B) P.S.3, (C) P.S.4 and (D) P.S.2.

Novel Enhancement of HVOF Thermal Sprayed Nanostructured WC-12Co / Inconel-625 Coatings for Tribocorrosion Applications | **Al-Harbi, Naif I**

221
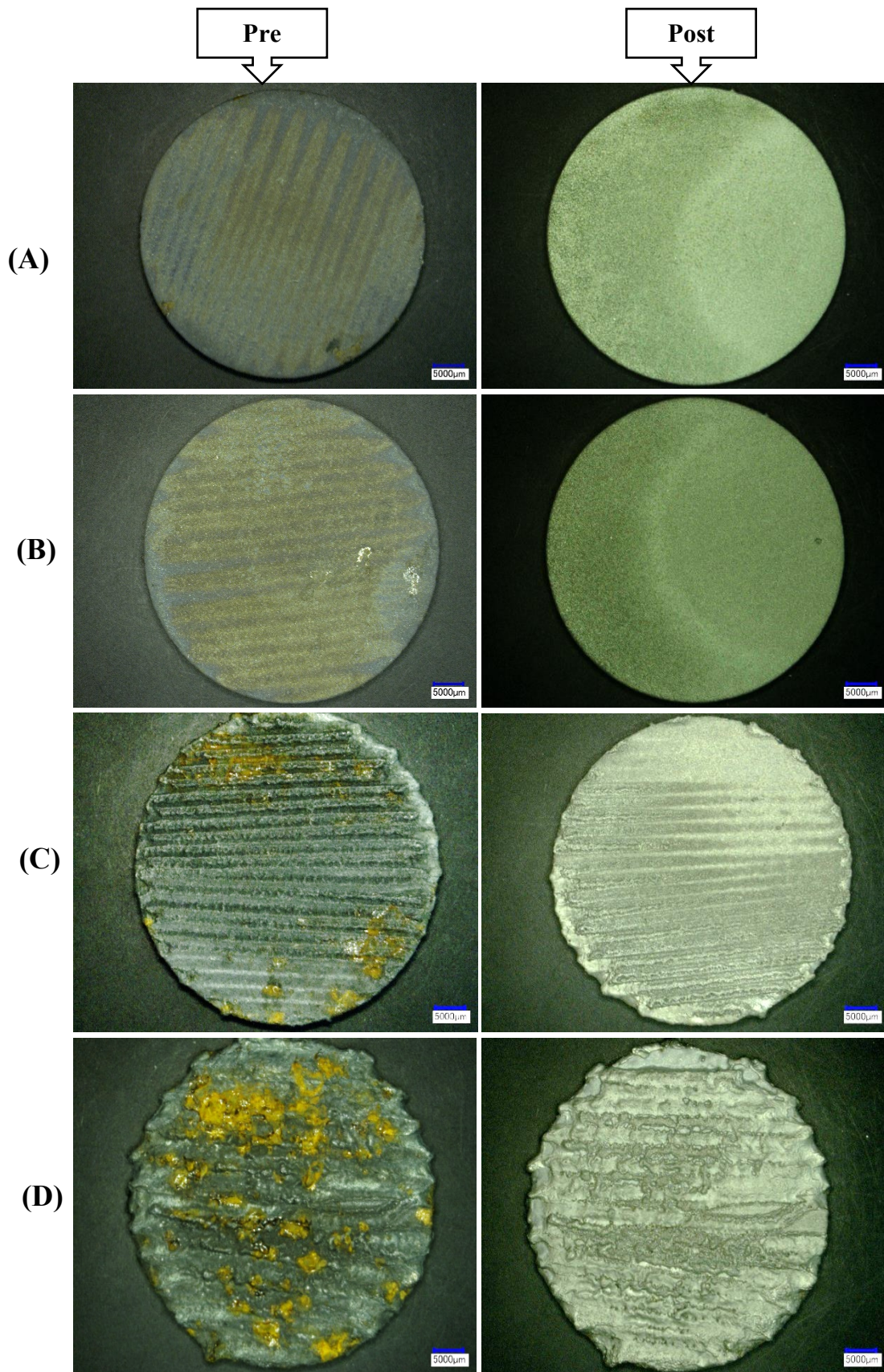
Figure 5-111: Optical photographs of laser-treated samples for the mixed coating pre (after contact with corrosion liquid) and post grit blasting. (A) P.S.12, (B) P.S.10, (C) P.S.8 and (D) P.S.6.

Novel Enhancement of HVOF Thermal Sprayed Nanostructured WC-12Co / Inconel-625 Coatings for Tribocorrosion Applications | **Al-Harbi, Naif I**

222

5.12.1 Development of the mathematical model for slurry erosion results

The design of experiment (DOE) method was used to compare the measured data on experimental slurry erosion with the process factors: laser power, focal position and scanning speed. Tables 5-15 and 5-16 show the resulting ANOVA of the slurry erosion for both laser-treated coating data. A quadratic model was chosen to fit the data, as it showed significant models (<0.05) for both coatings within high R^2 values of 0.964 and 0.93 for the monomial and the mixed coatings, respectively. Moreover, it is evident that lack of fit was not significant, the difference between predicted R^2 and adjusted R^2 being less than 0.2.

The ANOVA for both coatings indicated that laser power, followed by focal position, was the primary factor controlling slurry erosion for laser-treated coatings, with scanning speed having a negligible effect. Moreover, significant interactions took place up to the second order, in the focal position for the monomial coating and scanning speed for the laser-treated mixed coating. This indicates that the response is not linear but instead will be more sensitive to changes when the focal position is high, for the monomial coating, or the scanning speed is low, for the laser-treated mixed coating.

Source	Sum of Squares	DF	Mean Square	F value	Prob > F	
Model	0.7458	8	0.0932	27.22	< 0.0001	significant
A-Laser Power	*0.3698*	*1*	*0.3698*	*107.99*	*< 0.0001*	
B-Focal Position	*0.0639*	*1*	*0.0639*	*18.66*	*0.0025*	
C-Scanning Speed	*0.0020*	*1*	*0.0020*	*0.5704*	*0.4718*	
AB	*0.0452*	*1*	*0.0452*	*13.19*	*0.0067*	
BC	*0.0256*	*1*	*0.0256*	*7.48*	*0.0257*	
A²	*0.0256*	*1*	*0.0256*	*7.48*	*0.0256*	
B²	*0.1468*	*1*	*0.1468*	*42.88*	*0.0002*	
C²	*0.0458*	*1*	*0.0458*	*13.36*	*0.0064*	
Residual	*0.0274*	*8*	*0.0034*			
Lack of Fit	*0.0117*	*4*	*0.0029*	*0.7427*	*0.6099*	*not significant*
Pure Error	*0.0157*	*4*	*0.0039*			

R-Squared   **0.964**   Adj.R^2 = 0.92

Adeq. Precision = 15.04   Pred.R^2 = 0.79

Table 5-15: ANOVA analysis of the laser-treated monomial nWC-12Co coating slurry erosion data.

Novel Enhancement of HVOF Thermal Sprayed Nanostructured WC-12Co / Inconel-625 Coatings for Tribocorrosion Applications | **Al-Harbi, Naif I**

223

Source	Sum of Squares	DF	Mean Square	F value	Prob > F	
Model	0.3709	7	0.0530	17.12	0.0002	significant
A-Laser Power	*0.1461*	*1*	*0.1461*	*47.20*	*< 0.0001*	
B-Focal Position	*0.0308*	*1*	*0.0308*	*9.94*	*0.0117*	
C-Scanning Speed	*0.0048*	*1*	*0.0048*	*1.54*	*0.2466*	
AB	*0.0989*	*1*	*0.0989*	*31.96*	*0.0003*	
A²	*0.0156*	*1*	*0.0156*	*5.05*	*0.0513*	
B²	*0.0153*	*1*	*0.0153*	*4.95*	*0.0530*	
C²	*0.0607*	*1*	*0.0607*	*19.62*	*0.0016*	
Residual	*0.0279*	*9*	*0.0031*			
Lack of Fit	*0.0148*	*5*	*0.0030*	*0.9114*	*0.5512*	*not significant*
Pure Error	*0.0130*	*4*	*0.0033*			

R-Squared	**0.93**	Adj.R^2 = 087	
Adeq. Precision = 16. 3		Pred.R^2 = 0.78	

Table 5-16: ANOVA analysis of the laser-treated mixed coating slurry erosion data.

The final mathematical models for both laser-treated coatings' slurry erosion, in terms of coded factors that can be used to make predictions about the response for given levels of each factor, were found to be as follows:

nWC-12Co coating (Slurry erosion) = +0.51 - 0.22 * A +0.089 * B -0.016 * C -0.1 * AB -6.250E-003 * AC -0.080 * BC -0.078 * A² -0.19 * B² -0.1 * C² $Equation\ 5-22$

Mixed coating (Slurry erosion) = +0.56 + 0.14 * A - 0.062 * B - 0.024 * C - 0.16 * AB - 5.000E-003 * AC + 0.046 * BC + 0.061 * A² - 0.060 * B² - 0.12 * C² $Equation\ 5-23$

The foregoing equations can be used to rank dependence for the monomial nWC-12Co coating: –A > –B² > –AB = –C² > B > –BC > –A² > –C > –AC. For the slurry erosion response of the laser-treated monomial nWC-12Co coating, laser power (A) had the highest negative effect, followed by a positive effect for focal position (B) and scanning speed (–C), respectively. When squared, focal position (B²) had the highest negative effect, whereas as a paired factors interaction, within negative effect the laser power within the focal position (–AB) had the most significant impact on slurry erosion for the laser-treated monomial nWC-12Co coating.

Novel Enhancement of HVOF Thermal Sprayed Nanostructured WC-12Co / Inconel-625 Coatings for Tribocorrosion Applications | **Al-Harbi, Naif I**

224

Dependence for the laser-treated mixed coating can be ranked as follows: $-AB > A > -C^2 > -B > A^2 > -B^2 > BC > -C > -AC$. Laser power had the highest effect, both as itself (A) and with negative effect as a paired interaction with focal position ($-AB$). Focal position was next as an interaction and as itself with negative effect ($-AB$ and $-B^2$, respectively). When squared, within a negative effect, scanning speed and then focal position power ($-C^2$ and $-B^2$, respectively) had the most significant effects on slurry erosion.

Figure 5-112 is a normal plot for the laser-treated monomial nWC-12Co coating slurry erosion. The plot shows that the residuals have a linear relationship, which implies that they are normally distributed. Hence, an ANOVA can be carried out on observations for the dry erosion of this coating.

.
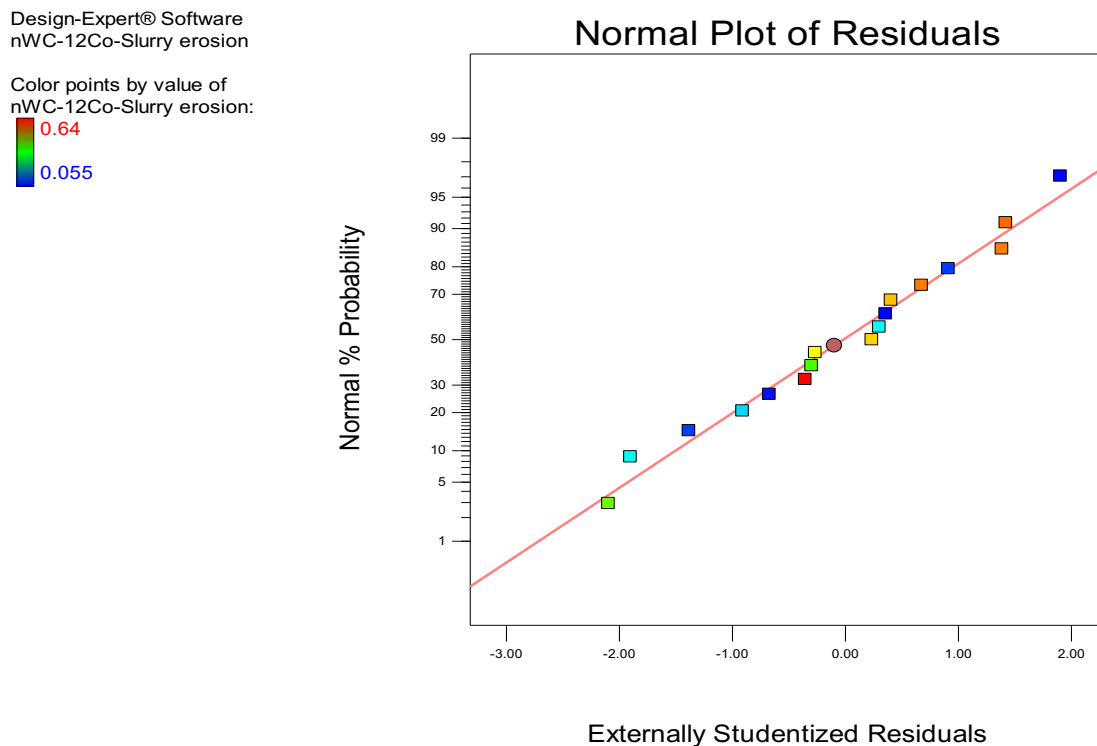
Figure 5-112: Normal plot residual of laser-treated monomial nWC-12Co coating for slurry erosion (g).

In addition, the relationship between the actual and predicted value is linear, indicating that the difference between them is small, as shown in Figure 5-113 for the monomial nWC-12Co coating (slurry erosion). The same was observed for the mixed-coating dry erosion, which for the sake of brevity, is provided in Appendix E of this research.

Novel Enhancement of HVOF Thermal Sprayed Nanostructured WC-12Co / Inconel-625 Coatings for Tribocorrosion Applications | **Al-Harbi, Naif I**

225
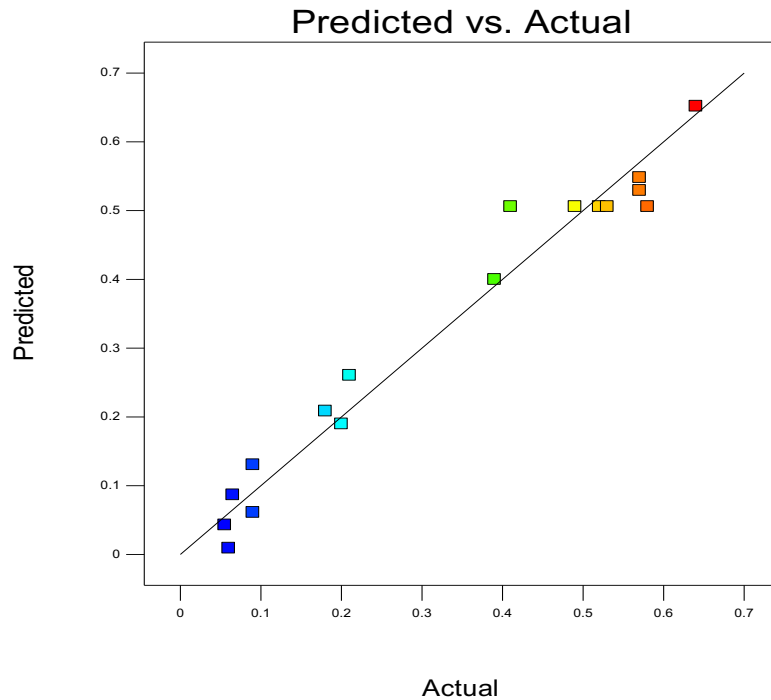
Figure 5-113: Predicted versus actual plot for laser-treated monomial nWC-12Co coating for dry erosion (g).

The final mathematical model determined by the DOE software for both laser-treated coatings will be used to predict the optimised values of slurry erosion response to the actual factors given in Equations 5-24 and 5-25.

nWC-12Co Coating (Slurry erosion) = -17.09425+0.010437 * Laser Power +0.71660 * Focal Position +0.016873 * Scanning Speed -2.12500E-004 * Laser Power * Focal Position -8.33333E-007 * Laser Power * Scanning Speed -2.13333E-004 * Focal Position * Scanning Speed -7.80000E-006 * Laser Power² -7.47000E-003 * Focal Position² -1.85333E-005 * Scanning Speed²   *Equation* 5 − 24

Mixed Coating (Slurry erosion) = -5.84466 + 0.011036 * Laser Power + 0.23159 * Focal Position + 4.51633E-003 * Scanning Speed - 3.14500E-004 * Laser Power * Focal Position- 6.66667E-007 * Laser Power * Scanning Speed + 1.23333E-004 * Focal Position * Scanning Speed + 6.09000E-006 * Laser Power² - 2.41400E-003 * Focal Position² - 2.13511E-005 * Scanning Speed²   *Equation* 5 − 25

Novel Enhancement of HVOF Thermal Sprayed Nanostructured WC-12Co / Inconel-625 Coatings for Tribocorrosion Applications | **Al-Harbi, Naif I**

226

5.12.2 DOE results of slurry erosion

Figures 5-114 to 5-116 show a perturbation plot effect of each of the three control factors (laser power, focal position and scanning speed) and the interactions of the most paired factors, the laser power within the focal position (AB) and the focal position within the scanning speed (BC), respectively, with the slurry erosion response for the laser-treated monomial nWC-12Co coating. The perturbation plot in Figure 5-114 shows that the slurry erosion decreased significantly with increased laser power (A) in an almost linear decay manner. The same thing happened when lowering the focal position height (B) (decreasing the laser beam size) and slowing the laser scanning speed (C), as clarified by the interaction contour plots in Figures 5-115 and 5-116 respectively. Meanwhile, by increasing the scanning speed, the energy per unit length to the treated surface will be reduced as a function of reducing the interaction time, and by decreasing the laser power and/or increasing the height/level of the focal position (increasing the beam size), the power density will be smaller. This finding can, in some way, allow us to say that the slurry erosion of the monomial nWC-12Co coating decreases as a function of increasing the energy input. This can be explained by the reasoning noted earlier: As the thermal energy input increases to a particular level, the coating layer becomes denser and has fewer microstructure defects. The outcomes include increasing the degree of the nWC-12Co coating particles' flattering and bonding, elimination of porosity and discrete splats structure, and reduction of the dramatic composition gradients between the Nano-size WC hard phase carbides and the cobalt matrix (particularly at the coating's outer surface). This therefore forms a barrier to the ingress of corrosive species to the underlying surface during the first stage in contact within the corrosive liquid, and remarkable resistance comes next during the second stage when the grit particles are sprayed to its surface. However, from Figure 5-115, interaction clearly occurs between the laser power (A) and the focal position (B) under the highest level (+45 mm) and the lowest focal position/beam size (+35 mm), so that under a particular level for the laser power ($\approx$ 330 W), the highest focal position starts to perform better in comparison to the lowest one. This may be attributed to two different factors; first, the hardness of the coating's outer surface is reduced as a result of the high degree of WC decarburisation under this high energy level, which weakens the coating's surface wear resistance, as reported by Rakhest et al. [142]. Second, the high focal position/beam size enables lower surface roughness, as has been found before, leading to better erosion resistance thanks to lowering of the friction coefficient during the grit blasting process.

Novel Enhancement of HVOF Thermal Sprayed Nanostructured WC-12Co / Inconel-625 Coatings for Tribocorrosion Applications | **Al-Harbi, Naif I**

227

Design-Expert® Software
Factor Coding: Actual
nWC-12Co-Slurry erosion (g)

Actual Factors
A: Laser Power = 250.00
B: Focal Position = 40.00
C: Scanning Speed = 225.00
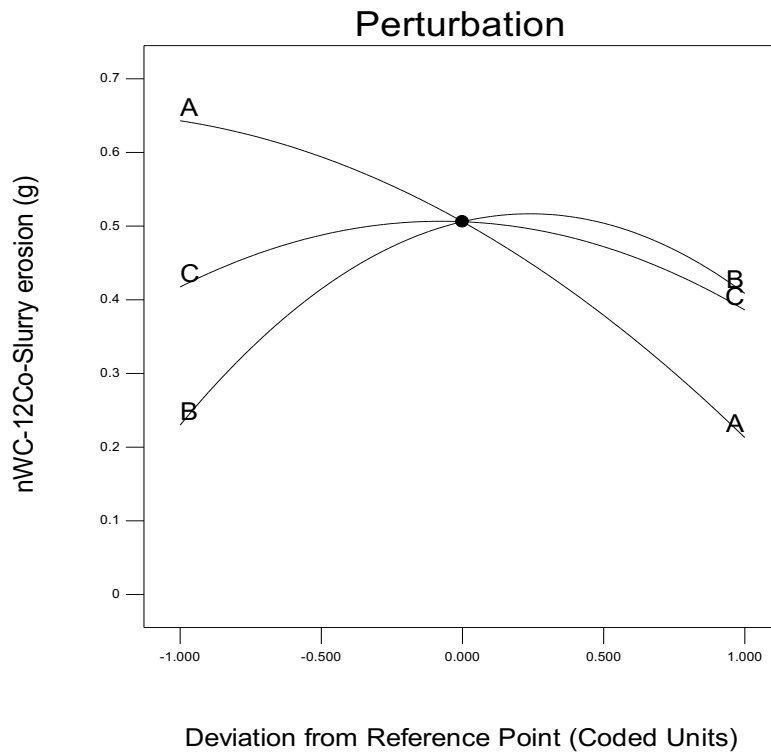
Figure 5-114: Perturbation plot for laser-treated monomial nWC-12Co coating slurry erosion results.

Design-Expert® Software
Factor Coding: Actual
nWC-12Co-Slurry erosion (g)

X1 = A: Laser Power
X2 = B: Focal Position

Actual Factor
C: Scanning Speed = 225.00

■ B- 35.00
▲ B+ 45.00
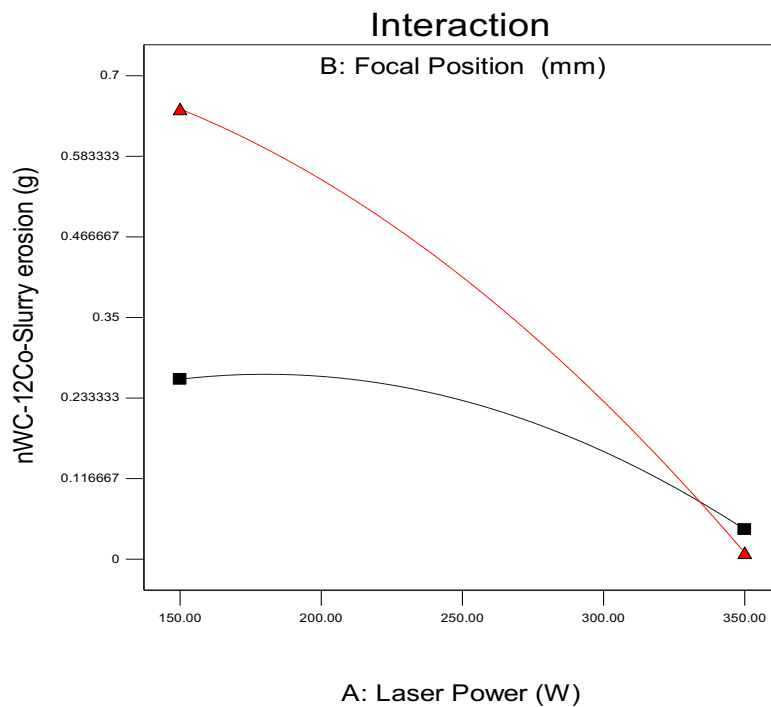
Figure 5-115: Interaction between the laser power and the focal position to the monomial nWC-12Co coating slurry erosion results.

Novel Enhancement of HVOF Thermal Sprayed Nanostructured WC-12Co / Inconel-625 Coatings for Tribocorrosion Applications | **Al-Harbi, Naif I**

228
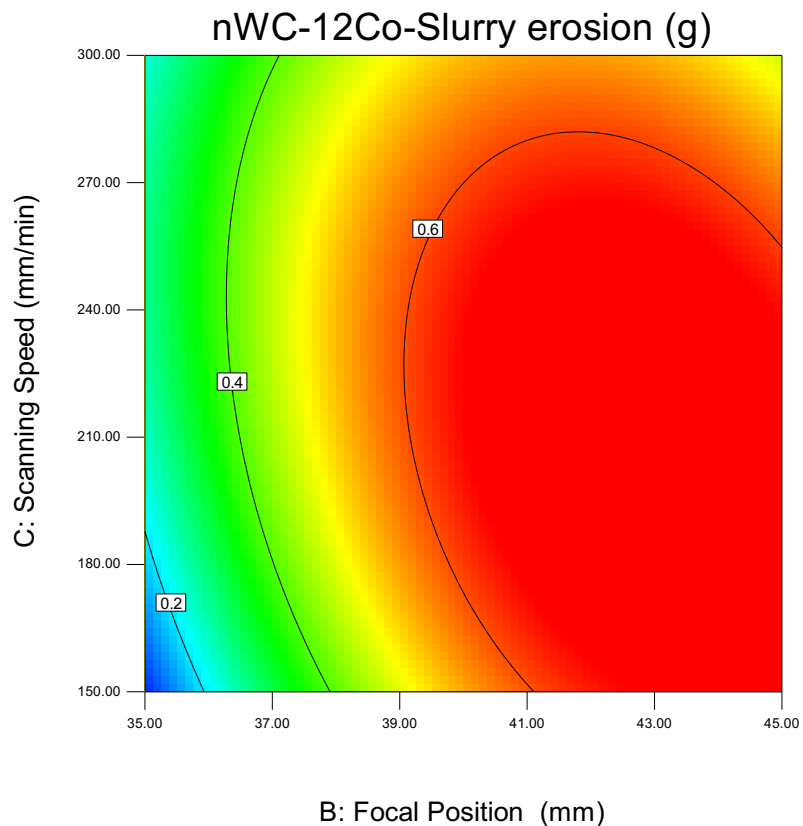
Figure 5-116: Contour plot of the laser-treated monomial nWC-12Co coating slurry erosion response versus the focal position and the laser power.

For the laser-treated mixed coating, the perturbation plot showing the effects of each of the three controlled factors can be seen in Figure 5-117; moreover, the contour plots displaying the most significant paired factors' effects as interaction (AB and BC) are presented in Figures 5-118 and 5-119 respectively. First, each of the three factors clearly show strongly similar effects on the slurry erosion response for the laser-treated mixed coating as on the dry erosion. In general, we can clearly see that treating the mixed coating under low specific energy will lead to the lowest mass losses. This is because the formation of gas pockets in the coating layer led to a high corrosion rate after contact with corrosive liquid. The perturbation plot in Figure 5-117 clearly evinces that as the laser power (A) increases, so does the amount of mass losses in a quadratic manner (A and A^2 terms in the coded equation), while losses decrease slightly in an exponential manner when increasing the focal position. Meanwhile, the effect of the scanning speed is obviously insignificant in terms of the slurry erosion for

Novel Enhancement of HVOF Thermal Sprayed Nanostructured WC-12Co / Inconel-625 Coatings for Tribocorrosion Applications | **Al-Harbi, Naif I**

229

the laser-treated mixed coating, which was confirmed earlier in the dependence ranking for the mathematical model in Equation 5– 25.
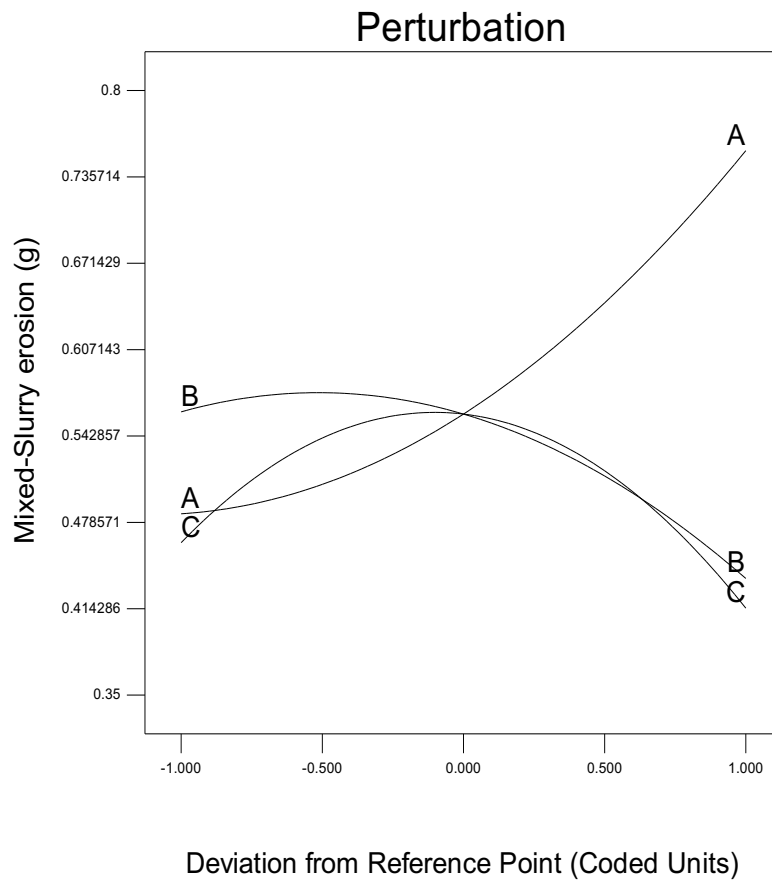
Figure 5-117: Perturbation plot for laser-treated mixed coating slurry erosion results.

Figures 5-118 and 5-119 shows the interaction plots at the focal position with laser power and the scanning speed, respectively, at medium level = 0 for the third factor. Clearly, both contour plots show that the slurry erosion response behaves more satisfactorily under a low specific energy level. Furthermore, similar to what was noticed in the dry erosion, the plots demonstrate and confirm that laser power is slightly more significant regarding slurry erosion, followed by scanning speed, with focal position as the lowest.

Novel Enhancement of HVOF Thermal Sprayed Nanostructured WC-12Co / Inconel-625 Coatings for Tribocorrosion Applications | **Al-Harbi, Naif I**

230
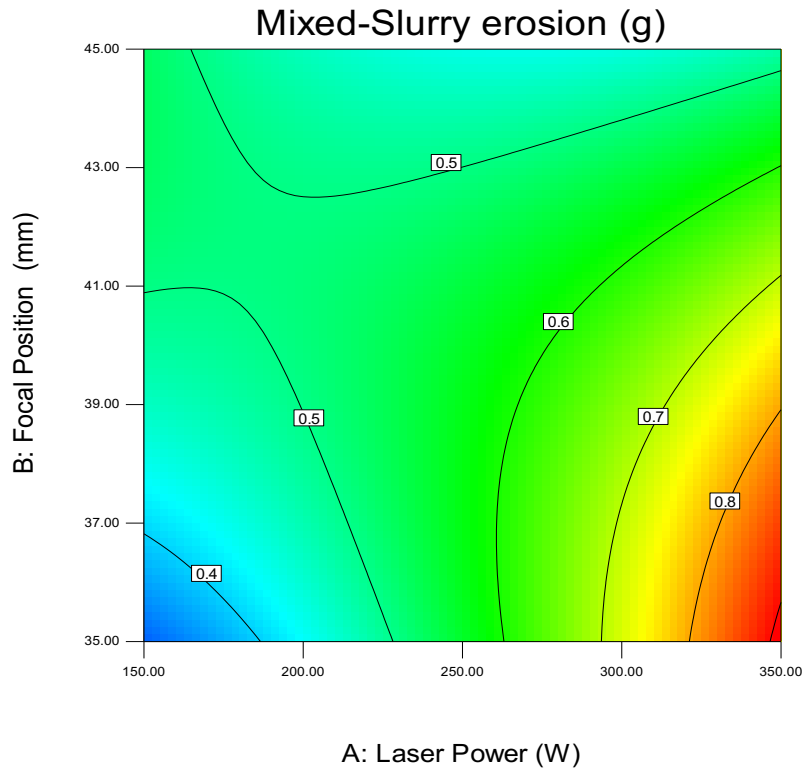
Figure 5-118: Contour plot of the laser-treated mixed coating slurry erosion response versus the focal position and the laser power.
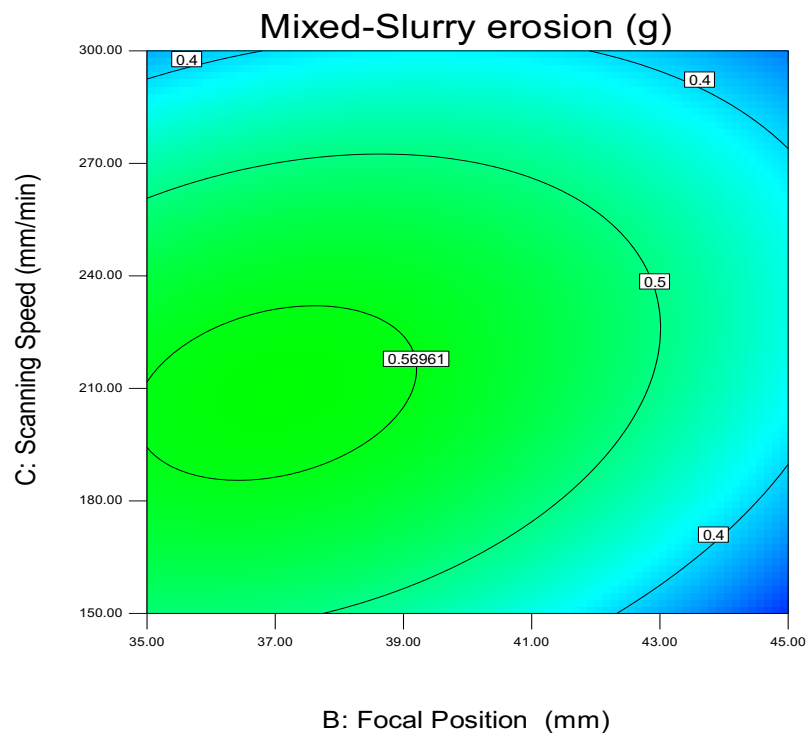
Figure 5-119: Contour plot of the laser-treated mixed coating slurry erosion response versus the scanning speed and the focal position.

Novel Enhancement of HVOF Thermal Sprayed Nanostructured WC-12Co / Inconel-625 Coatings for Tribocorrosion Applications | **Al-Harbi, Naif I**

231

5.13 Operating Cost Calculation

The approximate cost of the HVOF thermal spray coating process for each of the coating types under investigation in this research will be calculated, plus the addition of the laser treatment process, according to the DOE matrix (from Tables 3–6 of Chapter 3). The purpose is to evaluate the cost effectiveness of adding the laser process, based on the enhancement achieved in the coated properties, compared to the untreated ones. Only the variable costs were calculated, with the labour and overheads cost excluded because of their dependence on the location where a process may take place. The cost is based on producing, 1,000 samples 38 * 38 mm square, coated with a layer thickness of ≈ 270 μm (approximately between 28 to 32 coating passes) for each coating type.

5.13.1 Cost of the HVOF coating process

The approximate cost of coating 1,000 samples for each of the coating types was broken into various gases (propane, oxygen, nitrogen and compressed air), the amount of the coating materials used, the substrate surface preparation, the pre-heating of the substrate prior spraying process and the powder mixing for the mixed coating type.

By using the MultiCoat HVOF thermal spray system shown in Figure 3-10, 16 samples can be coated in one run, with each run taking almost one hour. As a result, 63 runs are required to produce 1,000 coating samples for each of the coating types. HVOF thermal spray coating runs can be costed as follows:

Step 1: Substrate surface preparation
The preparation of 1,000 substrate surface samples requires approximately four bags (each containing 25 kg) of the Guyson blasting media (Honite 13), and the process will take almost four hours for each coating type. The cost of the four bags is €314.8 and the cost of four hours of the blasting process is €8 (attributed to the electricity cost) [143]. The total cost of the surface preparation for 1,000 samples, for each coating type, will amount to €322.80.

Step 2: Substrates pre-heating
Prior to spraying the coating powder, the substrates must be preheated by hot air from the front face through the HVOF gun for approximately two minutes until the pre-heated

Novel Enhancement of HVOF Thermal Sprayed Nanostructured WC-12Co / Inconel-625 Coatings for Tribocorrosion Applications | **Al-Harbi, Naif I**

232

temperature is reached. The cost for 63 HVOF runs for each coating type would be €252 [143]. (worked out from details given in step 4 below).

Step 3: Powder mixing

This procedure is only applied to the mixed coating type using the V-shaped blender (shown in Figure 3-6). For 23 kg, with each 1 kg being blended for 30 minutes, the total time and cost for the mixing process would be 11.4 hours and €23 (attributed to the electricity cost) respectively.

Step 4: Cost of gases

The cost of using propane gas is almost €31 per hour, with €32 per hour for using nitrogen, €24 per hour for using oxygen and €3.2 per hour for compressed air (attributed to electricity cost), as reported by Stokes [143]. The total cost of the various gases for 63 HVOF thermal spray runs, for each coating, equals €5682.20.

Step 5: Cost of the coating materials

The weight of powder material required to spray each sample (38 x 38 mm = 1444 mm^2) with $270 \pm 10\mu m$ coating thickness and deposition efficiency of 70% (because some of the coating powders are wasted during the spraying process) is approximately 23 grams (Data obtained from Oerlikon Company). Meanwhile, the cost of 1 kg of (nano-structured) WC-12Co (Infralloy^{TM} S7412) is €149 and €93 for 1 kg of the Inconel 625 (Diamalloy 1005). Consequently, coating 1,000 samples from each coating type will cost €3,427 and €3,104 for the monomial and mixed coating respectively.

The total operation/variables approximate cost (excluding the labour cost) of spraying 1,000 samples from each coating type would therefore be €9,684 and €9,384 for the monomial and mixed coatings respectively. The spray gases, followed by the coating materials, almost form the main thermal spray costing process. However, should be noted that the optimisation of the deposition efficiency of the coating process, in terms of the waste of the coating material, will effect a significant reduction in the coating process.

Novel Enhancement of HVOF Thermal Sprayed Nanostructured WC-12Co / Inconel-625 Coatings for Tribocorrosion Applications | **Al-Harbi, Naif I**

233

5.13.2 Cost of the Laser operating process

The laser treatment operation cost of 1000 coated samples with the mentioned dimensions in the previous section, for each of the two coating materials, can be estimated as laser treatment per unit length according to Equation 5-26 [144]. The laser processing for this research work is carried out by a CO_2 laser system of 1.5 KW maximum output power and a system using static volume of laser gases of approximately 7.5 litres for every 72 hours. The operation cost for this type of laser system was reported by Havrilla et al. [145], under the categories listed in Table 5-17. The operation cost analysis used was similar to that of the HVOF coating process, did not include fixed costs such as laser system purchasing, labour costs, unscheduled breakdown and maintenance or PC hard disk replacement, while assuming 85% utilization. The "pf" for the first three cost elements in Table 5-17 represents the power factor of the AC electric power system used. Furthermore, small modifications to equation 5-26 include the change in coverage rate as a result of changing the focal position/beam size by dividing the total length of each focal position/beam size into 1 m sections.

Elements of cost	Calculations	Treatment cost (€/hr)
Laser electrical power	(20.88 kVA) (0.8 pf) (€ 0.1209/kWhr) (P/1.5)	1.346 x P
Motion controller power	(4.8 kVA) (0.8 pf) (€ 0.1209/kWhr)	0.464
Chiller electrical power	(11.52 kVA) (0.8 pf) (€ 0.1209/kWhr)	1.114
Exhaust system power	(0.9 kWhr) (€ 0.1209/ kWhr)	0.109
Laser gas LASPUR208	{(€1043.93/ bottle) / (1500 liter/bottle)}x 7.5Liter / 72 hr	0.072
Gas bottle rental	(€181.37/720 hr)	0.252
Chiller additives	(€284.80/year) / (8760 hr/year)	0.033
Argon (Shielding gas)	(5 litre/min) (60 min/h) (€12.174 x 10^{-3})	3.652
Nozzle tip	(€7.20/200 hr)	0.036
Exhaust system filters	(€5/100 hr)	0.05
Laser Focus lens	(€423/lens) / (1000 hr)	0.423
Maintenance labour (with overhead)	(12 hr/2000 hrs operation) (€50/hr)	0.30
Total operation cost per hour		6.51 + 1.346 x P €/hr

Table 5-17: Laser treatment operation cost breakdown.

Novel Enhancement of HVOF Thermal Sprayed Nanostructured WC-12Co / Inconel-625 Coatings for Tribocorrosion Applications | **Al-Harbi, Naif I**

234

$$\text{Laser processing [Euro/m]} = \frac{6.51 + 1.346 \text{ x P}}{(0.85) \times S[\text{mm/min}][60\text{min/hr}][\text{m/1000mm}]} \times \text{L(Ratio)} \quad Equation\ 5-26$$

Where;

P: The laser power used (KW), value from 0 to 1.5 KW.

S: The scanning speed (mm/min)

L(Ratio): The ratio of the change in the coverage rate as a function of changing the focal position/beam size.

5.13.3 Development of the mathematical model for laser operation cost data

The same statistical testing procedure was also performed for the laser operation cost response to optimize the laser parameters based in the cost criterion in the following section. A quadratic model was chosen to fit the data, as it showed significant models (<0.05), lack of fit not significant and the difference between predicted and adjusted R^2 being less than 0.2. In addition, a magnificent value for adequate precision (>40) can be seen in the ANOVA data in table 5-18. From the ANOVA data and the final mathematical model in terms of coded and actual factors shown in Equations 5-27 and 5-28 respectively, the results indicate that, of the three control factors in the laser processing under the selected levels, the scanning speed (C) has the highest impact in the laser processing cost as itself (-C), squared (C^2) and as an interaction in positive effect with the focal position (BC). These results agreed with those obtained by Benyounis and Hayat [86, 146]. However, the dependence for the laser operating cost from Equation 5-27 as a coded factor can be ranked as follows: $-C > C^2 > -B > BC > A > B^2 > -AC > -AB > A^2$. This shows clearly that the laser power as square (A^2) and as an interaction with scanning speed and focal position (-AC, -AB) had an insignificant impact on the laser operating process cost. Moreover, from the data determined by the DOE software, the operating cost of laser processing for 1000 samples of each coating type ranged between €567.40 and €1430.92, as per Tables (5-19 and 5-20). In conclusion, the additional cost of laser processing resulting in the worst case scenario, would be 17% of an additional cost on top of HVOF deposition.

Novel Enhancement of HVOF Thermal Sprayed Nanostructured WC-12Co / Inconel-625 Coatings for Tribocorrosion Applications | **Al-Harbi, Naif I**

235

Source	Sum of Squares	DF	Mean Square	F value	Prob > F	
Model	9.572E+05	7	1.367E+05	3363.86	< 0.0001	significant
A-Laser Power	2625.03	1	2625.03	64.58	< 0.0001	
B-Focal Position	87986.01	1	87986.01	2164.55	< 0.0001	
C-Scanning Speed	8.120E+05	1	8.120E+05	19975.01	< 0.0001	
AC	161.44	1	161.44	3.97	0.0774	
BC	5480.10	1	5480.10	134.82	< 0.0001	
B²	613.31	1	613.31	15.09	0.0037	
C²	47581.20	1	47581.20	1170.55	< 0.0001	
Residual	365.84	9	40.65			
Model	9.572E+05	7	1.367E+05	3363.86	< 0.0001	
Lack of Fit	348.00	3	116.00			
Pure Error	0.000	4	0.000			

R-Squared   **0.99**   Adj.R^2 = 0.99

Adeq. Precision = 193   Pred.R^2 = 0.99

Table 5-18: ANOVA analysis for the operating cost model of laser treatment of both coating types.

The final mathematical model determined by the DOE software for laser-treated coating operating cost in terms of coded and actual factors is given in equations 5-27 and 5-28.

Laser treating operating cost (Predicted) = +843.86 +18.11* A -104.87 * B -318.58 * C -1.98 * AB -6.35 * AC +37.01 * BC -0.71 * A² +12.09 * B² +106.19 * C² $Equation\ 5-27$

Laser treating operating cost (Actual) = +5119.40035 +0.56582 * Laser Power -80.87906 * Focal Position -16.47967 * Scanning Speed -3.96312E-003 * Laser Power * Focal Position - 8.47064E-004 * Laser Power * Scanning Speed +0.098704 * Focal Position * Scanning Speed -7.11158E-005 * Laser Power² +0.48359 * Focal Position² +0.018879 * Scanning Speed² $Equation\ 5-28$

Novel Enhancement of HVOF Thermal Sprayed Nanostructured WC-12Co / Inconel-625 Coatings for Tribocorrosion Applications | **Al-Harbi, Naif I**

236

5.14 Optimisation of Laser Process Parameters

The laser processing of the two coating types, under the selected control factors and levels, is a complex procedure, with multiple input and output properties for the different mechanical and erosion responses that are statically studied in this research. To obtain the overall optimum laser parameters, desirability approaches can be used throughout the design of the experimental software, as explained earlier in Chapter 3. The optimisation approach focuses on two different presentation/feature techniques (numerical and graphical optimisation). The numerical optimisation feature was assigned a point or a list of laser settings that yielded to the highest overall desirability for the various responses, based on their desirable criterion (i.e. the goal) and their importance ranking (out of five). The graphical optimisation feature is a form presenting the optimum laser setting for each of the responses, which are gathered from the numerical optimisation to be presented together graphically in plots, called "overlay plots", to provide a simpler understanding of the higher desirability region and to allow visual selection of the optimal laser processing conditions, according to a certain criterion.

Two criteria were used for the numerical and graphical optimisation of this research work. The difference between the two criteria is that, in the first (known as a quality criterion), no restriction applies to the mechanical and erosion responses' output quality as a result of the laser operation cost minimization . In the second, the laser operating cost is taken into consideration and its goal is set to a minimum, with the highest importance (referred to as a cost criterion).

5.14.1 Numerical optimisation

Tables 5-19 and 5-20 present the two numerical optimisation criteria for the laser-treated monomial and mixed coatings respectively. In these criteria, each factor and response has been given a specific goal and importance level. The main aim of both coating types in both criteria is to minimise the roughness, dry erosion and slurry erosion and to maximise the bending strength. The only difference between both criteria is that the target for the laser operating cost is minimised within the highest importance for the cost criterion. Therefore, the cost was set to be within a range because it conflicted with the responses for the quality criterion. Moreover, the observer should note that the upper and lower limit represent the limits of the factor levels chosen and the response values for each property obtained in this research from the laser processing, according to the DOE matrix created.

Novel Enhancement of HVOF Thermal Sprayed Nanostructured WC-12Co / Inconel-625 Coatings for Tribocorrosion Applications | **Al-Harbi, Naif I**

237

With the key goal of this research being to improve erosion wear (slurry and dry), the quality criterion has been given the highest importance, with the remaining mechanical properties assigned as secondary importance (3 out of 5) after cost, within the cost criterion.

Factor or response	Lower Limit	Upper Limit	First criterion (Quality)		Second criterion (Cost)	
			Goal	Importance	Goal	Importance
A-Laser Power (W)	150	350	Is in range	3	Is in range	3
B-Focal Position (mm)	35	45	Is in range	3	Is in range	3
C-Scanning Speed (mm/min)	150	300	Is in range	3	Is in range	3
Slurry erosion (g)	0.055	0.64	Minimize	5	Minimize	3
Dry erosion (g)	0.13	0.75	Minimize	5	Minimize	3
Bending (MPa)	580	738	Maximize	1	Maximize	1
Roughness (μm)	2.7	3.34	Minimize	1	Minimize	1
Laser Cost (Euro)	567.4	1430.92	Is in range	3	Minimize	5

Table 5-19: Criteria for numerical optimisation of laser-treated monomial nWC-12Co coating

Factor or response	Lower Limit	Upper Limit	First criterion (Quality)		Second criterion (Cost)	
			Goal	Importance	Goal	Importance
A-Laser Power (W)	150	350	Is in range	3	Is in range	3
B-Focal Position (mm)	35	45	Is in range	3	Is in range	3
C-Scanning Speed (mm/min)	150	300	Is in range	3	Is in range	3
Slurry erosion (g)	0.265	0.9	Minimize	5	Minimize	3
Dry erosion (g)	0.75	5.95	Minimize	5	Minimize	3
Bending (MPa)	570	650	Maximize	1	Maximize	1
Roughness (μm)	3.01	22.3	Minimize	1	Minimize	1
Laser Cost (Euro)	567.4	1430.92	Is in range	3	Minimize	5

Table 5-20: Criteria for numerical optimisation of laser-treated mixed coating.

Novel Enhancement of HVOF Thermal Sprayed Nanostructured WC-12Co / Inconel-625 Coatings for Tribocorrosion Applications | **Al-Harbi, Naif I**

238

Tables 5-21 and 5-22 show the overall optimal settings for the laser process parameters and their individual corresponding response value for both criteria of the monomial and mixed coating respectively. The results indicate that a more than optimal solution can be obtained, using laser processing to achieve the highest desirability value for the two criteria (for the five highest listed in the Tables). However, failure to act generally imposes a restriction on minimizing the laser operating cost (set to be within a range) in the quality criterion. The laser processing yields better values for each of the individual responses for both coating types. To the same extent, the responses most affected by imposing restrictions to minimise the laser operating cost are the slurry erosion and bending strength for the monomial nWC-12Co coating, and the slurry erosion for the mixed coating. It should be noted that A, B and C represent the laser power, focal position and scanning speed respectively. The units for each parameter are listed in Tables (5-19 and 5-20). However, a percentage reduction in the operating cost of approximately 230% and 30% could be achieved if the second criterion was implemented for the monomial and mixed coatings respectively.

	No.	A	B	C	Slurry erosion	Dry erosion	Bending	Roughness	Cost	Desirability
1st criterion (Quality)	1	350	37.24	150.00	0.04	0.13	727.70	2.70	1376	0.99
	2	350	37.11	150.00	0.03	0.12	727.10	2.69	1380	0.99
	3	350	37.15	151.01	0.04	0.13	726.50	2.71	1371	0.99
	4	350	36.26	150.02	0.02	0.06	722.60	2.65	1407	0.99
	5	350	36.07	150.00	0.03	0.05	721.40	2.64	1413	0.99
2nd criterion (Cost)	1	350	45.000	299.9	0.197	0.14	658.11	2.855	584.8	0.92
	2	349.9	44.962	300.0	0.193	0.136	658.11	2.854	585.1	0.92
	3	349.9	44.722	300.0	0.171	0.112	658.05	2.849	587.4	0.92
	4	349.9	44.646	299.9	0.164	0.105	658.02	2.848	588.1	0.92
	5	350	44.606	299.9	0.161	0.101	658.00	2.847	588.5	0.92

Table 5-21: Optimal Laser treatment conditions as obtained by Design-Expert for monomial nWC-12Co coating.

Novel Enhancement of HVOF Thermal Sprayed Nanostructured WC-12Co / Inconel-625 Coatings for Tribocorrosion Applications | **Al-Harbi, Naif I**

239

	No.	A	B	C	Slurry erosion	Dry erosion	Bending	Roughness	Cost	Desirability
1st criterion (Quality)	1	169.0	35	275.4	0.3	0.2	626.1	3.3	756.5	1
	2	168.2	35	274.9	0.3	0.2	626.1	3.3	757.8	1
	3	170.1	35	276.1	0.3	0.2	626.1	3.3	754.8	1
	4	167.2	35	274.3	0.3	0.2	626.0	3.3	759.4	1
	5	171.9	35	277.2	0.3	0.2	626.2	3.3	752.1	1
2nd criterion (Cost)	1	250	45	300	1.04	0.140	627.50	3.63	575.7	0.929
	2	250.3	45	300	1.04	0.136	627.51	3.64	575.7	0.928
	3	248.8	45	300	1.04	0.112	627.46	3.63	575.6	0.928
	4	251.8	45	300	1.05	0.105	627.56	3.64	575.9	0.928
	5	251.1	45	300	1.04	0.101	627.52	3.63	575.8	0.928

Table 5-22: Optimal Laser treatment conditions as obtained by Design-Expert for the mixed coating.

5.14.2 Graphical optimisation

As explained earlier, the range of each response has been obtained from the numerical optimisation results in the DOE software to attain the optimum results for each response as an individual in graphical form. This range can be graphical optimisation as overlay plots. The green highlighted areas in Figures 5-120 to 5-123 are the region that meet the first and second criteria for both coating types. Figures 5-120 and 5-121 are overlay plots for the laser-treated monomial and mixed coatings according to the first criterion (quality criterion), while Figures 5-122 and 5-123 are overlay plots according to the second criterion (cost criterion). These types of graphs are practical for technical use and can be given to an operator or research group as an example of a quick and simple visualisation tool for selecting the optimal laser operation condition to achieve the desired response values for each of these coating types.

Obviously, the regions identified for the first and second criteria for both coatings are completely different. Minimising the laser operating cost for the cost criterion in comparison

Novel Enhancement of HVOF Thermal Sprayed Nanostructured WC-12Co / Inconel-625 Coatings for Tribocorrosion Applications | **Al-Harbi, Naif I**

240

with the quality criterion for the monomial nWC-12Co coating (Figure 5-122 and 5-120 respectively) relies on using the highest laser scanning speed, 300 mm/min compared to 150 mm/min for the quality criterion, and increasing the coverage rate is a function of increasing the focal position/beam size. For the mixed coating, minimising the laser operating cost completely relies on increasing the coverage rate by increasing the focal position highest/beam size, as shown in Figure 5-123, in comparison to the quality criterion, which is shown in Figure 5-121.
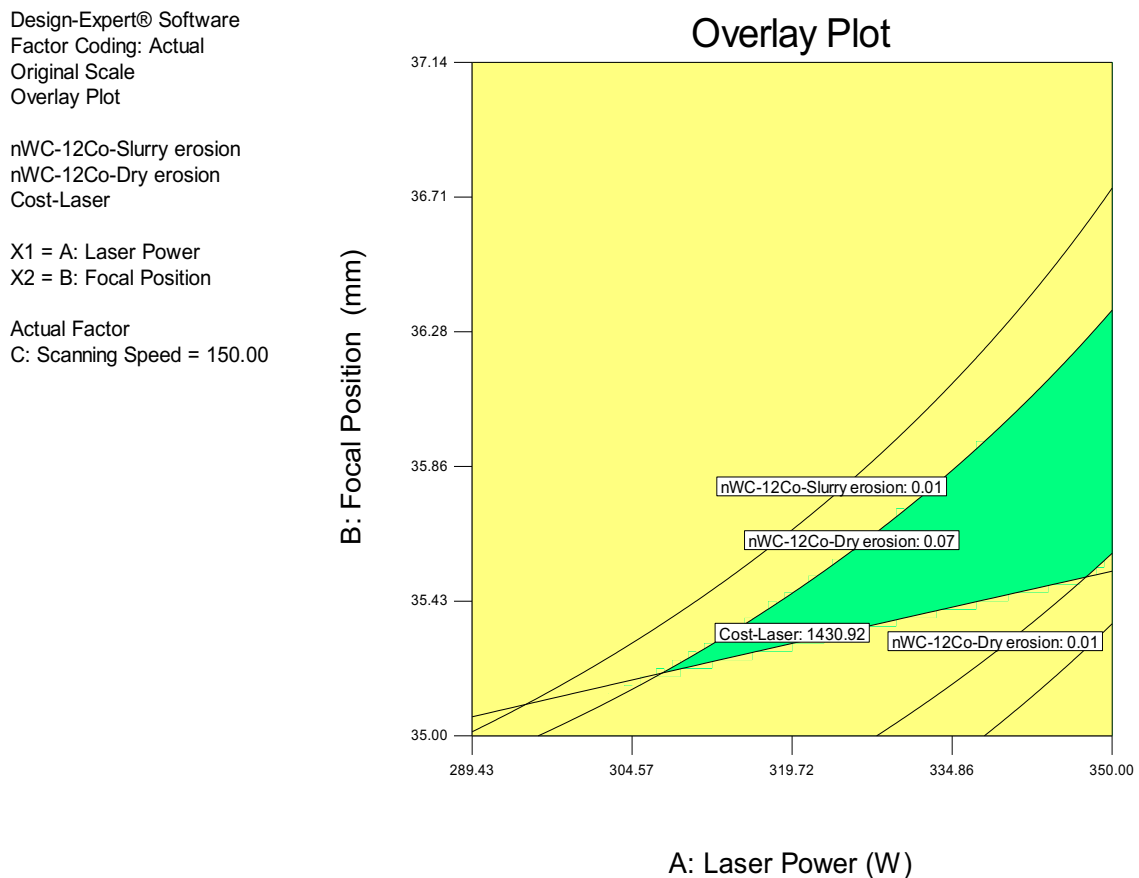
Figure 5-120: Overlay plot shows the region of optimal laser condition based on the first criterion (quality criteria) for the monomial nWC-12Co coating.

Novel Enhancement of HVOF Thermal Sprayed Nanostructured WC-12Co / Inconel-625 Coatings for Tribocorrosion Applications | **Al-Harbi, Naif I**

241

Overlay Plot

Mixed Coating - Bending: 620
Mixed Coating - Roughness: 3.9
Mixed Coating-Dry erosion: 0.32
Mixed Coating-Slurry erosion: 0.280394

B: Focal Position (mm)

A: Laser Power (W)

Figure 5-121: Overlay plot shows the region of optimal laser condition based on the first criterion (quality criteria) for the mixed coating.

Overlay Plot

nWC-12Co-Dry erosion: 0.01
nWC-12Co-Slurry erosion: 0
nWC-12Co-Dry erosion: 0.1
nWC-12Co-Slurry erosion: 0.1

B: Focal Position (mm)

A: Laser Power (W)

Figure 5-122: Overlay plot shows the region of optimal laser condition based on the second criterion (cost criteria) for the monomial nWC-12Co coating.

Novel Enhancement of HVOF Thermal Sprayed Nanostructured WC-12Co / Inconel-625 Coatings for Tribocorrosion Applications | **Al-Harbi, Naif I**

242

Design-Expert® Software
Factor Coding: Actual
Original Scale
Overlay Plot

Mixed Coating-Slurry erosion
Mixed Coating-Dry erosion
Mixed Coating - Roughness
Cost-Laser

X1 = A: Laser Power
X2 = B: Focal Position

Actual Factor
C: Scanning Speed = 300.00
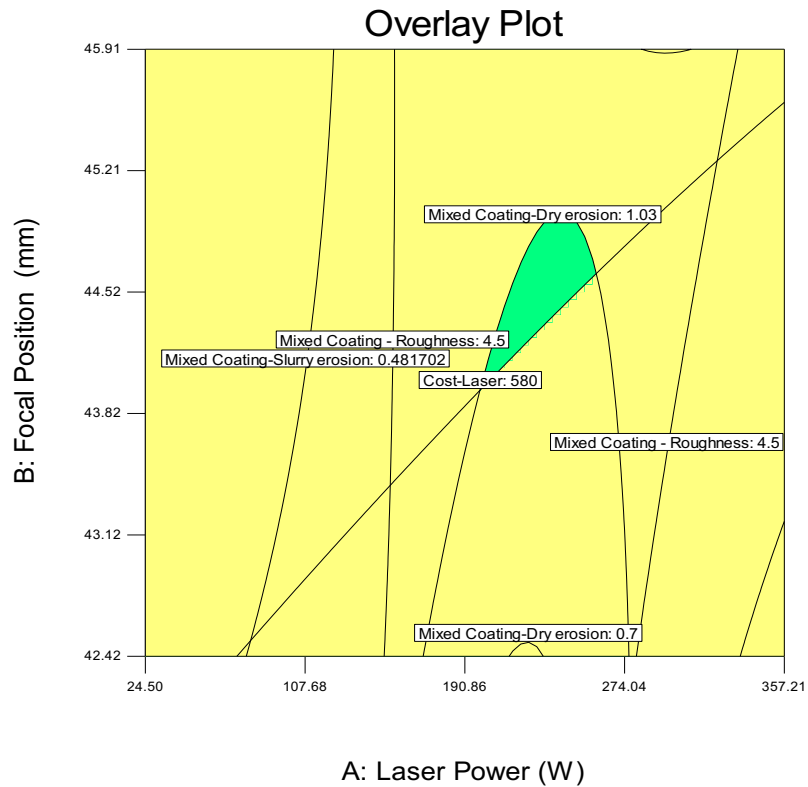
Figure 5-123: Overlay plot shows the region of optimal laser condition based on the second criterion (cost criteria) for the mixed coating.coating.

5.14.3 Practicality of the Research

The basis for this cost analysis to only evident if it is possible to coat flat/curved or internal components and to post laser treat them. For HVOF flat/curved and internal components are possible either directly using the HVOF or using an additional lence (Figure 5-124 (a)).

Similarly, laser treatment can be achieved either using a laser directly or via the use of mirrors (Figure 5-124 (b)). So the life of the components in Figure 2-5 can all be extended through the research.

Novel Enhancement of HVOF Thermal Sprayed Nanostructured WC-12Co / Inconel-625 Coatings for Tribocorrosion Applications | **Al-Harbi, Naif I**

243
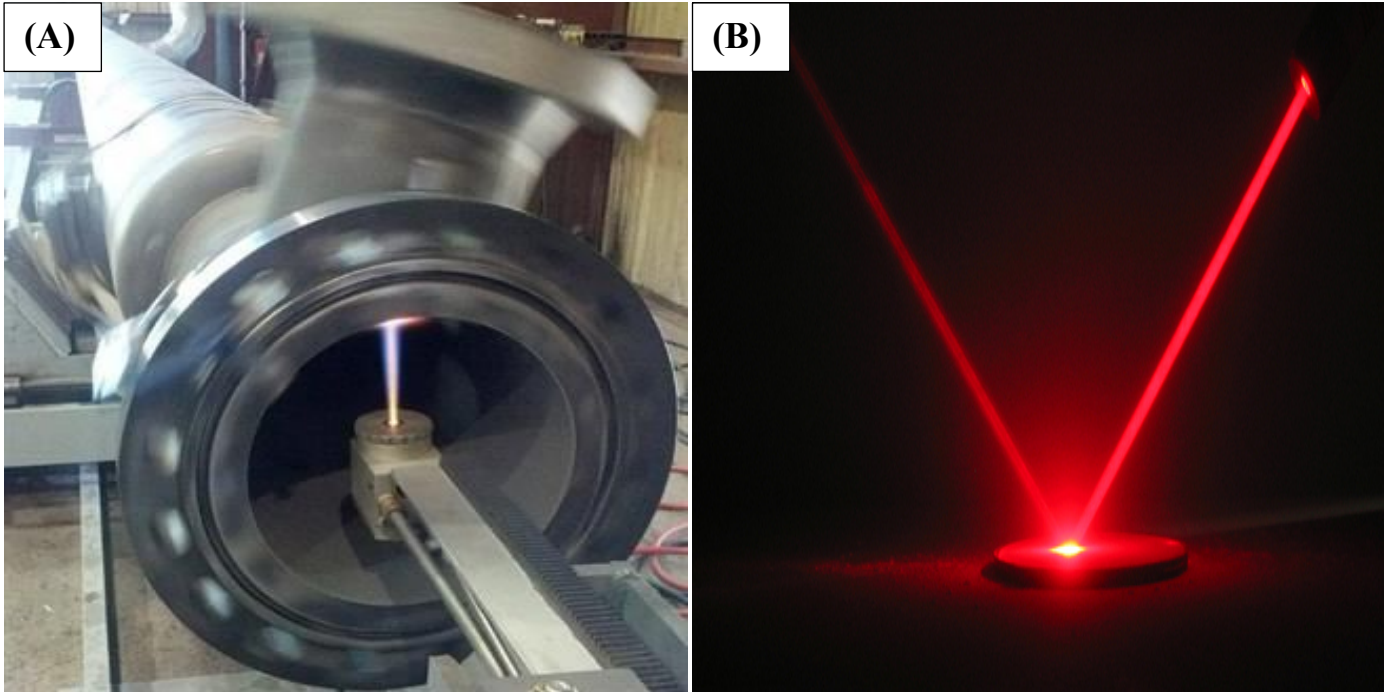
Figure 5-124: Examples shown the feasibility of treating curve components ; (A) HVOF coated for internal pipe region ,and (B) Laser reflection lens mirror [147, 148].

Novel Enhancement of HVOF Thermal Sprayed Nanostructured WC-12Co / Inconel-625 Coatings for Tribocorrosion Applications | **Al-Harbi, Naif I**

244

CHAPTER 6 - Conclusion and Recommendation for Future Work

6.1 Conclusion

The aim of this study was to improve the erosion and corrosion wear resistance and mechanical properties of HVOF thermal-sprayed coatings applied to AISI 4140 carbon steel substrate surfaces, post treated using a 1.5 kW CO_2 Rofin laser. This involved comparing the performance of the laser treated samples obtained to that of the as-sprayed components. The investigation was carried out on two different coating types: 100% tungsten carbide cobalt (nanostructured) WC-12Co (Infralloy™ S7412) and WC-12Co nanostructured powder mixed with a nickel chromium alloy (Diamalloy 1005-Inconel 625) at optimised weight percentage compositions of 75% and 25% respectively.

The researcher sought first to investigate the effects of laser processing conditions before identifying the optimal laser for the two coating materials—defined as those yielding enhanced erosion wear (dry and slurry erosion) and mechanical properties (hardness, bendability and surface roughness) through the design of experiment technique (DOE) via a Box-Behnken design featuring three levels (3^n) for three choice control factors and levels: laser power (150, 250 and 350 W), scanning speed (150, 225 and 300 mm/min) and focal point position/beam size (+35, +40 and +45 mm). This excluded the experimental data for the micro-hardening properties, which had not been statically analysed because they were only measured to link their values to the different properties evaluated in the research. The results indicated the possibility of improving the erosive wear and mechanical properties through proper selection of laser processing parameters. The outcomes of the work are summarised and presented in comparison to the objectives described in Section 1.2 as follows:

- From the results obtained for the operation windows created for both coatings to select the similar control factor levels and the melt-pool geometry DOE static analyses, one could clearly see that the melt pool dimensions (track width and depth D_m/t_c) increased with enhanced energy density (power/area). This was due to either increasing the power or reducing the beam size as a function of lowering the focal position, as well as with lengthening the beam resident time within the target surface as a result of reducing the scanning speed. In this case, the laser power was found to be the dominant factor for both

Novel Enhancement of HVOF Thermal Sprayed Nanostructured WC-12Co / Inconel-625 Coatings for Tribocorrosion Applications | **Al-Harbi, Naif I**

245

coatings in changing the melt-pool dimensions. Moreover, the changing ratio in the melt pool dimensions was found to be greater for the mixed coating in comparison to the monomial nWC-12Co coating response, for which the reason, as reported in two research studies [24, 47], can be attributed to the rise in the thermal conductivity with increasing WC concentration.

- The surface and cross-section views of the as-sprayed two coating types (monomial nWC-12Co and mixed) showed some unmelted particles with a high porosity level, micro-separation (porous strips) along the coating/substrate interface, micro-cracks and inhomogeneous distribution of the coating elements in the coating layer. However, in general, the monomial coating performed better, because of the lower amount of defects noted and the higher ratio of nano-scale hard phase carbide in the starting powder. After laser processing under different settings according to the DOE matrix (see Table 3–6), the surface and cross section of both coatings became denser and more homogeneous for several laser settings, with excellent sealing due to the melting of the unmelted particles in the as-sprayed coating layer. However, the improvement was greater for the monomial coating because the coating surface became rough and gas pockets started forming under a particular laser setting for the mixed coating, which was not the case for the monomial coating, where the size and magnitude of the gas pockets increased almost linearly with the increasing energy input.

- Prior to the laser processing, the average surface roughness was approximately 5.58 μm and 5.24 μm for the monomial and mixed coating respectively. After laser treatment, as a result of melting the coating top surface, the surface roughness reduced significantly to almost 100% for the monomial coating when treated by P.S.9 and P.S.8 (see Table 3–6) and approximately 55%, as was the case for P.S.1 and P.S.12 for the mixed coating. Furthermore, the surface roughness for the monomial nWC-12Co HVOF subjected to all of the laser settings reduced in comparison to its untreated counterpart, whereas this was not the case in the laser setting that yielded to a high energy input for the mixed coating because the surface became rough to an even greater extent than was measured for the untreated one. This may be attributed to a higher ratio of metallic binder matrices in the mixed coating, which could have caused the metallic binders to become unstable during the laser processing (the laser settings providing high-energy input). Moreover, apart from

Novel Enhancement of HVOF Thermal Sprayed Nanostructured WC-12Co / Inconel-625 Coatings for Tribocorrosion Applications | **Al-Harbi, Naif I**

246

the extent of the energy input effects, the larger the beam focus (a larger laser beam) the lower the surface roughness, as a result of reducing the number of laser tracks over the coating surface [121].

- A significant improvement was noted in the hardness after the laser treatment for a number of laser settings for both coatings as a result of eliminating a number of defects within the HVOF as-sprayed coatings, such as micro-cracks and porosity, as well as an improvement of the coating elements' homogeneity along both coating type cross-sections, especially the nano-scale WC hard particles.

- Notable an improvement was seen in the elastic limit for the two types of coating after laser treatment (under various settings). This can be attributed to the elimination of a number of coating microstructure defects that act as crack initiation (microcracks, voids, pore strips at the coating/substrate interface and so on) during the bending process and the improvement of the coating's microhardness. The P.S.6 laser setting for the monomial nWC-Co coating provided 738 MPa flexural strength in comparison to 622 MPa for the untreated type. Meanwhile, for the mixed coating, the improvement was limited by gas pocket formation, which notably acted as a crack initiator and had an inverse relationship with the bending strength response. However, the P.S.10 setting provided the highest elastic limit for the mixed coating and yielded additional 49 MPa flexural strength/elastic limit in comparison to the untreated mixed coating.

- An improvement in the dry and slurry erosion was considered to be the main objective of this research. A remarkable improvement in dry and slurry mass losses was noted for the laser-treated monomial nWC-12Co HVOF coating, reaching approximately a five- to six-fold reduction in mass, as was the case for P.S.9 and P.S.2 for the dry and slurry erosion respectively. For the mixed coating, the reduction improvement ratio was far lower than was observed in the laser-treated monomial coating. However, the P.S.7 laser setting for the dry erosion and P.S.10 for the slurry erosion yielded the lowest mass losses for the laser-treated mixed coating, with a reduction of 50–70% in mass losses compared to the untreated one. This can be attributed to a number of reasons, including the reduction in surface roughness and the improvement of the microhardness and homogeneity of the coating elements in the coating outer region.

Novel Enhancement of HVOF Thermal Sprayed Nanostructured WC-12Co / Inconel-625 Coatings for Tribocorrosion Applications | **Al-Harbi, Naif I**

247

- The laser parameters optimisation was carried out through the desirability approach in the design of the experimental software. Two criteria were used: the first (known as a quality criterion) where no restriction was applied to the mechanical and erosion responses' output quality. The second criterion was that the laser operating cost was taken into consideration and its goal was set to a minimum. The results indicate that an optimal solution could be obtained, and a number of laser settings (based on the overlay plot) showed a better predicted improvement to both the coating's mechanical and erosion properties than what was found in the research. For example, a number of laser settings provided an optimal monomial nWC-12Co coating (according to the quality criteria) in terms of dry and slurry erosion resistance with mass losses reductions of 0.02 and 0.06 g for the dry and slurry erosion respectively. This can be compared to the lowest values obtained under the laser setting created in the DOE matrix in this research work, which were 0.055 and 0.13 g respectively. Similarly, the dry erosion of the mixed coating, optimal laser settings provided a coating which only attained a mass loss of 0.2 g in comparison to 0.75 g for other settings used.

- Based on optimisation obtained, the mass loss reduction for both laser treated coatings under the predicted optimal condition, can demonstrate that the laser process is an efficient and economical process. As calculated earlier, under the selected levels and factors, an additional cost will not exceed 17% as compared to HVOF deposition.

6.2 Main Contributions from this Work

- The novelty of this research, in terms of a PhD study, is firstly attributed to the acquisition of detailed knowledge of the laser processing conditions' effects on these two coating materials, which had not been extensively studied previously.

- The design of experiment (DOE) software was used to analyse the experimental date and then provide the optimal laser processing conditions, according to a set of research objectives, particularly erosion and erosion/corrosion. This is an extremely novel approach, which has not been applied to post treated laser -coated products to date. This would bring about an opportunity to reduce the cost of scheduling maintenance plans, which are used to account for operational costs in the oil and gas industry. As an example,

Novel Enhancement of HVOF Thermal Sprayed Nanostructured WC-12Co / Inconel-625 Coatings for Tribocorrosion Applications | **Al-Harbi, Naif I**

248

most of the firms in this industry schedule their maintenance plans for thousands of miles of their pipelines by carrying out testing and inspection in a particular time period. Thus, any alteration characterized by extending this period will result in a significant increase in the net profit margin for the company. In addition, punitive damages and other legal penalties may be avoided where environmental contamination is present as a result of a wear- and corrosion-induced leak in an oil pipe. This could be effected by providing high-quality coating that would increase the MTBF (mean time between failures). A low MTBF indicates low service life and high repair costs and, eventually, high replacement costs, which will be expensed in the firm's account books. Increasing the mean time to repair will increase the time between one repair cycle and the next and will save the company billions of dollars in labour costs, new coating or parts replacement, loss of revenue because of disruption to the supply (unplanned shutdown), and loss of reliability.

- Finally, the evaluation of the total operation/variables cost (excluding the labour cost) of the HVOF spraying and laser processing of 1,000 samples for each coating type was determined. This is significant, as this determines the cost effectiveness of adding an additional processing technique (the laser process), to as-sprayed coatings, in order to further enhance their functionality. Research studies generally suggest alternative techniques or operating parameters in order to enhance such coatings used in Surface Engineering, without identifying their cost benefit.

6.3 Recommendation for Future Work

Despite the significant results that were obtained in this research, further recommendations can be suggested for any future work as follows:

• HVOF Coating

Future work could include reducing the ratio of the Inconel 625 (Ni-Cr-based alloy) mixture to the WC-12Co nanostructured powder to be less than 25%, as in the case of the mixed coating type, or using nanosized WC/metallic monomial coating within either a different WC grain size or a different cobalt metallic ratio and metallic materials (e.g. WC-15Co, WC-8Co and WC-CoCr) [42]. Such coatings could be compared to the results obtained in this research. Furthermore, as the heat treatment will be applied to the coating, the HVOF coating spray

Novel Enhancement of HVOF Thermal Sprayed Nanostructured WC-12Co / Inconel-625 Coatings for Tribocorrosion Applications | **Al-Harbi, Naif I**

249

parameters must be optimised, to ensure a high deposition efficiency in order to lower the overall HVOF coating process cost

• Laser Processing

Different laser systems (e.g. Diode, Yag and so on) or laser beam profiles (e.g. Diamond, Rectangular, Square beam geometry and so on) could be used to treat the coating layer [72], and the results could then be compared to what was achieved in the current study under a CO_2 laser system and elliptical beam geometry.

• Investigation

Further investigation can be carried out to evaluate the two coating types' properties pre and post laser treatment under various testing and conditions that were not covered in this research, such as corrosion properties, wear (adhesive, fretting and abrasive wear), various mechanical properties (tensile, fatigue and so on) and the modification in the residual stress levels in the coating as a function of the laser processing condition. This would expand its application to other areas other than oil and gas industries.

Novel Enhancement of HVOF Thermal Sprayed Nanostructured WC-12Co / Inconel-625 Coatings for Tribocorrosion Applications | **Al-Harbi, Naif I**

250

References

[1] Bartosik, M., Daniel, R., Zhang, Z., 2012, "Lateral Gradients of Phases, Residual Stress and Hardness in a Laser Heated Ti 0.52 Al 0.48 N Coating on Hard Metal," Surface and Coatings Technology, 206 (22) pp. 4502-4510.

[2] Bambha, R. P., Dansson, M. A., Schrader, P. E., 2013, "Effects of Volatile Coatings and Coating Removal Mechanisms on the Morphology of Graphitic Soot," Carbon, 61pp. 80-96.

[3] Tems, R., and Al-Zahrani, A., 2006, "Cost of Corrosion in Oil Production and Refining," Saudi Aramco Journal of Technology, pp. 2-14.

[4] WSJ News Graphics, (http://graphics.wsj.com/oil-barrel-breakdown/), 2018, "Barral Breakdown," (Access date 15/05/2018).

[5] OPEC, The Product Market Outlook Ahead of Winter, Monthly Oil Market Report, (https://www.opec.org/opec_web/static_files_project/media/downloads/publications /MOMR%20October%202016.pdf), 2016, (Access date 10/10/2018).

[6] Bach, F., Möhwald, K., Laarmann, A., 2006, "Modern surface technology," John Wiley & Sons, Germany, pp. 346.

[7] Rao, K., Somrvill, D., and Lee, D., 1986, "Properties and Characterization of Coatings made using «Jet-Cote» Thermal Spraying Technique," Adv.in Thermal Spraying: Proc.of the ITSC, 86 pp. 873-882.

[8] Tan, J. C., Optimisation of the HVOF Thermal Spray Process for Coating, Forming and Repair of Components, PhD Thesis, Dublin City University, Ireland. (1997; (http://doras.dcu.ie/16638/),.

[9] Oksa, M., Turunen, E., Suhonen, T., 2011, "Optimization and Characterization of High Velocity Oxy-Fuel Sprayed Coatings: Techniques, Materials, and Applications," Coatings, 1(1) pp. 17-52.

[10] Liu, Y., Fischer, T. E., and Dent, A., 2003, "Comparison of HVOF and Plasma-Sprayed Alumina/Titania Coatings— microstructure, Mechanical Properties and Abrasion Behavior," Surface and Coatings Technology, 167(1) pp. 6876.

[11] Yao, Z., Stiglich, J. J., and Sudarshan, T., 1999, "Nano-Grained Tungsten Carbide-Cobalt (WC/Co)," Materials Modification, pp. 1-27.

[12] Stokes, J., 2008, "The Theory and Application of the Sulzer Metco HVOF Thermal Spray Process, ISBN-1-87232753-2," Dublin City University, Ireland, pp. 3-134.

[13] Jafari, M., Enayati, M., Salehi, M., 2013, "Comparison between Oxidation Kinetics of HVOF Sprayed WC–12Co and WC–10Co–4Cr Coatings," International Journal of Refractory Metals and Hard Materials, 41pp. 78-84.

[14] METCO / Perkin Elmer, 1989, "Diamond Jet Process Manual,".

[15] Cho, J., Hwang, S., and Kim, K., 2006, "Corrosion Behavior of Thermal Sprayed WC Cermet Coatings having various Metallic Binders in Strong Acidic Environment," Surface and Coatings Technology, 200(8) pp. 2653-2662.

Novel Enhancement of HVOF Thermal Sprayed Nanostructured WC-12Co / Inconel-625 Coatings for Tribocorrosion Applications | **Al-Harbi, Naif I**

251

[16] Perry, J. M., Hodgkiess, T., and Neville, A., 2002, "A Comparison of the Corrosion Behavior of WC-Co-Cr and WC-Co HVOF Thermally Sprayed Coatings by in Situ Atomic Force Microscopy (AFM)," Journal of Thermal Spray Technology, 11(4) pp. 536-541.

[17] Al Hamed, A. Investigation of HVOF thermal sprayed micro/nanostructured WC-12Co mixed with inconel-625 nickel/chrome based coatings for erosion/corrosion applications, PhD Thesis. Dublin City University, Ireland. (2015; (http://doras.dcu.ie/20823/)),.

[18] Steen, W.M., 1991, "Laser Material Processing,"Springer, pp. 172-219.

[19] Poza, P., Múnez, C., Garrido-Maneiro, M., 2014, "Mechanical Properties of Inconel 625 Cold-Sprayed Coatings After Laser Remelting. Depth Sensing Indentation Analysis," Surface and Coatings Technology, 243pp. 51-57.

 [20] Yilbas, B., and Akhtar, S., 2012, "Laser Re-Melting of HVOF Coating with WC Blend: Thermal Stress Analysis," Journal of Materials Processing Technology, 212(12) pp. 2569-2577.

[21] Al-Taha, Z. Y., Investigation into Laser Re-Melting of Inconel 625 HVOF Coating Blended with WC, PhD Thesis, Dublin City University, Ireland., (2009; (http://doras.dcu.ie/2379/)), .

[22] Tems, R., and Al-Zahrani, A., 2006, "Cost of Corrosion in Oil Production and Refining," Saudi Aramco Journal of Technology, pp. 2-14.

[23] Al-Mutairi, S. A., Durability of Multi Layered Plasma and HVOF Coatings, PhD Thesis. Dublin City University, Ireland. (2013; (http://doras.dcu.ie/17715/)),.

[24] Chen, H., Xu, C., Zhou, Q., 2005, "Micro-Scale Abrasive Wear Behaviour of HVOF Sprayed and Laser-Remelted Conventional and Nanostructured WC–Co Coatings," Wear, 258(1) pp. 333-338.

[25] Haefer, R., 1987, "Surface and Thin Film Technology: Part I, Surface Coatings, "Springer, Heidelberg, Berlin, New York, London, Paris, Tokyo, Chap. 1.

 [26] Rakhes, M.M., Laser Surface Modification of HVOF Coatings for Improvement of Corrosion and Wear Performance. PhD Thesis. University of Manchester, UK. (2013, (https://www.escholar.manchester.ac.uk/uk-ac-man-scw:192267)),.

[27] Williams, J., 2005, "Engineering Tribology," Cambridge University Press, pp. 510.

[28] Ukpai, J., Erosion-Corrosion Characterisation for Pipeline Materials using Combined Acoustic Emission and Electrochemical Monitorin, PhD Thesis. University of Leeds, UK. (2014, (http://etheses.whiterose.ac.uk/7328/)),.

[29] Hailing, J., 1985, "Introduction: Recent Developments in Surface Coating and Modification Processes," MEP, London.

[30] Bhushan, B., and Gupta, B. K., 1991, "Handbook of Tribology: Materials, Coatings, and Surface Treatments," McGraw Hill, New York.

[31] Wank, A., 2006. "Basics of Thermal Spray Technology" GTV Verschleiss-Schutz GmbH, Luckenbach, Germany.

Novel Enhancement of HVOF Thermal Sprayed Nanostructured WC-12Co / Inconel-625 Coatings for Tribocorrosion Applications | **Al-Harbi, Naif I**

252

[32] Flame Spray Technology, "Thermal Spray Technology," (http://www.fst.nl/), 2016, (Access date 12/10/2018) pp. 15.

[33] Thermal Spray Technology,"Thermal Spray Society," (http://www.asminternational.org/documents/17679604/17683439/white+paper.pdf/fba0eade-d6db-4921-b42f-668965d7c70a), 2016 (Access date 12/09/2018) pp.9.

[34] Singh, H., Sidhu, T.S. and Kalsi, S.B.S., 2012. "Cold spray technology: future of coating deposition processes" Frattura ed Integrità Strutturale, (22), p.69.

[35] Fauchais, P., and Vardelle, A., 2012, "Thermal sprayed coatings used against corrosion and corrosive wear," Advanced plasma spray applications, In Tech .France.

[36] Zhengui, Y., Stiglich, J., and Sudarshan, T., 1998, "Nano-Grained Tungsten Carbide Cobalt (WC/Co)," Materials Modification, Inc, 2929.

[37] Sarin, V. K., 1981, "Cemented Carbide Cutting Tools," Advances in Powder Technology, pp. 253-288.

[38] Davidge R.W., 1979, "Mechanical Behaviour of Ceramics", Cambridge Univ. Press, ISBN 0-5212-1915-9.

[39] Kingery, W. D., M. K. Bowen, and D. R. Uhlmann, 1967, "Introduction to Ceramics", Wiley and Sons Publ. ISBN 0-4714-7860-1.

[40] Bernecki T.F., 1991, "Thermal Spray Coatings: Properties, Processes and Applications", Pittsburgh, USA, May 4-10.

[41] Ogwu, A., and Davies, T., 1993, "Electronic Structure Basis for Selection of Metal Binders for Hardmetal Systems," Materials Science and Technology, 9(3) pp. 213-217.

[42] N. Al Harbi, K. Y. Benyounis, L. Looney, J. Stokes, " Synthesis and Properties of Nanostructured cermet coatings, " Reference Module in Materials Science and Materials Engineering, Elsevier Ltd, 2018.

[43] Kumari, K., Anand, K., Bellacci, M., 2010, "Effect of Microstructure on Abrasive Wear Behavior of Thermally Sprayed WC–10Co–4Cr Coatings," Wear, **268**(11-12) pp. 1309-1319.

[44] Al-Hamed, A., Al-Fadhli, H., Al-Mutairi, S., 2013, "Investigation of HVOF Thermal Sprayed Nanostructured WC-12Co Mixed with Inconel-625 Coatings for Oil/Gas Applications," WIT Transactions on Engineering Sciences, **78**pp. 215-225.

[45] Gérard, B., 2006, "Application of Thermal Spraying in the Automobile Industry," Surface and Coatings Technology, **201**(5) pp. 2028-2031.

[46] Moskowitz, L., 1993, "Application of HVOF Thermal Spraying to Solve Corrosion Problems in the Petroleum Industry—an Industrial Note," Journal of Thermal Spray Technology, **2**(1) pp. 21-29.

Novel Enhancement of HVOF Thermal Sprayed Nanostructured WC-12Co / Inconel-625 Coatings for Tribocorrosion Applications | **Al-Harbi, Naif I**

253

[47] Sidhu, T., Prakash, S., and Agrawal, R., 2006, "Hot Corrosion Studies of HVOF NiCrBSi and Stellite-6 Coatings on a Ni-Based Superalloy in an Actual Industrial Environment of a Coal Fired Boiler," Surface and Coatings Technology, **201**(3-4) pp. 1602-1612.

[48] Hidalgo, V. H., Varela, F. B., Menéndez, A. C., 2001, "A Comparative Study of High-Temperature Erosion Wear of Plasma-Sprayed NiCrBSiFe and WC–NiCrBSiFe Coatings Under Simulated Coal-Fired Boiler Conditions," Tribology International, **34**(3) pp. 161-169.

[49] Reyes, M., and Neville, A., 2003, "Degradation Mechanisms of Co-Based Alloy and WC Metal–matrix Composites for Drilling Tools Offshore," Wear, **255**(7-12) pp. 1143-1156.

[50] Al-Hamed, A., Al-Fadhli, H., Al-Mutairi, J. Stokes., 2013, "Investigation of HVOF Thermal Sprayed Nanostructured WC-12Co Mixed with Inconel-625 Coatings for Oil/Gas Applications," WIT Transactions on Engineering Sciences, **78**pp. 215-225.

[51] W. M. Steen, 2003, "Laser Material Processing," Springer Science & Business Media, London, pp. 407.

[52] Kou, S., 2003, "Welding metallurgy," John Wiley & Sons, New Jeresy, pp. 480.

[53] Frenk, A., and Kurz, W., 1993, "High Speed Laser Cladding: Solidification Conditions and Microstructure of a Cobalt-Based Alloy," Materials Science and Engineering: A, 173(1-2) pp. 339-342.

[54] Liu, Z., Cabrero, J., Niang, S., 2007, "Improving Corrosion and Wear Performance of HVOF-Sprayed Inconel 625 and WC-Inconel 625 Coatings by High Power Diode Laser Treatments," Surface and Coatings Technology, 201(16) pp. 7149-7158.

[55] Kumari, S., Khanna, A. S., and Gasser, A., 2006, "The influence of laser glazing on morphology, composition and microhardness of thermal sprayed Ni-WC coatings," 4th International Surface Engineering Congress and Exhibition, Minnesota, August 2005, Proceedings, pp. 128 – 135.

[56] Zhang, S., Cho, T., Yoon, J., 2008, "Characterization of Microstructure and Surface Properties of Hybrid Coatings of WC–CoCr Prepared by Laser Heat Treatment and High Velocity Oxygen Fuel Spraying," Materials Characterization, 59(10) pp. 1412-1418.

[57] Wu, P., Zhou, C., and Tang, X., 2003, "Microstructural Characterization and Wear Behaviour of Laser Cladded Nickel-Based and Tungsten Carbide Composite Coatings," Surface and Coatings Technology, 166(1) pp. 84-88.

[58] Yilbas, B., Toor, I., Patel, F., 2013, "Effects of Laser Re-Melting on the Corrosion Properties of HVOF Coatings," Journal of Materials Engineering and Performance, 22(5) pp. 1505-1511.

[59] Tuominen, J., Vuoristo, P., Mäntylä, T., 2000, "Improving Corrosion Properties of High-Velocity Oxy-Fuel Sprayed Inconel 625 by using a High-Power Continuous Wave Neodymium-Doped Yttrium Aluminum Garnet Laser," Journal of Thermal Spray Technology, 9(4) pp. 513-519.

[60] Triantafyllidis, D., Li, L., and Stott, F., 2006, "Crack-Free Densification of Ceramics by Laser Surface Treatment," Surface and Coatings Technology, 201(6) pp. 3163-3173.

Novel Enhancement of HVOF Thermal Sprayed Nanostructured WC-12Co / Inconel-625 Coatings for Tribocorrosion Applications | **Al-Harbi, Naif I**

254

[61] Ahmed, N., Voisey, K., and McCartney, D., 2010, "Investigation into the Effect of Beam Shape on Melt Pool Characteristics using Analytical Modelling," Optics and Lasers in Engineering, 48(5) pp. 548-554.

[62] Safdar, S., Li, L., and Sheikh, M., 2007, "Numerical Analysis of the Effects of Non-Conventional Laser Beam Geometries during Laser Melting of Metallic Materials," Journal of Physics D: Applied Physics, 40(2) pp. 593.

[63]] Safdar, S., Li, L., Sheikh, M., 2006, "An Analysis of the Effect of Laser Beam Geometry on Laser Transformation Hardening," Journal of Manufacturing Science and Engineering, 128(3) pp. 659-667.

[64] Triantafyllidis, D., Li, L., and Stott, F., 2006, "Investigation of the Effects of Nonconventional Beam Geometries in Laser Surface Treatment of Ceramics: Experimental Analysis," Journal of Laser Applications, 18(3) pp. 267-274.

[65] Sheikh, M., and Li, L., 2010, "Understanding the Effect of Nonconventional Laser Beam Geometry on Material Processing by Finite Element Modelling," Proceedings of the Institution of Mechanical Engineers, Part C: Journal of Mechanical Engineering Science, 224(5) pp. 1061-1072.

[66] Kock, D., 2001, "Lasers Offer Unique Heat Treating Capabilities," Available from; ndustrial Heating(USA), **68**(10) pp. 75-78.

[67] Safdar, S., Li, L., and Sheikh, M., 2004, "Modelling the effects of laser beam geometry on laser surface treatment of metallic materials," Proceedings of the 34th International MATADOR Conference, Springer, pp. 273-280.

[68] Triantafyllidis, D., Li, L., and Stott, F., 2002, "Surface Treatment of Alumina-Based Ceramics using Combined Laser Sources," Applied Surface Science, 186(1) pp. 140-144.

[69] Safdar, S., Li, L., Sheikh, M., 2006, "Thermal History Analysis of Surface Heating of Mild Steel with Different Laser Beam Geometries," Proceedings of the Institution of Mechanical Engineers, Part C: Journal of Mechanical Engineering Science, 220(10) pp. 1549-1557.

[70] Triantafyllidis, D., Li, L., and Stott, F., 2006, "Investigation of the Effects of Nonconventional Beam Geometries in Laser Surface Treatment of Ceramics: Theoretical Analysis," Journal of Laser Applications, 18(2) pp. 161-168.

[71] Triantafyllidis, D., Li, L., and Stott, F., 2006, "Investigation of the Effects of Nonconventional Beam Geometries in Laser Surface Treatment of Ceramics: Experimental Analysis," Journal of Laser Applications, 18(3) pp. 267-274.

[72] N. Al Harbi, K. Y. Benyounis, L. Looney, J. Stokes, "Laser Surface Modification of Ceramic Materials, " Reference Module in Materials Science and Materials Engineering, Elsevier Ltd, 2018.

[73] Inframat Corporation, "Sprayable SuperfineTechnicalTungsten Carbide Cobalt – Infralloy™ Thermal Spray Information Powder S7412," (http://www.inframat.com/tech_information/infralloys7412_ti.pdf), (Access date 12/11/2018) pp. 1-2.

[74] Inframat Corporation, "Thermal Spray of Superfine Wc/Co Feedstocks with Improved Coating Properties," (http://www.inframat.com/tcc.htm#), (Access date 12/11/2018) pp. 1.

Novel Enhancement of HVOF Thermal Sprayed Nanostructured WC-12Co / Inconel-625 Coatings for Tribocorrosion Applications | **Al-Harbi, Naif I**

255

[75] Oerlikon Metco, "Nickel-Chromium Superalloy Thermal Spray Powders," (https://www.oerlikon.com/metco/en/products-services/coating-materials/coating-materials-thermal-spray/carbides/), (Access date 28/5/2018) pp. 1-5.

[76] Atarés, L., Depypere, F., Pieters, J., 2012, "Coating Quality as Affected by Core Particle Segregation in Fluidized Bed Processing," Journal of Food Engineering, 113(3) pp. 415-421.

[77] Bauman, I., Ćurić, D., and Boban, M., 2008, "Mixing of Solids in Different Mixing Devices," Sadhana, 33(6) pp. 721-731.

[78] Oerlikon Metco , "MultiCoat High Performance Thermal Spray Controller", Product Data Sheet. (https://www.oerlikon.com/metco/en/products-services/coating-equipment/thermal-spray/systems/hvof/hvof-multicoat/), (Access date 21/5/2018) pp. 1-8.

[79] Oerlikon Metco, "Thermal spray equipment guide", Product Data Sheet. (https://www.oerlikon.com/metco/en/products-services/coating-equipment/thermal-spray/systems/hvof/hvof-multicoat/), (Access date 22/5/2018) pp. 1-40.

[80] Oerlikon Metco, "Metco 9MP Series Thermal Spray Powder Feeders", Product Data Sheet. (https://www.oerlikon.com/metco/en/products-services/coating-equipment/thermal-spray/feeders/feeders-hvof/hvof-9mp/), (Access date 25/5/2018) pp. 1-8.

[81] Oerlikon Metco, "Diamond Jet Gas fuel HVOF Spray Guns", Product Data Sheet. (https://www.oerlikon.com/metco/en/products-services/coating-equipment/thermal-spray/spray-guns/spray-guns-hvof/hvof-diamond-jet/), (Access date 2/6/2018) pp. 1-4.

[82] Oerlikon Metco, "Diamond Jet DJC Series Semi-Automatic HVOF Controller", Product Data Sheet. (https://www.oerlikon.com/metco/en/products-services/coating-equipment/thermal-spray/systems/hvof/diamond-jet/), (Access date 17/6/2018) pp. 1-4.

[83] Oerlikon Metco, 2015,"The HVOF-GF Process and the influences of their spray parameters on coatings", Oerlikon Metco process manual.

[84] Liu, X., Du, D. and Mourou, G., 1997, "Laser ablation and micromachining with ultrashort laser pulses", IEEE J.Quant.Electron., Vol.33 (10), pp. 1706-1716.

[85] Ben Azouz, A., Microfluidic device prototyping via laser processing of glass and polymer materials, PhD Thesis. Dublin City University, Ireland. (2014; (http://doras.dcu.ie/19697/)),.

[86] Benyounis, K., Prediction and optimization of residual stresses, weld-bead profile and mechanical properties of laser welded components, PhD Thesis. Dublin City University, Ireland. (2006; (http://doras.dcu.ie/16941/)),.

[87] Box, G. E., and Behnken, D. W., 1960, "Some New Three Level Designs for the Study of Quantitative Variables," Technometrics, **2**(4) pp. 455-475.

[88] Anderson, M.J., and Whitcomb, P.J., 2016, "RSM simplified: optimizing processes using response surface methods for design of experiments," Productivity press, .

Novel Enhancement of HVOF Thermal Sprayed Nanostructured WC-12Co / Inconel-625 Coatings for Tribocorrosion Applications | **Al-Harbi, Naif I**

256

[89] Radiological and Environmental Management, "Scanning Electron Microscopic," (http://www.purdue.edu/rem/rs/sem.htm), (Access date 2/07/2018).

[90] Gatan, "EDS/EDX Techniques," http://www.gatan.com/techniques/edsedx), (Access date 4/07/2018).

[91] Zwick, "Instruction Manual for Material Testing Machine," https://www.zwick.com/composites/tensile-test-compression-test-flexure-test/flexure-tests, (Access date 4/07/2018).

[92] Colangelo, V. J., and Heiser, F., 1974, "Analysis of Metallurgical Failures," John Wiley & Sons, Inc., 1974, pp. 361.

[93] Kannatey-Asibu Jr, E., 2009, "Principles of laser materials processing," John Wiley & Sons, New Jersey.

[94] Zhou, S., Zeng, X., Hu, Q., 2008, "Analysis of Crack Behaviour for Ni-Based WC Composite Coatings by Laser Cladding and Crack-Free Realization," Applied Surface Science, 255(5) pp. 1646-1653.

[95] Wang, A., Wang, W., Xie, C., 2004, "CO 2 Laser-Induced Structure Changes on a Zircon Refractory," Applied Surface Science, 227(1) pp. 104-113.

[96] Goswami, G., Kumar, D., Grover, A., 1999, "Control of Defects during Laser Surface Alloying," Surface Engineering, 15(1) pp. 65-70.

[97] Kong, D. J., Yuan, F., and Miao, H., 2009, "Effects of Residual Stress on Interfacial Bonding Strength of WC Coating," Applied Mechanics and Materials, Anonymous Trans Tech Publ, 16, pp. 10-14.

[98] Tuominen, J., Vuoristo, P., Mäntylä, T., 2002, "Corrosion Behavior of HVOF-Sprayed and Nd-YAG Laser-Remelted High-Chromium, Nickel-Chromium Coatings," Journal of Thermal Spray Technology, 11(2) pp. 233.

[99] Pokhmurs' ka, H., 2003, "Crack Formation in Gas-Thermal Coatings Depending on the Conditions of their Laser Remelting," Materials Science, 39(1) pp. 64-68.

[100] Groysman, A., 2009, "Corrosion for everybody," Springer Science & Business Media, pp. 368.

[101] Magnani, M., Suegama, P., Espallargas, N., 2008, "Influence of HVOF Parameters on the Corrosion and Wear Resistance of WC-Co Coatings Sprayed on AA7050 T7," Surface and Coatings Technology, 202(19) pp. 4746-4757.

[102] Abdollah, S "Evaluating properties of corrosion resistance in thermal-sprayed (HVOF) coatings," PhD Thesis. University of Manchester, UK. 2008, (http://ethos.bl.uk/OrderDetails.do?uin=uk.bl.ethos.490179)) ,.

[103] Mateos, J., Cuetos, J., Fernandez, E., 2000, "Tribological Behaviour of Plasma-Sprayed WC Coatings with and without Laser Remelting," Wear, 239(2) pp. 274-281.

Novel Enhancement of HVOF Thermal Sprayed Nanostructured WC-12Co / Inconel-625 Coatings for Tribocorrosion Applications | **Al-Harbi, Naif I**

257

[104] Boudi, A., Hashmi, M., and Yilbas, B., 2006, "ESEM Evaluation of Inconel-625 Thermal Spray Coating (HVOF) Onto Stainless Steel and Carbon Steel Post Brine Exposure After Tensile Tests," Journal of Materials Processing Technology, 173(1) pp. 44-52.

[105] Al Fadhil, H., Stokes, J., Hashmi, S., 2005, "Post Test Analysis of Inconel-625 (HVOF) Coating using SEM and EDS After Exposure to Erosion-Corrosion Test," Microscopy and Microanalysis, 11(S02) pp. 1996-1997.

[106] Akesson, L., 1983, "An Experimental and Thermodynamic Study of the Co-W-C System in the Temperature Range 1470-1700 K", Science of Hard Materials, Springer, pp. 71-82.

[107] Karmaker, A., and Prasad, A., 2000, "Effect of Design Parameters on the Flexural Properties of Fiber-Reinforced Composites," Journal of Materials Science Letters, **19**(8) pp. 663-665.

[108] Li, H., Khor, K., and Cheang, P., 2002, "Titanium Dioxide Reinforced Hydroxyapatite Coatings Deposited by High Velocity Oxy-Fuel (HVOF) Spray," Biomaterials, **23**(1) pp. 85-91.

[109] Yilbas, B., Arif, A., and Gondal, M., 2005, "HVOF Coating and Laser Treatment: Three-Point Bending Tests," Journal of Materials Processing Technology, **164**pp. 954-957.

[110] Arif, A., and Yilbas, B., 2006, "Three-Point Bend Testing of HVOF Inconel 625 Coating: FEM Simulation and Experimental Investigation," Surface and Coatings Technology, **201**(3-4) pp. 1873-1879.

[111] Al-Anazi, D. M., Study of the Mechanical and Metallurgical Properties of AMDRY 9954 HVOF Coated Ti-6A1-4V Alloy, PhD Thesis, Dublin City University, Ireland. (2007; (http://doras.dcu.ie/16950)),.

[112] Watanabe, S., Amano, J., Tajiri, T., 1998, "Fatigue Cracks in HVOF Thermally Sprayed WC-Co Coatings," Journal of Thermal Spray Technology, **7**(1) pp. 93-96.

[113] Al-Fadhli, H., Analysis of the effect of bending, fatigue, erosion-corrosion and tensile stresses on HVOF coating of metallic surfaces, PhD Thesis, Dublin City University, Ireland. (2006; (http://doras.dcu.ie/17302/)),.

[114] White, J., Read, N., Ward, R., 2014, "Prediction of Melt Pool Profiles for Selective Laser Melting of AlSi10Mg Alloy," Materials Science and Technology Conference and Exhibition 2014, Anonymous pp. 1985-1992.
[115] Apfelberg, D.B., 1987, "Evaluation and installation of surgical laser systems," Springer, pp. 13-15.

[116] Ching, H. A., Choudhury, D., Nine, M. J., 2014, "Effects of Surface Coating on Reducing Friction and Wear of Orthopaedic Implants," Science and Technology of Advanced Materials, **15**(1) pp. 014402.

[117] Menezes, P., and Kailas, S., 2016, "Role of Surface Texture and Roughness Parameters on Friction and Transfer Film Formation when UHMWPE Sliding Against Steel," Biosurface and Biotribology, **2**(1) pp. 1-10.

[118] Al-Samarai, R. A., Haftirman, K. R. A., and Al-Douri, Y., 2012, "Evaluate the Effects of various Surface Roughness on the Tribological Characteristics Under Dry and Lubricated Conditions for Al-Si Alloy," Journal of Surface Engineered Materials and Advanced Technology, **2**(03) pp. 167.

Novel Enhancement of HVOF Thermal Sprayed Nanostructured WC-12Co / Inconel-625 Coatings for Tribocorrosion Applications | **Al-Harbi, Naif I**

258

[119] Al-Samarai, R. A., Haftirman, K. R. A., and Al-Douri, Y., 2012, "The Influence of Roughness on the Wear and Fric-Tion Coefficient Under Dry and Lubricated Sliding," Int.J.Sci.Eng.Res, **3**(4) pp. 1-6.

[120] Chikarakara, E., Naher, S., and Brabazon, D., 2010, "Process Mapping of Laser Surface Modification of AISI 316L Stainless Steel for Biomedical Applications," Applied Physics A, **101**(2) pp. 367-371.

[121] Yasa, E., and Kruth, J., 2011, "Application of Laser Re-Melting on Selective Laser Melting Parts," Advances in Production Engineering and Management, **6**(4) pp. 259-270.

[122] Formisano, A., Capece Minutolo, F., Caraviello, A., 2016, "Influence of Eta-Phase on Wear Behavior of WC-Co Carbides," Advances in Tribology, Hindawi.

[123] Chivavibul, P., Watanabe, M., and Kuroda, S., 2007, "316 Effect of carbide size and Co content on wear behavior of HVOF-sprayed WC-Co coatings," The Proceedings of the Materials and Mechanics Conference 2007, Anonymous The Japan Society of Mechanical Engineers, pp. 183-184.

[124] Safdar, S., Li, L., Sheikh, M., 2006, "An Analysis of the Effect of Laser Beam Geometry on Laser Transformation Hardening," Journal of Manufacturing Science and Engineering, **128**(3) pp. 659-667.

[125] Safari, M., 2014, "Numerical Investigation of the Effect of Process and Sheet Parameters on Bending Angle in the Laser Bending Process," World Journal of Mechanics, **4**(04) pp. 97.

[126] Paul, C., Gandhi, B., Bhargava, P., 2014, "Cobalt-Free Laser Cladding on AISI Type 316L Stainless Steel for Improved Cavitation and Slurry Erosion Wear Behavior," Journal of Materials Engineering and Performance, **23**(12) pp. 4463-4471.

[127] Li, J., Chen, C., and Wang, D., 2012, "Surface Modification of Titanium Alloy with Laser Cladding RE Oxides Reinforced Ti3Al–matrix Composites," Composites Part B: Engineering, **43**(3) pp. 1207-1212.

[128] Jayakumar, J., and Kumar, D. T. S., 2015, "Review Study of Laser Cladding Processes on Ferrous Substrates, 2015," International Journal of Advanced Multidisciplinary Research, **2**(6) pp. 72-87.

[129] Weng, F., Yu, H., Chen, C., 2015, "Microstructures and Wear Properties of Laser Cladding Co-Based Composite Coatings on Ti–6Al–4V," Materials & Design, **80**pp. 174-181.

[130] Weng, F., Yu, H., Chen, C., 2017, "Effect of Process Parameters on the Microstructure Evolution and Wear Property of the Laser Cladding Coatings on Ti-6Al-4V Alloy," Journal of Alloys and Compounds, **692**pp. 989-996.

[131] Hemmati, I., Ocelík, V., and De Hosson, J Th M, 2011, "The Effect of Cladding Speed on Phase Constitution and Properties of AISI 431 Stainless Steel Laser Deposited Coatings," Surface and Coatings Technology, **205**(21-22) pp. 5235-5239.

[132] Hutchings, I., 1992, "Tribology: Friction and Wear of Engineering Materials," Arnold, Pans.

[133] Strang, J., 2006, "Cast valve materials for seawater service nickel-aluminum bronze and its rivals," Proceedings of the valve world conference, Maastricht, Netherlands.
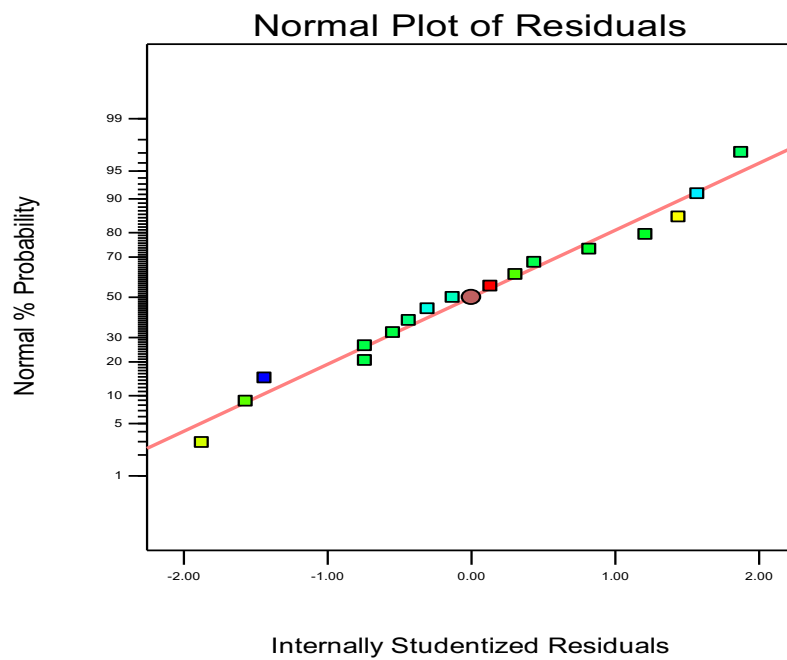
Novel Enhancement of HVOF Thermal Sprayed Nanostructured WC-12Co / Inconel-625 Coatings for Tribocorrosion Applications | **Al-Harbi, Naif I**

259

[134] Dawson, R., 1978, "Aluminium Bronze," Eng.Mater.Design, **22**(12) pp. 25-28.

[135] Callcut, V., 1989, "Aluminium Bronzes for Industrial Use," Metals and Materials, **5**(3) pp. 128-132.

[136] Nandakumar, M., Sudhakar, K., Natu, H., 2018, "Experimental Investigation of Slurry Erosion Characteristics of Laser Treated Nickel Aluminum Bronze," Materials Today: Proceedings, **5**(1) pp. 2641-2649.

[137] Hawthorne, H., Arsenault, B., Immarigeon, J., 1999, "Comparison of Slurry and Dry Erosion Behaviour of some HVOF Thermal Sprayed Coatings," Wear, **225**pp. 825-834.

[138] Tomlinson, W., and Linzell, C., 1988, "Anodic Polarization and Corrosion of Cemented Carbides with Cobalt and Nickel Binders," Journal of Materials Science, **23**(3) pp. 914-918.

[139] Singh, R., Kumar, M., Kumar, D., 2012, "Erosion and Corrosion Behaviour of Laser Cladded Stainless Steels with Tungsten Carbide," Journal of Materials Engineering and Performance, **21**(11) pp. 2274-2282.

[140] Rogne, T., Solem, T., and Berget, J., 1998, "Effect of Composition and Corrosion Properties of the Metallic Matrix on the Erosion-Corrosion Behaviour of HVOF Sprayed WC-Coatings," Corrosion 98, San Diego, NACE International.

[141] Perry, J. M., Hodgkiess, T., and Neville, A., 2002, "A Comparison of the Corrosion Behavior of WC-Co-Cr and WC-Co HVOF Thermally Sprayed Coatings by in Situ Atomic Force Microscopy (AFM)," Journal of Thermal Spray Technology, **11**(4) pp. 536-541.

[142] Rakhes, M., E. Koroleva, and Z. Liu., 2011, "Improvement of corrosion performance of HVOF MMC coatings by laser surface treatment," Surface Engineering, **27**(10) pp. 729-733.

[143] Stokes, J., Production of Coated and Free-Standing Engineering Components using the HVOF (High Velocity Oxy-Fuel) Process, PhD Thesis. Dublin City University, Ireland. (2003; (http://doras.dcu.ie/18232/)),.

[144] Eltawahni, H., Rossini, N., Dassisti, M., 2013, "Evalaution and Optimization of Laser Cutting Parametersfor Plywood Materials," Optics and Lasers in Engineering, **51**(9) pp. 1029-1043.

[145] Havrilla, D., and Anthony, P., 2000, "Laser Cutting Process Fundamentals and Troubleshooting Guidelines," Rofin Sinar Laser Publications, p. 5 1 .

[146] Eltawahni, H., Optimisation of process parameters of high power CO2 Laser cutting for advanced materials, PhD Thesis. Dublin City University, Ireland. (2011;(http://doras.dcu.ie/16609/)),

[147] Curtiss Wright , "HVOF Thermal Spray," (http://www.fwgts.com/blog/hvof-thermal-spray), (Access date 17/04/2019) .

[148] Atomic Rockets, "Lasers, Mirrors and Star Pyramids" (http://toughsf.blogspot.com/2018/05/lasers-mirrors-and-star-pyramids.html), (Access date 17/04/2019) pp. 1-5.

Novel Enhancement of HVOF Thermal Sprayed Nanostructured WC-12Co / Inconel-625 Coatings for Tribocorrosion Applications | **Al-Harbi, Naif I**

260

Appendices

Appendix A-1: Normal plot residual and Predicted versus actual plot for laser-treated mixed coating track width (mm).

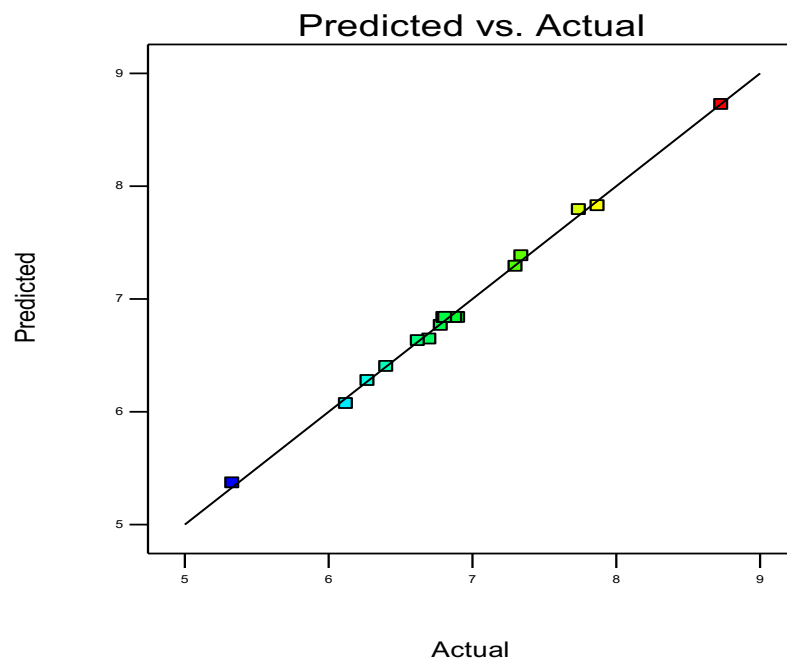Design-Expert® Software
Mixed Coating (Track Width)

Color points by value of
Mixed Coating (Track Width) :
8.73
5.33

Normal Plot of Residuals

Design-Expert® Software
Mixed Coating (Track Width)

Color points by value of
Mixed Coating (Track Width) :
8.73
5.33

Predicted vs. Actual

Novel Enhancement of HVOF Thermal Sprayed Nanostructured WC-12Co / Inconel-625 Coatings for Tribocorrosion Applications | **Al-Harbi, Naif I**

261

Appendix A-2: Normal plot residual and Predicted versus actual plot for laser-treated mixed coating (D_m / t_c).

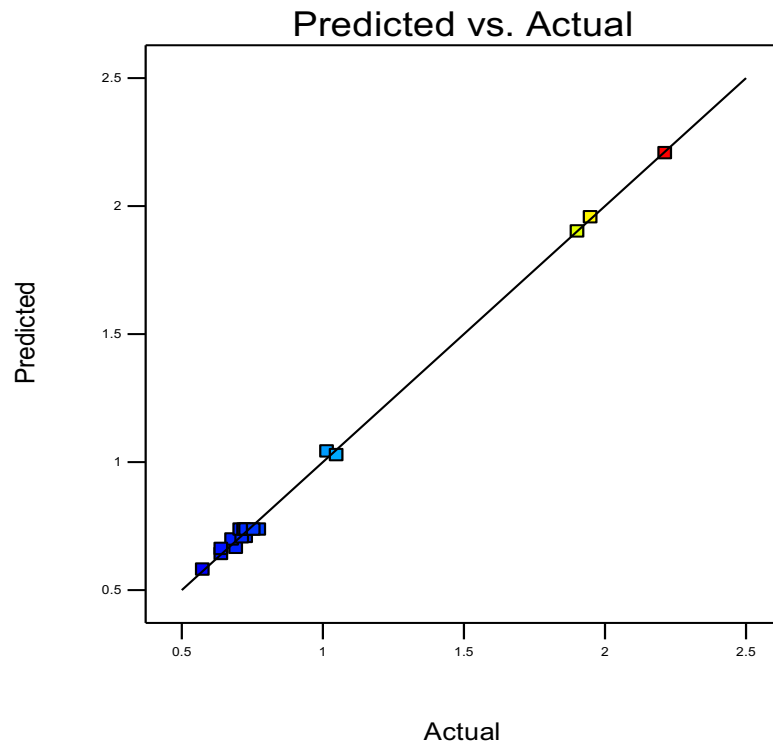Design-Expert® Software
Sqrt(Mixed Coating (Dm /tc))

Color points by value of
Sqrt(Mixed Coating (Dm /tc)):

2.214

0.574

Normal Plot of Residuals

Normal % Probability

Externally Studentized Residuals

Design-Expert® Software
Sqrt(Mixed Coating (Dm /tc))

Color points by value of
Sqrt(Mixed Coating (Dm /tc)):

2.214

0.574

Predicted vs. Actual

Predicted

Actual

Novel Enhancement of HVOF Thermal Sprayed Nanostructured WC-12Co / Inconel-625 Coatings for Tribocorrosion Applications | **Al-Harbi, Naif I**

262

Novel Enhancement of HVOF Thermal Sprayed Nanostructured WC-12Co / Inconel-625 Coatings for Tribocorrosion Applications | **Al-Harbi, Naif I**

263

Appendix C: Normal plot residual and Predicted versus actual plot for laser-treated mixed coating yield strength (MPa).

Design-Expert® Software
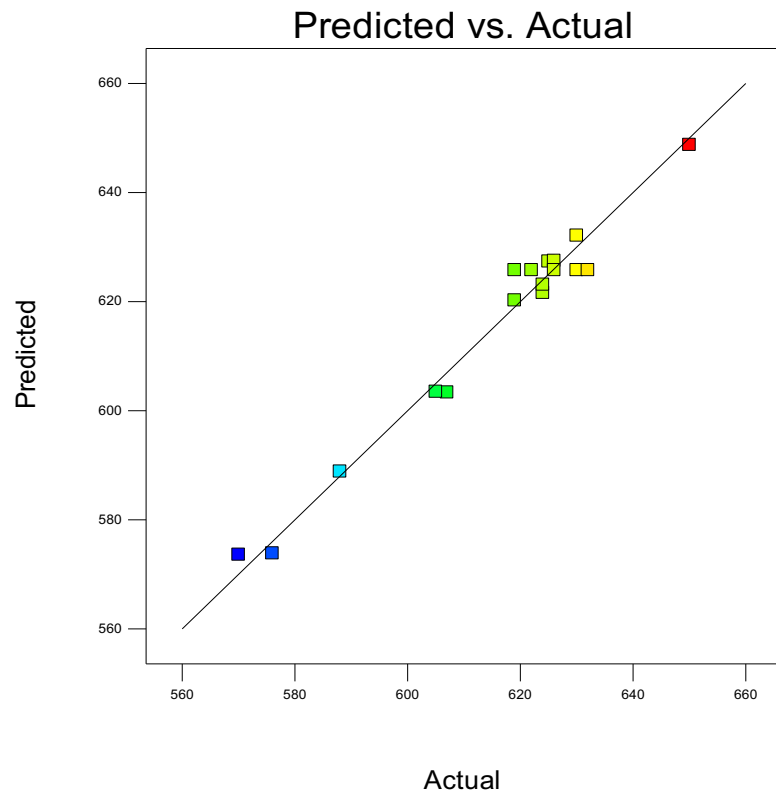Mixed Coating - Bending

Color points by value of
Mixed Coating - Bending:
650
570

Normal Plot of Residuals

Normal % Probability

Externally Studentized Residuals

Design-Expert® Software
Mixed Coating - Bending

Color points by value of
Mixed Coating - Bending:
650
570

Predicted vs. Actual

Predicted

Actual

Novel Enhancement of HVOF Thermal Sprayed Nanostructured WC-12Co / Inconel-625 Coatings for Tribocorrosion Applications | **Al-Harbi, Naif I**

264
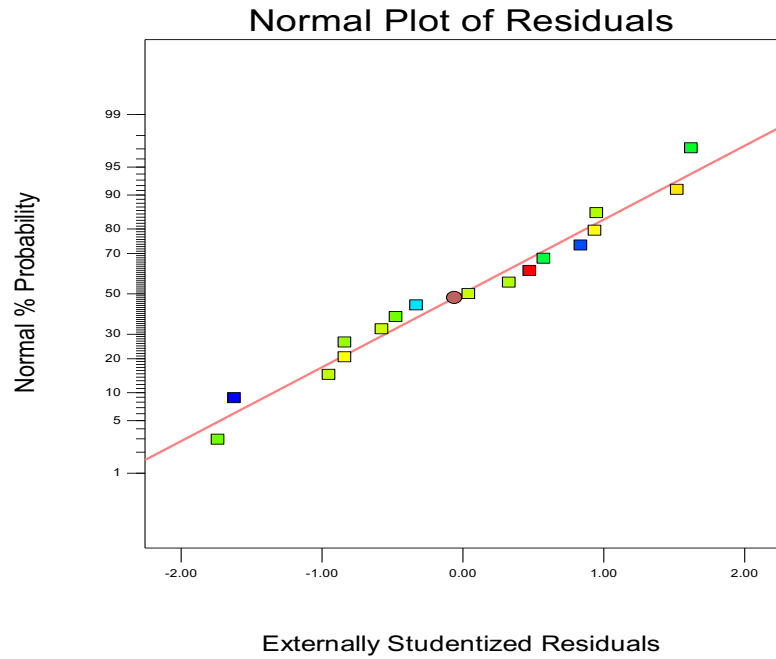
Appendix D: Normal plot residual and Predicted versus actual plot for laser-treated mixed coating dry erosion (g).

Design-Expert® Software
Mixed Coating-Dry Erosion

Color points by value of
Mixed Coating-Dry Erosion:

5.95

0.75

Normal Plot of Residuals

Normal % Probability (y-axis): 1, 5, 10, 20, 30, 50, 70, 80, 90, 95, 99

Externally Studentized Residuals (x-axis): -4.00, -2.00, 0.00, 2.00, 4.00

Design-Expert® Software
Mixed Coating-Dry Erosion

Color points by value of
Mixed Coating-Dry Erosion:

5.95

0.75

Predicted vs. Actual

Predicted (y-axis): 0, 1, 2, 3, 4, 5, 6

Actual (x-axis): 0, 1, 2, 3, 4, 5, 6

Novel Enhancement of HVOF Thermal Sprayed Nanostructured WC-12Co / Inconel-625 Coatings for Tribocorrosion Applications | **Al-Harbi, Naif I**

265
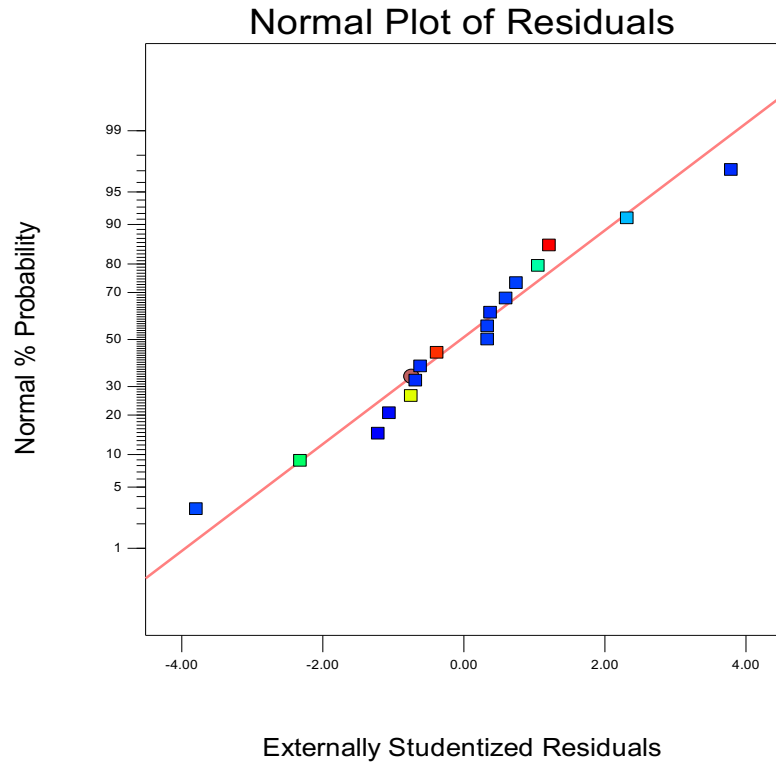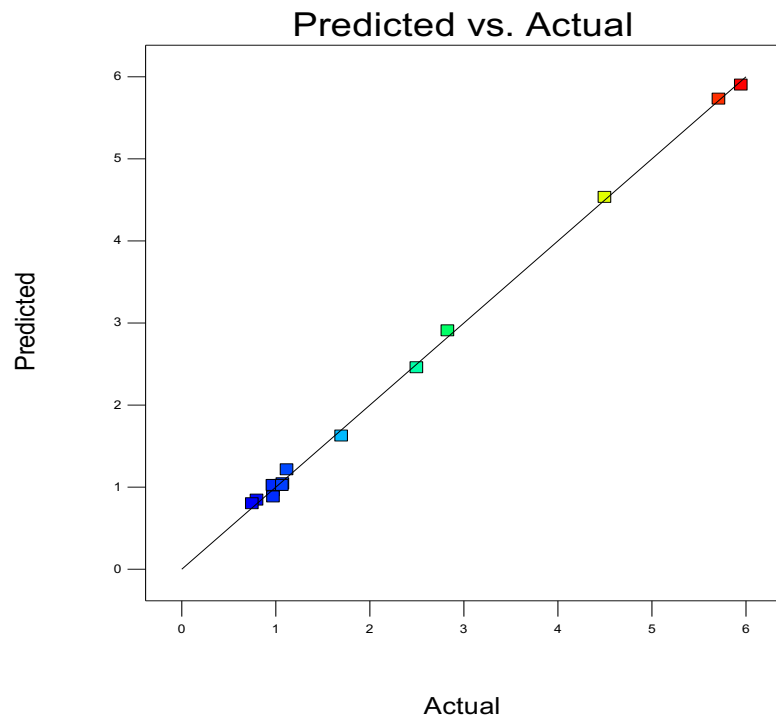
Appendix E: Normal plot residual and Predicted versus actual plot for laser-treated mixed coating slurry erosion (g).

Design-Expert® Software
Mixed-Slurry erosion

Color points by value of
Mixed-Slurry erosion:
0.9
0.265

Normal Plot of Residuals

Design-Expert® Software
Mixed-Slurry erosion

Color points by value of
Mixed-Slurry erosion:
0.9
0.265

Predicted vs. Actual

Novel Enhancement of HVOF Thermal Sprayed Nanostructured WC-12Co / Inconel-625 Coatings for Tribocorrosion Applications | **Al-Harbi, Naif I**

266